# CHARACTERIZING HELICOBACTER PYLORI FLAGELLAR MOTOR ACCESSORY STRUCTURES

by

#### KYLE ROSINKE

(Under the Direction of Timothy R. Hoover)

#### **ABSTRACT**

The bacterial flagellum is a complex nanomachine that functions in motility. In Helicobacter pylori, flagellum-mediated motility plays a critical role in colonizing the human stomach. This intricate structure spans from the cytoplasm, passes through both the inner and outer membranes, and extends to form an extracellular filament. The flagellar motor, located within the membrane-spanning region, facilitates proton translocation and axial rotation, driving motility. Key proteins within this motor are membrane-associated, either through transmembrane helices or lipid modifications, such as acyl chains in lipoproteins. Notably, the flagellar motor of *H. pylori* features several poorly characterized accessory structures, believed to be essential for the generation of high torque, which enables the bacterium to navigate the viscous environment of the gastric mucosa. This dissertation focuses on the characterization of these accessory proteins to enhance our understanding of their roles in *H. pylori* motility and pathogenesis. The first research chapter (Chapter 2) reports on the identification of *H. pylori* HP0838 as a lipoprotein that forms a previously uncharacterized ring-like motor accessory associated with the outer membrane. In the absence of HP0838, H. pylori B128 displayed a motilitydependent sensitivity to bacitracin, an antibiotic that is normally excluded by the outer membrane. We designated HP0838 as FapH (flagellum-associated protein in Helicobacter pylori) and the ring structure that it forms as the FapH ring, and hypothesize that the FapH ring helps to preserve the barrier function of the outer membrane during

flagellar rotation. In Chapter 3, bacitracin-resistant mutants of a *H. pylori* Δ*fapH* mutant were isolated and characterized. Mutations in the ferric uptake regulator (*fur*) and the lipopolysaccharide biosynthesis gene *lpxF* were found to suppress the bacitracinsensitivity of the *H. pylori* Δ*fapH* mutant. In Chapter 4, PflA and PflB were shown to form a set of spokes and ring-like structures that are associated with the flagellar stator units and presumably stabilize the stators. In addition, PflA was shown to interact with FlgY, which forms a novel motor accessory consisting of a ring and set of spokes that surround the MS-ring. We hypothesize that the FlgY ring acts as a bushing to stabilize the MS-ring as it rotates. In Chapter 5, loss of the previously uncharacterized lipoprotein HP0018 was shown to result in extensive formation of outer membrane vesicles that frequently formed long chains at the cell pole. Co-immunoprecipitation assays identified two enzymes involved in modification of cell wall peptidoglycan, AmiA and MltD, as potential HP0018 interaction partners. HP0018 may modulate the activity of AmiA or MltD, and in the absence of HP0018 the unregulated activity of these enzymes may alter the peptidoglycan layer in a manner that results in altered cell shape and hypervesiculation.

INDEX WORDS: Helicobacter pylori, motility, flagella, flagellar motor, protein, lipoprotein

Characterizing	Helicobacter p	<i>pylori</i> flac	ellar motor	accessory	structures

by

# Kyle Rosinke

A Dissertation Submitted to the Graduate Faculty of the University of Georgia in Partial Fulfillment of the Requirements for the Degree.

**Doctor of Philosophy** 

Athens, Georgia

2025

©2025

Kyle Rosinke

All Rights Reserved

### Characterizing Helicobacter pylori flagellar motor accessory structures

by

# Kyle Rosinke

Major Professor: Timothy R. Hoover

Committee:

Vincent J. Starai Christine Szymanski Jorge C. Escalante Stephen Trent

Electronic Version Approved:

Ron Walcott
Dean of the Graduate School
The University of Georgia
May 2025

### Acknowledgements

I would like to thank my grandfather, Elmer Hamann, for his financial and moral support, which made both my bachelor's degree and Ph.D. possible. I am also grateful to Dr. Neil Blackstone for his mentorship during my undergraduate studies and guidance toward graduate school. Special thanks to Dr. Tim Hoover for giving me the opportunity to join his lab during my fourth rotation and for his continued patience and guidance throughout my Ph.D. I would also like to acknowledge Dr. Vinny Starai for his valuable input on experimental design and troubleshooting. Lastly, I thank my dog, Flick, for unparalleled moral support.

# **Table of Contents**

Li	ist of Figures	vii
Li	ist of Tables	х
С	hapter 1: Introductory Chapter	1
	Helicobacter pylori history, prevalence, effect, and mode of colonization	1
	Flagellar-Driven Motility	4
	Flagellar gene regulation	7
	Flagella Localization	9
	Flagella Assembly and Structure	12
	The Flagellar Motor of H. pylori	21
	Flagellar Motor Function and Rotational Switching	27
	Bacterial Chemotaxis	31
	Translocation of flagellar proteins across the inner membrane	37
	Lipoprotein Sorting and processing	46
	The role of the H. pylori Flagella in Biofilm Formation	52
	Candidate Flagellar Genes in H. pylori	53
С	HAPTER SUMMARIES	55
	hapter 2: A Helicobacter pylori flagellar motor accessory is needed to maintain the barrier	
fι	Inction of the outer membrane during flagellar rotation	59
	ABSTRACT	60
	AUTHOR SUMMARY	60
	RESULTS	63
	DISCUSSION	76
	MATERIALS AND METHODS	80
	SUPPLEMENTARY MATERIALS	88
С	hapter 2 Appendix	108
	Examining interactions between known and potential flagellar motor proteins using the BAC system	<b>CTH</b> 108
	Incorportating formaldehyde cross-linking in the co-IP assay to search for FapH interaction partners	110
	Comparision of the $\Delta$ fapH pfl $A^*$ and $\Delta$ fapH pfl $A^T$ transcriptomes	112
	Using AlphaFold to model protein-protein interactions	118

Chapter 3: Inactivation of LpxF and Fur rescue bacitracin sensitivity in fapH deletion mutants	130
INTRODUCTION	130
RESULTS	131
CONCLUSIONS	139
SUPPORTING MATERIALS	140
Chapter 4: FlgY, PflA, and PflB form spoke-ring network in high-torque flagellar motor of Helicobacter pylori	150
ABSTRACT	151
SIGNIFICANCE STATEMENT	151
INTRODUCTION	152
RESULTS	155
DISCUSSION	163
MATERIALS AND METHODS	166
SUPPORTING INFORMATION	173
Chapter 4 appendix: <i>pfIA</i> repeat units	187
Chapter 5: Helicobacter pylori HP0018 has a Potential Role in Maintenance of the Cell Envelope	e191
ABSTRACT	192
INTRODUCTION	192
RESULTS	194
DISCUSSION	204
CONCLUSIONS	207
MATERIALS AND METHODS	207
SUPPLEMENTARY MATERIALS	213
Chapter 6: Conclusions and Future Directions	228
FapH, outer membrane associated flagellar motor accessory structures, and membrane permeability	228
Inner membrane associated flagellar motor structures and rod-cage connection	231
Role of a candidate cell division protein in outer membrane stability	232
REFERENCES	235

### **List of Figures**

#### **Chapter 1: Introductory Chapter**

- Figure 1.1: Scanning electron microscopy images of *H. pylori* B128 cells
- Figure 1.2: Molecular overview of motility in *H. pylori*
- Figure 1.3: Bacterial flagellar arrangements
- Figure 1.4: The Flagellar Basal Body
- Figure 1.5: The F-T3SS
- Figure 1.6: The *H. pylori* flagellar sheath
- Figure 1.7: Ion movement through the bacterial flagellar motor
- Figure 1.8: Rotational switching of the motor at the C-Ring
- Figure 1.9: Chemotaxis in bacteria with a peritrichous flagellation pattern
- Figure 1.10: Chemotaxis in H. pylori
- Figure 1.11: translocation of peptides containing a SPI or SPII signal sequence (SS) by the post-translational and co-translational pathways
- Figure 1.12: YidC insertase activity of a peptide with a SPI signal sequence
- Figure 1.13. SEC SPI and SPII characterization of proteins discussed in future chapters
- Figure 1.14: Translocation and processing of a prolipoprotein containing a SPII signal sequence in *E. coli*
- Figure 1.15: Lipoprotein trafficking in *H. pylori*

# Chapter 2: A *Helicobacter pylori* flagellar motor accessory is needed to maintain the barrier function of the outer membrane during flagellar rotation

- Figure 2.1. Organization of operons containing *fapH* in various members of Campylobacterota and the predicted lipoprotein signal peptides for the FapH homologs
- Figure 2.2. Electron micrographs of *H. pylori* B128 wild type and  $\Delta fapH pflA^T$  strain.
- Figure 2.3. Motility of H. pylori B128 wild type and  $\Delta fapH$  mutants and their sensitivity to bacitracin
- Figure 2.4. Architecture of the FapH ring in the *H. pylori* motor
- Figure 2.5. Identification of FapH interaction partners
- Figure S2.1. Characterization of flagellation patterns and growth rates of  $\Delta fapH$   $pflA^{T}$  and  $\Delta fapH$   $pflA^{*}$
- Figure S2.2. Predicted tertiary structures of PfIA, PfIA<sup>T</sup> and PfIA\*
- Figure S2.3. Reconstructed  $\Delta fapH$  mutants display sensitivity to bacitracin
- Figure S2.4. *In-situ* structures of the wild-type and  $\Delta fapH pflA^T$  motors
- Figure S2.5. AlphaFold modeling of FapH
- Figure S2.6. Assessment of protein-protein interactions in BACTH system on MacConkey-maltose agar
- Figure S2.7. Characterization of *H. pylori* Δ*hp1456* mutant
- Figure S2.8. Construction of the *H. pylori* B128 Δ*fapH* mutant
- Figure S2.9. DNA sequences of the insertions in plasmid pHel3 to generate plasmids pHel3-GG and pHel3-myc

#### **Chapter 2 Appendix**

Figure A2.1: Protein-protein interactions using BACTH assays

- Figure A2.2: FapH-myc formaldehyde cross linking
- Figure A2.3: RT-qPCR with hp0715
- Figure A2.4: AlphaFold structure prediction and error plot of FapH
- Figure A2.5: Alphafold2 multimer predictions
- Figure A2.6: PISA values from FapH-HP1456 AlphaFold generated models
- Figure A2.7: Modeled interactions of FapH with HP1454 and HP1456
- Figure A2.8: FapH-HP1456 output models with different interfaces
- Figure A2.9: Alignment and residue conservation of FapH
- Figure A2.10: Error plots of AlphaFold models
- Figure A2.11: PfIA-PfIB output models with similar interface
- Figure A2.12: PISA values from PfIA-PfIB AlphaFold generated models

# Chapter 3: Inactivation of LpxF and Fur rescue the bacitracin sensitivity in FapH deletion mutants

- Figure 3.1: Some FapH mutants are less sensitive to bacitracin
- Figure 3.2:  $\Delta fapH$  rescues sensitive to bacitracin in the  $\Delta fapH$  background
- Figure 3.3: Strain Flagellation when grown in 0.25% semi-solid agar
- Figure 3.4: Cell diameter measurements
- Figure 3.5: Incubation of  $\Delta fapH$  with 2-2' dipyridyl
- Figure S3.1: Unassociated flagella in Δ*fapH*
- Figure S3.2: Membrane morphology of strains

# Chapter 4: Cryo-electron tomography reveals how coordination between novel FlgY and PflA/PflB is required for flagellar motility in *Helicobacter pylori*.

- Figure 4.1. Cryo-ET analysis reveals distinct spoke-ring network in the *H. pylori* motor.
- Figure 4.2. FlgY is essential for formation of proximal and distal spokes in the *H. pylori* flagellar motor
- Figure 4.3. FlgY forms spoke-ring near the MS-ring
- Figure 4.4. PflA forms distal spokes and PflB forms distal ring structure in the *H. pylori* flagellar motor
- Figure 4.5. Model of the *H. pylori* flagellar motor shows distinct FlgY-PflA-PflB spoke-ring network that bridges the MS-ring and 18 stator complexes
- Figure S4.1. AlphaFold-predicted structures indicate that PfIA in *Campylobacterota* and MotK in *Cereibacter sphaeroides* possess similar domains and motifs
- Figure S4.2. AlphaFold-predicted structures suggest that FlgY in *Campylobacterota* and MotE in *C. sphaeroides* possess similar domains and motifs
- Figure S4.3. Asymmetric reconstruction of the *H. pylori* flagellar motor reveals 13 spokes around the MS-ring in periplasmic region
- Figure S4.4. PflA and PflB are essential for bacterial motility but not flagellar assembly in *H. pylori*
- Figure S4.5. *In-situ* structure of the Δ*pflB* flagellar motor
- Figure S4.6. Molecular interface between the MS-ring and FlgY ring
- Figure S4.7. AlphaFold-predicted model of *H. pylori* PflA-PflB<sub>2</sub> heterotrimer fits well into the *insitu* map
- Figure S4.8. SPR experiments indicate that the PfIA-PfIB complex in *H. pylori* interacts with components of the stator and cage
- Figure S4.9. Bacterial adenylate cyclase two-hybrid (BACTH) assay shows interactions of PflA and PflB with other motor components
- Figure S4.10. Construction of specific mutants in *H. pylori* B128

#### Chapter 4 appendix: pflA repeat units

Figure A4.1: PflA structure as predicted by AlphaFold monomer

Figure A4.2: PCR with internal pflA primers

Figure A4.3: Alignment of the pflA in H180-7 and the native pflA

#### Chapter 5: Helicobacter pylori HP0018 has a Potential Role in Maintenance of the Cell Envelope

Figure 5.1. TEM and SEM images of wild-type *H. pylori* B128, the non-motile  $\Delta hp0018$  mutant (H19), and the motile  $\Delta hp0018$  isolate (H23).

Figure 5.2. Motility of *H. pylori* strains in soft agar medium. *H. pylori* strains were stab inoculated into soft agar medium and incubated under microaerobic conditions for 7 d.

Figure 5.3. Flagella of strains H19 and H23

Figure 5.4. TEM images of OMVs isolated from wild type, H19, and H23

Figure 5.5. Localization of a HP0018-sfGFP fusion protein in *H. pylori* by fluorescent microscopy

Figure 5.6. AlphaFold2 predictions of protein-protein interactions between HP0018 and AmiA or MltD.

Figure S5.1. TEM images of the motile *H. pylori*  $\Delta hp0018$  mutant complemented with plasmid expressing the HP0018-myc fusion protein.

#### **List of Tables**

#### **Chapter 1: Intoductory Chapter**

Table 1.1. Helicobacter pylori flagellar, flagellar-associated and flagellar regulatory genes

# Chapter 2: A *Helicobacter pylori* flagellar motor accessory is needed to maintain the barrier function of the outer membrane during flagellar rotation

Table S2.1. Homologs of FapH, FlgP, and FlgH in *Helicobacter* species and other members of Campylobacterota with flagellar sheaths

Table S2.2: Mutations identified in  $\Delta fapH$  strains,  $\Delta flgP$  mutant, and  $\Delta hp1456$  mutant

Table S2.3. Proteins identified from third replicate of the co-immunoprecipitation assay with FapH-Myc protein

Table S2.4: Primer list

Table S2.5: Strains and Plasmids

#### **Chapter 2 Appendix**

Table A2.1. Genes that are differentially expressed in ΔfapH pflA\*

Table A2.2 or 2.3?

Table A2.2. Counts for DEGs in  $\triangle fapH pflA^*$ 

# Chapter 3: Inactivation of LpxF and Fur rescue the bacitracin sensitivity in FapH deletion mutants

Table S3.1: Strain WGS

# Chapter 4: Cryo-electron tomography reveals how coordination between novel FlgY and PflA/PflB is required for flagellar motility in *Helicobacter pylori*

Table S4.1. Mutations identified in the  $\Delta pflA$ ,  $\Delta pflB$ , and  $\Delta flgY$  strains

Table S4.2. Plasmids and *H. pylori* strains used in the study

Table S4.3. Primers used in the study

Table S4.4. Summary of cryo-ET data used in the study

#### Chapter 4 appendix: pflA repeat units

Table A4.1: pflA unassigned new junction evidence frequency

Table A4.2: pflA internal primers

#### Chapter 5: Helicobacter pylori HP0018 has a Potential Role in Maintenance of the Cell Envelope

Table 5.1. Proteins identified from co-IP assay with HP0018-myc-tagged protein

Table S5.1. Strains, plasmids, and primers generated for the study

Table S5.2. Mutations identified in the original H. pylori  $\Delta$ hp0018 mutant (strain H19) and a motile variant of the  $\Delta$ hp0018 mutant (strain H23) compared to wild-type H. pylori B128

Table S5.3. Proteins identified in OMV samples from wild-type H. pylori B128, non-motile  $\Delta hp0018$  mutant (strain H19), and motile  $\Delta hp0018$  isolate (strain H23)

# **Chapter 1: Introductory Chapter**

# Helicobacter pylori history, prevalence, effect, and mode of colonization

Helicobacter pylori was first characterized in 1982 by the clinical pathologist Dr. Barry Marshall and trainee doctor Professor Robin Warren (*Marshall and Warren 1984*). In his role as a clinical pathologist, Warren noticed a correlation between stomach inflammation and a helical, Gram-negative bacterium present in the inflamed tissue (*Watts 2005*). To test the hypothesis that the bacterium was responsible for the gastric inflammation, Dr. Warren teamed up with Professor Marshall. After encountering a great deal of skepticism from the scientific community regarding the hypothesis that a bacterium was responsible for peptic ulcers, Marshall performed an experiment on himself, swallowing a culture of *Campylobacter pylori*, later renamed *H. pylori*. He developed gastritis and a stomach biopsy revealed the presence of *H. pylori* in the tissue samples, fully satisfying Koch's postulates.

H. pylori is a human bacterial pathogen belonging to the phylum Campylobacterota that infects roughly half of the human population worldwide (Hooi et al. 2017). H. pylori is a helical-shaped diderm (Fig. 1.1) that uses multiple polar flagella for motility (Prashar et al. 2022). H. pylori colonizes the human stomach where infection may persist for years. Most of the H. pylori cells are found as free swimming in the mucus layer of the gastric epithelium, while a smaller proportion of bacterial cells attach to epithelial cells to form micro colonies (Fung et a. 2019, Kim and Blanke 2012). Of the cells that attach to the epithelium, a small percentage penetrate deep within the gastric glands (Fung et a. 2019, Keilberg et al. 2016), and some of these bacteria invade epithelial cells (Capurro et al. 2019, Dubois and Borén 2007). Bacteria that invade host cells can successfully recolonize the stomach following eradication treatment. H. pylori infection can develop into several diseases, including chronic gastritis, peptic ulcer disease, and gastric cancer (Wroblewski et al. 2010, Salama et al. 2013). The most serious of these, gastric cancer, is the third most common cancer worldwide (Plummer et al. 2015). The strong association of H.

*pylori* with this form of cancer led to the classification of the bacterium as a class 1 carcinogen by the International Agency for Research on Cancer.

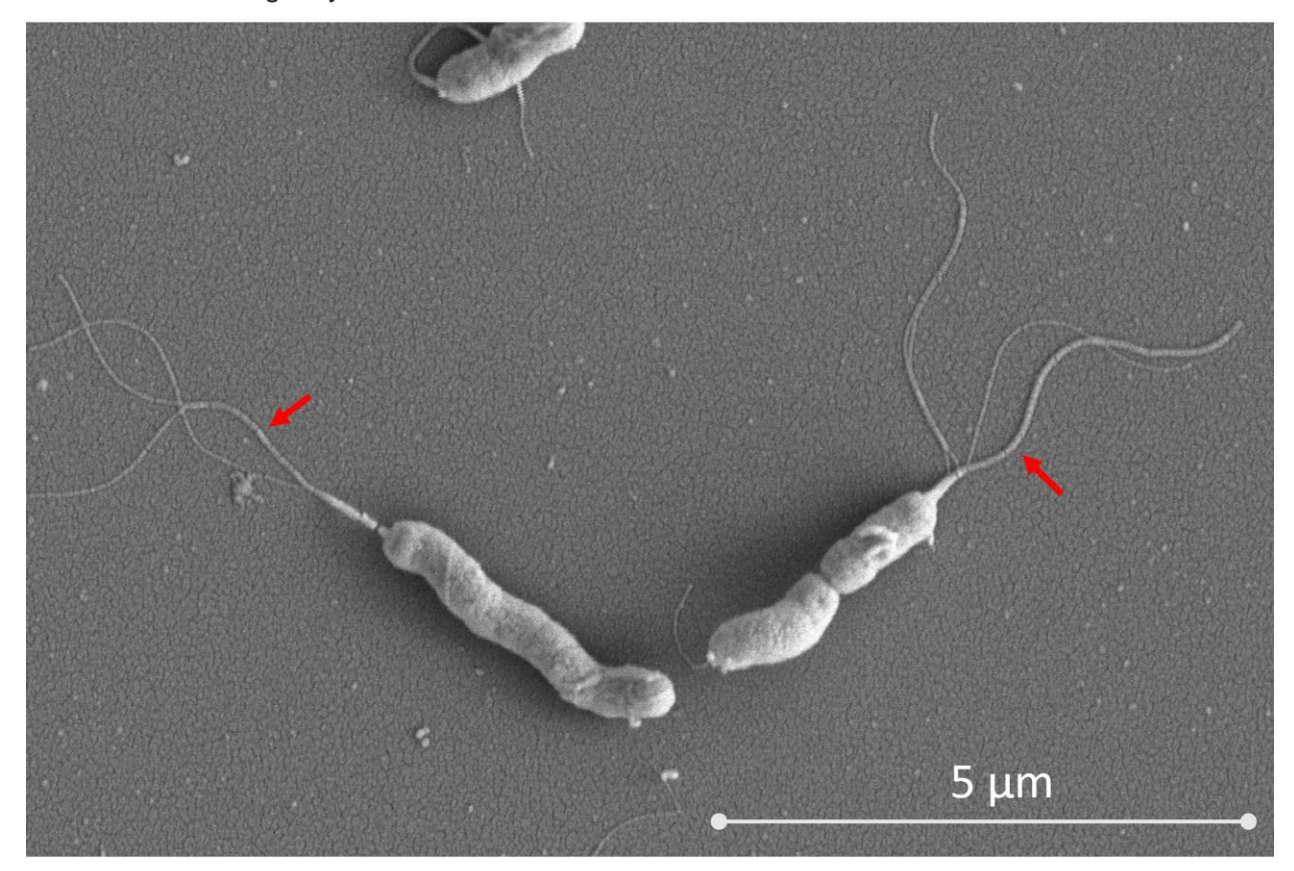


**Figure 1.1. Scanning electron microscopy images of** *H. pylori* **B128 cells.** Note the helical shape of the cells and the multiple flagella at one cell pole. The cell to the right is undergoing cytokinesis as evidenced by the invagination of the cell envelope at the mid-cell. Flagella are indicated with red arrows. Scanning electron microscopy images were taken by K. Rosinke.

An important adaptation of *H. pylori* to the acid environment of the stomach is the ability of the bacterium to buffer the pH inside and outside the cell. This buffering is accomplished through the urease, AmiR amidase, and AmiF formamidase enzymes (*Van Vliet et al. 2004*). Urease is made up of subunits A (UreA) and B (UreB), where UreA contains the active site and UreB assists in assembly and stabilization. The presence of urea in the stomach likely comes from saliva but may also come from diffusion from the blood stream. One study of healthy adults found that the average concentration of urea in saliva is 20.5 mg/dl, while the concentration of urea in plasma is 24.5 mg/dl (*Lasisi et al. 2016*). Saliva is produced at a rate of 0.3–0.4 ml/min, which means that between 288-384 ml is produced while awake (average 16 h per day), and 96 ml while asleep (average 8h per day) for a total of 384-480 ml of saliva produced per day

(*lorgulescu* 2009), which contains 1.3-1.6 mmol of urea. *H. pylori* transports the urea into the cell through a hydrogen gated Urel channel, where UreA hydrolyzes urea leading to the buffering of pH. Urease is also found outside the cell where it hydrolyzes urea to NH<sub>3</sub> forming an ammonia cloud that results in an increased pH around the cell. Gastric mucin forms a gel at low pH (< pH 4) due to cross-linking of mucin monomers through hydrophobic interactions. Gel formation of gastric mucin is important for the barrier function of gastric mucus. The localized increase in pH surrounding *H. pylori* cells due to urease activity results in a transition of the gastric mucin from a gel to sol phase, which allows the bacteria to penetrate the gastric mucus. (*Celli et al.* 2009, *Clyne et al.* 1995).

H. pylori binds to epithelial cell surface receptors via adhesions such as BabA, SabA (Backert et al. 2011), and HopQ (Javaheri et al. 2016, Königer et al. 2016). Once H. pylori binds to a host cell, it uses a Type 4 Secretion System (T4SS) to inject virulence factors into the cell. One of the best characterized H. pylori virulence factors is vacuolating cytotoxin A (VacA), which causes vacuolation by forming pores in the plasma membrane (Foegeding et al. 2016). Another well characterized virulence factor is cytotoxin-associated antigen A (CagA), which causes release of inflammatory cytokines (Königer et al. 2016). CagA associates with the inner membrane where it disrupts cell-to-cell signaling, resulting in damage to the junctions between epithelial cells (Ohnishi et al. 2008). H. pylori can also enter host cells through endocytosis, phagocytosis, or micropinocytosis, where it can evade or manipulate the host cell to avoid lysosomal degradation (Necchi et al. 2017). VacA assists in the ability of H. pylori to survive inside lysosomes and allows the intruder to vacuolate the cell from the inside-out.

H. pylori has several additional adaptations that allow it to successfully colonize the stomach. The morphology of H. pylori is often described as helical, with the function of swimming more efficiently though gastric mucus (*Martínez et al. 2016*). H. pylori has a bundle of polar flagella with powerful flagellar motors that assist the cell in swimming through the highly viscous gastric mucus layer. Together with altering the consistency of the mucosa, the shape of the cell and powerful flagella allow it to penetrate the viscous gastric mucus layer and successfully colonize the underlaying gastric epithelium.

Robert Koch in the late 1800's was the first scientist to describe and photograph bacterial flagella (*Munch 2003*). The Eukaryotic cilia, sometimes called a flagellum, was described by Antoine von Leeuwenhoek much earlier in the late 1600's. The protein composition (*Boivin and Mesrobeanu 1938, Weibull 1948, Weibull 1949, Weibull 1950, Weibull 1953*) and the function of the flagellum as a motility organelle was established by the mid 1900's (*Strict 1996*). In *H. pylori*, the motility machinery of chemotaxis and flagella are fine-tuned to the task of burrowing

through gastric mucus and colonizing the gastric epithelium. Although not typically thought of as a virulence factor, motility is required for successful host colonization (*O'Toole et al. 2000*). The flagella, and to a lesser extent the chemotaxis system, are the focus of the following sections.

## **Flagellar-Driven Motility**

#### **Definitions and abbreviations**

- Chemotaxis system Sensory system that communicates with the flagellum
- Flagellum Nanomachine used for motility
- Flagellar arrangement refers to the localization of flagella on the bacterial cell body
- Amphitrichous A single flagella at each cell pole
- Lophotrichous Multiple flagella at one cell pole
- Monotrichous A single flagella at one cell pole
- Peritrichous Multiple flagella distributed over the entire cell surface
- CW and CCW <u>Clockwise</u> and <u>Counterclockwise</u> are the two directions that a flagellum can rotate.

Flagellar-driven motility is locomotion caused by the rotation of one or more flagella, which provides propulsion. Bacterial motility involves an interplay between the chemotaxis system and flagellum (**Fig. 1.2**). Much of the motility research has been conducted in *Escherichia coli*, where Howard Berg's group and others made many important discoveries (*Berg 2003*). Flagellar arrangements vary considerably across species and result in different swimming behaviors (**Fig. 1.3**). Perhaps the most common polar flagellation pattern is monotrichous (i.e., a single flagellum at a cell pole), and is found in many well studied bacteria, such as *Vibrio cholerae* and *Pseudomonas aeruginosa* (*Thormann et al. 2022*). Some polarly flagellated bacteria have a single flagellum at each cell pole, called an amphitrichous pattern, such as in *Campylobacter jejuni*. *E. coli* has multiple flagella distributed over the entire cell body in an arrangement referred to as peritrichous (*Schuhmacher et al. 2015*). The swimming behavior of *E. coli* is described as run-and-tumble. When all the *E. coli* flagella are rotating in a counterclockwise (CCW) direction, the flagellar filaments wrap around the cell body and coalesce into a flagellar bundle, which results in smooth swimming or a run. Upon a switch in direction from CCW to clockwise (CW) in one or more of the flagella, the flagellar bundle comes apart causing reorientation (tumble) of the cell.

Details of flagellar directional switching are discussed in the flagellar motor and chemotaxis section.

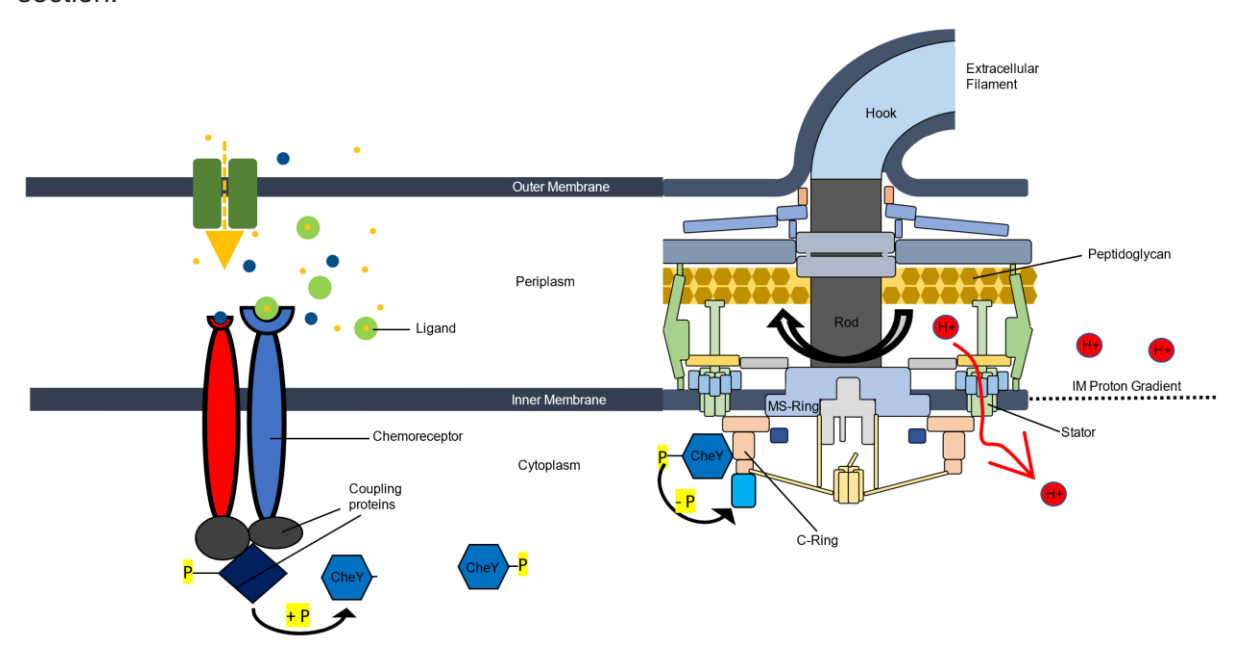


**Figure 1.2. Molecular overview of motility in** *H. pylori*. Signals are transmitted when a ligand binds a chemoreceptor. The signal is transmitted though coupling proteins to CheY. In *H. pylori* interaction of CheY-P with the C-ring of the flagellar motor results in CW rotation. In the absence of CheY-P, the motor rotates in a CCW direction. The opposite is true in *E. coli* where interaction of CheY-P with the motor stimulates CCW rotation and in absence of CheY-P the *E. coli* motor rotates CW. The torque used to rotate the flagellum is generated by proton flux through the stator units. Torque is transmitted through the axial motor components to the flagellar filament.

H. pylori has a lophotrichous arrangement of flagella, meaning it has several flagella at one cell pole (Marshall and Warren 1984, Bansil et al. 2023). This arrangement of flagella leads to a motility behavior described as run-reverse (Thormann et al. 2022). Using a single flagella or flagella bundle, the cell can operate as a pusher with the flagella rotating CCW, or as a puller where the flagella rotate CW while extended in front of the cell. A variation on run-reverse is run-reverse-flick, where the act of switching between pusher and puller motility causes the flexible hook to buckle, which reorients the cell by 90°. H. pylori swims faster when acting as a pusher (CCW) compared to as a puller (CW) (Antani et al 2021). H. pylori exhibits a run-reverse-reorient swimming behavior in viscous and aqueous solutions (Antani et al 2021, Constantino et al. 2016, Su and Liao 2020), where the flagellar bundle comes apart to re-orient the cell (Martínez et al. 2016, Constantino et al. 2016, Su and Liao 2020). H. pylori has fewer run reversal events

in viscous solution than in aqueous solution, although the reason for this is unknown (*Martínez et al. 2016*). *H. pylori* cell tracking experiments show that the helical shape of the cell body causes a characteristic oscillation swimming pattern due to the rotation of the cell body (*Constantino et al. 2016*). The rotation of the cell body in the opposite direction of flagellar rotation places net zero torque at the flagellar pole.

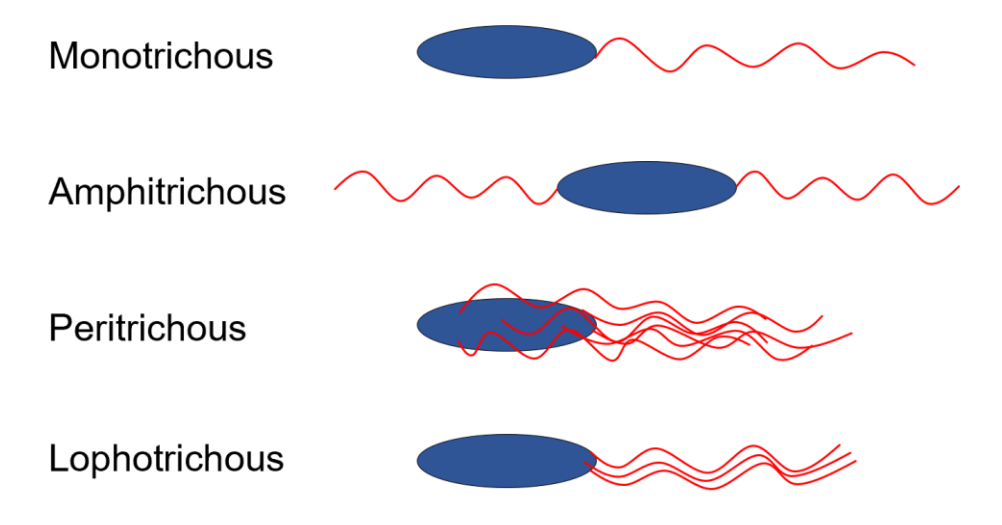


Figure 1.3. Bacterial flagellar arrangements. Cell bodies are blue and flagella are red. Representatives of each arrangement include: monotrichous, *V. cholerae* and *P. aeruginosa*; amphitrichous, *C. jejuni*; peritrichous, *E. coli* and *Bacillus subtilis*; lophotrichous, *H. pylori* and *Vibrio fischeri* (*Thormann et al. 2022*).

The helical body shape of *H. pylori* and *C. jejuni* is thought to allow the cells to swim faster than rod-shaped bacteria (*Karim et al. 1998*). While differences such as cell size, shape, and number of flagella vary, researchers found that the helical body of *H. pylori* confers up to a 20% increase in swimming speed compared to a rod-shaped *H. pylori* mutant that is deficient in helical shape determining peptidoglycan peptidases (*Sycuro et al. 2012*).

In some bacterial species, such as *C. jejuni* and *Helicobacter suis*, the flagella can wrap around the cell body where it acts as a pusher (*Grognot and Taute 2021*, *Thormann et al. 2022*). This type of swimming behavior, however, has not been reported for *H. pylori*. Wrapping of flagella around the cell body is thought to help the cell to escape dead ends or reorient the cell if trapped.

### Flagellar gene regulation

#### **Abbreviation and definitions**

- Transcriptional hierarchy refers to the temporal or spatial transcription of a set of genes.
   The genes that encode components of the bacterial flagellum are expressed in a transcriptional hierarchy so that genes are transcribed as their products are needed in flagellum assembly.
- Operon A unit of transcriptional organization. Genes within a single operon are often regulated and/or transcribed together.
- RpoD ( $\sigma^{80}$ ) The primary sigma factor in *H. pylori* and is directly involved in transcription of genes required early in flagellar assembly.
- RpoN ( $\sigma^{54}$ ) Alternative sigma factor that is responsible for transcription of genes involved midway in flagellar biosynthesis.
- FliA  $(\sigma^{28})$  Alternative sigma factor responsible for transcription of late flagellar genes.

In many bacteria, the flagellar gene transcriptional hierarchy is initiated by a master regulator that activates transcription of genes whose products are required for the earliest steps in flagellum assembly (*Smith and Hoover 2009*). Examples of master regulators involved in flagellar biogenesis include *E. coli* FlhCD and *V. cholerae* FlrA (*Bartlett et al. 1988, Prouty et al. 2001*). A master regulator has not been identified in *H. pylori* (*Tsang and Hoover 2014*). Flagellar genes in *E. coli* are organized within a few large operons. In contrast, *H. pylori* flagellar genes are scattered across the chromosome and are often in operons with genes unrelated to flagellum biogenesis or motility. Thus, many of the early flagellar genes may be expressed constitutively rather than temporally.

As indicated, RpoN is required for transcription of genes whose products are required midway through flagellar biogenesis. These RpoN-dependent flagellar genes encode the rod proteins (FlgB, FlgC, FlgJ), hook proteins (FlgE, FlgE2, FlgD, FlgL), the hook-length control protein (FliK), the minor flagellin (FlaB), and flagellin glycosylation protein (PseC) (*Niehus et al. 2004*). RpoN-dependent transcription requires a transcriptional activator that stimulates the isomerization of the closed complex between RpoN-RNAP holoenzyme and the promoter to the open promoter complex (*Popham et al. 1989*). FlgR is the transcriptional activator that stimulates transcription of the RpoN-dependent flagellar genes in *H. pylori* (*Spohn and Scarlato 1999*), and is a response regulator of a two-component system that includes the sensor kinase FlgS (*Beier and Frank 2000*). Results from multiple studies suggest that assembly of the flagellar-type III secretion system (f-T3SS) is required for expression of RpoN-dependent genes (*Tsang and Hoover 2014*).

Disrupting the f-T3SS genes *flil*, *fliQ*, or *flhB* (*Porwollik et al. 1999*; *Allan et al. 2000*) in *H. pylori* results in reduced expression of the RpoN-dependent gene *flaB* and *flgE*. Niehus and co-workers showed that disrupting *flhA*, which encodes another component of the f-T3SS, inhibits transcription of the RpoN regulon (*Niehus et al. 2004*). In *C. jejuni*, a member of the phylum Campylobacterota that is closely related to *H. pylori*, deletion of *flhA*, *flhB*, *fliP*, or *fliR* inhibits expression of a RpoN-dependent reporter gene (*Hendrixson et al. 2001*). Tsang and co-workers showed that a truncated FlhA protein supported expression of RpoN-dependent reporter genes in *H. pylori*, but not flagellum assembly (*Tsang et al. 2013*). Tsang and co-workers subsequently showed that FlgS binds a polypeptide corresponding to N-terminal region of FlhA with high affinity, but the polypeptide did not stimulate the autokinase activity of FlgS (*Tsang et al. 2015*). There are nine copies of FlhA in the flagellar protein export apparatus, and Tsang and co-workers proposed that binding of FlgS monomers to the FlhA subunits in the export apparatus may facilitate dimerization and subsequent activation of the autokinase activity of FlgS (*Tsang et al. 2015*).

In addition to the transcriptional control by the FlgS/FlgR two-component system, expression of the *H. pylori* RpoN-dependent flagellar genes may be modulated by HP0958 (*Ryan et al. 2005*, *Pereira and Hoover 2005*). HP0958 was initially identified in a high-throughput yeast two-hybrid screen as interacting strongly with RpoN (*Rain et al., 2001*). In the absence of HP0958, *H. pylori* G27 is non-motile due to the rapid turnover of RpoN (*Pereira and Hoover 2005*). HP0958 has been proposed to be a RpoN chaperone that facilitates the association of RpoN with core RNAP to form RpoN-RNAP holoenzyme (*Pereira and Hoover, 2005*). HP0958 also binds and destabilizes transcripts of the major flagellin gene, *flaA*, and has been proposed to negatively regulate *flaA* expression (*Douillard et al., 2008*).

In *E. coli* and *Salmonella enterica* the activity of FliA is negatively regulated by the anti-sigma factor FlgM (*Gillen and Hughes 1991*). FlgM is a filament-type substrate of the f-T3SS and is secreted from the cell upon completion of the rod-hook structure, which leads to transcription of  $\sigma^{28}$ -dependent genes (*Hughes et al. 1993*). Transcription of the late flagellar genes in *H. pylori* is dependent on FliA ( $\sigma^{28}$ ) (*Niehus et al. 2004*), and as occurs in *E. coli* and *S. enterica*, the activity of FliA is negatively regulated by FlgM (*Josenhans et al. 2002*). In contrast to *E. coli* and *S. enterica* though, *H. pylori* does not appear to secrete FlgM to alleviate its inhibitory effect on FliA (*Rust et al. 2009*).

### Flagella Localization

#### **Abbreviation and definitions**

- Flagellar Localization Refers to the location of the flagellum relative to the cell body.
- FlhF GTPase involved in regulation of flagellar assembly, particularly the formation and position of flagella.
- GTPase (Guanosine Triphosphatase) an enzyme that catalyzes the hydrolysis of guanosine triphosphate (GTP) into guanosine diphosphate (GDP) and inorganic phosphate (Pi).
- FlhG ATPase involved in regulating the number and placement of flagella. Interacts with FlhF.
- ATPase (Adenosine Triphosphatase) an enzyme that catalyzes the hydrolysis of adenosine triphosphate (ATP) to adenosine diphosphate (ADP) and inorganic phosphate (Pi).
- Hypoflagellation Phenotype in which fewer flagella than normal are produced.
- Hyperflagellation Phenotype in which more flagella than normal are produced.

In many polar flagellated bacteria, the location and number of flagella are determined at least partly by the cytoplasmic proteins FlhF and FlhG. *flhF* was first identified though in the peritrichously flagellated bacterium *Bacillus subtilis* as being involved in flagellar biogenesis, as a *B. subtilis* Δ*flhF* mutant was found to be non-motile and aflagellated (*Carpenter et al. 1992*). Since then, FlhF has been shown to prevent the mislocalization of flagella to non-polar sites in *Vibrio alginolyticus* (*Kusumoto et al. 2008*), *P. aeruginosa* (*Murray and Kazmierczak, 2006*) and *Pseudomonas putida* (*Pandza et al. 2000*). FlhF is a GTPase that belongs to the GTP-binding signal recognition particle (SRP) family, which includes FtsY and Ffh (*Carpenter et al. 1992*), proteins that are involved in targeting secreted and integral membrane proteins to the cell membrane (*Halic and Beckmann, 2005*). *flhG* was first identified in *P. aeruginosa*, originally called *fleN*, where it was found that a deletion of *flhG* resulted in hyperflagellation instead of the normal single polar flagellum, suggesting a role for FlhG in regulating flagellar number (*Dasgupta et al. 2000*). FlhG belongs to the MinD/ParA ATPase family (*Leipe et al. 2002*), members of which act in coordinating spatiotemporal processes such as cell division site selection and plasmid partitioning (*Lutkenhaus*, *2012*).

GFP-fusions of FlhF and FlhG localize to the flagellated cell pole in *V. alginolyticus*, and FlhG was reported to prevent localization of FlhF to the pole (*Kusumoto et al. 2008*). FlhF and FlhG

were also found to localize to the cell pole in *Vibrio parahaemolyticus*, but in this case FlhG was shown to be required for proper localization of FlhF (*Arroyo-Pérez and Ringgaard, 2021*). Mutations in the GTPase motifs in FlhF of *V. alginolyticus* and *C. jejuni* interfere with its localization to the cell pole and inhibit flagellum assembly (*Balaban et al. 2009, Kusumoto et al. 2009*). The mechanism by which FlhF prevents the mislocalization of flagella to non-polar sites is unknown, but the current model predicts the GTP-bound dimeric form of FlhF localizes to the cell pole where it recruits the MS-ring protein FliF or other flagellar proteins to the pole to initiate flagellum assembly (*Bange et al. 2007, Green et al. 2009, Kondo et al. 2018*). The mechanism by which FlhF localizes to the cell pole is not known for most bacterial species. Arroyo-Pérez and co-workers identified an integral membrane protein in three species of γ-proteobacteria (*V. parahaemolyticus, P. putida*, and *Shewanella putrefaciens*) that they designated FipA, which acts in concert with the polar landmark protein HubP/FimV to recruit FlhF to the cell pole (*Arroyo-Pérez et al. 2024*). *H. pylori* lacks homologs of HubP/FimV and FipA, and the mechanism by which FlhF localizes to the cell pole in *H. pylori* is unknown.

FlhF is needed for expression of  $\sigma^{54}$ -dependent and  $\sigma^{28}$ -dependent flagellar genes in *C. jejuni* and *H. pylori* (*Neihus et al. 2004, Balaban et al. 2009*). The requirement of FlhF for expression of the middle and late flagellar genes in *C. jejuni* and *H. pylori* presumably results from the failure of the *flhF* mutants to form flagellar assembly intermediates that regulate the transcriptional hierarchy controlling flagellar gene expression in these bacteria.

The crystal structure of FlhG from *Geobacillus thermodenitrificans* is very similar to *E. coli* MinD, sharing key active site motifs that are involved in ATP-binding and hydrolysis (*Schuhmacher et al. 2015*). *G. thermodenitrificans* FlhG forms a homodimer that is dependent on both ATP and lipid (*Schuhmacher et al. 2015*). FlhF and FlhG interact with each other (*Bange et al. 2007, Kusumoto et al. 2008*), and *B. subtilis* FlhG stimulates the GTPase activity of FlhF (*Bange et al. 2011*). Amino acid substitutions in *V. alginolyticus* FlhG that result in elevated ATPase activity inhibit flagellation, whereas mutations that inhibit FlhG ATPase activity result in hyperflagellation (*Ono et a. 2015*). These observations have led to the current model that FlhG regulates flagellar number by stimulating the GTPase activity of FlhF, converting it to the GDP-bound form that is unable to promote flagellum assembly (*Schuhmacher et al. 2015*).

In addition to regulating FlhF, FlhG appears to have other roles in some bacterial species. FlhG has been implicated in the assembly of the flagellar C-ring as *G. thermodenitrificans* was shown to interact with the C-ring proteins FliM/FliY and stimulate their assembly with FliG *in vitro* (*Schuhmacher et al. 2015*). In *C. jejuni*, deletion of *flhG* leads to increased production of minicells, and expression of an ATPase deficient FlhG variant inhibits cell division and leads to

cell elongation (*Balaban and Hendrixson, 2011*). *C. jejuni* lacks the Min system that prevents cell division near the cell poles in other bacteria, and FlhG appears to take over the role of the Min system in *C. jejuni*.

Like FlhF, FlhG has been reported to have roles in regulating gene expression. FlhG has been found to regulate flagellar biogenesis both at the transcriptional and post-transcriptional level. FlhG interacts directly with FleQ in *P. aeruginosa* (*Dasgupta et al. 2000*), and negatively regulates *flrA* (*Correa et al. 2005*), both master regulators of flagellar gene expression.

Most studies on FIhF and FIhG have been done in bacterial species that have a single polar flagellum or amphitrichous flagella, and little work on these proteins have been done in *H. pylori* or other lophotrichous-flagellated bacteria. Disrupting *flhG* in *H. pylori* 11A was reported to result in loss of motility and aflagellation (*van Amsterdam and van der Ende, 2004*). Gibson and coworkers, however, reported that deletion of *flhG* in *H. pylori* G27 did not inhibit motility, although it did alter the flagellation pattern so that there was a wider range in the number of flagella per cell compared to wild type (*Gibson et al. 2023*). The earlier report that disrupting *flhG* in *H. pylori* 11A prevented flagellar biosynthesis may have been due to polar effects on other flagellar genes as *flhF* and *flhG* are in an operon and upstream of flagellar genes *flgV*, *fliA*, *flgM*, and *fliY* in *H. pylori*. Similar to what has been reported for other bacteria, deletion of *flhF* in *H. pylori* G27 results in reduced motility, hypoflagellation, and mislocalized flagella to non-polar sites (*Gibson et al. 2023*).

## Flagella Assembly and Structure

#### **Abbreviation and definitions**

- Archetypal flagellum, flagellar motor refers to the structure found in E. coli or Salmonella, which is the most studied and simplest of flagellar structures.
- Basal body The portion of the flagellum that is located between the cytoplasm and outer membrane. Includes the flagellar motor.
- Flagellar motor The portion of the flagellum located between the IM and OM in the periplasmic space. Anchored to the peptidoglycan. Responsible for producing the force that drives the flagellar filament.
- Hook A flexible rotating linker that connects the axial motor components of the basal body to the flagellar filament. The hook is located at the terminus of the rod in proximity to the outer membrane and extends out of the cell.
- Flagellar filament The portion of the flagellum that is located outside the cell. Often longer than the length of the cell.
- F-T3SS Flagellar Type 3 Secretion System
- NF-T3SS Non-Flagellar Type 3 Secretion System

The bacterial flagellum is composed of 3 large components: the membrane-embedded basal body, hook, and filament. The basal body spans the periplasmic space and contains the flagellar protein export apparatus and flagellar motor, while the hook is anchored to the motor and extends away from the cell where it is connected to the flagellar filament (*Carroll and Liu 2020*).

The flagellum in diderms has a conserved core of structures, starting from the cytoplasm: the cytoplasmic export apparatus and C-ring, inner membrane imbedded MS-ring and stator units, the periplasmic rod, P-ring and L-ring (associated with the peptidoglycan and lipopolysaccharide layers, respectively, and collectively referred to as the LP-ring), the hook, and filament (Fig. 1.4A). Gram-positive bacteria have a similar flagellar architecture but lack the L- and P- rings since they do not possess an OM (*Mukherjee Kearns 2014*). Assembly of rod, hook, and filament requires a flagellar protein export apparatus, which is a type III secretion system (T3SS) located at the cytoplasmic base. The flagellar T3SS (F-T3SS) is housed at the base of the flagellum andtranslocates axial components of the flagellum (e.g., rod, hook, and filament proteins) across the inner membrane in a proton motive force-dependent manner (*Halte and Erhardt 2021*). Protein substrates are secreted across the inner membrane into the lumen of the nascent flagellum in an unfolded state and diffuse to the end of the nascent flagellum where they fold into

their tertiary structures and are incorporated into the growing flagellum. The F-T3SS can secrete several thousand amino acid residues per second (*lino*, 1974), which is significantly faster than the general secretory system (Sec system) that only secretes a few dozen amino acid residues per second (*Tomkiewicz et al. 2006*). Protein substrates for the F-T3SS share conserved  $\alpha$ -helices at their N- and C-termini that form an antiparallel coiled-coil structure (*Saijo-Hamano et a. 2019*).

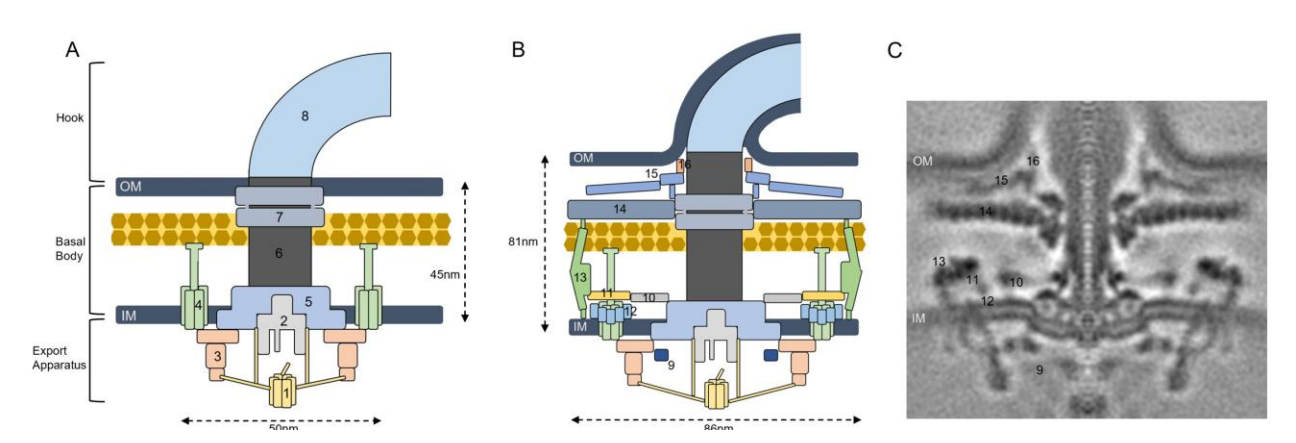


**Figure 1.4.** The Flagellar Basal Body. (A) The archetypal bacterial flagellum in diderms includes the F-T3SS (1, 2), C-ring (3), stator units (4), MS-ring (5) rod (6), LP-ring (7), and hook (8). (B) The basal body of *H. pylori* has additional structures that are not found in the archetypal basal body include the FlgV ring (9), proximal spokes (10), distal spokes (11), FliL ring (12), cage (13), basal disk (14), outer disk (15), and FapH ring (16). The filament is not shown. (**C**) Cryo-ET subtomogram image average of the *H. pylori* B128 flagellar motor. Image provided by Jun Liu.

The F-T3SS is structurally and functionally homologous to the Non-Flagellar Type III secretion system (NF-T3SS) found in the bacterial injectisome (*Wagner et al. 2010*). The injectisome uses a NF-T3SS to inject virulent effector proteins into host cells (*Wagner et al. 2018*). In addition to sharing structural and functional homology, components of the NF-T3SS and the F-T3SS share common ancestry (*Abby et al. 2012*). Of the core proteins found in both systems, nine share sequence homology while two others are structurally homologous (*Pallen and Matzke 2006*). Importantly, the evidence suggests that the NF-T3SS is monophyletic and branches from a point following the evolution of the F-T3SS (*Abby et al. 2012*). Additional evidence shows that the T3SS was initially used for the transport of flagellar proteins, and genomic analysis found the presence of flagellar genes in species that lack flagella, suggesting

that the F-T3SS evolved first (*Snyder et al. 2009, Ferris and Minamino 2006*). Interestingly, there is even evidence that suggests NF effectors can be secreted by the F-T3SS (*Lee and Galan 2004*). There are two proposed models for assembly of the NF-T3SS, the inside-out and outside-in models (*Diepold et al. 2010, Diepold et al. 2011, Wagner et al. 2010, Abby et al. 2012*). Given that the flagellum follows an inside-out model, this is the likely way that the NF-T3SS assembles (*Kubori et al. 1997, Macnab 2003*).

The F-T3SS (described above as the export apparatus) consists of FlhA, FlhB, FliP, FliQ, FliR, which make up the gate complex, FliH, FliI, FliJ that make up the ATPase complex (*Fukumura 2017, Minamino and Macnab 1999, Minamino and Macnab 2000, Carroll and Liu 2020*), and the FliP/FliR chaperone FliO (*Fabiani et al. 2017, Halte and Erhardt 2021*). FlgV is a protein identified by cryo-ET as associating with the MS-ring and C-ring with an unknown function (*Botting et al. 2023*). The export apparatus is responsible for the assembly of the axial flagellum including the rod, hook, and filament (*Inoue et al. 2018*). The ATPase complex, specifically FliH and FliI assist the hook protein FlgE and the hook-length protein FliK in docking at the gate complex. FliH has also been shown to be a negative regulator of FliI (*Imada et al. 2016*).

In *S. enterica*, the ATPase complex together is responsible for the docking of proteins associated with the growing hook and filament, and especially the junction and cap proteins FIgK, FIgL, and FIiD. In the absence of the ATPase complex monomers of the filament protein FIiC (FlaA in *H. pylori*) are leaked into the media due to the loss of the filament cap protein. Flil of the ATPase complex is not essential for flagellar assembly in *C. jejuni*, although it does enhance assembly and motility (*Henderson et al. 2020*). The gate complex harnesses proton motive force to translocate flagellar proteins across the membrane (*Inoue et al. 2018, Minamino et al. 2016, Minamino et al. 2011, Paul et al. 2008*). FlhA is the core of the gate complex and functions as the proton/protein antiporter through which the flagellar proteins to pass (*Minamino et al. 2021*), while FlhB has been shown to be critical for substrate specificity and docking of flagellar proteins (*Erhardt et al. 2017, Minamino et al. 2016, Minamino et al. 2011, Ferris et al. 2005*). The C-terminal domain of FlhA has been shown to interact with chaperones and the export substrates (*Bange et al. 2010, Xing et al. 2018, Inoue et al. 2019*).

Anchoring the FliH subunits of the ATPase complex is the C-ring (*Inoue et al. 2018*). The C-ring is the switch complex of the motor that interacts with the stators to change the direction of rotation and accept torque from the stators (*Carroll et al. 2020*). The C-ring is made up of 3 subunits; FliG, FliM, and FliN, and in some bacteria, including *H. pylori*, there is a fourth subunit

that is a FliN homologue and is referred to as FliY. Anchored within the C-ring is the MS-ring that accepts the torque from the C-ring following ion flow (*Carroll and Liu 2020*). The MS-ring is composed of monomers of FliF that interact intimately with the upper portion of the C-ring comprised of FliG (*Henderson et al. 2020*). FliF is anchored to the inner membrane by N and C terminal transmembrane helices. The export gate complex resides within the MS-ring.

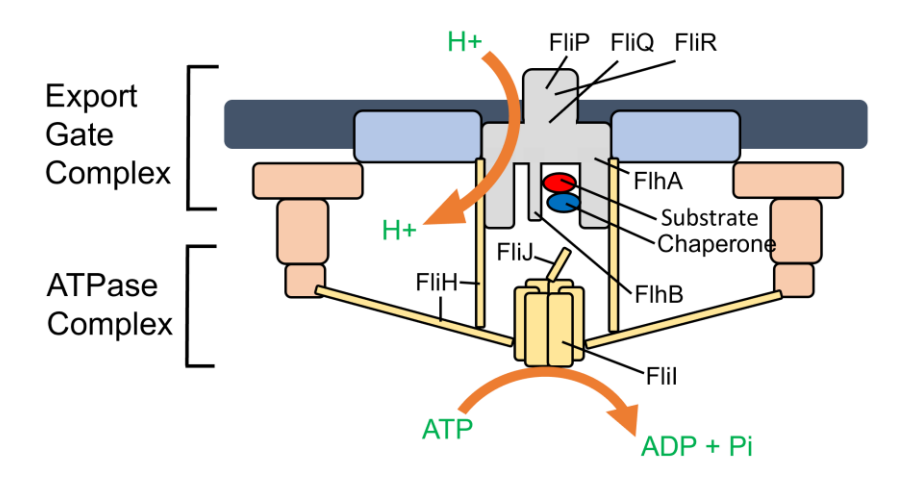


**Figure 1.5.** The F-T3SS. The F-T3SS consists of two major mulit-subunit components, the export gate complex (FlhA, FlhB, FliP, FliQ, and FliR) and the ATPase complex (FliH, FliI, and FliJ).

The MS-ring acts as a structural platform for the motor at the inner membrane and distributes torque to the motor driveshaft, which is the rod (*Carroll and Liu 2020*). The rod is the most proximal portion of the axial motor and is comprised of FlgB, FlgC, FlgF, FlgG, and FliE. The rod stretches from the MS-ring at its base to the OM and contains the central channel that the axial components of the motor transported by the gate complex travel through. The LP-ring composed of FlgI and FlgH, assembled with the help of the periplasmic chaperone FlgA, is a structure associated with the OM and peptidoglycan in the archetypal motor that is thought to act as a bushing for the rod (*Carroll and Liu 2020, Karlinsey et al. 1997*). In flagellar disassembly products, the LP-ring is found to be associated with the OM in the absence of the rod and inner membrane structures (*Kaplan et al. 2019, Kaplan et al. 2020*).

At the termination of the rod is the hook, a flexible structure made up of protofilaments of FIgE that behaves as a universal joint to allows the transfer of torque from the rod to the filament even when the axes of these flagellar components are perpendicular to each other. Each protofilament has the important ability to compress and extend as needed during flagellar rotation (*Samatey et al. 2004, Matsunami et al. 2016*). It has been demonstrated in some bacteria that

the hook can buckle in certain environments or during a specific rotational direction of the flagellar motor (**Son et al. 2013**). This bucking occurs when the hook is compressed, either during pulling motility or when the resistance from the environment is high. The buckling, referred to as a flick, is an example of controlled mechanical instability being utilized to reorient the bacterial cell, allowing the cell to change direction.

Before the hook is assembled with FIgE subunits the hook cap protein FIgD is put into place (*Inoue et al. 2018*). The hook cap allows for the assembly of the hook while preventing leakage of FIgE into the medium. Once the hook-length control protein FliK determines that the hook has reached its appropriate length, export of FIgE stops. FliK acts as a molecular ruler that is secreted intermittently to assess the length of the growing hook (*Erhardt et al. 2011*) and plays a pivotal role in substrate switching of the export apparatus along with autocleavage of FlhB (*Williams et al. 1996*). The hook-filament junction proteins FlgK and FlgL are then exported. Following completion of the hook assembly, FliD is exported where several copies assemble into the filament cap structure that prevents leakage of flagellins into the medium (*Nedeljkovi´c et al. 2021*).

The flagellar filament was first described as being comprised of numerous protein subunits referred to as flagellins in 1948 (Weibull 1948 and Kobayashi et al 1959), and the flagellins were subsequently named several years later (Astbury and Weibull 1955). The flagellins are elongated proteins (Nedeljkovi´c et al. 2021) that assemble into structures called protofilaments that make up the mature flagellum (O'Brien and Bennett 1972, Samatey et al. 2001, Wang et al. 2017). The protofilaments have either a left or right conformation as they wind down the length of the flagellum. The molecular weight of a flagellin protein ranges from 26-kDa to 115-kDa in Bacillus cereus and Desulfotalea psychrophila, respectively (II Kim et al. 2018, Beatson et al. 2006). Structurally, there is a great deal of homology in the terminal region of a flagellin, which are found near the center of the filament, while there is high variability in the remainder of the protein (LaVallie and Stahl 1989). Flagellins have different gene designations depending on the species, such as fliC in E. coli, hag in B. subtilis, and flaA in H. pylori (Nedeljkovi´c et al. 2021). About half of bacterial species have more than one flagellin gene, with Caulobacter crescentus having the most at 15 (Faulds-Pain et al. 2011). The highest number of different filament species present in a single cell is 7, which was reported in Rhizobium leguminosarum (Tambalo et al. 2010). In some species, flagellin genes are phase variable and therefore not expressed at the same time (Silverman et al. 1979). Phase variation of flagellins allows the cell to alter filament structure depending on environmental conditions (Ikeda et al. 2001, Horstmann et al. 2017). This variation in subunit selection affects the properties and geometry of the filament with the

result of modified swimming behavior (*Faulds-Pain et al. 2011, Kim et al. 2014, Kuhn et al. 2018*). In other species, such as *H. pylori* and *C. jejuni*, two different flagellins are expressed simultaneously and are present in a single filament, where the minor flagellin FlaB is located proximal to the hook and the major flagellin FlaA forms the rest of the filament. (*Kostrzynska et al. 1991, Wassenaar et al. 1994*). In *H. pylori*, FlaA and FlaB share only 58% amino acid similarity (*Schmitz et al. 1997*), while the flagellins of *C. jejuni* share a higher degree of similarity (*Alm et al. 1993*). The presence of both flagellins in the cell is required for optimal swimming characteristics (*Guerry et al. 1991, Kuhn et al. 2018*). Geis and co-workers were the first to characterize the *H. pylori* flagellar filament, which is typically 3-5 µm in length and contain a bulb-like structure at the distal end (*Geis et al. 1989*); while Kostrzynska and co-workers were the first to purify both the major and minor *H. pylori* flagellins (*Kostrzynska et al. 1991*). The flagellar hook protein FlgE was purified and characterized in 1994 (*O'Toole et al. 1994*), completing the characterization of the extracellular components of the *H. pylori* flagellum.

Flagellin glycosylation is responsible for the difference between the theoretical and experimentally determined molecular weights of isolated flagellins and was first characterized in 1998 in *P. aeruginosa* (*Brimer and Montie 1998*). In *C. jejuni* a difference of 6 kDa is found between experimental and predicted molecular weights of the flagellins (*Doig et al. 1996, Thibault et al. 2001, Logan et al. 2002*). The *C. jejuni* flagellins are heavily glycosylated with the sialic acid-like sugar 5,7-diacetoamido-3,5,7,9-tetradeoxy-L-*glycero*-α-L-*manno*-nonulosonic acid (pseudominic acid) and derivatives attached to serine and threonine residues through *O*-linkages. *H. pylori* flagellins are also glycosylated with pseudaminic acid, with most sites found in the protein core (*Schirm et al. 2003*). In both *C. jejuni* (*Goon et al. 2003*) and *H. pylori* glycosylation is essential for filament formation (*Schirm et al. 2003*).

A single filament is assembled from stacks of flagellins in 11 protofilaments that twist along a screw axis (*Yonekura et al. 2002*). Protofilaments can take either left or right-handed conformations based on interactions of flagellins within a single protofilament, independent of other protofilaments (*Kamiya et al 1980*). During flagellar rotation, the number of right- vs left-handed protofilaments determines the pitch of the superhelix, altering the swimming properties (*Calladine et al. 2013*). A straight filament reflects all the protofilaments locked in either right- or left-hand conformations, which results in a nonfunctional flagellum. The diameter of the native filament in *S. enterica* is roughly 230 Å (*Mimori et al 1995*).

The chaperone FliS plays an important role in both delivering flagellin to the T3SS as well as keeping flagellins in an unfolded state (*Nedeljkovi´c et al. 2021*). These properties prevent accumulation and polymerization of flagellin in the cytosol (*Khanra et al. 2016*), as well as

allowing for translocation of flagellin through the central pore of the growing filament (Auvray et al. 2001). At a diameter of 20-30 Å, a folded flagellin would not be able to traverse the central pore of the growing filament. At the export apparatus, FliS binds with FlhA to promote protein translocation of the complexed flagellin (Furukawa et al. 2016, Bange et al. 2010). In S. enteria, FliS suppressed the secretion of anti-sigma factor FlgM, suggesting a regulatory role for substrate switching of the export apparatus (Furukawa et al. 2016). The filament cap protein FliD also has a chaperone in FliT (Imada et al. 2010). FliT binds with the export apparatus proteins FlhA, FliI, and FliJ to elicit translocation of FliD, and also works as a negative transcriptional regulator of flagellar genes by inhibiting FlhDC. FliT is complexed with FlhDC, which is the master regulator for flagellar gene expression in E. coli and S. enterica, until the completion of hook-basal body, at which point FliT is released from FlhDC and is able to interact with FliH, FliI, FliJ (Nedeljkovi'c et al. 2021). The FliT-FliD-FliH-FliJ complex then binds to the base of the export gate. Once FliD is released, FliT is free to complex with FlhDC again. Later, FliT dissociates with FlhDC which leads to the activation of transcription from class II promoters. The proteins FliW1 and FliW2 were found in C. jejuni to bind the flagellins, performing a regulatory role along with FliS (Radomska et al. 2017).

The mechanism of filament self-assembly is still a matter of some debate, however, it appears that an injection-diffusion model is the most likely method (*Renault et al. 2017*). In this model, the proton-motive force (*Fig. 1.5*) supplied by the gate complex is used to push flagellins down the growing filament (*Stern and Berg 2013, Shibata et al. 2007*). Under this model, flagellar filament growth decay exponentially as the filament grows in length, limiting the maximum length the filament can achieve.

The archetypal flagellum is represented in the motors of *E. coli* and *S. enterica* and is found in all bacterial species that possess flagellar systems. Some bacteria have flagellar motors that have additional accessory structures. The additional structures of the *H. pylori* flagellar motor are discussed in the next section.

Table 1.1. <i>Helicobacter pylori</i> flagellar, flagellar-associated and flagellar regulatory genes			
Gene Name	Strain 26695	Sigmulon	Description
	Locus Tag		
flaA	HP0601	FliA	major flagellin
flaB	HP0115	RpoN	minor flagellin
flaG	HP0751	FliA	role in control of filament length
flgA	HP1477	RpoD	periplasmic chaperone involved in P-ring assembly
flgB	HP1559	RpoD/RpoN	proximal rod protein
flgC	HP1558	RpoD/RpoN	proximal rod protein
flgD	HP0907	RpoN	hook cap protein
flgE	HP0870	RpoN	hook protein
flgE2	HP0908	RpoN	potential second hook protein
flgG	HP1585	RpoD	distal rod protein
	HP1092	RpoD	
flgG	HP0325		flagellar basal-body rod protein
flgH		RpoD	L-ring protein
flgl	HP0246	RpoD	P-ring protein
flgJ (predicted)	HP1233	RpoN	muramidase/rod cap protein
flgK	HP1121	RpoN	hook-associated protein 1
flgL	HP0295	RpoN	hook-associated protein 3
flgM	HP1122	RpoD	anti- $\sigma^{28}$ factor
flgP	HP0837	RpoD	predicted basal disc protein
flgQ	HP0702	RpoD	predicted basal disc protein
flgR	HP0703	RpoD	response regulator for σ <sup>54</sup> -dependent genes
flgS	HP0244	RpoD	histidine kinase; transcription of $\sigma^{54}$ -dependent genes
flgV	HP1033b	RpoD	MS-ring associated cytosolic protein
flgY	HP0257	RpoD	Bushing proximal to the MS-ring
flgZ	HP0958	RpoD	prevents rapid turnover of σ <sup>54</sup>
fliA	HP1032	RpoD	sigma factor, σ <sup>28</sup>
fliD	HP0752	FliA	filament cap protein
fliE	HP1557	RpoD/RpoN	MS-ring/rod junction protein
fliF	HP0351	RpoD	MS-ring protein
fliG	HP0352	RpoD	rotor protein; C-ring component
fliH	HP0353	RpoD	flagellar export apparatus protein; regulator of Flil
flil	HP1420	RpoD	flagellar export apparatus protein; ATPase
fliJ (predicted)	HP0256	RpoD	flagellar export apparatus protein; co-chaperone
fliK	HP0906	RpoN	hook-length control protein
fliL	HP0809	RpoD	inner membrane protein associated with stator
fliM	HP1031	RpoD	C-ring component
fliN	HP0584	RpoD	C-ring component
fliO	HP0583	RpoD	FliP/FliR chaperone
fliP	HPG27_642	RpoD	flagellar export apparatus protein
fliQ	HP1419	RpoD	flagellar export apparatus protein
fliR	HP0173	RpoD	flagellar export apparatus protein
fliS	HP0753	FliA	flagellin chaperone
fliS	HP1076	RpoN	predicted co-chaperone with FliS
fliW1	HP1154	RpoN	predicted chaperone, binds flagellin
fliW2	HP1377	RpoN	Predicted chaperone, binds flagellin
fliY	HP1030	RpoD	C-ring component
flhA	HP1041	RpoD	flagellar export apparatus protein

flhB	HP0770	RpoD	flagellar export apparatus protein
flhF	HP1035	RpoD	GTPase required for localization of flagella to cell pole
flhG	HP1034	RpoD	ATPase that regulates GTPase activity of FlhF
motA	HP0815	RpoD	stator protein of flagellar motor
motB	HP0816	RpoD	stator protein of flagellar motor
pfIA	HP1274	RpoD	medial disc protein
pflB	HP1479	RpoD	proximal disc protein
pfIC	HP0036	RpoD	flagellar accessory structural protein
fapH	HP0838	RpoD	outer ring protein
pilN	HP0272	RpoD	cage protein
pilM	HP0271	RpoD	cage protein
pilO	HP0273	RpoD	cage protein
Other			
rpoN	HP0714	RpoD	sigma factor, σ <sup>54</sup>
pseC	HP0366	RpoN	pseudaminic acid biosynthesis
pseF	HP0326	RpoD	pseudaminic acid biosynthesis
pseH	HP0327	RpoD	pseudaminic acid biosynthesis
pseB	HP0840	RpoD	pseudaminic acid biosynthesis
psel	HP0178	RpoD	pseudaminic acid biosynthesis
Indicates sigma factor ( $\sigma$ 80 (RpoD); $\sigma$ 54 (RpoN); or $\sigma$ 28 (FliA)) required for transcription of the gene			

## The Flagellar Motor of *H. pylori*

#### **Abbreviation and definitions**

- Torque refers to the rotational force generated by the flagellar motor.
- *pflA* (<u>paralysed flagella A</u>) comprises an accessory structure in Campylobacterota flagellar motors in proximity to the stators and inner membrane.
- *pflB* (<u>paralysed flagella B</u>) comprises an accessory structure in Campylobacterota flagellar motors in proximity to the stators and inner membrane.
- flgP (<u>flagellar</u> protein <u>P</u>) comprises an accessory structure in Campylobacterota flagellar motors in proximity to the LP-Ring and outer membrane.
- FlgV ring A cytosolic structure associated with the C-ring in *H. pylori*.
- FliL ring A structure of nine FliL monomers that encircle the MotB portion of the stator unit in H. pylori.
- PilMNO Pilin homologues that constitute components of the cage in *H. pylori*.

The flagellar motor of *H. pylori* is one of the largest bacterial flagellar motors described to date, measuring 86 nm in diameter and 81 nm in height (**Fig. 1.4**). The *H. pylori* motor recruits 18 torque-generating stator units that produce an estimated 3,600 pN·nm of torque (*Celli et al. 2009, Qin et al. 2017*). In contrast, the *E. coli* motor is 50 nm in diameter and 45 nm in height (**Fig. 1.4**), and only recruits up to 11 stator units that produce ~1,300 pN·nm of torque (*Reid et al. 2006, DePamphilis and Adler 1971*). The stator units *H. pylori* are stably associated with the *H. pylori* motor and are clearly visible in *in-situ* structures of the *H. pylori* motor generated by cryo-ET and subtomogram averaging (*Qin et al. 2017*). In contrast, the stator units in *E. coli* motor exchange with a pool of unassociated stator units in the membrane and the number of motor-bound units increases as load on the motor increases (*Leake et al. 2006*).

The *H. pylori* motor has associated structures that are not present in the *E. coli* motor (**Fig. 1.4**), some of which are thought to assist in the recruitment and/or retention of stator units in the *H. pylori* motor. These *H. pylori* motor accessories include sets of proximal and distal spokes, PflB ring, L ring, and a periplasm-spanning cage (**Fig. 1.4B**). Another *H. pylori* motor accessory is the FlgV ring, which is located on the cytoplasmic side of the inner membrane near the C-ring and stator units and is required for wild-type motility in soft agar medium (*Botting et al. 2023*). Additional *H. pylori* motor accessories are associated with the OM, and these structures may have roles flagellar sheath biosynthesis or in protecting the cell envelope from stress resulting from flagellar rotation. Many of the *H. pylori* motor accessories are present in the motors of other

bacterial species, and as with the *H. pylori* motor, stator units are stably associated with the motors of many of these bacteria (*Chaban et al. 2018*). Thus, the following section discusses studies on *H. pylori* motor accessories, but also draws heavily on related studies of other bacteria. Much of what is known about *H. pylori* motor accessories is a result of studies with *C. jejuni*, which like *H. pylori*, is a member of the order Campylobacterales within the phylum Campylobacterota.

In 1994, *pflA* (<u>paralysed flagella A</u>) was identified in a phenotypic screen following insertional mutagenesis in *C. jejuni* where a kanamycin-resistance cassette was introduced leading to an abolition of flagellar function (*Yao et al. 1994*). Later a group used a transposon library to identify genes that resulted in the inability of *C. jejuni* to invade mammalian cells (*Gao et al. 2014*). After identification they performed co-immunoprecipitation experiments and named the protein that interacts with PflA PflB. Flagellation was confirmed by electron microscopy in these studies.

Genes encoding several motor accessory proteins were identified initially as novel flagellar genes in screens of *C. jejuni* mutant libraries. The first of these motor accessory genes was *pflA* (paralysed flagella A), which was identified as a gene that was required for motility by not flagellum assembly (Yao et al. 1994). Taking advantage of the need for *C. jejuni* to be motile to invade mammalian cells, Gao and co-workers screened a *C. jejuni* transposon library to identify novel flagellar genes (Gao et al. 2014). One of the genes identified in the screen was required for motility but not flagellum assembly and was designated as *pflB* (paralyzed flagella B) (Gao et al., 2014). PflB interacted with PflA in a co-immunoprecipitation (co-IP)-IP assay, and a PflA-GFP fusion localized to the cell poles (Gao et al., 2014). A high-resolution *in-situ* structure of the *C. jejuni* motor generated by single particle cryo-electron microscopy revealed that PflA and PflB are closely associated and form a set spoke-like structures and a rim-like structure, respectively, near the stator units (*Drobnič*, *T. et al.* 2023).

Hendrixson and co-workers identified 28 genes in a *C. jejuni* mutagenesis screen that resulted in motility defects (*Hendrixson et al. 2001*). A follow-up publication in 2007 characterized two of these genes that were in the same operon, and these genes were named *flgP* and *flgQ* since disrupting the genes resulted in loss of motility but did not block flagellum assembly (*Sommerlad and Hendrixson 2007*). FlgP is a lipoprotein and was identified to be present predominately in the outer membrane fraction, and localization of FlgP to the outer membrane was shown to be dependent on *flgQ* (*Sommerlad and Hendrixson, 2007*). FlgP was subsequently shown to be required for formation of the basal disk (*Beeby et al., 2016*). A recent high-resolution *in-situ* structure of the *C. jejuni* flagellar motor indicated that the basal disc is comprised of a dozen or more concentric rings (*Drobnic et al., 2023*). The innermost ring of the

basal disc is predicted to be composed of 17 sets of FlgP trimers and the other concentric rings are similarly predicted to be formed by FlgP trimers (Drobnic et al., 2023). Assembly of the basal disc is dependent on FlgQ since the basal disc is not formed in a  $\textit{C. jejuni } \Delta \textit{flgQ}$  mutant (Beeby et al., 2016). Although FlgQ has a predicted signal peptide and presumably localizes to the periplasmic space, it does not appear to form a motor accessory that needs to be made prior to the assembly of the basal disc (Drobnic et al., 2023). It has been proposed that FlgQ facilitates assembly of the basal disc by acting as a chaperone for FlgP or maintaining the stability of FlgP in its final location (Drobnic et al., 2023).

Although FliL is technically not a motor accessory protein since it is found in S. enterica and E. coli, the ring-structure formed by FliL was first visualized in in-situ structures the H. pylori and Borrelia burgdorferi flagellar motors (Tachiyama et al., 2022, Guo et al., 2022). The FliL ring is a motor accessory in H. pylori and other bacteria. FliL is an integral membrane protein that has a single transmembrane helix and a large C-terminal periplasmic region (FliL<sub>C</sub>). *In-situ* structures of the H. pylori and B. burgdorferi motors showed that FliLc forms a ring made up of nine monomers that encircles the plug/linker regions of the MotB dimer of the stator unit (Tachiyama et al. 2022, Guo et al. 2022). Homologs of fliL are found in a variety and bacterial species and was originally identified in E. coli where it was shown to not be required for swimming but necessary for swarming motility (Partridge et al. 2023). The function of the FliL ring in H. pylori and other bacteria is not clear. but FliLc is structurally similar stomatin/prohibitin/flotillin/HflK/C (SPFH) domain of stomatin family proteins, some of which modulate the activities of ion channels in various organisms (*Takekawa et al. 2019*). Thus, FliL<sub>C</sub> may have a role in regulating proton flow through the stator units, and therefore torque output. FliL was originally reported to be required for motility in H. pylori (Tachiyama et al. 2022), but a later report showed that a highly motile variant of H. pylori G27 had a nonsense mutation early in the fliL coding sequence and failed to assemble the FliL ring (Botting et al., 2023). Another study using H. pylori SS1 showed that a strain with a mutation in fliL that resulted in removal of most of the protein sequence retained motility in soft agar medium, whereas strains with mutations that resulted in the retention of the entire transmembrane helix were severely defective in motility (*Liu* et al. 2022).

Recent work by Liu and coworkers identified three proteins, PilM, PilN, and PilO, as structural components of the *H. pylori* flagellar motor where they constitute a portion of the cage structure (*Liu et al. 2024*). Interestingly, the *H. pylori* proteins are homologues of components of the type-IV pilus found in some bacteria. *H. pylori*  $\Delta pilN$  and  $\Delta pilO$  mutant had enhanced motility in soft agar medium compared with the wild type, while deletion of pilM had no effect on motility.

In-situ structures of the motors in the deletion mutants generated by cryo-ET were missing components of the cage accessory structure in proximity to the inner membrane, but a portion of the cage that appears to contact the basal disk was still present (*Liu et al., 2024*). The researchers concluded that PilMNO regulates the ability of the cell to decrease motility in soft agar medium and form microcolonies under certain conditions, possibly through interaction with surface sensing proteins (*Liu, et al., 2024*).

To examine the evolution of the flagellar motor, Chaban and co-workers used sequence homology of conserved flagellar motor proteins to build a phylogenetic tree for motor accessory structures (*Chaban et al. 2018*). The researchers placed members of Campylobacterota as either precursors or descendants of *C. jejuni* by searching for homologues of *flgP*, *flgQ*, *pflA*, and *pflB*. Cryo-ET analysis led the authors to conclude that the flagellar motor of *Wolinella succinogenes* was an evolutionary intermediate of *C. jejuni* and *H. pylori*. The phylogeny analysis revealed that *W. succinogenes* is in the same clade as *Helicobacter* species, although like *C. jejuni* it has 17 stator units compared with 18 in *H. pylori*. All three motor have a basal disk and cage-like periplasmic spanning structures, while the *W. succinogenes* motor differs from *C. jejuni* in the location of the medial ring. Chaban and co-workers examined the motility of several species in media of different viscosities and found that bacteria with larger motors such as *C. jejuni* are more successful at navigating this media. A later section on chemotaxis will discuss the evolutionary history of *H. pylori* and *C. jejuni* and how it differs from flagellar motor evolution.

## The *H. pylori* Flagellar Sheath

#### **Abbreviation and definitions**

 Flagellar Sheath – A structure that surrounds the flagellar filament. Typically seen as a continuation of the outer membrane and composed of lipids but can also be composed of protein.

Of all the aspects of bacterial flagellar research, the flagellar sheath may be the most enigmatic (*Chu et al. 2020*). The exact function of the flagellar sheath is unknown in any bacterial species and may even vary between species. In the case of *H. pylori*, the most plausible functions of the sheath include protection of the filament from depolymerization resulting from exposure to gastric acid, and adherence to the gastric epithelium. In other species, the sheath may protect the filament from detection of flagellins by the host innate immune system (*Yoon and Mekalanos 2008*), or even offer protection from flagellotropic phages, which require flagellar rotation for attachment (*Guerrero-Ferreira et al. 2011*). In the majority of bacterial species, the flagellar sheath is an extension of the OM, but prior to this understanding, researchers speculated that the sheath was comprised of the outer portion of the cell wall (*Sjoblad et al. 1983*). Exceptions to the membranous sheath includes proteinaceous sheaths, but these are relatively uncommon (*Lefevre et al. 2010*). Also, the flagella of spirochetes are periplasmic so technically are sheathed (*Wolgemuth 2015*).

Early analysis of the flagellar sheath from *Bdellovibrio bacteriovorus* found that levels of nonadecenoic acid were slightly enriched and levels of β-hydroxymyristic acid were reduced compared with the LPS from the cell body (*Thomashow and Rittenberg 1985*). A later group found that in *Vibrio anguillarum* a specific LPS antigen localizes exclusively to the cell pole (*Norqvist and Wolf-Watz 1993*). These early studies indicated that the LPS composition of the flagellar sheath varies from the cell body. In *H. pylori*, the sheath contains high amounts of cardiolipin relative to the cell body (*Chu 2019*). Cardiolipin is a phospholipid that accumulates in areas of the membrane with negative curvature. Additional analysis indicated that myristic acid and cyclopropane nonadecanoic acid, fatty acids found in cardiolipin, are elevated in the sheath (*Hirai et al. 1995*).

An area of interest has to do with the proteome of the flagellar sheath. Some researchers have found proteins that localize exclusively to the flagellar sheath, such as porins and predicted adhesions (*Bari et al. 2012*). These are interesting because they can inform as to the purpose of why a cell would have a sheathed flagellum. In the case of *H. pylori*, the story begins in 1988 with

H. pylori adhesion A (HpaA), although there are conflicting reports as to whether it localizes specifically to the sheath (*Evans et al. 1988, O'Toole, et al. 1995, Lundstrom et al. 2001*). The prevalence of hpaA is interesting as the gene is found in gastric but not enterohepatic Helicobacter species, suggesting co-occurrence of sheathed Helicobacter with this gene (*Bansil et al. 2023*). A more compelling development came much later when Radin and coworkers found a large protein that localizes exclusively to the flagellar sheath using immunogold labeling EM and fluorescent microscopy (Radin et al. 2013). This protein FaaA (Flagellar-associated autotransporter A) is a type V autotransporter with a secreted passenger domain and beta-barrel domain that inserts into the OM (*Meuskens et al. 2019*). Interestingly, an faaA mutant had reduced motility, defects in flagellum biosynthesis, and colonization deficiencies (Radin et al. 2013).

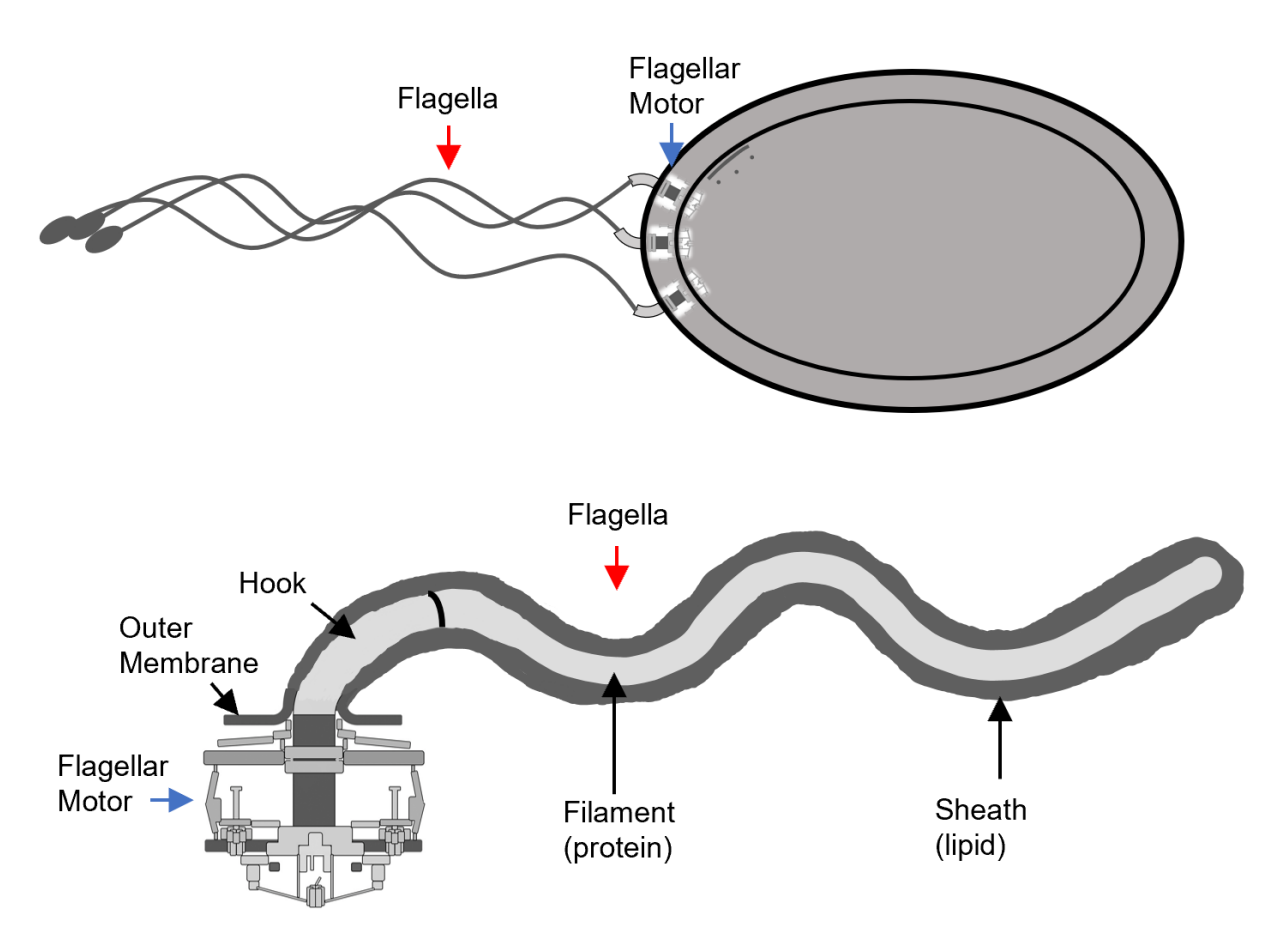


**Figure 1.6.** The *H. pylori* flagellar sheath. The flagellar sheath in *H. pylori* is contiguous with the outer membrane and completely surrounds the proteinaceous filament. The flagellar motor (blue) and flagella (red) are indicated in the figure in the figure.

The *H. pylori* flagellar sheath was first described in a 1989 publication (*Goodwin et al.* 1985), and a later study reported the sheath to have a similar protein, phospholipid, and LPS composition to the outer membrane, with some differences in protein and fatty acid composition (*Geis et al.* 1993). Flagellar sheaths are found almost exclusively in bacteria with polar flagella (Fig. 1.4), where bacteria that have multiple polar flagella, each flagellum has its own sheath (*Chu et al.* 2020). The end of the *H. pylori* flagellum contains a bubble-like distortion referred to as a bulb, found in several other species as well (*Geis et al.* 1989). The composition, structure, and function of the bulb are unknown. *Helicobacter* species that possess flagellar sheaths have distinct phylogenetic clustering from those that are unsheathed and all gastric species examined have sheathed flagella, while enterohepatic species are known to have either sheathed and unsheathed flagella (*Berthenet et al.* 2019). Little is known about flagellar sheath biosynthesis in any bacterial species. *In-situ* structures of nascent *H. pylori* flagella indicate the developing basal body causes a distortion in the OM that leads to the formation of the sheath, which suggests sheath biosynthesis and flagellum biosynthesis are coupled (*Qin et al.* 2017).

## Flagellar Motor Function and Rotational Switching

#### **Abbreviations and Definitions**

- Ion Motive Force (IMF) A force generated by the movement of ions from one side of the membrane to the other. In the case of the flagellar motor, this is a flow of ions through the stator units from the periplasm to the cytoplasm.
- Proton Motive Force (PMF) A form of IMF involving the translocation of protons.
- Stator units The torque-generating units of the flagellar motor found spanning the inner membrane. Each stator is composed of MotA:MotB or in 5:2 stoichiometry.
- C-ring The cytosolic ring structure at the base of the flagellar motor that determines the direction of rotation. The C-Ring together with the MS-ring form the rotor of the flagellar motor to transmit torque to the rod.
- Che-Y The cytosolic signaling protein that interacts with the C-ring to determine the direction of rotation.

Maximum torque generation varies between flagellar motors from 350 pN·nm in *C. crescentus* to 4,000 pN·nm in the motors of spirochetes (*Li and Tang 2006, Nakamura et al. 2014*). This variation in torque is attributed to structural features of the motor including the number of stator

complexes and the motor's diameter (*Beeby et al. 2016*). In the motors studied thus far, *E. coli* and *H. pylori* represent the least and greatest number of associated stator units, at 11 and 18, respectively. In the *E. coli* motor, the stators are not stably maintained within the motor but are recruited as the load on the motor demands (*Nord et al. 2017*, *Wadhwa et al. 2019*). In other bacterial species, including *H. pylori*, the stator units are stably associated with the motor under a range of load conditions (*Chaban et al. 2018*).

The basal body of the bacterial flagella contains the flagellar motor and torque generating stator units that harness ion motive force (IMF) to generate torque (**Fig. 1.7**). Stators that use proton-motive force (PMF) are composed of MotA and MotB, while stators that are sodium driven are composed of PomA and PomB subunits, all in a 5:2 stoichiometry of A to B subunits (*Tang et al. 1996, Santiveri et al. 2020*). The stators share sequence homology with the transport proteins ExbBD (*Kojima and Blair, 2001*). This section will focus on the proton-driven motor, as it is more common and is the type of motor found in *H. pylori*. A stator functions similarly to ATP synthase, where a periplasmic ion is transported through the stator and is deposited in the cytoplasm. The movement of the ion is driven by a charge gradient difference between the periplasm and cytoplasm.

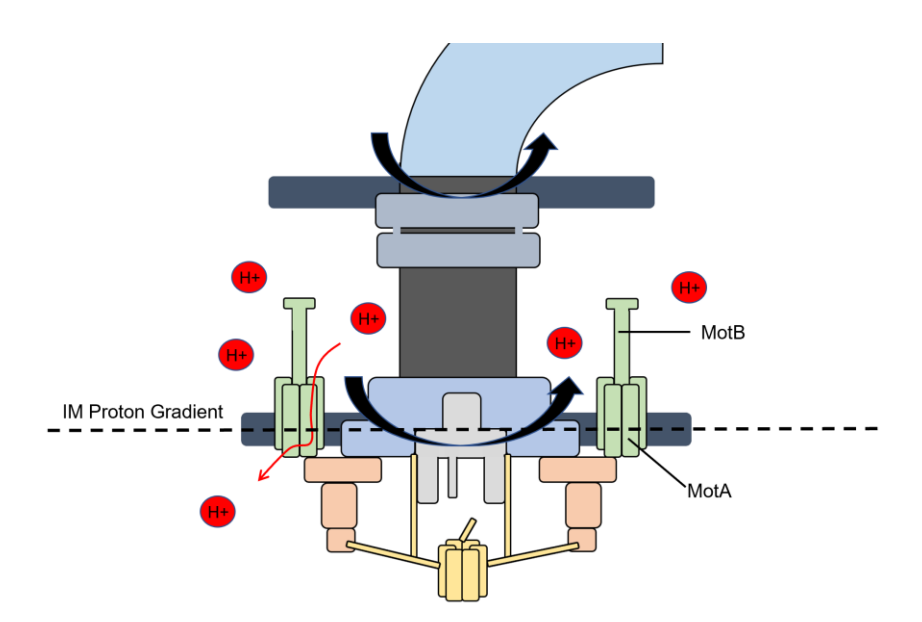


Figure 1.7. Ion movement through the bacterial flagellar motor. Protons or other ions flow through a stator motor unit down a gradient from high concentration in the periplasm to low concentration in the cytoplasm as illustrated by the red arrow. Each stator is composed of MotA:MotB in 5:2 stoichiometry. Proton movement through the stator results in the rotation of the

MotA pentamer to generate torque, which is transmitted to the rotor formed by the C-ring and MS-ring.

MotA forms a ring that imbeds within the inner membrane while MotB anchors the peptidoglycan at one end, passes through the MotA ring, and anchors the IM with a transmembrane helix at the other (*Santiveri et al. 2020*). The domains of MotB include a C-terminal, peptidoglycan-binding domain (PGB) that anchors the stator to the cell wall, a periplasmic linker, a plug domain, and an N-terminal, MotA interaction domain (*Roujeinikova, et al. 2008*). The plug domain allows the stator to adopt an active or inactive state. In the active state the MotB PGB domain binds to the cell wall and the plug domain becomes unplugged, activating the ion translocation function of the stator (*Hosking et al. 2006*). The ion channel is composed of neutral and negatively charged residues, allowing a proton to move from periplasm to cytoplasm by moving along these energetically-favorable side chains (*Santiveri et al. 2020*). The channel is opened or closed by the aromatic ring of a phenylalanine in MotA.

The MotB chains that reside within the active MotA ring have highly conserved residues that are critical for the ability of the stator to transport protons from the periplasm to the cytoplasm (*Zhou and Blair 1997*). A negatively charged aspartic acid at position 33 in *S. enterica* (position 22 in *C. jejuni*) is responsible for accepting the proton from the periplasm and moving it through the ion channel to the cytoplasmic side (*Santiveri et al. 2020*). This proton-accepting portion of the motor is highly conserved where an alanine substitution at Asp-33 in MotB results in the abolishment of motility (*Zhou and Blair 1997*). The translocation of protons is an intricate process orchestrated by the two MotB subunits within each stator. When the Asp-33 on one MotB chain accepts a proton, the result is movement of the MotA in a single direction, by 36 degrees, as the result of Brownian motion (*Santiveri et al. 2020*). Following this rotation, the Asp-33 of the opposite MotB chain releases a proton, where the proton travels through a MotA channel lined with acidic residues. This chain will then accept another proton and the process will repeat.

The stator interacts with the C-ring, which determines the direction of motor rotation (*Carroll et al. 2020*). The C ring has 3 subunits in most flagellar motors; a proximal FliG portion, a middle FliM portion, and a distal FliN portion (*Fig. 1.8*). FliG interacts with both the stator and MS-ring, allowing for the transit of torque to the motor drive shaft. FliM interacts with CheY-P (CheY-phosphate) and FliN interacts with the ATPase portion of the export apparatus (*Fig. 1.8*). The motor is in a counterclockwise rotation until CheY-P interacts with FliM resulting in clockwise rotation. Binding of CheY-P causes a conformational change of the C-ring that changes its interaction with the stator unit (*Chang et al. 2020*). A portion of FliG<sub>C</sub> (C-terminal domain) called

the torque helix has highly conserved negatively charged residues that interact with the positively charged residues on one of the MotA subunits (*Santiveri et al. 2020, Carroll et al. 2020*). When the C-ring undergoes conformational change the torque helix flips 180 degrees. In counterclockwise rotation the torque helix interacts with the inside surface of MotA and in clockwise rotation it interacts with the outside surface of MotA (*Hu et al. 2022, Santiveri et al. 2020, Zhou and Blair 1997, Lee et al. 2010, Chang et al. 2020*). The reorientation of the torque helix and the reversal of the charge interaction of the C-ring with the stator leads to the C-ring rotating in the opposite direction. The rotating C-ring is connected to the IM associated MS-ring, which is connected to the axial rod (*Carroll and Liu 2020*). The torque generated by the proton flow through the stator units is transferred to the rod and out of the cell through the filament.

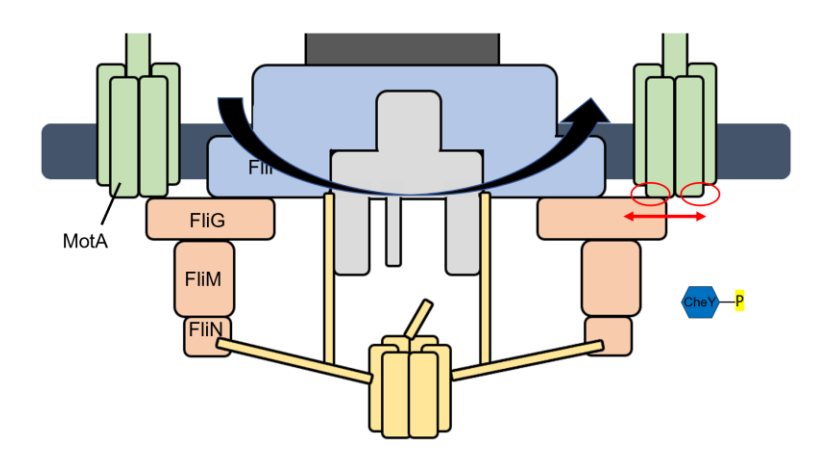


**Figure 1.8. Rotational switching of the motor at the C-Ring.** The torque helix of FliG can interact with either of two different regions of the stator unit (red circles), changing the diameter of the C-ring (red arrows) and direction of rotation of the rotor. The rotor rotates in a counterclockwise rotation when FliG interacts with the inside of the stator as shown in the figure. Upon binding of CheY-P to FliM, a conformational change within the C-ring causes FliG to engage the outside of the stator and results in clockwise rotation of the rotor.

#### **Bacterial Chemotaxis**

#### **Abbreviations and Definitions**

- Chemotaxis Movement of a bacterial cell towards or away from a signal as a result of the cell sensing that signal.
- Chemoreceptor Sensory proteins that receive an environmental signal, triggering a chemotaxis pathway. Typically have sensory domains in the periplasm but can also be entirely cytosolic.
- Coupling Protein Cytosolic proteins that relay signal between the chemoreceptor and histidine kinase CheA.
- CheA Transmits signal from the coupling protein to CheY in the form of a phosphate.
- CheY CheY-P is a periplasmic protein that interacts directly with the C-Ring of the flagellar motor.

Bacterial taxis is motility guided by environmental sensing, which biases the otherwise random swimming of a cell towards more optimal environments (*Beeby et al. 2020*). Different forms of taxis include phototaxis (light), aerotaxis (oxygen), gravitaxis (gravity), rheotaxis (flow), magenetotaxis (magnetism), and chemotaxis (chemicals). Chemotaxis machinery can sense chemicals, pH, osmolarity, temperature, and redox potential (*Bi et al. 2018*). Because chemotaxis is the only documented taxis used by *H. pylori*, chemotaxis will be the focus on in this section.

The bacterial flagellar system works at the direction of the chemotaxis system, where directionality is determined in a cascading series of events to either direct the bacterium towards attractants or away from repellents (*Bi et al. 2018*). There are 17 types of conserved chemotaxis systems, each with a distinct combination of signaling proteins (*Wuichet and Zhulin 2010*). Ternary complexes composed of transducer-like proteins called chemoreceptors, their histidine kinases, and adaptors are the tools of chemotaxis (*Fig. 1.9*). Sensory complexes of chemoreceptors form receptor trimers and dimers that assemble in arrays. The sensitivity of the arrays is such that a change of less than 1% over background conditions can lead to a chemotactic response (*Colin and Sourjik 2017*, *Bi and Sourjik 2018*). The complexes that include the chemoreceptors also include the histidine kinase CheA and adaptor CheW which regulates CheA (*Bi et al. 2018*). Attractants interact with a chemoreceptor that then inhibits the CheA autophosphorylation, while binding of repellents to a chemoreceptor activates CheA autophosphorylation. CheA can donate its phosphate to CheY, leading CheY-P to interact with the flagellar motor at the switch complex by donating its phosphate group. This interaction leads to clockwise rotation (*Fig. 1.9B*), while an unphosphorylated CheY does not interact with the C-

ring resulting in counterclockwise rotation (Fig. 1.9A). *H. pylori* mutants in *cheA* or *cheY* are non-chemotactic and are unable to colonize animal models (*Barak et al. 2004*). Some bacteria modulate the sensitivity of the chemotaxis system through the methyltransferase CheR and methylesterase CheB. CheR methylates kinase-off receptors while CheB demethylates kinase-on receptors. The negative feedback allows the cell to constantly adapt to a wide range of background stimulus strengths. The rates of CheR and CheB activity are slower than the time scale of signaling which allows the cell to compare current environmental conditions with those several seconds in the past, functioning as a type of memory system (*Parkinson et al. 2015, Bi et al. 2018*). Many bacteria have additional signaling proteins including CheZ, FliY, CheC, CheV, CheD, and CheX. These additional proteins typically have auxiliary roles to the core set of proteins (*Ortega and Zhulin 2016, Bi et al. 2018*). Unlike the flagellar system, the chemotaxis system is conserved between archaea and bacteria (*Wuichet and Zhulin 2010*). The chemotaxis system is thought to have been introduced to archaea through horizontal gene transfer.

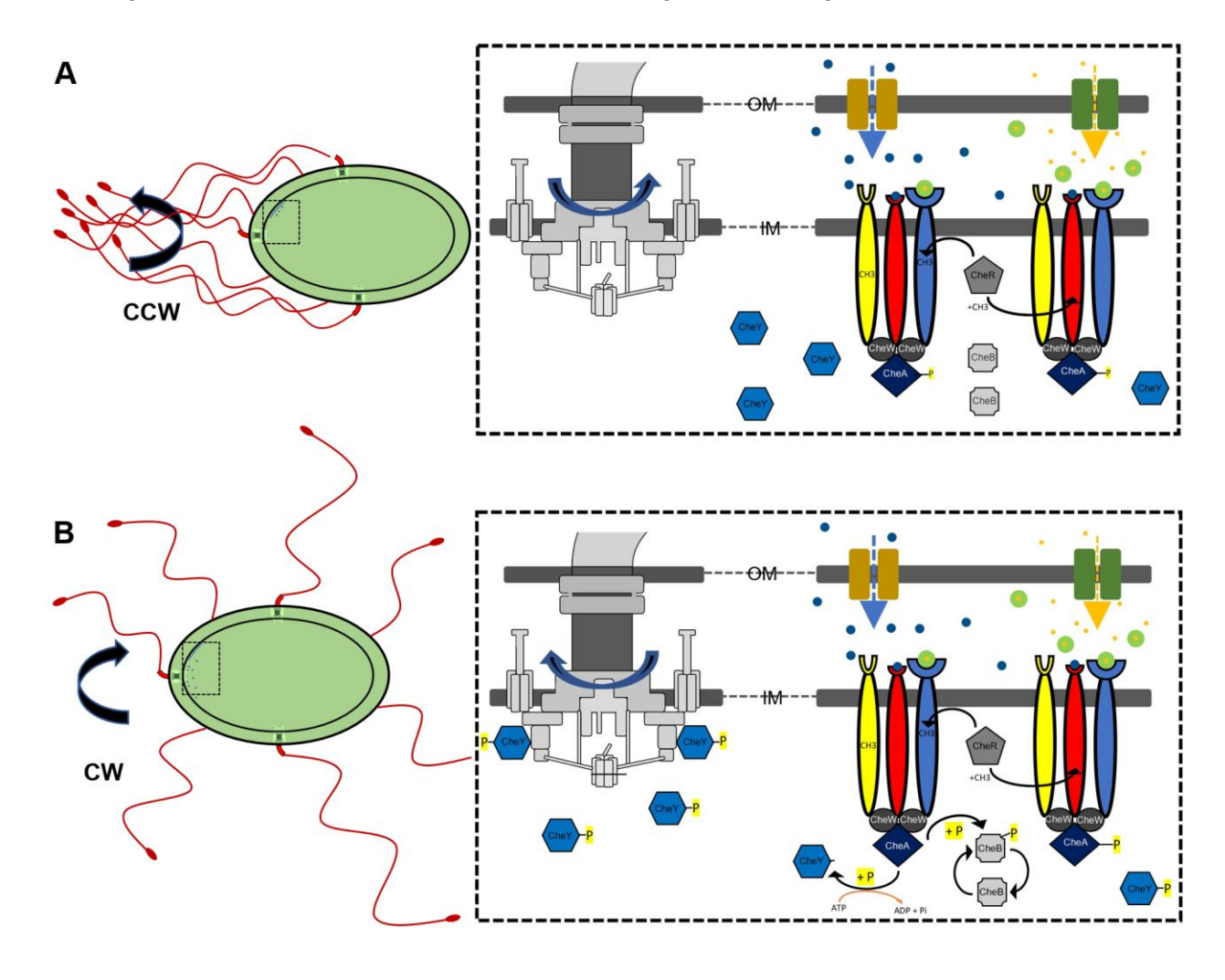


**Figure 1.9. Chemotaxis in bacteria with a peritrichous flagellation pattern**. Chemoreceptors bind ligands which begins signal transduction that causes the flagellar motor to rotate clockwise or counter clockwise. *E. coli* and *S. enterica* are represented by this type of motility.

Bacterial chemoreceptors usually span from the periplasm to the cytoplasm (Fig. 1.9, chemoreceptors are colored cylinders in yellow, red, and blue), and possess a periplasmic sensory domain that receives the signal, a methylation helix for signal adjustment, and a cytoplasmic signaling tip (Bi et al. 2018). Chemoreceptors are grouped by the length of the signaling domain and are represented by the number of helical heptads (H); 24H, 28H, 36H, 40H, 44H, and 52H. (Wuichet et al. 2007). Molecules can interact with chemoreceptors in several ways, with interactions of the periplasmic sensory region being the most common (Fig. 1.9, colored circles in the periplasm). Chemical ligands can interact with the sensory region by direct or indirect binding. In direct binding, the chemical ligand binds directly to the tip of the receptor (Fig. 1.9, red receptor and blue ligand), which allows for a highly sensitive response over a wide dynamic range primarily because of methylation dependent adaptation (Colin and Sourjik 2017, Bi et al. 2018). Despite the sensitivity of direct binding, it is less commonly used than indirect binding, which utilizes a binding protein that mediates between the ligand and receptor (Fig. 1.9, blue receptor, green binding protein, orange ligand). The dynamic range of indirect binding is not as sensitive as direct binding because receptors cannot adjust binding affinities for binding proteins, although its regulatory flexibility is greater because the cell can adjust the levels of the binding proteins (Neumann et al. 2010, Bi et al. 2018). The differences in chemotactic systems include the composition of the signaling pathway and number of pathways, the number of receptors, the specificities of the receptors, and the differences in how the signal is relayed (Ortega et al. 2017, Wuichet and Zhulin 2010, Bardy et al. 2017, Bi et al. 2018). In E. coli, Tar and Tsr are the most common receptors and sense amino acids and other stimuli, while the less common Trg, Tap, and Aer sense sugars, dipeptides, and redox potentials, respectively (Parkinson et al. 2015, Bi et al. 2018).

In most species of Campylobacterales, including *H. pylori*, the single taxis system is chemotaxis (*Ortega et al. 2017, Liu and Ottemann 2022*). Chemotaxis in *H. pylori* responds primarily to pH, diverting the cell from areas of low pH to areas of higher pH, or towards urea, which the cell can metabolize to create ammonia and bicarbonate, two alkaline compounds (*Mizote et al. 1997, Worku et al. 2004, Huang et al. 2015*). Other studies have identified compounds such as mucin, amino acids, and cholesterol as attractants for *H. pylori*, while

repellents include salts, metal ions, and quorum autoinducer-2 (*Ortega et al. 2017, Worku et al. 2004, Wunder et al. 2006, Rader et al. 2011, Collins et al. 2016, Sanders et al. 2013*).

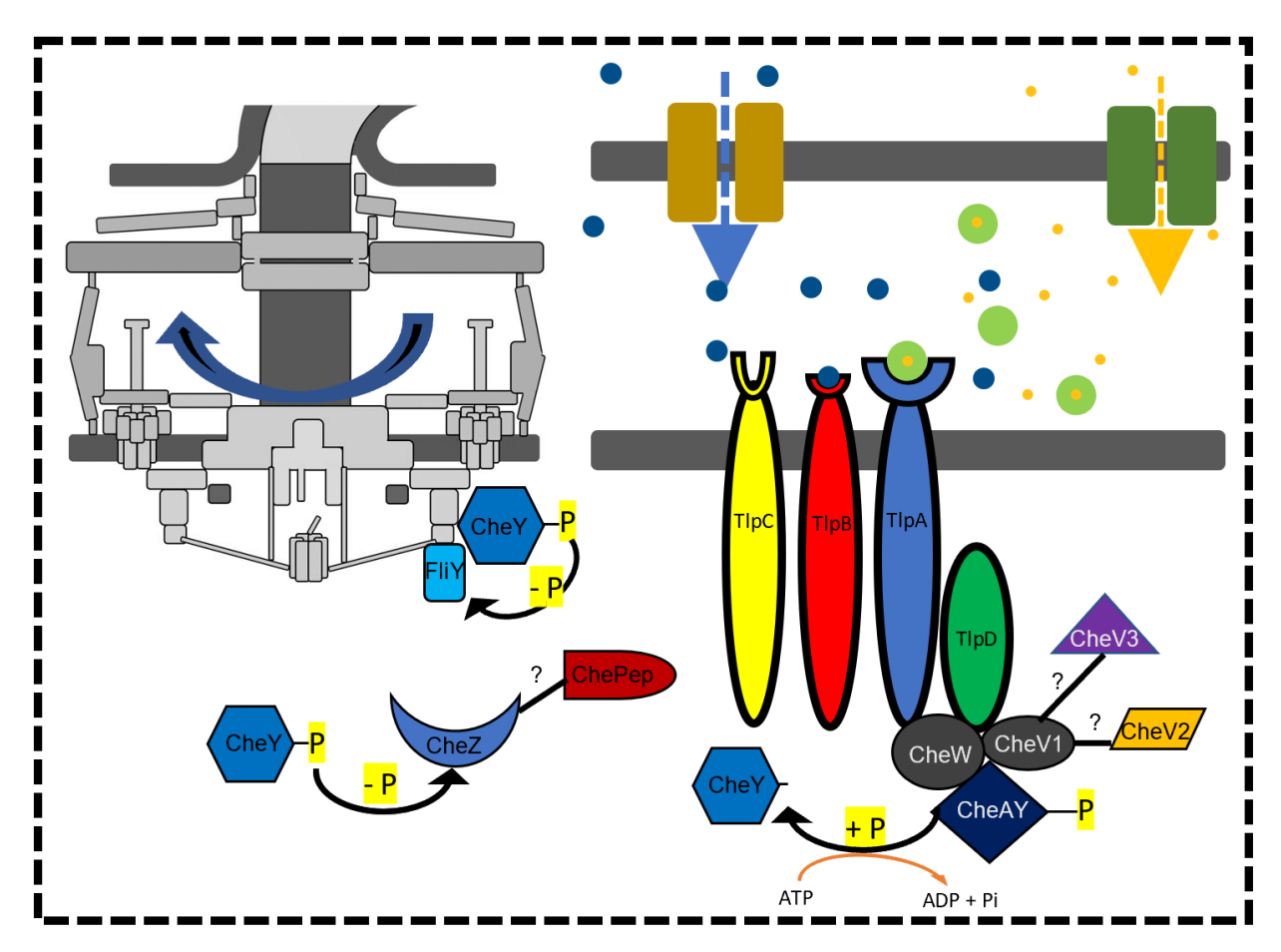


**Figure 1.10. Chemotaxis in** *H. pylori*. Chemotaxis begins with either direct or indirect binding of the ligand (blue and yellow circles) to the chemoreceptor (TlpABC). The signal of the ligand's binding is transmitted to the coupling protein CheW, then to CheAY-P. CheAY-P will donate its phosphate to CheY, which then interacts with the flagellar motor. CheV1 may assist in signal transduction between CheW and CheAY. The function of CheV2 and CheV3 is unknown. ChePep is involved in dephosphorylation of CheY-P and CheZ is a phosphatase. FliY is also a phosphatase of CheY-P. Methylation of chemoreceptors does not occur in *H. pylori*.

The chemotactic system in *H. pylori* includes the chemoreceptors, coupling proteins, a kinase, and a response regulator (**Fig. 1.10**). *H. pylori* has a set of 4 chemoreceptors, compared to the 5 in *E. coli* and 10 in *C. jejuni* (*Ortega et al. 2017*). TlpA, TlpB, and TlpC are membrane spanning receptors, while TlpD is cytosolic. Mutation or deletion of either chemoreceptor has the result of reducing or eliminating the bacterium's ability to colonize or persist in the stomach

(Anderman et al. 2002, Rolig et al. 2012, Behrens et al. 2013, Croxen et al. 2006, Mcgee et al. 2005, Williams et al. 2007). The chemoreceptors interact with coupling proteins that relay signals to the sensor kinase CheA. In H. pylori these coupling proteins are CheW, CheV1, CheV2, and CheV3, but only the functions of CheW and CheV1 are well characterized (Pittman et al. 2001, Terry et al. 2006, Lowenthal et al. 2009, Abedrabbo et al. 2017). The number of cheV genes in the Helicobacteracae family ranges from one to four (Liu and Ottemann 2022). CheV1, CheV2, and CheV3 are hybrids of CheW that contain a C-terminal response regulator-like domain (Rec) and a N-terminal CheW domain, while CheW contains a single domain (Pittman et al. 2001, Pinas et al. 2016). Evidence suggests that the affinity of the coupling proteins for individual chemoreceptors may vary (Ortega and Zhulin 2016). Deletion mutants in cheW and cheV1 are severely compromised in soft agar chemotaxis assays, while mutants in cheV2 and cheV3 show only mild motility defects (*Lowenthal et al. 2009*). Studies on the interaction between the coupling proteins, chemoreceptors, and CheA reveal strong interactions between CheW and CheV1 as well as strong interaction of both of these proteins with CheA (Abedrabbo et al. 2017). TlpD (used as a model for all four chemoreceptors) interacts with CheW and CheV1, while CheV1 has weak interaction with CheV2 and CheV3. Abedrabbo and co-workers found that when incubated with either one or both CheW and CheV1, CheA phosphorylation is significantly increased, suggesting that these proteins are intermediary between the chemoreceptors and sensor kinase. CheW, CheV1, and CheA are also involved in localizing the chemosensory complex to the membrane and cell pole, and stability of the complex in H. pylori cells. In H. pylori, it is thought that CheV3 has a similar role as CheW in mediating interactions between some chemoreceptors and CheA. The role of CheV1 and CheV2 are not well understood, but they are thought to catalyze the removal of phosphate from CheAY (Jimenez-Pearson et al. 2005). Many questions still remain regarding the function of the coupling proteins, such as: what is the role of CheV2 and CheV3 in signal transduction; does each coupling protein have greater affinity for one or more chemoreceptor; does the relative abundance or function of each coupling protein shift with different environmental conditions?

The histidine kinase CheA and adapter CheW of the chemotactic ternary signaling complex in *H. pylori* are similar to those in *E. coli* (*Lertsethtakarn et al. 2011*). As in *E. coli*, mutation of CheA, CheW, or the response regulator CheY reduces chemotaxis or motility (*Foynes et al. 2000, Pittman et al. 2001, Terry et al. 2005*). *H. pylori* CheA differs from the canonical CheA in that it has an additional REC domain at the C-terminus and lacks sequence conservation in the P2 CheY binding domain (*Foynes et al. 2000, Wuichet and Zhulin 2010*). CheA is referred to as CheAY if it contains this additional REC domain. *H. pylori* contains an additional chemotaxis

protein called ChePep that is responsible for the efficient dephosphorylation of CheY-P (*Howitt et al. 2011*). ChePep interacts closely with the phosphatase CheZ where localization of CheZ to the cell pole is reliant on ChePep (*Lertsethtakarn et al. 2015*). The loss of either CheZ or ChePep results in an increase in hyper reversals, suggesting elevated levels of CheY-P in the absence of CheZ or ChePep. *H. pylori* contains the additional accessory protein FliY, a phosphatase that accelerates the autodephosphorylation activity of CheY. (*Lertsethtakarn et al. 2011*). FliY is located at the C-ring and shares homology to FliN.

Two widespread chemotaxis proteins, the methyltransferase CheR and the methylesterase CheB are absent in H. pylori (Lertsethtakarn et al. 2011, Parkinson et al. 2015, Liu and Ottemann 2022). A significant number of species in Helicobacteraceae lack genes for cheB and cheR, while species in Campylobacteraceae retain them. Analysis of the Campylobacterota phylum suggests that the ancestor of the phylum had cheA, cheR, and cheB, and the phylum is monophyletic (Waite et al. 2017). Modern species that lack cheR and cheB underwent gene loss. The authors were interested in knowing if ecological niche had a role in the retention of cheR and cheB. They found in the characterized species of Helicobacter that all enterohepatic species have cheR and cheB, while all gastric species lack the genes. The authors proposed that cheR and cheB are predictive to ecological niche. In addition, they found that genome size is also predictive of where the bacterium resides with enterohepatic species having an average genome size of 2.05 Mbp and gastric species having 1.65 Mbp. The authors hypothesize that the niche is responsible for the selection against cheR and cheB. H. pylori must cross the mucus membrane to colonize the gastric epithelium, and without cheR and cheB the cells may have longer straighter runs that allow for more efficient colonization. The streamlining of the H. pylori genome may play a role as well, since H. pylori doesn't have competitors in the harsh stomach environment it is unnecessary to have a more sensitive chemotaxis system.

# Translocation of flagellar proteins across the inner membrane

#### Abbreviations and definitions

- F-T3SS flagellar type III secretion system
- Sec bacterial translocation machinery for preproteins
- YidC bacterial membrane insertion machinery
- Tat bacterial translocation machinery for folded proteins
- SRP signal recognition particle
- RNC Ribosome-nascent chain complex
- PMF proton motive force
- ATP adenosine triphosphate
- SP signal peptide
- SPI signal peptidase I
- SPII signal peptidase II
- MD mature domain
- TF chaperone trigger factor
- GTP Guanosine triphosphate
- TMH transmembrane helix
- REMP redox enzyme maturation proteins

In the assembly of the bacterial flagellum, the axial components of the flagellum are transported across the inner membrane by the F-T3SS. Other flagellar basal body proteins, including the MS-ring protein, LP-ring proteins, and stator unit proteins, as well as the proteins that form the periplasmic motor accessory structures (**Fig. 1.4**) are transported across the membrane by other means. The other pathways of protein translocation in bacteria include the Lol pathway for lipoproteins, the Sec (<u>Sec</u>retory), YidC, and the Tat (<u>Twin-arginine translocation</u>) systems (*De Geyter et al. 2019*).

There are two pathways by which proteins are translocated: the co-translational pathway and the post-translational pathway (*Muller et al. 2001, Hartl et al. 1990*), where hydrophobicity is the discriminating factor in which pathway the peptide will take (*Lee and Bernstein 2001, Peterson et al. 2003*). The co-translation pathway involves membrane-bound proteins being translocated directly from the ribosome into the membrane, where insertion into the membrane is

mediated by either the SecYEG or YidC translocon, or sometimes both in complex (*Cymer et al.* 2015). A translocon is a protein channel through which proteins pass for secretion or insertion into the membrane. Translocons have the ability to either shield hydrophobic residues from the aqueous environment allowing them to embed into the membrane, or shield hydrophilic residues from lipids as they pass through the protein channel. Both SecYEG and YidC are translocons, with SecYEG involved in protein secretion and inserting lipoproteins and transmembrane helices (TMH), while YidC only functions as an insertase for TMHs.

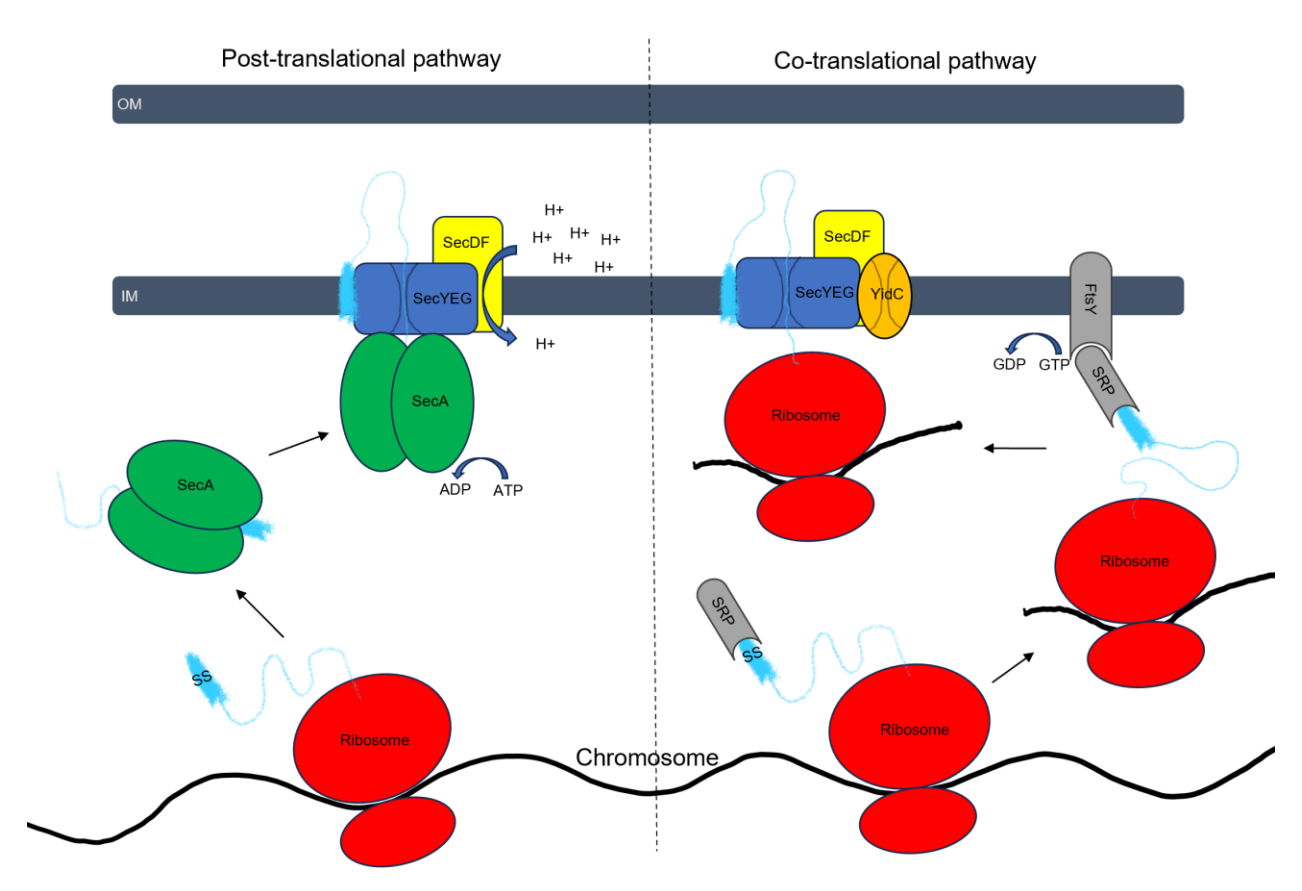


Figure 1.11. Translocation of peptides containing a SPI or SPII signal sequence (SS) by the post-translational and co-translational pathways. Diagrammed is models of the post-translational and co-translational pathways. In summary, peptides are translocated after dissociation with the ribosome in the post translational pathway (left), while peptide association with the ribosome is maintained during translocation in the co-translational pathway (right).

The ubiquitous Sec system, found in bacteria, archaea, and eukaryotes can mediate both post- and co-translational translocation (Fig. 1.11) and is responsible for translocation of the majority of the bacterial exportome (Collinson et al. 2015, De Geyter et al. 2019). The Sec machinery harnesses both ATP hydrolysis and PMF to translocate proteins in an unfolded state. The translocon SecYEG is a heterotrimer where SecY forms the largest portion and core of the translocation channel (Cannon et al. 2005). Translocation is initiated when the N-terminal region of a protein with a signal peptide (SP) interacts with SecY (Van Den Berg et al. 2004). The SP is located at the N-terminal end, while the mature domain (MD) refers to the remainder of the peptide (Chatzi et al. 2013, von Heijne 1990). The SP consists of 3 regions: (i) an N-terminal positively charged region; (ii) a central hydrophobic region; (iii) and an end-terminal hydrophilic region that contains the signal peptidase recognition site (Cranford-Smith and Huber 2018). There are two signal peptidases, SPI and SPII, with SPI targeting proteins to the OM and SPII involved in targeting of lipoproteins, most of which that end up in the OM. SecE partially surrounds SecY and enhances its stability (Kihara et al. 1995), while the function of SecG is unknown (van der Sluis et al. 2006). The cytoplasmic SecA ATPase motor protein assists SecYEG in the initiation of translocation of all proteins taking the post-translational pathway, and in some cases has a role in co-translational initiation (Qi and Bernstein 1999, Rapoport 2007). Translocation is controlled by a plug domain and a ring of hydrophobic resides that are part of SecY (Van Den Berg et al. **2004**). The widening of the lateral gate of SecY allows translocation of the unfolded peptide while preventing passage of small molecules (Park and Rapoport 2011). Along with movement of the plug domain by the SP, the lateral gate of SecY widens in response to SecA binding, thereby allowing translocation of the protein (Van Den Berg et al. 2004, Zimmer et al. 2008, Hizlan et al. 2012). While SecYEG provides the channel and control over initiation of peptide translocation, SecDF has a role in proton translocation (Arkowitz and Wickner 1994, Tsukazaki et al. 2011). Proton flux leads to conformational changes in the periplasmic domains of SecDF, which is thought to ratchet the peptide through the SecY channel from the periplasmic side (Tsukazaki et al. 2011).

The post-translational pathway involves peptides being released from the ribosome before being targeted for translocation where the SP interacts with the channel of SecY initiating translocation (*Hartl et al. 1990, Gouridis et al. 2009, Hizlan et al. 2012*). Peptides can be assisted to the SecYEG translocon by SecA (*Brundage 1990*), the export chaperone SecB, SecA-SecB complexes, or the general chaperone trigger factor (TF) (*Tsirigotaki 2017, Crane and Randall 2017*), leading to initiation that is characterized by a conformational change of SecYEG distinct from SecA (*Zimmer et al. 2008, Park et al. 2014*, *Gogala et al. 2014*). During

translocation, large conformational changes have been observed in SecYEG and SecA (Zimmer et al. 2008). Protein secretion is broken down into two distinct parts: initiation and translocation, where initiation involves unlocking of SecYEG and translocation when the peptide passes through the complex. ATP hydrolysis at SecA is required for both initiation and translocation of the peptide (Schiebel 1991) and is stimulated by SecYEG (Lill et al. 1989). PMF is critical for late-stage translocation of the peptide and has been found to function in the absence of ATP hydrolysis. Research in eukaryotic systems suggests that protein translocation abides by a Brownian motor mechanism (*Dudek et al. 2015, Matlack et al. 1999*), but in bacteria, which lack periplasmic ATP, the story is more complex. There is limited experimental evidence for the mechanism of action of protein secretion in bacteria, but the two leading theories are the power stroke and diffusion models. The power stroke model is one where the peptide goes through steps as molecules of ATP are hydrolyzed at SecA leading to binding, forward movement, and release of the peptide. The diffusion model is characterized by the hydrolysis of ATP at SecA biasing the direction of movement of the peptide through the channel with PMF powering the peptide through the channel. Of the two models, the ratcheting mechanism of the diffusion model is most similar to that seen in eukaryotic systems (Dudek et al. 2015) and has advantages over the power-stroke model (Simon et al. 1992), but further experimental evidence is needed.

The co-translational pathway occurs in conjunction with translation. To begin the cotranslational pathway, the SP is recognized by the ribosome-bound signal recognition particle (SRP) as the peptide exits the ribosome (Tsirigotaki 2017, Steinberg et al. 2018, Saraogi and Shan 2014, Kuhn et al. 2017). The SRP has a role in initiation in the translocation of membrane proteins where it recognizes a hydrophobic polypeptide segment, either a signal sequence or TMH (Flanagan et al. 2003). Binding of the polypeptide to SRP causes a structural change leading to the ribosome-nascent chain-SRP (RNC-SRP) binding to the SRP receptor FtsY, which then binds the translocon (Saraogi and Shan 2014, Kuhn et al. 2017). Binding of SRP to FtsY brings the RNC in close proximity to SecYEG leading to the formation of an unstable intermediary complex (Tsirigotaki 2017, Kuhn et al. 2017). SRP-FtsY binding induces GTP hydrolysis leading to the formation of a stable SRP-RNC-FtsY complex (Steinberg et al. 2018, Saraogi and Shan 2014, Kuhn et al. 2017). SRP and FtsY dissociate, allowing the ribosome to bind SecY directly (Steinberg et al. 2018, Saraogi and Shan 2014, Kuhn et al. 2017), where the SP then enters the SecYEG pore to begin translocation (Tsirigotaki 2017, Steinberg et al. 2018, Kuhn et al. 2017). Inner membrane proteins with TMHs are inserted by SecYEG when a SP binds the lateral gate of SecY, with the nascent chain inserting into SecY as a hairpin loop (Kuhn et al. 2017). As TMHs occupy the lateral gate, hydrophilic residues remain unfolded within the aqueous channel

(*Tsirigotaki 2017, Kuhn et al. 2017*). The TMHs slide into the inner membrane and the SP is cleaved by the signal peptidase.

Like the Sec system, the YidC system is highly conserved and found in Bacteria, Archaea, and eukaryotes. YidC acts as an insertase without the need for an energy source (Fig. 12), and instead is thought to use hydrophobic forces to facilitate the insertion of TMHs (*Dalbey et al. 2014*). YidC is involved in the insertion of some singular protein domains when complexed with SecYEG, yet the number of proteins that only require YidC for insertion is limited, despite YidC being more plentiful than SecYEG in *E. coli* (*Gallusser and Kuhn 1990, van der Laan et al. 2003, Facey et al. 2007, Celebi et al. 2006*). Of the 972 proteins found in the *E. coli* K12 inner membrane, only 2 have been found to be translocated exclusively by YidC, while 68 are translocated by Sec and YidC complexed (*De Geyter et al. 2019, Orfanoudaki and Economou 2014*). YidC can function to direct proteins that lack an SP to the membrane through three mechanisms; (i) the first involves the SRP, which facilitates membrane targeting (*Facey et al. 2007*); (ii) second, YidC can act as a ribosome receptor itself that directly accepts the membrane protein (*Jia et al. 2003*); (iii) and third, involves an electrostatic mechanism where the positively

charged ends of a peptide interact directly with the negatively charged lipid heads facilitated by YidC (*Gallusser and Kuhn 1990*).

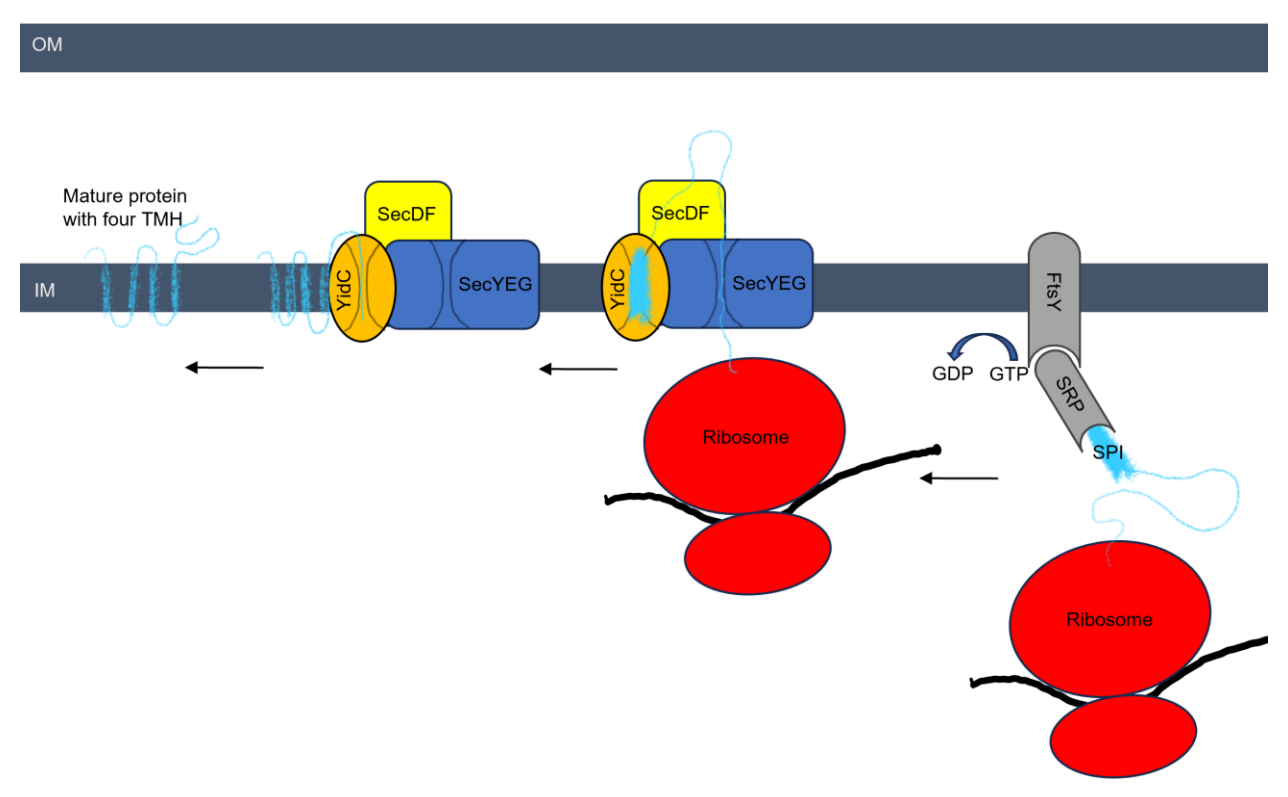


Figure 1.12. YidC insertase activity of a peptide with a SPI signal sequence. YidC complexed with the Sec machinery inserts a protein with a signal sequence into the membrane due to the protein containing highly hydrophobic regions. **Note**: only YidC complexed with Sec through the SRP targeted pathway is shown. YidC interacting directly with the ribosome not complexed with Sec machinery or interacting with the SRP are not shown. YidC can also translocate proteins that do not contain a SPI signal sequence.

Proteins that are translocated only by YidC have one or two short TMHs where the energetic gain of inserting a TMH may help with the energetic cost of translocating a hydrophilic periplasmic region (*Serek et al. 2004, Hennon et al. 2015*). YidC complexes with Sec to translocate proteins with TMHs when the energetic cost is too high for YidC alone (*Hennon et al. 2015*). When complexed with Sec, YidC may facilitate integration of TMHs, help with the packing of helical bundles, and remove TMHs from the Sec channel (*Dalbey et al. 2014, Hennon et al. 2015*). YidC can either directly complex with SecYEG or through a SecDFYajC bridge (*Dalbey et al. 2014*). Substrates that only require YidC for translocation can be crosslinked to SecYEG, suggesting that YidC may never function independently of the Sec machinery (*Dalbey et al.* 

2014). In terms of whether a TMH will be translocated by either Sec or YidC, negatively charged residues in the TM region are a YidC determinant, while positively charged residues are a YidC/Sec determinant (*Price and Driessen 2010, Zhu et al. 2013*). Experiments show that altering the charge of the exposed residues of a TMH can change it from a YidC-dependent to independent peptide, and vice versa (*Gray et al. 2011*). The strongest determinant for whether a protein will be inserted dependent on YidC is a moderate hydrophobicity of the TM regions (*Ernst et al. 2011, Zhu et al. 2013*).

The crystal structure of YidC shows that it has a hydrated cleft that extends over halfway across the membrane where it is exposed to both the cytosol and lipid bilayer (*Kumazaki et al. 2014*, *Wickles et al. 2014*). YidC may translocate peptides where a hydrophilic tail or loop region can remain in the cleft while TMHs slide into the membrane (*Seitl et al. 2014*, *Wickles et al. 2014*). Free energy change calculations indicate that destabilization of the membrane around the YidC translocon resulting from insertion of TMHs into the membrane may allow the polar region in the hydrated cleft to pop across the remaining membrane to the periplasmic side. A comparative analysis of the energy contribution of the YidC and SecYEG translocons showed the  $\Delta$ G of nonpolar residues was similar, while the  $\Delta$ G of polar resides was 2-fold higher when translocation is mediated by YidC, suggesting TMHs are more lipid exposed during YidC mediated translocation (*Ojemalm 2013, Xie et al. 2007*).

YidC is thought to be involved in the assembly of membrane protein complexes since some complexes fail to form or have reduced levels in its absence (*van der Laan et al. 2003, Wickstrom et al. 2011*). In the absence of YidC, (i) the level of F1Fo ATP synthase is decreased by 60% due to YidC being necessary to subunits a, b, and c insertion (*van der Laan et al. 2003*); (ii) cytochrome bo oxidase levels are decreased by 50% due to YidC being necessary for insertion of CyoA (*Wickstrom et al. 2011*); (iii) NADH dehydrogenase 1 levels are decreased by 30% (*Wickstrom et al. 2011*); and (iv) the MalFGK2 maltose transporter levels are decreased by 94% (*Wickstrom et al. 2011*). Cytochrome bo oxidase subunits CyoA and CyoB copurify with YidC (*Price et al. 2010*). When complexed with YEG, YidC is thought to act as a foldase for the packing of TMHs of proteins that have multiple membrane spanning segments (*Nagamori 2004, Wagner et al. 2008, Zhu et al. 2013*).

The Tat system, in contrast to the Sec system, is used to secrete proteins in folded conformations across the membrane (*Collinson et al. 2015*). Proteins destined for the Tat system have a N-terminal cleavage SP that is recognized by two arginines at the N-terminus (*Chaddock et al. 1995*). The Tat system utilizes PMF for secretion, but does not require ATP (*Santini et al. 1998, Yahr and Wickner 2001*). The Tat system is known to export 32 folded proteins in *E. coli* 

K12 (*De Geyter et al. 2019, Ball et al. 2016*). Proteins exported by Tat end up as soluble periplasmic proteins, periplasmic proteins associated with the inner membrane, or are lipoproteins (*Shruthi 2010*), and these are often substrate binding proteins, transporters, or enzymes.

The Tat system is comprised of TatA, TatB, TatC, TatD, and TatE subunits but most organisms have a subset of these (*Palmer et al. 2010*). Gram-negative bacteria typically have TatA, TatB, and TatC (*Hamsanathan and Musser 2018*). The Tat translocase only assembles during substrate binding and dissociates once translocation is complete (*Cline 2015, Berks 2015*). Export of Tat substrates is assisted by redox enzyme maturation proteins (REMPs) which are chaperones that can assist in targeting, protecting the SP, and prevent premature folding of substrates (*Cherak and Turner 2017, Kuzniatsova 2016, Stevens and Paetzel 2012*). Initiation begins when the SP is targeted to the TatB-TatC receptor where TatC binds the twin-arginine motif which results in recruitment and oligomerization of TatA (*Zoufaly et al. 2012*). Translocation of a substrate occurs slowly, then the SP is cleaved and the TatA oligomers dissociate (*Cline 2015, Berks 2015*). Tat has a proofreading ability that assesses the conformational flexibility of substrates and only exports the more rigid ones (*Jones et al. 2016*). Tat will not transport a protein that has not acquired its proper final folded state (*Berks 2015*).

*H. pylori* proteins discussed in later chapters are predicted to be transported by either the Sec or Lol systems. HP1454 and PflA are predicted to have Sec/SPI signal peptides, while FlgP, FapH, HP1456, and HP0018 are predicted to have Sec/SP2 signal peptides. A typical SP is 20-30 amino acids in length, has 1-8 positively charged residues at the start (N), followed by 4-16 residues making a helical hydrophobic core (H), then there is a slightly polar domain with a preference for cysteine at the end (C) (*Chatzi et al. 2013*). The SP C-terminal domain contains the SPase cleavage site. The N-terminal cleavage sequence is found in *Figure 9*. FapH as it is annotated in *H. pylori* B128 is not predicted to have a SP or be a lipoprotein by SignalP – 6.0, but this is likely due to an annotation error in the translational start site as FapH in *H. pylori* 26695 is a predicted lipoprotein (*Fig. 13*).

PfIB lacks a SP and has a hydrophobic alpha helix 60 residues from the N-terminus that is a predicted TMH. The lack of a signal sequence and the presence of predicted transmembrane regions means PfIB is likely translocated and inserted into the membrane by YidC without the assistance of SRP (**Fig. 12**). The TMH is 22 amino acids in length and is rich in leucine, isoleucine, and a single tyrosine, with neutral amino spaced between. This helix orients the side groups of the hydrophobic amino acids towards the membrane when predicted by Alphafold. I predict that PfIB is translocated by a SecYEG-YidC complex. YidC would recognize and insert the TMH, then

the large periplasmic region could be translocated by SecYEG (*Kuhn et al. 2017, Kuhn and Kiefer 2018*).

SEC SP1
HP1454: N-MKKIILACLMAFVGANLSA/E
PfIA: N-MWLKSKIFLLMGLLSHSLNA/L
HP0257: N-MRKILLMGLILQALFSEEA/A
SEC SP2
FIgP: N-MRLHTAFFGINSLLVATLLISG/C+1
FapA: N-MTLFFVS/C+1
FapA (26695): N- MRYFRSAFLLFFMTLFFAS/C+1
HP1456: N-MKNQVKKILGMSVIAAMVIVG/C+1
HP0018: N-MKIFVLLMSVILGISLTG/C+1

Positive charge Hydrophobic Polar

Figure 1.13. SEC SPI and SPII characterization of proteins discussed in future chapters.

Proteins that possess a SPI signal sequence are transported across the inner membrane, while proteins that have a SPII signal sequence are transported across the inner membrane and lipidated. SPI proteins end up as periplasmic proteins, while SPII proteins are membrane bound to either the outer leaflet of the inner membrane, or either the inner or outer leaflet of the outer membrane. The amino acid composition of the signal peptide determines the destination of the protein. Dashed lines indicate signal peptide cleavage site.

# Lipoprotein Sorting and processing

#### **Abbreviations and definitions**

- IM inner membrane
- OM- outer membrane
- Monoderm A bacterium having a single membrane, typically with a thick layer of peptidoglycan. Gram positive
- Diderm A bacterium having two membranes, IM and OM. Gram negative
- SP signal peptide
- SPI signal peptidase I
- SPII signal peptidase II
- Lgt Phosphatidylglycerol:prolipoprotein diacylglyceryl transferase
- Lsp Prolipoprotein signal peptidase
- Lnt apolipoprotein N-acyltransferase
- PG phosphatidylglycerol
- PE Phosphatidylethanolamine
- CL cardiolipin
- ABC transporter ATP-binding cassette transporter

Lipoproteins are a family of acetylated proteins in bacteria where the acylation spatially confines the protein to a membrane (*Grabowicz 2019, Buddelmeijer 2015*). Therefore, in monoderms (Gram-positive bacteria) all lipoproteins are associated with the inner (plasma) membrane (IM), while in diderms (i.e., Gram-negative bacteria) lipoproteins can be associated with either the inner or outer membrane (OM). Lipoprotein modification occurs in the IM by the action of three membrane-bound enzymes (*Wu et al. 1982*). Lipoproteins contain an invariant cysteine residue that is the target of modification, and immediately upstream is a lipobox where SPII cleaves the SP (*Babu et al. 2006*), leading to the lipidated cysteine becoming the N-terminus of the protein.

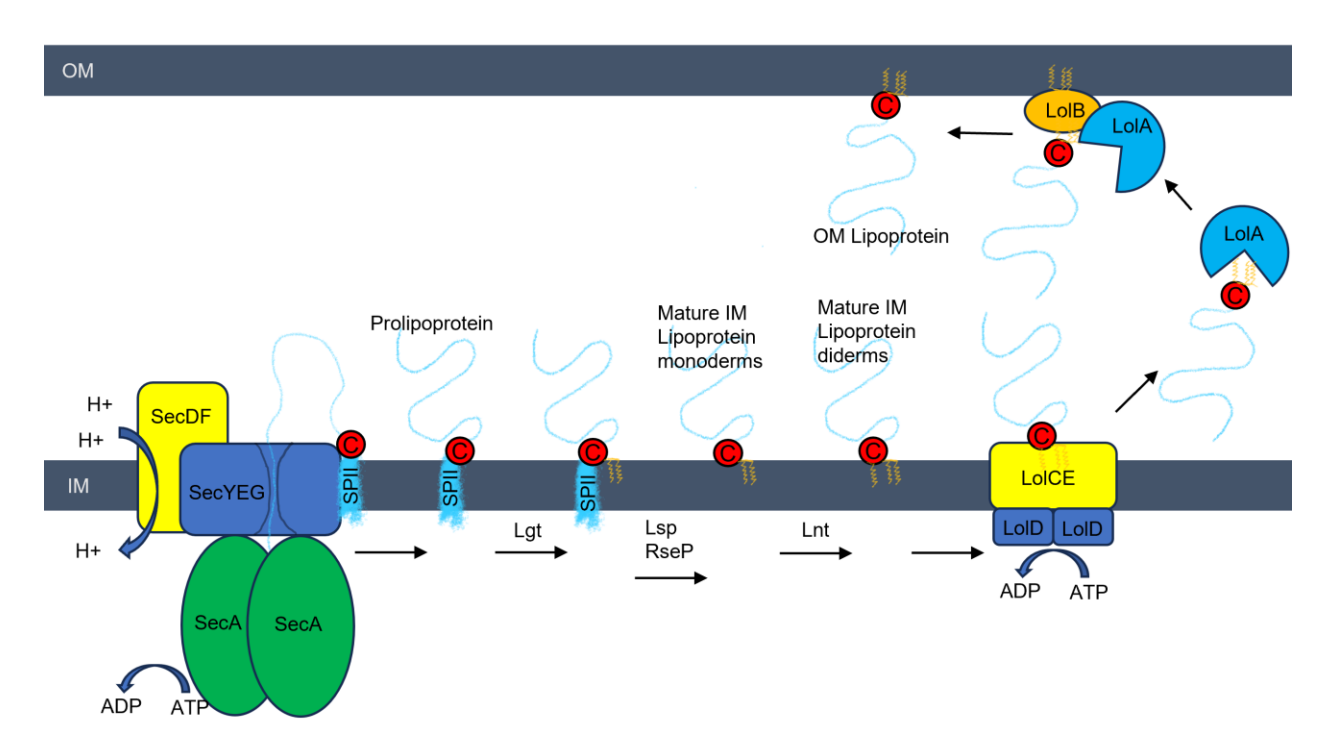


Figure 1.14. Translocation and processing of a prolipoprotein containing a SPII signal sequence in *E. coli*. Prolipoproteins are translocated to the periplasmic side of the inner membrane by the Sec system. The prolipoprotein is then lapidated by Lgt, the SP is released by Lsp, and the SP is cleaved by RseP. In monoderms the lipoprotein is mature after SP cleavage, while in diderms additional lipidation is carried out by Lnt. In diderms most lipoproteins are then transported to the OM by the Lol system, where LolE recruits the lipoprotein, LolC recruits LolA, and LolD uses ATP hydrolysis to transfer the lipoprotein from the IM to LolA. LolA then transports the lipoprotein across the periplasm where it interacts with LolB, and LolB inserts the lipoprotein into the OM. There is evidence that the Lol system is not the exclusive system of lipoprotein transport to the OM.

Prolipoproteins are translocated to the IM from the cytosol by the Sec or Tat system (**Fig. 1.14**). Once in the IM the enzyme Lgt attaches a diacyl moiety (a *sn*-1,2-diacylglyceryl group) retrieved from phosphatidylglycerol (PG) to the sulfhydryl group of the invariant cysteine residue next to the lipobox, resulting in a thioether-linked diacylglyceryl-prolipoprotein with a *sn*-glycerol-1-phosphate byproduct (*Tokunaga et al. 1982, Sankaran and Wu 1994, Mao et al. 2016, Buddelmeijer 2015*). The mechanism of Lgt lipidation is unknown. PG is the sole acyl donor for lipidation, as PE and CL are not used as substrates (*Sankaran and Wu 1994*). The lipid moiety of lipoproteins varies by the fatty acid composition of the phospholipids in each bacterium. Next, the enzyme LspA (SPase II) releases the SP from the α-amino group of the diacylated product

(*Inouye et al. 1983, Vogeley et al. 2016*), after which the SP is cleaved by peptidase RseP (*Saito et al. 2011*). Following release of the SP, the diacylated cysteine becomes the N-terminal residue (Cys<sup>+1</sup>) of the mature lipoprotein. Lipoproteins of monoderms have reached the end of processing and their final destination, while diderms undergo further processing, and for most lipoproteins, trafficking to the OM.

Lipoproteins in diderms have additional processing where a 3<sup>rd</sup> acyl group is added to Cys<sup>+1</sup> by the enzyme Lnt (*Noland et al. 2017*, *Wiktor et al. 2017*). As with Lgt the source of acyl groups is phospholipids, but Lnt uses PE instead of PG. First, the active site cysteine of Lnt reacts with the sn-1 of PE resulting in a thioesteracyl-enzyme intermediate and a lysophospholipid byproduct (*Jackowski and Rock 1986, Hillmann et al. 2011*), then the acyl group is transferred to the lipoprotein (*Gupta et al. 1991*). In addition to acylation, some bacteria are known to glycosylate their lipoproteins (*Espitia and Mancilla 1989, Wehmeier et al. 2009, Brulle et al. 2010*).

Most lipoproteins in diderms must traverse to the OM (*Grabowicz 2018, Konovalova and Silhavy 2015*). In fact, 90% of all lipoproteins in *E. coli* are trafficked to the OM, where the majority reside in the inner leaflet (*Horler et al. 2009*). Successful trafficking of lipoproteins to the OM is essential in diderms, where the buildup of these lipoproteins in the IM can be lethal (*Yakushi 1997*). The characterized pathway used to traffic lipoproteins from the IM, across the periplasm, to the OM is called the Lol (*Localization of lipoproteins*) pathway (*Okuda and Tokuda 2009*).

The LoI pathway moves lipoproteins from the IM to OM and has components in the IM, periplasm, and OM (*Narita and Tokuda 2017*). The *E. coli* LoI pathway is composed of LoIABCDE, with the ATP-binding cassette (ABC) transporter LoICDE in the IM, LoIA as a soluble periplasmic chaperone protein, and lipoprotein acceptor LoIB, which is itself a lipoprotein residing in the OM.

The trafficking of lipoproteins begins with a lipoprotein interacting with LoIE in the IM (*Mizutani et al. 2013*). While LoIE recruits the lipoprotein, LoIC recruits LoIA to the IM complex by trapping it in its periplasmic loop (*Mizutani 2013, Okuda and Tokuda 2009*). In bacteria that have LoIDF in place of LoICDE, two monomers of LoIF take the place of LoICE, where LoIF monomers each perform both of the functions. LoID is the ATPase component of the system where the energy derived from ATP hydrolysis is thought to be necessary to remove the acyl chains of the lipoprotein from the IM lipid bilayer and transfer the protein to LoIA (*Yakushi 2000, Ito et al. 2006, Taniguchi and Tokuda 2008*). In order for LoIA to shield the lipoprotein from the aqueous environment, the hydrophobic cavities of LoIA and LoIC line up in a mouth-to-mouth orientation (*Okuda and Tokuda 2009*). The lipoprotein moves with LoIA within the periplasm until

it contacts LoIB, where the lipoprotein is transferred to LoIB, where trafficking is completed when the lipoprotein is imbedded within the OM (*Matsuyama et al. 1997*). Interestingly, the function of LoIB does not depend on it being imbedded within the OM, but to guarantee accurate unidirectional transport it must be within the OM (*Tsukahara et al. 2009*).

When LoIA and LoIB were first discovered they were described as essential proteins, where deletion mutants were nonviable and reducing levels of each protein led to a decrease in cell viability (*Tajima et al. 1998*). The story appears to be the same for LoICDE (*Yakushi 2000*). LoIB depletion studies showed that lipoproteins mislocalized to the IM and accumulated along with LoIA in the periplasm (*Tanaka et al. 2001*). The thinking behind the essentiality of the LoI pathway was that in its absence mislocalization of some lipoproteins may be toxic or distort the cell envelope. There are several well-known essential OM lipoproteins, including BamBCDE, Lpt, Lpp, that need to properly localize for cell viability (*Malinverni et al. 2006, Wu et al. 2006, Konovalova et al. 2017, Okuda et al. 2016*).

Recent work in E. coli has discovered that while LolCDE are essential, LolA and LolB can be deleted (Grabowicz and Silhavy 2017). This work showed that LoIAB are not completely essential but are needed for efficient trafficking to prevent buildup of toxic OM lipoproteins in the IM. In the absence of LoIAB, two proteins were found to build up in the IM, Lpp and OsmB. In their absence, Lpp forms toxic PG crosslinks to the IM, and OsmB may form pores in the IM dissipating PMF. Additionally, Bam lipoproteins were able to reach the OM in the absence of LolAB. These revelations are exciting because they show that there is an alternative trafficking route to LoIAB. While the alternative trafficking route remains unidentified, it seems to be that LoIAB evolved for the purpose of increased trafficking efficiency of potentially toxic lipoproteins like Lpp and OsmB (Grabowicz 2019). Interestingly, many diderms lack a LoIB homologue, but Lpp and OsmB are found exclusively in diderms that have LoIAB homologues (Grabowicz 2018). IoIB homologues are not found outside of beta and gamma-Proteobacteria. Recent work shows that LoIA and LoIB are derived from a single ancestor and share bifunctionality, and the C. vibriodes LoIA has important structural features of both LoIA and LoIB (Smith et al. 2023). The C. vibriodes LoIA has both chaperone and insertion activity. The authors also showed that the E. coli LolA demonstrates bifunctionality with minor sequence changes. Therefore, in species that lack a lolB homolgue, LolA may function to both transport and insert lipoproteins.

Liporprotein transport of *H. pylori* differs in some ways from that of *E. coli* (**Fig. 1.14**). In *H. pylori*, as well as *Alpha-*, *Beta-*, and some *Gamma-* and *Delta-* proteobacteria, a single *IoIF* gene takes the place of both *IoIC* and *IoIE* (*LoVullo et al. 2015*). Another difference is that *H. pylori* lacks a *IoIB* homologue. The lack of LoIB suggests that LoIA plays the role of both

chaperone and lipoprotein insertase. The evidence suggests that *lgt, lspA, lolA*, and *lolF* are essential, while *Int* is not essential in *H. pylori* (*McClain et al. 2020*). *Int* appears to not be essential in species that have a *lolF* homologue. The nonessential status of *Int* in species that lack *lolF* suggests that the Lol system in these species, specifically the LolF protein, has greater affinity towards diacylated lipoproteins compared with triacylated lipoproteins. **Figure 1.15** shows lipoprotein trafficking in *H. pylori*.

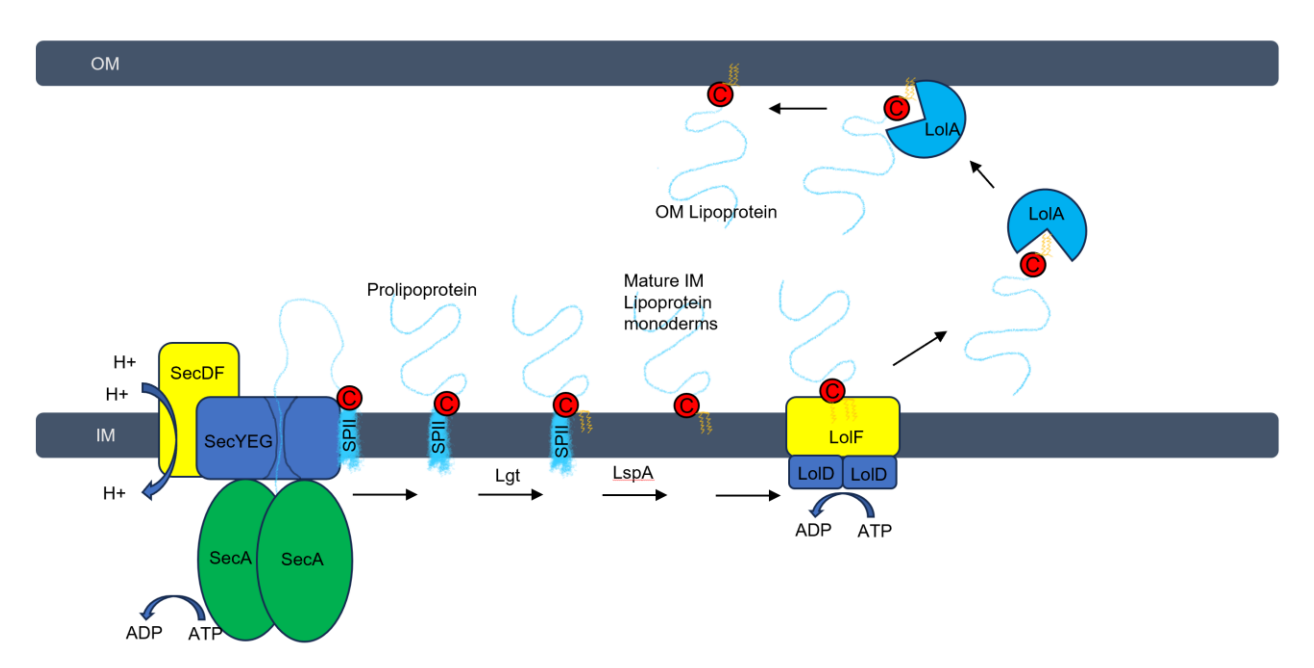


**Figure 1.15. Lipoprotein trafficking in** *H. pylori*. In contrast to *E. coli*, lipoprotein trafficking does not require Lnt to add a third acyl chain to the lipoprotein in *H. pylori*, despite a proposed *Int* homologue. Additionally, LoIF substitutes for LoICE and there is no LoIB homolog.

How does the cell decide which lipoproteins should be retained in the IM and which should be trafficked to the OM? There are two theories that seek to describe this process; the first model involves a LoI avoidance signal within the peptide chain, while the second model involves the acylation state of the acyl groups on Cys<sup>+1</sup>.

Research dating back to the 1980s found that gene fusion experiments with heterologous proteins could be targeted to the OM by fusion with an N-terminal sequence from OM lipoproteins (Yamaguchi 1988). Further work during this period found that the amino acid following Cys<sup>+1</sup> was all that was necessary to correctly localize lipoproteins in *E. coli* (*Gennity and Inouye 1991*, *Terada et al. 2001*). Specifically, it was an aspartic acid (Asp<sup>+2</sup>) that was necessary for IM

retention. This became known as the +2-rule for avoidance of the Lol machinery. Despite there being strong biochemical evidence for the function of Asp to associate with phospholipids (*Hara et al. 2003*), researchers found that other residues could take the place of Asp<sup>+2</sup>, including Trp Phe, Pro, Gly, and Tyr (**Seydel 1999**). Researchers believe that the +2-rule hinged on the residue of that position not being able to properly interact with LolCDE (*Sakamoto et al. 2010*). An important issue arose around the research into Lol avoidance signals; the signals seem to vary widely between bacterial species. *Pseudomonas aeruginosa* loosely obeys the +2-rule, where Asp<sup>+2</sup> is a retention signal but generally uncommon (*Narita and Tokuda 2017, Lewenza et al. 2008, Tanaka et al. 2007*). Additionally, the residues in the +3 and +4 position appear to be important for proper localization in *P. aeruginosa*. Further, *Borrelia burgdorferi* has a different Lol avoidance signal where an acidic N-terminal region is employed (*Schulze and Zuckert 2006*).

The hypothesis of a N-terminal Lol avoidance sequence is compelling due to its simplicity, but the current body of research in E. coli suggests a coincidence in that these native IM lipoproteins have an Asp+2. There are several studies that complement each other and illustrate that the Lol avoidance theory has major flaws. Work in E. coli sought to express the efflux pumps MexAB-OprM and MexCD-OprJ from P. aeruginosa and assess their activity (Srikumar et al. 1998, Mine et al. 1998, Tikhonova et al. 2002). These tripartite pumps efflux antibiotics and are built of an ABC transporter (MexB and MexD), and an IM component (MexA and MexC) that connects to an OM component (OprM and OprJ). When these proteins are expressed in E. coli the cells display a drug resistance phenotype, demonstrating that the complexes are correctly assembled and functioning. Importantly, neither MexA nor MexC contain the Asp+2 that is thought to be key to IM retention of lipoproteins in E. coli. Despite not adhering to the +2 rule, MexA and MexC were able to remain in the IM and avoid trafficking by the Lol system. Another study looked to express the E. coli LolCDE in P. aeruginosa and evaluate lipoprotein sorting (Lorenz et al. 2019). They found that essential lipoproteins were able to localize correctly, including ones that did not contain Asp+2. These studies provide compelling evidence that the early steps of lipoprotein sorting do not depend on a specific amino acid sequence. Lorenz et al. hypothesized that lipoprotein retention in the IM likely depends on a strong interaction of phospholipids in the IM with the acyl chains of the lipoprotein, in contrast, lipoproteins that form weak interactions with the IM are extracted and exported to the OM (Lorenz et al. 2019).

Recent research has identified the acylation state of lipoproteins as a determinant for OM trafficking. The LolCDE complex in *E. coli* has very low affinity for diacyl-form lipoproteins (*Grabowicz 2018*). Lnt is an IM enzyme that adds a third acyl group to a lipoprotein in diderms and its deletion has been found to be lethal in *E. coli* (*Noland et al. 2017*, *Wiktor et al. 2017*).

Researchers found that the lethal *Int* deletion can be overcome by expressing the transacylase Lit, which restored OM trafficking possibly by the addition of a third acyl group that is necessary for LolCDE recognition (*Armbruster and Meredith 2017*). Some bacteria are found to not require the LolCDE complex, but these bacteria produce native triacyl-form lipoproteins (*LoVullo et al. 2015, Gwin et al. 2018*). In contrast to the LolCDE complex, the LolDF complex seems to recognize triacylated lipoproteins. A possibility is that N-terminal acylation of lipoproteins plays a regulatory function in diderms.

### The role of the *H. pylori* Flagella in Biofilm Formation

Biofilm formation is a topic of importance in medicine, dentistry, industry, and environmental science. As a medical concern, biofilms can foster antibiotic resistant strains, can lead to persistent infections in infected individuals both in tissues and on medical devices, and can cause dental diseases. *H. pylori* biofilm formation has been documented *in vitro* (*Stark et al. 1999*), in wastewater (*Moreno and Ferrus 2012*), and in the human stomach (*Carron et al. 2006*, *Coticchia et al. 2006*). A search of PubMed using the keywords "*Helicobacter pylori*" and "biofilm" lists 290 results, yet a very small percentage of these papers have investigated the role of the flagella in biofilm formation and structure.

Flagellar rod, hook, and filament genes have been found to be upregulated in *H. pylori* biofilms compared with planktonic cells (*Hathroubi et al. 2018*). Cell envelope genes that are upregulated in biofilm cells compared with planktonic cells include the flagellar genes *flgL*, *flgK*, *flgM*, *flaG*, *flaB*, *flgE1*, *flgB*, *fliL*, *fliK*, and *fliD*. These flagellar genes have greater upregulation than any other cell envelope genes. SEM micrographs demonstrate that flagellar filaments are present in clumps of mostly coccoid cells, as a tangled mess of structures. The filaments can be seen emanating from the pole of some cells and contacting several other cells. The researchers characterized a *fliM* deletion mutant by SEM and found the strain to be severely impaired in biofilm formation. FliM, a C-ring component, is required for formation of an intact flagellum. They also characterized a *motB* deletion mutant and found this strain to be better at forming biofilms than the *fliM* mutant, but worse than wild type, suggesting that in the absence of motility the flagella are still able to have a structural role in the biofilm.

The mechanism underlying flagellar function in biofilm formation and maintenance in *H. pylori* is unknown but may have to do with proteins found in the flagellar sheath. Recall from the section on the flagellar sheath that some proteins are known to localize exclusively to the sheath

in *H. pylori*. It is possible that uncharacterized proteins, such as adhesions, localize to the flagellar sheath and assist in biofilm formation.

It is not clear if the current list of adhesions found in *H. pylori* have a role in biofilm formation or only the adhesion of individual cells to the epithelium. Adhesions BabA, SabA, and HopQ have not been found to localize specifically to the flagellar sheath, however, these proteins may localize to both the OM and sheath to increase the surface area of the cell that can be used for adherence.

## Candidate Flagellar Genes in H. pylori

Since the identities of the proteins that comprise many of the accessory structures in  $H.\ pylori$  motor are unknown, much of my research focused on identifying candidates for motor accessory proteins. Candidate proteins that I investigated to varying degrees during my graduate studies included HP0838 (which we named flagellum-associated protein in Helicobacter pylori [FapH]), HP0018, HP0097, HP1454, HP1456, and HP1457. Chapter 1 focuses on characterizing  $\Delta fapH$  mutants in  $H.\ pylori$ , and association of FapH with FlgP, HP1454, HP1456, and HP1457. Of these FapH interaction partners, HP1456 appeared to be the most physiologically relevant based on the results from co-immunoprecipitation and bacterial and two-hybrid assays, as well as its predicted structural similarity to the motor accessory proteins FlgP and FlgT ( $Drobnic et al.\ 2023$ ). HP1456 is encoded in an operon with genes encoding HP1454, HP1455, HP1456, and HP1457, all uncharacterized proteins in  $H.\ pylori$ . HP1454 and HP1455 are predicted to have SPI signal sequences and HP1456 and HP1457 are predicted to have SPII signal sequences, suggesting that these proteins localize to the IM, periplasm, or OM.

Currently, there is no evidence to suggest that any of the proteins listed above are flagellar proteins, except FapH. HP1456, also called Lpp20, has been studied for its antigenic properties in both culture and in animal models. A PubMed search of Lpp20 identified 33 publications with the search term present, as recent as March 2024. These publications can be classified as follows: (27) antigen investigation, immune response, vaccine development, antibody preparation, related antigenic proteins; (3) nano particle target; and (3) protein and gene characterization of Lpp20.

Lpp20 was characterized as being a major antigen of *H. pylori* in rabbit hyperimmune antisera (*Kostrzynska et al. 1994*). This group identified Lpp20 as accumulating in membrane vesicles, having a N-terminal 21 amino acids as being consistent with a lipoprotein, and they found that unprocessed and processed forms of the proteins were different sizes, of 19,701 and

18,283, respectively. The amino acid sequence of Lpp20 has been found to have similarities with peptidoglycan-associated lipoproteins. The acyl chains of Lpp20, derived from membrane phospholipids, were found to consist exclusively of C16:0 and C18:0 cyclopropane-containing fatty acids, while membrane phospholipids contain primarily C14:0 and C19:0 (*McClain et al. 2024*). Evidence to show that Lpp20 is either an adhesion, surface exposed, or released is lacking, as the protein has only been found in OM membrane fractions of in OMVs. Therefore, little characterization of Lpp20 has been conducted since the protein was identified in 1994. Lpp20 is a lipoprotein that is ~18k-Da in size, has acyl chains that differ from the composition of the OM, and is antigenic in animal models and therefor a vaccine candidate. What is not known is the physiological role of Lpp20 in *H. pylori*, if it is needed for colonization, or if it is an effector protein.

# **CHAPTER SUMMARIES**

# Chapter 2: A *Helicobacter pylori* flagellar motor accessory is needed to maintain the barrier function of the outer membrane during flagellar rotation

Rosinke K, Tachiyama S, Mrásek J, Liu J, Hoover TR. A *Helicobacter pylori* flagellar motor accessory is needed to maintain the barrier function of the outer membrane during flagellar rotation. PLoS Pathog. 2025 Jan 10;21(1):e1012860. doi: 10.1371/journal.ppat.1012860.

**Aim 1**: Characterize  $\Delta hp0838$  and determine if it is necessary for flagellar or sheath biosynthesis.

**Aim 2**: Probe for interaction partners of HP0838

Summary: H. pylori hp0838 encodes a previously uncharacterized lipoprotein and is in an operon with flqP, which encodes a motor accessory protein. Deletion analysis of hp0838 in H. pylori B128 showed that the gene is not required for motility in soft agar medium, but the mutant displayed a reduced growth rate and an increased sensitivity to bacitracin an antibiotic that is normally excluded by the OM. Introducing a plasmid-borne copy of hp0838 into the H. pylori  $\Delta$ hp0838 mutant suppressed the fitness defect and antibiotic sensitivity of the strain. A variant of the Δhp0838 mutant containing a frameshift mutation in pflA, which resulted in paralyzed flagella, displayed wild-type growth rate and resistance to bacitracin and vancomycin, suggesting the fitness defect and antibiotic sensitivity of the  $\Delta hp0838$  mutant are dependent on flagellar rotation. Comparative analysis of *in-situ* structures of the wild type and Δ*hp0838* mutant motors revealed the  $\triangle hp0838$  mutant motor lacked a previously undescribed ring structure with 18-fold symmetry located near the outer membrane. Based on these observations, we designated HP0838 as FapH (flagellum-associated protein in Helicobacter pylori) and the ring structure that it forms as the FapH ring. We hypothesize that the FapH ring helps to preserve OM barrier function during flagellar rotation. FapH homologs are present in many members of the phylum Campylobacterota and may have similar roles in protecting the OM from damage due to flagellar rotation in these bacteria

# Chapter 3: Inactivation of LpxF and Fur rescue bacitracin sensitivity in *fapH* deletion mutants

**Aim 1**: Isolate  $\Delta$ *fapH* motile suppressors that are not sensitive to bacitracin.

**Aim 2**: Assess which genetic variants rescue the drug sensitivity phenotype.

**Summary**: Picking up where **Chapter 2** left off,  $\Delta fapH pfIA^*$  ( $\Delta fapH$  in this chapter) was used to screen for suppressors that were resistant to bacitracin. WGS was performed on the bacitracin-resistant suppressors and mutations that were suspected of suppressing the drug sensitivity were identified in the iron regulatory gene *fur*. Mutants were created in  $\Delta fapH$  and the wild-type background where  $\Delta fur$  was introduced, and those mutants were assessed for sensitivity to bacitracin. In addition to drug sensitivity, the morphology of the strains was assessed by TEM. I found that the absence of *fur* in the  $\Delta fapH$  background suppressed the sensitivity to bacitracin, suggesting a loss of flagellar gene regulatory control was the cause. The other finding in **Chapter 3** is that during the construction of some new  $\Delta fapH$  mutants resulted is isolates that were less motile and lacked sensitivity to bacitracin. WGS revealed that these isolates had mutations in *lpxF* that introduced an early stop codon in the signal peptide of the protein. *lpxF* is involved in removing a phosphate from lipid A, and may affect the hydrophobicity of the cell envelope.

# Chapter 4: Cryo-electron tomography reveals how coordination between novel FlgY and PflA/PflB is required for flagellar motility in *Helicobacter pylori*

Revised manuscript submitted 12/24/24 to PNAS

**Aim 1**: Characterize  $\Delta pflA$ ,  $\Delta pflB$ ,  $\Delta flgY$  deletion mutants in *H. pylori*.

Aim 2: Perform cryo-ET and determine the motor architecture of each deletion mutant.

**Summary**: To colonize the human stomach, *Helicobacter pylori* must generate exceptionally high rotational torque for flagellar rotation and migration in the gastric mucus layer. In various members of the phylum Campylobacterota, conserved accessory proteins contribute to flagellar motor assembly and function. Here, we identify the positions of flagellar motor components FlgY, PflA, and PflB and determine that these conserved proteins are essential for motor assembly and wild-

type motility in *H. pylori*. Cryo-electron tomography and subtomogram averaging reveal that 13 dimers of FlgY near the MS-ring form a small ring with spokes that interact with 18 copies of PflA, which similarly form spoke-like structures. The spokes of FlgY and PflA form a mesh-like architecture that presumably stabilizes the MS-ring during flagellar rotation. In the periplasmic region, 18 copies of PflB form a large ring structure that is a potential scaffold for the stator units and key cage components. Deletion of *pflA* and *plfB* in *H. pylori* B128 established that both PflA and PflB are essential for the stable association of stator units with the motor. A combination of high-resolution structures from cryo-ET and AlphaFold prediction suggested that the C-terminal side of PflA, at its interface with FlgY, is dynamic and undergoes conformational changes. Overall, these results demonstrate how highly conserved accessory proteins in the flagellar motor coordinate to achieve bacterial motility in distinct niches, such as human gastric mucus layer.

# Chapter 5: *Helicobacter pylori* HP0018 has a Potential Role in Maintenance of the Cell Envelope

Rosinke K, Starai VJ, Hoover TR. *Helicobacter pylori* HP0018 has a potential role in the maintenance of the cell envelope. Cells. 2024 Aug 27;13(17):1438. doi: 10.3390/cells13171438.

**Aim 1**: Characterize Δ*hp0018* in *H. pylori* 

**Aim 2**: Identify interaction partners of HP0018

Aim 3: Assess localization of HP0018

**Summary**: *H. pylori* is a bacterial pathogen that colonizes the human stomach where it can cause a variety of diseases. *H. pylori* uses a cluster of sheathed flagella for motility, which is required for host colonization in animal models. The flagellar sheath is continuous with the outer membrane and is found in most *Helicobacter* species identified to date. HP0018 is a predicted lipoprotein of unknown function that is conserved in *Helicobacter* species that have flagellar sheaths but is absent in *Helicobacter* species that have sheath-less flagella. Deletion of *hp0018* in *H. pylori* B128 resulted in formation of long chains of outer membrane vesicles, which were most evident in an aflagellated variant of the  $\Delta hp0018$  mutant that had a frameshift mutation in *fliP*. Flagellated cells of the  $\Delta hp0018$  mutant possessed what appear to be a normal flagellar sheath, suggesting that HP0018 is not required for sheath formation. Cells of the  $\Delta hp0018$  mutant were also less helical in shape compared to wild-type cells. A HP0018-super folder green fluorescent fusion protein expressed in the *H. pylori*  $\Delta hp0018$  mutant formed fluorescent foci at the cell poles and lateral sites. Co-immunoprecipitation assays with HP0018 identified two enzymes involved in

modification of cell wall peptidoglycan, AmiA and MltD, as potential HP0018 interaction partners. HP0018 may modulate the activity of AmiA or MltD, and in the absence of HP0018 the unregulated activity of these enzymes may alter the peptidoglycan layer in a manner that results in altered cell shape and hypervesiculation.

# Chapter 2: A *Helicobacter pylori* flagellar motor accessory is needed to maintain the barrier function of the outer membrane during flagellar rotation

1

Rosinke K, Tachiyama S, Mrásek J, Liu J, Hoover TR. A *Helicobacter pylori* flagellar motor accessory is needed to maintain the barrier function of the outer membrane during flagellar rotation. PLoS Pathog. 2025 Jan 10;21(1):e1012860. doi: 10.1371/journal.ppat.1012860.

K.R. contributed with the mutant construction and characterization, TEM, motility and EoP assays, growth rate analysis, co-IP, BACTH assays, AlphaFold analysis, idea generation, writing, editing.

<sup>&</sup>lt;sup>1</sup> Reprinted here with the permission of publisher

### **ABSTRACT**

The Helicobacter pylori flagellar motor contains several accessory structures that are not found in the archetypal Escherichia coli and Salmonella enterica motors. H. pylori hp0838 encodes a previously uncharacterized lipoprotein and is in an operon with flqP, which encodes a motor accessory protein. Deletion analysis of hp0838 in H. pylori B128 showed that the gene is not required for motility in soft agar medium, but the mutant displayed a reduced growth rate and an increased sensitivity to bacitracin, which is an antibiotic that is normally excluded by the OM. Introducing a plasmid-borne copy of hp0838 into the H. pylori Δhp0838 mutant suppressed the fitness defect and antibiotic sensitivity of the strain. A variant of the  $\Delta hp0838$  mutant containing a frameshift mutation in pflA, which resulted in paralyzed flagella, displayed wild-type growth rate and resistance to bacitracin, suggesting the fitness defect and antibiotic sensitivity of the  $\Delta hp0838$ mutant are dependent on flagellar rotation. Comparative analysis of in-situ structures of the wild type and  $\Delta hp0838$  mutant motors revealed the  $\Delta hp0838$  mutant motor lacked a previously undescribed ring structure with 18-fold symmetry located near the outer membrane. Given its role in formation of the motor outer ring, HP0838 was designated FapH (flagellar accessory protein in Helicobacter pylori) and the motor accessory formed the protein was named the FapH ring. Our data suggest that the FapH ring helps to preserve OM barrier function during flagellar rotation. Given that FapH homologs are present in many members of the phylum Campylobacterota, they may have similar roles in protecting the OM from damage due to flagellar rotation in these bacteria.

#### **AUTHOR SUMMARY**

H. pylori causes a variety of gastric diseases in humans, including peptic ulcer disease, chronic gastritis, gastric cancer, and mucosa-associated lymphoid tissue lymphoma. Treatment of H. pylori infections is complicated by the need to combine multiple antibiotics and the rising occurrence of antibiotic resistance in clinical isolates, which underscores the need for new treatment options against this widespread and cancerogenic pathogen. The H. pylori flagellar motor shares core components with the E. coli flagellum, but has evolved additional accessories that help the bacterium navigate the highly viscous gastric mucus layer. We report here on a previously uncharacterized ring-like H. pylori motor accessory associated with the outer membrane that is formed by the lipoprotein FapH. In the absence of FapH, H. pylori displays an increased sensitivity to bacitracin, an antibiotic that is normally excluded by the outer membrane. The increased antibiotic sensitivity of the fapH mutant is dependent on a functional flagellum,

suggesting that the FapH ring protects the OM from damage resulting from flagellar rotation. These findings identify the FapH ring as a potential target for novel therapeutics that may potentiate the activity of existing antibiotics in the treatment of *H. pylori* infections.

# INTRODUCTION

H. pylori is a Gram-negative bacterial pathogen of the phylum Campylobacterota that colonizes the gastric mucosa of approximately half of the human population worldwide (*Hooi et al. 2017*). H. pylori infection is the causative agent of chronic gastritis and peptic ulcer disease, as well as a major risk factor for gastric cancer (*Atherton and Blaser 2009, Cover and Blaser 1992, Kuipers 1997*). The H. pylori flagellum is an essential virulence factor as flagellum-mediated motility is required for host colonization of the bacterium in animal models (*Eaton et al. 1992, Ottemann and Lowenthal 2002*).

The bacterial flagellum consists of three major components: the basal body, hook, and filament. The basal body contains a rotary motor, which depending on the species uses energy from the proton motive force or a sodium ion gradient to generate torque (Berg 2003, Biquet-Bisquert et al. 2021, Manson et al. 1977). The torque generated by the motor is transferred from the rotor to the filament via the rod and hook. The filament is a rigid helical structure that acts as a propeller to push the cell forward as the filament rotates. Conserved core structures of the basal body include a flagellar type III secretion system (fT3SS) that transports axial components (e.g., rod, hook, and filament proteins) across the cell membrane, C-ring (rotor and switch complex), MS-ring (rotor component), torque generating MotA/MotB or PomA/PomB stator units, P- and Lrings (bushings), and rod (driveshaft) (Carroll and Liu 2020, Zhao et al. 2014). The H. pylori motor, the largest bacterial flagellar motor described to date, accommodates 18 stator units that produce an estimated 3,600 pN·nm of torque (Celli et al. 2009) In addition to the conserved core motor structures, high-resolution in-situ structures of the motors of H. pylori and other bacteria determined by cryo-electron tomography (cryo-ET) and subtomogram averaging reveal structures that are not present in the archetypal E. coli and S. enterica motors (Carroll and Liu 2020, Beeby et al. 2016, Chaban et al. 2018, Quin et al. 2017). Functions for the motor accessories are largely unknown, but possible roles include recruitment and retention of stator units in the motor, stabilization of stator-rotor interactions, and protection of the cell envelope from the high torque generated by the motor (Carroll and Liu 2020, Beeby et al. 2016, Chaban et al. 2018, Quin et al. 2017).

The flagellar motor is anchored within the cell envelope and traverses the OM in all diderms with the exception of the spirochetes. Depending on the species, the flagellar motor can rotate from hundreds to over 1,000 revolutions per second (*Manson 2010*), rotational speeds that are comparable to those of a household blender. The bacterial cell body counterrotates to the direction of the flagellar motor rotation (*Manson 2010*). The rotation of the flagellum and counterrotation of the cell body has the potential to exert stress on the OM. The OM is an asymmetrical lipid bilayer with an outer leaflet populated by lipopolysaccharide (LPS) or lipooligosaccharide and an inner leaflet composed of glycerophospholipids (GPLs). The lipid asymmetry is important for OM barrier function and the intrusion of GPLs into the outer leaflet increases the permeability of the OM to harmful compounds that are normally excluded by the OM such as certain antibiotics and bile salts (*Silhavy et al. 2010*). We hypothesize that in the absence of protective mechanisms the stress exerted on the OM by flagellar rotation facilitates the flipping of GPLs from the inner leaflet to the outer leaflet of the OM and thereby compromise OM barrier function.

In the *S. enterica* motor, the flagellar LP-ring bushing complex aligns and balances the flagellar rod as it rotates and is formed by multiple copies of FlgH and FlgI, which form the L-ring and P-ring, respectively (*Johnson et al. 2021*, *Tan et al. 2021*). The L-ring forms a pore in the OM through which the rod passes. Hydrophobic and charged interactions between an α-helix of FlgH and the lipid A moiety of LPS fixes the protein in the outer leaflet of the OM (*Johnson et al. 2021*). *S. enterica* FlgH is a lipoprotein and the diacylglycerol attached to the side chain of the N-terminal cysteine residue of the protein aligns laterally to the L-ring and packs against hydrophobic amino acid residues of the protein. Rather than forming a typical membrane bilayer, the LPS layer and lipid moieties of FlgH form a hydrophobic band that encircles the L-ring (*Johnson et al. 2021*). The atypical membrane structure surrounding the L-ring may help to preserve OM barrier function by preventing the entry of GPLs into the outer leaflet of the OM during flagellar rotation.

The architecture of the *H. pylori* L-ring differs from that of *S. enterica*. *H. pylori* FlgH is not a lipoprotein, and the L-ring in the *H. pylori* motor is located below the OM rather than embedded in the OM (*Qin et al. 2017*). Thus, if the *S. enterica* L-ring has a role in protecting the OM from flagellum-mediated damage, the *H. pylori* L-ring does not appear to be positioned for such a function. The *H. pylori* flagellum also differs from the *S. enterica* flagellum in that the filament of *H. pylori* flagellum is surrounded by a membranous sheath that is contiguous with the OM. The flagellar sheath is a feature that *H. pylori* shares with many other bacteria, including most *Helicobacter* and *Vibrio* species (*Chu et al. 2020*). Fuerst proposed two models for the behavior of the sheath during flagellar rotation (*Fuerst 1980*). In one model, the sheath rotates with the

filament, which requires that the sheath be rigid and the junction of the sheath and OM to be fluid. The other model proposes the filament rotates freely within a wave-propagating sheath. This second model requires the sheath to be flexible enough to allow for distortions caused by the rotating filament but rigid enough to prevent the sheath from detaching from the cell. Regardless of which model most accurately describes the behavior of the sheath as the filament rotates, rotation of sheathed flagella is a significant generator of outer membrane vesicles in *Vibrio* species (*Aschtgen et al. 2016, Brennan et al. 2014*), suggesting that flagellar rotation does indeed exert stress on the OM in bacteria with sheathed flagella.

The H. pylori flagellar motor has accessories associated with the H. pylori L-ring that may help to preserve OM barrier function as the flagella rotate. We provide evidence here that a ring-like motor accessory associated with the OM in H. pylori is formed by a lipoprotein that we designate FapH (flagellum-associated protein in Helicobacter pylori). Deletion of fapH in H. pylori B128 resulted in increased sensitivity to bacitracin, an antibiotic that is normally excluded by the OM. The antibiotic sensitivity of the  $\Delta fapH$  mutant was suppressed by introducing a copy of fapH on a shuttle vector into the strain. In addition, the antibiotic sensitivity of the  $\Delta fapH$  mutant was dependent on functional flagella as a H. pylori  $\Delta fapH$  mutant with paralyzed flagella due to a mutation in pflA displayed wild-type resistance to bacitracin. Taken together, these findings suggest that in the absence of the FapH ring, OM barrier function is compromised by rotation of the flagella. The breakdown in OM barrier function presumably results from the intrusion of GPLs into the outer leaflet of the OM, making the OM more permeable to bacitracin. FapH homologs are present in several other Campylobacterota, and these fapH homologs may function in protecting the OM from damage due to flagellar rotation in these bacteria.

## **RESULTS**

### fapH (hp0838) is conserved in Helicobacter species and linked to flgP

H. pylori HP0838 (FapH) is a predicted lipoprotein encoded by a gene immediately downstream of flgP, which encodes a flagellar motor accessory protein that forms the basal disk in Campylobacter jejuni and Aliivibrio fischeri (Beeby et al. 2016). In the genomes of other Helicobacter species that we examined, a fapH homolog is located immediately downstream of a flgP homolog (Fig. 2.1 and Table S2.1). Further analysis of FapH using the Position-Specific Iterative (PSI)-BLAST tool identified FapH homologs in other members of the phylum Campylobacterota (Table S2.1). In contrast to the synteny of fapH and flgP in Helicobacter species, however, fapH and flgP only display synteny in Wolinella succinogenes for the other

Campylobacterota that we examined (**Fig. 2.1 and Table S2.1**). Notably, the *W. succinogenes fapH* homolog is in an operon with six other genes known or predicted to be involved in flagellum assembly (**Fig. 2.1**), suggesting a role for *fapH* in flagellar function. As with *H. pylori* FapH, all of the FapH homologs that were examined have predicted lipoprotein signal peptides (**Table S2.1**). Given the synteny between *flgP* and *fapH* in *Helicobacter* species and *W. succinogenes*, close association of *fapH* with several flagellar genes in *W. succinogenes*, and the predicted periplasmic location of FapH, we hypothesized that FapH is a flagellar motor accessory protein.

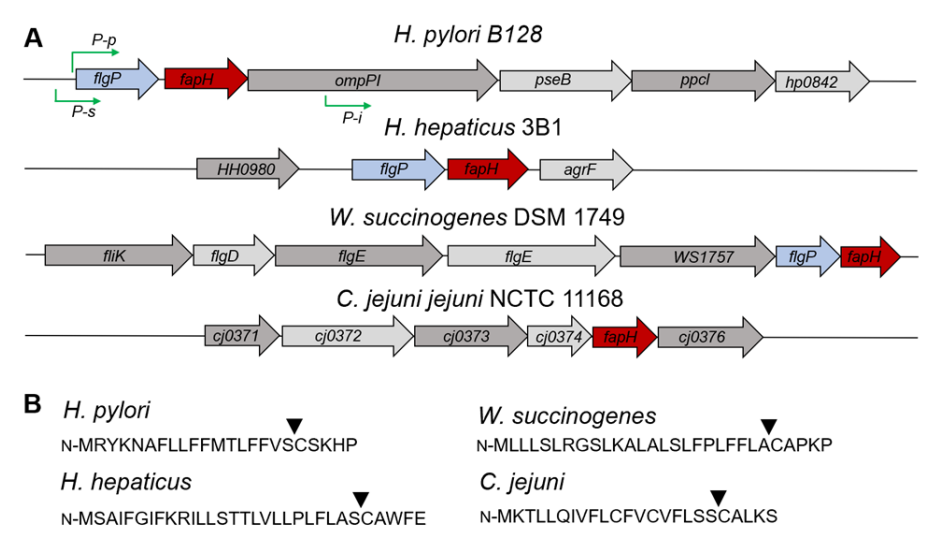


Figure 2.1. Organization of operons containing *fapH* in various members of Campylobacterota and the predicted lipoprotein signal peptides for the FapH homologs. (A) In many genomes, *fapH* is located immediately downstream of *flgP*. Approximate locations of predicted promoters for the operon containing *fapH* in *H. pylori* B128 are indicated (green arrows), which is based on a transcriptional start site database determined from the *H. pylori* 26695 transcriptome (*Sharma et al.* 2010). *P-p*: primary promoter, *P-s*: secondary promoter, *P-i*: internal promoter. (B) Predicted lipoprotein signal peptides of the FapH homologs. Amino acids sequences of the FapH homologs were analyzed for signal peptides and their cleavage sites using the SignalP-6.0 server (https://services.healthtech.dtu.dk/service.php?SignalP) (*Teufel et al.* 2022). Locations of the cleavage sites in the FapH homologs are indicated by the arrow.

In examining the FIgP homologs of various *Helicobacter* species, we noted that many of the FIgP homologs possess predicted lipoprotein signal peptides, while others have signal peptides that are cleaved by signal peptidase I and are not predicted lipoproteins (**Table S2.1**). This differentiation followed a morphological distinction as *Helicobacter* species that have sheathed flagella (FS<sup>+</sup> species) typically possessed a FIgP homolog predicted to be a lipoprotein, while the FIgP homologs in *Helicobacter* species with sheath-less flagella (FS<sup>-</sup> species) lacked a

predicted lipoprotein signal peptide. Two FlgP homologs in FS<sup>+</sup> Helicobacter species that we examined were not predicted to have signal peptides, but this may be due to incorrect assignments for the translational start sites as selecting alternative upstream translational start sites resulted in protein sequences with predicted lipoprotein signal peptides. Some species of Campylobacterota (*C. jejuni, Nautilia profundicola*, and *Sulfurospirillum deleyianum*) have FlgP homologs that are predicted lipoproteins, while the FlgP homologs in other species have signal peptides predicted to be cleaved by signal peptidase I (*W. succinogenes* and *Sulfurimonas gotlandica*) (**Table S2.1**).

#### FapH is not essential for motility in *H. pylori*

To determine if FapH plays a role in flagellar biosynthesis or function, fapH was deleted in H. pylori B128 and the flagellation and motility of the resulting mutant was assessed. Examination of the  $\Delta fapH$  mutant by transmission electron microscopy (TEM) and cryo-ET revealed the cells were indistinguishable from wild type in the localization and number of flagella (Fig. 2.2 and Fig. S2.1A and S2.1B). The flagellar sheaths of the  $\Delta fapH$  mutant appeared to be intact, suggesting that FapH is not required for sheath biosynthesis. The H. pylori B128  $\Delta fapH$  mutant was impaired in its motility in soft agar medium as it generally produced no discernible swim halo following a 7-d incubation (Fig. 2.3A). Migration of bacterial cells from the point of inoculation in soft agar medium involves both the ability to swim and chemotaxis. In our hands, a chemotaxis deficient H. pylori B128  $\Delta cheA$  mutant forms a small, but readily discernible, swim halo following a 7-d incubation ( $Botting\ et\ al.\ 2023$ ). Thus, the failure of the  $\Delta fapH$  mutant to form a swim halo was not due to loss of chemotaxis, but instead resulted from the inability of the mutant to swim in the soft agar medium.

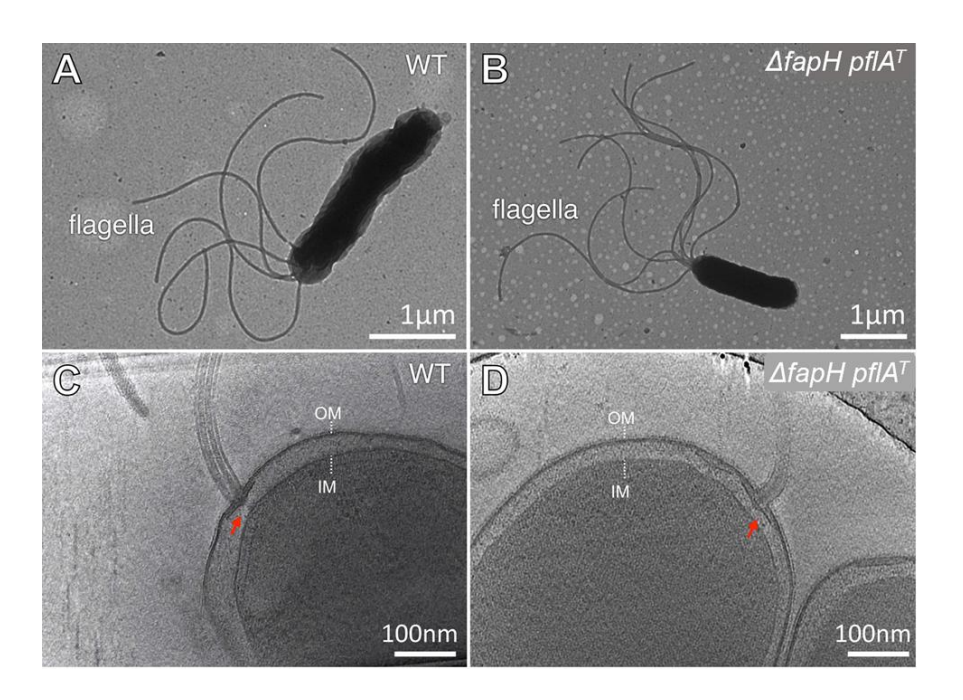


Figure 2.2. Electron micrographs of *H. pylori* B128 wild type and  $\Delta fapH$   $pflA^T$  strain. TEM images of representative cells of *H. pylori* B128 wild type (**A**) and  $\Delta fapH$   $pflA^T$  mutant (**B**). Cryo-ET reconstructions of *H. pylori* B128 wild type (C) and  $\Delta fapH$   $pflA^T$  mutant cells (**D**). Flagellar basal bodies in cryo-ET reconstructions are shown by red arrows.

Small swim halos were sometimes observed on soft agar medium plates inoculated with the  $\Delta$  fapH mutant, suggesting that motile suppressors of the  $\Delta$  fapH mutant were arising. To enrich for motile variants of the  $\Delta$  fapH mutant, cells from the edge of the small swim halos were used to inoculate fresh soft agar plates. Over the course of several passages in soft agar medium the average swim halo diameter of the  $\Delta$  fapH mutant increased from ~5 mm to ~35 mm, and clonal isolates from the cells at the edges of these swim halos were obtained.

Whole genome sequencing (WGS) of the original  $\Delta fapH$  mutant revealed an insertion of a guanosine at position 1429 in pflA (paralysed flagellar protein A) (Table S2.2). PflA is required for motility in *C. jejuni* and *H. pylori*. *In-situ* structures of the *C. jejuni* motor generated by cryo-ET and single particle cryo-electron microscopy (cryo-EM) suggest PflA forms a set of spoke-like structures that are closely associated with the stator units (*Beeby et al. 2016, Drobnic et al. 2023*). Stator units are not visible in the *in-situ* structure for the motor of the *C. jejuni*  $\Delta pflA$  mutant, suggesting that PflA is required for the recruitment and/or retention of the stator units within the motor (*Beeby et al. 2016*). The insertion in pflA shifted the reading frame and introduced a stop codon four codons downstream of the insertion, which is predicted to result in expression of a

truncated PfIA that is shortened by 325 amino acid residues (**Fig. S2.2B**). We hereafter refer to the original, non-motile  $\Delta fapH$  mutant as the  $\Delta fapH$   $pfIA^T$  strain. Introducing pfIA on a shuttle vector into the  $\Delta fapH$   $pfIA^T$  strain (hereafter designated as  $\Delta fapH$   $pfIA^T$ /ppfIA) restored motility in soft agar medium to near wild-type levels (**Fig. 2.3A**), indicating that the frameshift mutation in pfIA was responsible for the loss of motility in the  $\Delta fapH$   $pfIA^T$  strain. Moreover, these data indicated that FapH is not essential for motility in soft agar medium.

WGS analysis of a  $\Delta$ fapH motile variant that produced a robust swim halo revealed a deletion of a cytosine at nucleotide position 1393 in *pflA* (**Table S2.2**), which restored the reading frame following the insertion of the guanosine at position 1429 and allowed for the expression of a full-length PflA variant in which the amino acid sequence from Leu-465 to Ile-476 (L<sup>465</sup>FSMEGNTQEKI<sup>476</sup>) is altered to F<sup>465</sup>FPWRGTRKKKS<sup>476</sup>. PflA monomer structure predicted by AlphaFold 2 (*Jumper et al. 2021*) possesses a  $\beta$ -sandwich domain near the N-terminus and a tetratricopeptide repeat (TPR) domain that comprises most of the remainder of the protein (**Fig. S2A**). The altered sequence in PflA is primarily within a loop between  $\alpha$ -helices 16 and 17 in the TPR domain, and the predicted tertiary structure of the PflA variant (hereafter referred to as PflA\*) is essentially identical to that of wild-type PflA (**Figs. S2.2A and S2.2C**). Given that the isolate expressing PflA\* was highly motile and the amino acid substitutions did not impact the predicted tertiary structure of PflA, we proceeded to analyze further the motile isolate, hereafter referred to as the  $\Delta$ fapH pflA\* strain.

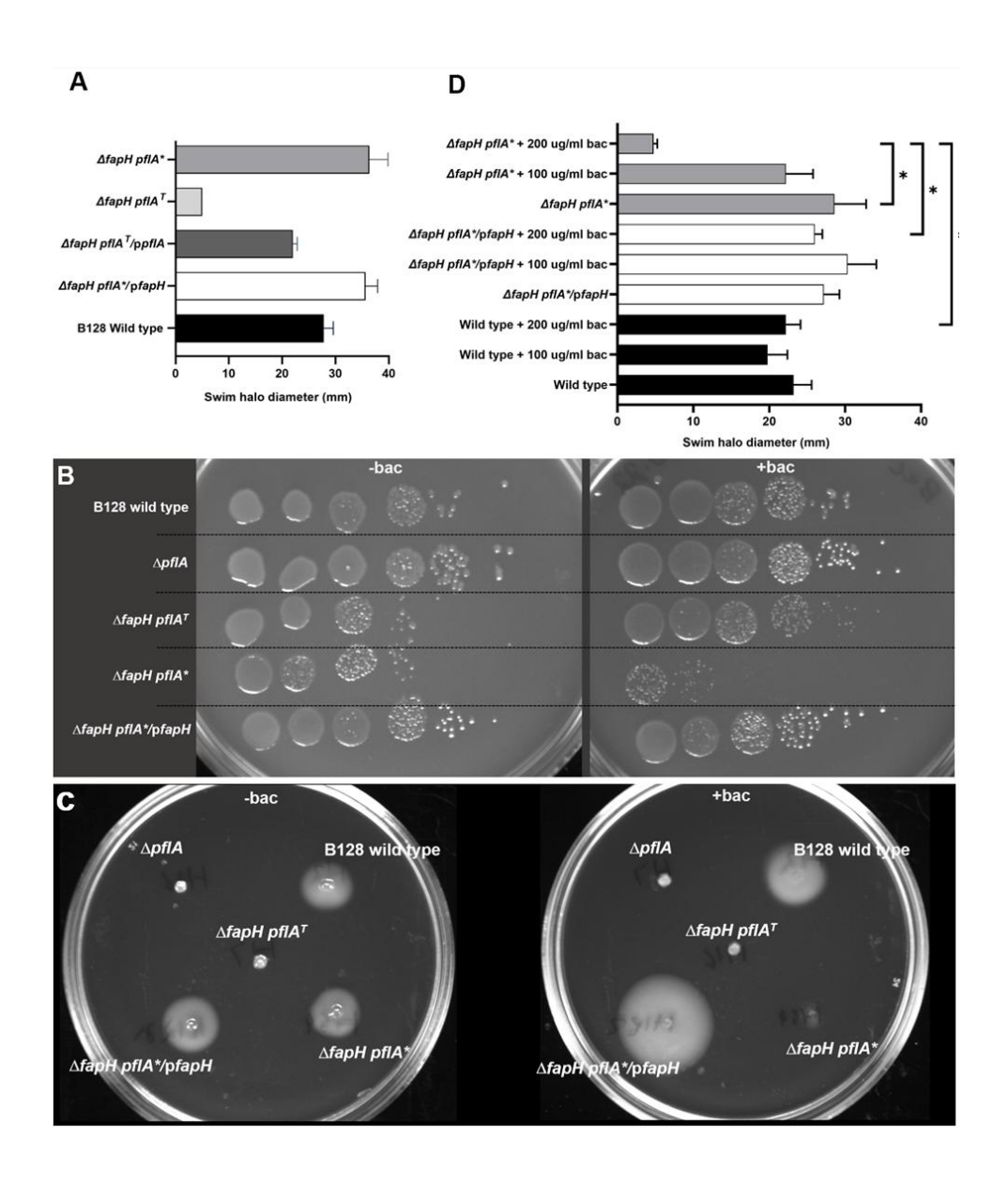


**Figure 2.3. Motility of** *H. pylori* **B128 wild type and** Δ*fapH* mutants and their sensitivity to bacitracin. (**A**) Motilities of wild type,  $\Delta fapH$   $pflA^T$ ,  $\Delta fapH$   $pflA^*$ ,  $\Delta fapH$   $pflA^T$ /pflA, and  $\Delta fapH$   $pflA^*$ /pfapH were assessed by stab inoculating the strains in soft agar medium and then measuring the diameters of the resulting swim halos following a 7-d incubation period. Bars indicate mean values for the diameters of the swim halos and the error bars indicate the standard error of the mean (SEM). At least 4 replicates were used in motility assays. (**B**) Efficiency of plating assays were done with *H. pylori* strains (indicated in **A**) on TSA (-bac) or TSA supplemented with 200 μg/ml bacitracin (+bac). Cells from freshly grown cultures of the strains were resuspended in tryptic soy broth to the same cell densities (OD<sub>600</sub>). Ten-fold serial dilutions of the resuspensions

(10<sup>0</sup> to 10<sup>-5</sup>) were then spotted onto the media, and the cultures were incubated for 7 d. The  $\Delta pfIA$  mutant was included to demonstrate that disrupting pfIA was not responsible for the increased sensitivity to bacitracin. (**C**) Growth of *H. pylori* strains in soft agar medium in the absence (-Bac) and presence of 200 μg/ml bacitracin (+Bac). (**D**) *H. pylori* B128 wild type,  $\Delta fapH pfIA^*$ , and  $\Delta fapH pfIA^*/pfapH$  were stab inoculated into soft agar medium that contained 0, 100, or 200 μg/ml bacitracin and the diameters of the resulting swim halos were measured following a 7-d incubation period. Bars indicate mean values for swim halo diameters and the error bars indicate the SEM.The asterisk indicates statistically significant differences in swim halo diameters as determined using a two-sample t test (p-value <0.0001). At least 3 replicates were done for each sample.

#### The $\Delta fapH pfIA^*$ strain has reduced fitness

Although our data indicated that fapH is not required for H. pylori motility, we wished to determine if loss of fapH resulted in other phenotypic traits. Examination of the  $\Delta fapH$   $pflA^*$  strain by TEM indicated that it was indistinguishable from wild type and the parental  $\Delta fapH$   $pflA^T$  strain in the number of flagella per cell (**Fig. S2.1A**). Unexpectedly, the mean length of the flagellar filaments in the  $\Delta fapH$   $pflA^*$  strain was slightly, but significantly, longer than those of the  $\Delta fapH$   $pflA^T$  strain and wild type (**Fig. S2.1B**).

To determine if loss of FapH impacted the growth rate of H. pylori, we compared the growth rates of wild type, the non-motile  $\Delta fapH$   $pflA^T$  strain, and the motile  $\Delta fapH$   $pflA^*$  strain. Growth rates for cultures of wild type and  $\Delta fapH$   $pflA^T$  strain were similar (mean doubling time was ~6 h; **Fig. S2.1C**). By contrast, the growth rate of the  $\Delta fapH$   $pflA^*$  strain was significantly slower with a mean doubling time of ~13 h (**Fig. S2.1C**). To determine if deletion of fapH was responsible for the slower growth rate of the  $\Delta fapH$   $pflA^*$  strain, fapH was introduced into the strain on the shuttle vector pHel3 to generate the strain that we hereafter refer to as  $\Delta fapH$   $pflA^*/pfapH$ . Strain  $\Delta fapH$   $pflA^*/pfapH$  had a growth rate similar to that of wild type and the  $\Delta fapH$   $pflA^T$  strain (**Fig. S2.1C**). Taken together, these data suggest the loss of FapH results in a motility-dependent reduction of fitness in H. pylori.

### Strain $\Delta fapH pfIA^*$ , but not $\Delta fapH pfIA^T$ , has increased sensitivity to bacitracin

The LPS in the outer leaflet of the OM forms an effective barrier to hydrophobic antibiotics and other noxious chemicals, and increased sensitivity to these compounds is often indicative of the intrusion of GPLs into the outer leaflet of the OM (*Silhavy et al. 2010*). Bacitracin is a cyclic polypeptide antibiotic that interferes with peptidoglycan biosynthesis by binding undecaprenyl-

pyrophosphate to disrupt the undecaprenyl-phosphate cycle and thereby inhibit synthesis of the peptidoglycan precursor molecule lipid II (*Stone and Strominger 1971*). In an efficiency of plating assay, the motile  $\Delta fapH pflA^*$  strain displayed increased sensitivity to bacitracin compared to, wild type, the non-motile  $\Delta fapH pflA^T$  strain, the motile  $\Delta fapH pflA^*/pfapH$  strain, and the  $\Delta pflA$  mutant, (**Fig. 2.3B**). These data demonstrate that loss of FapH in *H. pylori* results in increased sensitivity to bacitracin and the antibiotic sensitivity is dependent on a functional flagellum. Moreover, these data show that disrupting pflA has no discernible effect on bacitracin sensitivity.

Sensitivity of the *H. pylori* strains to bacitracin was examined further under conditions where motility was assessed simultaneously by inoculating the strains in soft agar medium that contained bacitracin. *H. pylori* strains were inoculated into soft agar medium that contained 0, 100, or 200 µg/ml bacitracin and the subsequent swim halos were measured. Consistent with the results from the efficiency of plating assays, the  $\Delta fapH plfA^*$  strain displayed increased sensitivity to bacitracin as the swim halo diameter of the strain was markedly decreased in the presence of the antibiotic at a concentration of 200 µg/ml, while swim halo formation by wild type was unaffected (**Figs. 2.3C**). Although the  $\Delta fapH pflA^T$  strain did not form a swim halo since its flagella are paralyzed, colony growth of the strain in the soft agar medium containing bacitracin was dense indicating that the strain was resistant to bacitracin under the assay conditions (**Fig. 2.3C and 2.3D**). As observed in the efficiency of plating assay (**Fig. 2.3B**), the  $fapH pflA^*/pfapH$  strain was resistant to bacitracin in the motility-based assay indicating that the loss of FapH was responsible for the antibiotic sensitivity of the  $\Delta fapH pflA^*$  strain (**Figs. 2.3C and 2.3D**).

To address the possibility that PflA\* is required for the antibiotic sensitivity of the  $\Delta fapH$  pflA\* strain, we generated additional  $\Delta fapH$  mutants in H. pylori B128 and examined the sensitivity of the resulting strains to bacitracin. The resulting  $\Delta fapH$  mutants were motile and sensitive to bacitracin (**Fig. S2.4**). WGS of the strains indicated that they did not have secondary mutations in any known flagellar gene, including pflA (**Table S2.2**). These findings indicate that the sensitivity of H. pylori to bacitracin upon disruption of fapH is not dependent on the PflA variant PflA\*.

### FapH forms a flagellar motor accessory associated with the OM

Given the sensitivity of the  $\Delta fapH$   $pflA^*$  and  $\Delta fapH$  strains to antibiotics that are normally excluded by the OM, we hypothesized that FapH is required to form a motor accessory that helps to preserve OM barrier function during flagellar rotation. To address this hypothesis, we compared *in-situ* structures of the motors of wild-type H. pylori B128, the  $\Delta fapH$   $pflA^*$  strain that were determined by cryo-electron-ET and subsequent subtomogram averaging.

The motor of the  $\triangle fapH pflA^T$  strain contained many of the core components and accessories that were present in the wild-type motor, but lacked many of the periplasmic components of the motor (**Fig. S2.4A and S2.4B**). Since the periplasmic components are missing in the *in-situ* structure for the motor of the *C. jejuni*  $\triangle pflA$  mutant (**Beeby et al. 2016**), we infer that the truncation of PflA in  $\triangle fapH pflA^T$  was responsible for the motor assembly and motility defects in the strain.

Comparing the *in-situ* structures of the motors of wild type and  $\Delta fapH$   $pflA^*$  revealed that the motors of the two strains were identical with the exception of a globular density near the junction of the OM and flagellar sheath that was missing in the motor of the  $\Delta fapH$   $pflA^*$  strain (**Fig. 2.4A-2.4B**). Perpendicular cross-sectional imaging revealed that the globular densities form a ring-like structure with 18-fold symmetry, and we designate the structure as the FapH ring (**Figs. 2.4D** and **2.4E**). The FapH ring subunits are anchored on a motor accessory that we refer to as the outer disk and extend towards the OM (**Fig. 2.4C**).

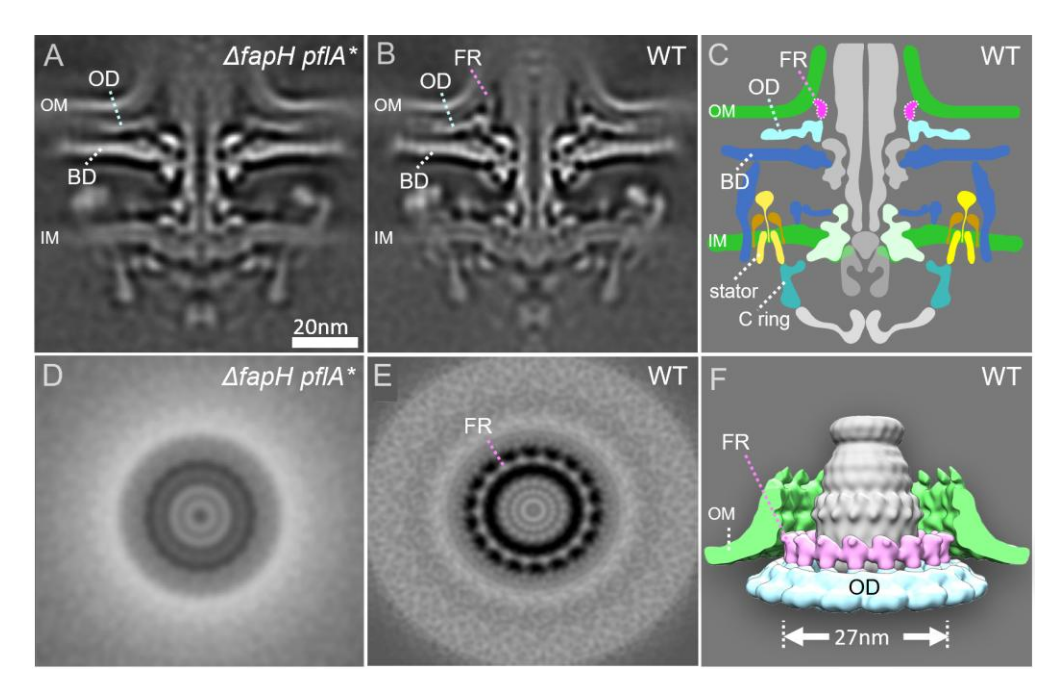


Figure 2.4. Architecture of the FapH ring in the *H. pylori* motor. (A and B) *In-situ* structures of the flagellar motors from  $\Delta fapH$   $pflA^*$  and wild-type cells were determined using subtomogram averaging, respectively. Medial slices through the motor structures indicate the  $\Delta fapH$   $pflA^*$  motor is composed of all motor components, except globular densities in the outer membrane region. (C) A model showing the location of the FapH ring and outer disk structures. (D) Cross section through the globular densities in the  $\Delta fapH$   $pflA^*$  motor. (E) Cross section through the globular densities in the wild-type motor. (F) 3D model of the FapH ring adjacent to the outer membrane. FR – FapH ring, OD – outer disk, BD – basal disk, OM – outer membrane, IM – inner membrane.

The tertiary structure of FapH predicted by Alphafold2 (*Jumper et al. 2021*) indicates  $\alpha$ -helices near the N-terminus and at the C-terminus that are separated by a domain comprised of two  $\beta$ -sheets linked by three short  $\alpha$ -helices (**Fig. S2.5A**). The N-terminal  $\alpha$ -helix of FapH is dominated by acidic amino acid residues, while the C-terminal  $\alpha$ -helix and surface of the  $\beta$ -sheet domain contain several basic amino acid residues (**Fig. S2.5B**). The predicted tertiary structure of FapH fit well into the density of the FapH ring subunits (**Fig. S2.5C**), suggesting that each subunit represents a FapH monomer. From the modeling of the FapH tertiary structure on the FapH ring subunits, the  $\beta$ -sheet domain of FapH contacts the outer disk, while the N-terminal and C-terminal  $\alpha$ -helices are distal to the outer disk and located at the top of the FapH ring subunits. Consistent with the proposed orientation of FapH, the N-terminus is closely associated with the OM, which would allow the acyl side chains of the FapH lipoprotein to insert into the OM.

#### **Identification of FapH interaction partners**

We sought to identify proteins that interact with FapH to gain a better understanding of how FapH protects the barrier function of the OM from flagellum-mediated damage. Moreover, given the close association of the FapH ring and outer disk, we reasoned that FapH interaction partners that we identified would be good candidates for outer disk components. FapH was reported to interact with HP1409/HP0426 (these proteins are duplicated in H. pylori 26695) and the basal disk protein FlgP in a high-throughput yeast two-hybrid screen (Rain et al. 2001). HP1409 and HP0426 are predicted cytoplasmic proteins and are unlikely to interact with FapH within the context of the flagellar basal body. To identify additional FapH interaction partners, we expressed a c-Myc-tagged FapH protein in the ΔfapH pfIA\* strain and performed coimmunoprecipitation (co-IP) assays with cell extracts of the strain. Examination of the immunoprecipitated proteins by SDS-PAGE followed by Coomassie blue staining revealed a few prominent protein bands in the sample that contained the FapH-Myc fusion protein (Fig. 2.5A, lanes 4 and 5) that were not apparent in the sample prepared with cell extracts from wild-type H. pylori B128, which served as a negative control (Fig. 2.5A, lanes 2 and 3). Proteins in three of these bands were identified by peptide mass fingerprinting. FapH was the only identified protein in the ~26-kDa band, which was the most intense band on the gel. Two proteins, HopD and FtsH, were identified in the ~70-kDa band. HopD is one of five β-barrel OM proteins (HopA, HopB, HopC, HopD, and HopE) in H. pylori that are identified as porins and are structurally homologous with the E. coli OmpF porin (Lienlaf et al. 2010). FtsH is an integral membrane, ATP-dependent zinc metallopeptidase that functions in quality control of integral membrane proteins (*Langklotz* et al. 2012). HP1456 (also referred to as Lpp20), a predicted lipoprotein of unknown function, was

the only identified protein in the ~15-kDa band. A crystal structure for *H. pylori* HP1456 indicated that the protein is elongated and bent, consisting of a three-stranded anti-parallel β-sheet flanked by three α-helices on one side and a short α-helix on the other side (*Vallese et al. 2017*). Drobnič and co-workers reported that the predicted tertiary structures of *C. jejuni* FlgP and *Vibrio alginolyticus* FlgT are very similar to that of *H. pylori* HP1456 (*Drobnič et al. 2023*). Like FlgP, FlgT forms a disk-like motor accessory (*Terashima et al. 2013*).

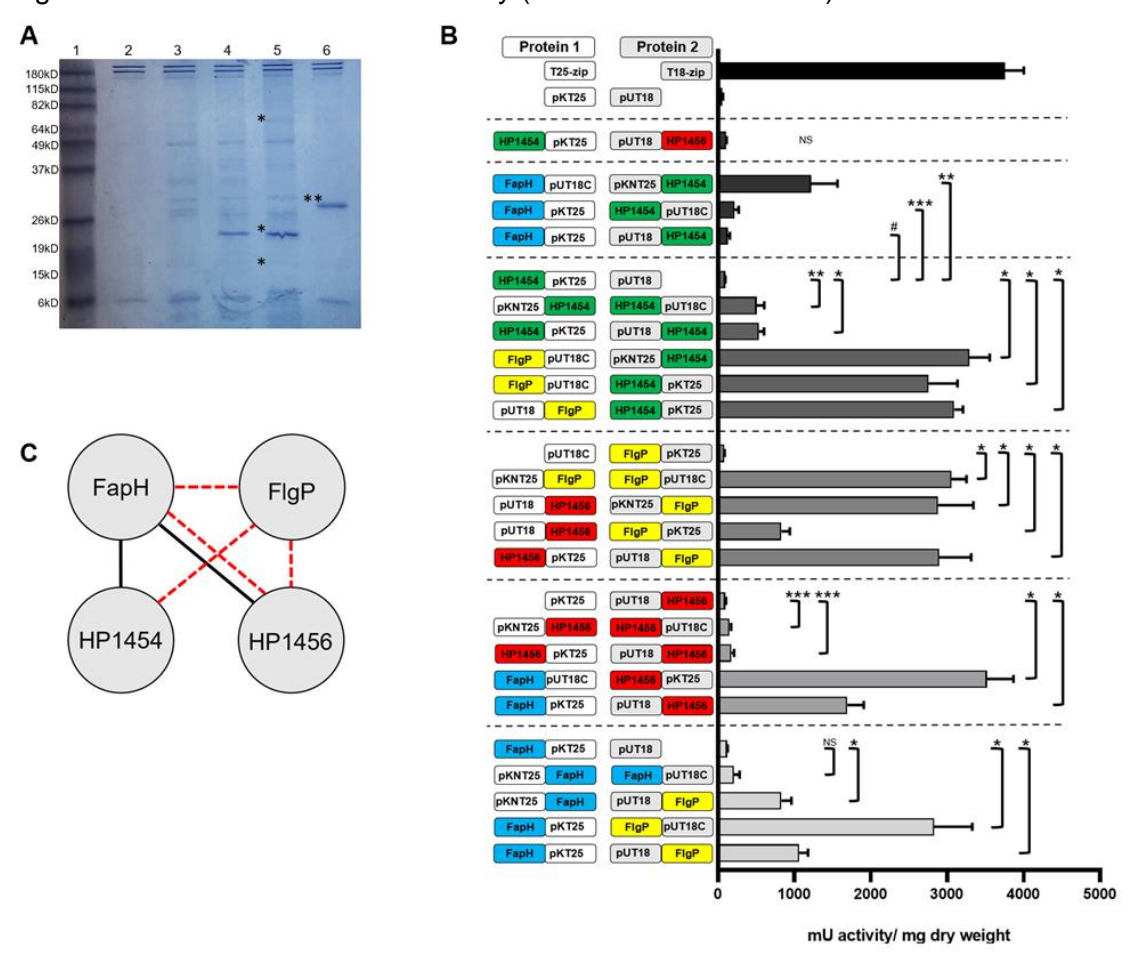


Figure 2.5. Identification of FapH interaction partners. (A) SDS-PAGE gel of proteins isolated from co-IP assay using anti-myc antibody. Lane 1 contained the molecular weight standards. Sizes of the protein standards are indicated to the left of the gel. Lanes 2 and 3 are negative controls and are samples from the co-IP assay with cellular extracts prepared from wild type *H. pylori* B128 and correspond to 5 μl and 10 μl of loaded sample, respectively. Lanes 3 and 4 are samples from the co-IP assay with cellular extracts prepared *H. pylori* B128 strain expressing the FapH-myc fusion protein and correspond to 5 μl and 10 μl loaded sample, respectively. Lane 6 is the positive control of a c-myc tagged *E. coli* protein (indicated by \*\*) that served as a positive control for the co-IP assay and was supplied with the Pierce c-Myc Tag Magnetic IP/co-IP kit.

Protein bands in lane 5 that were excised and analyzed to identify proteins present are indicated by an asterisk (\*). HopD and FtsH were identified in the top band, the middle band corresponded to the FapH-myc protein, and HP1456 was identified in the lower band. (B) Results from βgalactosidase assays for strains with select combinations of adenylate cyclase T15 and T25 fragments fused to FapH, FlqP, HP1454, and HP1456. The cartoons shown on the y-axis illustrate the orientation of the adenylate cyclase fragments and H. pylori proteins in the fusion proteins relative to each other. In the cartoons, FapH is indicated in blue, FlgP is indicated in yellow, HP1456 is indicated in red, and HP1454 is indicated in green. pKNT25 and pKT25 indicate the adenylate cyclase T25 fragment at the N-terminus or C-terminus of the fusion protein, respectively. pUT18 and pUT18C indicate the adenylate cyclase T18 fragment at the N-terminus or C-terminus of the fusion protein, respectively. An E. coli strain containing the BACTH vectors pKT25 and pUT18 served as a negative control, and an E. coli strain bearing plasmids that expressed the T25-zip andT18-zip proteins served as a positive control. The bars indicate the average β-galactosidase activity for each strain and the error bars indicate the SEM. At least 3 replicates were done for each sample. A single asterisk (\*) indicates a p-value of < 0.0001, two asterisks (\*\*) indicate a p-value of < 0.001, and three asterisks (\*\*\*) indicated a p-value of < 0.005. Significance of interaction between pKNT25-FlgP and FlgP-pUT18C is compared with pKT25 and pUT18. For the FapH-FlgP interactions, 7 of the 8 possible plasmid combinations produced significantly elevated levels of β-galactosidase activity, but only 3 of the 7 strains are shown in the figure. (C) Protein-protein interaction map constructed from co-IP and BACTH experiments. Solid black lines indicate interactions observed in co-IP assays involving the FapH-myc protein and dashed red lines indicate interactions observed in the BACTH assay.

Additional proteins that were pulled-down in the co-IP assays used for the fingerprinting analysis, as well as co-IP samples from two additional replicates were identified by analyzing the total protein content of the samples by mass spectroscopy (**Table S2.3**). Notably, HP1456 was identified in all three replicates of the co-IP assay and FlgP was identified in one of the three replicates. HP1454, which is encoded in the same operon as HP1456, was identified in two of the replicates of the co-IP assay. HP1454 is a secreted protein composed of three distinct domains (*Quarantini et al. 2014*), the first of which is structurally similar to HP1456 (*Vallese et al. 2017*).

Since FlgP was identified in one of the replicates of the co-IP assay with the FapH-Myc fusion protein, we used a co-IP assay to determine if FapH was pulled-down with FlgP and to also identify other potential FlgP partners. For these co-IP assays, we used cell extracts prepared from a *H. pylori* B128  $\Delta$  flgP mutant that expressed FlgP-myc fusion protein. A caveat of the experiment was the  $\Delta$  flgP mutant was aflagellated. WGS of the  $\Delta$  flgP mutant revealed that the strain had a

single nucleotide deletion within a homopolymeric tract of eight guanosines in *fliP*, which encodes a component of the flagellar protein export apparatus. Slipped-strand mispairing-mediated mutagenesis within this poly(G)-tract in *fliP* was reported previously for *H. pylori* 26695, and was suggested as a mechanism for switching between "on" and "off" phases for flagellation and motility (*Josenhans et al. 2000*). Despite the mutation in *fliP*, we proceeded with co-IP assays with the expectation that FlgP can associate with at least some of its interaction partners in the absence of the axial components of the motor. Mass spectrometry analysis of the proteins pulled-down in two biological replicates of the co-IP assay with the FlgP-myc protein identified several potential FlgP interaction partners (**Table S2.3**). Notably, FapH was identified in both replicates of the co-IP assay. Other proteins of interest identified from the co-IP assay with the FlgP-myc protein included HP1456 and HP1454.

To examine the validity of the protein interactions predicted from the co-IP assays, we examined the interactions of FapH with selected proteins using the bacterial adenylate cyclase two-hybrid (BACTH) assay (*Karimova et al. 1998*). The BACTH assay is based on the reconstitution of adenylate cyclase (CyaA) activity where two complementary fragments from the catalytic domain of the *Bordetella pertussis* CyaA toxin are brought into proximity by interacting proteins that are fused to the CyaA fragments. Reconstitution of CyaA activity leads to production of cAMP, which is assessed by monitoring the expression of cAMP-dependent genes in an *E. coli cyaA* mutant. We constructed vectors that expressed FapH, HP1454, HP1456, or FlgP fused to the N- or C-termini of the *B. pertussis* CyaA fragments T18 and T25. In constructing the expression vectors, the sequences encoding the signal peptides of the *H. pylori* proteins were omitted to avoid secretion of the fusion proteins into the periplasm.

All possible combinations of expression vectors in the *E. coli* reporter strain BTH101 were examined by culturing the cells on McConkey agar medium that contained 1% maltose (**Fig. S2.6**), and β-galactosidase activities were measured for strains with plasmid combinations that produced pink or red colonies on McConkey-maltose agar medium (**Fig. 2.5B**). Consistent with the co-IP data that suggested interactions between FapH and HP1456, five of the eight combinations of FapH-CyaA and HP1456-CyaA fusion proteins reconstituted active CyaA as demonstrated by the significantly higher β-galactosidase activities in strains harboring these vector combinations versus the negative control (**Fig. 2.5B**). In addition, three of the eight combinations of FapH-CyaA and HP1454-CyaA fusion proteins reconstituted active CyaA (**Fig. 2.5B**). Consistent with the results from the co-IP assays with both the FapH-myc and FlgP-myc proteins as well as the reported interactions between FlgP and FapH in a yeast two-hybrid assay (*Rain et al. 2001*), seven of the eight combinations of FapH-CyaA and FlgP-CyaA fusion proteins

reconstituted active CyaA (**Fig. 2.5B**). FlgP also interacted with HP1454 and HP1456 in the BACTH system, as well as itself (**Fig. 2.5B**). The strong interaction of FlgP with itself is consistent with the assembly of FlgP monomers to form the basal disk. Additional results from the BACTH assays suggest that HP1454 interacts weakly to moderately with itself but does not interact with HP1456 (**Fig. 2.5B**). In addition to interacting with FlgP and FapH, HP1456 interacted weakly with itself (**Fig. 2.5B**). Results of the protein-protein interaction studies are summarized in **Figure 2.5C**.

Given the interactions between FapH and HP1456 in the co-IP and BACTH assays (**Fig. 2.5**) as well as the structural similarity between HP1456 and the disk-forming motor accessory proteins FlgP and FlgT (*Drobnič et al. 2023*), HP1456 seemed a good candidate for an outer disk protein. To address the hypothesis that HP1456 forms the outer disk of the *H. pylori* motor, we generated an unmarked deletion of hp1456 in *H. pylori* B128 and characterized the resulting mutant. The number of flagella produced by the  $\Delta hp1456$  mutant and the motility of the mutant in soft agar medium were the same as observed for wild type (**Figs. S2.7A-C**). In addition, the  $\Delta hp1456$  mutant displayed wild-type resistance to bacitracin (**Fig. 2.S7D**), indicating that HP1456 is not required by FapH to protect the barrier function of the OM from flagellum-mediated damage. The *in-situ* structure of the  $\Delta hp1456$  mutant motor was indistinguishable from that of wild type (**Figs. S2.7E and S2.7F**), indicating that HP1456 is not required for assembly of the outer disk. Thus, despite being a promising candidate HP1456 is not an outer disk component.

# **DISCUSSION**

The flagellar motors of H. pylori and other bacteria contain accessory structures that are not present in the archetypal E. coli and S. enterica motors (Carroll and Liu 2020, Beeby et al. 2016, Chaban et al. 2018, Quin et al. 2017). The functions and protein components for many of these motor accessories have yet to be determined. We report here on a previously uncharacterized ring-like structure in the H. pylori motor that is associated with the OM and is dependent on the lipoprotein FapH for its assembly. In the absence of the FapH ring, H. pylori displays an increased sensitivity to bacitracin that is dependent on a functional flagellum. In support of this thesis, the motile  $\Delta fapH$   $pflA^*$  strain, but not the non-motile, parental strain  $\Delta fapH$   $pflA^T$ , displayed increased sensitivity to bacitracin compared to wild type (Fig. 2.3B-D). Moreover, introducing fapH into the  $\Delta fapH$   $pflA^*$  strain on a shuttle vector suppressed the antibiotic sensitivity of the strain (Fig. 2.3B-D), indicating that loss of fapH was responsible for the increased antibiotic sensitivity of the strain. Although the  $PflA^*$  variant has a 12 amino acid sequence that differs from the wild-type sequence, a couple of lines of evidence indicate this alteration in PflA is neither responsible nor required for the antibiotic sensitivity of the  $\Delta fapH$   $pflA^*$  mutant. Firstly, introducing

a plasmid-borne copy of fapH into  $\Delta fapH$   $pflA^*$  suppressed the bacitracin-sensitivity of the strain, indicating the PflA\* variant is not responsible for the antibiotic sensitivity of the strain. Secondly, the  $\Delta fapH$  mutants that were generated subsequent to the isolation and characterization of  $\Delta fapH$   $pflA^*$  were sensitive to bacitracin and have the wild-type pflA allele, indicating that the PflA\* variant is not required for the antibiotic sensitivity of the H. pylori fapH mutant.

Bacitracin inhibits peptidoglycan biosynthesis by binding undecaprenyl-pyrophosphate within the periplasmic space (*Stone and Strominger 1971*) and is normally excluded by the OM. In various bacterial species, mutations that lead to the accumulation of GPLs in the outer leaflet of the OM result in increased sensitivity to bacitracin and other antibiotics due to the increased permeability of the OM to these compounds (*Silhavy et al. 2010, Davies et al. 2019, Roier et al. 2016*). The increased sensitivity of  $\Delta fapH pflA^*$  and  $\Delta fapH$  mutants to bacitracin suggests the lipid asymmetry of the OM is compromised in these strains. We hypothesize that in the absence of the FapH ring, stress exerted on the OM and flagellar sheath by the rotation of the flagella and the counterrotation of the cell body facilitates the intrusion of GPLs into the outer leaflet of the OM and compromises the barrier function of the OM.

Given the importance of lipid asymmetry for OM barrier function, bacteria have evolved various systems for removing GPLs that make their way into the outer leaflet of the OM. One mechanism for removing GPLs from the outer leaflet of the OM in E. coli and other bacteria is the maintenance of lipid asymmetry (Mla) system, which consists of the OM lipoprotein MlaA, the periplasmic chaperone MlaC, and the inner membrane complex MlaFEDB (Malinverni and Silhavy 2009). MIaA extracts GPLs from the outer leaflet of the OM and transfer them to MIaC for transport across the periplasmic space to the MlaFEDB complex, which inserts the GPLs into the inner membrane (Malinverni and Silhavy 2009). H. pylori possesses homologs of MlaF (HP1465), MIaE (HP1466), and MIaD (HP1464) but lacks a MIaB homolog as has been reported for other members of the phylum Campylobacterota (Roier et al. 2016). Although homologs of MlaA and MlaC have been reported in C. jejuni 11168 and 488 (Davies et al. 2019), H. pylori lacks homologs to both of these proteins, suggesting that the H. pylori Mla system differs somewhat from the well-characterized Mla system in E. coli and other bacteria. A second mechanism used by E. coli to remove GPLs from the outer leaflet of the OM is the enzyme PagP, which acylates the lipid A moiety of LPS at the position 2 R-3-hydroxymyristate chain with a GPLderived palmitoyl group (Bishop et al. 2000). H. pylori, however, lacks a PagP homolog.

A third mechanism for removing GPLs from the outer leaflet of the OM is the phospholipase PldA, which catalyzes the hydrolysis of acyl ester bonds in GPLs that enter the outer leaflet of the OM to generate lysophospholipids and free fatty acids (*Dekker 2000*,

Nishijima et al. 1977, Snijer et al. 1999). H. pylori possesses a PldA homolog, but aspects of the enzyme differ somewhat from E. coli PldA. For example, H. pylori PldA is proposed to be a virulence factor as a H. pylori SS1 pldA mutant was unable to colonize mice (Dorrell et al. 1999). H. pylori PldA also appears to have additional enzymatic activities as the H. pylori SS1 pldA mutant was reported to have reduced phospholipase activity, as well as reduced lecithinase and hemolytic activities compared to the parental strain (Dorrell et al. 1999). The lecithinase activity was assessed by observing zones of clearing around H. pylori grown on egg yolk agar (Dorrell et al. 1999), suggesting PldA was secreted in amounts that were sufficient to hydrolyze the egg yolk lecithin. Expression of H. pylori pldA is phase variable as a result of slippage during DNA replication within a homopolymeric (G) tract located about two-thirds of the way into the open reading frame of the gene (Tannaes et al. 2001). Changes in the length of the (G) tract result in reversible frameshifts, which manifest in translation of the full-length, active PldA or a truncated, inactive enzyme (Tannaes et al. 2001).

The H. pylori B128 genome sequence in the NCBI database indicates the poly(G)-tract in pldA is 7 nucleotides in length, whereas the poly(G)-tract in the wild-type B128 strain used in our studies is 10 nucleotides in length. In both cases though, *pldA* is predicted to be in the 'off' phase. WGS of the  $\Delta fapH pfIA^T$  and  $\Delta fapH pfIA^*$  strains indicated the poly(G)-tract in pldA increased from 10 to 11 nucleotides in 67% and 63% of the reads for that region, respectively (Table S2), indicating that pldA had switched to the 'on' phase in most of the cells in the populations of these strains. Increased PldA activity resulting from pldA switching to the 'on' phase may have compensated for any breakdown in the OM lipid asymmetry. WGS of the  $\Delta fapH$  mutant and its parental fapH::kanR-sacB strain, however, revealed that while the poly(G)-tract in pldA was reduced from 10 to 9 nucleotides in >90% of the reads for that region (Table S2), pldA remained in the 'off' phase in these strains. It is possible that reducing the poly(G)-tract to 9 nucleotides allowed for low level expression of full-length PIdA due to the ribosome shifting one nucleotide backward (-1, in the direction of the 5'-end of the transcript) while translating the poly(G)-tract. Translational frameshifting results from the ribosome shifting either one nucleotide forward (+1, in the direction of the 3'-end of the transcript) or one nucleotide backward, but most case studies on translational frameshifting involve -1 shifting (Atkins et al. 2016). Although increased PldA activity in the fapH mutants may have helped to mitigate disruptions in OM lipid asymmetry, the Mla pathway plays a more critical role in maintaining the lipid asymmetry of the OM in E. coli as loss the Mla pathway results in a slight increase in OM permeability, whereas loss of PldA has no effect (*Malinverni and Silhavy 2009*). The apparent disruption in OM barrier function in the  $\Delta$ *fapH* plfA\* and ΔfapH mutants suggest the systems for maintaining OM lipid asymmetry were

overwhelmed in these strains. Alternatively, the disruption in lipid asymmetry of the OM in the fapH mutants may have been localized near the flagella and OM lipid asymmetry was maintained over the bulk of the cell surface.

An intriguing question is what is the mechanism by which the FapH ring protects the OM from flagellum-dependent damage? One possibility is that the lipid moieties of FapH secure GPLs in the inner leaflet of the OM and prevent them from flipping into the outer leaflet. Additional *H. pylori* motor accessories associated with the OM, including the basal disk and outer disk, may function similarly to protect the OM from flagellum-mediated damage. The *C. jejuni* and *H. pylori* basal disk protein FlgP is a predicted lipoprotein. A high-resolution *in-situ* structure of the *C. jejuni* flagellar motor revealed that the basal disk is comprised of a dozen or more concentric rings, with the innermost ring consisting of 17 trimeric repeats of 51 FlgP protomers (*Drobnič et al. 2023*). Thus, the *H. pylori* basal disk is predicted to be formed by hundreds of FlgP protomers, and such an extensive network of lipoproteins may stabilize the OM around the base of the flagellum.

An alternative mechanism by which the FapH ring may protect the barrier function of the OM from flagellum-mediated damage is that it acts as a bushing to balance the flagellum rotates. The FapH ring is positioned near the base of the hook and may keep the hook aligned as the flagellum rotates to help to protect the integrity of the OM and flagellar sheath in this region.

Although FIgP, HP1456, and HP1454 were identified as FapH interaction partners in the co-IP assays and BACTH assays (**Fig. 2.5**), the significance of these protein-protein interactions is unclear. It is possible that FapH recruits HP1456 and/or HP1454 to the base of the sheath to assist in stabilizing the region as the flagella rotate. If that is the case, the recruitment of HP1456 does not appear to be a major contributing factor to OM stability since the Δ*hp1456* mutant displayed wild-type resistance to bacitracin (**Fig. S2.7**). FIgP has a large unstructured region at the N-terminus that allows the lipoprotein to anchor in the OM and form the basal disk well below the OM (*Drobnič et al. 2023*) (also see **Figs. 42.A-2.4C**). Thus, although the basal disk is not intimately associated with the FapH, the unstructured N-terminal region for some of the FIgP protomers are positioned to associate potentially with the FapH ring. Moreover, little is known about the assembly of the flagellar motor accessories in *H. pylori*, and interactions between FapH and FIgP may be important for FapH ring assembly.

While the flagellar sheath may potentiate flagellum-mediated damage to the OM in *H. pylori*, flagellar rotation may also present problems in maintaining the barrier function of the OM in diderms that have sheath-less flagella. Since FapH is restricted to members of the phylum Campylobacterota, bacterial species outside the phylum presumably rely on different mechanisms to protect the OM from flagellum-mediated damage. In bacteria that lack a flagellar

sheath, the L-ring forms a pore in the OM through which the flagellar rod passes, which may afford protection to the OM as the flagellum rotates. A high-resolution structure of the *S. enterica* flagellar basal body revealed that the LPS acyl chains and lipid moieties of FlgH form a hydrophobic band that encompasses the L-ring and is thinner than the canonical lipid bilayer (*Johnson et al. 2021*). An additional protein density was associated with the outside of the *S. enterica* L-ring, and this protein was identified as the lipoprotein YecR (*Johnson et al. 2021*). The authors of the study postulated a potential role for YecR in L-ring assembly, but their analysis of a *yecR* mutant indicated that YecR was not required for formation of the L-ring (*Johnson et al. 2021*). It is possible that like FapH, YecR has a role in protecting the OM from flagellum-mediated damage.

As our knowledge of the structural diversity of bacterial flagellar motors has grown, it has become clear that more work needs to be done to understand the roles of flagellar motor accessory structures. The characterization of motor accessories will undoubtedly lead to the discovery of novel mechanisms for regulating motor function or mitigating cellular damage resulting from action of the motor as we demonstrated here for the FapH ring of the *H. pylori* motor. Such new information will provide insight into how bacteria have sculpted the motor to address the demands imposed on them by specific ecological niches or by morphological variations in flagellum structure, such as the flagellar sheath.

## **MATERIALS AND METHODS**

**Bacterial strains and culture conditions.** *E. coli* NEB® Turbo cells (New England Biolabs, Ipswich, MA, USA, which were used for cloning procedures, were grown on LB medium supplemented with ampicillin (100 μg/ml) or kanamycin (30 μg/ml) as required. *H. pylori* strains used in the study were derived from *H. pylori* B128 (kindly provided by Richard M. Peek, Jr.). and are listed along with plasmids used in the study in **Table S2.5**. Liquid cultures of *H. pylori* were grown at 37°C with shaking in brain heart infusion (BHI) supplemented with 5% heat-inactivated horse serum (Gibco; Thermo Fisher Scientific, Waltham, MA, USA) in serum vials that contained an atmosphere consisting of 5% CO<sub>2</sub>, 10% H<sub>2</sub>, 10% O<sub>2</sub>, and 75% N<sub>2</sub>. *H. pylori* strains were grown on solid medium under an atmosphere consisting of 10% CO<sub>2</sub>, 6% O<sub>2</sub>, and 84% N<sub>2</sub> at 37°C on tryptic soy agar supplemented with 5% heat-inactivated horse serum (TSA-HS). Growth medium for *H. pylori* was supplemented with kanamycin (30 μg/ml), bacitracin (100 or 200 μg/ml), or 5% sucrose (w/v) as needed.

**PCR methods.** Genomic DNA (gDNA) from *H. pylori* B128 was purified using the Wizard genomic DNA purification kit (Promega, Madison, WI, USA) and used as the template for PCR using PrimeSTAR DNA polymerase (Takara Bio, San Jose, CA, USA) or Phusion DNA polymerase (New England Biolabs). To facilitate cloning into the pGEM-T Easy vector (Promega), amplicons were incubated with *Taq* polymerase (Promega) at 72° C for 10 min to add A overhangs at the 3'-ends.

Construction of *H. pylori* B128 ΔfapH, ΔflgP, and Δhp1456 mutants. Regions flanking fapH were amplified from H. pylori B128 gDNA using primer pair 59 and 60 (for upstream region) and primer pair 61 and 62 (for downstream region; Table S2.4). Primers 60 and 61 were complementary at their 5'-ends and introduced Xhol and Nhel restriction sites for subsequent introduction of a kan<sup>R</sup>-sacB cassette. The amplicons corresponding to the regions upstream and downstream of fapH were joined together by overlapping PCR, A overhangs were added to the 3'-ends of the resulting amplicon, which was then ligated into pGEM-T Easy (Promega) to generate plasmid pKR10 (Fig. S2.8). Plasmid pKR3 is a derivative of pJC038 (Chu et al. 2019) that carries a kan<sup>R</sup>-sacB cassette where sacB is under control of the H. pylori ureA promoter. In pKR3, the H. pylori urel promoter was introduced at the end of the cassette in an outward orientation to compensate for potential polar effects on genes that are downstream of the kan<sup>R</sup>sacB insertion. The kanR-sacB cassette was excised from plasmid pKR3 by digesting with Nhel and Xhol (New England Biolabs) and then introduced into the Nhel and Xhol sites in plasmid pKR10 to generate plasmid pKR11, which was introduced by natural transformation into H. pylori B128. Since plasmid pKR11 does not replicate in *H. pylori*, transformants in which fapH had been replaced with the kan<sup>R</sup>-sacB cassette by homologous recombination were enriched by selecting for kanamycin resistance. Replacement of fapH with the kan<sup>R</sup>-sacB cassette was confirmed by PCR using primer pair 59 and 62. One of the kanamycin-resistant isolates in which fapH was replaced with the kan<sup>R</sup>-sacB cassette, which was designated strain H6, was transformed with the suicide vector pKR10. Transformants in which the kanR-sacB cassette was replaced with the unmarked deletion of fapH resulting from homologous recombination between plasmid pKR10 and the chromosome were counter-selected on TSA-HS supplemented with 5% sucrose as described (Copass et al. 1997) Sucrose-resistant isolates were screened for kanamycinsensitivity on TSA-HS supplemented with kanamycin, and deletion of fapH in kanamycin sensitive isolates was confirmed by PCR using primer pair 59 and 62 and DNA sequencing of the resulting amplicon (Eton Biosciences, Research Triangle, NC, USA). A H. pylori B128 strain in which fapH was deleted was designated as strain H16.

An unmarked deletion of flqP in H. pylori B128 was constructed following the protocol used for constructing the  $\triangle fapH$  mutant. Regions flanking flgP were amplified from H. pylori B128 gDNA using primer pair 39 and 40, and primer pair 41 and 42. The resulting amplicons were joined together by overlapping PCR and cloned into pGEM-T Easy to generate plasmid pKR4 (Fig. **S2.8**). The kan<sup>R</sup>-sacB cassette was introduced into plasmid pKR4 to generate the suicide vector pKR9, which was introduced into H. pylori B128 to replace flqP with the kan<sup>R</sup>-sacB cassette through homologous recombination to yield strain H5. Replacement of flgP with the kan<sup>R</sup>-sacB cassette was confirmed by PCR using primer pair 39 and 42. The suicide vector pKR4 was introduced into H5 to replace the kan<sup>R</sup>-sacB cassette in the flgP locus with the unmarked deletion of flqP in plasmid pKR4 using the sucrose counter-selection as described above. Sucroseresistant isolates were screened for kanamycin-sensitivity on TSA-HS supplemented with kanamycin, and deletion of flqP in kanamycin sensitive isolates was confirmed by PCR using primer pair 39 and 42 and DNA sequencing of the resulting amplicon. A H. pylori B128 strain in which flgP was deleted was designated as strain H6. gDNA from strain H6 was prepared and provided to the SeqCenter (Pittsburgh, PA, USA) for whole genome Illumina sequencing. The resulting genome sequence data were analyzed using the breseg computational pipeline (Deatherage and Barrick 2014).

An unmarked deletion of hp1456 in H. pylori B128 was constructed following the protocol used for constructing the \(\Delta fapH\) mutant. Regions flanking \(hp1456\) were amplified from \(H.\) \(pylori\) B128 gDNA using primer pair 195 and 196, and primer pair 197 and 198. The resulting amplicons were joined together by overlapping PCR and cloned into pGEM-T Easy to generate plasmid pKR67. The kan<sup>R</sup>-sacB cassette was introduced into plasmid pKR67 to generate the suicide vector pKR77, which was introduced into *H. pylori* B128 to replace *hp1456* with the kan<sup>R</sup>-sacB cassette through homologous recombination to yield strain H143. Replacement of hp1456 with the kan<sup>R</sup>-sacB cassette was confirmed by PCR using primer pair 195 and 198. The suicide vector pKR67 was introduced into H143 to replace the kan<sup>R</sup>-sacB cassette in the hp1456 locus with the unmarked deletion of hp1456 in plasmid pKR67 using the sucrose counter-selection as described above. Sucrose-resistant isolates were screened for kanamycin-sensitivity on TSA-HS supplemented with kanamycin, and deletion of hp1456 in kanamycin sensitive isolates was confirmed by PCR using primer pair 195 and 198 and DNA sequencing of the resulting amplicon. A H. pylori B128 strain in which hp1456 was deleted was designated as strain H145. gDNA from strain H145 was prepared and provided to the SeqCenter (Pittsburgh, PA, USA) for whole genome Illumina sequencing. The resulting genome sequence data were analyzed using the breseg computational pipeline (**Deatherage and Barrick 2014**).

Complementation of mutants. To facilitate complementation assays in *H. pylori*, we modified the shuttle vector pHel3 (*Heuermann and Haas 1998*) for Golden Gate cloning that employed tandem sites for the Type IIS restriction enzyme BspQ1 (**Fig. S2.9**). The modified plasmid, which we designated pHel3-GG, contains the *fliF* promoter upstream of the tandem BspQ1 sites where the cloned gene is introduced. The *fliF* promoter is flanked by unique BamHI and Nhel sites that can be used to replace the *fliF* promoter with other promoters if desired.

Primers 169 and 170 were used to amplify *fapH* from *H. pylori* B128 gDNA (**Table S2.4**). The primers introduced BspQ1 sites immediately upstream and downstream of the start and stop codons of *fapH*, respectively. The resulting amplicon and pHel3-GG were digested together with BspQ1 (New England Biolabs) for 1 h at 50°C, after which the amplicon and vector were ligated using Fast-Link DNA ligase (Biosearch Technologies, Hoddeson, UK) for 30 min at room temperature. The reaction mix was incubated with BspQ1 to digest any uncut pHel3-GG vector, and the reaction mix was then used for transformation of *E. coli*. A plasmid containing the expected insert, designated as pKR54, was verified by restriction enzyme digestion and sequencing of the inserted DNA.

Primers 159 and 160 were used to amplify *pflA* from *H. pylori* B128 gDNA. The primers introduced BspQ1 sites immediately upstream and downstream of the start and stop codons of *pflA*, respectively. The resulting amplicon was cloned into pHel3-GG as described above. A plasmid containing the expected insert, designated as pKR50, was verified by restriction enzyme digestion and sequencing of the inserted DNA. Plasmids pKR54 and pKR50 were introduced by natural transformation into various *H. pylori* strains for complementation assays.

Construction of c-Myc tagged FapH and FlgP proteins. To facilitate construction of a c-Myc-tagged FapH in *H. pylori*, we modified the shuttle vector pHel3 (*Heuermann and Haas 1998*) to allow for the introduction of the c-Myc epitope at the C-terminus of the protein (Fig. S2.9). The modified plasmid, which we designated pHel3-Myc, contains the *fliF* promoter upstream of the tandem BspQ1 sites for Golden Gate cloning followed by a sequence encoding a flexible linker, c-Myc epitope, and DDDDK epitope. Primers 162 and 163 were used to amplify *fapH* from *H. pylori* B128 gDNA (Table S2.4). The primers introduced BspQ1 sites immediately upstream and downstream of the start and stop codons of *fapH*, respectively. The resulting amplicon and plasmid pHel3-Myc were digested together with BspQ1 and ligated using Fast-Link DNA ligase as described above. The reaction mix was incubated with BspQ1 to digest uncut pHel3-Myc

vector and the reaction mix was then used for transformation of *E. coli*. A plasmid containing the expected insert, designated as pKR55, was verified by restriction enzyme digestion and sequencing of the inserted DNA.

To construct a c-Myc-tagged FlgP, primers 78 and 79 were used to amplify *flgP* from *H. pylori* B128 gDNA. The resulting amplicon and plasmid pHel3-Myc were digested with BspQ1 and ligated together to generate plasmid pKR23. The *flgP-myc* chimeric gene in plasmid pKR23 was confirmed by DNA sequencing.

**Motility assay.** Motility was evaluated using a semisolid medium containing Mueller-Hinton broth (MHB), 10% heat-inactivated horse serum, 20 mM MES (2-(4-morpholino)-ethane sulfonic acid) (pH 6.0), and 0.4%-0.6% Noble agar. A minimum of three technical replicates were used to assess the motility of each strain. *H. pylori* strains grown on TSA-HS for 2 d were stab-inoculated into the motility agar and incubated at 37° C under an atmospheric condition consisting of 10% CO<sub>2</sub>, 6% O<sub>2</sub>, and 84% N<sub>2</sub>. The diameters of the resulting swim halos were measured 7 d post-inoculation and a two-sample t-test was used to determine statistical significance. For motility-base antibiotic resistance assays, bacitracin was included in the soft agar medium.

**Efficiency plating assay.** *H. pylori* strains were grown on TSA-HS, then resuspended in MHB. The densities of each cell suspension were adjusted to an  $OD_{600}$  of ~0.50. Cell suspensions were diluted serially, 3 µl of each dilution were plated onto TSA-HS and TSA-HS supplemented with bacitracin, and the cultures were incubated for 5 d under a microaerobic atmosphere. A minimum of two replicants were done for each strain and tested condition.

**Co-immunoprecipitation procedure.** Wild-type *H. pylori* B128 and the *H. pylori* strains expressing either the FapH-Myc or FlgP-Myc fusion proteins were grown on TSA-HS plates, harvested, and resuspended in 7 ml phosphate-buffer saline (PBS) with Pierce Protease Inhibitor (Thermo Fisher Scientific). Cells were lysed at 18,000 psi with a French press and the resulting cell lysate was centrifuged at 7,700 x g for 10 min to remove unlysed cells and cell debris. The resulting supernatant was centrifuged at 100,000 x g to pellet membrane vesicles, which were subsequently resuspended in PBS buffer containing 50 mM n-dodecyl-β-D-maltoside (DDM) (Chem-Impex International, Wood Dale, IL, USA). The solution was diluted to 20 mM DDM and the insoluble material was pelleted by centrifugation at 10,000 x g for 10 min and the resulting supernatant was used for the co-IP procedure using the Pierce c-Myc Tag Magnetic IP/Co-IP kit (Thermo Fisher Scientific) as described by the supplier. Samples were incubated with the

magnetic beads either overnight at 4°C or at room temperature for 30 min. Magnetic beads with bound proteins were washed at least 10 times with a 1:20 solution of Buffer 2 (supplied with the kit) containing 20 mM DDM. Proteins were eluted from the magnetic beads using 100 μl of 1x non-reducing sample buffer (supplied with the kit) followed by incubation at 95-100°C for 5 to 10 min. Samples were loaded on a 12% SDS-PAGE gel and proteins were visualized by staining with Coomassie Brilliant Blue R-250. Protein bands were excised from the gel and submitted to the University of Georgia Proteomics and Mass Spectrometry Facility for protein identification by peptide mass fingerprinting analysis.

Transmission electron microscopy. *H. pylori* strains were grown to late-log phase ( $OD_{600} \sim 1.0$ ) in MHB supplemented with 5% heat-inactivated horse serum. Cells from 1 mL of culture were pelleted by centrifugation (550 x g) then resuspended in 125 µL of PBS. Cells were fixed by adding 50 µL of 16% EM grade formaldehyde and 25 µL of 8% EM grade glutaraldehyde to the cell resuspension. Following incubation at room temperature for 5 min, 10 µL of the cell suspension were applied to a 300 mesh, formvar-coated copper grid and incubated at room temperature for 5 min. The cell suspension was wicked off the grids using a filter paper, and the grids were washed 3 times with 10 µL of water. Cells were stained by applying 10 µL of 1% uranyl acetate to the grids for 30 s. After removing the stain with filter paper, the grids were washed three times with 10 µL of water and then air-dried. Cells were visualized using a JEOL JEM 1011 transmission electron microscope. The number of flagella per cell were determined for at least 100 cells for each strain. Flagellar lengths were determined using Fiji ImageJ.

**Cryo-ET sample preparation.** *H. pylori* strains were grown on Columbia agar plates supplemented with 5% horse red blood cells at 37°C under microaerobic conditions. Bacteria from the agar medium were resuspended in PBS and mixed with 10 nm of BSA gold tracers (Aurion, Wageningen, NL). The mixtures were deposited on freshly grow-discharged cryo-EM grids (Quantifoil R2/1a. Cu 200 mesh and then frozen into liquid ethane by using a manual plunger as described previously (*Qin et al. 2017, Chu et al. 2019*).

Cryo-ET data collection and processing. Frozen-hydrated specimens were visualized in a 300kV Titan Krios G2 transmission electron microscope (Thermo Fisher Scientific) equipped with a K3 summit direct detection camera and a BioQuantum energy filter (Gatan). Tilt series images were acquired at 42,000x magnification (corresponding to a pixel size of 2.148 Å at the specimen level) and ~4.5 µm defocus using SerialEM (*Mastronarde 2005*) and FastTomo script (*Tan et al.* 

**2021**) based on a dose-symmetric scheme from -48° to +48° in 3° increments (**Xu 2021**). The total accumulative dose for each tilt series was ~60 e<sup>-</sup>/Å<sup>2</sup>. MotionCor2 (**Zheng et al. 2017**) was used to correct the beam induced motion. IMOD (**Kremer et al. 1996**) was used to create image stacks and align all images in each tilt series by tracing the gold tracer beads. Gctf (**Zhang 2016**) was used for the defocus estimation for all images in the tilt series, and then the ctfphaseflip function in IMOD was used for contrast transfer function (CTF) correction (**Xiong et al. 2009**).

**Subtomogram averaging.** Tomo3D (*Agulleiro and Fernandez 2015*) was used to generate 3D reconstructions with the simultaneous iterative reconstruction technique (SIRT), and a total of 268, 225, and 134 tomograms were reconstructed from the wild type,  $\Delta fapH \ pflA^T$ , and  $\Delta fapH \ pflA^T$ , respectively. 6 x binned tomograms were used to select 824, 640, and 525 flagellar motors from the wild-type,  $\Delta fapH \ pflA^T$ , and  $\Delta fapH \ pflA^T$ , respectively. After the particle picking, tomograms with weighted back projection (WBP) were used for the initial subtomogram averaging with the i3 suite (*Winkler 2007, Winkler et al. 2009*). For further structural analysis, 4 x binned subtomograms were used to refine the intact motor structures.

FapH modeling in the intact flagellar motor. Alphafold 2 was used to generate a structural prediction for FapH (*Jumper et al. 2021, Varadi et al. 2022*). The predicted structure deemed the best model was used to fit into the intact motor structure derived from subtomogram averaging by using the "fit in map" option in UCSF ChimeraX software (*Goddard et al. 2018*). All models examined had the signal peptides removed.

Whole genome sequencing and analysis. gDNA from the *H. pylori* strains was purified using the Wizard genomic DNA purification kit (Promega) and submitted to the SeqCenter (Pittsburgh, PA, USA) for genomic library preparation and Illumina sequencing. Reads for *H. pylori* gDNA sequence were mapped using the *breseq* computational pipeline (*Deatherage and Barrick 2014*) with the published NCBI genome for *H. pylori* B128 (Accession no.: NZ\_CP024951.1).

**Construction of plasmids for BACTH assays.** The Bacterial Adenylate Cyclase Two-Hybrid (BACTH) System Kit (Euromedex, Souffelweyersheim, France) was used to detect and characterize protein-protein interactions *in vivo*. Primer pairs 208/209, 2010/211, 212/213, and 214/215 (**Table S2.4**) were used to amplify *hp1454*, *hp1456*, *fapH*, and *flgP*, respectively, from *H. pylori* B128 gDNA. The forward primers corresponded to sequences immediately following the regions that encoded the predicted signal peptides to prevent secretion of the recombinant

proteins. Following the addition of A's to the 3'-ends, the resulting amplicons were ligated into pGEM-T Easy. The resulting plasmids were designated pKR69, pKR70, pKR71, and pRK72 (Table S2.5), and the inserted DNA sequences were confirmed by sequencing. BamHI-KpnI fragments from these plasmids were cloned into BamHI and KpnI sites in the BACTH vectors pKT25, pKNT25, pUT18, andpUT18C) to generate plasmid pRK96 though pRK112. DNA fragments that were cloned into the BACTH vectors were sequenced to confirm that the plasmid constructs were correct. *E. coli* reporter strain BTH101 (Euromedex) was used for cotransformation of BACTH plasmids. Eight combinations of plasmids were co-transformed and screened in BTH101 for each of the following protein-protein interaction pairs: FapH-FlgP, FapH-HP1454, FapH-HP1456, FlgP-HP1454, FlgP-HP1456, HP1454-HP1456, FlgP-FlgP, HP1454-HP1454, and HP1456-HP1456, for a total of 72 different combinations. Transformants were plated onto McConkey agar supplemented with 1% (w/v) maltose, 100 μg/ml ampicillin, 50 μg/ml kanamycin, and 0.5 mM isopropyl-β-D-thiogalactopyranoside (IPTG).

**β-galactosidase Assay.** Cultures of *E. coli* BTH101 harboring various combinations of BACTH plasmids were grown at 30°C to mid- to late-log phase in LB supplemented with ampicillin (50 µg/ml), kanamycin (25 µg/ml), and 0.5 mM IPTG. Cells were diluted five-fold in M63 medium (15 mM (NH<sub>4</sub>)<sub>2</sub>SO<sub>4</sub>,100 mM KH<sub>2</sub>PO<sub>4</sub>, 1.8 μM FeSO<sub>4</sub>, 1 mM MgSO<sub>4</sub>, and 4 μM thiamine) containing 0.2% maltose as the carbon source in a final volume of 2.5 ml and OD<sub>600</sub> readings were recorded for each culture. Cells were permeabilized by adding 30 µl of toluene and 35 µl of a 0.1% sodium dodecylsulfate solution then incubating for 30-40 min at 37°C with shaking. The permeablized cells were diluted 10-fold in PM2 buffer (70 mM Na<sub>2</sub>HPO<sub>4</sub>, 30 mM NaH<sub>2</sub>PO<sub>4</sub>, 1 mM MgSO<sub>4</sub>, 0.2 mM MnSO<sub>4</sub>, 100 mM β-mercaptoethanol, pH 7.0) to a final volume of 1 ml and placed in 5 ml glass tubes. Cells were incubated for 5 min in a water bath at 28°C, and the enzymatic reaction was started with the addition of 0.25 ml of 13 mM o-nitrophenol-β-galactoside (ONPG) in PM2 buffer. Enzyme reactions were stopped at various recorded times by the addition of 0.5 mL of 1 M Na<sub>2</sub>CO<sub>3</sub>, and then the OD<sub>420</sub> values were recorded for each sample. The enzymatic activity (A; units (in nmol ONPG hydrolyzed min<sup>-1</sup>)/ml) was calculated according to the instructions provided by the BACTH kit supplier using the formula  $A = 200 \times (OD_{420} / min of incubation) \times dilution factor.$ The factor 200 in the formula is the inverse of the OD<sub>420</sub> for 1 µM o-nitrophenol using a 1 cm light path, which is 0.0045 at pH 11.0. The dilution factor for each was 10. Specific activities (SA) expressed in units per mg dry weight were calculated by considering 1 ml of culture at OD<sub>600</sub> = 1 corresponds to 300  $\mu$ g dry weight bacteria and using the formula SA = A / (OD<sub>600</sub> x 0.3 mg dry

weight per  $OD_{600}$ ). Each strain was assayed with at least three replicates, and a two-sample *t*-test was used to determine statistical significance.

# **Acknowledgements**

We thank the following people for their contributions: Vincent Starai, Jack Botting, and Doreen Nguyen for helpful discussions; Robert Maier for providing access to equipment; and Stéphane Benoit for the strains used in the BACTH assays. This work was supported by NIH grant Al140444 to T.R.H., and NIH grants Al087946 and Al132818 to J.L. Proteomics data generated in the study were supported by instrument grant NIH S10 OD025118 to the University of Georgia Proteomics and Mass Spectrometry Facility.

# SUPPLEMENTARY MATERIALS

Table S2.1. Homologs of FapH, FlgP, and FlgH in *Helicobacter* species and other members of Campylobacterota with flagellar sheaths

species+A3:F32	aFapH homolog accession	bsignal peptide prediction	<sup>a</sup> FlgP homolog accession #	<sup>b</sup> signal peptide prediction	flgP-FapH synteny
Helicobacter pylori	WP_001268506.1	Sec/SPII (1.00)	WP_001236618.1	Sec/SPII (1.00)	yes
Helicobacter acinonychis	WP_011578069.1	Sec/SPII (1.00)	WP_011578068.1	Sec/SPII (1.00)	yes
Helicobacter ailurogastricus	WP_053945035.1	Sec/SPII (1.00)	WP_053941682.1	Sec/SPII (0.993)	yes
Helicobacter anseris	WP_115578244.1	Sec/SPII (0.997)	WP_115578245.1	Sec/SPII (0.984)	yes
Helicobacter aurati	WP_104763506.1	Sec/SPII (1.00)	WP_115582549.1	Sec/SPII (1.00)	yes
Helicobacter baculiformis	WP_104751740.1	Sec/SPII (0.999)	WP_233708949.1	<sup>c</sup> other (1.00); Sec/SPII (1.00)	yes
Helicobacter bilis	WP 005217292.1	Sec/SPII (1.00)	WP 077388503.1	Sec/SPII (1.00)	yes
Helicobacter bizzozeronii	WP_013889620.1	Sec/SPII (0.986)	WP_104628845.1	Sec/SPII (0.965)	yes
Helicobacter brantae	WP 115569802.1	Sec/SPII (1.00)	RDU70366.1	Sec/SPII (1.00)	yes
Helicobacter canis	WP_084330889.1	Sec/SPII (0.998)	WP_150336683.1	Sec/SPII (1.00)	yes
Helicobacter cetorum	WP_014658887.1	Sec/SPII (1.00)	WP_014661575.1	Sec/SPII (1.00)	yes
Helicobacter cholecystus	WP 104724631.1	Sec/SPII (1.00)	WP 104724630.1	Sec/SPII (1.00)	ves
Helicobacter cinaedi	WP 002957383.1	Sec/SPII (0.887)	WP 014666253.1	Sec/SPII (1.00)	ves
Helicobacter cynogastricus	WP 104750309.1	Sec/SPII (1.00)	WP 104750398.1	Sec/SPII (0.918)	yes
Helicobacter equorum	WP_104694233.1	Sec/SPII (0.797)	WP_115571536.1	Sec/SPII (1.00)	yes
Helicobacter felis	WP_013469510.1	Sec/SPII (1.00)	CBY83146.1	Sec/SPII (0.999)	yes
Helicobacter fennelliae	WP_023946537.1	Sec/SPII (1.00)	WP_034549153.1	Sec/SPII (0.853)	yes
Helicobacter heilmannii	CCM10801.1	Sec/SPII (1.00)	CCM10800.1	Sec/SPII (0.996)	yes
Helicobacter hepaticus	WP 011115818.1	Sec/SPII (1.00)	WP 011115819.1	Sec/SPII (1.00)	yes
Helicobacter himalayensis	WP_066386686.1	Sec/SPII (0.979)	WP_231860284.1	Sec/SPII (1.00)	yes
Helicobacter jaachi	WP_034352443.1	Sec/SPII (0.999)	WP_034352442.1	Sec/SPII (1.00)	yes
Helicobacter japonicus	WP 034362244.1	Sec/SPII (1.00)	WP 034362246.1	Sec/SPII (1.00)	ves
Helicobacter labetoulli	WP 121727297.1	Sec/SPII (0.898)	WP 014666253.1	Sec/SPII (1.00)	yes
Helicobacter macacae	WP 023927489.1	Sec/SPII (0.991)	WP 023927488.1	Sec/SPII (0.999)	yes
Helicobacter magdeburgensis	WP_034586686.1	Sec/SPII (0.999)	WP_138129097.1	Sec/SPII (1.00)	yes
Helicobacter marmotae	WP_233706655.1	Sec/SPII (1.00)	WP_104700435.1	Sec/SPII (1.00)	yes
Helicobacter muridarum	WP_034557117.1	Sec/SPII (1.00)	WP_034557115.1	Sec/SPII (1.00)	yes
Helicobacter mustelae	WP 013023615.1	Sec/SPII (1.00)	WP 013023614.1	Sec/SPII (0.948)	yes
Helicobacter pametensis	WP 051420501.1	Sec/SPII (1.00)	WP 027326760.1	Sec/SPII (1.00)	yes
Helicobacter rappini	WP_005217292.1	Sec/SPII (1.00)	WP_004085965.1	Sec/SPII (1.00)	yes
Helicobacter saguini	WP_052062339.1	Sec/SPII (1.00)	WP_034570145.1	Sec/SPII (1.00)	yes
Helicobacter salomonis	WP 104751259.1	Sec/SPII (1.00)	WP 233709791.1	<sup>c</sup> other (1.00); Sec/SPII (0.998)	ves
Helicobacter suis	WP 006564908.1	Sec/SPII (1.00)	WP 163532053.1	Sec/SPII (0.980)	ves
Helicobacter trogontum	WP 034321248.1	Sec/SPII (1.00)	TLD97124.1	Sec/SPII (1.00)	ves
Helicobacter typhlonius	WP_034325957.1	Sec/SPII (1.00)	WP_034325956.1	Sec/SPII (1.00)	ves
				(1100)	,
Helicobacter species with ur	sheathed flagella				
Helicobacter apodemus	WP 108910962.1	Sec/SPII (0.899)	WP 108910963.1	Sec/SPI (0.999)	yes
Helicobacter burdigaliensis	WP 121764719.1	Sec/SPII (1.00)	WP 121764718.1	Sec/SPI (0.999)	yes
Helicobacter canadensis	WP 006655834.1	Sec/SPII (0.545)	WP 006656899.1	Sec/SPI (0.999)	ves
Helicobacter ganmani	WP 115551484.1	Tat/SPII (0.596)	WP 115551483.1	Sec/SPI (0.998)	ves
Helicobacter mesocricetorum	WP_104722701.1	Sec/SPII (0.997)	WP_104722702.1	Sec/SPI (0.999)	yes
Helicobacter pullorum	WP 005020762.1	Sec/SPII (0.971)	WP_005020761.1	Sec/SPI (0.999)	ves
Helicobacter rodentium	WP 026943429.1	Tat/SPII (0.871)	WP 034550981.1	Sec/SPI (0.998)	ves
Helicobacter valdiviensis	PZT48166.1	Sec/SPII (1.00)	PZT48174.1	Sec/SPI (0.997)	yes
Helicobacter winghamensis	WP_006802619.1	Sec/SPII (1.00)	WP_040498531.1	Sec/SPI (0.999)	yes
J 1 10.0		/		()	
Other representatives of Car	mpylobacterota				
Aliarcobacter butzleri	NLO18110.1	Sec/SPII (1.00)			n/a
Campylobacter jejuni	EFC32131.1	Sec/SPII (1.00)	EFC32730.1	Sec/SPII (1.00)	no
Nautilia profundicola	WP 015901819.1	Sec/SPII (1.00)	WP 187146597.1	Sec/SPII (1.00)	no
Sulfurimonas gotlandica	WP_008335553.1	Sec/SPII (1.00)	WP_008336442.1	Sec/SPI (0.999)	no
Sulfurospirillim deleyianum	WP_012855937.1	Sec/SPII (1.00)	WP_012856125.1	Sec/SPII (1.00)	no
Wolinella succinogenes	WP 011139560.1	Sec/SPII (1.00)	WP 011139561.1	Sec/SPI (0.999)	ves

<sup>&</sup>lt;sup>a</sup>GenBank accession number

Footnote 1: A FapH homolog in *Steptomyces sulfonofaciens* (WP\_229925214.1) was identified in the PSI-BLAST analysis, but this protein appears to be incorrectly annotated as it shares 100% identity with *H. pylori* FapH.

Footnote 2: Two FlgP homologs in FS+ *Helicobacter* species are not predicted to have signal peptides, but this may be due to incorrect assignments for the translational start sites of these flgP homologs as selecting alternative upstream translational start sites resulted in protein sequences with predicted lipoprotein signal peptides.

Table S2.2: Mutations identified in  $\Delta fapH$  strains,  $\Delta flgP$  mutant, and  $\Delta hp1456$  mutant.

ΔfapH pflA <sup>T</sup> (lab strain H16)						
NCBI	26695 locus	Gene/ description	Mutation	<sup>a</sup> lmpact	<sup>b</sup> Frequency	
designation	tag			•		

<sup>&</sup>lt;sup>b</sup>Prediction from SignalP-6.0 for type of signal peptide: Sec/PI - predicted signal peptide; Sec/SPII - predicted lipoprotein signal peptide; Tat/SPII - predicted TAT lipoprotein signal peptide; other (no signal peptide). Likelihood of prediction is indicated in parentheses.

<sup>&</sup>lt;sup>c</sup>Sec/SPII site predicted using alternative translational start site.

CV725_RS00010	HP1527	comH, competence protein	Δ1 bp (708/1440 nt)	Val236fs	95%
CV725_RS00960	HP1274	pflA, paralyzed flagella protein	+G (1428/2406 nt)	Ala477fs	<mark>92.9%</mark>
CV725_RS02305	HP0427	US of <i>hp04</i> 27 (hypothetical protein),	+GTTGGATGATTGG		97.4%
CV725_RS02315	23S rRNA	US of 23S rRNA gene	ATG		
			intergenic (-234/-736)		
mreC	HP1372	mreC, rod shape-determining	codon-220	Tyr220His	97.7%
		protein	( <u>T</u> AC→ <u>C</u> AC)		
CV725_RS02745	HP0098	thrC, threonine synthase	codon-417	Glu417Lys	96.3%
		, , , , , , , , , , , , , , , , , , , ,	( <u>G</u> AA→ <u>A</u> AA)	, ,	
CV725_RS04505	HP0475	modD, molybdenum ABC transport	codon-155	Leu155Leu	96%
		protein	(TT <u>A</u> →TT <u>G</u> )		
CV725_RS04785	HP0838	fapH	codon-18	Val18Ala	84.1%
			(G <u>T</u> C→G <u>C</u> C)		
			Δ515 bp (69-584/618	deletion	
			nt)		
CV725_RS05360	HP0726	DS of hp0726 outer membrane	(T) <sub>20→19</sub>		84.6%
CV725_RS05365	HP0725	protein, US of hopP	intergenic (+121/-173)		
		·	,		
CV725_RS06350	HP0527	cag pathogenicity island protein	codon-936	Thr936Thr	95.6%
		(cag7)	(AC <u>G</u> →AC <u>C</u> )		
			codon-752	Thr752Thr	97.8%
			(AC <u>C</u> →AC <u>G</u> )		
			codon-742	Ala742Ala	98.5%
			(GC <u>T</u> →GC <u>C</u> )		
CV725_RS06500	HP0499	pldA, phospholipase A pseudogene	(G) <sub>10→11</sub>	phase 'off' to	67.1%
			(683/1070 nt)	phase 'on'	
babA	HP1243	US of babA, DS of tRNA_fMet	(T) <sub>13→12</sub>		91.2%
CV725_RS06645	tRNA_fMet	, =	intergenic (-131/+149)		
CV725_RS08550	HP1412	DS of hp1412 (hypothetical protein),	(C) <sub>11→10</sub>		96.8%
queF	HP1413	DS of queF	intergenic (+11/+121)		
,		,	, , , , , , , , , , , , , , , , , , ,		
ΔfapH pfIA* (lab	strain H54. pa	arental strain H16)			ı
CV725_RS00010	HP1527	comH, competence protein	Δ1 bp (708/1440 nt)	Val236fs	98.8%
*CV725 RS00395	HP1451	spollIJ-associated protein	+T (689/798 nt)	Tyr230fs	98.1%
CV725_RS00395 CV725_RS00960	HP1274	pflA, paralyzed flagella protein	+G (1428/2406 nt)	offsetting fs	98.4%
CV725_R300900	ПР 12/4	pina, paratyzeu nagena protein	△1 bp (1391/2406 nt)		
mof	LID4000	DC of mot UC of 5=4000		mutations	98.5%
maf CV725_RS01150	HP1239	DS of <i>maf</i> , US of <i>hp1239</i> (hypothetical protein)	(A) <sub>13→14</sub> intergenic (+61/+394)		80.5%
_	HP1240		codon-220	Turagollic	98.8%
mreC	HP1372	mreC, rod shape-determining protein	codon-220 ( <u>T</u> AC→ <u>C</u> AC)	Tyr220His	90.0%
CV725_RS02745	HP0098	thrC, threonine synthase	codon-417	Glu417Lys	98.9%
	5555		( <u>G</u> AA→ <u>A</u> AA)		30.070
*tlpB	HP0103	tlpB, methyl-accepting chemotaxis	codon-26	Gly26Glu	98.6%
upo	111 0 100	protein	(GGG→GAG)	Oly 2001u	30.070
*0\/705_0000745	HP0298	dppA, dipeptide ABC transporter,	(T) <sub>10→9</sub>	Phe10fs	96.4%
*CV725_RS03745	111 0230	periplasmic dipeptide-binding protein	coding (30/1644 nt)	1 116 1015	30.470
*0./705 300 /0	LD1020		coding (30/1644 nt)	Alo16\/ol	00 50/
*CV725_RS04335	HP1028	hypothetical protein	Codon-16 (G <mark>C</mark> T→G <u>T</u> T)	Ala16Val	98.5%
CV725_RS04505	HP0475	modD, molybdenum ABC transport	codon-155	Leu155Leu	99.1%
3 7 7 Z O_ 1 (O O 7 O O O	' 5-7.5	protein	(TT <u>A</u> →TT <u>G</u> )	Logrooled	00.170
CV725_RS04600	HP0875	US of katA, US of frpB	(A) <sub>5→6</sub>		83.4%
CV725_RS04605	HP0876	OO OI Kath, OO OI IIPB	intergenic (-34/-290)		03.470
CV725_RS04785	HP0838	<i>fapH</i>	codon-18	Val18Ala	99.1%
JV120_N304100	111 0000	тарі і	(G <u>T</u> C→G <mark>C</mark> C)	VaiTOAla	33.170
	<u> </u>	l	( <u>01</u> 0→0 <u>0</u> 0)		1

			Δ515 bp (69-584/618	deletion	
CV725_RS06350	HP0527	cag pathogenicity island protein	nt) codon-752	Thr752Thr	96.2%
CV725_RS06350	HP0527	(cag7)		111/52111	96.2%
		(cagr)	(AC <mark>C</mark> →AC <u>G</u> )	A1-740A1-	00.00/
			codon-742	Ala742Ala	99.3%
01/705 0000500	1100100		(GC <u>T</u> →GC <u>C</u> )		00.00/
CV725_RS06500	HP0499	pldA, phospholipase A pseudogene	(G) <sub>10→11</sub>	phase 'off' to	62.8%
	1104040	110 (/ / 4 50 (/5)) (/4 /	(683/1070 nt)	phase 'on'	00.00/
babA	HP1243	US of babA, DS of tRNA_fMet	$(T)_{13\to 12}$		86.2%
CV725_RS06645	tRNA_fMet		intergenic (-131/+149)		
CV725_RS08550	HP1412	DS of hp1412 (hypothetical protein),	(C) <sub>11→10</sub>		94.6%
queF	HP1413	DS of queF	intergenic (+11/+121)		
familialian acab	 	00.7)			
fapH::kan-sacB	•		1 (1-101-11)	1	T ====:
CV725_RS00720	HP1322	DS of HP1321 conserved	(ATACATAA) <sub>10→5</sub>		99.7%
CV725_RS00725	HP1321	hypothetical ATP-binding protein	intergenic (-194/+7)		
		and US of HP1322 hypothetical			
		protein.			
CV725_RS02305	HP0427	US of hp0427 (hypothetical protein),	+32 bp		90.5%
CV725_RS02315	23S rRNA	US of 23S rRNA gene	intergenic (-234/-736)		
CV725_RS02465	HP1375		(C) <sub>14→13</sub>	restore full-	88.3%
		N-6 DNA methylase	pseudogene (3224/337	length ORF	
			2 nt)		
CV725_RS04600	HP0875	US of HP0875 katA, US of HP0876	(A) <sub>5→6</sub>		94.4%
CV725_RS04605	HP0876	frpB	intergenic (-34/-290)		
CV725_RS04785	HP0838	fapH	codon-18	Asp201Asp	100.0%
			(GA <u>T</u> →GA <u>C</u> )		
			Δ515 bp (69-584/618	deletion	
			nt)		
CV725_RS06350	HP0527	cag pathogenicity island protein	codon-752	Thr752Thr	87.5%
		(cag7)	(AC <u>C</u> →AC <u>G</u> )		
			codon-742	Ala742Ala	82.1%
			(GC <u>T</u> →GC <u>C</u> )		
CV725_RS06500	HP0499	pldA, phospholipase A pseudogene	(G) <sub>10→9</sub>	phase 'off' to	93.7%
			(683/1070 nt)	phase 'off'	
CV725_RS07515	HP1412	DS of HP1412 hypothetical protein	(C) <sub>11→10</sub>		96.0%
queF	HP1413	and DS of queF	intergenic (+11/+121)		
		ental strain H180-7)			
CV725_RS00720	HP1322	DS of HP1321 conserved	(ATACATAA) <sub>10→5</sub>		99.6%
CV725_RS00725	HP1321	hypothetical ATP-binding protein	intergenic (-194/+7)		
		and US of HP1322 hypothetical			
		protein.			
CV725_RS02305	HP0427	US of hp0427 (hypothetical protein),	A→G		86.2%
CV725_RS02315	23S rRNA	US of 23S rRNA gene	intergenic (-235/-735)		
			,		
CV725_RS02465	HP1375		(C) <sub>14→13</sub>	restore full-	92.3%
		N-6 DNA methylase	pseudogene (3224/337	length ORF	
			2 nt)	-	
CV725_RS03080	HP0164	arsS, histidine kinase	(G) <sub>11→12</sub>		80.8%
			coding (1261/1281 nt)		
	l .	I .	<u> </u>	I	1

01/705 500 (000	1100000	THE (HESSE / // HE (HESSE)	I (a)	1	00.00/
CV725_RS04600	HP0875	US of HP0875 katA, US of HP0876	(A) <sub>5→6</sub>		92.8%
CV725_RS04605	HP0876	frpB	intergenic (-34/-290)		
CV725_RS04785	HP0838	fapH	codon-18	Val18Ala	100%
			(G <u>T</u> C→G <u>C</u> C)		
			codon-201	Asp201Asp	99.0%
			(GA <u>T</u> →GA <u>C</u> )		
			Δ515 bp (69-584/618	deletion	100%
			nt)		
CV725_RS06350	HP0527	cag pathogenicity island protein	codon-742	Ala742Ala	82.3%
CV723_N300330	111 0321			Alai 42Ala	02.570
01/705 0000500	1100400	(cag7)	(GC <u>T</u> →GC <u>C</u> )		00.00/
CV725_RS06500	HP0499	pldA, phospholipase A pseudogene	(G) <sub>10→9</sub>	phase 'off' to	93.3%
			(683/1070 nt)	phase 'off'	
CV725_RS07515	HP1412	DS of HP1412 hypothetical protein	<b>(C)</b> <sub>11→10</sub>		98.0%
queF	HP1413	and DS of queF	intergenic (+11/+121)		
ΔfapH (lab strain	H181-9, pare	ental strain H180-7)			
CV725 RS00720	HP1322	DS of HP1321 conserved	(ATACATAA) <sub>10→5</sub>		100%
CV725_RS00725	HP1321	hypothetical ATP-binding protein	intergenic (-194/+7)		10070
07720_11000720	111 1321	and US of HP1322 hypothetical			
		1			
01/705 000005	1100407	protein.	00.1		00.00/
CV725_RS02305	HP0427	US of <i>hp0427</i> (hypothetical protein),	+32 bp		89.3%
CV725_RS02315	23S rRNA	US of 23S rRNA gene	intergenic (-234/-736)		
CV725_RS02465	HP1375		(C) <sub>14→13</sub>	restore full-	84.3%
		N-6 DNA methylase	pseudogene (3224/337	length ORF	
			2 nt)		
CV725_RS04600	HP0875	US of HP0875 katA, US of HP0876	(A) <sub>5→6</sub>		97.1%
CV725_RS04605	HP0876	frpB	intergenic (-34/-290)		
CV725_RS04780	HP0839	outer membrane protein P1 (ompP1)	+30bp	Insertion	100%
		, (ep)	coding (494-523/1764		
			nt		
CV725_RS04785	HP0838	fapH	codon-18	Val18Ala	100%
CV723_N304703	111 0030	Тарт	(G <u>T</u> C→G <u>C</u> C)	VaiTOAla	10076
				A = == 004 A = ==	00.40/
			codon-201	Asp201Asp	99.1%
			(GA <u>T</u> →GA <u>C</u> )		
			Δ515 bp (69-584/618	deletion	100%
			nt)		
CV725_RS06350	HP0527	cag pathogenicity island protein	codon-752	Thr752Thr	82.6%
		(cag7)	(AC <mark>C</mark> →AC <u>G</u> )		
CV725_RS06500	HP0499	pldA, phospholipase A pseudogene	(G) <sub>10→9</sub>	phase 'off' to	95.2%
_			(683/1070 nt)	phase 'off'	
CV725_RS07515	HP1412	DS of HP1412 hypothetical protein	(C) <sub>11→10</sub>		98%
queF	HP1413	and DS of queF	intergenic (+11/+121)		3070
CV725_RS07950	HP1562	iron(III) ABC transporter, periplasmic	Codon-180	Glu180Asp	100%
07720_1\307330	111 1302			GluTouAsp	10070
		iron-binding protein (ceuE)	(GA <u>G</u> →GA <u>T</u> )		
Δhp1456 (lab str					
CV725_RS00365	HP1465	LPP20 family lipoprotein	455 bp→25 bp	Gene	100%
			coding (48-502/528 nt)	deletion	
CV725_RS00720	HP1322	DS of HP1321 conserved	(ATACATAA) <sub>10→5</sub>		98.3%
CV725_RS00725	HP1321	hypothetical ATP-binding protein	intergenic (-194/+7)		
<u> </u>	1	1 7 P Jan	l	I	I

		and US of HP1322 hypothetical protein.			
babA	HP1243	babA	Coding-718 (AGA→CGC)	Arg718Arg	100%
			Coding-719	Arg719Arg	100%
			(AG <u>A</u> →AG <u>G</u> ) Coding-720	Leu720Leu	100%
			(CT <u>C</u> →CT <u>T</u> ) Coding-727	Tyr727Tyr	98.6%
			(TA <u>C</u> →TA <u>T</u> )		
CV725_RS02465		hypothetical protein	(C) <sub>14→13</sub> pseudogene (3224/337 2 nt)	restore full- length ORF	91.8%
hcpE	HP0235	Sel1-like repeat protein HcpE	+CAGGGTGTTTT coding (384/1068 nt)	Frameshift, out of frame	93.7%
pyrG CV725_RS03950	HP0349 HP0350	US of HP0349 <i>pyrG</i> , US of HP0350 hypothetical protein	(A)17→16 intergenic (-94/-161)		91.9%
CV725_RS04600 CV725_RS04605	HP0875 HP0876	US of HP0875 katA, US of HP0876 frpB	(A) <sub>5→6</sub> intergenic (-34/-290)		92.6%
CV725_RS06350	HP0527	cag pathogenicity island protein (cag7)	codon-752 (AC <u>C</u> →AC <u>G</u> )	Thr752Thr	91.5%
CV725_RS06500	HP0499	pldA, phospholipase A pseudogene	(G) <sub>10→11</sub> (683/1070 nt)	phase 'off' to phase 'on'	86.5%
CV725_RS07515 queF	HP1412 HP1413	DS of HP1412 hypothetical protein and DS of queF	(C) <sub>11→10</sub> intergenic (+11/+121)		97.1%
CV725_RS07535	HP1416	lipopolysaccharide 1,2- glucosyltransferase (rfaJ)	Coding-26 (G <u>G</u> C→G <u>A</u> C)	Gly26Asp	99.8%

<sup>&</sup>lt;sup>a</sup>"fs" indicates frameshift

Table S2.3. Proteins identified from third replicate of the co-immunoprecipitation assay with FapH-Myc protein. Not shown due to length of the table. See publication for table.

<sup>&</sup>lt;sup>b</sup>Frequency is the number of times the mutation was identified relative to the total number of reads for that sequence.

<sup>\*</sup>Not found in strain H16.

Displaying mutations that are found in > 80% of reads and any mutations in known flagellar genes.

Secondary flagellar mutations are highlighted in yellow.

			Score	#
Date	Strain	Protein	Mascot	peptides
6.13.23	FapA-myc H116	FapA	75	2
	FapA-myc H116	FlgP	125	4
10.25.23	FapA-myc H116	FapA	1004	8
	FapA-myc H116	HP1456	150	1
3.8.23	FlgP-myc H89	FlgP	1080	10
	FlgP-myc H89	HP1456	216	6
	FlgP-myc H89	FapA	214	6
	FlgP-myc H89	HP1454	68	5
	FlgP-myc H89	HP1457	61	3
11.13.23	FlgP-myc H89	FlgP	1102	13
	FlgP-myc H89	HP1456	555	6
	FlgP-myc H89	HP1454	443	7
	FlgP-myc H89	HP1457	163	3
	FlgP-myc H89	FapA	97	1
12.6.23	FapA-myc H116	FapA	8968	16
	FapA-myc H116	HP1456	2266	11
	FapA-myc H116	FlgP	863	8
	FapA-myc H116	PflC	521	8
	FapA-myc H116	HP1457	474	5
	FapA-myc H116	HP1454	164	3

Table S2.4: Primer list

Primer Name	Primer	Primer sequence
	description	
Primer 35	pGEM-Kan-sacB	5'AATTTTTGTTTGGAAGGAAAAGGCACA3'
	R w urelP OH	
Primer 36	pGEM-Kan-sacB	5'TAAGGAGCGTTGCTCCTAAAAAATCGT3'
	F w ure/P OH	
Primer 37	urelP F w Kan-	5'GCGATAGAGTTTGGCATGGTGTTTGTG3'
	sacB OH	
Primer 38	urelP R w Kan-	5'AAATTGGAGTGATAATGGTGGCCACGA3'
	sacB OH	
Primer 39	flgP US F	5'GCACTATTTTCACTATCATAGGGAT3'
Primer 40	flgP US R	5'GAATTCGATTATCCTCGAGGGCATTTTCCTTAAAATGAGTTCAT3'
Primer 41	flgP DS F	5'GATAATCGAATTCGCTAGCTTTTTTTTGTCTCTTGCTCCAAGCA3'
Primer 42	flgP DS R	5'AGGGTTCGATCCTAATAGCAATTTT3'
Primer 59	hp0838 US F	5'CCCATTTATCCCCCAACCAATTTCA3'
Primer 60	<i>hp0838</i> US R w	5'GAATTCGATTATCCTCGAGTGCTTGGAGCAAGAGGCAAAAAAAA
	linker	

Primer 61	<i>hp0838</i> DS F w	5'GATAATCGAATTCGCTAGCAAGATAATGAAAACGCTGACAGCGA3'
	linker	
Primer 62	hp0838 DS R	5'GAAGCGAGGTTACGACTTTTTGAT3'
Primer 78	flgP US R for myc	5'ATTAAGTTTTTGTTCTCCTCTCGCTCCGCTCAAAATGCGA3'
Primer 79	flgP DS F for	5'AGTGAAGAAGATCTTTAAACTCTCTTACTCTATAATCATGCGG3'
	pHel3-myc	
Primer 159	pflA F w BspQl	5'CCGCTCTTCCATGTGGCTTAAGTCAAAAATCTTTC3'
	ОН	
Primer 160	pflA R w BspQl	5'CCGCTCTTCCGTTATGACTCCTTGTTTTTCAATAAA3'
	ОН	
Primer 162	<i>hp0838</i> F w	5'AAGCTCTTCCATGCGGTATTTTAGAAGTG3'
	BspQI OH	
Primer 163	<i>hp0838</i> R w	5'AAGCTCTTCAACCTTGGAGCTCGCTGTC3'
	BspQI OH for	
	pHel3-myc	
Primer 169	<i>hp0838</i> F w	5'AAGCTCTTCCATGCGGTATTTTAGAAGTGCTTTT3'
	BspQI OH	
Primer 171	<i>hp0838</i> R w	5'AAGCTCTTCTTTATTGGAGCTCGCTGTCAGCGT3'
	BspQI OH	
Primer 195	hp1456 US F	5'TCAGATGTTATTAATGACACCACGC3'
Primer 196	hp1456 US R	5'GAATTCGATTATCCTCGAGGCTGCTATCACACTCATTCCTAAAA3'
Primer 197	hp1456 DS F	5'GATAATCGAATTCGCTAGCAAGAGTTGGGCATGGTTAAAAAGTA3'
Primer 198	hp1456 DS R	5'TATAGGCCTTGCTATACCACTTAGG3'
Primer 200	pHel3 F	5' CTCGGTATAATCTTACCTATCACCT 3'
Primer 201	pHel3 R	5'CCTTTGAGTGAGCTGATACGAATTA3'
Primer 208	hp1454 BACTH F	5'GAGGATCCCGAGCCTAAGTGGTATAGCAA3'
Primer 209	hp1454 BACTH R	5'CGGTACCCGTAGCCCCGTATTGCCTT3'
Primer 210	hp1456 BACTH F	5'GAGGATCCCTGCAGCCATGCCCCAAAATCAG3'
Primer 211	hp1456 BACTH R	5'CGGTACCCGCTTTTTAACCATGCCCAACTCTTCGCG3'
Primer 212	hp0838 BACTH F	5'GAGGATCCCTGCTCCAAGCACCCTTTTTCTAAGC3'
Primer 213	hp0838 BACTH R	5'CGGTACCCGTTGGAGCTCGCTGTCAGCGT3'
Primer 214	hp0837 BACTH F	5'GAGGATCCCTGCAGTCTCTTTAAAAAGCGTAACACT3'
Primer 215	hp0837 BACTH R	5'CGGTACCCGTCCTCGCTCCGCTCAAAA3'
Primer 234	hp1456 US R for	5'aagctcttcaATGAAAAATCAAGTTAAAAAAATTT3'
	myc	
Primer 236	hp1456 DS F for	5'aagctcttcaaccCTTTTTAACCATGCCCAA3'
	pHel3-myc	

**Table S2.5: Strains and Plasmids** 

H. pylori	Relevant genotype	Source
strains		
B128 Wild type (lab	H. pylori B128 wild-type	Richard M.
strain H2)		Peek, Jr.
flgP::kanR-sacB(	H. pylori B128 flgP::kan <sup>R</sup> -sacB	Current
lab strain H5)		study
fapH::kanR-	H. pylori B128 hp0838::kan <sup>R</sup> -sacB	Current
sacB(lab strain H6)		study
ΔflgP (lab strain	H. pylori B128 ΔflgP fliP261; fliP in "off" phase	Current
H14)		study
ΔfapH pflAT (lab	H. pylori B128 Δhp0838 pflA1429; single nucleotide insertion at position 1429	Current
strain H16)	in <i>pflA</i>	study
ΔfapH pflA* (lab	motile variant of H16; Δhp0838 pflA1393; single nucleotide deletion at position	Current
strain H54)	1393 and a single nucleotide insertion at position 1429 in pflA	study
<i>ΔfapH pflA</i> * (lab	motile variant of H16; Δhp0838 pflA1393; single nucleotide deletion at position	Current
strain H55)	1393 and a single nucleotide insertion at position 1429 in pflA	study
<i>ΔfapH pflA</i> * (lab	motile variant of H16; Δhp0838 pflA1393; single nucleotide deletion at position	Current
strain H70)	1393 and a single nucleotide insertion at position 1429 in pflA	study
<i>ΔfapH pflA</i> * (lab	motile variant of H16; Δhp0838 pflA1393; single nucleotide deletion at position	Current
strain H73)	1393 and a single nucleotide insertion at position 1429 in pflA	study
FlgP-myc (lab	H14 bearing plasmid pKR23; FlgP-myc fusion protein expressed from plasmid	Current
strain H89)	pKR23	study
ΔfapH pflAT/pPflA	H16 bearing plasmid pKR50; wild-type pflA allele expressed from plasmid	Current
(lab strain H114)	pKR50	study
ΔfapH	H16 bearing plasmid pKR54; hp0838 expressed from plasmid pKR54	Current
pflAT/pFapH (lab		study
strain H115)		
FapH-myc (lab	H16 bearing plasmid pKR55; HP0838-myc fusion protein expressed from	Current
strain H116)	plasmid pKR55	study
ΔfapH pflA*/pFapH	H54 bearing plasmid pKR54; hp0838 expressed from plasmid pKR54	Current
(lab strain H122)		study
ΔfapH (lab strain	H. pylori B128 hp0838::kan <sup>R</sup> -sacB	Current
H180 -isolate 7)		study
ΔfapH (lab strain	H. pylori B128 Dhp0838	Current
H181 -isolate 4 and		study
9)		
hp1456::kanR-	H. pylori B128 hp1456::kanR-sacB	Current
sacB( lab strain		study
H143)		

Δhp1456 (lab strain	H. pylori B128 Δhp1456	Current
H145)		study
HP1456-myc (lab strain H170)	H145 bearing plasmid pKR119; HP1456-myc fusion protein expressed from plasmid pKR119	
Plasmids	Description or genotype	Source
pKR4	flgP deletion, US, DS, pGEM, amp <sup>R</sup> . Primers 39, 40, 41, 42.	Current
		study
pKR9	flgP deletion, US, DS, Kan-sacB, pGEM, amp <sup>R</sup> . Primers 39, 40, 41, 42.	Current
		study
pKR10	hp0838 deletion, US, DS, pGEM, amp <sup>R</sup> . Primers 59, 60, 61, 62.	Current
		study
pKR11	hp0838 deletion, US, DS, Kan-sacB, pGEM, amp <sup>R</sup> . Primers 59, 60, 61, 62.	Current
		study
pKR23	flgP-myc, pGEM, amp <sup>R</sup> , 3.6kb, Primers 78 and 79.	Current
		study
pKR50	pflA complement in P49, kanR, 8.0kb, primers 159, 160	Current
		study
pKR54	hp0838 complement in P49, kan <sup>R</sup> , 6.1kb, primers 164, 169	Current
		study
pKR55	hp0838-myc (C-term) in P48, kan <sup>R</sup> , 6.1kb, primers 163, 169	Current
		study
pKR67	hp1456 deletion, US, DS, pGEM, ampR. Primers 195, 196, 197, 198	Current
		study
pKR77	hp1456 deletion, US, DS, Kan-sacB, pGEM, ampR. Primers 195, 196, 197, 198	Current
		study
pKR119	HP1456-myc, pGEM in P48, Kan <sup>R</sup> , 6.1kb, Primers 234 and 236	Current
		study
BACTH Strains	Description or genotype	Source
and Plasmids		
E69	DHMI. F-, cya-854, recA1, endA1, gyrA96 (Nal r), thi1, hsdR17, spoT1, rfbD1,	Stéphane
	glnV44(AS).	Benoit
E70	BTH101. F-, cya-99, araD139, galE15, galK16, rpsL1 (Str r), hsdR2, mcrA1,	Stéphane
	mcrB1.	Benoit
pKR62	pKT25 (sequence w M13 F/R), Kan <sup>R</sup> , 3442bp	Stéphane
		Benoit
pKR63	pKNT25 (sequence w M13 F/R), Kan <sup>R</sup> , 3469bp	Stéphane
		Benoit
pKR64	pUT18 (sequence w M13 F/R), Amp <sup>R</sup> , 3023bp	Stéphane
		Benoit

pKR65	pUT18C (sequence w M13 F/R), Amp <sup>R</sup> , 3017bp	Stéphane
pririoo	por roc (osquence winter rivy), rump , correp	Benoit
pKR69	hp1454 in p-GEM w BamHI and KpnI overhangs. Amp <sup>R</sup> , 3.9kb. Primers 208	Current
	and 209.	study
pKR70	hp1456 in p-GEM w BamHI and KpnI overhangs. Amp <sup>R</sup> , 3.5kb. Primers 210	Current
	and 211.	study
pKR71	hp0838 in p-GEM w BamHI and KpnI overhangs. Amp <sup>R</sup> , 3.6kb. Primers 212	Current
	and 213.	study
pKR72	flgP in p-GEM w BamHI and KpnI overhangs. Amp <sup>R</sup> , 3.6kb. Primers 214 and	Current
	215.	study
pKR96	hp0838 digested P71 + pKT25 P62 Kan <sup>R</sup>	Current
		study
pKR97	hp0838 digested P71 + pKNT25 P63 Kan <sup>R</sup>	Current
		study
pKR98	hp0838 digested P71 + pUT18 P64 Amp <sup>R</sup>	Current
		study
pKR99	hp0838 digested P71 + pUT18C P65 Amp <sup>R</sup>	Current
		study
pKR100	hp1456 digested P70 + pKT25 P62 Kan <sup>R</sup>	Current
		study
pKR101	hp1456 digested P70 + pKNT25 P63 Kan <sup>R</sup>	Current
		study
pKR102	hp1456 digested P70 + pUT18 P64 Amp <sup>R</sup>	Current
		study
pKR103	hp1456 digested P70 + pUT18C P65 Amp <sup>R</sup>	Current
		study
pKR104	Positive control pKT25.zip. Kan <sup>R</sup>	Current
		study
pKR105	Positive control pUT18c.zip. Amp <sup>R</sup>	Current
		study
pKR106	flgP digested P72 + pKT25 P62 Kan <sup>R</sup>	Current
		study
pKR107	flgP digested P72 + pKNT25 P63 Kan <sup>R</sup>	Current
		study
pKR108	flgP digested P72 + pUT18 P64 Amp <sup>R</sup>	Current
		study
pKR109	flgP digested P72 + pUT18C P65 Amp <sup>R</sup>	Current
		study
pKR110	hp1454 digested P69 + pKT25 P62 Kan <sup>R</sup>	Current
		study

pKR111	hp1454 digested P69 + pKNT25 P63 Kan <sup>R</sup>	Current
		study
pKR112	hp1454 digested P69 + pUT18 P64 Amp <sup>R</sup>	Current
		study
pKR113	hp1454 digested P69 + pUT18C P65 Amp <sup>R</sup>	Current
		study

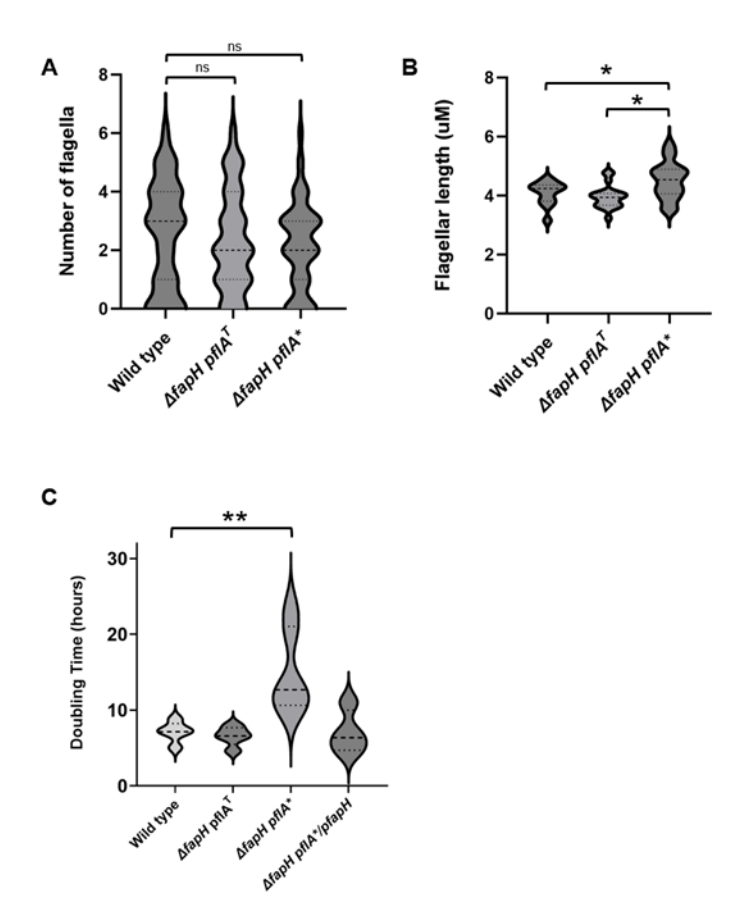


**Figure S2.1.** Characterization of flagellation patterns and growth rates of Δ*fapH pflA*<sup>T</sup> and Δ*fapH pflA*\*. (**A**) Number of flagella per cell for *H. pylori* B128 wild type, Δ*fapH pflA*<sup>T</sup>, and Δ*fapH pflA*\*. Cells were visualized by TEM and the number of flagella per cell (n=100) were counted for each strain. An ANOVA analysis of the data indicated there was no significant difference between the strains in the number of flagella per cell. ns – not significant. (**B**) Lengths of the flagellar filaments were measured using ImageJ. The asterisk (\*) indicates a *p*-value < 0.005. (**C**) Growth rates of *H. pylori* strains in brain heart infusion (BHI) supplemented with 5% heat-inactivated horse serum were determined by measuring OD<sub>600</sub> values of the cultures at various times. Calculated

doubling times for the strains were: wild type B128 - 7.1 h;  $\Delta fapH pflA^T$  - 6.6 h;  $\Delta fapH pflA^*$  - 13.1 h;  $\Delta fapH pflA^*/pfapH$  - 7.0 h. The \*\* indicate a *p*-value < 0.05.

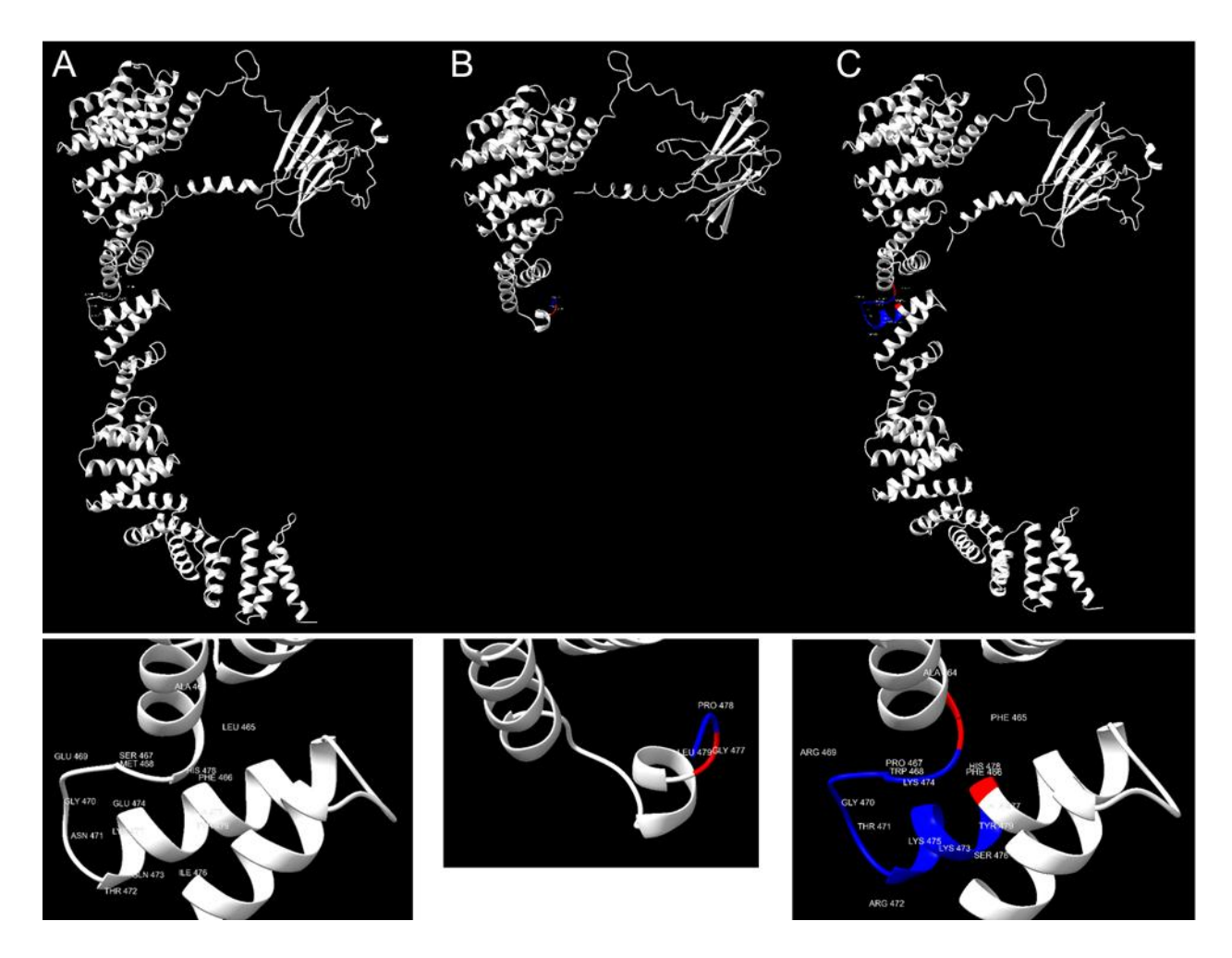


Figure S2.2. Predicted tertiary structures of PfIA, PfIA<sup>T</sup> and PfIA\*. The predicted structures are shown for the native PfIA (**A**), truncated PfIA expressed in  $\Delta fapH$   $pfIA^T$  (**B**), PfIA\* variant expressed in  $\Delta fapH$   $pfIA^*$  (**C**) using AlphaFold (*Jumper et al. 2021*). Close ups of the regions where the PfIA proteins differ are shown below each modeled structure. Red coloring indicates residues where mutations occurred and blue coloring indicates resides that are changed downstream of where the mutations occur.

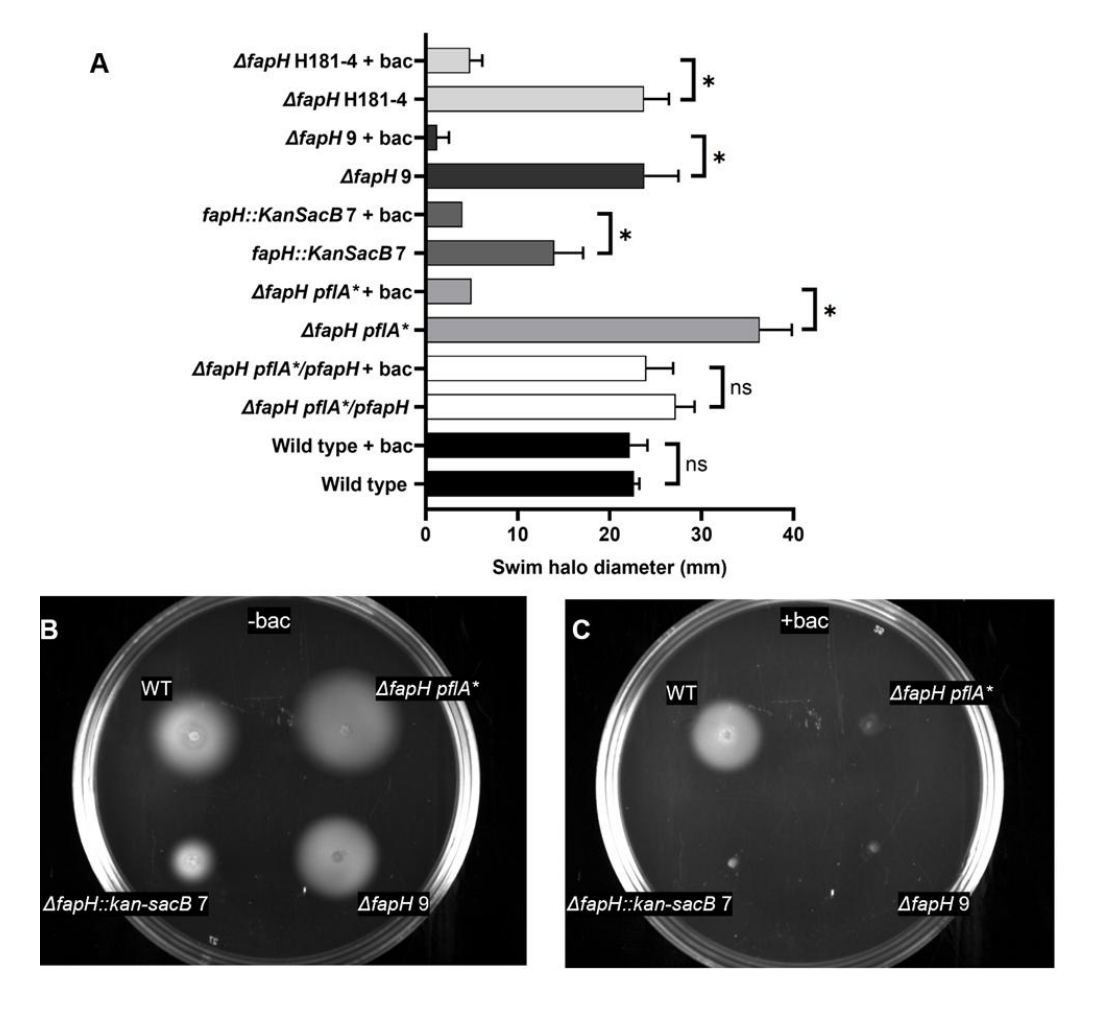
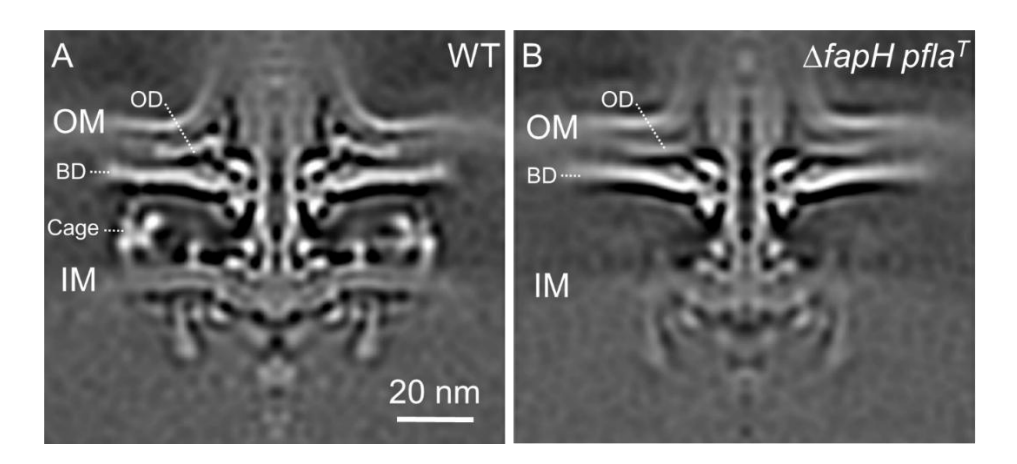
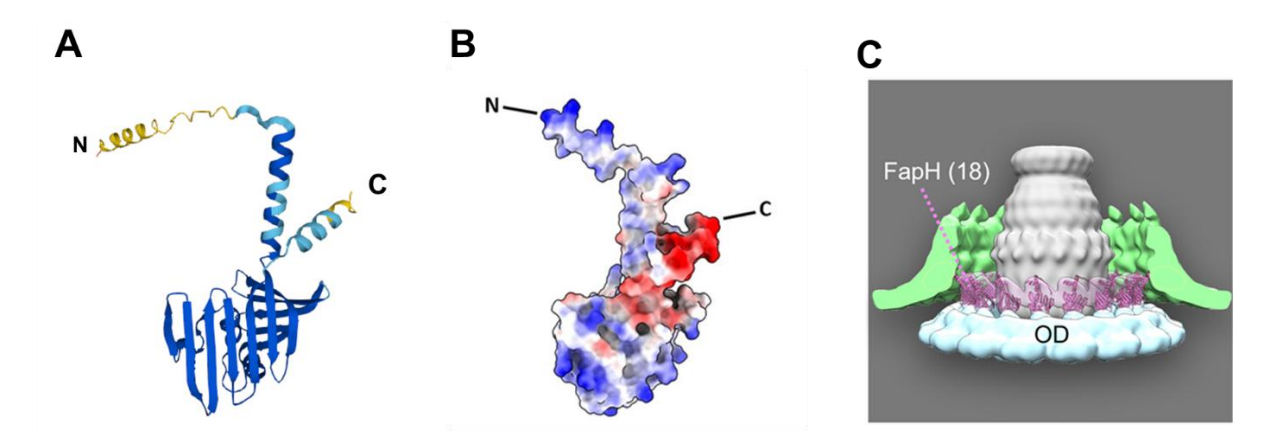


Figure S2.3. Reconstructed Δ*fapH* mutants display sensitivity to bacitracin. (A) *H. pylori* B128 wild type,  $\Delta fapH$   $pflA^*$ , a strain with the kan<sup>R</sup>-sacB cassette inserted into fapH ( $\Delta fapH$ :kansacB 7), and two isolates with unmarked deletions of fapH (designated  $\Delta fapH$  4 and  $\Delta fapH$  9) were stab inoculated into soft agar medium that contained 0 or 200 μg/ml bacitracin and the diameters of the resulting swim halos were measured following a 7-d incubation period. Bars indicate mean values for swim halo diameters and the error bars indicate the SEM. The asterisk indicates statistically significant differences in swim halo diameters as determined using a two-sample t test (p-value <0.0001). At least 5 replicates were done for each sample. (**B** and **C**) Growth and motility of t0.0001). At least 5 replicates were done for each sample. (**B** and **C**) 9 in soft agar medium in the absence (**B**) and presence (**C**) of 200 μg/ml of bacitracin.



**Figure S2.4.** *In-situ* structures of the wild-type and  $\Delta$  *fapH pfIA*<sup>T</sup> motors. Medial slices through *in-situ* structures of *H. pylori* B128 wild type (panel **A**; WT) and  $\Delta$  *fapH pfIA*<sup>T</sup> (panel **B**) motors determined by subtomogram averaging of 786 and 640 particles for wild type and  $\Delta$  *fapH pfIA*<sup>T</sup> motors, respectively. Electron densities corresponding to periplasmic accessory structures are absent in the  $\Delta$  *fapH pfIA*<sup>T</sup> motor. Local refinement variation results in variable appearance of the motors. Basal disk (BD), outer disc (OD), cage, outer membrane (OM), and inner membrane (IM) structures are labeled.



**Figure S2.5. AlphaFold modeling of FapH.** (**A**) Ribbon diagram of predicted FapH structure predicted by AlphaFold (*Jumper et al. 2021*). The N-terminal signal peptide is included in the structure. (**B**) Charge distribution of FapH. Regions of the protein that are dominated by acidic amino acid residues are indicated in red, while regions dominated by basic amino acid residues are indicated in blue. (**C**) Fitting of predicted FapH structure on subunits of FapH ring. The base of the flagellar sheath is shown in green. OD – outer disk.



Figure S2.6. Assessment of protein-protein interactions in BACTH system on MacConkeymaltose agar. The strains on these plates are the ones that are indicated in Figure 5, which shows the results of the  $\beta$ -galactosidase assays for these strains. Strain descriptions are in **Table S5**. Each plate included a positive control (Pos), which was the strain bearing the plasmids that expressed the T25-zip and T18-zip fusion proteins. Each plate also included a negative control (E229), which was the strain bearing the pKT25 and pUT18 BACTH vectors. (A) FapH-FlgP interactions. Strain E233 is a negative control that carries pUT18 and a plasmid expressing the FapH-T25 fusion protein. Strain E173 expresses the T25-FapH and T18-FlgP fusion proteins, strain E172 expresses the FapH-T25 and FlgP-T18 fusion proteins, and strain E171 expresses the FapH-T25 and T18-FlqP fusion proteins. (B) FapH-HP1456 interactions. Strain E236 is a negative control that carries pKT25 and a plasmid expressing the T18-HP1456 fusion protein. Strain E185 express the FapH-T18 and HP1456-T25 fusion proteins, and strain E179 expresses the FapH-T25 and T18-HP1456 fusion proteins. (C) FlgP-HP1456 interactions. Strain E234 is a negative control that carries pUT18C and a plasmid expressing the FlgP-T25 fusion protein. Strain E193 expresses the T18-HP1456 and T25-FlgP fusion proteins, strain E192 expresses the T18-HP1456 and FIgP-T25 fusion proteins, and strain E188 expresses the HP1456-T25 and T18-FIgP fusion proteins. (D) FlqP-HP1454 interactions. Strain E235 is a negative control that carries

pUT18 and a plasmid expressing the HP1454-T25 fusion protein. Strain E219 expresses the FlgP-T18 and T25-HP144 fusion proteins, strain E218 expresses the FlgP-T18 and HP1454-T25 fusion proteins, and strain E216 expresses the T18-FlgP and HP1454-T25 fusion proteins. (**E**) FapH-HP1454 interactions. Strain E204 expresses the FapH-T25 and HP1454-T18 fusion proteins, and strain E196 expresses the FapH-T25 and T18-HP1454 fusion proteins. (**F**) FlgP-FlgP interactions. Strain E234 is a negative control that carries pUT18C and a plasmid expressing the FlgP-T25 fusion protein. Strain E224 expressed the T25-FlgP and FlgP-T18 fusion proteins, strain E223 expresses the T25-FlgP and T18-FlgP fusion proteins, and strain E222 expresses the FlgP-T25 and FlgP-T18 fusion proteins.

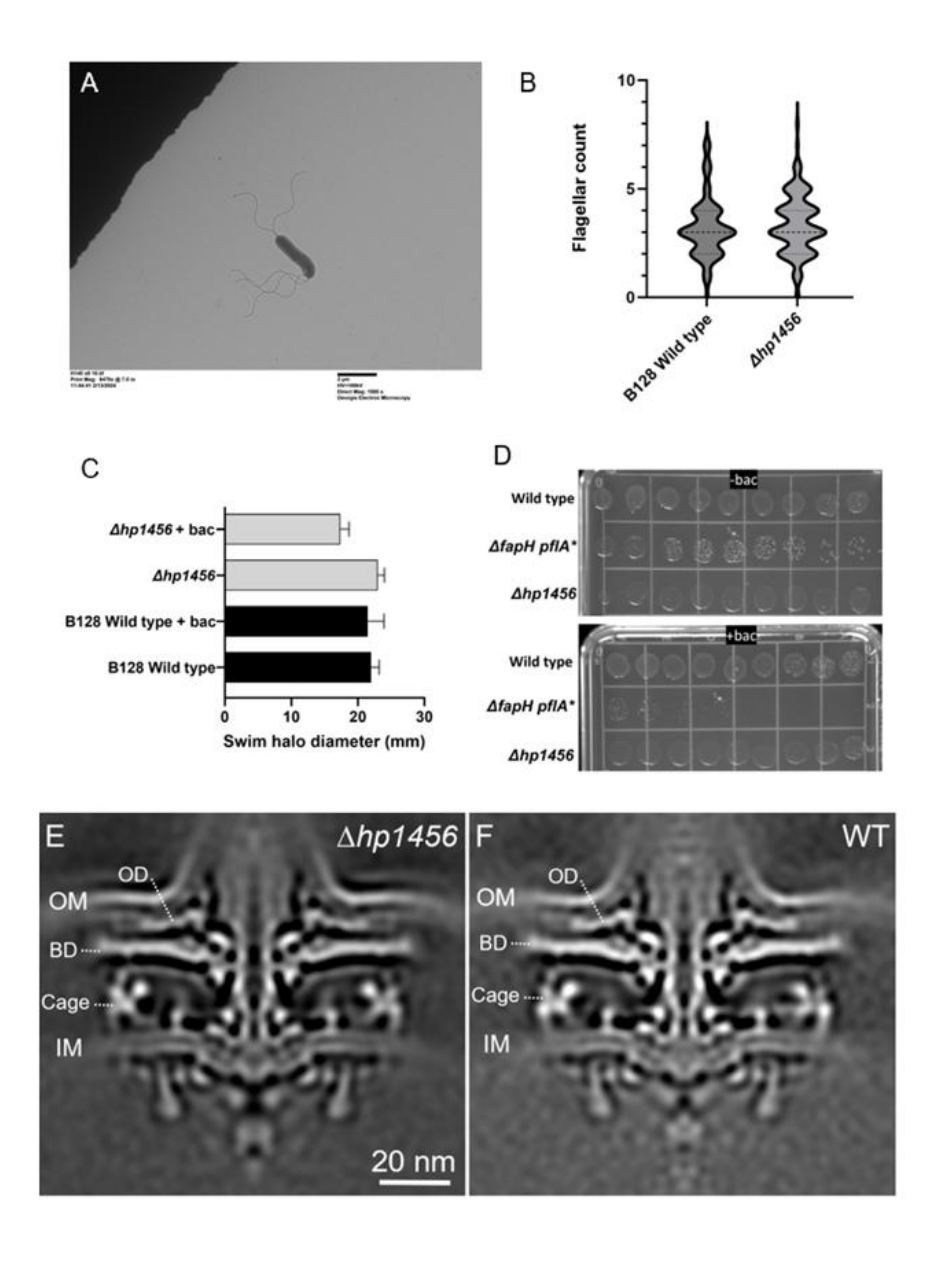
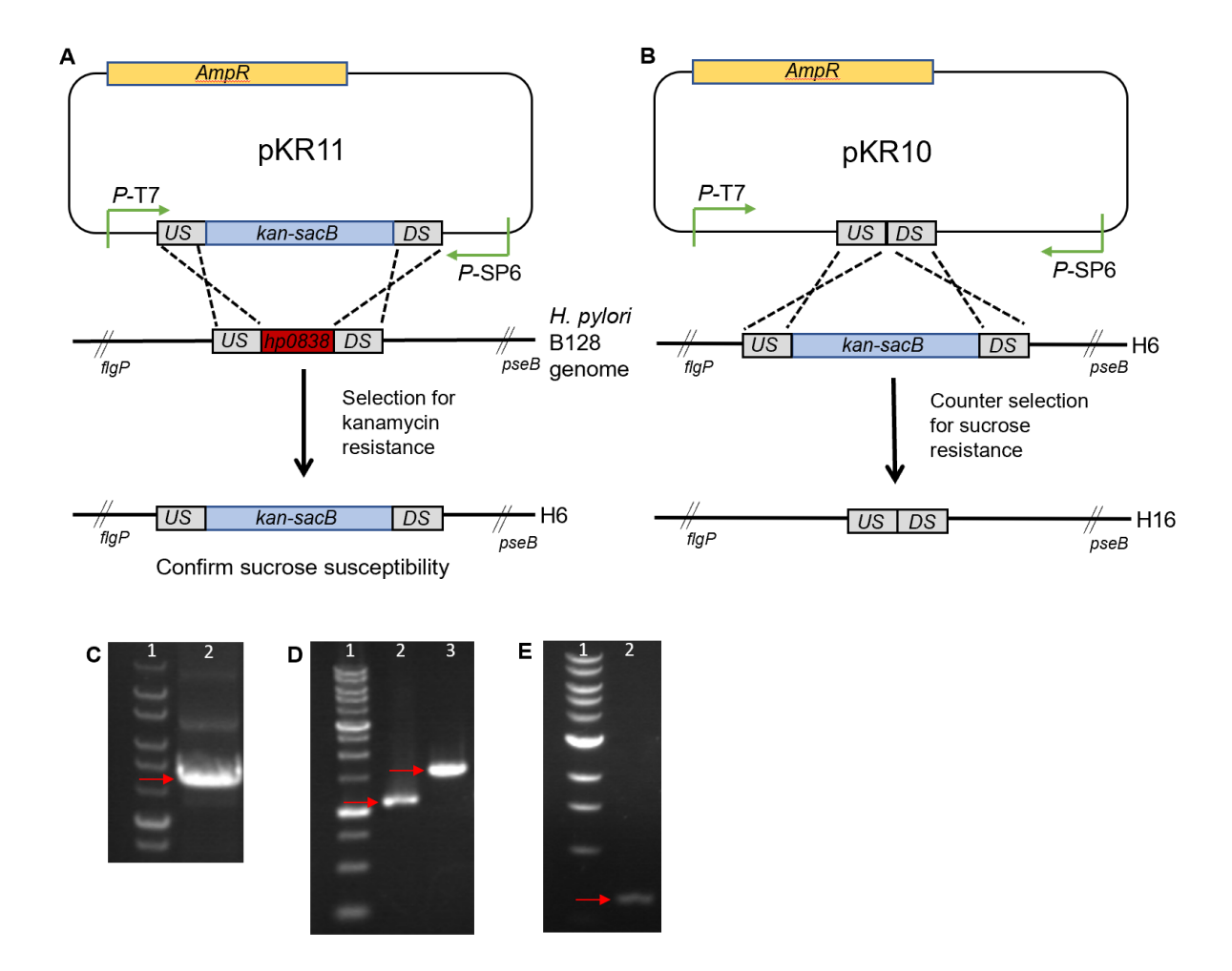


Figure S2.7. Characterization of H. pylori Δhp1456 mutant. (A) TEM of a H. pylori Δhp1456 mutant cell. (B) Cells were visualized by TEM and the number of flagella per cell were counted for each strain (n=80 for wild type, n=129 for  $\Delta hp1456$  mutant). An ANOVA analysis of the data indicated there was no significant difference between the strains in the number of flagella per cell. (C) H. pylori Δhp1456 mutant and B128 wild type were stab inoculated into soft agar medium that contained no bacitracin or 200 µg/ml bacitracin (+ bac) and the diameters of the resulting swim halos were measured following a 7-d incubation period. Bars indicate mean values for swim halo diameters. The average swim halo diameters for the two strains in the absence or presence of bacitracin were not significantly different as determined using a two-sample t test. At least 5 replicates were done for each sample. (D) Efficiency of plating assays with H. pylori  $\Delta hp1456$ mutant and B128 wild type on TSA-HS (-bac) and TSA-HS supplemented with 200 µg/ml bacitracin (+bac). Cells from freshly grown cultures of the strains were resuspended in tryptic soy broth to the same cell densities. Ten-fold serial dilutions of the resuspensions (10<sup>o</sup> to 10<sup>-8</sup>) were then spotted onto the media, and the cultures were incubated for 7 d. (E and F) Medial sliced view of subtomogram averaged in-situ structures of flagellar motors from  $\Delta hp1456$  mutant (E) and wildtype H. pylori B128 (F). OD - outer disk, BD - basal disk, OM- outer membrane, IM - inner membrane.



**Figure S2.8. Construction of the** *H. pylori* B128 Δ*fapH* mutant. (A and B) Construction of an unmarked deletion in *hp0838*. In strain H6, *hp0838* has been replaced with the kan<sup>R</sup>-sacB cassette (A), which was replaced with the unmarked deletion of *hp0838* to generate strain H16 (B). (C) The arrow indicates the predicted 4-kbp PCR product in lane 2 resulting from amplification of region around *hp0838* using gDNA from strain H6 and primers 59 and 62. Goldbio 1kbp DNA ladder is shown in the lane 1. (D) Arrows indicate PCR products of expected sizes resulting from amplification of region around *hp0838* in strains H16 (lane 2; expected size 1 kbp) and H2 (lane 3; expected size 1.5 kbp) using primers 59 and 62. Goldbio 1kb DNA ladder is shown in lane 1. (E) PCR with H122 (lane 1) using primers 169 and 171. NEB 1kDa DNA ladder. 618 bp band (H122). gDNA PCR products were confirmed by sequencing (Eton Biosciences).

### Α

#### BamHI

### В

#### BamHI

### C

ggt tet get gge age get gea ggg tea ggt gaa ttt gaa eaa aaa ett ate tet gaa gaa G S A G S A A G S G E F E Q K L I S E E gat ett gat gae gat gae aaa taa D L D D D K -

Figure S2.9. DNA sequences of the insertions in plasmid pHel3 to generate plasmids pHel3-GG and pHel3-myc. (A) The DNA sequence was synthesized and inserted into the BamHI and Xhol sites of the H. pylori shuttle vector pHel3 (Heuermann and Haas 1998) by Azenta Life Sciences to create plasmid pHel3-GG. Sequence in red contains the predicted promoter for fliF in H. pylori 26695. Sequence between Nhel and Ncol sites is the Shine-Dalgarno sequence from H. pylori 26695 ureA. Tandem BspQ1 sites are indicated in blue, with the underlined sequence corresponding to the BspQ1 site on the top strand and the italicized sequence corresponding to the BspQ1 site on the bottom strand. Start codon for the cloned gene of interest is within the Ncol site and the stop codon is indicated in green. The sequence introduces a unique Nhel site that can be used in conjunction with the unique BamHI for switching the promoter in the vector. (B) The DNA sequence was synthesized and inserted into the BamHI and XhoI sites of the H. pylori shuttle vector pHel3 by Azenta Life Sciences to create plasmid pHel3-myc. In addition to the features described for pHel3-GG, the synthetic DNA introduced a coding sequence for a flexible glycine- and serine-rich linker (Waldo et al. 1999), c-myc epitope, and a DDDDK epitope between the tandem BspQI sites (indicated in blue) and stop codon (indicated in green). (C) Nucleotide and amino acid sequences for flexible linker (amino acid sequence in purple), c-myc epitope (amino acid sequence in red), and DDDDK epitope (in blue).

### **Chapter 2 Appendix**

In addition to the data presented above on the characterization of FapH, I carried out a number of additional studies on FapH that are summarized in the following section. These studies included: (i) using the BACTH assay to examine protein-protein interactions for flagellar motor proteins that are localized closely to the FapH ring; (ii) using formaldehyde crosslinking in co-IP assays to identify FapH interaction partners; (iii) examining the transcriptomes of  $\Delta$  fapH pfIA\* and  $\Delta$  fapH pfIAT by RNA-seq; and (iv) modeling interactions of FapH with other proteins using AlphaFold 2.

## Examining interactions between known and potential flagellar motor proteins using the BACTH system

In addition to using the BACTH system to examine interactions between FapH, FlgP, HP1454, and HP1456 (**Fig. 2.5**), I expanded the scope of the study to assess protein-protein interactions involving FlgH, FlgI, FlgQ, and HP1457. FlgH and FlgI were chosen for these studies since they form the LP-ring, which is relatively close to the FapH ring (**Figs. 1.4**, and **2. 4**). FlgQ was chosen for the studies since it appears to be required for assembly of the basal disk in *C. jejuni* (**Beeby et al. 2016**) and therefore may interact with FlgP or other motor accessory proteins. HP1457 is an uncharacterized predicted lipoprotein and was chosen for the studies since itwhich was identified as a potential FapH interaction partner in the co-IP experiments (**Table S2.3**).

*E. coli* strains bearing combinations of plasmids expressing the *H. pylori* proteins fused to the adenylate cyclase T25 or T18 fragments were streaked on MaConkey agar supplemented with 1% maltose. Nearly all of the strains were a beige color (**Fig. A2.1A**), indicating no interaction between the *H. pylori* proteins. Some combinations resulted in pink colonies due to strong interaction between the proteins, such as Flgl-Flgl and FlgH-FlgH, while others had a faint pink color such as Flgl-FapH and HP1457-HP1457. The strong self-interactions between Flgl and FlgH makes sense as such interactions are involved in assembly of the LP-ring. All of the combinations

that elicited a pink color, as well as some that did not to serve as negative controls, were assessed further by measuring the  $\beta$ -galactosidase activity. **Figure A2.1B** shows the results of these assays with each protein fusion indicated as Protein 1 or Protein 2. Unfortunately, very few of the combinations resulted in a statistically significant result in the assay. The only combinations that resulted in  $\beta$ -galactosidase activities significantly higher than background were those that involved FlgI-FlgI, FlgH-FlgI, or HP1457-HP1457 combinations. FlgQ failed to interact with any protein in the BACTH system, including itself.

There are a number of possible reasons for the failure to observe protein interactions in the BACTH assay, including issues with protein expression, stability, and folding. The most likely explanation, however, may be that the proteins examined do not interact *in vivo*.

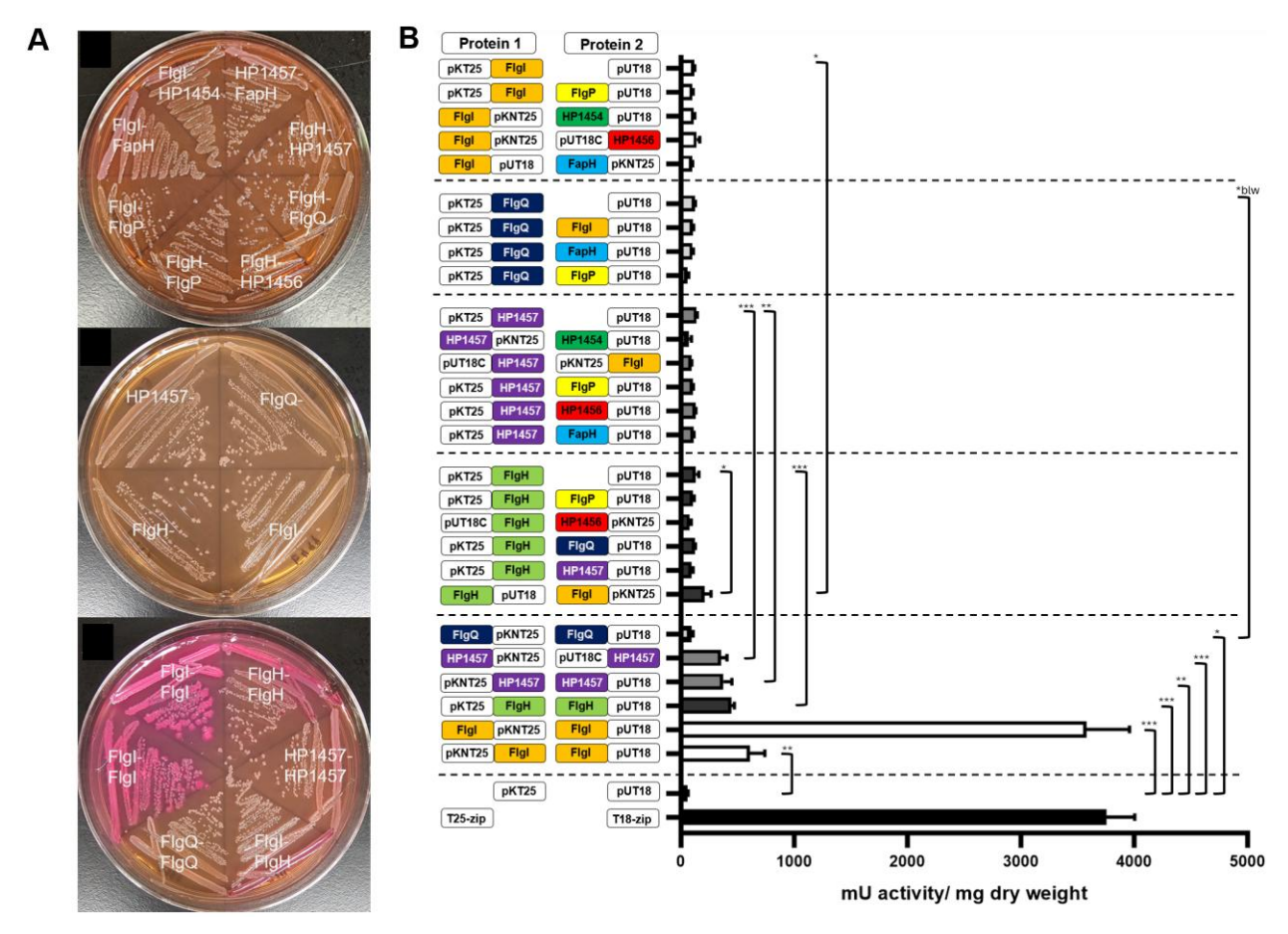


Figure A2.1. Assessing interactions various known and potential flagellar motor proteins using the BACTH system. (A) protein-protein co-transformants isolation streaked to MaConkey agar with 1% maltose. Interacting proteins display a pink color, while proteins that do not interact appear colorless. (B) Results from β-galactosidase assays for strains with select combinations of adenylate cyclase T15 and T25 fragments and fused to FapH, FlgP, HP1454, HP1456, FlgH, FlgI,

HP1457, FlgQ. The cartoons shown on the y-axis illustrate the orientation of the adenylate cyclase fragments and H. pylori proteins in the fusion proteins relative to each other. FlgH – light green, FlgI – orange, FapH – light blue, FlgQ – dark blue, FlgP – yellow, HP1454 – green, HP1456 – red, HP1457 – purple. pKNT25 and pKT25 indicate the adenylate cyclase T25 fragment at the N-terminus or C-terminus of the fusion protein, respectively. pUT18 and pUT18C indicate the adenylate cyclase T18 fragment at the N-terminus or C-terminus of the fusion protein, respectively. An E. coli strain containing the BACTH vectors pKT25 andpUT18 served as a negative control, and an E. coli strain bearing plasmids that expressed the T25-zip andT18-zip proteins served as a positive control. The bars indicate the average β-galactosidase activity for each strain and the error bars indicate the SEM. At least 3 replicates were done for each sample.T25.zip and T18-zip represent the positive control. \*\*\* indicates a P-value of <0.0001, \*\* indicates a P-value of <0.001, \* indicates a P-value of <0.005.

## Incorportating formaldehyde cross-linking in the co-IP assay to search for FapH interaction partners

Formaldehyde crosslinking is a technique used to study protein-protein interactions by covalently linking interacting proteins in close proximity within a cell. Formaldehyde is small and highly reactive and can penetrate the cell membrane. It works by forming methylene bridges between the amino groups (such as lysine residues) of proteins that are spatially close. These covalent bonds freeze the interactions, preserving the native protein complexes. The crosslinked proteins can then be extracted and analyzed including by methods such as immunoprecipitation. Formaldehyde crosslinking is mainly used in chromatin immunoprecipitation (ChIP) to examine protein-DNA and protein-protein interactions *in vivo*.

Whole cell lysates from FapH-myc and WT samples were treated with formaldehyde to examine protein-protein interactions. The co-IP assay (**Chapter 2, Materials and Methods**) was modified to include a a formaldehyde incubation and glycine quench. The whole cell lysate was incubated with 0.5% formaldehyde for 30 minutes at room temperature then quenched by the addition of glycine to a final concentration of 200 mM. 1.2 M glycine. Following the glycine quench, the protocol continued as previously described (**Chapter 2, Materials and Methods**).

The results of the crosslinking experiment were two new bands in the FapH-myc X-link lane when viewed after a Western blot (Fig. A2.2). The bands were not seen on the SDS-PAGE

gel with Coomassie staining. FapH-myc appears as a ~20kDa band and the new faint bands are at ~45kDa and ~50kDa. The lower band could be FapH interacting with itself, while the upper band is likely FapH interacting with a slightly larger unidentified protein. Alternatively, the lower band may be FapH interacting with the slightly smaller FlgP or HP1456, and the upper band may be FapH interacting with itself. In this case the bands could appear larger because of how the gel ran. Since the bands were not visible with Coomassie staining we were unable to excise the bands and submit them for protein fingerprinting to identify the proteins in the bands.

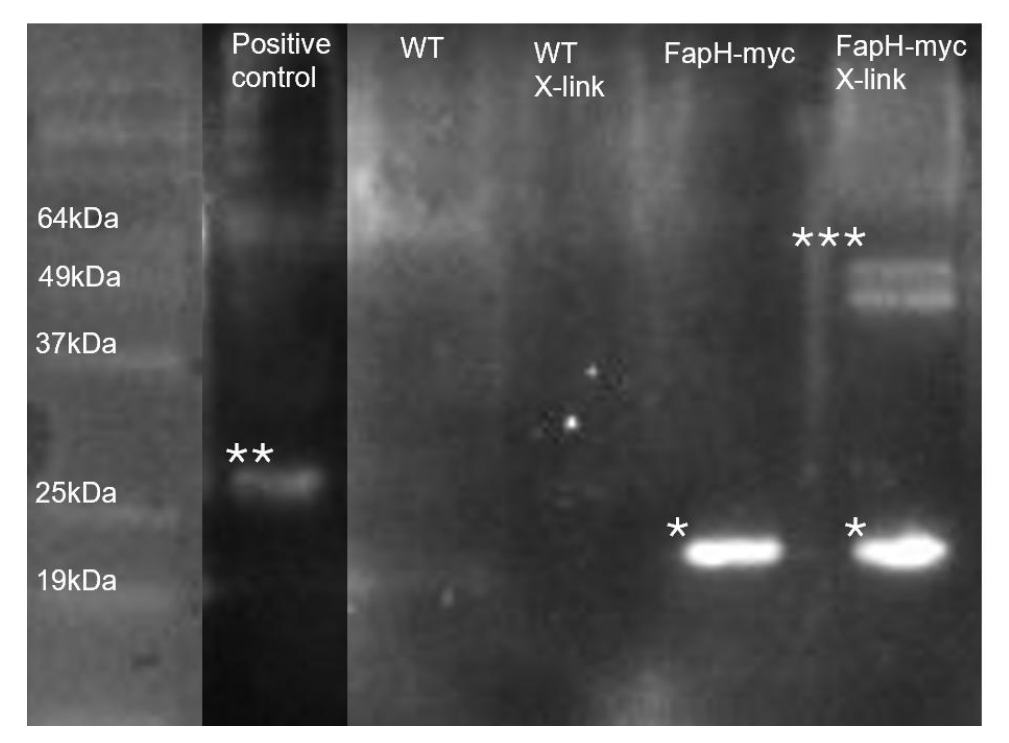


Figure A2.2. Results from co-IP assay following FapH-myc formaldehyde cross-linking. Western blot of an SDS-PAGE gel of the results of a co-immunoprecipitation assay with FapH-myc cell lysates with formaldehyde incubation. \*\*\* indicates two bands that are seen in the FapH-myc sample that was exposed to formaldehyde. The contents of these bands are unknown. \*\* indicates the positive control *E. coli* protein of a known size (**Fig. 2.5**). \* Indicates FapH as confirmed by Coomassie staining. Formaldehyde crosslinking of the wild type whole cell lysate did not produce any new bands.

## Comparision of the $\Delta fapH$ $pflA^*$ and $\Delta fapH$ $pflA^T$ transcriptomes

To examine how the loss of fapH in H. pylori cells with functional flagella impacted global gene regulation, we compared the transcriptome of the motile  $\Delta fapH pfIA^*$  (H54) with those of the non-motile  $\Delta fapH$   $pflA^T$  (H16) and wild-type H. pylori B128 (H2). For the transcriptome comparisons, three biological replicates were used for each strain to prepare RNA samples for RNA-seq assays and subsequent analysis. H. pylori strains WT,  $\Delta fapH$   $pflA^T$ , and  $\Delta fapH$ pfIA\*were grown to mid-log phase (OD<sub>600</sub> ~0.5) in BHI supplemented with 5% heat-inactivated horse serum. RNA was purified using the Direct-zol RNA MiniPrep Plus kit (Zymo Research). RNA concentrations were determined using Qubit 4. RNA samples were submitted to the SegCenter (Pittsburgh, PA), where cDNAs were prepared from the RNA samples and sequenced, and the DNA sequencing data were further processed by the SeqCenter as follows. Quality control and adapter trimming was performed with bcl-convert, which is a proprietary Illumina software used to convert bcl files to basecalls. Read mapping was performed with HISAT2 (Kim et al. 2019). Read quantification was performed using Subread's featureCounts functionality (Liao et al. 2014). Read counts loaded into R (R Core Team 2020) and were normalized using edgeR's (Robinson et al. 2010) Trimmed Mean of M values (TMM) algorithm. Subsequent values were then converted to counts per million (cpm). Differential expression analysis was performed using edgeR's exact test for differences between two groups of negative-binomial counts with an estimated dispersion value of 0.1.

The SeqCenter identified 49 genes that were differentially expressed (differentially expressed genes; DEGs) in  $\Delta fapH$   $pflA^*$  versus wild type (WT) and 43 DEGs in  $\Delta fapH$   $pflA^*$  compared to  $\Delta fapH$   $pflA^T$ . For many of the identified DEGs, however, the false discovery rate (FDR) was high due to outliers in the biological replicates. The FDR refers to the estimated likelihood that a gene identified as differentially expressed is not truly different between the groups. For example, an FDR of 0.05 means that there is a 5% chance that a gene that was identified as differentially expressed is a false positive. Therefore, wedefined DEGs initially as ones that had an FDR of  $\leq 0.05$ . Nine DEGs were identified in the comparison of  $\Delta fapH$   $pflA^*$  versus WT, and six DEGs were identified in the comparison of  $\Delta fapH$   $pflA^T$  using this criterion (**Table A2.1**). The p-values for the statistical analysis of sequencing data for these

genes were <0.0003, and fold-change values for the normalized read counts of the genes ranged from ~2.5-fold to ~9-fold. Only one of the DEGs, *hofH* (encodes a β-barrel outer membrane protein), was found in both comparisons (**Table A2.1**). As expected, one of the DEGs identified in the comparison of  $\Delta fapH$   $pflA^*$  versus WT was fapH (**Table A2.1**). Using a lower stringency for the FDR ( $\leq$ 0.16) and a p-value of  $\leq$ 0.005 expanded the number of DEGs to 20 and 14 in the comparison of  $\Delta fapH$   $pflA^*$  with WT and  $\Delta fapH$   $pflA^T$ , respectively (**Table A2.1**). All of these DEGs were identified in the analysis done by the SeqCenter. In the expanded list of DEGs, the number of DEGs that were in common in the two comparisons increased to six. These six genes are *hofH*, CV725\_00055, hp1070, hp1521, mltD, and lptB; the first two genes were down-regulated in  $\Delta fapH$   $pflA^*$  and the last four genes were up-regulated in  $\Delta fapH$   $pflA^*$  (**Table A2.1**). For both the high stringency FDR and the lower stringency FDR groups, the read counts for the DEGs in the biological replicates were uniform and did not have obvious outliers (**Table A2.2**).

Many of the genes that were differentially expressed in  $\Delta fapH$  pflA\* versus WT and/or  $\Delta fapH pfIA^{T}$  are involved in cell envelope assembly or maintenance. The altered expression of these genes in  $\Delta fapH pflA^*$  likely reflects a response of the strain to OM stress. Four of the DEGs (hopA, hopQ1, hopQ2, and hofH) encode β-barrel OM proteins. Three of the DEGs encoding OM proteins (hopQ1, hopQ2, and hopA) were up-regulated in  $\Delta$ fapH pflA\* compared to  $\Delta$ fapH pflAT, while hofH was down-regulated in  $\Delta fapH$  pflA\* compared to both WT and  $\Delta fapH$  pflAT (**Table** A2.1). HopQ1, HopQ2, and HopA each have a predicted extracellular SabA adhesion domain that functions as sugar-binding adhesion domain for attachment to host cells (*Paraskevopoulou* et al. 2021). HopQ1 recognizes isoforms of the carcinoembryonic antigen-related cell adhesion molecule family (CEACAM) as host cell receptors (Koniger et al. 2016, Jahaheri et al. 2016). Binding of HopQ to CEACAM receptors facilitates the delivery of cytotoxin-associated antigen A into epithelial cells, which results in the secretion of inflammatory cytokine IL-8. While we did not have the SeqCenter prepare a comparative analysis of the WT and  $\Delta fapH pfIA^T$  transcriptomes, hopQ1, hopQ2, and hopA appear to be down-regulated in  $\Delta$ fapH pflA<sup>T</sup> compared to WT (average cpm for hopQ1 in  $\Delta$ fapH pflA<sup>T</sup> was 905 ± 185 versus 2425 ± 454 in WT; average cpm for hopQ2 in  $\Delta$ fapH pflA<sup>T</sup> was 1016 ±281 versus 2833 ± 342 in WT; and average cpm for hopA in  $\Delta$ fapH  $pflA^{T}$  was 1036 ± 349 versus 2993 ± 1087 in WT). Given that  $\Delta fapH$   $pflA^{T}$  has paralyzed flagella, these findings suggest that expression of hopQ1, hopQ2, and hopA is up-regulated in cells that have functional flagella, which may be a strategy that planktonic H. pylori cells use to promote attachment to host epithelial cells.

Additional genes involved in cell envelope assembly or maintenance included *lptB*, *algC*, *hp0350*, *hp1162*, and *mltD*. *lptB*, which was up-regulated in  $\Delta$ *fapH pflA*\* in both transcriptome

comparisons, encodes the ATPase component of an ABC transporter that extracts LPS molecules from the inner membrane for transport to the OM (*Ruiz et al. 2008, Narita and Tokuda 2009*). It is possible that *lptB* is up-regulation of *lptB* in ΔfapH pflA\* to restore the lipid homeostasis of the OM. IptB is immediately upstream of and in an operon with rpoN, which encodes the alternative sigma factor RpoN that is required for transcription of a subset of *H. pylori* flagellar genes (*Neihus* et al. 2004). rpoN was up-regulated in  $\Delta fapH$  pflA\* compared to  $\Delta fapH$  pflA<sup>T</sup> (Table A2.1). Consistent with the up-regulation of *rpoN* in Δ*fapH pflA*\*, some RpoN-dependent flagellar genes (flaB, flqE, flqL, and flqK) were also up-regulated slightly, although the FDR values for these genes were above the 0.16 cutoff. FlaB is a minor flagellin, and increased expression of FlaB in ΔfapH pflA\* may have accounted for the longer flagellar filaments observed for this strain (Fig. S2.1B). hp0350 was down-regulated in  $\Delta$ fapH pflA\* compared to WT (**Table A2.1**). HP0350 is one of four predicted PAP2 enzymes (type 2 phosphatidic acid phosphatases) found in H. pylori, although the physiological role of HP0350 is unknown and Gasiorowski and co-workers were unable to identify activity of the enzyme on any of the substrates they tested (Gasiorowski et al. 2019). algC, which was up-regulated in  $\Delta fapH$  pflA\* compared to  $\Delta fapH$  pflAT (**Table A2.1**), is involved in fucose biosynthesis in H. pylori and knocking out the gene results in truncated LPS (Liu et al. **2022**). hp1162, which was also down-regulated in  $\Delta$ fapH pflA\* compared to WT (**Table A2.1**), encodes a DedA superfamily protein. DedA family members have roles in flipping both GPLs and the lipid carrier undecaprenyl phosphate across lipid bilayers (Roney and Rudner 2023, Li et al. **2021**). Similar to the altered expression of *lptB* in  $\Delta$ *fapH pflA*\*, the down-regulation of *hp1162* may have been in response to restoring lipid homeostasis of the OM. Finally, MltD is a lytic murein transglycosylase, and these enzymes catalyze the the non-hydrolyic cleavage of the glycosidic bond between the N-acetylmuramic acid and N-acetylglucosamine subunits in peptidoglycan, and have roles in cell wall synthesis, remodeling, and degradation (*Dik et al. 2017*).

Other DEGs of interest included ftsH and hp1070, which is immediately downstream of ftsH, both of which were up-regulated in  $\Delta fapH$   $pflA^*$  (**Table A2.1**). FtsH is an integral membrane, ATP-dependent zinc metallopeptidase that degrades a set of short-lived proteins as well as misassembled membrane proteins (*Langklotz et al. 2012*). HP0170 is a small protein (84 amino acids) of unknown function that possesses a single TM helix. The up-regulation of ftsH in  $\Delta fapH$   $pflA^*$  may have been in response to cell envelope stress in the strain. Additional DEGs of interested included hp0963, hp0965, and hp0966, three genes that encode dynamin-like proteins. Each of these genes were down-regulated in  $\Delta fapH$   $pflA^*$  compared to  $\Delta fapH$   $pflA^T$  (**Table A2.1**). Dynamins and dynamin-like proteins are GTPases that have roles in various processes in eukaryotes, including budding of transport vesicles, division of organelles, and cytokinesis

(*Praefcke and McMahon 2004*). Based on the cpm values for these genes, they appear to be expressed at relatively low levels (**Table A2.1**). The physiological roles of dynamin-like proteins in bacteria are poorly understood, but they have been found to facilitate membrane vesicle-aassociated toxin secretion in *E. coli* (*Michie et al. 2014*) and counteract membrane stress resulting from exposure to antibiotics and phage in *Bacillus subtilis* (*Sawant et al. 2016*). If the *H. pylori* dynamin-like proteins play a role in counteracting membrane stress, it is somewhat counterintuitive why these genes would be down-regulated in  $\Delta fapH pflA^*$ .

Transcript levels of three of the genes identified as differentially expressed (*lptB*, *hp0586*, and *mltD*) were examined by qRT-PCR to confirm the results of the RNA-seq analysis. RNA was prepared as described above. cDNA was synthesized with the iScript cDNA Synthesis Kit (Bio-Rad). RT-qPCR was performed using a 7500 Fast Real-Time PCR System (Applied Biosystems, Waltham, MA) and the FastSYBR Green Master Mix (Applied Biosystems).  $\Delta\Delta$ Ct was used as previously described to plot the data (*Livak and Schmittgen 2001*). Primers used are listed in **Table A2.3** Analysis of the RNA samples prepared from  $\Delta$ fapH pflA\*,  $\Delta$ fapH pflA<sup>T</sup>, and WT by qRT-PCR confirmed that the levels of *lptB*, *hp0586*, and *hp1572* transcripts were elevated in  $\Delta$ fapH pflA\* (**Fig. S3**).

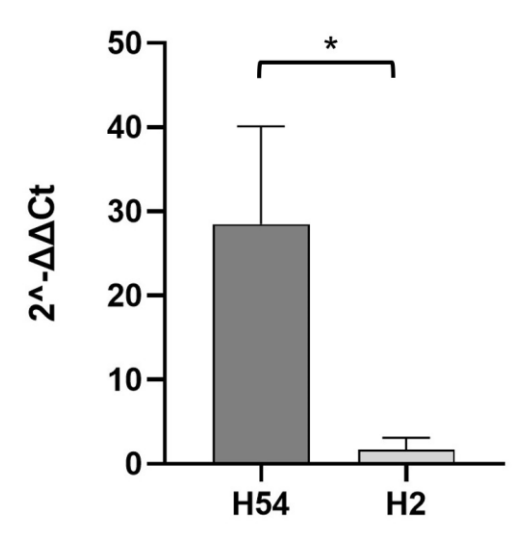


**Figure A2.3.** RT-qPCR with *IptB*. qPCR was performed using primers 243 and 244 to amplify 150 bp of hp0715 using samples with an OD<sub>600</sub> of 0.5-0.7. The samples with the highest and lowest values were removed from the graph. The ΔΔCt method was used as previously described (*Livak and Schmittgen 2001*) with rpoA (hp1263) used as the control gene, WT used as the control strain, and  $\Delta fapH pfIA^*$  used as the experimental strain.

Table A2.1. Genes that are differentially expressed in  $\Delta fapH pflA^*$ .

Locus tag	Gene	Description	<sup>a</sup> log₂FC	<i>p</i> -value	<sup>b</sup> FDR
∆fapH pflA* ve	rsus wild ty	/pe			
CV725_04785	fapH	motor accessory protein FapH	1.83	8.44E-06	0.00925
CV725_02335		adenine-specific DNA methyltransferase	3.01	1.94E-05	0.00925
CV725_00020	hp1526	exodeoxyribonuclease III	2.14	2.35E-05	0.00925
CV725_01560	hofH	outer membrane protein	3.19	2.36E-05	0.00925
CV725_02330		restriction endonuclease	2.72	4.10E-05	0.0128
CV725_00055		DUF4065 domain-containing protein	1.58	7.63E-05	0.0199
CV725_00045	hp1521	type III restriction enzyme	-2.07	1.62E-04	0.0327
CV725_06150	hp0565	DUF417 domain-containing protein	-1.82	1.67E-04	0.0327
CV725_07915	mltD	lytic transglycosylase	-1.31	2.10E-04	0.0367
CV725_04120	hp1070	hypothetical protein	-0.98	3.50E-04	0.0548
CV725_03770	appD	dipeptide ABC transporter	-1.28	5.93E-04	0.0844
CV725_04125	ftsH	metalloprotease	-1.06	7.06E-04	0.0884
CV725_01675		nuclease, psuedogene	-1.11	7.34E-04	0.0884
CV725_03760	dppB	dipeptide ABC transporter	-1.34	9.41E-04	0.104
CV725_04190	hp1057	outer membrane β-barrel protein	1.23	9.92E-04	0.104
CV725_01585	hp1162	DedA family protein	0.86	1.55E-03	0.149
CV725_03955	hp0350	phosphatidic acid phosphatase family protein	0.86	1.61E-03	0.149
CV725 05415	lptB	LPS export ABC transporter	-1.38	1.83E-03	0.156
CV725_05965	hp0600	ABC transporter, ATP-binding protein	1.22	1.89E-03	0.156
CV725_02235	dnaK	protein chaperone	1.44	2.03E-03	0.159
ΔfapH pfIA* ve	rsus ∆ <i>fapH</i>	pfIA <sup>T</sup>			
CV725_01515	hopQ-1	outer membrane protein	-2.48	4.47E-06	0.00618
CV725_05385	hopQ-2	outer membrane protein	-2.67	7.89E-06	0.00618
CV725_03410	hopA	outer membrane protein	-2.86	2.34E-05	0.0122
CV725_00055	•	DUF4065 domain-containing protein	1.60	6.96E-05	0.0273
CV725_01560	hofH	outer membrane protein	2.48	1.44E-04	0.0452
CV725_00955	algC	phosphomannomutase	-1.90	1.88E-04	0.0492
		/phosphoglucomutase			
CV725_07015	hp0965	dynamin-like GTPase	1.29	2.62E-04	0.0573
CV725_04120	hp1070	hypothetical protein	-1.00	3.20E-04	0.0573
CV725_00045	hp1521	type III restriction enzyme	-1.87	3.29E-04	0.0573
CV725_07020	hp0966	dynamin-like GTPase	1.25	4.09E-04	0.0631
CV725_07915	mltD	lytic transglycosylase	-1.19	4.43E-04	0.0631
CV725_07010	hp0963	dynamin-like GTPase	1.14	5.17E-04	0.0675
CV725_05420	rpoN	RNA polymerase sigma factor RpoN	-1.29	6.04E-04	0.0728
CV725_05415	lptB	LPS export ABC transporter	-1.46	1.25E-03	0.140

<sup>&</sup>lt;sup>a</sup>Log2 fold-change. A positive value indicates the gene is down-regulated in  $\Delta$ fapH  $pfIA^*$  (strain H54) compared to wild type (WT) or  $\Delta$ fapH  $pfIA^T$  (strain H16). A negative value indicates the gene is up-regulated in  $\Delta$ fapH  $pfIA^*$  (strain H54) compared to wild type (WT) or  $\Delta$ fapH  $pfIA^T$  (strain H16). <sup>b</sup>False discovery rate.

Table A2.2. Counts for DEGs in  $\Delta fapH pfIA^*$ .

Locus tag	Gene	Description	<sup>a</sup> H54_1	<sup>a</sup> H54_2	<sup>a</sup> H54_3	<sup>a</sup> WT_1	<sup>a</sup> WT_2	<sup>a</sup> WT_3
∆fapH pflA*	versus wild	d type						
CV725_04	fapH	motor accessory	112.41	110.31	149.18	503.20	412.57	402.49
785	-	protein FapH						

	mothyltropofe		42.77	93.36	345.17	480.60	552.89
	methyltransferase						
p1526	exodeoxyribonucleas e III	54.62	55.67	44.79	165.33	269.14	246.99
ofH	outer membrane protein	181.18	138.51	205.22	1206.0 8	2386.1 1	1201.92
	restriction endonuclease	70.15	64.21	173.85	522.43	760.60	744.63
	DUF4065 domain-	31.38	35.38	24.99	114.85	81.58	78.59
p1521	type III restriction	198.61	223.74	188.02	32.39	73.19	40.24
p0565	DUF417 domain-	2078.58	1357.73	947.68	483.36	400.70	352.58
nltD	lytic transglycosylase	663.88	640.52	966.83	304.45	352.80	256.55
p1070	hypothetical protein	325.60	332.07	342.72	178.80	170.27	156.17
ррД	dipeptide ABC	208.12	182.42	310.05	93.36	113.34	81.14
sH	metalloprotease	3014.39	2427.93	3033.88	1499.9 4	1580.9 7	995.84
	nuclease,	30.53	40.90	29.86	17.58	15.10	14.23
ррВ	dipeptide ABC	474.14	355.28	703.84	224.15	235.20	144.06
p1057	outer membrane β-	56.94	62.33	47.06	125.44	175.82	89.81
p1162	DedA family protein	158.57	122.28	139.66	289.64	210.29	262.33
p0350	phosphatidic acid phosphatase family	341.76	526.15	390.86	719.23	701.48	860.01
otB	LPS export ABC	198.08	153.60	187.59	77.42	46.99	83.37
p0600	ABC transporter,	9.72	18.94	11.58	33.11	35.50	25.45
naK	protein chaperone	1497.00	1831.85	1843.54	3543.0 9	2838.0 6	7630.61
ersus A <i>far</i>	oH nfIA <sup>T</sup>						
	outer membrane	3784.23	5061.71	6331.83	725.14	895.82	1096.64
opQ-2	outer membrane	5013.74	5193.56	9220.86	933.96	783.64	1329.38
орА	outer membrane	5704.87	6739.86	10124.5	1331.9 9	650.48	1127.20
	DUF4065 domain-	31.38	35.38	24.99	1059 1	82.49	90.25
ofH	outer membrane	181.18	138.51	205.22	482.43	1276.5 7	1176.61
lgC	phosphomannomutas e	640.32	652.38	415.64	118.29	159.57	180.78
p0965	dynamin-like GTPase	37.61	35.90	30.62	87.76	94.05	73.84
p1070	hypothetical protein	325.60	332.07	342.72	136.44	169.54	195.02
p1521	type III restriction enzyme	198.61	223.74	188.02	35.70	65.31	65.73
	01521 00565 01070 0pD 0H 001057 01162 00350 0tB 00600 0naK 0pQ-1 0pQ-2 0pA 0fH 0gC 00965	e III  offH outer membrane protein restriction endonuclease DUF4065 domain-containing protein type III restriction enzyme  outer membrane protein type III restriction enzyme  outer membrane protein lytic transglycosylase outer membrane β-barrel protein  outer membrane grotein  outer membrane protein  outer membrane protein	e III outer membrane protein restriction endonuclease DUF4065 domain- containing protein 181.18 07521 type III restriction enzyme 07565 DUF417 domain- containing protein 07566 DUF417 domain- containing protein 0757 DUF418 ABC transporter 0758 dipeptide ABC transporter 0758 dipeptide ABC transporter 0759 dipeptide ABC transporter 0759 Outer membrane β- Deal dipeptide ABC transporter 0759 DedA family protein 0757 DedA family protein 0757 DedA family protein 0757 DedA family protein 0758 DedA family protein 0759 DedA family protein 0759 DedA family protein 0759 DedA family protein 0759 DedA family protein 0750 DedA	e III   outer membrane protein   restriction endonuclease   DUF4065 domain-containing protein   198.61   223.74   223	e III	c   III	Bill   Outer membrane protein   181.18   138.51   205.22   1206.0   2386.1   1   1   1   1   1   1   1   1   1

CV725_07	hp0966	dynamin-like GTPase	15.32	16.96	13.20	75.26	109.21	75.82
020								
CV725_07	mltD	lytic transglycosylase	663.88	640.52	966.83	347.30	270.05	380.32
915								
CV725_07	hp0963	dynamin-like GTPase	15.32	16.96	13.20	35.82	34.03	30.27
010	-	-						
CV725_05	rpoN	RNA polymerase	191.22	259.12	260.61	113.24	85.99	90.44
420		sigma factor RpoN						
CV725_05	lptB	LPS export ABC	198.08	153.60	187.59	96.77	51.64	47.72
415		transporter						

<sup>&</sup>lt;sup>a</sup>Values are normalized to number of counts per one million reads (cpm). Values for the three biological replicates used for each strain are indicated in the table.

Table A2.3: RT-qPCR primers

Primer 241	hp0586 F	5'CGCTTGATATTGCTGGCAAT3'
Primer 242	hp0586 R	5'CCTCCTTTTCCTAAAACGAGAT3'
Primer 243	hp0715 F	5'CTGATTGGATTAAACATCGGCG3'
Primer 244	hp0715 R	5'CTTGCGCACCAAAGTGTTTT3'
Primer 249	hp1572 F	5'AAAAGCCCTTTCATCACCCATG3'
Primer 250	hp1572 R	5'GGGATGATTAAGCGCTGGTG3'
Primer 239	rpoA F	5'TTGCACACCCTTTTATTCCAATCC3'
Primer 240	rpoA R	5'CCAATGACAATGAGCGCATG3'

### Using AlphaFold to model protein-protein interactions

To follow up on the results from the co-IP and BACTH assays from this chapter, I modeled interactions actions between various proteins using AlphaFold 2.3.1. Specifically, I used AlphaFold to model FapH-HP1456 and FapH-HP1452 interactions. AlphaFold is a powerful computational tool for investigating protein structure (*Jumper et al. 2021*). Prior to the advent of AlphaFold, protein structure prediction tools were reliant on datasets of experimentally determined structures. AlphaFold and all subsequent version is open source, and the documentation is easily found online (<a href="https://github.com/google-deepmind/alphafold">https://github.com/google-deepmind/alphafold</a>). Structure prediction of novel proteins was impossible with the best tools available. AlphaFold uses multiple bioinformatic and Al tools to assemble 3D protein structures. First, AlphaFold uses a protein's amino acid sequence as the input. Next, AlphaFold creates a multiple sequence alignment (MSA) of the input amino acid sequence with related sequences. The MSA is used to look for structural patterns among related proteins. Next, AlphaFold uses a neural network based on transformers to process the

sequential data. AlphaFold then combines the MSA and transformer-based architecture to predict the distances between amino acids, which are then used to create a rough protein structure. AlphaFold refines the protein structure prediction using a neural network-based refinement module to increase accuracy. The final output is a 3D model of the protein's structure down to the location of individual atoms. Many AlphaFold structures are now found online (<a href="https://alphafold.ebi.ac.uk/">https://alphafold.ebi.ac.uk/</a>) and can be compared with the experimentally determined crystal structures. The tertiary structure of the AlphaFold models is highly accurate, but the orientation of amino acid side chains is inconsistent.

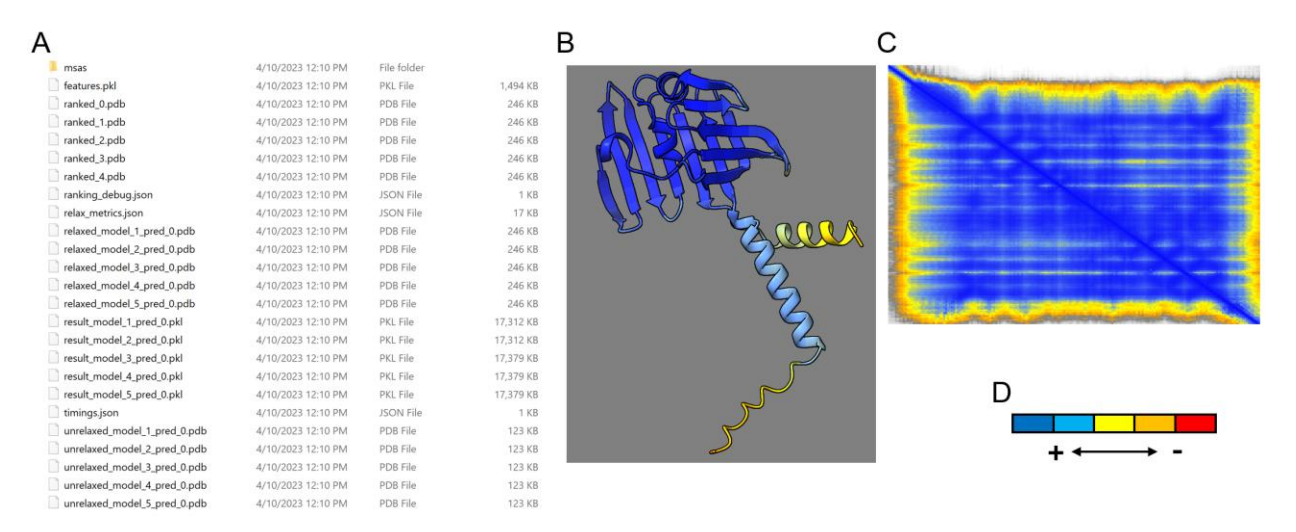


Figure A2.4: AlphaFold structure prediction and error plot of FapH. (A) Output files produced from. (B) AlphaFold2 monomer Predicted structure and (C) Predicted Aligned Error (PAE) plot. The plot represents the predicted error in the position of each residue in a protein structure when compared to the true structure, essentially showing how confident AlphaFold is about the relative positions of different parts of the protein, with darker colors (blue) indicating high confidence (low error) and lighter colors (yellow) indicating low confidence (high error) for each residue pair when aligned against each other. The structure and error plot are for ranked\_0.pdb. (D) High (blue) to low (red) confidence.

Understanding the strengths and weaknesses of AlphaFold is important when using the tool. The predictions have become increasingly accurate since the launch of Alphafold2, at the expense of a large amount of computing power. Most predictions can be done in a short time, less than an hour, while others, such as when using the multimer tool, can take several days when requesting the maximum amount of computing power on the Sapelo2 cluster. AlphaFold multimer allows the prediction of protein-protein interactions or protein complexes by inputting two or more amino acid sequences. Both the AlphaFold monomer and multimer tools do an excellent job of

predicting the tertiary protein structure. The main limitation of AlphaFold is the placement and orientation of the amino acid side chains, which is problematic for predicting protein-protein interactions.

The scripts for executing AlphaFold monomer and multimer on the Sapelo2 high performance computing cluster are similar. The first difference is the input file for monomer has one amino acid sequence, while multimer has two or more amino acid sequences. The second difference is that multimer has one additional command line (uniport\_database\_path) and requires the multimer preset. Each AlphaFold tool has an output of structural predictions ranked from best to worst (ranked\_0 - ranked\_4), additional models that were generated to build the final ranked\_ models (result\_model, unrelaxed\_model) and error plots of those structures (Fig. A2.4A). The final structural prediction is in pdb file format with an accompanying error plot (Fig. A2.4B-C). The confidence is ranked by color, blue being best and red being worst (Fig. A2.4D). The confidence can be taken to mean the fold and position of that region of the protein in space. The highest likelihood prediction is always called ranked\_0, with the less likely structures being called ranked\_1, ranked\_2, and so on.

AlphaFold multimer struggles with predicting the interaction of proteins that do not have experimentally verified structures. Figure A2.5 shows how the same input produces different structural predictions. Figures A2.5A and A2.5B represent ranked\_0 while Figures A2.5C and **A2.5D** represent ranked 5, of twenty-six generated predictions. These two predictions show an interface at different areas of both proteins. The ranked\_0 is often significantly different from other models using the same inputs. The error plots show that FapH contains a single domain while HP1456 has two domains (Figs. A2.5B and A2.5D). The error plots are divided into 4 quadrants with FapH in the top left, HP1456 in the bottom right, and the top right and bottom left showing the relative location of residues in one sequence with residues in the other sequence (Figs. A2.5B and A2.5D). The quadrant for FapH has a single block of blue, while the quadrant for HP1456 has a white gap between the two domains. The top right and bottom left quadrants show the confidence of the location of an amino acid on one chain relative to the location of an amino acid on the other chain. Therefore, these error plots show that the models are confident in the fold of each protein individually (top left, bottom right), but not confident in the location of the chain relative to the other chain (top right, bottom left). This low confidence in the interaction is evident in the yellow, orange, gray, and white coloring in the top right and bottom left quadrants of the error plots where ranked\_0 is more confident than raned\_5 in the location of these residues (Figs. A2.5B and A2.5D).

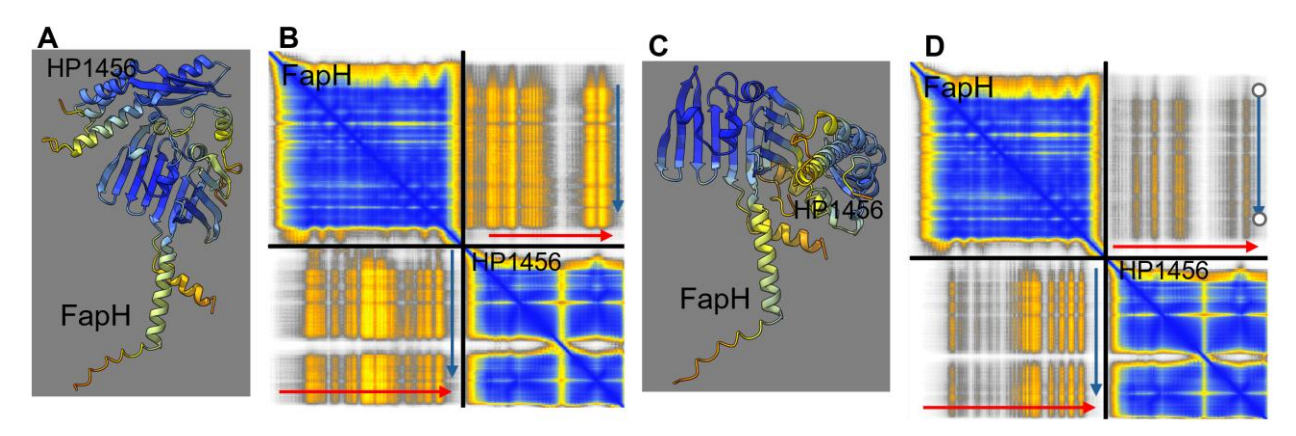
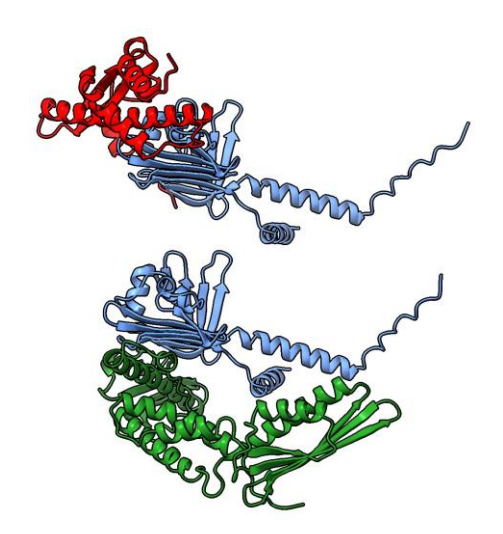


Figure A2.5: Alphafold2 multimer predictions. (A, B) FapH and HP1456 ranked\_0, (C, D) FapH and HP1456 ranked\_5. Prediction aligned error (PAE) score (B and D) of the model for interactions between FapH and HP1456 where the x and y acis indicate amino acid positions within the folded protein. Blue indicates high confidence while yellow and orange are low confidence. The labeled top left and bottom right quadrants indicate error within the distance of amino acids within that protein. In the bottom left and top right quadrants (B and D), the red arrows indicate the increasing residue number of chain A (FapH), while the blue arrow indicates the increasing residue number of chain B (HP1456). This means that the direction the arrows point indicate the proximity of amino acids, increasing in number from the N to C terminus. The significance of the orange/yellow coloring in the bottom left and top right quadrants indicates low confidence in the proximity of amino acids on either chain to one another, suggesting the final protein complex is low confidence.

PDBePISA (Proteins, Interfaces, Structures and Assemblies) is a tool for assessing the probability of a predicted protein-protein interaction from a PDB file. PISA provides a variety of information, including the P-value of the solvent free energy gain or interface specificity ( $\Delta^i$ G P-value, less than 0.5 is significant), the solvent free energy gain ( $\Delta^i$ G kcal/mol), the interface area (A²), and displays all interfacing residues and any bonds they form (**Fig. A2.6**). For many models generated by AlphaFold2 multimer the ranked\_0 model does not have the most convincing PISA outputs (**Fig. A2.6**). The  $\Delta^i$ G P-value and  $\Delta^i$ G kcal/mol for ranked\_5 and ranked\_9 are more favorable than for ranked\_0. Ranked\_0 consistently differs from the other models in the number of hydrogen bonds (N<sub>HB</sub>), salt bridges (N<sub>SB</sub>), and disulfide bonds (N<sub>DS</sub>). Ranked\_0 has 8 hydrogen bonds and 10 salt bridges, while ranked\_5 and ranked\_9 have fewer. Maximizing these bonds appears to be an important characteristic that AlphaFold2 multimer uses in assessing confidence.

ranke	d_0															
##		Stru	cture 1		×		Stru	cture :	2	interface	$\Delta^{i}G$	$\Delta^{i}G$	$N_{HB}$	N <sub>SB</sub>	$N_{\text{DS}}$	CSS
NN «»	Range	<sup>i</sup> N <sub>at</sub>	<sup>i</sup> N <sub>res</sub>	Surface A <sup>2</sup>		Range	<sup>i</sup> N <sub>at</sub>	<sup>i</sup> N <sub>res</sub>	Surface A <sup>2</sup>	area, A <sup>2</sup>	kcal/mol	P-value				
1 0	Α	133	33	13407	<b>◊</b>	В	122	33	10273	1135.2	-1.9	0.542	8	10	0	0.000
ranke	d_5															
##		Stru	icture 1	<u> </u>	×		Str	ucture	2	interface	ΔĠ	$\Delta^{i}G$	$N_{HB}$	N <sub>SB</sub>	$N_{\text{DS}}$	CSS
NN «»	Range	<sup>i</sup> N <sub>at</sub>	$^{\mathrm{i}}\mathrm{N}_{\mathrm{res}}$	Surface A <sup>2</sup>		Range	<sup>i</sup> N <sub>at</sub>	<sup>i</sup> N <sub>res</sub>	Surface A <sup>2</sup>	area, A <sup>2</sup>	kcal/mol	P-value				
1 0	Α	135	32	13062	<b>\Q</b>	R	151	35	10244	4252.2		0 446	_	0	0	0.000
		133	52	13002		D	TOT	20	10244	1253.3	-6.0	0.416	/	8	0	0.000
ranke		155	32	13062			131	22	10244	1253.3	-6.0	0.416	/	8	0	0.000
			octure 1		×			ucture		interface	_6.θ Δ <sup>i</sup> G	Δ <sup>i</sup> G	N <sub>HB</sub>	N <sub>SB</sub>		CSS
ranke	d_9		ıcture 1			Range			2				N <sub>HB</sub>			

Figure A2.6: PISA values from FapH-HP1456 AlphaFold generated models. <a href="https://www.ebi.ac.uk/pdbe/pisa/">https://www.ebi.ac.uk/pdbe/pisa/</a> The PISA tool gives a range of outputs when interactions are assessed from a PDB file.



**Figure A2.7: Modeled interactions of FapH with HP1454 and HP1456.** The models show the predicted interface as determined by AlphaFold multimer 2.3.1. FapH – blue, HP1456- red, HP1454 – green.

#### Results

I was interested to know if AlphaFold would support-protein-protein interactions obtained by experimental methods (Chapter 1) and identify important residues in that interaction. If the structure of two proteins is known, the surface residues can be examined to determine the rate of evolution, assuming the residues in the interface will evolve more slowly. Interface residues of interacting proteins evolve more slowly because mutations of these residues can interfere with the interaction of the proteins. The rate of evolution is calculated by the percentage of all surface conserved/all surface residues vs interface conserved/all interface residues and assessed (*de* 

Juan et al. 2013). Chapter 1 details how FapH is found to interact with HP1454 and HP1456 through co-immunoprecipitation and in BACTH β-galactosidase assays. I began by using AlphaFold2 multimer version 2.3.1 on the Sapelo2 high performance computing cluster with the amino acid sequences of FapH and HP1456. The ranked\_0 models of each interaction suggest that HP1454 and HP1456 may interact with different faces of FapH (Fig. A2.7).

The input of FapH and HP1456 into AlphaFold2 multimer resulted in twenty-five ranked\_ output files that showed many different orientations of the proteins (**Fig. A2.8**). Six of these models are displayed in **Figure A2.8** with FapH colored white and HP1456 colored red. Of the models displayed, ranked\_0 is the highest probability model, and HP1456 is seen to interact with FapH in four different orientations resulting in four different interfaces.

After obtaining the AlphaFold models I performed an alignment for both FapH and HP1456 of close homologues in *Helicobacter* species using the (PSI)-BLAST tool (**Fig. A2.9**). The species selected included homologues of FapH that were conserved to 56% sequence identity. This cutoff was chosen as lower cutoffs were found to not support coevolution, likely due to divergence in the species. All the species selected are gastric *Helicobacter* species. Only the residues with exact conservation (\*) were used for coevolution analysis.

Next, PISA was used to assess the energetic likelihood of ranked\_0 (**Table A2.4**). The PISA outputs did not support the model of ranked\_0 FapH-HP1456 due to a  $\Delta^i$ G P-value of 0.542, which is not significant. A PISA P-value is a measure of probability of interface specificity with a value of <0.5 being significant (<a href="https://www.ebi.ac.uk/pdbe/pisa/">https://www.ebi.ac.uk/pdbe/pisa/</a>). **Table A2.4** and **Figure A2.10** show the PISA results and AlphaFold error plots for other interactions investigated.

 $\Delta^i G$  P-value indicates the P-value of the observed <u>solvation free energy gain</u>. The P-value measures the probability of getting a lower than observed  $\Delta^i G$ , when the interface atoms are picked randomly from the protein surface, such as to amount to the observed interface area. The P-value is a measure of interface specificity, showing how surprising, in energy terms, the interface is.

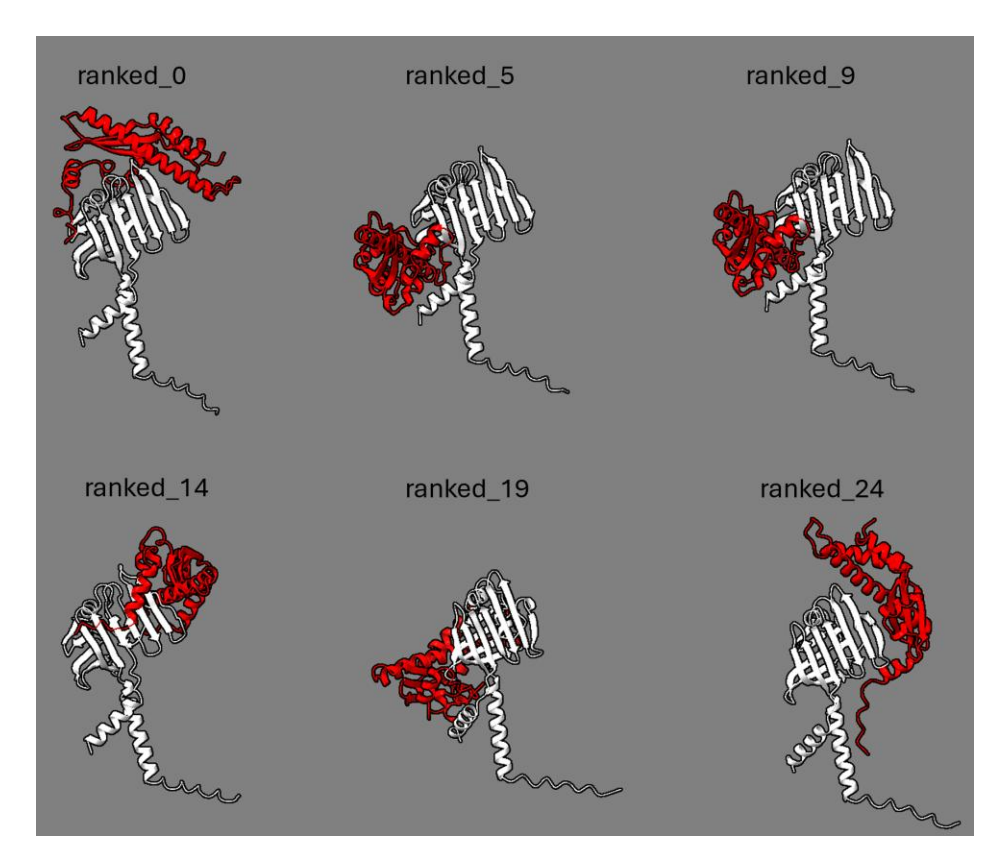


Figure A2.8: FapH-HP1456 output models with different interfaces. FapH is colored white and HP1456 red. The signal peptide of each protein was removed prior to the modeling: this is the first 7 residues on FapH N-terminal to C1 and the first 21 residue of HP1456 N-terminal to C1.

After obtaining the PISA outputs, the residues were identified that were involved in the interacting interface and compared with the conserved residues in the alignment (**Fig. A2.9**). The degree of conservation was calculated by the percentage of all surface conserved/all surface residues vs interface conserved/all interface residues. For the FapH-HP1456 model 25.4% of surface residues and 48.4% of surface interface residues of FapH are conserved, while 28.3% of surface residues and 36.3% of surface residues of HP1456. This greater conservation at the interface for both proteins using the ranked\_0 model suggests that FapH and HP1456 have coevolved.

It is difficult to say if the results of the coevolution analysis are reliable, because of the variation in the interface of the AlphaFold output models (**Fig. A2.8**). In some metrics ranked\_0 performs well; the coevolution analysis, while in others it performs less well than the other ranked\_models; the PISA analysis. This appears to be the case with some modeled interactions but not all. In the case of the PfIA-PfIB modeled interaction, all the ranked\_models show a similar interface and interfacing residues, with PfIA displayed in red and PfIB in white (**Fig. A2.11**). We

see that the N-terminal region of PfIA, composed of beta strands and loops, becomes wedged between two domains of PfIB. The PISA values for these models are also similar, with favorable  $\Delta^i$ G kcal/mol and  $\Delta^i$ G P-values for ranked\_0, ranked\_5, and ranked\_9 (**Fig. A2.12**). Compared to the FapH-HP1456 models, the PISA values of PfIA-PfIB models seem more convincing (**Fig. A2.12**).

۸		
A Hcetorum_81%	mqylksafllfflalffvscskhpfskqtpkt	32
HpyloriB128	MTLFFVSCSKHPFSKQTPKT	20
Hacinonychis_93%	mryfrstfslflmalfliscskhpfskqtpkt	32
hsalomonis_58%	pktpk-pksth	25
Hbaculiformis_57%	maqvrsrhhfclrflgtlalgfllvscahkkspkpksahkqh	42
Hsuis_56%	mvrrflalilfgvlvsachhqvkpkkphkvhkpkthrprkpkkpekpkkth	51
Hailurogastricus_57%	mwgrllavglfgflvsachhqpkpekphkshkphkph	37
Hheilmannii_57%	hlvvglfglllsachhqpkvakpkkphhh	29
	: .:. :* ::	
Hcetorum_81%	-raqikaneehkkrqetlnalrqfkliyintpvfrfydygtiktdkshnieitlykl	88
HpyloriB128	-REQIRQEEANKKREETLNALRQFRLIYINTPVFRFYDYGTIKTDKDHNIEVTLYKL	76
Hacinonychis_93%	-reqirqeearkkreetlnalrqfkliyintpvfrfydygtiktdrsrniavtlykl	88
hsalomonis_58%	kklfiaksaaqrkqeaetarkkaleqfkliyiytpvlrfydygtiehtkegdlrivlyql	85
Hbaculiformis_57%	kklfikksaeqrkleaevarkkaleqfkliyiytpvlrfydygtinhtkegdvqlvlyql	102
Hsuis_56%	kkvfikkstaerkaeqqaqirkelakfkliyiytpvfrfydygaigrnkegdlelvlykl	111
Hailurogastricus_57%	kkffikksyaerqreqeakikqelakfkliyiytpvlrfydygtigrtkegdlelvlykl	97
Hheilmannii_57%	kkifikksyaqrqreeaakirqelekfkliyiytpvlrfydygtigrtkegdlelvlykl	89
	: *: : * :*:**** ***:*******	
Hcetorum_81%	sqkvgdifmtkrticftrkcsakwlvardlfgkvsyadlfddivlgrdifkglgkrhltp	148
HpyloriB128	SQRVGDIYMTKRNICFSQKCSAKWIAARDLFGKVSYGDLFDDIVLGRDIFKGLGKRHLTP	136
Hacinonychis_93%	sqkvgdiymtkrsvcfsqkcsakwivardlfgkvsygdllddivlgrdifkglgkrhltp	148
hsalomonis_58%	skkageilikknylcfsgicsakwsaardlfgkvsygdlfddivlgrdifqgvgkrieps	145
Hbaculiformis_57%	skkvgevvikknylcfsgicsakwsaardlfgkvsygdlfddivlgrdifkgigkriepn	162
Hsuis_56%	skhfgdivikknyicfsgtcsakwvaardmfgevsygdlfddivlgrdifqgigkqiqpn	171
Hailurogastricus_57%	skrlgdivikknyicfsgtcmakwsaardmfgkvsygdlfddivlgrdifqgmgkqiapn	157
Hheilmannii_57%	shrfgdiiikknyicfsgtcmakwsaardmfgkvsygnlfddivlgrdifhglgkqiapn	149
	* *	
Hcetorum_81%	eyviqrfqksgdiilyerkkglisfqnltqriairieqyepslqdlednenadkelp	205
HpyloriB128	EYVIQRFQKSGEIILYERKNDLISFQNLTQKIAIRIEPYEPSLQDLEDNENADSELQ	193
Hacinonychis_93%	gyviqrfqksgeiilyerknglisfqnltqkiairiepyepslqdlednenadselq	205
hsalomonis_58%	gaviqrfmqngelifyerkpdkilfqnmstgtaiviqqyhp	186
Hbaculiformis_57%	geivqrfvengeviyyerkpgkilfqnmstgtaiviqqyhp	203
Hsuis_56%	gvllqrfiengqmiyyerspekilfqnmttgvaiviqpyhpq	213
Hailurogastricus_57%	gtliqrfvengeliyyernpekilfqnmttgvaivfeayhpq	199
Hheilmannii_57%	gtliqrfvengqliyyertfgktlfqnmttgvaivfeayhpq	191
	::*** :.*::* ***: ** :: *.*	

### FapA-HP1456, 56% FapA

C1, I18, L34, F36, L38, I39, Y40, I41, T43, P44, V45, R47, F48, Y49, D50, Y51, G52, I54, L66, Y67, L69, S70. G74, K80, C84, F85, C89, A91, K92, W93, A96, R97, D98, F100, G101, V103, S104, Y105, L108, D110, D111, I112, V113, L114, G115, R116, D117, I118, F119, G121, G123, K124, Q134, R135, F136, G140, I143, Y145, E146, R147, F154, Q155, N156, A162, I163, Y168, P170

Surface - 46/181, 25.4%

Surface interface - 16/33, 48.4%

Solvent Inaccessible

Figure A2.9: Alignment and residue conservation of FapH. (A) Alignment of 7 FapH homologues. Homologues were identified using the (PSI)-BLAST tool at <a href="https://blast.ncbi.nlm.nih.gov/Blast.cgi">https://blast.ncbi.nlm.nih.gov/Blast.cgi</a>. (B) PISA displays surface, surface interacting, and solvent inaccessible residues. The residues C1, I18, etc are conserved, the surface interface residues are highlighted in <a href="yellow">yellow</a>, and the solvent inaccessible residues are highlighted in <a href="yellow">green</a>.

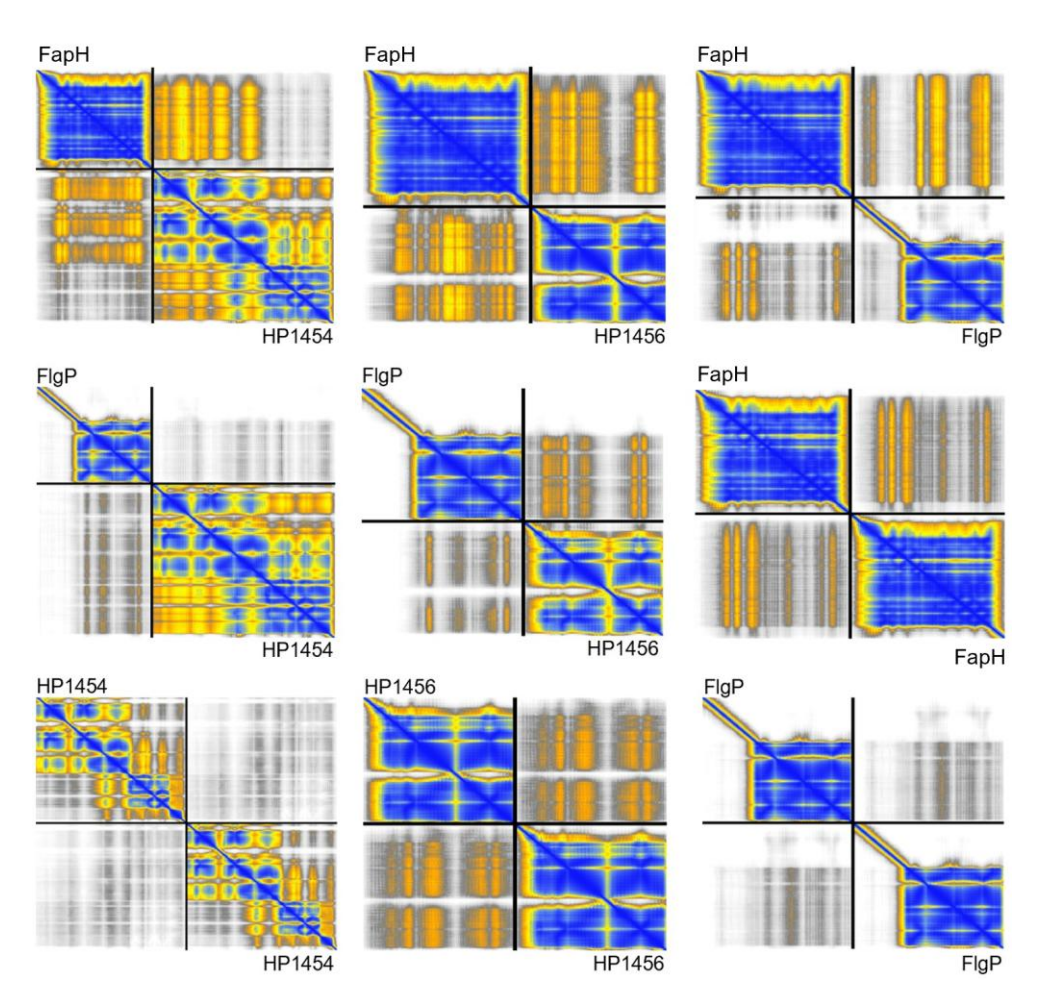


**Figure A2.10:** Error plots of AlphaFold models. AlphaFold2 multimer 2.3.1 was used to predict protein-protein interactions. The plots from the highest likelihood ranked\_0 is shown.

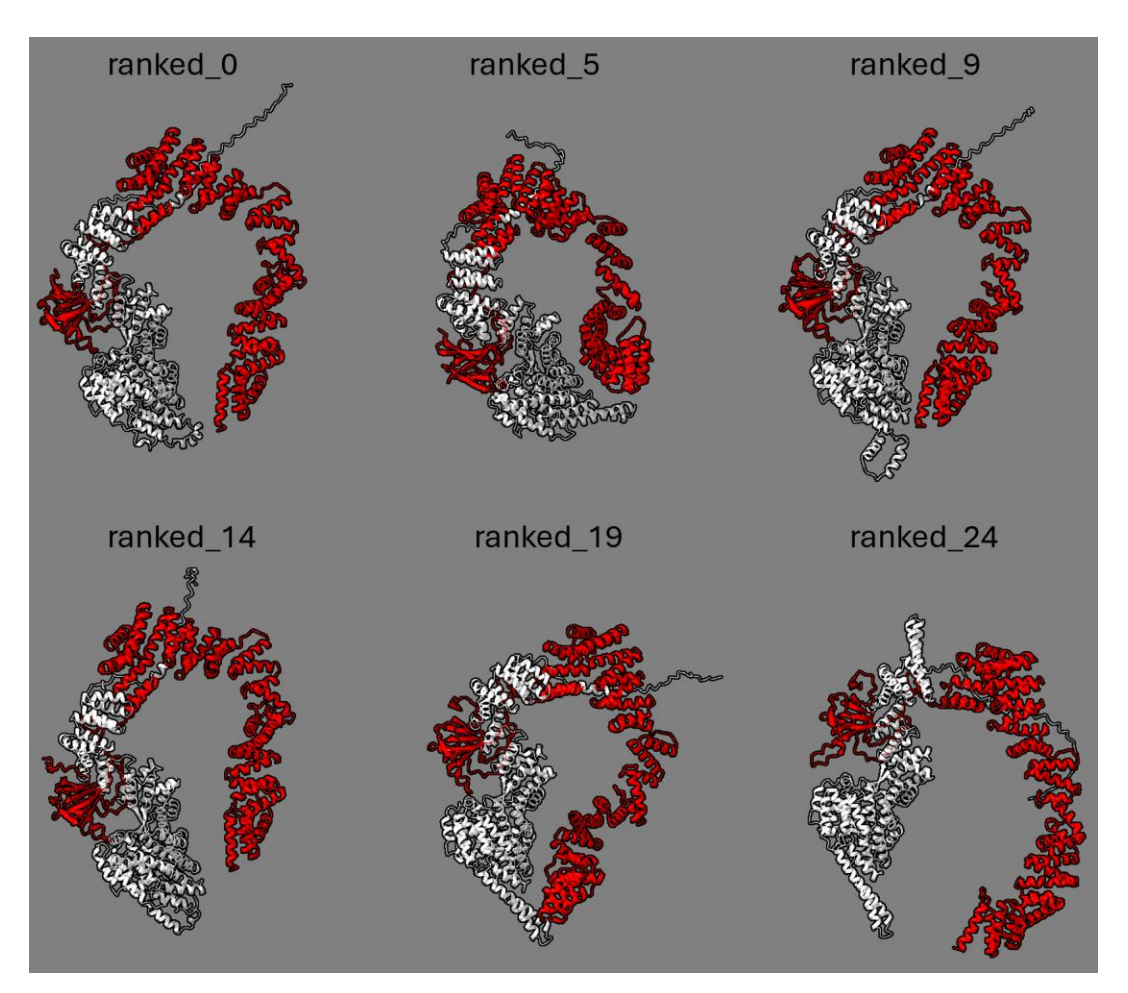


**Figure A2.11: PfIA-PfIB output models with similar interface.** PfIA is red and PfIB is white. The PfIB transmembrane helix of residues 62-84 and the residues 1-62 were removed prior to modeling. <a href="https://services.healthtech.dtu.dk/services/TMHMM-2.0/">https://services.healthtech.dtu.dk/services/TMHMM-2.0/</a>

ranke	d_0															
##		Stru	cture 1		×		Str	ucture 2		interface	$\Delta^{i}G$	$\Delta^{i}G$	$N_{HB}$	$N_{\text{SB}}$	$N_{DS}$	CSS
NN «»	Range	<sup>i</sup> N <sub>at</sub>	<sup>i</sup> N <sub>res</sub>	Surface A <sup>2</sup>		Range	<sup>i</sup> N <sub>at</sub>	<sup>i</sup> N <sub>res</sub>	Surface A <sup>2</sup>	area, A <sup>2</sup>	kcal/mol	P-value				
1 0	Α	459	111	48469	<b>\Q</b>	В	483	128	43659	4661.2	-47.2	0.025	34	13	0	0.000
ranke	d_5															
##		Stru	cture 1		×		Str	ucture 2		interface	ΔĠ	$\Delta^{i}G$	$N_{HB}$	$N_{SB}$	$N_{DS}$	CSS
NN «»	Range	<sup>i</sup> N <sub>at</sub>	<sup>i</sup> N <sub>res</sub>	Surface A <sup>2</sup>		Range	<b>N</b> at	<sup>i</sup> N <sub>res</sub>	Surface A <sup>2</sup>	area, A <sup>2</sup>	kcal/mol	P-value				
1 0	Α	455	109	47983	<b>\Q</b>	В	474	128	42854	4637.6	-47.5	0.021	44	12	0	0.000
ranke	d_9															
##		Stru	cture 1		×		Str	ucture 2		interface	ΔĠ	$\Delta^{i}G$	$N_{HB}$	N <sub>SB</sub>	$N_{\text{DS}}$	CSS
NN «»	Range	<sup>i</sup> N <sub>at</sub>	$^{I}N_{res}$	Surface A <sup>2</sup>		Range	<b>N</b> at	<sup>i</sup> N <sub>res</sub>	Surface A <sup>2</sup>	area, Å <sup>2</sup>	kcal/mol	P-value				
1 0	Α	457	113	48829	<b>\Q</b>	В	472	128	44230	4742.3	-43.8	0.065	43	14	0	0.000

Figure A2.12: PISA values from PfIA-PfIB AlphaFold generated models. <a href="https://www.ebi.ac.uk/pdbe/pisa/">https://www.ebi.ac.uk/pdbe/pisa/</a>

Table A2.4: PISA assessment of protein-protein interactions

Interaction	Interface area, Å <sup>2</sup>	Δ <sup>i</sup> G kcal/mol	Δ <sup>i</sup> G P-value	<b>N</b> нв	NsB
FapH-HP1454	1094.7	-6.4	0.252	3	8
FapH-HP1456	1135.2	-1.9	0.542	8	10
FapH-FlgP	2556.8	-32.8	0.119	15	9
FlgP-HP1454	588.1	-1.0	0.618	10	6
FlgP-HP1456	837.3	-1.2	0.730	8	7
FapH-FapH	1287.9	-3.1	0.451	9	14
HP1454-HP1454	2222.8	-15.8	0.118	18	8
HP1456-HP1456	1688.8	-3.2	0.550	17	9
FlgP-FlgP	659.1	-2.8	0.805	1	0

Interface area,  $\mathring{A}^2$  – The total accessible surface areas of isolated and interfacing structures, divided by two.  $\Delta^i G$  kcal/mol – The solvation free energy gain by formation of the interface.  $\Delta^i G$  P-value – The P-value of the solvation free energy gain, a measure of interface specificity showing how surprising the interface is in energy terms. P=0.5 – not surprising. P>0.5 - less hydrophobic than could be. P<0.5 – surprising hydrophobicity, interface can be interaction specific. NHB – Number of potential hydrogen bonds. NSB – Number of potential salt bridges. https://www.ebi.ac.uk/pdbe/pisa/

### Concluding remarks on the unpublished data on FapH

The results from the further characterization of FapH provided some interesting points for follow up studies to address the basis for the phenotype of the H. pylori  $\Delta fapH$  mutant. In addition, following up on the results of these studies may lead to the identification of candidates for H. pylori motor accessory proteins, such as the protein(s) that form the outer disk. Key findings from these studies include the following.

- Examining interactions between known flagellar motor proteins (FlgI, FlgH, FlgP, and FapH) and HP1456 or HP1454 using the BACTH system failed to provide evidence for these proteins being novel motor accessory proteins. In addition, we failed to identify convincing interactions between FlgP and FlgQ, despite the previous report that FlgQ is required for assembly of the basal disk in *C. jejuni* (ref).
- Several models for FapH-HP1456 and FapH-HP1454 interactions were generated using AlphaFold (indicate the figures), and a number of these models were predicted to be energetically favorable (indicate the figures). These data support the notion that FapH interacts with HP1456 and HP1454 in *H. pylori*, although the physiological relevance of such interactions remains unclear.
- Including a formaldehyde cross-linking step in the co-IP assay with the FapH-myc protein revealed two cross-linked species of ~40 kDa and ~50 kDa in size that were pulled down with the FapH-myc protein (**Fig. A2.2**). Although we did not attempt to identify the proteins in the cross-linked, potential candidates for cross-linked species include FapH-FapH (predicted size of ~50 kDa), FapH-FlgP (predicted size of ~45 kDa), and FapH-1456 (predicted size of ~42 kDa). Alternatively, the cross-linked species may include a different protein, which may be the protein that forms the outer disk.
- Comparing the transcriptomes of ΔfapH pflA\*, ΔfapH pflA<sup>T</sup>, and wild type revealed that many of the DEGs in ΔfapH pflA\* are involved in cell envelope assembly or maintenance. The differential expression of some of these genes in ΔfapH pflA\* may have been in response to disruption in lipid homeostasis of the OM, such as the up-regulation of the LPS transport gene lptB (Table A2.1).

# Chapter 3: Inactivation of LpxF and Fur rescue bacitracin sensitivity in *fapH* deletion mutants

### INTRODUCTION

Chapter 2 describes how FapH forms a flagellar motor accessory that we refer to as the FapH ring and is situated between the flagellar hook and OM. In the absence of FapH the cells become sensitive to bacitracin, an antibiotic that is typically excluded by the OM. Bacitracin is a cyclic polypeptide antibiotic that interferes with peptidoglycan biosynthesis by binding undecaprenyl-pyrophosphate to disrupt the undecaprenyl-phosphate cycle and thereby inhibit the synthesis and flipping of the peptidoglycan precursor molecule lipid II (*Kahn et al. 2011*). In various bacterial species, mutations that lead to the accumulation of GPLs in the outer leaflet of the OM result in increased sensitivity to antibiotics such as bacitracin due to the increased permeability of the OM to these antibiotics (*Silhavy et al. 2010, Davies et al. 2019, Roier et al. 2016*).

I sought to investigate further the role of FapH in OM stability and permeability by isolating and characterizing variants of the  $\Delta fapH$  mutant that suppress the bacitracin sensitivity of the mutant. Both frameshift and missense mutations in the iron regulatory gene *fur* were identified in the bacitracin-resistant variants of  $\Delta fapH$ . Fur is involved in regulating expression of flagellar genes in *H. pylori* (*Danielli et al. 2006*) and differs from *E. coli* Fur in that it regulates gene expression in both the iron bound (Fe-Fur) and non-iron bound (apo-Fur) forms (*Kang et al. 2024*). Deleting *fur* in the  $\Delta fapH$  mutant suppressed the bacitracin sensitivity of the mutant, indicating that the loss of Fur was sufficient to suppress the bacitracin-sensitivity of the  $\Delta fapH$  mutant. Three of the bacitracin-resistant  $\Delta fapH$  variants had a missense mutation in *fur* that changed Asp-135 to Asn. *H. pylori* Fur contains three distinct metal-binding sites that are designated S1, S2, and S3. Asp-135 is adjacent to His-134, which is one of the amino acid residues that coordinate the metal ion in the S3 binding site (*Vitale et al. 2011*) Including the iron chelator 2,2'-dipyridyl in the medium suppressed the bacitracin sensitivity of the  $\Delta fapH$  mutant, which taken together with the antibiotic resistance of the  $\Delta fapH$  variants that express the Fur<sup>D135N</sup>

mutant, suggests that loss of metal binding at the S3 site in Fur phenocopies the *fur* deletion. Two of the newly constructed  $\Delta fapH$  mutants from **Chapter 2** did not have any mutations in *fur*, but both had a nonsense mutation in *lpxF* that introduced a stop codon early in the coding region of the gene. LpxF is a phosphatase that removes the 4'-phosphate on the lipid A molecule to generate the major species of lipid A in *H. pylori*, which has a single phosphate at position 1 (**Stead et al. 2008**). Thus, the nonsense mutation in *lpxF* is expected to result in lipid A being phosphorylated at both the 1 and 4' positions, which corresponds to the minor lipid A species in *H. pylori* (**Stead et al. 2008**). The phosphates at the 1 and 4' positions in the lipid A moiety would be able to ion pair with divalent metal cations, which may stabilize the outer leaflet of the OM in the  $\Delta fapH$  mutant as the flagella rotates.

### **RESULTS**

In our previous work we showed that motile  $\Delta fapH$  strains, but not non-motile  $\Delta fapH$  strains with a truncated PfIA were sensitive to bacitracin (*Rosinke et al. 2024*). We constructed a  $\Delta fapH$  strain that had a restored reading frame and full length PfIA ( $\Delta fapH pfIA^*$ ) where 11 residues of PfIA were altered from the native version. This PfIA\* had an indistinguishable tertiary structure from the native PfIA, but we were concerned that the bacitracin-sensitive phenotype may have been the result of this strain. We showed that a reconstructed  $\Delta fapH$  without secondary flagellar mutations was motile and sensitive to bacitracin. Additionally, the flagellar motor structures associated with PfIA appeared indistinguishable from the wild type. We concluded that the PfIA in  $\Delta fapH pfIA^*$  functioned as a native PfIA. The WGS of this strain can be found in **Table S1**. We used a  $\Delta fapH pfIA^*$  mutant to conduct a suppressor search for resistance to bacitracin. We did this by inoculating semi-solid agar medium with  $\Delta fapH pfIA^*$ , incubating for 7 d, selecting cells at the edge of the swim halo, and repeating the inoculation. After 2 passages the result was a robust swim halo where cells were taken and streaked for clonal isolates. For the remainder of this chapter we will refer to the  $\Delta fapH pfIA^*$  genetic background as  $\Delta fapH$ .

Loss of LpxF may suppress the bacitracin sensitivity of the  $\Delta fapH$  mutant. It was described in Chapter 2 how  $\Delta fapH$  mutants were constructed with secondary mutations in the flagellar gene PflA. A suppressor search yielded a motile variant with a full length PflA that had 12 amino acids changed. The result was a protein predicted by AlphaFold to fold into the native shape, despite these mutations. To be sure that the bacitracin sensitivity seen in this  $\Delta fapH$  was due to the loss of FapH and not a mutated PflA, new  $\Delta fapH$  mutants were constructed that lacked secondary flagellar mutations. These  $\Delta fapH$  mutants ( $\Delta fapH$  4 and 9) were motile and sensitive to bacitracin

(Fig. S2.3). Additional  $\Delta fapH$  isolates were generated that were less motile and lacked the same level of sensitivity to bacitracin as  $\Delta fapH$  isolates 4 and 9 (Figs. S2.3, 3.1). WGS of two of the bacitracin-resistant variants of the  $\Delta fapH$  mutant (H181-2 and H181-11 in Table S3.1) revealed a mutation in IpxF that changed codon 14 from TGG (codes for tryptophan) to a TGA stop codon, which effectively results in a IpxF null mutant. Hereafter, H181-2 and H181-11 are referred to as  $\Delta fapH IpxF$ -2 and  $\Delta fapH IpxF$ -11, respectively. As shown in Figure 3.1A,  $\Delta fapH IpxF$ -2 and  $\Delta fapH IpxF$ -11 are more resistant to bacitracin than the  $\Delta fapH$  parental strain. The only other mutations found in  $\Delta fapH IpxF$  mutants are in arsS (H181-2) and serS (H181-11) (Table S3.1). ArsS is a histidine kinase in the ArsRS two-component system, which regulates the expression of genes involved in pH homeostasis (Loh and Cover 2006), while SerS is a serine-tRNA ligase. It seems unlikely that the mutations in arsS and serS are responsible for suppressing bacitracin-sensitivity of the  $\Delta fapH$  mutant given the roles of these genes. Given the role of LpxF in lipid A biosynthesis, the nonsense mutation in IpxF seems to be the most likely candidate for suppressing the bacitracin sensitivity of the  $\Delta fapH$  mutant.

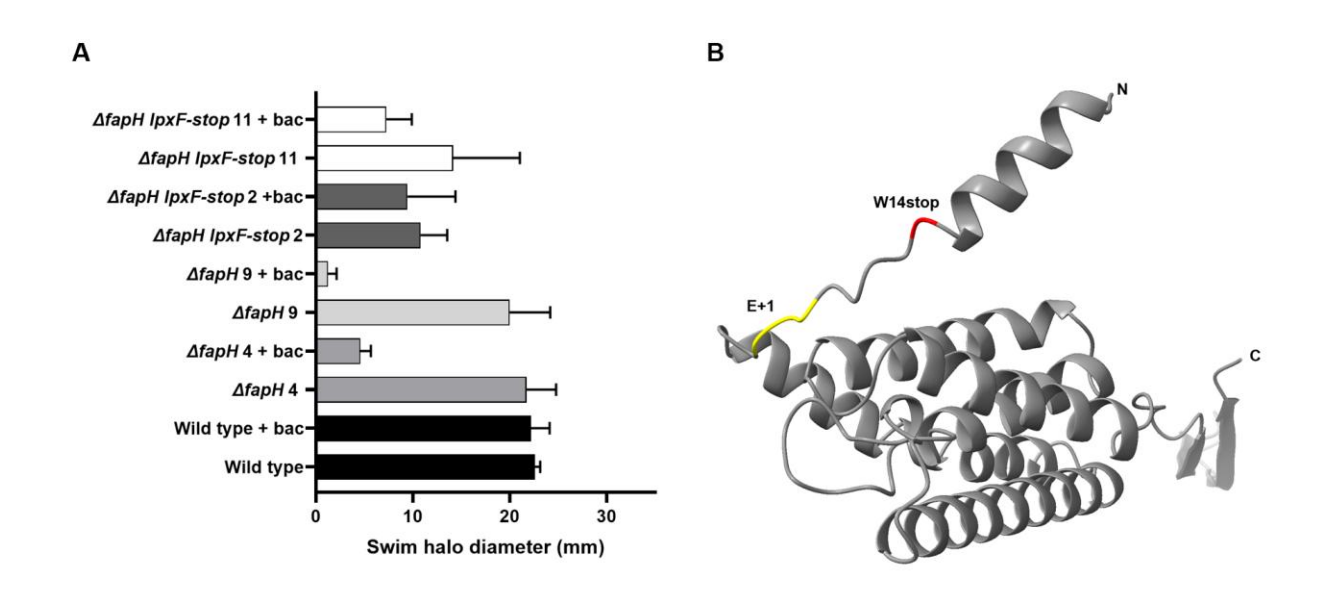


Figure 3.1:  $\triangle$  fapH mutants with a null *lpxF* have reduced motility and less sensitivity to bacitracin.  $\triangle$  fapH 4 and 9 from Chapter 2 (Fig. S2.3) are more motile and sensitive to bacitracin that  $\triangle$  fapH isolates 2 and 11 have a mutation in the phosphatase LpxF at residue 14 changing a tryptophan to a stop codon, indicated as *lpxF-stop*. (A) Motility of isolates with and without the *lpxF* mutation. (B) Structure of LpxF as predicated by AlphaFold. In red is the location of the trp14

where a stop codon is introduced in isolates 2 and 11. Trp14 is located within the signal sequence of LpfX. The yellow indicates the location of SPI cleavage, with the new N-terminus of glutamic acid indicated as E+1.

Mutations in *fur* rescue bacitracin sensitivity in  $\Delta fapH$ . WGS from twelve  $\Delta fapH$  bacitracin resistant clonal isolates (H150-H161) revealed each strain had either a frameshift or missense mutation in *fur*, which encodes the ferric uptake regulator (**Table S1**). The twelve isolates (i.e., strains H150-H161) displayed varying degrees of resistance to bacitracin, but all were significantly more resistant to bacitracin compared to the  $\Delta fapH$  parental strain (**Fig. 3.2A**). Nine of the isolates had an additional adenosine within a homopolymeric run of 8 A's located in nucleotide positions 55-62, resulting in a frameshift at codon 21 (**Table S1**). *H. pylori* Fur is 150 amino acid residues in length, and the frameshift results in a severe truncation of the protein.

Three of the bacitracin-resistant isolates (H154, H156, and H160) had a missense mutation in *fur* that changed Asp-135 to Asn. Gilbreath and co-workers performed site-directed mutagenesis on residues of *H. pylori fur* thought to be important for iron binding including aspartic acid 135 (*Gilbreath et al. 2013*). According to their model aspartic acid 135 lies directly in the S3 structural metal-binding site that is occupied in both the Fe-Fur and *apo*-Fur forms (*Gilbreath et al. 2013*). Mutations of residues in this S3 region of *fur* shared similar regulatory phenotypes. Under iron-replete conditions levels of *amiE* were higher than in wild type and no change in iron levels following chelation, resulting in a  $\Delta fur$ -life phenotype for the regulation of *amiE*, a Fe-Fur repressed gene used for assessing Fe-Fur regulation (*Carpenter et al. 2007, Carpenter et al. 2010*). Gilbreath and co-workers concluded that S3 residues including Asp-135 are involved in proper metal ion coordination in the *apo*-Fur form (*Gilbreath et al. 2013*).

To test if inactivation of Fur was responsible for rescuing the sensitivity to bacitracin in  $\Delta fapH$ , fur was deleted in the mutant and wild type backgrounds (**Fig. 3.2C**). Similar to the wild type and complementation strains,  $\Delta fur$  showed no increased sensitivity to bacitracin or a motility defect. However, when  $\Delta fur$  was introduced into the  $\Delta fapH$  mutant background the loss of Fur resulted in reduced sensitivity to bacitracin, where the cells were able to swim out from the point of inoculation (**Fig. 3.2C**).

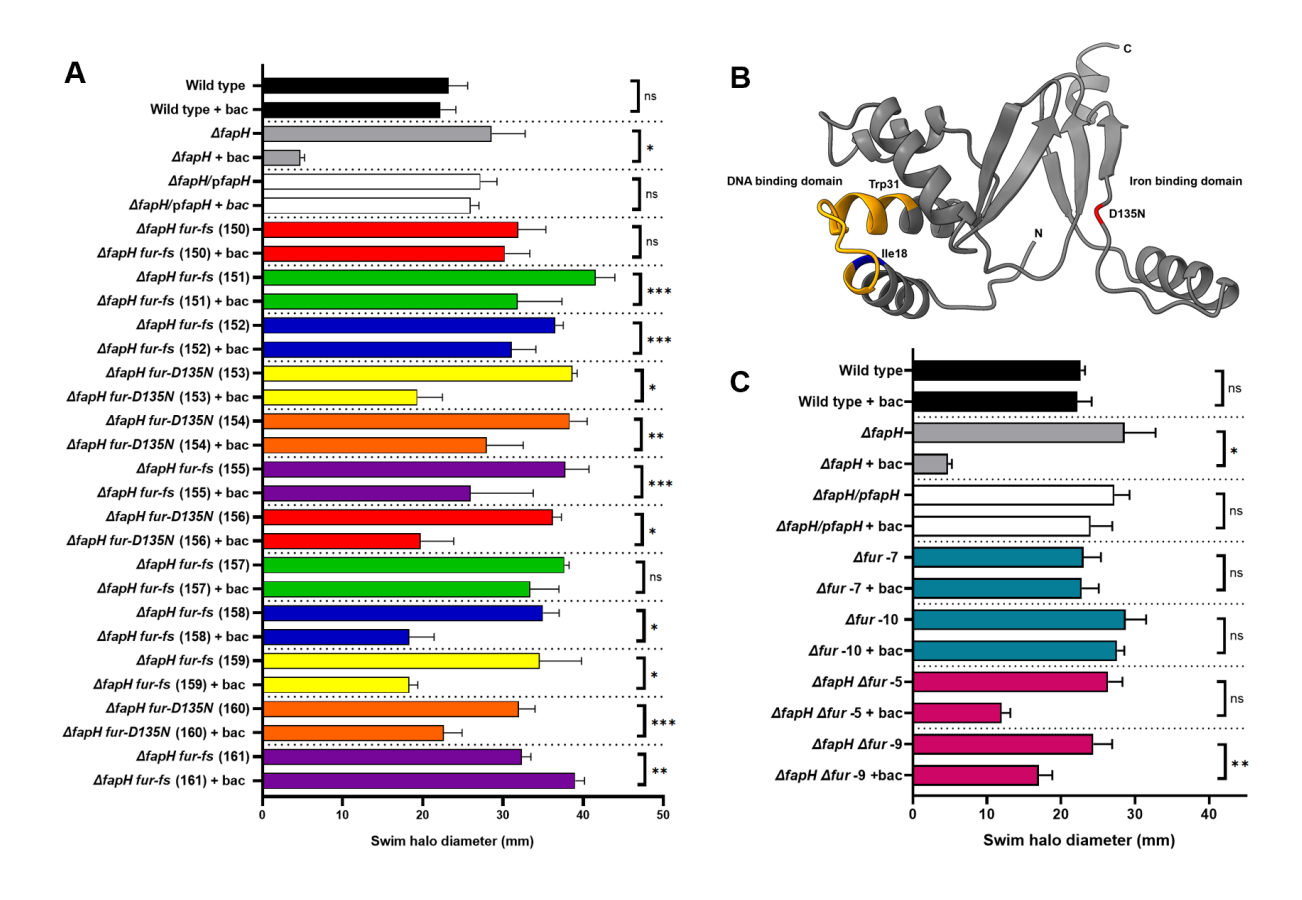


Figure 3.2: Deletion of *fur* suppresses the bacitracin sensitivity of the  $\Delta$ *fapH* mutant. (A) Isolates (150-161) identified during a suppressor search that have either a frameshift mutation (55/453 nt) resulting in a premature stop codon or a SNP D135N in the iron binding domain. The result of motility assays for each isolate with and without the presence of bacitracin is shown. \* - <0.0001, \*\* - <0.001, \*\*\* - <0.05 (B) AlphaFold model of *fur* from *H. pylori* 26695 (Jumper et al. 2021). Red D135N indicates the mutation found in bacitracin-resistant  $\Delta$ *fapH* isolates. Blue Ile18 indicates the mutation found in bacitracin-resistant  $\Delta$ *fapH* isolates, where the gold is the residues that are mutated as the result of the mutation at residue 19 that introduces a stop codon at Trp31. (C) Graphical representation of *fur* mutants in motility assays with or without the addition of bacitracin.  $\Delta$ *fur* isolates 7 and 10 have non significant differences in bacitracin sensitivity compared to the wild type and  $\Delta$ *fapH/pfapH* complementation strains. Compared to  $\Delta$ *fapH*,  $\Delta$ *fapH*  $\Delta$ *fur* isolates 5 and 9 have greater motility in the presence of bacitracin, suggesting less sensitivity to the antibiotic.

When cultured in semi-solid medium, the  $\Delta fapH$  and  $\Delta fapH$   $\Delta fur$  mutants have fewer flagella compared to the  $\Delta fur$  mutant. We considered that deletion of fur may result in a reduction in the number of flagella per cell, which might account for the increased resistance to

bacitracin in the motility-based antibiotic sensitivity assay (Fig. 3.2C). Since we were examining antibiotic sensitivity in semi-solid agar medium, we thought it prudent to likewise examine the flagellation of the H. pylori strains under the same growth condition. We previously reported that the H. pylori ΔfapH mutant had wild type flagellation when cells were grown in liquid culture (**Rosinke et al. 2025**). Interestingly, cells of the  $\Delta$ fapH mutant isolated from the semi-solid agar medium displayed reduced flagellation compared to wild type (Fig. 3.3). The bacitracin-resistant variants of the ΔfapH mutant isolated from the semi-solid agar medium also displayed reduced flagellation compared to wild type (Fig. 3.3A). The reduced flagellation of the bacitracin-resistant variants was observed when the cultures were grown either in the absence or presence of bacitracin (**Fig. 3.3A**). Similarly, the  $\Delta fapH$   $\Delta fur$  mutant, but not the  $\Delta fur$  mutant, displayed reduced flagellation when isolated from the semi-soft agar medium (Fig. 3.3B). When imaging cells of the ΔfapH mutant taken from semi-solid agar it was clear that many flagella were not associated with cells, while wild type displayed a greater number of flagella per cell and unassociated flagella were rarelyobserved (Fig. S3.1). The number of flagella per cells displayed by the  $\Delta fapH \Delta fur$  mutant was similar to that observed with the  $\Delta fapH$  mutant, and unassociated flagella were also also commonly observed with this strain. The number of flagella per cell for the  $\Delta fur$  strains were similar to that of wild type (Fig. S3.1), and as with wild type, unassociated flagella are not commonly seen with the  $\Delta fur$  strains. It should be noted that the  $\Delta fapH$  strain that was complemented with a plasmid-borne copy of fapH displayed an intermediate flagellation phenotype that was between that of the wild type and  $\Delta fapH$  strains, which was largely due to the absence of cells that had 4 or more flagella (Fig. 3.3A).

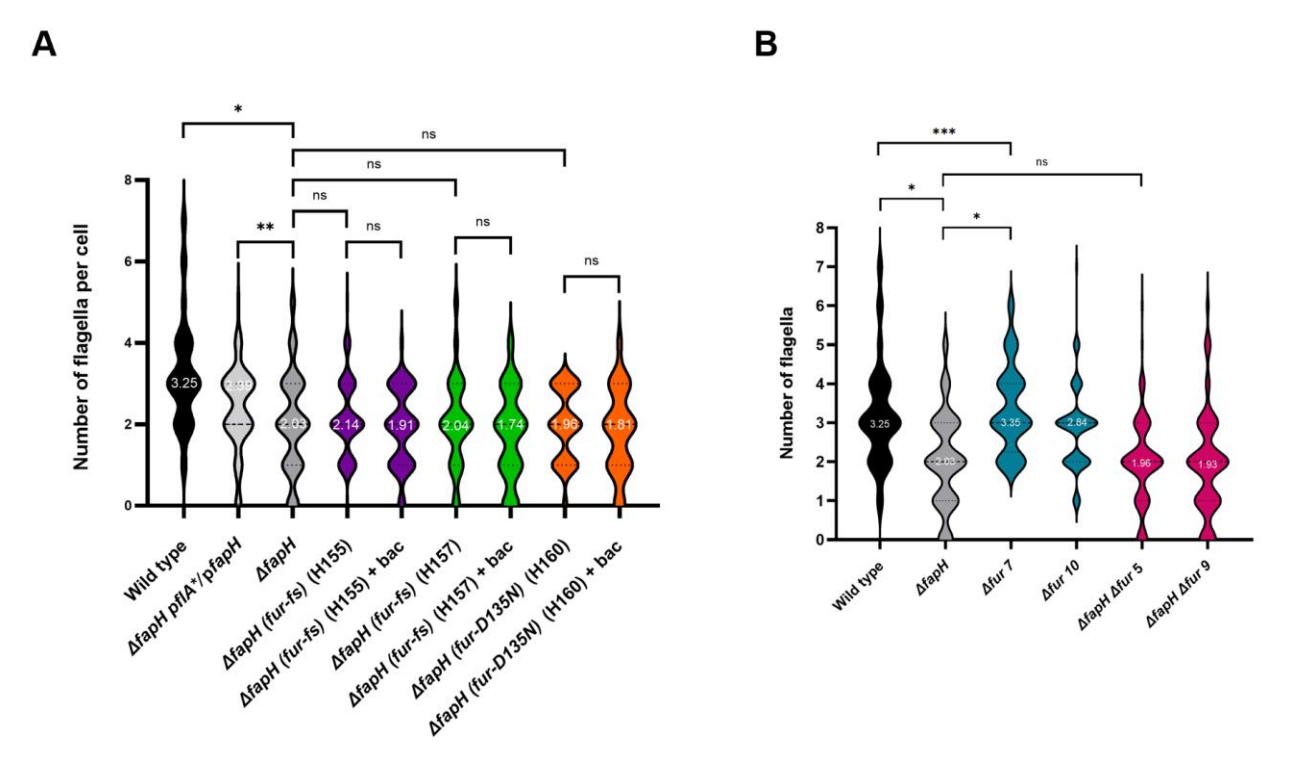


Figure 3.3: Strain Flagellation when grown in 0.25% semi-solid agar. (A)  $\Delta fapH$  and  $\Delta fapH$  bacitracin resistant isolates have reduced flagellation compared with wild type and the complement strain. (B)  $\Delta fur$  has comparable flagellation to wild type and  $\Delta fapH$   $\Delta fur$  has similar flagellation to  $\Delta fapH$ . \* indicates a P-value <0.0001, while \*\* indicates a P-value <0.005.

The reduced number of flagella per cell in  $\Delta fapH$  strains grown in semi-solid agar compared to liquid culture may be the result of the flagella being ejected or shearing off during flagellar rotation. The wild-type flagellation and absence of unassociated flagella in  $\Delta fapH$  grown in liquid culture may have been due to the lower viscosity of the liquid medium or it may have been that a significant portion of the cells in the liquid medium were not swimming.

### Cells of the strains with $\Delta fapH$ and $\Delta fur$ mutations are thinner than wild-type cells.

Examination of TEM images of cells of the  $\Delta fapH$ ,  $\Delta fapH$   $\Delta fur$ , and  $\Delta fur$  strains harvested from semi-solid agar medium differed somewhat in appearance compared to wild-type cells. Cells of all strains examined a dark, electron dense region in the center that was surrounded by a lighter, less electron dense region that may correspond to the periplasmic space (**Fig. 3.3A-E**). In wild type, the lighter region was significantly thicker compared to cells of the  $\Delta fapH$ ,  $\Delta fapH$   $\Delta fur$ , and  $\Delta fur$  strains. The lighter region of the  $\Delta fapH$  mutant was particularly thin compared to wild type, and in some places appeared discontinuous (**Fig. 3.3B**). The increased thickness of the lighter

region may have contributed to cell width as the wild-type cells were significantly wider than cells of  $\Delta fapH$ ,  $\Delta fapH \Delta fur$ , and  $\Delta fur$  mutants (**Fig. 3.3F-G**). Interestingly, the average cell width of wild type and the  $\Delta fapH$  mutant were indistinguishable when the strains were grown in liquid medium (**Fig. 3.3F**)

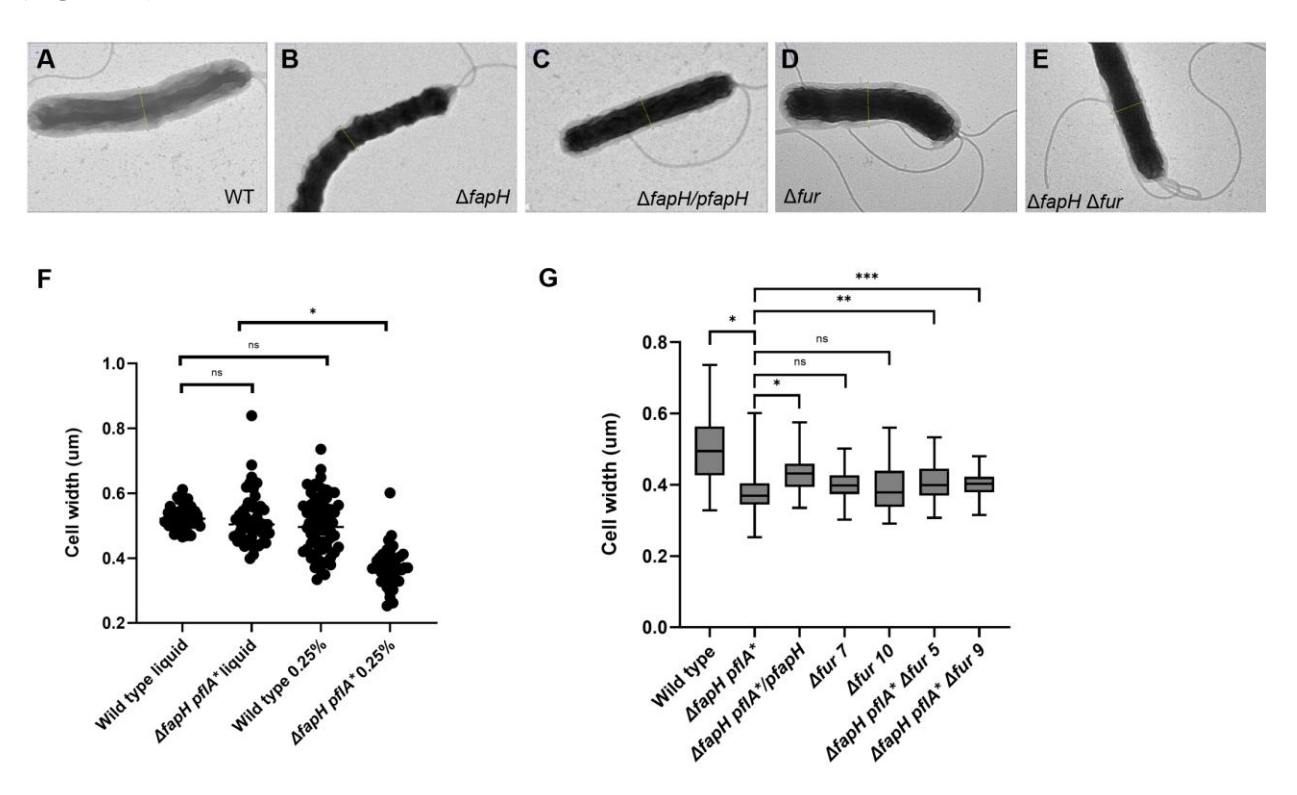


**Figure 3.4: Cell width measurements.** The cell diameter of (**A**) wild type, (**B**)  $\Delta$  fapH, (**C**)  $\Delta$  fapH/pfapH, (**D**)  $\Delta$  fur, and (**E**)  $\Delta$  fapH  $\Delta$  fur was determined by measuring the center of each cell. Cells that had a septum were not measured. (**A-E**) Examples of each measurement are seen as the line at the center of the cell. The inner membrane of the cell appears as dark, while the outer membrane due to a wash step after staining is seen as a lighter shade of gray. Many examples were present where  $\Delta$  fapH,  $\Delta$  fur, and  $\Delta$  fapH  $\Delta$  fur had less outer membrane material, often appearing as thin or absent in some regions of the cell. (**E**) Scatter plot comparing the wild type and  $\Delta$  fapH grown in liquid or 0.25% semi-solid agar. \* Indicates a P-value of <0.0001. (**F**) Box and whisker plot of width of cells grown in 0.25% semi-solid agar. \* Indicates a P-value of <0.0001, \*\* indicates a P-value of <0.005, \*\*\* indicates a P-value of <0.05. Cells measure: wild type -66,  $\Delta$  fapH -42,  $\Delta$  fapH pflA\*/pfapH -51,  $\Delta$  fur 7-20,  $\Delta$  fur 10-27,  $\Delta$  fapH  $\Delta$  fur 5-57,  $\Delta$  fapH  $\Delta$  fur 9-38.

**2,2'-Dipyridyl rescues bacitracin sensitivity in**  $\Delta$ *fapH*. The observation that the  $\Delta$ *fapH* mutant that expressed the Fur<sup>D135N</sup> variant had increased resistance to bacitracin compared to the  $\Delta$ *fapH* 

parental strain (Fig. 3.2A) suggested that apo-Fur was able to suppress the antibiotic sensitivity of the  $\Delta$  fapH mutant. To address this hypothesis, we attempted to determine if depeting ferrous iron in the growth medium suppressed the sensitivity of the ΔfapH mutant to bacitracin. 2,2'dipyridyl is a chelator that binds ferrous iron with high specificity. Since iron is required for growth of H. pylori, we initially examined the growth of wild-type H. pylori B128 in semi-solid growth medium that contained 2,2'-dipyridyl ranging in concentration from 25 µM to 100 µM. H. pylori B128 failed to grow in the medium containing 100 µM 2,2'-dipyridyl, but grew well at lower concentrations of the chelator (data not shown). Wild type formed a robust swim halo in semisolid growth medium containing bacitracin and supplemented with 25 µM, 50 µM, or 75 µM 2,2'dipyridyl (**Fig. 3.5A**). At concentrations of 25  $\mu$ M or 50 uM 2,2'-dipyridyl, the  $\Delta$ fapH mutant failed to form a swim halo in the presence of bacitracin, but at a concentration of 75 µM 2,2'-dipyridyl the  $\triangle$ fapH mutant formed a robust swim halo in the presence of bacitracin (**Fig. 3.5A**). Statistically, 75 uM 2,2'-dipyridyl was non-significant compared with  $\Delta fapH \Delta fur$  in the presence of bacitracin (Fig. 3.5B). Taken together, these data strongly suggest that culture conditions that result in the formation apo-Fur phenocopy the fur deletion in suppressing the bacitracin sensitivity of the  $\Delta fapH$ mutant.

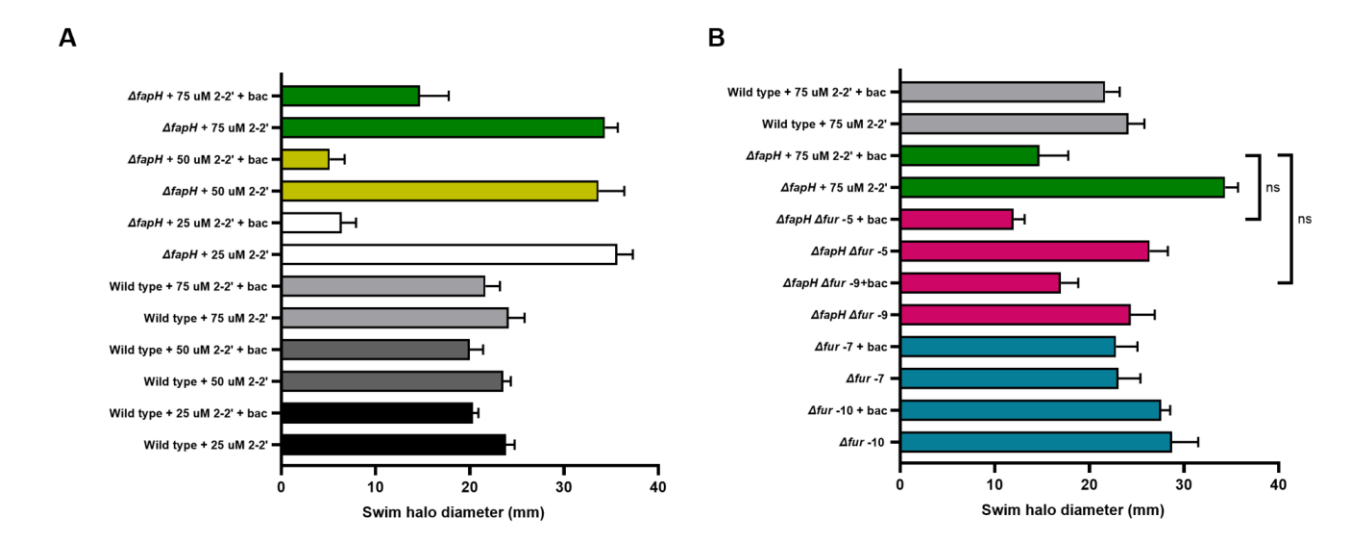


Figure 3.5: Addition of 2,2'-dipyridyl to the growth medium suppresses the bacitracin sensitivity of the  $\Delta$  fapH mutant. Motility assays in semi-solid agar after 7 days of incubation in the presence of 2-2' dipyridyl. (A) Assays were performed with the metal chelator 2,2'-dipyridyl at difference concentrations. (B) Comparison of wild type and  $\Delta$  fapH with 75 uM 2,2'-dipyridyl and  $\Delta$  fapH  $\Delta$  fur, with and without bacitracin.  $\Delta$  fapH inoculated to medium containing 25 or 50 uM of 2-2" dipyridyl had growth at the point of inoculation but no visible swim halo.

### **CONCLUSIONS**

We show here that mutations in *fur* that are predicted to result in either failure to express full-length Fur or the expression of a Fur variant that is deficient in metal-binding (i.e., FurD<sup>135N</sup>) suppress the bacitracin sensitivity of the *H. pylori*  $\Delta$  fapH mutant (**Fig. 3.2**). *H. pylori* Fur is a global regulator that controls expression of many genes and is unusual in that both the apo- and holoforms of the protein are involved in gene regulation (*Kang et al. 2024*). Our data suggest that mutations that result in loss of holo-Fur is sufficient for suppressing the bacitracin sensitivity of the  $\Delta$  fapH mutant. Consistent with this hypothesis, the addition of the ferrous iron chelator 2,2'-dipyridyl to the growth medium suppressed the bacitracin sensitivity of the  $\Delta$  fapH mutant (**Fig. 3.5**). It is unclear how disrupting Fur function suppresses the bacitracin sensitivity of the  $\Delta$  fapH mutant, but it presumably results from altered expression of one or more gene. Further investigation into genes in the Fur regulon should provide insight into this issue.

A couple  $\Delta fapH$  isolates had the same nonsense mutation in IpxF that introduced a stop codon early in the coding sequence of the gene. The  $\Delta fapH \Delta IpxF$  strains (**Fig. 3.1**) have reduced motility and reduced sensitivity to bacitracin compared to  $\Delta fapH$ . LpxF catalyzes the removal of a phosphate from the 4' position of lipid A (**Stead et al. 2008**). Although we did not confirm that disrupting IpxF was responsible for suppressing the bacitracin sensitivity of the  $\Delta fapH$  mutant, the IpxF mutation was the best candidate for such a suppressor. The presence of phosphate moieties at both the 1 and 4' positions in lipid A may stabilize the outer leaflet of the OM and help to preserve the barrier function of the OM in the absence of the FapH ring. A top priority for future studies will be to confirm that loss LpxF is able to suppress the bacitracin sensitivity of the  $\Delta fpaH$  mutant.

# **SUPPORTING MATERIALS**

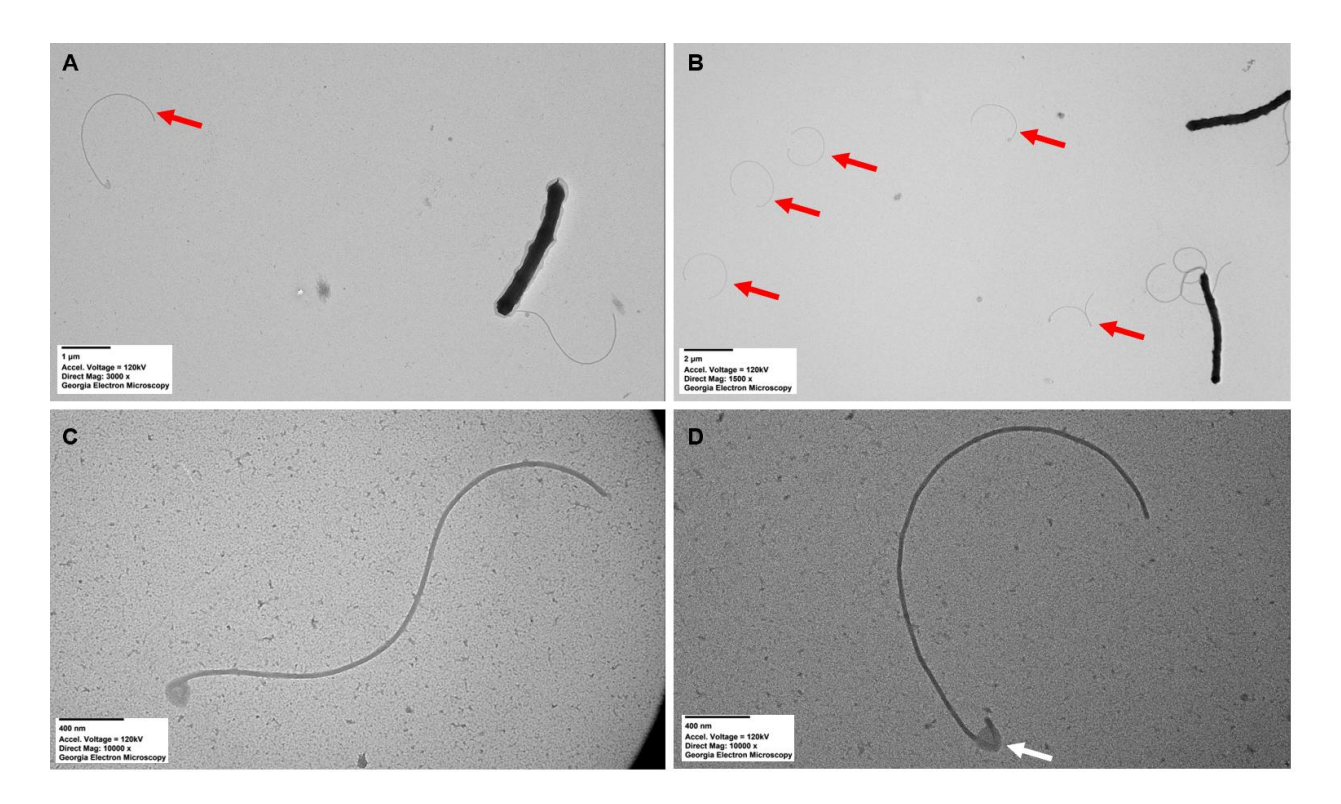


**Figure S3.1: Unassociated flagella in \Delta** *fapH*. (**A and B**) Unassociated flagella as seen by TEM in  $\Delta$  *fapH* grown in semi-solid agar as indicated by red arrows. (**C and D**) Higher magnification of unassociated flagella. (**D**) Some unassociated flagella have structures at one end that appear to be the remnants of membrane and the hook or possibly the bulb (white arrow).

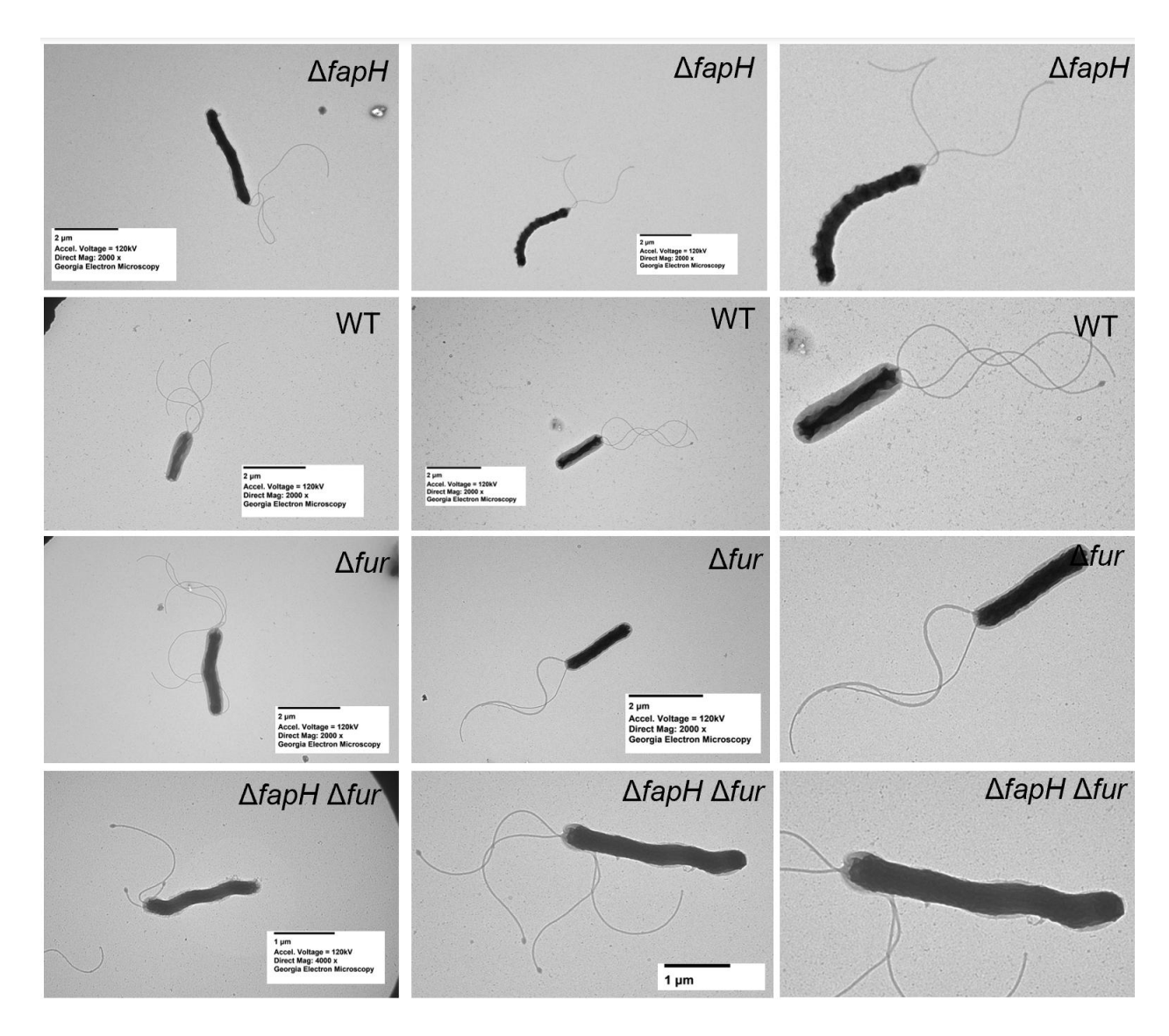


**Figure S3.2: Membrane morphology of strains**. Examples of the different outer membrane morphologies in  $\Delta fapH$ , Wild type,  $\Delta fur$ , and  $\Delta fapH$   $\Delta fur$ . The inner membrane is seen as the dark area of the cell, while the outer membrane is seen as the lighter gray area of the cell. This contrast is due to the water wash step following staining with 1% uranyl acetate that removes the stain from the outer membrane, making it appear lighter than the unwashed inner membrane.

Table S3.1: Strain WGS

ΔfapH pfIA* (H54	)				
CV725_RS00010	HP1527	comH, competence protein	Δ1 bp (708/1440 nt)	Val236fs	98.8%
*CV725 RS00395	HP1451	spoIIIJ-associated protein	+T (689/798 nt)	Tyr230fs	98.1%
CV725_RS00960	HP1274	pflA, paralyzed flagella protein	+G (1428/2406 nt)	offsetting fs	98.4%
_			Δ1 bp (1391/2406 nt)	mutations	98.5%
maf	HP1239	DS of maf, US of hp1239	(A) <sub>13→14</sub>		80.5%
CV725_RS01150	HP1240	(hypothetical protein)	intergenic (+61/+394)		
mreC	HP1372	mreC, rod shape-determining protein	codon-220 (TAC→CAC)	Tyr220His	98.8%
CV725_RS02745	HP0098	thrC, threonine synthase	codon-417 ( <u>G</u> AA→ <u>A</u> AA)	Glu417Lys	98.9%
*tlpB	HP0103	tlpB, methyl-accepting chemotaxis protein	codon-26 (G <u>G</u> G→G <u>A</u> G)	Gly26Glu	98.6%
*CV725_RS03745	HP0298	dppA, dipeptide ABC transporter, periplasmic dipeptide-binding protein	(T) <sub>10→9</sub> (30/1644 nt)	Phe10fs	96.4%
*CV725_RS04335	HP1028	hypothetical protein	codon-16 (GCT→GTT)	Ala16Val	98.5%
CV725_RS04505	HP0475	<i>modD</i> , molybdenum ABC transport protein	codon-155 (TT <u>A</u> →TT <u>G</u> )	Leu155Leu	99.1%
CV725_RS04600 CV725_RS04605	HP0875 HP0876	US of katA, US of frpB	(A) <sub>5→6</sub> intergenic (-34/-290)		83.4%
CV725_RS04785	HP0838	fapH	codon-18 (G <u>T</u> C→G <u>C</u> C) Δ490	Val18Ala Deletion	99.1%
CV725_RS06350	HP0527	cag pathogenicity island protein	соdon-752	Thr752Thr	96.2%
CV725_RS06350	HF0327	(cag7)	(AC <u>C</u> →AC <u>G</u> )		
			codon-742 (GC <u>T</u> →GC <u>C</u> )	Ala742Ala	99.3%
CV725_RS06500	HP0499	pldA, phospholipase A pseudogene	(G) <sub>10→11</sub> (683/1070 nt)	phase 'off' to phase 'on'	62.8%
babA	HP1243	US of babA, DS of tRNA_fMet	(T) <sub>13→12</sub>		86.2%
CV725_RS06645	tRNA_fMet		intergenic (-131/+149)		
CV725_RS08550	HP1412	DS of hp1412 (hypothetical protein),	(C) <sub>11→10</sub>		94.6%
queF	HP1413	DS of queF	intergenic (+11/+121)		
ΔfapH pfIA* (H150)			•	II.	1
NCBI designation	26695 locus tag	Gene/ description	Mutation/annotation	Impact	Frequency
CV725_RS00040	NA	Site-specific DNA-methyltransferase, pseudogene	(G) <sub>14→12</sub> (1452/2053 nt)	No effect	94.8%
CV725_RS00720	HP1321	DS of HP1321 conserved	(ATACATAA) <sub>10→5</sub>	Impact	99.2%
CV725_RS00725	HP1322	hypothetical ATP-binding protein and US of HP1322 hypothetical protein.	intergenic (-194/+7)	unknown	
CV725_RS08420	HP1353	Type ISP C-terminal specificity domain, pseudogene	(C) <sub>14→13</sub> (3223/3372 nt)	No effect	93.4%
CV725_RS03925	HP0337	hypothetical protein	(A) <sub>7→8</sub> (62/339 nt)	Asn19-fs	98%
	HP1027	Ferric uptake regulation	(A) <sub>8→9</sub> (55/453 nt)	Ile18-fs	97.4%
fur	111 1021	protein (fur).	(7 t)0=3 (007 100 m)		

ΔfapH pfIA* (H151)					
NCBI	26695	Gene/ description	Mutation/annotati	Impact	Frequency
designation	locus tag		on		
CV725_RS00040	NA	Site-specific DNA-methyltransferase,	(G) <sub>14→13</sub>	phase 'off' to	91.4%
		pseudogene	(1453/2053 nt)	phase 'on'	
CV725_RS00720	HP1321	DS of HP1321 conserved	(ATACATAA) <sub>10→5</sub>	Impact	100%
CV725_RS00725	HP1322	hypothetical ATP-binding protein and	intergenic (-194/+7)	unknown	
		US of HP1322 hypothetical protein.			
CV725_RS08420	HP1353	Type ISP C-terminal	(C) <sub>14→13</sub>	No effect	88.6%
		specificity domain,	(3223/3372 nt)		
		pseudogene			
fur	HP1027	Ferric uptake regulation protein (fur).	(A) <sub>8→9</sub> (55/453 nt)	lle18-fs	97.1%
CV725_RS05120	HP0771	hypothetical protein.	(T) <sub>8→9</sub> (59/738 nt)	Phe19-fs	97.2%
A.C. 11. (14. (11. 1. 1. 1. 1. 1. 1. 1. 1. 1. 1. 1. 1.					
Δ <i>fapH pfIA</i> * (H152 <u>)</u> NCBI	) 26695	Gene/ description	Mutation/annotation	Impact	Frequency
designation	locus tag	Gener description	Widtation/annotation	IIIIpact	riequency
CV725_RS00040	NA	Site-specific DNA-methyltransferase,	(G) <sub>14→13</sub>	phase 'off' to	90.3%
		pseudogene	(1453/2053 nt)	phase 'on'	
CV725_RS00720	HP1321	DS of HP1321 conserved	(ATACATAA) <sub>10→5</sub>	Impact	99.6%
CV725_RS00725	HP1322	hypothetical ATP-binding protein and	intergenic (-194/+7)	unknown	
_		US of HP1322 hypothetical protein.			
CV725_RS08420	HP1353	Type ISP C-terminal specificity	(C) <sub>14→13</sub>	No effect	91.9%
		domain, pseudogene	(3223/3372 nt)		
fur	HP1027	Ferric uptake regulation protein (fur).	(A) <sub>8→9</sub> (55/453 nt)	lle18-fs	96.7%
CV725_RS05120	HP0771	hypothetical protein.	(T) <sub>8→9</sub> (59/738 nt)	Phe19-fs	96%
hefC	HP0607	efflux RND transporter permease	Codon-808	Ala808Val	99.5%
		subunit HefC.	(G <u>C</u> T→G <u>T</u> T)		
ΔfapH pflA* (H153)		Lorent description	Modelinglessetation	1 1	l <b>-</b>
NCBI	26695	Gene/ description	Mutation/annotation	Impact	Frequency
designation	locus tag	0:4 :6: DNIA :4 !4 .6	(0)		04.00/
CV725_RS00040	NA	Site-specific DNA-methyltransferase,	(G) <sub>14→13</sub>	phase 'off' to	91.6%
01/705 5000700	LIBAGGA	pseudogene	(1453/2053 nt)	phase 'on'	22.22/
CV725_RS00720	HP1321	DS of HP1321 conserved	(ATACATAA) <sub>10→5</sub>	Impact	99.3%
CV725_RS00725	HP1322	hypothetical ATP-binding protein and	intergenic (-194/+7)	unknown	
01/705 - 5004000	_	US of HP1322 hypothetical protein.	44001	- ··	00.00/
CV725_RS01830		HP1117 family Sel1-like repeat protein	Δ108 bp (231-338/771 nt)	Truncation	99.8%
CV725_RS08420	HP1353	Type ISP C-terminal specificity	(C) <sub>14→13</sub>	No effect	92.4%
CV723_N300420	1111333	domain, pseudogene	(3223/3372 nt)	No ellect	92.470
fur	HP1027	Ferric uptake regulation protein (fur).	(3223/3372 ftt) (A) <sub>8→9</sub> (55/453 nt)	lle18-fs	100%
CV725_RS05120	HP0771	hypothetical protein	Δ27 bp (68-94/738 nt)	Truncation	100%
		SurA N-terminal domain protein;	Codon-		
CV725_RS05665	HP0659	- I	398 ( <u>C</u> GC→ <u>T</u> GC)	Arg398Cys	100%
		predicted periplasmic peptidyl-prolyl cis-trans isomerase.			
	1	CISTUALIS ISUITICIASE.			
	†			i de la companya de	1
ΔfapH ofIA* (H154)	)				1
Δ <i>fapH pfIA</i> * (H154)		Gene/ description	Mutation/annotation	Impact	Frequency
NCBI	26695	Gene/ description	Mutation/annotation	Impact	Frequency
		Gene/ description  Site-specific DNA-methyltransferase,	Mutation/annotation (G) <sub>14→12</sub>	Impact No effect	Frequency 94.5%

CV725_RS00720	HP1321	DS of HP1321 conserved	(ATACATAA) <sub>10→5</sub>	Impact	99%
CV725_RS00725	HP1322	hypothetical ATP-binding protein and	intergenic (-194/+7)	unknown	3370
01720_71000720	111 1022	US of HP1322 hypothetical protein.	3 1 ( 1 , 7	dillitiowii	
CV725_RS08420	HP1353	Type ISP C-terminal specificity	(C) <sub>14→13</sub>	No effect	90.1%
CV723_N300420	111 1333	domain, pseudogene	(3223/3372 nt)	NO effect	90.176
fur	HP1027	Ferric uptake regulation protein (fur).	$C \rightarrow T (\underline{G}AC \rightarrow \underline{A}AC)$	Asp135Asn	99.7%
	HP0771		$\Delta 27 \text{ bp } (68-94/738 \text{ nt})$		100%
CV725_RS05120		hypothetical protein.		Truncation	
hefC	HP0607	efflux RND transporter permease	Codon-808	Ala808Val	99.7%
		subunit HefC.	(G <u>C</u> T→G <u>T</u> T)		
A f!! f! A+ /!!4 F.F.					
ΔfapH pflA* (H155		Const description	Mutation/appatation	lumpost	
NCBI	26695	Gene/ description	Mutation/annotation	Impact	Frequency
designation	locus tag		(0)		
CV725_RS00040	NA	Site-specific DNA-methyltransferase,	(G) <sub>14→13</sub>	phase 'off' to	92.2%
		pseudogene	(1453/2053 nt)	phase 'on'	
CV725_RS00385	HP1453	outer membrane beta-barrel	(T) <sub>17→16</sub>	Unknown	80.5%
mnmE		protein/tRNA	intergenic (-105/+113)		
		uridine-5-carboxymethylaminomethyl			
		(34) synthesis GTPase MnmE			
CV725_RS00720	HP1321	DS of HP1321 conserved	(ATACATAA) <sub>10→5</sub>	Impact	99.5%
CV725_RS00725	HP1322	hypothetical ATP-binding protein and	intergenic (-194/+7)	unknown	
		US of HP1322 hypothetical protein.			
CV725_RS08420	HP1353	Type ISP C-terminal specificity	(C) <sub>14→13</sub>	No effect	91.4%
		domain, pseudogene	(3223/3372 nt)		
CV725_RS03700	HP0289	vacuolating cytotoxin	Codon-670	Gly670Arg	100%
		domain-containing protein.	( <u>G</u> GG→ <u>A</u> GG)		
fur	HP1027	Ferric uptake regulation protein (fur).	(A) <sub>8→9</sub> (55/453 nt)	lle18-fs	94.9%
CV725_RS05120	HP0771	hypothetical protein.	(T) <sub>8→9</sub> (59/738 nt)	Phe19-fs	94.7%
CV725_RS07860	HP1581	methicillin resistance protein (Ilm).	Codon-43	Pro43Thr	100%
		у по	( <u>C</u> CA→ <u>A</u> CA)		
			/		
ΔfapH pfIA* (H156	)	L		- L	l .
NCBI	26695	Gene/ description	Mutation/annotation	Impact	Frequency
designation	locus tag	p			
CV725_RS00040	NA	Site-specific DNA-methyltransferase,	(G) <sub>14→13</sub>	phase 'off' to	90.4%
_		pseudogene	(1453/2053 nt)	phase 'on'	
CV725_RS00720	HP1321	DS of HP1321 conserved	(ATACATAA) <sub>10→5</sub>	Impact	99.7%
CV725_RS00725	HP1322	hypothetical ATP-binding protein and	intergenic (-194/+7)	unknown	
01720_7.000720		US of HP1322 hypothetical protein.			
rpsR	HP1244	DS of HP1244 rpsR 30S ribosomal	(A) <sub>13→14</sub>	Unknown	80.3%
babA	HP1243	protein S18 and US of HP1243 outer	intergenic (+195/-132)	Jimilowii	30.070
	111 12 10	membrane protein <i>babA</i>	, ,		
CV725_RS08420	HP1353	Type ISP C-terminal specificity	(C) <sub>14→13</sub>	No effect	89.8%
07720_1\300420	111 1333	domain, pseudogene	(3223/3372 nt)	INO GUECE	03.070
fur	HP1027	Ferric uptake regulation protein (fur).	$C \rightarrow T (\underline{G}AC \rightarrow \underline{A}AC)$	Asp135Asn	100%
		hypothetical protein.	$\Delta 27 \text{ bp } (68-94/738 \text{ nt})$		
CV725_RS05120	HP0771	1 *:		Truncation	100%
hefC	HP0607	efflux RND transporter permease	Codon-71	Gly71Arg	100%
		subunit HefC.	( <u>G</u> GG→ <u>A</u> GG)		
A famil m#1A+ /114 ==					
ΔfapH pflA* (H157	-	Canal dagarintian	Mutation/ann=t=t!=:	Impost	
NCBI designation	26695	Gene/ description	Mutation/annotation	Impact	Frequency
นธอเษาเลเเบา	locus tag				

CV725_RS00040	NA	Site-specific DNA-methyltransferase,	(G) <sub>14→13</sub>	phase 'off' to	93.5%
		pseudogene	(1453/2053 nt)	phase 'on'	
CV725_RS00720	HP1321	DS of HP1321 conserved	(ATACATAA) <sub>10→5</sub>	Impact	98.8%
CV725_RS00725	HP1322	hypothetical ATP-binding protein and	intergenic (-194/+7)	unknown	
		US of HP1322 hypothetical protein.			
CV725_RS08420	HP1353	Type ISP C-terminal specificity	(C) <sub>14→13</sub>	No effect	88.1%
		domain, pseudogene	(3223/3372 nt)		
fur	HP1027	Ferric uptake regulation protein (fur).	(A) <sub>8→9</sub> (55/453 nt)	lle18-fs	94.8%
CV725_RS05120	HP0771	hypothetical protein.	(T) <sub>8→9</sub> (59/738 nt)	Phe19-fs	93.3%
CV725_RS06910	HP0947	hypothetical protein	+T coding (173/363 nt)	Lys58-fs	100%
ΔfapH pfIA* (H158	•	T	T	T -	T _
NCBI	26695	Gene/ description	Mutation/annotation	Impact	Frequency
designation	locus tag				
CV725_RS00040	NA	Site-specific DNA-methyltransferase,	(G) <sub>14→13</sub>	phase 'off' to	96.5%
		pseudogene	(1453/2053 nt)	phase 'on'	30.9%
CV725_RS00720	HP1321	DS of HP1321 conserved	(ATACATAA) <sub>10→5</sub>	Impact	100%
CV725_RS00725	HP1322	hypothetical ATP-binding protein and	intergenic (-194/+7)	unknown	
		US of HP1322 hypothetical protein.			
CV725_RS02330	HP1370	biotin synthase/type III restriction	(C) <sub>13→14</sub>	No effect	85%
CV725_RS02335	NA	enzyme.	intergenic (-243/-51)		
CV725_RS08420	HP1353	Type ISP C-terminal specificity	(C) <sub>14→13</sub>	No effect	65.5%
		domain, pseudogene	(3223/3372 nt)		
fur	HP1027	Ferric uptake regulation protein (fur)	(A) <sub>8→9</sub> (55/453 nt)	lle18-fs	99.5%
CV725_RS05120	HP0771	hypothetical protein.	Δ27 bp (68-94/738 nt)		100%
hefC	HP0607	efflux RND transporter permease	Codon-642	Asn64Asp	100%
		subunit HefC.	( <u>A</u> AT→ <u>G</u> AT)		
A.C. 11 (1A+ /114=0					
ΔfapH pfIA* (H159		Ta	T	T	· _
NCBI	26695	Gene/ description	Mutation/annotation	Impact	Frequency
designation	locus tag	16: DAIA di 16: 6	(0)		0.5.00/
CV725_RS00040	NA	Site-specific DNA-methyltransferase,	(G) <sub>14→13</sub>	phase 'off' to	95.9%
		pseudogene	(1453/2053 nt)	phase 'on'	
CV725_RS00720	1		(1-1-1-1-1)		
CV725_RS00725	HP1321	DS of HP1321 conserved	(ATACATAA) <sub>10→5</sub>	Impact	99.1%
37720_11000720	HP1321 HP1322	DS of HP1321 conserved hypothetical ATP-binding protein and	(ATACATAA) <sub>10→5</sub> intergenic (-194/+7)	Impact unknown	99.1%
	HP1322	DS of HP1321 conserved hypothetical ATP-binding protein and US of HP1322 hypothetical protein.	intergenic (-194/+7)	unknown	
CV725_RS02330	HP1322 HP1370	DS of HP1321 conserved hypothetical ATP-binding protein and US of HP1322 hypothetical protein. biotin synthase/type III restriction	intergenic (-194/+7) (C) <sub>13→14</sub>	•	99.1%
CV725_RS02330 CV725_RS02335	HP1322 HP1370 NA	DS of HP1321 conserved hypothetical ATP-binding protein and US of HP1322 hypothetical protein. biotin synthase/type III restriction enzyme.	intergenic (-194/+7)  (C) <sub>13→14</sub> intergenic (-243/-51)	unknown  No effect	88.3%
CV725_RS02330	HP1322 HP1370	DS of HP1321 conserved hypothetical ATP-binding protein and US of HP1322 hypothetical protein. biotin synthase/type III restriction enzyme.  Type ISP C-terminal specificity	intergenic (-194/+7)  (C) <sub>13→14</sub> intergenic (-243/-51)  (C) <sub>14→13</sub>	unknown	
CV725_RS02330 CV725_RS02335 CV725_RS08420	HP1322 HP1370 NA HP1353	DS of HP1321 conserved hypothetical ATP-binding protein and US of HP1322 hypothetical protein. biotin synthase/type III restriction enzyme.  Type ISP C-terminal specificity domain, pseudogene	intergenic (-194/+7)  (C) <sub>13→14</sub> intergenic (-243/-51)  (C) <sub>14→13</sub> (3223/3372 nt)	unknown  No effect  No effect	88.3% 89.4%
CV725_RS02330 CV725_RS02335 CV725_RS08420 fur	HP1322  HP1370 NA  HP1353  HP1027	DS of HP1321 conserved hypothetical ATP-binding protein and US of HP1322 hypothetical protein. biotin synthase/type III restriction enzyme.  Type ISP C-terminal specificity domain, pseudogene Ferric uptake regulation protein (fur)	intergenic (-194/+7)  (C) <sub>13→14</sub> intergenic (-243/-51)  (C) <sub>14→13</sub> (3223/3372 nt)  (A) <sub>8→9</sub> (55/453 nt)	unknown  No effect  No effect  Ile18-fs	88.3% 89.4% 98.1%
CV725_RS02330 CV725_RS02335 CV725_RS08420	HP1322 HP1370 NA HP1353	DS of HP1321 conserved hypothetical ATP-binding protein and US of HP1322 hypothetical protein. biotin synthase/type III restriction enzyme.  Type ISP C-terminal specificity domain, pseudogene	intergenic (-194/+7)  (C) <sub>13→14</sub> intergenic (-243/-51)  (C) <sub>14→13</sub> (3223/3372 nt)	unknown  No effect  No effect	88.3% 89.4%
CV725_RS02330 CV725_RS02335 CV725_RS08420 fur CV725_RS05120	HP1322 HP1370 NA HP1353 HP1027 HP0771	DS of HP1321 conserved hypothetical ATP-binding protein and US of HP1322 hypothetical protein. biotin synthase/type III restriction enzyme.  Type ISP C-terminal specificity domain, pseudogene Ferric uptake regulation protein (fur)	intergenic (-194/+7)  (C) <sub>13→14</sub> intergenic (-243/-51)  (C) <sub>14→13</sub> (3223/3372 nt)  (A) <sub>8→9</sub> (55/453 nt)	unknown  No effect  No effect  Ile18-fs	88.3% 89.4% 98.1%
CV725_RS02330 CV725_RS02335 CV725_RS08420  fur CV725_RS05120  ΔfapH pfIA* (H160	HP1322  HP1370 NA  HP1353  HP1027  HP0771	DS of HP1321 conserved hypothetical ATP-binding protein and US of HP1322 hypothetical protein. biotin synthase/type III restriction enzyme.  Type ISP C-terminal specificity domain, pseudogene Ferric uptake regulation protein (fur) hypothetical protein.	intergenic (-194/+7)  (C) <sub>13→14</sub> intergenic (-243/-51)  (C) <sub>14→13</sub> (3223/3372 nt)  (A) <sub>8→9</sub> (55/453 nt)  (T) <sub>8→9</sub> (59/738 nt)	unknown  No effect  No effect  Ile18-fs Phe19-fs	88.3% 89.4% 98.1% 94.8%
CV725_RS02330 CV725_RS02335 CV725_RS08420  fur CV725_RS05120  ΔfapH pfIA* (H160 NCBI	HP1322  HP1370 NA  HP1353  HP1027  HP0771  D)  26695	DS of HP1321 conserved hypothetical ATP-binding protein and US of HP1322 hypothetical protein. biotin synthase/type III restriction enzyme.  Type ISP C-terminal specificity domain, pseudogene Ferric uptake regulation protein (fur)	intergenic (-194/+7)  (C) <sub>13→14</sub> intergenic (-243/-51)  (C) <sub>14→13</sub> (3223/3372 nt)  (A) <sub>8→9</sub> (55/453 nt)	unknown  No effect  No effect  Ile18-fs	88.3% 89.4% 98.1%
CV725_RS02330 CV725_RS02335 CV725_RS08420 fur CV725_RS05120 ΔfapH pflA* (H160 NCBI designation	HP1322  HP1370 NA  HP1353  HP1027  HP0771  26695 locus tag	DS of HP1321 conserved hypothetical ATP-binding protein and US of HP1322 hypothetical protein. biotin synthase/type III restriction enzyme.  Type ISP C-terminal specificity domain, pseudogene Ferric uptake regulation protein (fur) hypothetical protein.  Gene/ description	intergenic (-194/+7)  (C) <sub>13→14</sub> intergenic (-243/-51)  (C) <sub>14→13</sub> (3223/3372 nt)  (A) <sub>8→9</sub> (55/453 nt)  (T) <sub>8→9</sub> (59/738 nt)  Mutation/annotation	unknown  No effect  No effect  Ile18-fs Phe19-fs  Impact	88.3% 89.4% 98.1% 94.8%
CV725_RS02330 CV725_RS02335 CV725_RS08420  fur CV725_RS05120  ΔfapH pfIA* (H160 NCBI	HP1322  HP1370 NA  HP1353  HP1027  HP0771  D)  26695	DS of HP1321 conserved hypothetical ATP-binding protein and US of HP1322 hypothetical protein. biotin synthase/type III restriction enzyme.  Type ISP C-terminal specificity domain, pseudogene Ferric uptake regulation protein (fur) hypothetical protein.  Gene/ description  Site-specific DNA-methyltransferase,	intergenic (-194/+7)  (C) <sub>13→14</sub> intergenic (-243/-51)  (C) <sub>14→13</sub> (3223/3372 nt)  (A) <sub>8→9</sub> (55/453 nt)  (T) <sub>8→9</sub> (59/738 nt)  Mutation/annotation  (G) <sub>14→13</sub>	unknown  No effect  No effect  Ile18-fs  Phe19-fs  Impact  phase 'off' to	88.3% 89.4% 98.1% 94.8%
CV725_RS02330 CV725_RS02335 CV725_RS08420  fur CV725_RS05120  ΔfapH pflA* (H160 NCBI designation CV725_RS00040	HP1322  HP1370 NA  HP1353  HP1027  HP0771  D)  26695 locus tag  NA	DS of HP1321 conserved hypothetical ATP-binding protein and US of HP1322 hypothetical protein. biotin synthase/type III restriction enzyme. Type ISP C-terminal specificity domain, pseudogene Ferric uptake regulation protein (fur) hypothetical protein.  Gene/ description  Site-specific DNA-methyltransferase, pseudogene	intergenic (-194/+7)  (C) <sub>13→14</sub> intergenic (-243/-51)  (C) <sub>14→13</sub> (3223/3372 nt)  (A) <sub>8→9</sub> (55/453 nt)  (T) <sub>8→9</sub> (59/738 nt)   Mutation/annotation  (G) <sub>14→13</sub> (1453/2053 nt)	unknown  No effect  No effect  Ile18-fs Phe19-fs  Impact  phase 'off' to phase 'on'	88.3% 89.4% 98.1% 94.8% Frequency
CV725_RS02330 CV725_RS02335 CV725_RS08420  fur CV725_RS05120  ΔfapH pfIA* (H160 NCBI designation CV725_RS00040  CV725_RS00720	HP1322  HP1370 NA  HP1353  HP1027  HP0771  D)  26695 locus tag  NA  HP1321	DS of HP1321 conserved hypothetical ATP-binding protein and US of HP1322 hypothetical protein. biotin synthase/type III restriction enzyme. Type ISP C-terminal specificity domain, pseudogene Ferric uptake regulation protein (fur) hypothetical protein.  Gene/ description  Site-specific DNA-methyltransferase, pseudogene DS of HP1321 conserved	(C) <sub>13→14</sub> intergenic (-194/+7)  (C) <sub>13→14</sub> intergenic (-243/-51)  (C) <sub>14→13</sub> (3223/3372 nt)  (A) <sub>8→9</sub> (55/453 nt)  (T) <sub>8→9</sub> (59/738 nt)   Mutation/annotation  (G) <sub>14→13</sub> (1453/2053 nt)  (ATACATAA) <sub>10→5</sub>	unknown  No effect  No effect  Ile18-fs  Phe19-fs  Impact  phase 'off' to phase 'on'  Impact	88.3% 89.4% 98.1% 94.8%
CV725_RS02330 CV725_RS02335 CV725_RS08420  fur CV725_RS05120  ΔfapH pflA* (H160 NCBI designation CV725_RS00040	HP1322  HP1370 NA  HP1353  HP1027  HP0771  D)  26695 locus tag  NA	DS of HP1321 conserved hypothetical ATP-binding protein and US of HP1322 hypothetical protein. biotin synthase/type III restriction enzyme.  Type ISP C-terminal specificity domain, pseudogene Ferric uptake regulation protein (fur) hypothetical protein.  Gene/ description  Site-specific DNA-methyltransferase, pseudogene DS of HP1321 conserved hypothetical ATP-binding protein and	intergenic (-194/+7)  (C) <sub>13→14</sub> intergenic (-243/-51)  (C) <sub>14→13</sub> (3223/3372 nt)  (A) <sub>8→9</sub> (55/453 nt)  (T) <sub>8→9</sub> (59/738 nt)   Mutation/annotation  (G) <sub>14→13</sub> (1453/2053 nt)	unknown  No effect  No effect  Ile18-fs Phe19-fs  Impact  phase 'off' to phase 'on'	88.3% 89.4% 98.1% 94.8% Frequency
CV725_RS02330 CV725_RS02335 CV725_RS08420  fur CV725_RS05120  AfapH pfIA* (H160 NCBI designation CV725_RS00040  CV725_RS00720 CV725_RS00725	HP1322  HP1370 NA  HP1353  HP1027  HP0771  D)  26695 locus tag  NA  HP1321 HP1322	DS of HP1321 conserved hypothetical ATP-binding protein and US of HP1322 hypothetical protein. biotin synthase/type III restriction enzyme.  Type ISP C-terminal specificity domain, pseudogene Ferric uptake regulation protein (fur) hypothetical protein.  Gene/ description  Site-specific DNA-methyltransferase, pseudogene DS of HP1321 conserved hypothetical ATP-binding protein and US of HP1322 hypothetical protein.	(C) <sub>13→14</sub> intergenic (-194/+7)  (C) <sub>13→14</sub> intergenic (-243/-51)  (C) <sub>14→13</sub> (3223/3372 nt)  (A) <sub>8→9</sub> (55/453 nt)  (T) <sub>8→9</sub> (59/738 nt)  Mutation/annotation  (G) <sub>14→13</sub> (1453/2053 nt)  (ATACATAA) <sub>10→5</sub> intergenic (-194/+7)	unknown  No effect  No effect  Ile18-fs Phe19-fs  Impact  phase 'off' to phase 'on' Impact unknown	88.3% 89.4% 98.1% 94.8% Frequency 94.2% 99%
CV725_RS02330 CV725_RS02335 CV725_RS08420  fur CV725_RS05120  ΔfapH pfIA* (H160 NCBI designation CV725_RS00040  CV725_RS00720	HP1322  HP1370 NA  HP1353  HP1027  HP0771  D)  26695 locus tag  NA  HP1321	DS of HP1321 conserved hypothetical ATP-binding protein and US of HP1322 hypothetical protein. biotin synthase/type III restriction enzyme.  Type ISP C-terminal specificity domain, pseudogene Ferric uptake regulation protein (fur) hypothetical protein.  Gene/ description  Site-specific DNA-methyltransferase, pseudogene DS of HP1321 conserved hypothetical ATP-binding protein and	(C) <sub>13→14</sub> intergenic (-194/+7)  (C) <sub>13→14</sub> intergenic (-243/-51)  (C) <sub>14→13</sub> (3223/3372 nt)  (A) <sub>8→9</sub> (55/453 nt)  (T) <sub>8→9</sub> (59/738 nt)   Mutation/annotation  (G) <sub>14→13</sub> (1453/2053 nt)  (ATACATAA) <sub>10→5</sub>	unknown  No effect  No effect  Ile18-fs  Phe19-fs  Impact  phase 'off' to phase 'on'  Impact	88.3% 89.4% 98.1% 94.8% Frequency

CV725_RS08420	HP1353	Type ISP C-terminal specificity	(C) <sub>14→11</sub>		81.9%
0 <u></u>		domain, pseudogene	pseudogene (3222-32		011070
		,,,,,,,,,,,,,,,,,,,,,,,,,,,,,,,,,,,,,,,	24/3372 nt)		
fur	HP1027	Ferric uptake regulation protein (fur)	C→T ( <u>G</u> AC→ <u>A</u> AC)	Asp135Asn	100%
CV725_RS05120	HP0771	hypothetical protein. In frame?	Δ27 bp	Truncation	100%
			coding (68-94/738 nt)		
CV725_RS06720	HP0911	DS of ATP-dependent helicase/US of	(T) <sub>14→15</sub>	No effect	85%
alpA	HP0912	Hop family adhesin AlpA (HopC).	intergenic (+380/-206)		
CV725_RS06910	HP0947	hypothetical protein (No hits for HP	Codon-114	Ala114Thr	100%
		designation)	( <u>G</u> CC→ <u>A</u> CC)		
ΔfapH pfIA* (H161	)				
NCBI	26695	Gene/ description	Mutation/annotation	Impact	Frequency
designation	locus tag				
CV725_RS00040	NA	Site-specific DNA-methyltransferase,	(G) <sub>14→13</sub>	phase 'off' to	85.9%
		pseudogene	(1453/2053 nt)	phase 'on'	
CV725_RS00720	HP1321	DS of HP1321 conserved	(ATACATAA) <sub>10→5</sub>	Impact	99.7%
CV725_RS00725	HP1322	hypothetical ATP-binding protein and	intergenic (-194/+7)	unknown	
		US of HP1322 hypothetical protein.			
CV725_RS00915	HP1284	glycosyltransferase family 9 protein	Codon-236	Gly236Val	98.9%
		ADP-heptose:LPS	(G <u>G</u> C→G <u>T</u> C)		
		heptosyltransferase			
CV725_RS02330	HP1370	biotin synthase/type III restriction	(C) <sub>13→14</sub>	No effect	84.6%
CV725_RS02335	NA	enzyme.	intergenic (-243/-51)		
CV725_RS08420	HP1353	Type ISP C-terminal specificity	(C) <sub>14→13</sub>	No effect	91.8%
		domain, pseudogene	(3223/3372 nt)		
fur	HP1027	Ferric uptake regulation protein (fur).	(A) <sub>8→9</sub> (55/453 nt)	lle18-fs	96.8%
CV725_RS05120	HP0771	hypothetical protein	(T) <sub>8→9</sub> (59/738 nt)	Phe19-fs	93.1%
Δfur (H177 7)					
NCBI	26695	Gene/ description	Mutation/annotation	Impact	Frequency
designation	locus tag				
CV725_RS00720	HP1321	DS of HP1321 conserved	(ATACATAA) <sub>10→5</sub>	unknown	100%
CV725_RS00725	HP1322	hypothetical ATP-binding protein and	intergenic (-194/+7)		
		US of HP1322 hypothetical protein.			
CV725_RS02305	HP0427	US of <i>hp0427</i> (hypothetical protein),	A→G	No effect	89.7%
CV725_RS02315	23S rRNA	US of 23S rRNA gene	intergenic (-235/-735)		
				_	
fur	HP1027	Ferric uptake regulation protein (fur).	Δ436	Gene	100%
01/=== 500//000			(4)	Deletion	22.20/
CV725_RS04600	HP0875	US of katA, US of frpB	(A) <sub>5→6</sub>		93.9%
CV725_RS04605	HP0876		intergenic (-34/-290)		
motA	HP0815	motA	Codon-201	Gly201Asp	99.3%
			(G <u>G</u> C→G <u>A</u> C)		
CV725_RS06350	HP0527	cag pathogenicity island protein	Codon-1226	Leu1226Leu	99.5%
		(cag7)	( <u>T</u> TA→ <u>C</u> TA)		
			codon-752	Thr752Thr	89.5%
			(AC <u>C</u> →AC <u>G</u> )		
			codon-742	Ala742Ala	80.8%
			(GC <u>T</u> →GC <u>C</u> )		
CV725_RS06500	HP0499	pldA, phospholipase A pseudogene	(G) <sub>10→8</sub>	phase 'off' to	98.2%
	I		(683/1070 nt)	phase 'on'	I

CV725_RS07515	HP1412	DS of HP1412 hypothetical protein	(C) <sub>11→10</sub>		96.1%
queF	HP1413	and DS of queF	intergenic (+11/+121)		
,		'	,		
Δfur (H177 10)					
NCBI	26695	Gene/ description	Mutation/annotation	Impact	Frequency
designation	locus tag				
CV725_RS00720	HP1321	DS of HP1321 conserved	(ATACATAA) <sub>10→5</sub>	unknown	99.6%
CV725_RS00725	HP1322	hypothetical ATP-binding protein and	intergenic (-194/+7)		
		US of HP1322 hypothetical protein.			
rpsS		30S ribosomal protein S19/50S	(G)5→4	No effect	99.6%
rpIV		ribosomal protein L22	intergenic (+5/-5)	·	
CV725_RS00895	HP1288	pantothenate kinase	-T (81/351 nt)	Phe27-fs	99.3%
fur	HP1027	Ferric uptake regulation protein (fur).	Δ436	Gene Deletion	100%
CV725_RS04600	HP0875	US of katA, US of frpB	(A) <sub>5→6</sub>		91.9%
CV725_RS04605	HP0876		intergenic (-34/-290)		
motA	HP0815	motA	Codon-201	Gly201Asp	100%
01.55			(G <u>G</u> C→G <u>A</u> C)		
CV725_RS06350	HP0527	cag pathogenicity island protein	Codon-1226	Leu1226Leu	99.6%
		(cag7)	( <u>T</u> TA→ <u>C</u> TA) Codon-936	Thr936Thr	97.1%
			$(ACG \rightarrow ACC)$	11119301111	97.170
			codon-752	Thr752Thr	95.4%
			$(ACC \rightarrow ACG)$	11117 02 1111	33.470
			codon-742	Ala742Ala	96.3%
			(GC <u>T</u> →GC <u>C</u> )		
CV725_RS06500	HP0499	pldA, phospholipase A pseudogene	(G) <sub>10→7</sub> (683/1070 nt)		85.1%
			(G) <sub>10→11</sub>		80.1%
CV725_RS07515	HP1412	DS of HP1412 hypothetical protein	(683/1070 nt) (C) <sub>11→10</sub>		96.1%
queF	HP1413	and DS of queF	intergenic (+11/+121)		90.176
quei	111 1413	and bo or quer	intergenic (+11/+121)		
ΔfapH pflA* Δfur (	 H179 5)		<u>l</u>		
NCBI	26695	Gene/ description	Mutation/annotation	Impact	Frequency
designation	locus tag				, , , , , , , , , , , , , , , , , , , ,
	NA	Site-specific DNA-methyltransferase,	(G) <sub>14→13</sub>	phase 'off' to	89.5%
		pseudogene	(1453/2053 nt)	phase 'on'	
CV725_RS00720	HP1321	DS of HP1321 conserved	(ATACATAA) <sub>10→5</sub>	unknown	99.5%
CV725_RS00725	HP1322	hypothetical ATP-binding protein and	intergenic (-194/+7)		
		US of HP1322 hypothetical protein.			
maf	HP1239	DS of maf, US of hp1239	(A) <sub>13→16</sub>		83.9%
CV725_RS01150	HP1240	(hypothetical protein)	intergenic (+74/+381)		
CV725_RS02330	HP1370	biotin synthase/type III restriction	(C) <sub>13→14</sub>	No effect	88.4%
CV725_RS02335	NA	enzyme.	intergenic (-243/-51)	NI- W	00.007
CV725_RS08420	HP1353	Type ISP C-terminal specificity domain, pseudogene	(C) <sub>14→13</sub> (3223/3372 nt)	No effect	89.3%
	<u> </u>		(0)		86.7%
CV725_RS03080	HP0164	arsS, histidine kinase	(G) <sub>11→12</sub> coding (1261/1281 nt)		00.770
CV725_RS03080 fur	HP0164 HP1027	arsS, histidine kinase  Ferric uptake regulation protein (fur).		Gene Deletion	100%

CV725_RS05175 rny	HP0761	5-formyltetrahydrofolate cyclo-ligase ribonuclease Y	Codon-208 (TA <u>C</u> →TA <u>T</u> )	Tyr208Tyr	99.2%
CV725_RS07655 labA	HP0026 HP0025	citrate synthase/Hop family adhesin LabA	(T)17→16 intergenic (+379/-149)		83.3%
ΔfapH pflA* Δfur (	 H179 9)				
CV725_RS00040	NA	Site-specific DNA-methyltransferase, pseudogene	(G) <sub>14→13</sub> (1453/2053 nt)	phase 'off' to phase 'on'	89.7%
CV725_RS00720 CV725_RS00725	HP1321 HP1322	DS of HP1321 conserved hypothetical ATP-binding protein and US of HP1322 hypothetical protein.	(ATACATAA) <sub>10→5</sub> intergenic (-194/+7)	unknown	99.6%
CV725_RS08420	HP1353	Type ISP C-terminal specificity domain, pseudogene	(C) <sub>14→13</sub> (3223/3372 nt)	No effect	89.4%
CV725_RS03080	HP0164	arsS, histidine kinase	(G) <sub>11→12</sub> coding (1261/1281 nt)		80.3%
fur	HP1027	Ferric uptake regulation protein (fur).	Δ436	Gene Deletion	100%
CV725_RS04785	HP0838	fapH	Δ490	Deletion	100%
CV725_RS05175 rny	HP0761	5-formyltetrahydrofolate cyclo-ligase ribonuclease Y	Codon-208 (TA <u>C</u> →TA <u>T</u> )	Tyr208Tyr	100%
CV725_RS05825	HP0628	sel1 repeat family protein	(C)7→6 coding (505/1059 nt)	Gly169-fs	95.6%
CV725_RS06350	HP0527	cag pathogenicity island protein (cag7)	Codon-936 (AC <u>G</u> →AC <u>C</u> )	Thr936Thr	96.9%
CV725_RS07655 labA	HP0026 HP0025	citrate synthase/Hop family adhesin LabA	(T)17→16 intergenic (+379/-149)		83.1%
ΔfapH (lab strain			T.,		T
CV725_RS00720 CV725_RS00725	HP1322 HP1321	DS of HP1321 conserved hypothetical ATP-binding protein and US of HP1322 hypothetical protein.	(ATACATAA) <sub>10→5</sub> intergenic (-194/+7)		99.0%
CV725_RS02305 CV725_RS02315	HP0427 23S rRNA	US of hp0427 (hypothetical protein), US of 23S rRNA gene	C→T intergenic (-235/-735)		81.6%
CV725_RS02465	HP1375	N-6 DNA methylase	(C) <sub>14→13</sub> pseudogene (3224/337 2 nt)	restore full- length ORF	91.8%
CV725_RS03080	HP0164	arsS, histidine kinase	(G) <sub>11→12</sub> coding (1261/1281 nt)		85.7%
CV725_RS04600 CV725_RS04605	HP0875 HP0876	US of HP0875 katA, US of HP0876 frpB	(A) <sub>5→6</sub> intergenic (-34/-290)		93.0%
CV725_RS04785	HP0838	fapH	codon-18 $(G\underline{T}C \rightarrow G\underline{C}C)$ codon-201 $(GA\underline{T} \rightarrow GA\underline{C})$	Val18Ala Asp201Asp	100% 99.4%
			Δ515 bp (69-584/618 nt)	deletion	100%
CV725_RS06500	HP0499	pldA, phospholipase A pseudogene	(G) <sub>10→9</sub> (683/1070 nt)	phase 'off' to phase 'off'	94.8%
CV725_RS07515 queF	HP1412 HP1413	DS of HP1412 hypothetical protein and DS of queF	(C) <sub>11→10</sub> intergenic (+11/+121)		96.4%
lpxF	HP1580	membrane-associated phospholipid phosphatase	G→A (TG <u>G</u> →TG <u>A</u> )	W14stop	100%

ΔfapH (lab strain	H181-11)				
serS	HP1480	serine-tRNA ligase	C→G (TC <u>C</u> →TC <u>G</u> )	Ser352Ser	99.6%
CV725_RS00720 CV725_RS00725	HP1322 HP1321	DS of HP1321 conserved hypothetical ATP-binding protein and US of HP1322 hypothetical protein.	(ATACATAA) <sub>10→5</sub> intergenic (-194/+7)		98.2%
CV725_RS02305 CV725_RS02315	HP0427 23S rRNA	US of <i>hp0427</i> (hypothetical protein), US of 23S rRNA gene	+32 bp intergenic (-234/-736)		92.3%
CV725_RS02465	HP1375	N-6 DNA methylase	(C) <sub>14→13</sub> pseudogene (3224/337 2 nt)	restore full- length ORF	90.5%
CV725_RS04600 CV725_RS04605	HP0875 HP0876	US of HP0875 katA, US of HP0876 frpB	(A) <sub>5→6</sub> intergenic (-34/-290)		95.6%
CV725_RS04785	HP0838	fapH	codon-18 $(G\underline{T}C \rightarrow G\underline{C}C)$ codon-201 $(GA\underline{T} \rightarrow GA\underline{C})$	Val18Ala Asp201Asp	99.7%
			Δ515 bp (69-584/618 nt)	deletion	100%
CV725_RS06350	HP0527	cag pathogenicity island protein (cag7)	codon-752 (AC <u>C</u> →AC <u>G</u> ) codon-742	Thr752Thr Ala742Ala	91.2% 95.5%
CV725_RS06500	HP0499	<i>pldA</i> , phospholipase A pseudogene	$(GC\underline{T} \rightarrow GC\underline{C})$ $(G)_{10\rightarrow 9}$	phase 'off' to	95.1%
CV725_RS07515	HP1412	DS of HP1412 hypothetical protein	(683/1070 nt) (C) <sub>11→10</sub>	phase 'off'	94.5%
queF	HP1413	and DS of queF	intergenic (+11/+121)		34.0 /0
lpxF	HP1580	membrane-associated phospholipid phosphatase	G→A (TG <u>G</u> →TG <u>A</u> )	W14stop	99.3%

<sup>&</sup>lt;sup>a</sup>"fs" indicates frameshift

Displaying mutations that are found in > 80% of reads and any mutations in known flagellar genes.

Secondary flagellar mutations are highlighted in yellow.

<sup>&</sup>lt;sup>b</sup>Frequency is the number of times the mutation was identified relative to the total number of reads for that sequence.

<sup>\*</sup>Not found in strain H16.

# Chapter 4: FlgY, PfIA, and PfIB form spoke-ring network in high-torque flagellar motor of *Helicobacter pylori*

2

Shoichi Tachiyama<sup>a,b,1</sup>, Kyle Rosinke<sup>c,1</sup>, Mohammad F. Khan<sup>d,e</sup>, Xiaotian Zhou<sup>d</sup>, Yue Xin<sup>d</sup>, Jack M. Botting<sup>a,b</sup>, Jian Yue<sup>a,b</sup>, Anna Roujeinikova<sup>d,e</sup>, Timothy R. Hoover<sup>c,\*</sup>, and Jun Liu<sup>a,b,\*</sup>

<sup>&</sup>lt;sup>2</sup> Submitted to PNAS on 2/24/2025

<sup>&</sup>lt;sup>1</sup> S.T. and K.R. contributed equally to this work. PNAS in review. K.R. contributed to this work in mutant construction and characterization, BACTH assays, meetings, discussions, and writing of the manuscript.

# **ABSTRACT**

Helicobacter pylori has evolved distinct flagellar motility to colonize the human stomach. Rotation of the H. pylori flagella is driven by one of the largest known bacterial flagellar motors. In addition to the core motor components found in Escherichia coli and Salmonella enterica, the flagellar motor in *H. pylori* possesses many accessories that enable the bacteria to penetrate the gastric mucus layer. Here, we leverage cryo-electron tomography (cryo-ET) with molecular genetics and biochemical approaches to characterize three motor accessory proteins, FlqY, PflA, and PflB, and their roles in H. pylori flagellar assembly and motility. Comparative analyses of in-situ flagellar motor structures from pflA, pflB, and flgY mutants and wild-type H. pylori reveal that FlgY forms a 13-fold proximal spoke-ring around the MS-ring, and that PfIA and PfIB form an 18-fold distal spoke-ring enclosing 18 torque-generating stator complexes. A combination of individual structures predicted by AlphaFold and experimentally confirmed protein-protein interactions with *in-situ* motor structures enabled us to build a pseudo-atomic model of the *H. pylori* motor. Our model suggests that the FlgY spoke-ring functions as a bearing around the rotating MS-ring and as a template for stabilizing the PfIA-PfIB spoke-ring, thus enabling the recruitment of 18 stator complexes for high-torque generation in each motor. Overall, our study sheds light on how this novel spoke-ring network between the MS-ring and stator complexes enables the unique motility of *H. pylori*. As these accessory proteins are conserved in the phylum Campylobacterota, our findings apply broadly to a better understanding of how polar flagella help bacteria thrive in gastric and enteric niches.

# SIGNIFICANCE STATEMENT

Flagellar motility is essential for *Helicobacter pylori* to penetrate and colonize the lining of the human stomach. The flagella in *H. pylori* differ from those in model systems such as *Escherichia coli* and *Salmonella* due to the presence of many uncharacterized motor accessories that likely contribute to *H. pylori*'s unique adaptations and remarkable ability to migrate and persist in the gastric mucosa. Here, we discover that three accessory proteins – FlgY, PflA, and PflB – form a distinct spoke-ring network between the rotor and stator in the *H. pylori* flagellar motor. Importantly, we provide direct evidence that this novel spoke-ring network plays a critical role in retaining 18 torque-generating stator complexes to maximize torque generation and enable the robust motility of *H. pylori*.

# INTRODUCTION

Helicobacter pylori is a Gram-negative bacterial pathogen that colonizes the gastric epithelium in about half of the human population worldwide (Hooi et al. 2017). H. pylori infection can lead to peptic ulcers and is a major risk factor for stomach cancer (Cover and Blaser 1992, Kuipers 1997, Atherton and Blaser 2009). To colonize the stomach, H. pylori requires flagellar motility to migrate through the highly viscous mucosal layer and reach the surface of epithelium cells (Eaton et al. 1992, Eaton et al. 1996, Ottemann and Lowenthal 2002, Schreiber et al. 2004). Motility of H. pylori is driven by one of the bacterium's most distinctive characteristics: a unipolar bundle of sheathed flagella. Although core components of flagella are conserved across species, H. pylori has evolved unique adaptations in its sheathed flagella that contribute to its crucial ability to traverse the highly viscous gastric mucosa for successful colonization in the human stomach.

The flagellum has been extensively characterized in model systems such as Escherichia coli and Salmonella enterica. It comprises three main parts: the flagellar motor, hook, and filament (*Minamino and Imada 2015*). The flagellar motor is composed of nearly 20 different types of proteins, with conserved core flagellar motor structures that include the stator complex, MS-ring, C-ring, LP-ring, and rod observed in various bacterial species (Chen et al. 2011, Carroll and Liu 2020). The stator complex, which generates torque, is formed by five MotA subunits and two MotB subunits (Santiveri et al. 2020, Deme et al. 2020, Hu et al. 2022). FliL is a stator-associated protein found in many bacteria, including S. enterica where it is dispensable for swimming but is essential for flagellar mediated swarming (Attmannspacher et al. 2008). FliL has a single transmembrane (TM) helix periplasmic domain that resembles and the stomatin/prohibitin/flotillin/HflK/C (SPFH) domain of mouse stomatin (Takekawa et al. 2019), a protein that regulates the activity of acid-sensing ion channels. Cryo-electron tomography (cryo-ET) and subtomogram averaging revealed that FliL forms a ring that encircles the MotB dimer and acts as a scaffold for the stator units in the motors of H. pylori and the spirochete B. burgdorferi (Tachiyama et al. 2022, Guo et al. 2022). The MS-ring is formed by the membrane protein FliF that possesses a set of ring-building motifs (RBMs) with variable stoichiometries and has predicted TM helices close to the N and C termini (Tan et al. 2021, Johnson et al. 2020). The C-ring is a switch complex located in the cytoplasmic region of the motor. The C-ring consists of three proteins FliG, FliM, and FliN in E. coli and S. enterica. The H. pylori C-ring contains FliG, FliM, and FliN, as well as FliY, which shares homology with FliN (Lowenthal et al. 2009). Together with the MS-ring, the C-ring forms the rotor that transmits rotational power from the stator units to the rod, hook, and filament. The rod serves as a drive shaft. The hook is a universal

joint between the rod and filament which functions as a propeller to push the cell forward as the filament rotates. The LP-ring is formed by multiple subunits of FlgH, and FlgI and acts as a bushing complex to align and balance the rod as it rotates (*Johnson et al. 2021, Tan et al. 2021, Yamaguchi et al. 2021*). The P-ring portion of the LP-ring complex is formed by FlgI and is associated with the peptidoglycan layer. In *E. coli* and *S. enterica*, the L-ring, formed by FlgH, creates a pore in the outer membrane, through which the rod passes. In *H. pylori*, the filament is surrounded by a membranous sheath contiguous with the outer membrane, and the L-ring is positioned below the outer membrane (*Qin et al. 2017*).

The flagellar motors of many bacteria, including *H. pylori*, possess accessory structures (*Chen et al. 2011, Carroll and Liu 2020, Qin et al. 2017*), many located in the periplasm near the MS-ring and stator units. One such motor accessory in *H. pylori* is a cage that surrounds the stator units and many periplasmic components (*Qin et al. 2017*). A recent study indicates that PilN-PilO heterodimers are responsible for the bottom part of the cage (*Liu et al. 2024*). Another *H. pylori* motor accessory protein, FlgV, is required to form a cytoplasmic ring near the junction of the MS-ring and C-ring that may enhance torque transmission (*Botting et al. 2023*). Although cryo-ET and subtomogram averaging have provided fine structural details of the motor accessories in *H. pylori*, proteins that are responsible for the unique adaptations remain to be identified or further characterized.

Comparing structure-function relationships in flagellar motors across species is a fruitful approach and essential to understanding the functions of these accessories. *Campylobacter jejuni* is closely related to *H. pylori*, as both species belong to the phylum Campylobacterota, and the motors of the two bacteria are structurally similar (*Beeby et al. 2016*, *Chaban et al. 2018*, *Drobnič et al. 2023*). Among the several novel flagellar genes identified through genetic screens in *C. jejuni* (*Gao et al. 2014*), *pflA* (paralyzed flagella protein A) and *pflB* (paralyzed flagella protein B) are essential for motility but not flagellar assembly (*Gao et al. 2014*, *Yao et al. 1994*, *Gupta 2006*). Recent *in-situ* structures of the *C. jejuni* motor achieved by cryo-ET and cryo-electron microscopy (cryo-EM) revealed that PflA and PflB are closely associated with each other and form spoke- and rim-like structures, respectively, near the stator complexes (*Beeby et al. 2016*, *Drobnič et al. 2023*). The *in-situ* structure of the *C. jejuni* motor revealed an additional accessory near PflA that was designated the E-ring though its component protein(s) are unknown (*Drobnič et al. 2023*).

A recent study from *Cereibacter sphaeroides* (previously named *Rhodobacter sphaeroides* and belonging to the phylum Pseudomonadota) suggested that MotE and MotK are accessory

proteins required for motility but not assembly of the polar flagella (*Velez-Gonzalez et al. 2024*). MotE and MotK also interact with the polar flagellum stator protein MotB (*Velez-Gonzalez et al. 2024*). Another study from *Ensifer meliloti* (formerly *Sinorhizobium meliloti*, another member of the phylum Pseudomonadota) suggested that MotE serves as a new chaperone specific for the periplasmic motility protein MotC (*Eggenhofer et al. 2004*). Intriguingly, predicted structures of PflA from *H. pylori* and *C. jejuni* possess the structural components found in MotK, namely an N-terminal β-sandwich domain connected by a long, unstructured linker to a C-terminal tetratricopeptide repeat (TPR) domain (*Drobnič et al. 2023*) (Fig. S4.1). *H. pylori* does not have a homolog of MotC identifiable by BLAST. However, the predicted structure of MotC consists of an extended TPR domain, similar to the predicted structures of the C-terminal domains of MotK and PflA. Thus, these predicted structures suggest that PflA is homologous to MotK and possibly to MotC.

C. jejuni CJJ881176-1448 was identified as a potential flagellar gene based on its requirement for host cell invasion and localization at the cell pole, and was designated flgY (**Gao et al. 2014**). The predicted structures of C. jejuni FlgY and its homolog in H. pylori (HP0257) are almost identical to the structure of MotE, which forms a homodimer in C. sphaeroides and E. meliloti (**Velez-Gonzalez et al. 2024, Eggenhofer et al. 2004**) (**Fig. S4.2**). Based on these observations and analyses, we hypothesized that FlgY, PflA, and PflB are motor accessory proteins in H. pylori.

Here, we combine cryo-ET and subtomogram averaging with molecular genetics and biochemical approaches to characterize the structures and functions of FlgY, PflA, and PflB in *H. pylori*. We find that FlgY forms a 13-fold periplasmic spoke-ring around the MS-ring. PflA and PflB form a distinct periplasmic, 18-fold spoke-ring that appears critical for recruitment and stabilization of 18 stator complexes. Supported by protein structure prediction with AlphaFold and experimental protein-protein interactions, we built a pseudo-atomic model of the *H. pylori* flagellar motor that provides a structural basis for understanding how a novel network of accessory proteins enables distinctive flagellar assembly and motility required for *H. pylori* to navigate the viscous environment of the gastric mucosa.

# **RESULTS**

### PfIA and PfIB are essential for specific flagellar assemblages and motility in *H. pylori*.

Our previous *in-situ* structure of the *H. pylori* motor revealed a cage that encloses 18 distal spoke structures and 18 stator units, each surrounded by a FliL ring in the periplasm (*Tachiyama et al. 2022, Qin et al. 2017*). While the periphery of the *H. pylori* motor shows 18-fold symmetry, the structures between the 18-fold spokes and MS-ring were poorly defined (*Tachiyama et al. 2022, Qin et al. 2017*) (Figs. S4.3A, B). To reveal detailed structures between the MS-ring and cage in the periplasm, we used extensive subtomogram classification and refinement to determine the asymmetric structure of the *H. pylori* motor (Figs. 4.1A-D). Different from the distal spokes with 18-fold symmetry, a structure with 13 spokes – here designated proximal spokes – surrounds the MS-ring (Figs. 4.1A-D and S4.3C, D). The proximal and distal spokes appear to interact with each other with different conformations at their symmetry-mismatched interface (Figs. 4.1C, D and S3D).

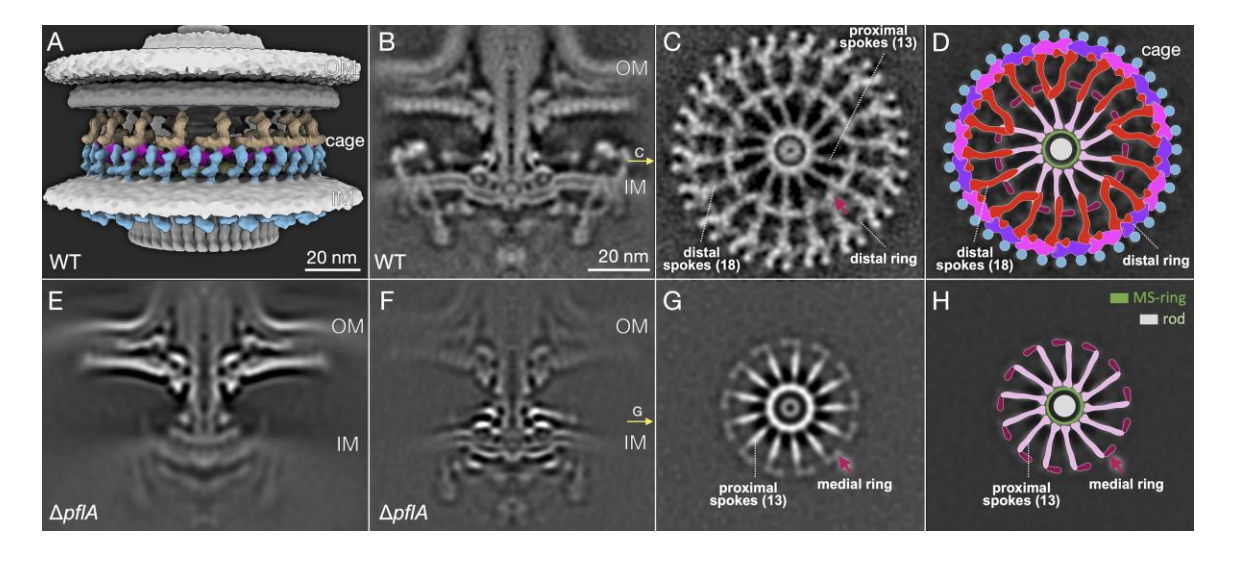


Figure 4.1. Cryo-ET analysis reveals distinct spoke-ring network in the *H. pylori* motor. (A, B) 3D view and central section of wild-type motor structure obtained using asymmetric reconstruction. Cage-like structure is shown in color in (A). (C) Cross-section view of periplasmic region reveals 13 proximal spokes around MS-ring, 18 distal spokes, and distal ring. Dark red arrow in the panel (C) indicates medial ring between proximal spokes and distal spokes. (D) Cartoon representation shows proximal spokes (pink), distal spokes (red), distal ring (magenta/purple), cage (blue), medial ring (dark red) and MS-ring (green) with rod (light gray). (E-H) The flagellar motor structure in the  $\Delta pflA$  mutant shows that the cage, distal spokes, and distal ring are absent. The 13 proximal spokes and medial ring are well resolved in the refined

structure shown in two perpendicular slices (**F** and **G**). **(H)** Cartoon representation allows comparison of structural phenotype of the  $\Delta pflA$  mutant with wild type (**D**).

As the accessory proteins PfIA and PfIB were suggested to interact with the stator units in C. jejuni (Beeby et al. 2016, Chaban et al. 2018, Drobnič et al 2023), their homologs are likely involved in forming some accessories identified in the H. pylori motor. We generated unmarked deletions of pfIA and pfIB in H. pylori B128 and characterized the phenotypes of the resulting mutants. As expected, the *H. pylori* Δ*pflA* (*Bijlsma et al. 1999*) and Δ*pflB* mutants were flagellated (Figs. S4.4A-G) but non-motile in soft agar medium (Figs. S4.4H). The ΔpflB mutant displayed flagellation like wild-type H. pylori B128, while the  $\Delta pflA$  mutant produced fewer flagella (Fig. **S4.4G**). Whole genome sequencing (WGS) of the  $\Delta pflA$  and  $\Delta pflB$  mutants confirmed the targeted genes were deleted (**Table S4.1**). WGS also indicated that the  $\Delta pf/B$  mutant did not have mutations in any other known flagellar genes, but the  $\Delta pflA$  mutant had acquired a secondary mutation in which portions of flil and the upstream gene were deleted (Table S4.1). Flil is a cytoplasmic ATPase complex that is part of the flagellar type III secretion system (fT3SS) that transports axial components of the flagellum (e.g., rod, hook, and hook-associated and filament proteins) across the inner membrane (Minamino and Macnab 1999, Minamino and Macnab **2000**). The mutation of *flil* was presumably responsible for the reduced flagellation of the  $\Delta pflA$ mutant but is not expected to have affected the motor structure since the periplasmic flagellar motor accessories are transported across the inner membrane by the Sec system rather than the fT3SS. The  $\Delta pfIA$  mutant also had a missense mutation in motB that replaced the non-conserved residue Gly<sup>106</sup> in the linker region with arginine (**Table S4.1**) (**De Mot and Vanderleyden 1994**), a substitution that likely did not impact the function of MotB.

We determined *in-situ* motor structures for both  $\Delta pflA$  and  $\Delta pflB$  mutants by cryo-ET and subtomogram averaging. Both mutants lacked the stator units, cage, distal ring, and distal spokes, while the proximal spokes remained associated with the MS-ring (**Figs. 4.1E-H** and **S4.5**). Comparing the *in-situ* structures from the two mutants with wild type revealed striking differences and the profound impacts of PflA and PflB as well as a novel ring – designated medial ring – at the distal ends of the proximal spokes (**Figs. 4.1E-H** and **S5**). Taken together, these results show that PflA and PflB are essential for formation of the 18 distal spokes, ring adjacent to the cage, and stator complexes and that other accessory proteins are required to form the 13 proximal spokes and medial ring in the *H. pylori* motor.

### FIgY is responsible for formation of the proximal spokes in the H. pylori motor.

Given that *C. sphaeorides* MotE is a predicted periplasmic motor accessory protein and that MotE and FlgY of *C. jejuni* and *H. pylori* are structurally similar (**Fig. S4.2**), we postulated that FlgY is a motor accessory protein in *H. pylori*. To test this hypothesis, we generated an unmarked deletion of *flgY* in *H. pylori* B128 and examined the phenotype of the resulting mutant. WGS of the  $\Delta flgY$  mutant confirmed *flgY* had been deleted and that the strain acquired a secondary mutation in *motA* that replaced the non-conserved residue Gly<sup>201</sup> with aspartate (**Table S4.1**). Based on the structure of the *C. jejuni* stator complex (*Santiveri et al. 2020*), Gly<sup>201</sup> in *H. pylori* MotA is located on the cytoplasmic side of the inner membrane and immediately adjacent to TM helix 4, and the aspartate substitution at this position likely does not impact the assembly of periplasmic motor accessories.

The H. pylori ∆flgY mutant was less motile in soft agar medium, and the diameter of the swim halo produced by the mutant was about half of that generated by wild type (Fig. 4.2A). Examination of the  $\triangle flgY$  mutant by cryo-ET revealed the strain was well flagellated (Fig. 4.2B), with the number of flagella per cell indistinguishable from that of wild type H. pylori B128 (Table **S4.4**). These findings agree with previous reports that the FlgY homolog MotE is not required for flagellum assembly in C. sphaeroides or E. meliloti (Velez-Gonzalez et al. 2024, Eggenhofer et **al. 2004**). The *in-situ* global averaged structure of the  $\Delta f \mid gY$  motor somewhat resembles those of the  $\Delta pfIA$  and  $\Delta pfIB$  mutants as the distal spokes are absent (Fig. 4.2C). However, unlike in the  $\Delta pfIA$  and  $\Delta pfIB$  mutants, the proximal spokes and medial ring are absent from the  $\Delta fIgY$  motor (Figs. 4.2D-F). While the cage and distal ring are present in the motor of the  $\Delta flgY$  mutant, the densities corresponding to these structures are not as distinct as those in the wild-type motor (Figs. 4.1C and 4.2E). Further classification showed that the cage is only present in a small portion of the motors, suggesting that the cage and distal ring are less stable in the absence of the proximal and distal spokes. Moreover, the stator units are not resolved in our averaged structures, suggesting that they are likely unstable in the absence of the proximal and distal spokes (Fig. 4.2D). Taken together, these results indicate that FlgY is required for formation of the proximal spokes and medial ring and that it plays a role in stably assembling the distal spokes and ring and, in turn, the stator complexes. This diminished recruitment and/or retention of stator units within the  $\Delta flgY$  motor likely accounts for the reduced motility of the strain in soft agar medium (Fig. 2A).

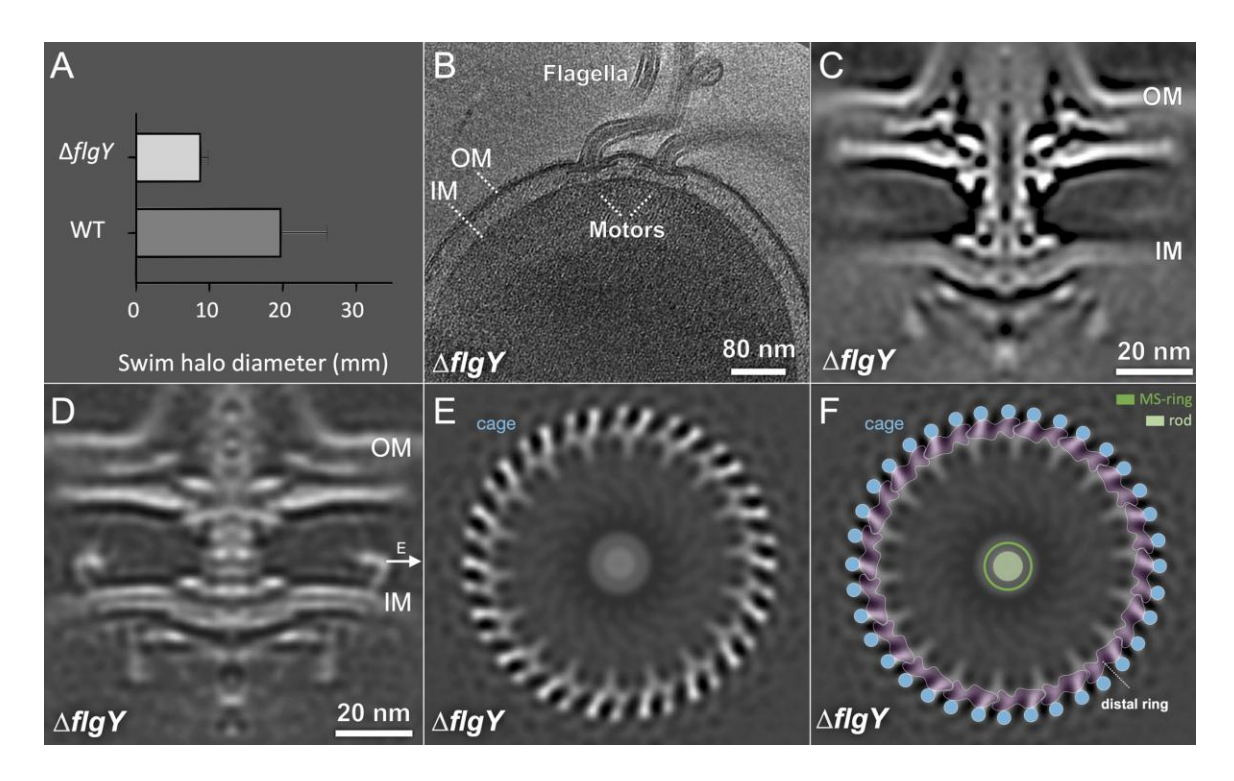


Figure 4.2. FlgY is essential for formation of proximal and distal spokes in the *H. pylori* flagellar motor. (A) Diameters of swim halos of wild type and  $\Delta flgY$  mutant (n=2) on semi-solid agar 7 days post-inoculation. (B) Section of cryo-ET image of  $\Delta flgY$  mutant shows flagellar filaments and motor. (C) Global averaged motor structure of  $\Delta flgY$  mutant. (D-F) Class average of  $\Delta flgY$  motor reveals cage shown in medial slice (D) and cross-section (E) views, as well as cartoon model (F) with cage colored blue and distal ring purple.

### FIgY dimers form the proximal spoke-ring around the MS-ring.

To understand how FlgY contributes to formation of the proximal spokes, 13-fold symmetry expansion and focused refinement in unbinned subtomograms were performed to determine *insitu* structures of the proximal spokes at 1.1 nm resolution (**Figs. 4.3A, B**). The 13 proximal spokes form a ring with 26 subunits around the  $\beta$ -collar of the MS-ring, with a ~0.6 nm gap between the two structures (**Figs. 4.3B-F**). A dimer model of FlgY predicted with a high confidence score by AlphaFold3 (*Abramson et al. 2024*) fits reasonably well into the densities of the proximal spoke (**Figs. 4.3C, D** and **S4.2**). Specifically, the globular C-terminal domains of the FlgY dimers appear to associate with each other and form the ring around a negatively charged region in the  $\beta$ -collar of the MS-ring (FliF residues 293-311) (**Figs. 4.3D** and **S4.6**). The MS-ring-facing interior surface of the FlgY ring contains a ring of positively charged lysine residues and negatively charged glutamic acid and aspartic acid (**Fig. S4.6**), suggesting potential electrostatic interactions

between the MS-ring and FlgY ring. The N-terminal domains of the FlgY dimer extend toward the distal spokes (**Figs. 4.3B, C**), which are not resolved in the map, likely due to the symmetry mismatch between the 13-fold proximal spokes and 18-fold distal spokes. To understand how the 13 FlgY dimers assemble in the motor, we built their models in the asymmetric map (**Figs. 4.3E-H**). In the asymmetric map, the interior of the motor has uneven spaces between each proximal spoke (**Fig. 4.1C**). Thus, the N-terminal domains appear flexible, allowing interaction with 13 of the 18 distal spokes despite the symmetry mismatch (**Figs. 4.3E-G**). Taken together, our data suggest that each of the proximal spokes is formed by a FlgY dimer and that the 13 FlgY dimers form a ring around the MS-ring through their C-terminal domains as well as function as a template for assembly of the distal spokes through their flexible N-terminal domains.

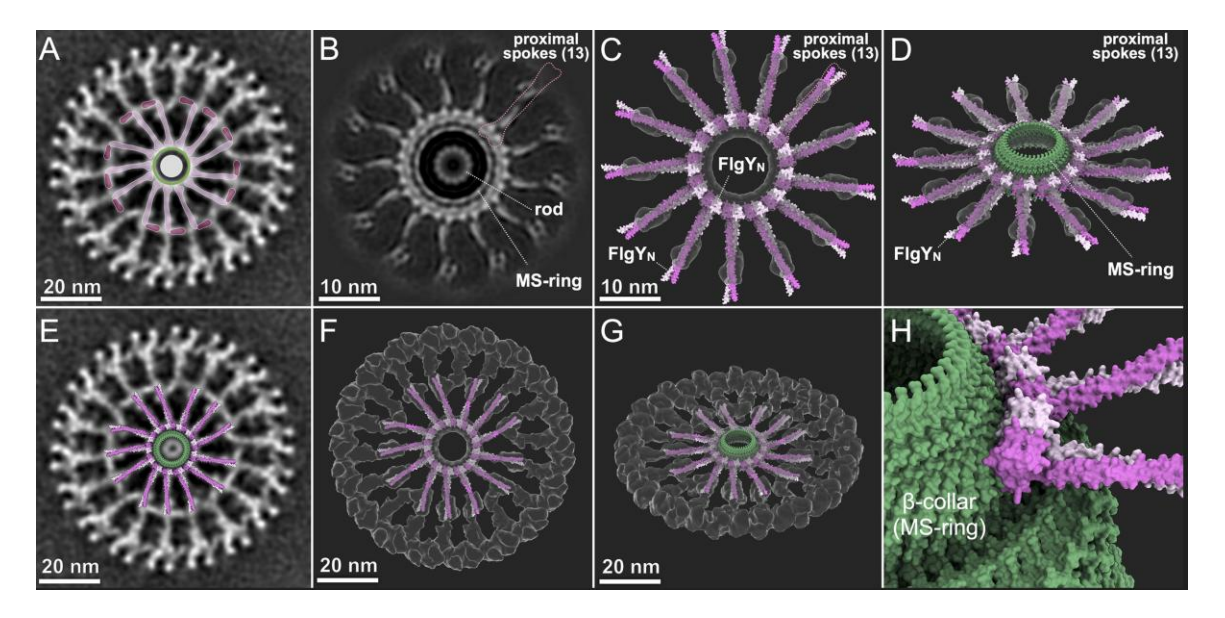
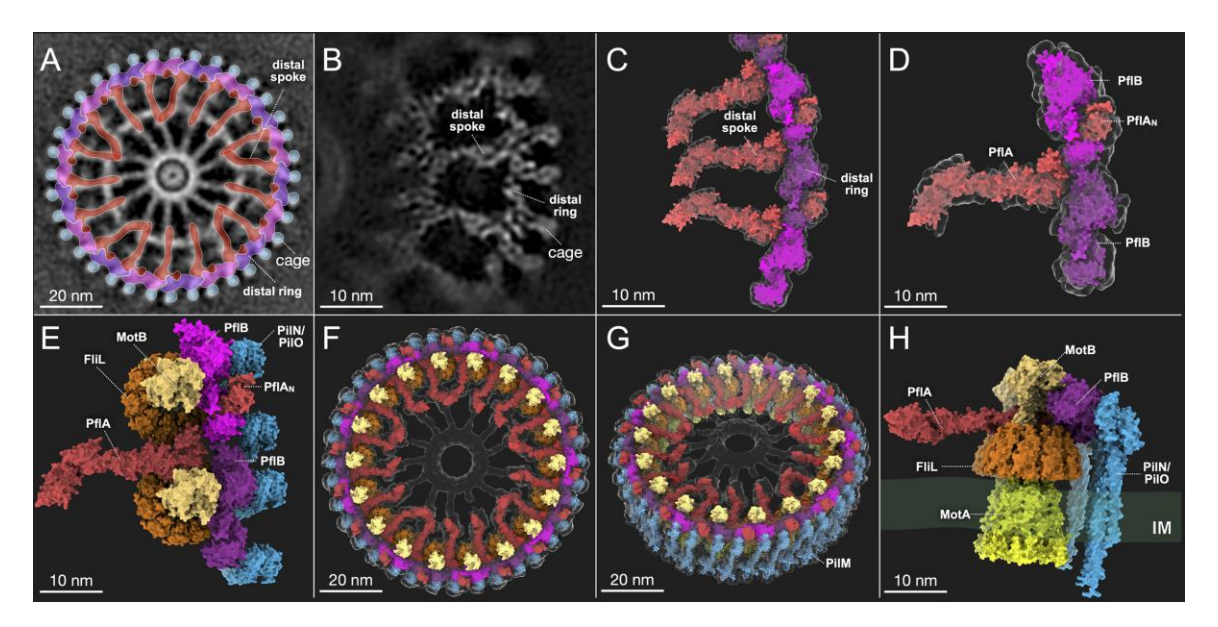


Figure 4.3. FlgY forms spoke-ring near the MS-ring. (A-B) Focused refinement of periplasmic region highlighted in pink in panel (A) reveals high-resolution structure of proximal spokes (B) that contains 26 copies of globular densities forming a small ring near the MS-ring. Pink dot line indicates FlgY dimer. (C-D) Top and tilted views show model of FlgY spoke-ring with C13 symmetry produced by docking AlphaFold predicted structure of *H. pylori* FlgY dimer (light/dark pink) (Fig. S4.2) into cryo-ET density (transparent regions). FlgY<sub>N</sub> indicates the N-terminal domain of FlgY dimer. (E) Refined FlgY model built based on asymmetric reconstruction. (F-H) Top and tilted views of asymmetric FlgY spoke-ring model. The density map is from the structure of the asymmetric reconstruction. (H) Close-up view of interface between FlgY (pink) and β-collar (green) of the MS-ring.

### PfIA and PfIB form the distal spoke-ring critical for stator recruitment and retention.

To better resolve the 18 distal spokes and their interactions with stator complexes and the cage, we deployed 18-fold symmetry expansion. Then, focused refinement was performed for only one side of the motor in unbinned subtomograms to determine *in-situ* structures of the distal spoke and its adjacent flagellar components at 1.0 nm resolution (**Figs. 4.4A, B**). One distal spoke connects with two subunits of the distal ring, which together form a T-shaped structure (**Fig. 4.4B**). As PfIA is predicted to be elongated, whereas PfIB is more compact, we postulate that the T-shaped structure is formed by one PfIA and two PfIB protomers (**Fig. 4.4B**). Although the stator complex, FliL ring (**Tachiyama et al. 2022**), and cage subunits (**Liu et al. 2024**) were previously resolved in the *in-situ* structure of the *H. pylori* motor, it had remained challenging to specifically define individual PfIA and PfIB molecules. Fortunately, AlphaFold-predicted structure of a heterotrimer complex consisting of one PfIA subunit and two PfIB subunits has a high confidence score (**Abramson et al. 2024**) (**Fig. S4.7**). Importantly, the predicted PfIA-PfIB<sub>2</sub> model matches the T-shaped structure very well (**Fig. S4.7**), thus serving as an initial model for further fitting into the density of one distal spoke and two distal ring subunits (**Figs. 4.4C**, **D**). Overall, 18 PfIA molecules form the distal spokes and PfIB molecules form the distal ring (**Fig. 4.4C**).



**Figure 4.4.** PfIA forms distal spokes and PfIB forms distal ring structure in the *H. pylori* flagellar motor. Focused refinement of the distal spoke and ring region highlighted in red, magenta, and purple in panel (**A**) reveals high-resolution structure of distal spokes and subunits of distal ring (**B**). Modeled T-shaped PfIA-PfIB<sub>2</sub> heterotrimers (**Fig. S7**) docked into refined map (**C**), with close-up view of single docked unit shown in (**D**). PfIA is shown in red and two PfIB

molecules in magenta and dark magenta. **(E)** Top view of PfIA-PfIB model shown with other motor components, including two MotA/B stator complexes, two FliL rings (*Tachiyama et al. 2022, Guo et al. 2022*), and four PilN/PilO cage subunits (*Liu et al. 2024*). (**F** and **G**) Top and tilted views show 18 PfIA spokes, 18 PfIB subunits, 18 stator complexes, 18 FliL rings, and 36 PilN/PilO cage units in the *H. pylori* motor. The density map is from the asymmetric reconstruction structure. **(H)** Side view of the model shown in (**E**).

The distal ring surrounds the stator complexes and is itself surrounded by the cage. Specifically, each PflB molecule is located between one FliL ring and two cage subunits (**Fig. 4.4E**). Together with recent models of the stator complex, FliL ring, and PilO/PilN cage subunit (**Fig. 4.4E**), we show for the first time how 18 PflA-PflB complexes tightly interact with each other to form the distal spoke-ring next to the bottom portion of the cage formed by 36 PilO/PilN cage subunits (*Liu et al. 2024*) (**Figs. 4.4F-H**). Importantly, the PflA-PflB spoke-ring perfectly encloses 18 stator complexes and 18 FliL rings, likely stabilizing them for maximal torque generation.

### Overall architecture of the distinct spoke-ring network in the *H. pylori* motor.

To better understand the interactions among three accessory proteins (FlgY, PflA, PflB) and core flagellar components in the *H. pylori* flagellar motor, we built a pseudo-atomic model (**Figs. 4.5A-C**) based on our current findings (**Figs. 4.3 and 4.4**) and recent works (*Tachiyama et al. 2022, Liu et al. 2024, Botting et al. 2023*). Notably, the N-terminal domains of each FlgY dimer interact with the C-terminal domain of PflA, enabling formation and stabilization of the distal spokes. Five of the 18 PflA molecules appear to interact with FlgY dimers in a different conformation, wherein the C-terminal TPR domain of PflA adopts a bent shape and interacts with a neighboring PflA-FlgY complex due to the symmetry mismatch between the 13 proximal spokes and 18 distal spokes (**Figs. 4.5B, C** and **S4.3D**). Our model of the *H. pylori* motor includes the core components (MS-ring, C-ring, and stator complexes) as well as many motor accessories (proximal spokes, distal spoke-ring, and cage) and reveals many protein-protein interactions potentially important for flagellar assembly and function in *H. pylori*.

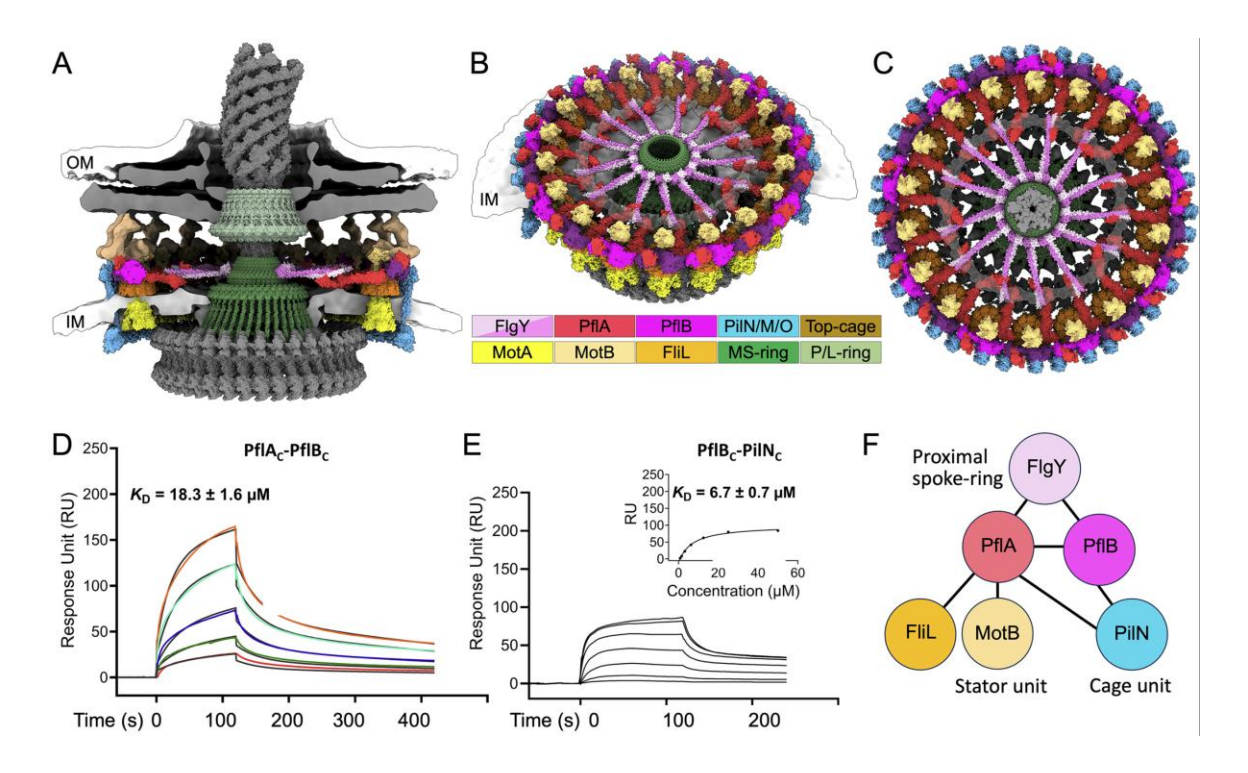


Figure 4.5. Model of the *H. pylori* flagellar motor shows distinct FlgY-PflA-PflB spoke-ring network that bridges the MS-ring and 18 stator complexes. (A-C) AlphaFold-predicted structures of FlgY, PflA, PflB, and other known components (*Santiveri et al. 2020, Tachiyama et al.17, Guo et al. 2022, Liu et al. 2024, Moon et al. 2016*) were used to build this model. (A) Cross-section view in same orientation as in Fig. 1B. (B) Tilted view with top part of motor and front part of cage removed to reveal periplasmic components. (C) Top view shows distinct periplasmic spoke-ring network formed by FlgY, PflA, and PflB. Inner membrane (IM) was omitted for clarity. (D) Binding affinity between PflA<sub>C</sub> and PflB<sub>C</sub> measured by fitting SPR data to kinetic model. PflB<sub>C</sub> was immobilized on the chip, and PflA<sub>C</sub> concentrations were 5, 10, 20, 40 and 60 μM. (E) Steady-state SPR binding analysis shows that PflB<sub>C</sub> also interacts with cage component PilN<sub>C</sub>. (F) Schematic of all pairwise interactions detected in SPR experiments (Fig. S4.8).

We sought to validate the protein-protein interactions predicted by our model using surface plasmon resonance (SPR) (**Fig. S4.8**) and the bacterial adenylate cyclase two-hybrid (BACTH) system (**Fig. S4.9**). Analysis of the SPR data showed that PfIA proteins lacking the N-terminal  $\beta$ -sandwich domain (PfIAc, the TPR domain of PfIA) and the periplasmic C-terminal domain of PfIB (PfIBc) bind to each other with a dissociation constant in a physiologically relevant range ( $K_D$ =18.3±1.6  $\mu$ M; **Fig. 4.5D**). Interactions between PfIA and PfIB were confirmed by results from

the BACTH assays (**Fig. S4.9**). This result aligns with previous findings in the closely related species *C. jejuni*, where PfIA and PfIB interact. It also explains the similar *in-situ* structures and identical motility phenotypes of the  $\Delta pfIA$  and  $\Delta pfIB$  mutants, indicating that both proteins are essential for motor function (**Figs. 4.1E-H** and **S4.5**).

SPR analysis also indicated that both PflA<sub>C</sub> and PflB<sub>C</sub> interact with the periplasmic MotB<sub>C</sub> with  $K_D$  values of 24.7±1.3 µM and 28.2±3.3 µM, respectively (**Figs. S4.8A, B**) and that PilN<sub>C</sub> binds to both PflB<sub>C</sub> ( $K_D$ =6.7±0.7 µM) and full-length PflA ( $K_D$ =12.2±3.8 µM (*Liu et al. 2024*) (**Figs. 4.5E** and **S4.8C, D**). These findings support our model, wherein the N-terminal side of the TPR domain of PflA is positioned next to the coiled-coil region of MotB, and both PflB and the N-terminal  $\beta$ -sandwich domain of PflA are located between MotB and the cage (**Figs. 4.4A-C**). We also investigated interactions of the soluble variants of PflA and PflB with periplasmic FliL<sub>C</sub>, a scaffold protein involved in stator stabilization and activation (*Tachiyama et al. 2022*). SPR suggests an interaction between PflA<sub>C</sub> and the FliL ring (**Figs. 4.4C** and **S4.8E**). No detectable interaction was observed between PflB<sub>C</sub> and FliL<sub>C</sub> under the same experimental conditions. These findings are consistent with results from the BACTH assays, which suggest that FliL interacts with PflA but not PflB (**Fig. S4.9**). From the SPR studies, we cannot exclude the possibility that PflB and FliL interact in the motor via their N-terminal regions, which were not included in the expressed protein constructs. To reconcile these findings, in our model, PflB<sub>C</sub> is located at a slightly higher position than PflA (**Fig. 4.4H**), leaving a space between PflB<sub>C</sub> and the FliL ring.

In our *H. pylori* motor model, FlgY connects with PflA<sub>C</sub>. SPR analysis of purified recombinant proteins revealed that PflA interacts with FlgY *in vitro* (**Figs. 4.5F** and **S4.8F**). However, PflB also interacts with FlgY *in vitro* though PflB is not in immediate proximity to FlgY in our model (**Figs. 4.5A-C**, **5F**, and **S4.8G**). Results from the BACTH assay did not reveal interactions between FlgY and PflA or PflB (**Fig. S4.9**). It is possible that the PflB-FlgY interaction occurs transiently during motor assembly but is not maintained in the final structure, where competing interactions with other proteins may impose spatial constraints that keep PflB and FlgY separated.

## DISCUSSION

Flagellar motility is essential for *H. pylori* to successfully colonize the human stomach (*Eaton et al. 1992, Eaton et al. 1996, Ottemann et al. 2002, Schreiber et al. 2004*). This motility is driven by one of the largest flagellar motors in bacteria. Different from *E. coli* and *S. enterica*, *H. pylori* possesses many accessory structures in the flagellar motor that enable high torque through 18

stator complexes and contribute to its remarkable ability to penetrate and persist in the gastric mucosa (Hu et al. 2022, Tachiyama et al. 2022, Qin et al. 2017, Liu et al. 2024, Botting et al. **2023**). However, specific adaptations in *H. pylori* remain poorly understood at the molecular level. Here, we combined cryo-ET with molecular genetics and biochemical approaches to reveal how three key accessory proteins (FlqY, PflA, and PflB) form a distinct spoke-ring network bridging the MS-ring and 18 stator complexes in the periplasmic region of the H. pylori flagellar motor. Furthermore, leveraging *in-situ* motor structures derived from cryo-ET and AlphaFold predictions, we built a model to show for the first time how FlgY, PflA, and PflB interact with the core flagellar components in H. pylori (Figs. 4.5A-C). Specifically, 13 copies of the FlgY homodimer form the proximal spoke-ring complex around the MS-ring (Fig. 4.3), while 18 copies of PfIA and 18 copies of PfIB form a distal ring-spoke, with the latter located between the cage and 18 stator complexes (Figs. 4.4F, G). Notably, each distal spoke adopts a different orientation at its interface with the proximal spokes (Figs. 4.4A, F), suggesting that both the C-terminal TPR domain of PfIA and the N-terminal helix of FlgY are flexible (Figs. 4.5C, S4.1, and S4.2). This raises the possibility that the periplasmic scaffold of the H. pylori flagellar motor is dynamic and that PflA protomers exchange binding partners during flagellar rotation or chemotaxis-driven changes in rotational direction.

The FlgY spoke-ring likely plays an important role in H. pylori given its remarkable structure and location (Figs. 4.5A-C). We propose that the FlgY spoke-ring functions as a molecular bearing to separate the rotating MS-ring from non-rotating periplasmic components, including the PfIA-PfIB spoke-ring and PiIN-PiIO cage. In the conserved core structure, the LPring is believed to act as a molecular bushing that maintains the coaxial alignment of the rod as it rotates. Consistent with this model, a high-resolution structure revealed a small gap between the rod and LP-ring that is wide enough for the rod to rotate freely within the flagellar motor (Yamaguchi et al. 2021). Moreover, surface-exposed Asp, Glu, and Lys residues in the center of the L-ring form negatively and positively charged regions that face the negatively charged surface of the rod (Yamaguchi et al. 2021). Thus, the electrostatic potentials of the L-ring interior and rod surface suggest that the interplay of repulsive and attractive forces balances the rod and enables it to rotate smoothly (Yamaguchi et al. 2021). Our structures of the FlqY spoke-ring and MS-ring are consistent with the bushing model for the LP-ring and rod (Yamaguchi et al. 2021), as there is a small gap (~0.6 nm) between the rotating and non-rotating units (Fig. 4.3B). In addition, Lys<sup>131</sup>, Lys<sup>134</sup>, and Lys<sup>165</sup> in the globular domain of FlgY are predicted to form a positively charged surface, and Glu<sup>140</sup> and Asp<sup>167</sup> on the same domain are predicted to form a negatively charged surface. These positively and negatively charged residues are relatively conserved and adjacent

to the negatively charged surface of the MS-ring (**Fig. S4.6**), creating an interaction interface resembling that between the LP-ring and rod. Furthermore, our *H. pylori* flagellar motor model predicts extensive interactions between PflA and PflB and further suggests these proteins are dependent on each other to form the extensively interconnected spoke-ring. As *H. pylori* rotates flagellar filaments in highly viscous environments, we speculate that the rod in the motor is not always on the central axis due to resistance from the environment. Thus, the flexibility of the PflA/FlgY interface may provide a cushion allowing the motor to tolerate some deviance in the position of the axial components, like a car's suspension system. It is also possible that the proximal and distal spokes play a role in flagellar mechanosensing by transferring signals from the MS-ring to distal components of the motor.

The distinct spoke-ring is also essential for recruitment and/or retainment of the stator units and their associated FliL rings within the motor, as stator units are absent from both the  $\Delta pflA$  and  $\Delta pflB$  mutants (**Figs. 4.1E-H** and **S4.5**), which also accounts for the non-motile phenotype of these strains (**Fig. S4.4**). The model is consistent with our SPR and BACTH experiments indicating that the PflA-PflB complex interacts with MotB and FliL (**Figs. 4.5D** and **S4.8** and **S4.9**). Assembly of the distinct spoke-ring network in the *H. pylori* flagellar motor appears to help ensure maximal stator occupancy, which in turn allows for the higher torque generation necessary for bacterial motility in viscous gastric mucus.

Our structural model of the *H. pylori* flagellar motor differs somewhat from the recently proposed structure of the *C. jejuni* flagellar motor (*Drobnič et al. 2023*). Most notably, the *C. jejuni* model lacks the symmetry mismatch between the proximal and distal spokes that we demonstrate in the *H. pylori* flagellar motor. Given that the flagellar motors possess distinct components with variable stoichiometries, a symmetry mismatch is not surprising in *H. pylori*. However, how this adaptation in variable stoichiometries affects flagellar motility is an open question. Beyond *C. jejuni*, FlgY and PflA homologs have been identified in members of the Pseudomonadota, namely *E. meliloti* and *C. sphaeroides*, where they are known as MotE and MotK, respectively (*Velez-Gonzalez et al. 2024*, *Eggenhofer et al. 2004*). Additionally, we identified a distant homolog of FlgY in spirochetes by position-specific iterative BLAST (PSI-BLAST). The spirochetal FlgY homolog FlbB is a flagellar motor protein necessary for downstream assembly of large parts of the spirochete-specific flagellar collar structure (*Chu et al. 2019*) FlbB is also predicted to share the N-terminal coiled-coil and C-terminal globular domain found in other MotE-like proteins (*Fig. S4.2*). The conservation of flagellar accessory structures

across phyla and a wide range of environmental niches suggests that they fulfill a broadly required functional role warranting further investigation.

### MATERIALS AND METHODS

Strains and growth conditions. *E. coli* NEB® Turbo (New England Biolabs, Ipswich, MA, USA) cells used for cloning were grown on LB medium supplemented with ampicillin (100 μg/ml) or kanamycin (30 μg/ml) as required. *H. pylori* strains and plasmids used in the study are listed in **Table S4.2**. *H. pylori* B128 (kindly provided by Dr. Richard M. Peek, Jr.) served as the parental strain for mutant construction. Unless stated otherwise, *H. pylori* was cultured at 37°C under microaerobic conditions (10% CO<sub>2</sub>, 8% O<sub>2</sub>, 82% N<sub>2</sub>) on tryptic soy agar supplemented with 5% heat-inactivated horse serum (Gibco; Thermo Fisher Scientific, Waltham, MA, USA) (TSA-HS medium) or in brain heart infusion (BHI) (Becton, Dickinson and Company, Sparks, MD, USA) broth with 5% heat-inactivated horse serum in sealed vials with an atmosphere of 5% CO<sub>2</sub>, 10% H<sub>2</sub>, 10% O<sub>2</sub>, and 75% N<sub>2</sub>. *E. coli* BL21 (DE3) strain for overexpression of recombinant proteins was purchased from Merck Millipore (Burlington, MA, USA).

**PCR methods.** Genomic DNA (gDNA) from *H. pylori* B128 was purified using the Wizard genomic DNA purification kit (Promega, Madison, WI, USA) and used as the template for PCR using PrimeSTAR DNA polymerase (Takara Bio, San Jose, CA, USA) or Phusion DNA polymerase (New England Biolabs). To facilitate cloning into the pGEM-T Easy vector (Promega), amplicons were incubated with *Taq* polymerase (Promega) at 72°C for 10 min to add A overhangs at the 3'-ends.

Construction of *H. pylori* B128 Δ*pflA*, Δ*pflB* and Δ*flgY* mutants. Upstream and downstream regions flanking *pflA* were amplified from *H. pylori* B128 gDNA using primer pairs 43/44 and 45/46 (Table S4.3). Primers 44 and 45 were complementary at their 5'-ends and introduced Xhol and Nhel restriction sites for kan<sup>R</sup>-sacB cassette insertion. The amplicons upstream and downstream of *pflA* were joined via overlapping PCR, treated with Taq polymerase to add A overhangs to their 3'-ends, and ligated into pGEM-T Easy (Promega) to generate plasmid pKR5 (Fig. S4.10). Plasmid pKR3 is a derivative of pJC038 (*Copass et al. 1997*) that carries a kan<sup>R</sup>-sacB cassette where *sacB* is under control of the *H. pylori ureA* promoter. In pKR3, the *H. pylori ureI* promoter was introduced at the end of the cassette in an outward orientation to compensate for potential polar effects on genes that are downstream of the kan<sup>R</sup>-sacB insertion. The kan<sup>R</sup>-sacB cassette from pKR3 was cloned into the Nhel and Xhol sites of pKR5 to generate plasmid pKR7, which

was introduced by natural transformation into *H. pylori* B128. Since plasmid pKR7 does not replicate in *H. pylori*, transformants in which *pflA* had been replaced with the kan<sup>R</sup>-sacB cassette by homologous recombination were enriched by selecting for kanamycin resistance. Replacement of *pflA* with the kan<sup>R</sup>-sacB cassette was confirmed by PCR using primer pair 43 and 46. One of the kanamycin-resistant isolates in which *pflA* was replaced with the kan<sup>R</sup>-sacB cassette (designated strain H3), was transformed with the suicide vector pKR5. Transformants in which the kan<sup>R</sup>-sacB cassette was replaced with the unmarked deletion of *pflA* resulting from homologous recombination between pKR5 and the chromosome were counter-selected on TSA-HS supplemented with 5% sucrose as described (*Deatherage and Barrick 2014*). Sucrose-resistant isolates were screened for kanamycin sensitivity on TSA-HS, and *pflA* deletion in kanamycin-sensitive isolates was confirmed by using primer pair 43 and 46 to amplify the region around the *pflA* locus and Sanger sequencing of the resulting amplicon (Eton Biosciences, Research Triangle, NC, USA). The *H. pylori* B128 strain with the unmarked deletion of *pflA* was designated strain H7.

Unmarked deletions of *pflB* and *flgY* in *H. pylori* B128 were constructed following the same protocol as for the  $\Delta pflA$  mutant. To construct the *pflB* deletion mutant, regions flanking *pflB* were amplified using primer pairs 224/225 (upstream), and 226/227 (downstream). The amplicons were joined via overlapping PCR and cloned into pGEM-T Easy to generate plasmid pKR61. The kan<sup>R</sup>-sacB cassette was introduced into pKR61 to generate the suicide vector pKR83, which was used to replace *pflB* with the kan<sup>R</sup>-sacB cassette in *H. pylori* B128 through homologous recombination, yielding strain H146. Replacement of *pflB* with the kan<sup>R</sup>-sacB cassette was confirmed by PCR using primer pair 224 and 227. The suicide vector pKR61 was introduced into H146 to replace the kan<sup>R</sup>-sacB cassette in the *pflB* locus with the unmarked deletion of *pflB* using the sucrose counter-selection as described above. Sucrose-resistant isolates were screened for kanamycin sensitivity, and deletion of *pflB* in kanamycin-sensitive isolates was confirmed by using primer pair 224 and 227 to amplify the region around the *pflB* locus and Sanger sequencing (Eton) the resulting amplicon. The *H. pylori* B128 strain in which *pflB* was deleted was designated strain H147.

To construct the *flgY* deletion mutant, regions flanking *flgY* were amplified using primer pairs 266/267 and 268/269. The amplicons were joined using overlapping PCR and cloned into pGEM-T Easy to generate plasmid pKR132. The kan<sup>R</sup>-sacB cassette was introduced into pKR132 to generate the suicide vector pKR133, which was used to replace *flgY* with the kan<sup>R</sup>-sacB cassette through homologous recombination to yield strain H165. The suicide vector pKR132 was

introduced into H165 to replace the kan<sup>R</sup>-sacB cassette in the *flgY* locus with the unmarked deletion of *flgY* in plasmid pKR132 using the sucrose counter-selection. Deletion of *flgY* in sucrose-resistant, kanamycin-sensitive isolates was confirmed by amplifying the region around the flgY locus using primer pair 266 and 269 and Sanger sequencing (Eton) the resulting amplicon. The *H. pylori* B128 strain in which *flgY* was deleted was designated strain H166.

Whole genome sequencing and analysis. gDNA from the *H. pylori* deletion mutants was purified using the Wizard genomic DNA purification kit (Promega) and submitted to the SeqCenter (Pittsburgh, PA, USA) for genomic library preparation and Illumina sequencing. Reads for *H. pylori* gDNA sequence were mapped to the published NCBI genome for *H. pylori* B128 (Accession no.: NZ\_CP024951.1) using the *breseq* computational pipeline (*Karimova et al. 1998*).

**Motility assay.** The motility of *H. pylori* strains was assessed by stab inoculating them into a soft agar medium consisting of Mueller-Hinton broth (Hardy Diagnostics, Santa Maria, CA, USA) (MHB), 10% heat-inactivated horse serum, 20 mM 2-[N-morpholino]ethane sulfonic acid (MES) pH 6.0 and 0.25% Noble agar. Prior to inoculation, *H. pylori* cells were cultured under microaerobic conditions on TSA-HS for 2 d at 37°C. The inoculated plates were then incubated under microaerobic conditions at 37°C to allow the cells to migrate from the point of inoculation and multiply. After 7 d, the diameters of the swim halos were measured. Each strain was tested in at least three replicates, and a two-sample t-test was used to determine statistical significance.

Transmission electron microscopy. *H. pylori* strains were grown to late-log phase ( $OD_{600} \sim 1.0$ ) in MHB supplemented with 5% heat-inactivated horse serum. Cells from 1 ml of culture were pelleted by centrifugation at 550 ×g, resuspended in 125 µl of 0.1 M phosphate-buffered saline (PBS) and fixed by adding 50 µl of 16% (v/v) EM grade formaldehyde and 25 µl of 8% (v/v) EM grade glutaraldehyde. Following a 5-min incubation at room temperature, 10 µl of the suspension was applied to a 300 mesh, formvar-coated copper grid and incubated at room temperature for 5 min. The cell suspension was then wicked off with filter paper, and the grids were washed 3 times with 10 µl of water. Cells were stained with 10 µl of 1% uranyl acetate for 30 s, followed by washing with water and air-drying. Cells were visualized using a JEOL JEM 1011 transmission electron microscope, and the number of flagella per cell (n=100+) was determined for each strain.

Construction of plasmids for BACTH assays. The Euromedex (Souffelweyersheim, France) Bacterial Adenylate Cyclase Two-Hybrid (BACTH) System Kit (*Bonny et al. 2024*) was used to detect and characterize protein-protein interactions *in vivo*. Primer pairs 216/217, 218/219, 220/221, and 302/303 (**Table S4.3**) were used to amplify *pflA*, *pflB*, *fliL*, and *flgY*, respectively,

from *H. pylori* B128 gDNA. The forward primers corresponded to sequences immediately downstream of the predicted signal peptides to prevent recombinant protein secretion. Amplicons were A-tailed and ligated into pGEM-T Easy, resulting in plasmids pKR73, pKR74, pKR75, pKR160 (**Table S4.2**). The Xbal and Kpnl fragment from pKR160 and BamHl-Kpnl fragments from pKR73, pKR74, pKR75, and pKR160 were cloned into BACTH vectors (pKT25, pKNT25, pUT18, and pUT18C). Cloned DNA fragments were sequenced by Eton to confirm that the plasmid constructs were correct. The *E. coli* reporter strain BTH101 was used for cotransformation of BACTH plasmids. Combinations of plasmids were co-transformed into BTH101 and screened for protein-protein interactions on McConkey agar supplemented with 1% (w/v) maltose, 100 μg/ml ampicillin, 50 μg/ml kanamycin, and 0.5 mM isopropyl-β-D-thiogalactopyranoside (IPTG).

**β-galactosidase assay for BACTH analysis.** Cultures of *E. coli* BTH101 harboring various combinations of BACTH plasmids were grown at 30°C to mid- to late-log phase in LB supplemented with ampicillin (50 µg/ml), kanamycin (25 µg/ml), and 0.5 mM IPTG. Cells were diluted five-fold in M63 medium (15 mM (NH<sub>4</sub>)<sub>2</sub>SO<sub>4</sub>,100 mM KH<sub>2</sub>PO<sub>4</sub>, 1.8 µM FeSO<sub>4</sub>, 1 mM MgSO<sub>4</sub>, and 4 µM thiamine) containing 0.2% maltose as the carbon source in a final volume of 2.5 ml, and OD<sub>600</sub> readings were taken for each culture. Cells were permeabilized by adding 30 μl of toluene and 35 μl of a 0.1% sodium dodecylsulfate solution. The tubes were plugged with cotton and incubated for 30-40 min at 37°C with shaking. The cultures were then diluted 10-fold in PM2 buffer (70 mM Na<sub>2</sub>HPO<sub>4</sub>, 30 mM NaH<sub>2</sub>PO<sub>4</sub>, 1 mM MgSO<sub>4</sub>, 0.2 mM MnSO<sub>4</sub>, 100 mM βmercaptoethanol, pH 7.0) to a final volume of 1 ml and placed in 5 ml glass tubes. Cells were incubated for 5 min in a water bath at 28°C, and the enzymatic reaction was started by adding 0.25 ml of 13 mM o-nitrophenol-β-galactoside (in PM2 buffer. Reactions were stopped by adding 0.5 mL of 1 M Na<sub>2</sub>CO<sub>3</sub>, and OD<sub>420</sub> values were measured. The enzymatic activity (A; units (i.e., nmol o-nitrophenol hydrolyzed min-1)/ml) was calculated according to instructions provided by BACTH kit supplier using the formula  $A = 200 \times (OD_{420} / min of incubation)$  dilution factor. The factor 200 in the formula is the inverse of the OD<sub>420</sub> for 1 µM o-nitrophenol using a 1 cm light path, which is 0.0045 at pH 11.0. The dilution factor for each sample was 10. Specific activities (SA) expressed in units per mg dry weight were calculated by considering 1 ml of culture at OD<sub>600</sub> = 1 corresponds to 300  $\mu$ g dry weight bacteria and using the formula SA = A / (OD<sub>600</sub> x 0.3 mg dry wt per OD<sub>600</sub>). Each strain was assayed with at least three replicates, and a two-sample t-test was used to determine statistical significance.

Protein expression and purification. Full-length PflA, the C-terminal TPR domain of PflA (PfIA<sub>C</sub>), and the C-terminal periplasmic domains of H. pylori MotB (MotB<sub>C</sub>), FliL (FliL<sub>C</sub>), PilN (PilN<sub>C</sub>, residues 41–177), and PflB (PflB<sub>C</sub>) were purified as previously described (**Zhou et al. 2024, Chan** et al. 2018, Roujeinikova 2008, Mastronarde 2005). The codon-optimized sequence of FlgY (HP0257 lacking the N-terminal 16-aa signal peptide, UniProt ID O25038) was synthesized and inserted into the pET151/D-TOPO vector to incorporate an N-terminal TEV-cleavable His6-tag by GenScript USA Inc. E. coli BL21(DE3) cells were transformed with the vector, grown in LB with 50 μg/mL ampicillin at 310 K to an OD<sub>600</sub> of 0.8, and protein overexpression was induced for 4 hrs with 1 mM IPTG. The cells were then harvested by centrifugation at 4,500×g for 15 min at 277 K. The cells were lysed by sonication in 20 mM Tris-HCl pH 8.0, 300 mM NaCl, 10 mM imidazole, 2 mM phenylmethanesulfonyl fluoride, and the clarified lysate - free of cell debris - was loaded onto a 5 ml Hi-Trap Chelating HP column (Cytiva, Malborough, MA, USA). The column was washed with 20 column volumes of buffer containing 20 mM sodium phosphate pH 7.4, 300 mM NaCl and 40 mM imidazole, and the protein was eluted with buffer containing 20 mM Tris-HCl pH 8.0, 300 mM NaCl and 500 mM imidazole. The His6 tag was cleaved off using His-tagged TEV protease (Invitrogen; Thermo Fisher Scientific, Waltham, MA, USA), and the uncleaved protein, His<sub>6</sub> tag, and TEV protease were removed by passing the mix through the Hi-Trap Chelating HP column. The protein was then passed through the Superdex 200 HiLoad 26/600 gel-filtration column (GE Healthcare) in buffer containing 10 mM HEPES-NaOH pH 7.4 and 150 mM NaCl.

Surface plasmon resonance (SPR). SPR experiments were performed at  $25^{\circ}$ C using Biacore T200 (Cytiva). The CM5 sensor chips (Cytiva) were used for all interactions except PflA<sub>C</sub>/PflB<sub>C</sub>, for which a CMD500m chip (XanTec bioanalytics GmbH, Dusseldorf, Germany) was used. The surfaces of flow cells were activated for 10 min using a 1:1 mixture of 0.1 M N-hydroxysuccinimide (NHS) and 0.1 M 1-ethyl-3-(3-diethylaminopropyl)-carbodiimide (EDC) at a flow rate of 5  $\mu$ l/min. The ligand (PflA, PflA<sub>C</sub> or PflB<sub>C</sub>) was diluted to 10  $\mu$ g/ml in buffer containing 10 mM sodium acetate pH 5.0 and immobilized in the target cells using amine-coupling chemistry. To block any remaining activated carboxyl groups on the surface, both target and reference cells were treated with a 15-minute injection of 1 M ethanolamine-HCl (pH 8.0) at a flow rate of 5  $\mu$ l/min. In the binding kinetics assay, approximately 200 response units (RU) were immobilized, while for steady-state binding analysis, the immobilization level was approximately 1000 RU. The analyte was buffer-exchanged into SPR running buffer (10 mM HEPES-NaOH pH 7.4 and 150 mM NaCl for MotB<sub>C</sub>, PilN<sub>C</sub> and FlgY; 10 mM HEPES-NaOH pH 7.4 and 300 mM NaCl for FliL<sub>C</sub> and PflA<sub>C</sub>) and injected onto the surface in target and reference cells at a flow rate of 30  $\mu$ l/min. To inhibit nonspecific binding of

MotB<sub>C</sub> and FIgY to the sensor surfaces, 0.5% (w/v) bovine serum albumin solution was injected over the surfaces at a flow rate of 30  $\mu$ l/min for 60 seconds before injecting the analyte. In the binding kinetics assay, the contact time and dissociation times were 120 and 300 s. Steady-state binding measurements were performed with contact and dissociation times of 120 s each. The surface was regenerated between measurements at different protein concentrations with a 60-s injection of 50 mM HCl (for MotBC, PilNC, and FlgY) or 50 mM NaOH (for FliLC and PflAC) to fully release the analyte from the previous flow. Experiments were conducted in triplicate, and consistency between replicates was used to confirm the stability of the immobilized ligand in the regeneration buffer. To account for non-specific binding, the response from the reference cell was subtracted from that of the target cell. The binding affinity ( $K_D$ ) value was estimated by fitting experimental data to either a steady-state binding model or a two-state reaction kinetic model using the Biacore T200 Evaluation software (version 3.2.1).

Cryo-ET sample preparation. *H. pylori* G27 as streaked on Columbia blood based agar plates containing 5% defibrinated horse blood and antibiotics (50 µg/mL cycloheximide, 10 µg/mL vancomycin, 5 µg/mL cefsulodin, and 2.5 units/ml polymyxin B). Mutant strains ( $\Delta flgY$ ,  $\Delta pflA$ ,  $\Delta pflB$ ) were streaked on tryptic soy agar plates containing 5% heat-inactivated horse serum. All strains were grown at 37°C in a 10% CO<sub>2</sub> atmosphere for 2 days, re-streaked on fresh plates and grown for an additional day. Cells from agar plates were resuspended in PBS and adjusted to an OD<sub>600</sub> of 1.0. The bacterial suspension was mixed with BSA-coated 10 nm Gold Tracer beads (Aurion Biotech, Cambridge, MA, USA), and 5 µL was deposited on glow-discharged cryo-EM grids (Quantifoil, Cu, 200 mesh, R2/1). To form a thin layer of frozen specimens, grids were blotted at the back with filter paper (Whatman<sup>TM</sup>) and immediately plunge-frozen in a liquid ethane-propane mixture using a homemade plunger.

**Cryo-ET data collection.** Images of frozen-hydrated *H. pylori* specimens were recorded using a Titan Krios G2 300 kV transmission electron microscope (Thermo Fisher Scientific) equipped with a field emission gun, K3 detector, and GIF BioQuantum imaging filter (Gatan, Pleasanton, CA, USA). SerialEM software (*Xu and Xu 2021*) was used for the automated acquisition of tilt series images at ×42,000 magnification with a physical pixel size of 2.15 Å, 4.9-5.2 μm defocus, and the dose fraction mode set to record 10 frames per image. The microscope stage was tilted from -48° to +48° in 3° increments using the dose-symmetric scheme in FastTomo script (*Zheng et al. 2017*).

Cryo-ET data processing and subtomogram averaging. Motioncorr2 (Kremer et al. 2016) was used to correct for image drift caused by the electron beam during the data collection. IMOD software was used to create image stacks and align images in each tilt series by tracking fiducial gold beads (Mastronarde and Held 2017, Zhang 2016). Gctf (Xiong et al. 2009) waC-terminals used to estimate defocus, and the 'ctfphaseflip' function in IMOD was used to correct the contrast transfer function (CTF) (Agulleiro and Fernandez 2015). 6x binned tomograms were reconstructed using Tomo3D (Winkler 2007). The simultaneous iterative reconstruction technique (SIRT) was employed to manually select flagellar motors from tomograms. In total, 567, 196, 333, 300 tomograms were reconstructed for WT,  $\Delta flgY$ ,  $\Delta pflA$ , and  $\Delta pflB$  strains, respectively. For the subtomogram averaging, 1635, 708, 975, 814 flagellar motors were selected from tomograms for WT,  $\Delta flgY$ ,  $\Delta pflA$ , and  $\Delta pflB$  strains, respectively. Subtomogram averaging was performed using the i3 package (Winkler 2009, Morado et al. 2016, Goddard et al. 2018). Initial averaged structures were determined using the positions of flagellar motors and 6× binned tomograms with Weighted Back Projection (WBP). For further structural analysis, subtomogram averaging was performed using the i3 package to analyze 2x binned subtomograms. To determine high-resolution structures, the C13 and C18 symmetry expansions were performed to increase the particle numbers for the proximal spoke and distal spoke-ring regions, respectively. Then, the focused refinement was performed for the proximal spoke and distal spoke-ring structures in unbinned subtomograms separately (Figs. 4.3B and 4.4B). For the focused refinement, molecular masks were applied for reference structures to improve the structural resolution. For the distal spoke-ring structure (Fig. 4.4B), only one side of the motor was used to refine the structure. The resolution was estimated by Fourier Shell Correlation (FSC).

Building atomic model of *H. pylori* flagellar motor. Electron density maps for globally and locally refined structures were generated using ChimeraX (*Pettersen et al. 2021*, *Johnson et al. 2024*) (University of California, San Francisco). AlphaFold3 (*Abramson et al. 2024*) was used to predict the structures of the FlgY homodimer (Fig. S4.5) and PflA-PflB<sub>2</sub> heterotrimer (Fig. S4.6). The FlgY model was fit into the electron densities for the proximal spoke and the ring near the MS-ring (Fig. 4.3D), and 13 FlgY homodimer copies were generated using the symmetry command in ChimeraX. The PflA-PflB<sub>2</sub> model (Fig. S4.6) was fit into the density map for the locally refined structure (Fig. 4.4B) and modified to improve the agreement with the density (Figs. 4.4C-E), particularly in PflA<sub>C</sub> (Fig. S4.6). For the pseudo-atomic model of the *H. pylori* flagellar motor (Fig. 4.4), both FlgY and PflA-PflB complex models were fit into the density map for the globally averaged structure. The predicted or experimentally determined structures of other

known components, FliL (*Tachiyama et al. 2022*), PilN-PilO heterodimer (*Liu et al. 2024*), PilM (*Liu et al. 2024*), MotA and MotB (*Guo et al. 2022*) were also fit into the density maps. As the Cring in the *H. pylori* flagellar motor comprises 39 subunits (*Botting et al. 2023*), we built the MS-ring and C-ring structures with 39-fold symmetry in *H. pylori* based on the *Salmonella* MS-ring (*Tan et al. 2021*) and C-ring structures (PDB: 8uox) (*Moon et al. 2016*). Other flagellar components including LP-ring (*Tan et al. 2021*) (PDB: 7cbl), rod and export apparatus (*Tan et al. 2021*) (PDB: 7e80), and curved hook (*Shibata et al. 2019*) (PDB: 6k3i) were used to build a complete flagellar motor model in *H. pylori*.

#### **ACKNOWLEDGMENTS**

This work was supported by the National Institutes of Health grants AI140444 (TRH), AI087946 (JL), and AI132828 (JL), and the Australian Research Council grant DP210103056 (AR). The funders had no role in study design, data collection and analysis, decision to publish, or preparation of the manuscript. We thank Jennifer Aronson, Beile Gao, and Xueyin Feng for critical reading of the manuscript.

# SUPPORTING INFORMATION

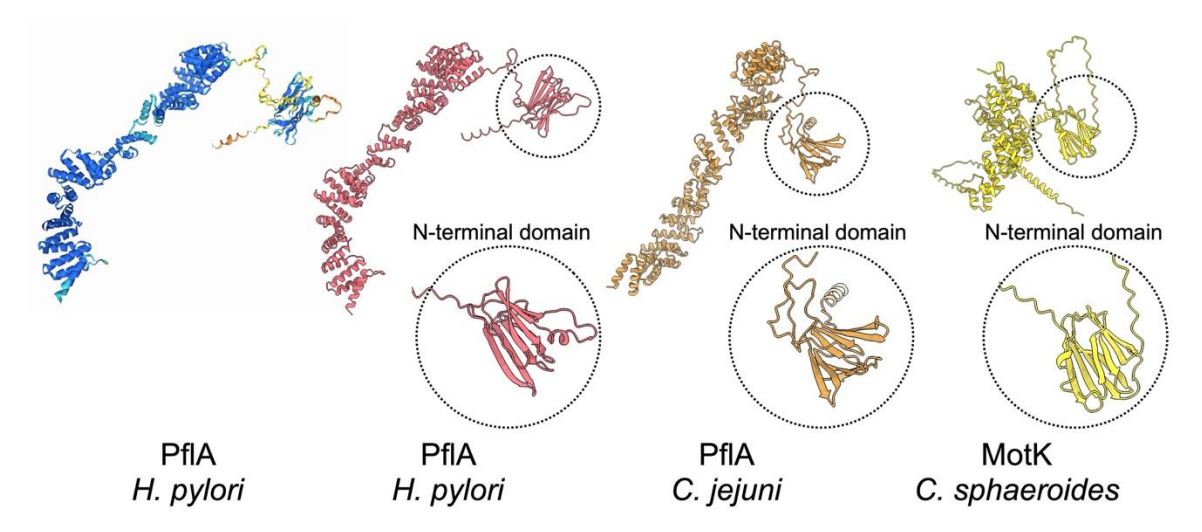


Figure S4.1. AlphaFold-predicted structures indicate that PflA in *Campylobacterota* and MotK in *Cereibacter sphaeroides* possess similar domains and motifs. (*Left*) Model of *H. pylori* PflA colored according to confidence level of structure prediction (with blue indicating high confidence and red indicating low confidence). Predicted structures of *H. pylori* PflA (red), *C. jejuni* 

PfIA (orange), and *C. sphaeroides* MotK (yellow) are presented in the right panels. All three proteins possess a sandwich domain (encircled) in their N-terminal regions and TPR motifs in their C-terminal regions.

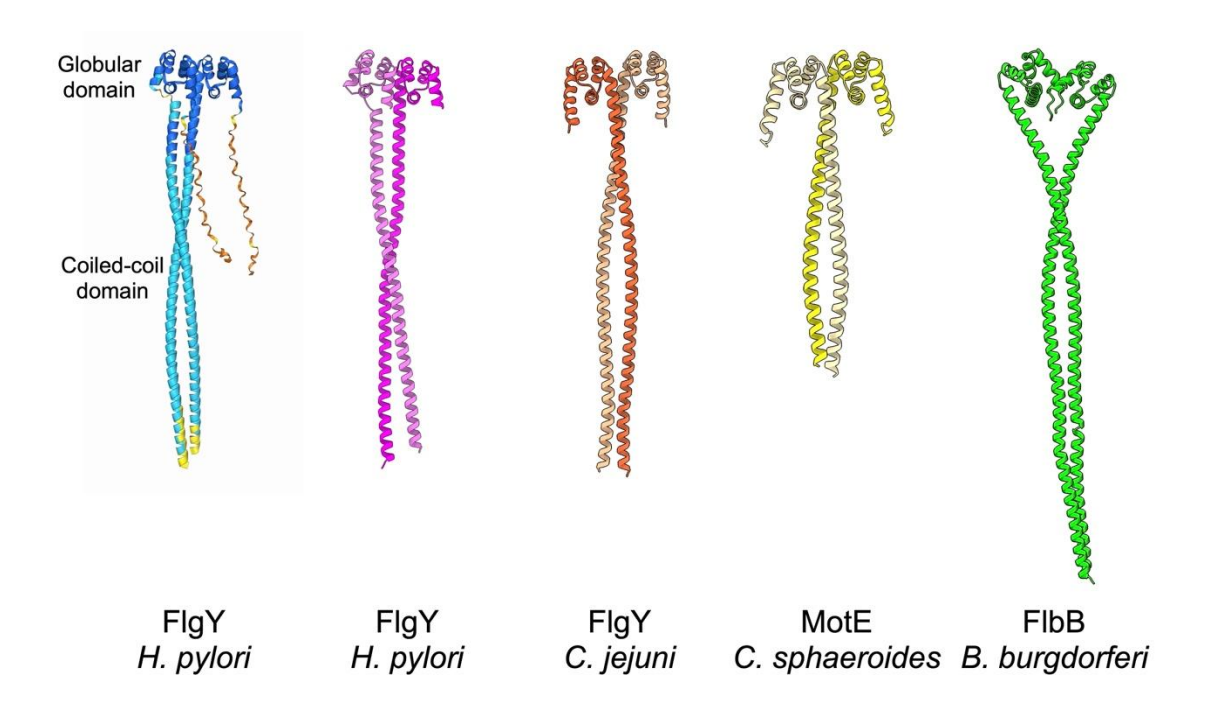


Figure S4.2. AlphaFold-predicted structures suggest that FlgY in *Campylobacterota* and MotE in *C. sphaeroides* possess similar domains and motifs. (*Left*) Model of *H. pylori* FlgY dimer colored according to confidence level of structure prediction. Predicted dimers of *H. pylori* FlgY (pink), *C. jejuni* FlgY (orange), *C. sphaeroides* MotE (yellow) and *B. burgdorferi* FlbB (green) are presented in the right panels. All four proteins are predicted to possess N-terminal coiled-coil domain and C-terminal globular domain.

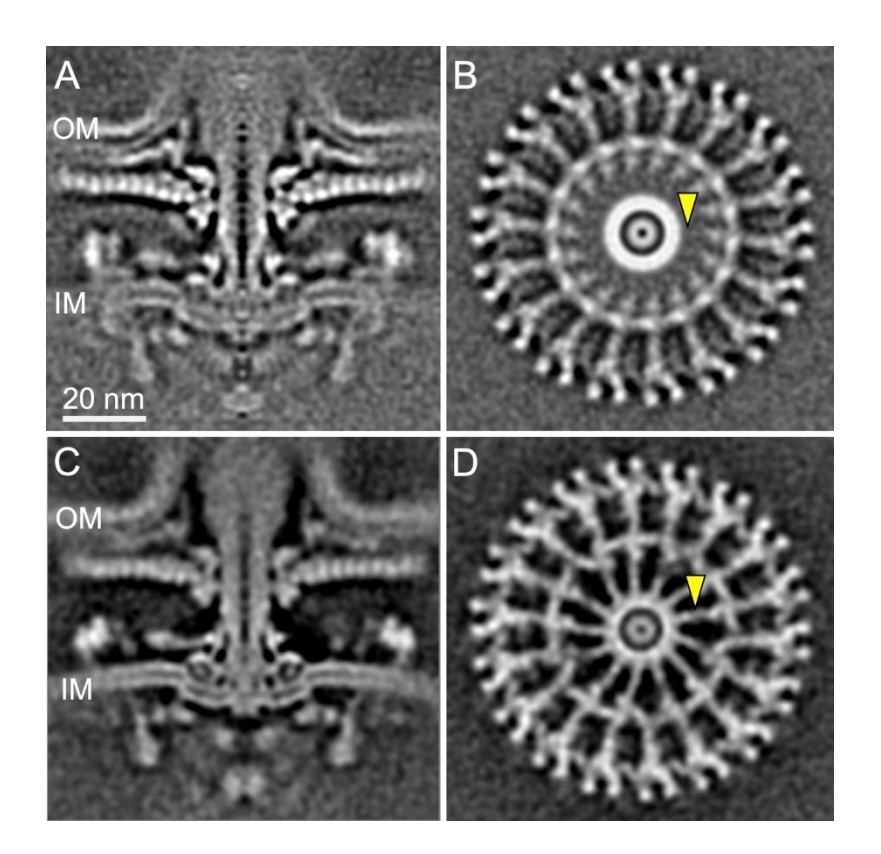


Figure S4.3. Asymmetric reconstruction of the *H. pylori* flagellar motor reveals 13 spokes around the MS-ring in periplasmic region. (A) Initial motor structure determined by applying 18-fold symmetry reveals distal spokes and cage units while the proximal spokes are not resolved in the region (yellow arrow) between the MS-ring and distal spokes. (C-D) Asymmetric reconstruction without 18-fold symmetry applied clearly resolves 13 copies of proximal spoke (yellow arrow) in this region. It is also apparent that there is flexible region where proximal spokes and distal spokes are joined.

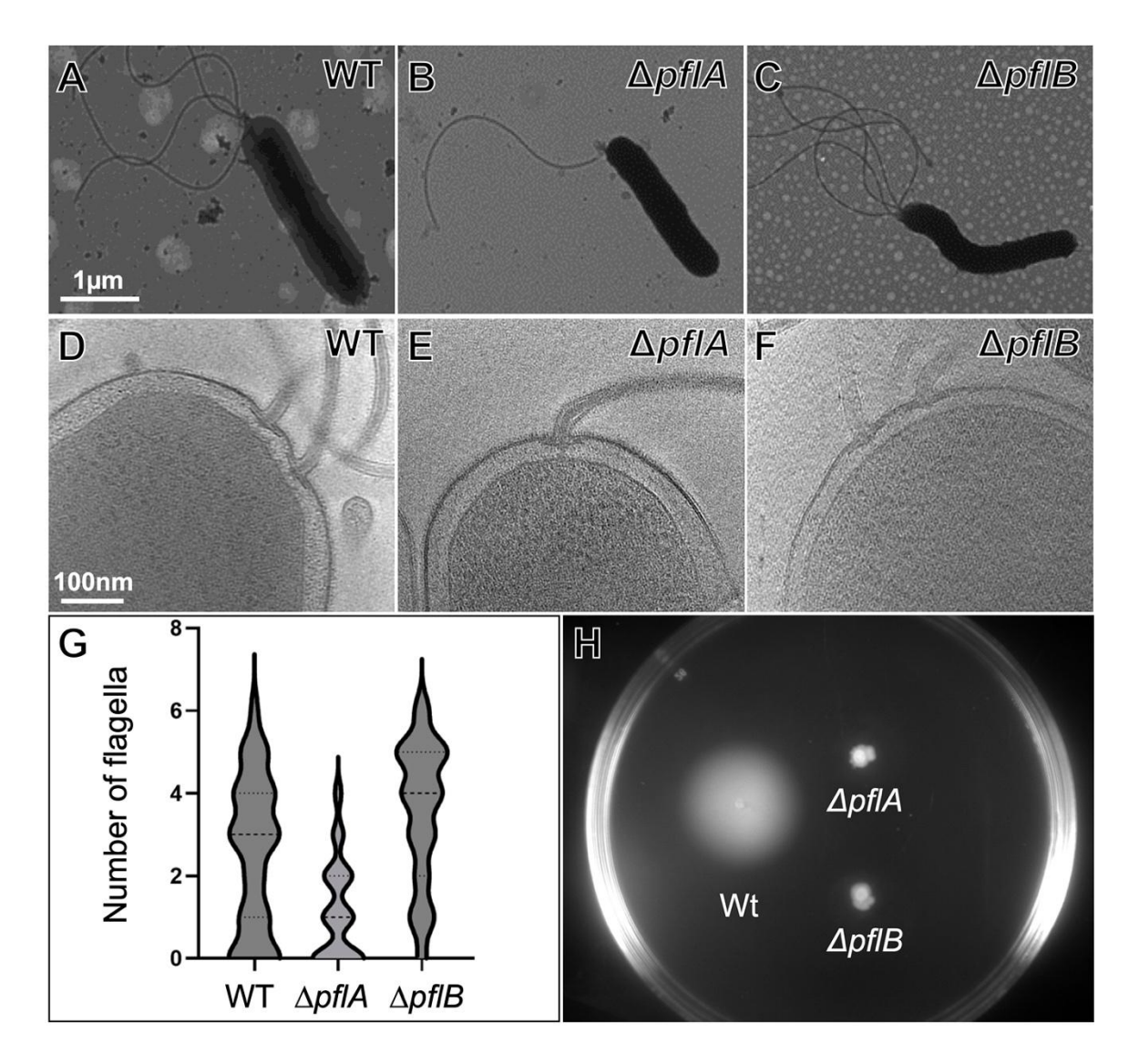


Figure S4.4. PfIA and PfIB are essential for bacterial motility but not flagellar assembly in *H. pylori*. TEM images of WT (**A**),  $\Delta pfIA$  mutant (**B**), and  $\Delta pfIB$  mutant (**C**) strains show flagellar filaments at the bacterial poles, respectively. Cryo-ET reconstructions from WT (**D**),  $\Delta pfIA$  mutant (**E**), and  $\Delta pfIB$  mutant (**F**) reveal the motors at the base of the filaments, respectively. (**G**) Number of flagella estimated by TEM is 3.21 (n=80) in WT, 1.13 (n=99) in  $\Delta pfIA$ , and 3.52 (n=102) in  $\Delta pfIB$ , respectively. (**H**) Results of bacterial motility assay on semi-solid (0.25%) agar.

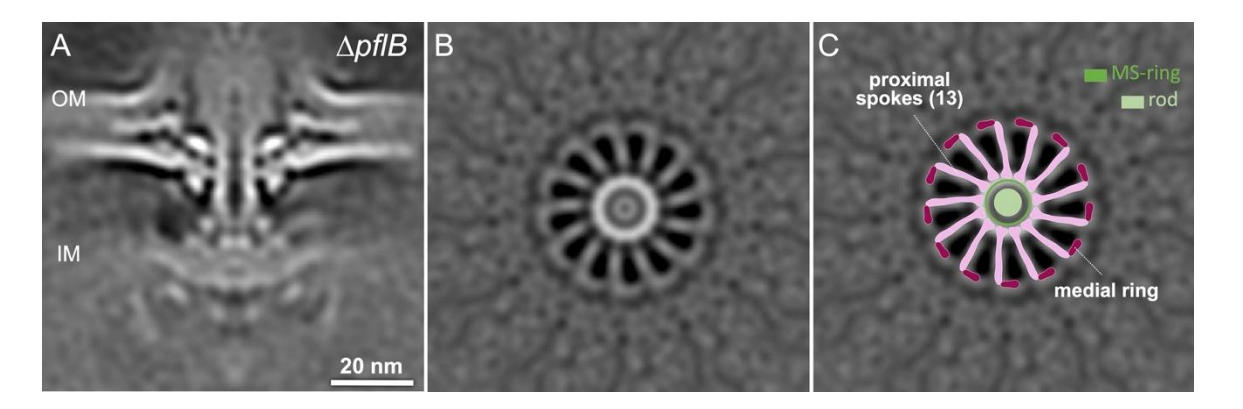


Figure S4.5. *In-situ* structure of the  $\triangle pflB$  flagellar motor. Medial slice (**A**) and cross-section (**B**) views of the *in-situ* structure of the  $\triangle pflB$  motor show 13 spokes and medial ring. However, the  $\triangle pflB$  motor appears to lack cage, distal ring, and distal spoke structures. (**C**) Cartoon model shows the proximal spokes (pink) and medial ring (dark red).

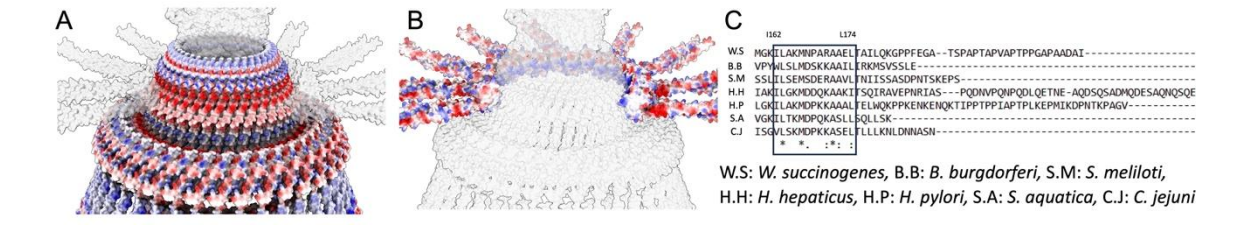


Figure S4.6. Molecular interface between the MS-ring and FlgY ring. (A) The MS-ring has negatively charged area (red) at its interface with the FlgY ring. (B) Globular domain of the FlgY dimer has both positively (blue) and negatively (red) charged residues that face the MS-ring. (C) Sequence alignment of the C-terminal globular regions of FlgY homologues from different species shows conserved region.

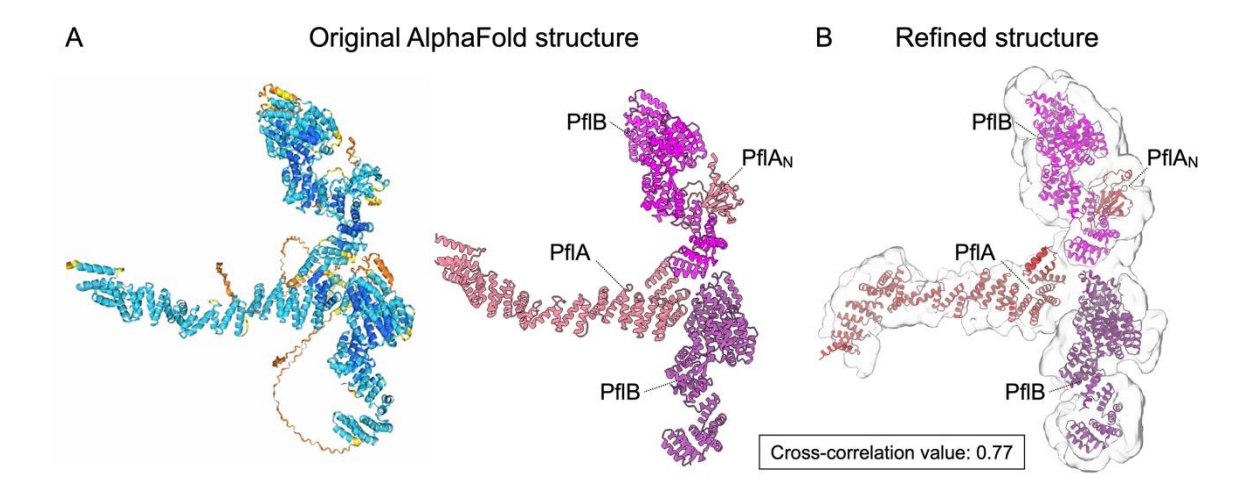


Figure S4.7. AlphaFold-predicted model of *H. pylori* PflA-PflB<sub>2</sub> heterotrimer fits well into the *in-situ* map. (A) AlphaFold-predicted model of PflA/PflB<sub>2</sub> heterotrimer colored with structure prediction confidence levels is shown in the left panel. One PflA (pink) appears to interact with two adjacent PflB molecules (magenta and dark purple) as shown in the right panel. (B) Refined model of the PflA-PflB<sub>2</sub> heterotrimer fits well into our *in-situ* map. Cross correlation value was estimated as 0.77.

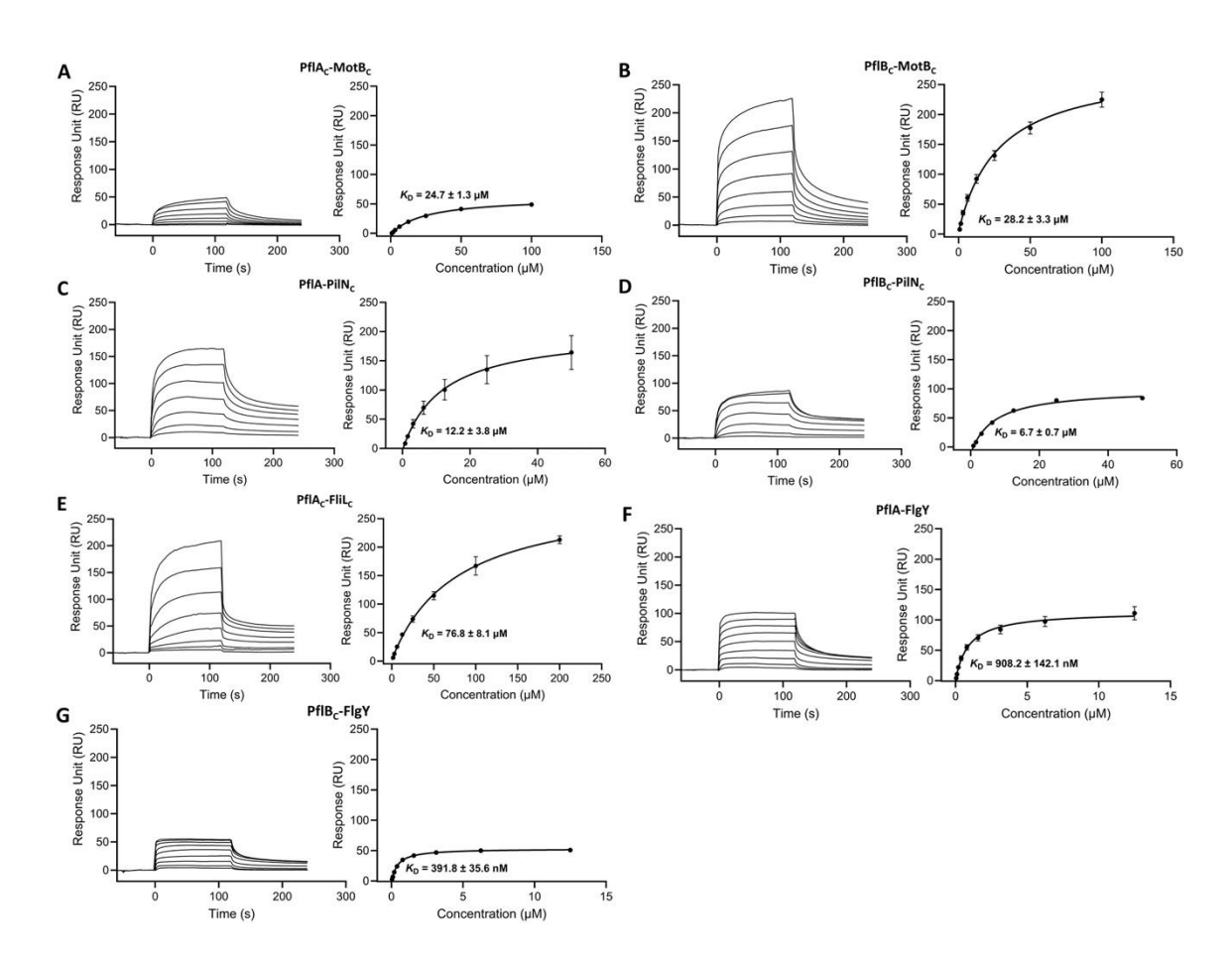


Figure S4.8. SPR experiments indicate that the PfIA-PfIB complex in *H. pylori* interacts with components of the stator and cage. Representative sensograms and equilibrium dissociation constant (KD) determinations for interactions between: (A) PfIA<sub>C</sub> and MotB<sub>C</sub> (MotB<sub>C</sub> concentrations were 0.8, 1.6, 3.1, 6.3, 12.5, 25, 50 and 100 μM), (B) PfIB<sub>C</sub> and MotB<sub>C</sub>, (C) PfIA and PiIN<sub>C</sub> (PiIN<sub>C</sub> concentrations were 0.8, 1.6, 3.1, 6.3, 12.5, 25 and 50 μM), (D) PfIB<sub>C</sub> and PiIN<sub>C</sub>, (E) PfIA<sub>C</sub> and FIiL<sub>C</sub> (FIiL<sub>C</sub> concentrations were 1.6, 3.1, 6.3, 12.5, 25, 50, 100 and 200 μM), (F) PfIA and FIgY (FIgY concentrations were 0.05, 0.1, 0.2, 0.4, 0.8, 1.6, 3.1, 6.3 and 12.5 μM), and (G) PfIB<sub>C</sub> and FIgY.

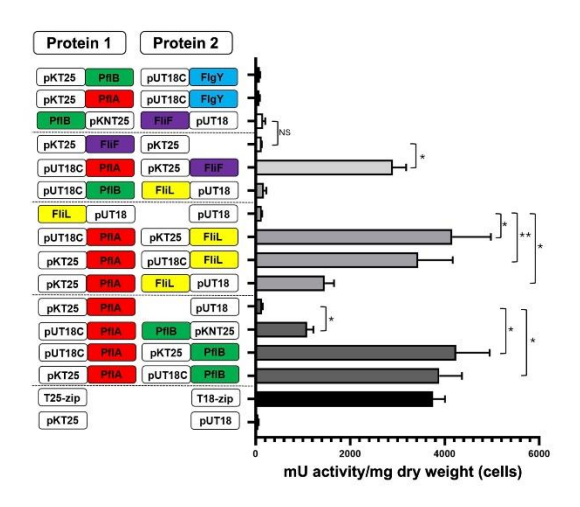


Figure S4.9. Bacterial adenylate cyclase two-hybrid (BACTH) assay shows interactions of PfIA and PfIB with other motor components. Coding regions of pfIA, pfIB, fliL, and flgY were cloned into BACTH vectors (pKT25, pKNT25, pUT18, and pUT18C) to generate four combinations of chimeric genes for each flagellar gene. Combinations of resulting plasmids were introduced into E. coli reporter strain BTH101. Strains harboring various plasmid combinations were assessed for reconstituted adenylate cyclase activity resulting from interactions between flagellar proteins. This was accomplished by examining ability of strains to catabolize maltose (generating red or pink colonies on McConkey-maltose agar) and induce lacZ expression (measured by β-galactosidase activity assays). β-galactosidase assays for strains with reconstituted adenylate cyclase activity as well as select plasmid combinations failed to reconstitute this activity. Schematics of various recombinant protein combinations indicate BACTH vector, flagellar protein (PfIA in red, PfIB in green, FliL in yellow, and FlgY in blue), and orientation of flagellar proteins (i.e., at N- or C-terminus of the recombinant protein). An E. coli strain bearing the BACTH vectors pKT25 and pUT18 served as a negative control, and an E. coli strain bearing plasmids that expressed the T25-zip andT18-zip fusion proteins served as a positive control. Single asterisk (\*) indicates P-value of < 0.0001, two asterisks (\*\*) indicate Pvalue of <0.0001.

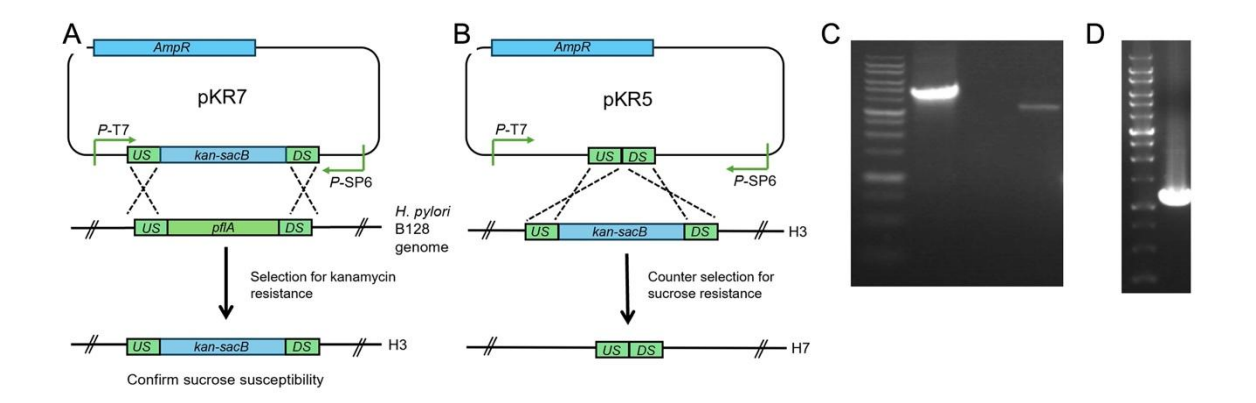


Figure S4.10. Construction of specific mutants in *H. pylori* B128. (A and B) Construction of unmarked deletion in pflA. (C) Phusion gDNA PCR amplification of H3 (lane 1) and H2 (lane 3) using primers 43/46. Bands are at 4kb (H3) and 3.5kb (H2). DNA ladder: Goldbio 1kb. (D) Phusion gDNA PCR amplification of H7 (lane 1) with primers 43/46. Band is at 1.2kb. H3 – pflA::kan-SacB. H2 - B128 wild type. H7 -  $\Delta pflA$ . Same general procedure was used to construct  $\Delta pflB$  and  $\Delta flgY$  mutants.

Table S4.1. Mutations identified in the  $\Delta pflA$ ,  $\Delta pflB$ , and  $\Delta flgY$  strains

∆ <i>pflA</i> mutant					
NCBI designation	locus tag in <i>H. pylori</i> 26695	Gene/ description	Mutation	<sup>a</sup> lmpact	<sup>b</sup> Frequency
CV725_RS00960	HP1274	pfIA	coding (62-2391/2406 nt) 2330 bp→23 bp	gene deletion	98.9%
CV725_RS02305 CV725_RS02315	HP0427 23S rRNA	US of hp0427 US of 23S rRNA gene	intergenic (-234/-736) +GTTGGATGATTGGA TG	unknown	95.7%
CV725_RS03080	HP0165	histidine kinase ArsS	(C) <sub>11→13</sub> (1261/1281 nt)	Pro424fs	90.6%
motB	HP0816	motB	codon- 106 ( <u>G</u> GC→ <u>C</u> GC)	Gly106Arg	97.7%
CV725_RS06500	HP0499	<i>pldA</i> , phospholipase A, pseudogene	(G) <sub>10→9</sub> (683/1070 nt)	remains phase 'off'	87.5%
babA CV725_RS06645	HP1243 tRNA_fMet	US of <i>babA</i> , DS of tRNA_fMet	(T) <sub>13→12</sub> intergenic (-131/+149)	unknown	83.9%
CV725_RS08550 queF	HP1412 HP1413	DS of hp1412 DS of queF	(C) <sub>11→10</sub> intergenic (+11/+121)	unknown	95.5%

0.4			<u> </u>		T
CV725_RS07725	HP0013	7-cyano-7-deaza guanine synthase	codon- 325 (TA <u>C</u> →TA <u>T</u> )	Tyr325Tyr	98.5%
flil	HP0809	flagellar protein export ATPase Flil	coding (168/1305 nt)	new junction	98.2%
CV725_RS00550	HP1421	type II/IV secretion system ATPase subunit	coding (560/915 nt)		
∆ <i>pfIB</i> mutant		<del>,</del>	<del>,</del>	<del>,</del>	
CV725_RS00245	HP1479	pflB	2474 bp→25 bp coding (26-2499/2535 nt)	Deletion	100%
CV725_RS00720	HP1322	hypothetical protein/	(ATACATAA) <sub>10→5</sub> intergenic (-194/+7)	unknown	100%
CV725_RS00725	HP1321	ATP-binding protein	mergeme ( 10 mm)		
CV725_RS04600 CV725_RS04605	HP0876 HP0875	TonB-dependent receptor/catalase	(A) <sub>5→6</sub> intergenic (-34/-290)	unknown	93.3%
CV725_RS06500	HP0499	pldA, phospholipase A, pseudogene	(G) <sub>10→9</sub> (683/1070 nt)	remains phase 'off'	84.7%
CV725_RS07485 CV725_RS07495	23S HP1409	23S ribosomal RNA/DUF262 protein	62 bp→G intergenic (-749/-224)	unknown	100%
CV725_RS08550	HP1412	DS of hp1412	(C) <sub>11→10</sub>		96.1%
queF	HP1413	DS of queF	intergenic (+11/+121)		
∆flgY mutant	_	1	T	T	1
CV725_RS00720	HP1322	hypothetical protein/	(ATACATAA) <sub>10→5</sub> intergenic (-194/+7)	unknown	99.5%
CV725_RS00725	HP1321	ATP-binding protein	milergeriic (-134/+1)		
CV725_RS03540	HP0257	flgY	611 bp→29 bp	deletion	100%
hopJ	HP0477	Hop family outer membrane protein HopJ/HopK	codon-182 (A <u>G</u> C→A <u>C</u> C)	Ser182Thr	99.3%
CV725_RS04600 CV725_RS04605	HP0876 HP0875	TonB-dependent receptor/catalase	(A) <sub>5→6</sub> intergenic (-34/-290)	unknown	92.3%
motA	HP0815	motA	codon-201 (G <u>G</u> C→G <u>A</u> C)	Gly201Asp	99.3%
oipA	HP0638	outer membrane protein OipA	Δ81 bp coding (174-254/958 nt )	Δlle59-Asn85	100%
CV725_RS06500	HP0499	pldA, phospholipase A, pseudogene	(G) <sub>10→11</sub> (683/1070 nt)	phase 'off' to phase 'on'	86.4%

CV725_RS08550	HP1412	DS of hp1412	(C) <sub>11→10</sub>	95.8%
queF	HP1413	DS of queF	intergenic (+11/+121)	

<sup>&</sup>lt;sup>a</sup>"fs" indicates frameshift

Table S4.2. Plasmids and H. pylori strains used in the study

Plasmids		
Name	Description	Reference
pKR3	pGEM-T Easy carrying the kan <sup>R</sup> -sacB cassette with <i>urel</i> promoter, Kan <sup>R</sup> , Amp <sup>R</sup>	(Rosinke et al. 2024)
pKR5	pGEM-T Easy carrying overlapping PCR product of <i>pflA</i> flanking regions, Amp <sup>R</sup>	current study
pKR7	pKR5 derivative with kan <sup>R</sup> -sacB cassette inserted into the <i>pflA</i> flanking regions, Kan <sup>R</sup> , Amp <sup>R</sup>	current study
pKR61	pGEM-T Easy carrying overlapping PCR product of <i>pflB</i> flanking regions, Amp <sup>R</sup>	current study
pKR83	pKR61 derivative with kan <sup>R</sup> -sacB cassette inserted into the <i>pflB</i> flanking regions, Kan <sup>R</sup> , Amp <sup>R</sup>	current Study
pKR132	pGEM-T Easy carrying overlapping PCR product of flgY flanking regions, Amp <sup>R</sup>	current study
pKR133	pKR132 derivative with kan <sup>R</sup> -sacB cassette inserted into the <i>pflB</i> flanking regions, Kan <sup>R</sup> , Amp <sup>R</sup>	current study
pKR73	pGEM-T Easy carrying <i>pflA</i> , Amp <sup>R</sup>	current study
pKR74	pGEM-T Easy carrying <i>pflB</i> , Amp <sup>R</sup>	current study
pKR75	pGEM-T Easy carrying <i>fliL</i> , Amp <sup>R</sup>	current study
pKR160	pGEM-T Easy carrying flgY, Amp <sup>R</sup>	current study
pKT25	carries T25 fragment of <i>Bordetella pertussis cya</i> , multicloning site (MCS) at 3'-end of <i>cya</i> fragment; Kan <sup>R</sup>	Karimova et al. 2001)
pKNT25	carries T25 fragment of <i>B. pertussis cya</i> , MCS at 5'-end of <i>cya</i> fragment; Kan <sup>R</sup>	(Karimova et al. 2001)
pUT18	carries T18 fragment of <i>B. pertussis cya,</i> MCS at 5'-end of <i>cya</i> fragment; Amp <sup>R</sup>	(Karimova et al. 2001)
pUT18C	carries T18 fragment of <i>B. pertussis cya,</i> MCS at 3'-end of <i>cya</i> fragment; Amp <sup>R</sup>	(Karimova et al. 2001)

<sup>&</sup>lt;sup>b</sup>Reads from the gDNA sequencing were mapped using the *breseq* computational pipeline with the published NCBI genome for *H. pylori* B128. Frequency is the number of times the mutation was identified relative to the total number of reads for the sequence. Only mutations found in > 80% of reads are indicated.

pKT25-zip	pKT25 derivative expressing leucine zipper of GCN4-T25 fragment fusion; Kan <sup>R</sup>	(Karimova et al. 2001)
pUT18C-zip	pUT18C derivative expressing leucine zipper of GCN4-T18 fragment fusion; Amp <sup>R</sup>	(Karimova et al. 2001)
pKR79	pKT25 derivative expressing T25 fragment-PflB fusion; Kan <sup>R</sup>	current study
pKR80	pKNT25 derivative expressing PflB-T25 fragment fusion; Kan <sup>R</sup>	current study
pKR81	pUT18 derivative expressing PflB-T18 fragment fusion; Amp <sup>R</sup>	current study
pKR82	pUT18C derivative expression T18 fragment-PflB fusion; Amp <sup>R</sup>	current study
pKR83	pKT25 derivative expressing T25 fragment-PflA fusion; Kan <sup>R</sup>	current study
pKR85	pKNT25 derivative expressing PfIA-T25 fragment fusion; Kan <sup>R</sup>	current study
pKR86	pUT18 derivative expressing PfIA-T18 fragment fusion; Amp <sup>R</sup>	current study
pKR87	pUT18C derivative expression T18 fragment-PflA fusion; Amp <sup>R</sup>	current study
pKR88	pKT25 derivative expressing T25 fragment-FliL fusion; Kan <sup>R</sup>	current study
pKR89	pKNT25 derivative expressing FliL-T25 fragment fusion; Kan <sup>R</sup>	current study
pKR90	pUT18 derivative expressing FliL-T18 fragment fusion; Amp <sup>R</sup>	current study
pKR91	pUT18C derivative expression T18 fragment-FliL fusion; Amp <sup>R</sup>	current study
pKR161	pKT25 derivative expressing T25 fragment-FlgY fusion; Kan <sup>R</sup>	current study
pKR162	pKNT25 derivative expressing FlgY-T25 fragment fusion; Kan <sup>R</sup>	current study
pKR163	pUT18 derivative expressing FlgY-T18 fragment fusion; Amp <sup>R</sup>	current study
pKR164	pUT18C derivative expression T18 fragment-FlgY fusion; Amp <sup>R</sup>	current study
H. pylori stra	ins	
H2	H. pylori B128 wild type	Richard M. Peek, Jr.
H3	H. pylori B128 pflA::kan <sup>R</sup> -sacB	current study
H7	H. pylori B128 ΔpflA	current study
H146	H. pylori B128 pflB::kan <sup>R</sup> -sacB	current study
H147	H. pylori B128 ΔpflB	current study
H165	H. pylori B128 flgY::kan <sup>R</sup> -sacB	current study
H166	H. pylori B128 ΔflgY	current study

Table S4.3. Primers used in the study

Primers				
Number	Target/Direction	Sequence		
35	kan <sup>R</sup> -sacB cassette/reverse	5' AATTTTGTTTGGAAGGAAAAGGCACA3'		
36	kan <sup>R</sup> -sacB cassette/forward	5' TAAGGAGCGTTGCTCCTAAAAAATCGT3'		

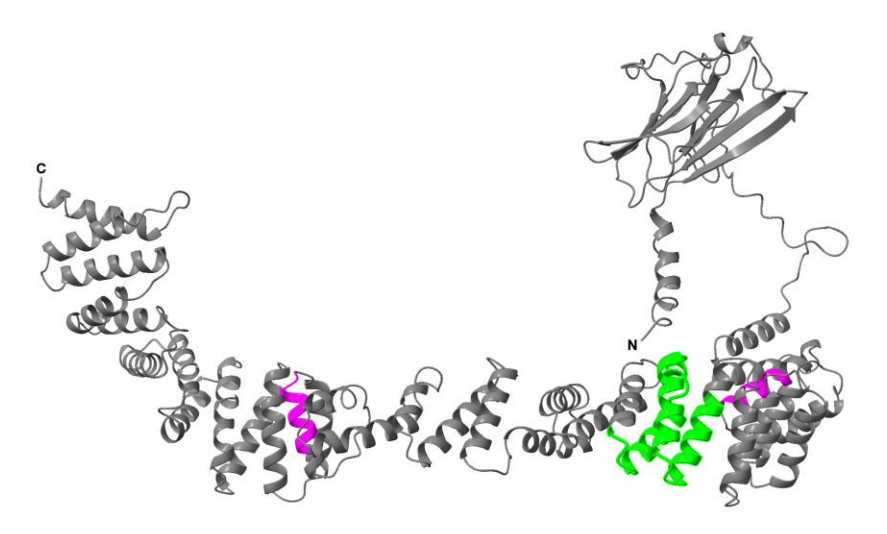
27	urolD E w Kon oo-D	ELCCCATACACTTTCCCATCCTCTTTCTCC
37	ureIP F w Kan-sacB OH	5' GCGATAGAGTTTGGCATGGTGTTTGTG3'
38	ureIP R w Kan-sacB OH	5' AAATTGGAGTGATAATGGTGGCCACGA3'
43	pflA upstream region/forward	5' ATGTTTGTTTATTGGTTCATGTTCG3'
44	pflA upstream region/reverse	5 'GAATTCGATTATCCTCGAGAGCCCATTAAAAGAAAGATTTTTGA3'
45	pflA downstream region/forward	5' GATAATCGAATTCGCTAGCGATCAAACAAACGCATGGCAAAATT3'
46	pflA downstream region/reverse	5' CTGATACGCTTCTAGGGCATTGACT3'
224	pflB upstream region/forward	5' CCTAAAGAAAGCGATGTTATGCAAG3'
225	pflB upstream region/reverse	5' GAATTCGATTATCCTCGAGATGAATTTTGCTCTTCATTCA
226	pflB downstream region/forward	5' GATAATCGAATTCGCTAGCTTAAACCAAGAAGAAAAGGGCGA3'
227	pflB downstream region/reverse	5' CACGCTCTTTTAAAAGGCTCATG3'
266	flgY upstream region/forward	5' TTTCTACAAGCCCTGAAAGAGAAG 3'
267	flgY upstream region/reverse	5' GAATTCGATTATCCTCGAGCAGACCCAATAACAAGATTTTACGC 3'
268	flgY downstream region/forward	5' GATAATCGAATTCGCTAGCAAGATCCTAACACCAAAGAGCCT 3'
269	flgY downstream region/forward	5' CGCTTCTAATCTCTCTAAAACTCGC 3'
216	pflA (for BACTH plasmids)/forward	5'GAGGATCCCCTCACGCTCACGCAAG3'
217	pflA (for BACTH plasmids)/reverse	5'CGGTACCCGTGACTCCTTGTTTTTGAATAAATTCA3'
218	pflB (for BACTH plasmids)/forward	5'GAGGATCCCAAAAAAGAAAATAAACAAACTTCTT3'
219	pflB (for BACTH plasmids)/reverse	5'CGGTACCCGTTCTAAAAACTCGCCCTT3'
222	fliL (for BACTH plasmids)/forward	5'GAGGATCCCAATAAGGAAGAATCTAAAGAAAACG3'
223	fliL (for BACTH plasmids)/reverse	5'CGGTACCCGTTGGATGATAAAATCAGTGAAAAAG3'
303	flgY (for BACTH plasmids)/forward	5'ACTCTAGAGGCGCAAGAATTGTTGCAATG3'
302	flgY (for BACTH plasmids)/reverse	5'CGGTACCCGTACCCCTGCAGGCTCTTTG3'

Table S4.4. Summary of cryo-ET data used in the study

Bacterial strains	wT	∆pfIA	∆pflB	∆flgY
Microscope	300kV Titan/Krios	300kV Titan/Krios	300kV Titan/Krios	300kV Titan/Krios
Magnifications	×42,000	×42,000	×42,000	×42,000
Tilt angles with steps	± 48° with 3° steps			
Total doses	65 e <sup>-</sup>	65 e <sup>-</sup>	65 e <sup>-</sup>	65 e <sup>-</sup>
No. of tomograms	576	196	333	300
No. of motors	1635	708	975	814

# Chapter 4 appendix: pflA repeat units

During construction of  $\Delta fapH$  mutants in Chapter 2, I found that some isolates had variants called by Breseq under Unassigned New Junction Evidence in pflA. Unassigned New Junction Evidence refers to structural variation in the genome that cannot be linked to a known genetic feature and may indicate complex genetic rearrangements. Causes can be insertions deletions, inversions, translocations, complex rearrangements, or sequencing artifacts. Of 8 ΔfapH isolates that were motile and sensitive to bacitracin, 4 had Unassigned New Junction Evidence for pflA (Table A4.1). The frequency that this mutation was called was 49.7% (H180-4), 44.5% (H180-7), 46.2% (H180-10), and 52.1% (H180-12). The frequency of the mutation was difficult to understand because if selection were occurring, we would expect a higher percentage of reads to contain the mutation, yet half of the isolates did not contain this mutation at all, and the other half had frequencies around 50%. We were not sure if this was real or a sequencing artifact. Sequencing artifacts can be caused by low-quality reads or misaligned sequences. The skew, a measure of the imbalance between the forward and reverse read coverage ranges from 0.2 to 0.7 in these strains (Table **A4.1**). Typically, a skew of <0.5 is considered acceptable, but considering the total number of reads is important. PflA is a tetratricopeptide repeat (TRP) domain-containing protein. The TRP motif consists of 3-16 tandem repeats of a degenerated amino acid sequence of 34 amino acid residues (Lamb et al. 1995). The region of the new junction predicted by Breseg resulted in a tandem repeat of a 58 amino acid sequence in the protein and is indicated by green in Fig. A4.1.



**Figure A4.1. PfIA structure as predicted by AlphaFold monomer**. In purple are the locations of the internal primers in **Table A4.2**. In green is the location of the repeat region predicted by Breseq.

We were unsure if this Unassigned New Junction Evidence was calling an insertion, deletion, or rearrangement, so I designed primers that flanked the new junction shown by Breseq (**Table A4.2**). The primers are indicated by the purple regions in **Fig. A4.1**. PCR using the internal pfIA primers of the  $\Delta fapH$  isolates indicated different band sizes in samples that contained the pfIA new junction evidence (**Fig. 4.2**). The band in sample 7 is roughly 200 bp larger than the band in sample 2. We would have expected that the isolates that contained the new junction evidence at ~50% would contain two bands, but surprisingly they only contained the single larger band (**Fig. 4.2**). Oddly, the wild type sample contained two bands, as we would have expected in the isolates that contained the new junction (**Fig. A4.2**).

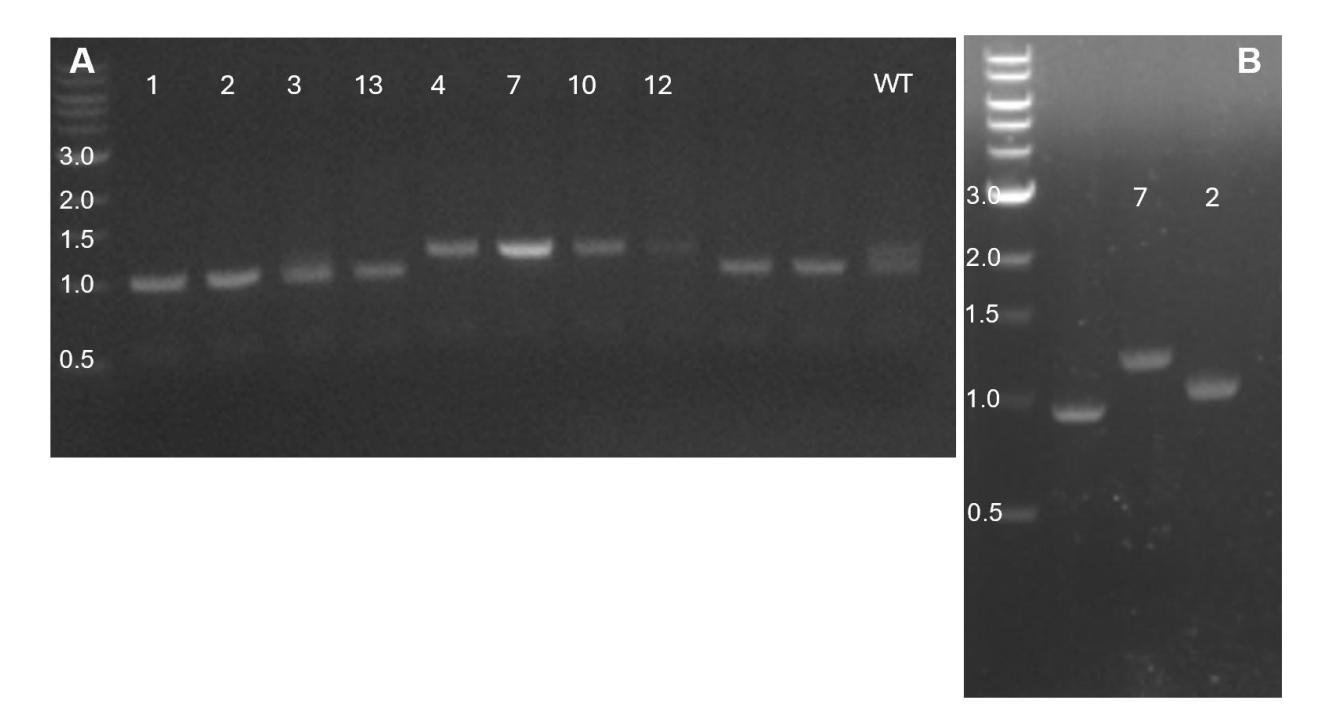


**Figure A4.2. PCR with internal** *pflA* **primers.** WGS from isolates 1, 2, 3, and 13 does not predict a *pflA* unassigned new junction evidence, while WGS from isolates 4, 7, 10, and 12 indicates the new junction evidence. (**A**) PCR using the internal *pflA* primers shows different band sizes between 1, 2, 3, 13 and 4, 7, 10, 12. (**B**) Another gel showing the difference in band sizes between isolates 7 and 2, with the band being larger for sample 7.

The PCR products from samples 7 and 2 were submitted for Eton sequencing and then an alignment was performed between the results of sample 7. The results show a 174 bp

duplication in the H180-7 sample where the text in italics indicates the duplicated bases (**Fig. A4.3**). It seems unlikely that both the WGS and sequencing of the PCR products are providing false data, so it seems the evidence suggests that in some strains PfIA is slightly longer than in the native form. I was able to find examples of this in other strains as well, not just  $\Delta fapH$  isolates. If correct, the PfIA distal spoke would be slightly longer in the strains where the duplication occurs (**Fig. 4.4**). It is not clear if the observed changes in the number of repeating units within the PfIA sequence has any relevance in flagellar motor assembly and/or function. PfIA is an elongated protein that forms the distal spokes that link the spoke-ring structure associated with the MS-ring and the flagellar motor cage (**Fig. 4.4**). The duplication within PfIA that we observed in some of the  $\Delta fapH$  strains is predicted to increase the length of the protein (**Fig. A4.1**), and thereby alter the length of the distal spokes. It is possible that altering the length of the distal spokes is a mechanism that *H. pylori* uses to modulate torque generation or some other motor function.

H180_7 pflA	GAAAACAACAATTACAAACAGGCCATGCGCTATTACAAACGCATTCTTTTAGAATACAAA GAAAACAACAATTACAAACAGGCCATGCGCTATTACAAACGCATTCTTTTTAGAATACAAA	163 900
H180_7 pflA	AATTCCCGCTACGCTCCTTTAGCCCAAATGCGTTTGGCCATTGAAGCGGCTGAAGGCTCT AATTCCCGCTACGCTCCTTTAGCCCAAATGCGTTTGGCCATTGAAGCGGCTGAAGGCTCT	223 960
H180_7 pflA	GATTTGAGCAACGCTAACATGCTTTTTAAAGAAGCTTTTTCTAACGCCAAAGACAAAGAG GATTTGAGCAACGCTAACATGCTTTTTAAAGAAGCTTTTTCTAACGCCAAAGACAAAGAC *********************	283 1020
H180_7 pflA	AGCGCGAGTGAAATCGCGCTTAATTGGGCTGAAGCAGAGATAAACTATCAAAACTTTAAT AGCGCGA <mark>G</mark> TGAAATCGCGCTTAATTGGGCTGAAGCAGAGATAAACTATCAAAACTTTAAT	343 1080
H180_7 pflA	AACGCTAAATACCTCATTGATAAGGTGGTTCAATCCAACCCAGATTATATTTCTACGCAT AACGCTAAATACCTCATTGATAAGGTGGTTCAATCCAACCCAGATTATATTTCTACGCAT	403 1140
H180_7 DflA	AGCGAATCAGCCCTAGACTTGCTCAAGTTATTGAAAAAAAA	463 1200
H180_7 pflA	AGTGAAATCGCGCTTAATTGGGCTGAAGCAGAGATAAACTATCAAAACTTTAATAACGCT ATTGAGATCGCTCACTTGCTCTTTAATCAACATGATGATGATGAAACCTAAAGAGCAAGCG * **** ***** * * * * * * * * * * * * *	523 1260
H180_7 pflA	AAATACCTCATTGATAAGGTGGTTCAATCCAACCCAGATTATATTTCTACGCATAGCGAA CTCTATGATTTAGGGGCCTTCT * * *** ** ** ***	583 1282
H180_7 pflA	TCAGCCCTAGACTTGCTCAAGTTATTGAAAAAAAACCAGATGAATGCAAGCGCGATTGAG	643 1282
H180_7 DflA	ATCGCTCACTTGCTCTTTAATCAAGATGATGACTTGAAAGCTAAAGAGCAAGCGCTCTAT	703 1282
H180_7 RflA	GATTTAGGGGGCGTTGTATGCAAGGATCAAGGACTTTAAGAACGCCCACCTTTACAACCTATGCAAGGATCAAGGACTTTAAGAACGCCCACCTTTACAACCT	763 1325
H180_7 pflA	GCAATATTTGCAAGATCATGCGGAATTGGGATAAAGTCTCTGTCGTTAGAATGCGCGATG GCAATATTTGCAAGATCATGCGGAATT-GGATAAAGTCTCTGTCGTTAGAATGCGCGATG	823 1384
H180_7 pflA	AAAAAGCCCTTTTTTCCATGGAGGGGAACACGCAAGAAAAATCGCCCACTAAAAAAGCCCTTTTTTCCATGGAGGGGAACACGCAAGAAAAAATCGCCCACTATGACAAAA	875 1444
H180_7 pflA	TCATTCAAAATTTCCCTAATTCTAATGAAGCCCTAAAGGCTTTAGAATTGAAAGCCCAAC	875 1504
H180_7	TCTTGTTTGAAAATAAGCGTTACGCTGAAGTGTTAGGCATGCAAAAAAATTTTGCCTAAAG	875 1564

Figure A4.3. Alignment of the pflA in H180-7 and the native pflA. An alignment was performed sequencing with the results the of the PCR products (https://www.ebi.ac.uk/jdispatcher/). Nucleotides in red, boldface, and underlined indicate where the new junction was indicated from the gDNA sequencing results. Sequences in red (not boldface or underlined) indicate the 10-bp inverted repeats in the wild-type sequence. Sequence in italics indicates a 174-bp duplication in H180\_7 sequence. Sequence in green indicates sequence alignment between pflA and H180\_7 that Clustal Omega should have aligned instead of trying to align the duplicated region

Table A4.1. *pflA* unassigned new junction evidence frequency

Strain	Reads	Frequency	Skew
H180-4	182	49.7%	0.2
H180-7	226	44.5%	0.6
H180-10	181	46.2%	0.4
H180-12	139	52.1%	0.7

Table A4.2. pflA internal primers

Primer 304: pflA F	5' TTTATTAGAAATTATCGCATTAGG 3'
Primer 305: pflA R	5' ATGCGAAATACAAGCAATCA 3'

# Chapter 5: *Helicobacter pylori* HP0018 has a Potential Role in Maintenance of the Cell Envelope

3

Rosinke K, Starai VJ, Hoover TR. *Helicobacter pylori* HP0018 Has a Potential Role in the Maintenance of the Cell Envelope. Cells. 2024 Aug 27;13(17):1438. doi: 10.3390/cells13171438. PMID: 39273010; PMCID: PMC11394524.

K.R. contributed to this chapter in mutant construction and characterization, TEM, SEM, fluoresnce microscopy, co-IP assays, writing, and editing.

<sup>&</sup>lt;sup>3</sup> Reprinted here with permission of publisher.

# **ABSTRACT**

Helicobacter pylori is a bacterial pathogen that colonizes the human stomach where it can cause a variety of diseases. H. pylori uses a cluster of sheathed flagella for motility, which is required for host colonization in animal models. The flagellar sheath is continuous with the outer membrane and is found in most Helicobacter species identified to date. HP0018 is a predicted lipoprotein of unknown function that is conserved in Helicobacter species that have flagellar sheaths but is absent in Helicobacter species that have sheath-less flagella. Deletion of hp0018 in H. pylori B128 resulted in formation of long chains of outer membrane vesicles, which were most evident in an aflagellated variant of the Δhp0018 mutant that had a frameshift mutation in fliP. Flagellated cells of the  $\Delta hp0018$  mutant possessed what appear to be a normal flagellar sheath, suggesting that HP0018 is not required for sheath formation. Cells of the  $\Delta hp0018$  mutant were also less helical in shape compared to wild-type cells. A HP0018-super folder green fluorescent fusion protein expressed in the *H. pylori* Δhp0018 mutant formed fluorescent foci at the cell poles and lateral sites. Co-immunoprecipitation assays with HP0018 identified two enzymes involved in modification of cell wall peptidoglycan, AmiA and MltD, as potential HP0018 interaction partners. HP0018 may modulate the activity of AmiA or MltD, and in the absence of HP0018 the unregulated activity of these enzymes may alter the peptidoglycan layer in a manner that results in altered cell shape and hypervesiculation.

### INTRODUCTION

Helicobacter pylori is a Gram-negative bacterium (i.e., diderm) that belongs to the phylum Campylobacterota. H. pylori colonizes the human stomach where it can cause peptic ulcer disease and chronic gastritis (Cover and Blaser 1992, Blaser et al 1993, Kuipers et al. 1997). In addition, H. pylori is a major risk factor for gastric cancer and mucosa-associated lymphoid tissue lymphoma (Moss et al. 2017) Several virulence factors have been identified in H. pylori, many of which are lipoproteins that have roles in adhesion (O'Toole et al. 1995, Odenbreit et al. 1999), virulence (Fischer 2011, McClain et al. 2020), and cell migration in gastric cancer cells (Vallese et al. 2017).

As with other diderms, *H. pylori* release outer membrane vesicles (OMVs), which are nanoparticles derived from the outer membrane that range in size from 20 to 300 nm and are part of normal bacterial growth both in vitro and in vivo (*Sartorio et al. 2021*). The composition of OMVs has been described in several bacterial species, and includes phospholipids, lipopolysaccharide, outer membrane proteins, periplasmic proteins, and peptidoglycan, as well

as cytoplasmic components, including DNA and RNA (*Sidhu et al. 2008, Kaparakis et al. 2010, Olofsson et al. 2010, Lappann et al. 2013, Aguilera et al. 2014, Roier et al. 2016, Zavan et al. 2019*). OMVs have reported roles in a broad range of physiological processes, including cell-to-cell communication, nutrient acquisition, quorum sensing, horizontal gene transfer, interbacterial killing, toxin delivery, and stress response (*Sartorio et al. 2021*).

H. pylori uses a cluster of polar flagella for motility, which is required for colonization in model animal systems (*Eaton et al. 1992, Ottemann and Lowenthal 2002*). The *H. pylori* flagellum is encased in a membranous sheath that is contiguous with the outer membrane, a feature that is shared with many other *Helicobacter* species (*Chu et al. 2020*). In a previous study, we identified a number of protein homologs that are prevalent in *Helicobacter* species that have flagellar sheaths (FS<sup>+</sup> species) but are absent or underrepresented in *Helicobacter* species that lack flagellar sheaths (FS<sup>-</sup> species) (*Gibson et al. 2022*). One of the proteins found in FS+ *Helicobacter* species but absent in FS<sup>-</sup> *Helicobacter* species is HP0018, a predicted lipoprotein of unknown function. *Campylobacter jejuni Cj0089* is a predicted lipoprotein of unknown function and a homolog of HP0018. The two proteins share 27% amino acid identity over 82% of their lengths, and both proteins contain a tetratricopeptide repeat (TPR) motif. TRP-containing proteins participate in a variety of cellular processes, including cell cycle control, transcriptional regulation, mitosis, protein transport, protein folding, and regulation of steroid receptor function (*Blatch and Lassie 1999, D'Andrea and Regan 2003*).

To determine if HP0018 had a role in flagellar sheath formation, we deleted the hp0018 homolog in H. pylori B128 and characterized the phenotype of the resulting mutant. The original  $\Delta hp0018$  mutant was aflagellated due to a single nucleotide deletion in homopolymeric tract of cytidines in fliP, which encodes a component of the flagellar type III secretion system that transports axial components of the flagellum (e.g., rod, hook, and filament proteins) across the cell membrane (Fan et al. 1997). The aflagellated  $\Delta hp0018$  mutant produced large amounts OMVs (i.e., hypervesiculated) that tended to form long chains at the cell pole. Flagellated  $\Delta hp0018$  cells in which fliP had reverted to the 'on' phase appeared to have a normal flagellar sheath, suggesting that HP0018 is not required for sheath formation. In addition to being hypervesiculated, cells of the  $\Delta hp0018$  mutant were less helical in shape compared to wild-type cells. Co-immunoprecipitation assays identified the peptidoglycan hydrolases MltD and AmiA as potential HP0018 interaction partners. We hypothesize that HP0018 regulates the activity of MltD or AmiA, and the unregulated activity of these enzymes in the absence of HP0018 affects the structure of the cell envelope.

# **RESULTS**

#### Deletion of hp0018 In H. pylori B128 Results in a Hypervesiculation Phenotype

HP0018 is a predicted lipoprotein of unknown function that is prevalent in FS<sup>+</sup> *Helicobacter* species but is absent or underrepresented in FS<sup>-</sup> *Helicobacter* species (*Gibson et al. 2022*). The HP0018 prolipoprotein is 469 amino acids in length and is encoded in an operon by itself (*Sharma et al. 2010*). *hp0018* homologs are widespread among *H. pylori* strains as a blastp search of the Joint Genome Institute's Integrated Microbial Genomes & Microbiomes database (https://img.jgi.doe.gov/) using the Homolog Display feature of the website identified *hp0018* homologs with high confidence (bit scores >824, E-values = 0.0, homology across the full-length of the protein) in 766 *H. pylori* genome sequences. Little is known about flagellar sheath biogenesis, and given that as a lipoprotein HP0018 likely localizes to the periplasm, it was a good candidate for having a role in sheath formation. To investigate the function of HP0018, we introduced an unmarked deletion of the *hp0018* homolog in *H. pylori* B128 (CV725\_07715) and characterized the resulting mutant (designated as strain H19).

Motility of strain H19 was assessed by inoculating it into soft agar medium and allowing the cells to swim from the point of inoculation and multiple to produce a zone of growth or swim halo. Strain H19 produced no swim halo or a very small swim halo compared to wild type when inoculated into soft agar medium. Cell morphologies of H19 and wild-type H. pylori B128 were examined by TEM and SEM using cells from cultures grown in liquid medium to mid-logarithmic phase. Most of the H19 cells were aflagellated (Figs. 5.1B and 5.1E), although flagellated cells were occasionally seen. The H19 cells produced abundant amounts of OMVs (Fig. 5.1B). Examining over 200 H19 cells from three biological replicates by TEM, ~90% of the cells had OMVs associated with the cell surface. In contrast, < 10% of the wild-type cells examined by TEM (n >200; three biological replicates) had OMVs associated with the cell surface (Fig. 5.1A). Interestingly, the H19 cells frequently produced chains of OMVs that tended to localize near the cell pole (**Figs. 5.1B, 5.1G, and 5.1H**). The OMV chains were unique to the  $\Delta hp0018$  mutant as we did not observe any such structures associated with wild-type cells. Detached chains of OMVs were often observed by TEM and SEM (Figs. 5.1E and 5.1I), suggesting that the OMV chains were sheared readily from the cells as they were prepared for electron microscopy. The formation of OMVs is part of bacterial growth, and previous studies revealed that OMV formation in H. pylori increases as cultures enter stationary phase (Olofsson et al. 2010, Zavan et al. 2019). Thus, the large amounts of OMVs produced by the H19 cells in logarithmic growth phase compared to wild-type cells was notable. Moreover, the chains of OMVs formed by the H19 cells seems to be

a unique phenotype as we are unaware of previous reports describing such morphological features in *H. pylori*. Another morphological distinction of the H19 cells was they were less helical than wild-type cells, which was most evident in the SEM images (**Figs. 5.1D and 5.1E**).

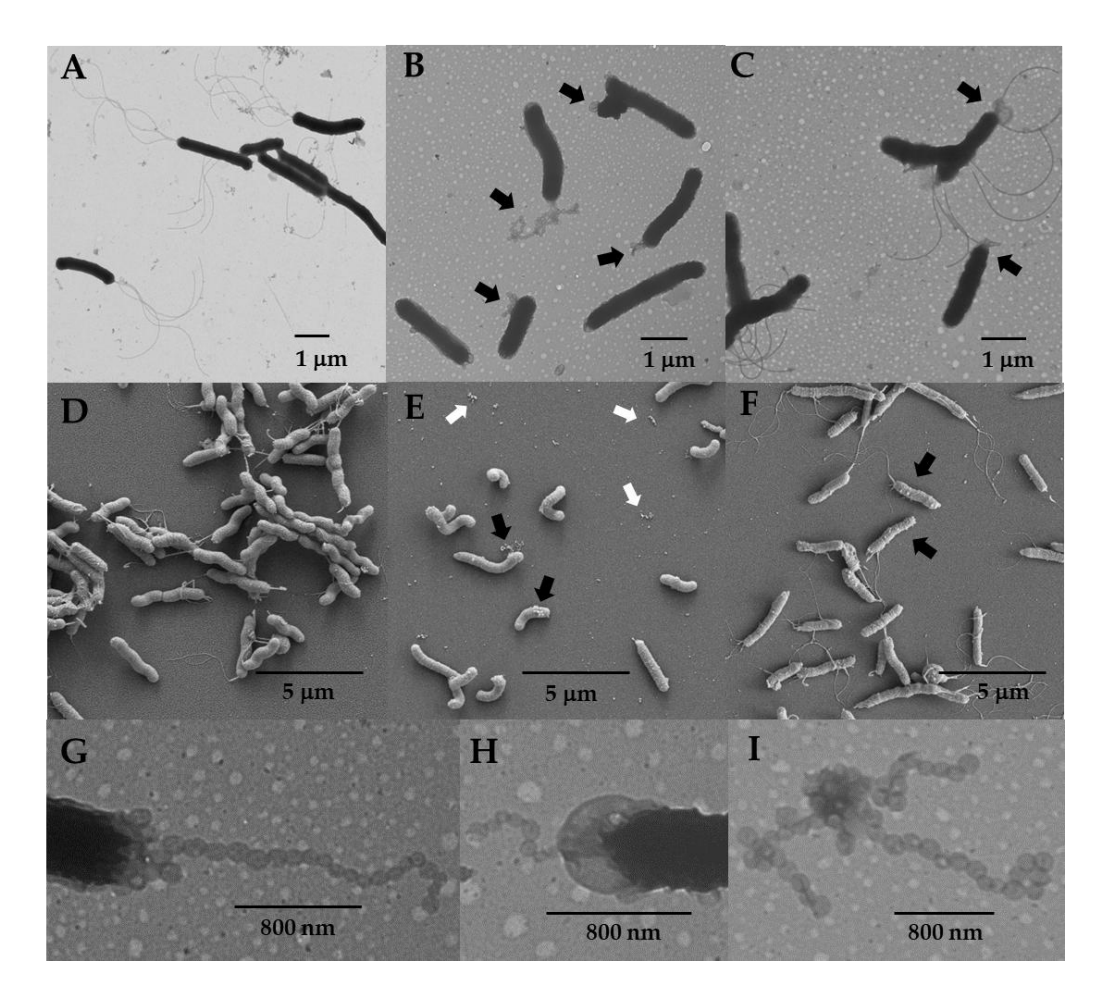


**Figure 5.1. TEM and SEM images of wild-type** *H. pylori* B128, the non-motile Δhp0018 mutant (H19), and the motile Δhp0018 isolate (H23). (A and D) TEM and SEM images, respectively, of wild-type *H. pylori* B128 cells. Note that the cells in the panel are flagellated. (**B** and **E**) TEM and SEM images, respectively, of H19. Note the chains of OMVs near the cell poles for many of the cells, which are indicated by the black arrows. Material that we infer to be free OMVs are indicated by the white arrows in panel E. (**C and F**) TEM and SEM images, respectively, of strain H23. Note the majority of the cells are flagellated and some of the cells appear to have OMVs on the cell surface (black arrows). (**G-I**) Close up TEM images of chains of OMVs attached to cells (panels **G and H**) or detached from cells (panel I). Images shown in panels G-I are of strain H19. Magnification for the SEM images was 15,000 x.

#### HP0018 is Not Required for Motility in Soft Agar Medium but Enhances Motility

To examine the basis of the motility defect of strain H19, motile variants of H19 were isolated by inoculating the strain into soft agar medium and incubating for 7 d to allow small swim halos to develop. Cells from the edge of the swim halo were used to inoculate fresh soft agar medium, which resulted in a larger swim halo. The process was repeated two more times, after which clonal isolates were obtained by streaking cells from the edge of the swim halo on TSA-HS medium. One of the motile isolates (designated as strain H23) was analyzed further. Strain H23 produced swim halos that were significantly larger than those formed by the parental H19 strain, but smaller than those generated by wild type (Fig. 5.2). Introducing a copy of hp0018 fused to a sequence encoding the c-myc epitope into strain H23 on the shuttle vector pHel3 (plasmid bearing the hp0018-myc fusion was designated as pKR66) restored motility of the strain in soft agar to the wild-type level (Fig. 5.2). Swim halo formation results from cells migrating from the point of inoculation in soft agar medium, which involves both swimming and chemotaxis. It is unclear if the smaller swim halos generated by strain H23 is due to an impairment in swimming or chemotaxis. Cells of strain H23 bearing plasmid pKR66 did not form the large amounts of OMVs when grown to mid-logarithmic phase that was observed with the original strain H23 (Fig. S5.1). Taken together, these results demonstrated that the HP0018-myc fusion suppressed the both the motility defect in soft agar medium and hypervesiculation phenotype of the  $\Delta hp0018$  mutant.

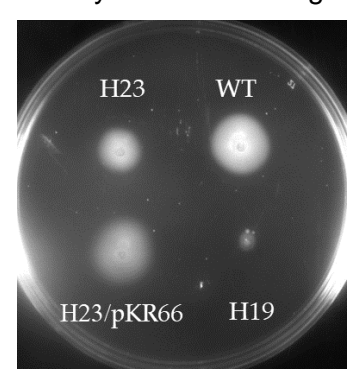


Figure 5.2. Motility of *H. pylori* strains in soft agar medium. *H. pylori* strains were stab inoculated into soft agar medium and incubated under microaerobic conditions for 7 d. Strains shown on the plate are wild-type *H. pylori* B128 (WT), H19 (non-motile  $\Delta hp0018$  mutant), H23 (motile  $\Delta hp0018$  isolate), and H23 carrying a derivative of plasmid pHel3 bearing a copy of  $\Delta hp0018$  (H23/pKR66).

As expected, cells of the H23 cells were well flagellated (**Figs. 5.1C and 5.1F**). Similar to H19, the H23 cells were less helical than the wild-type cells (**Figs 5.1D and 5.1F**). Flagella of the

H23 cells, as well as the occasional flagellated H19 cells, were sheathed and many had the characteristic bulb-like structure at their ends (**Fig. 5.3**), indicating that HP0018 is not required for sheath formation. H23 cells typically had OMVs on the cell surface (**Fig. 5.1C**), but the chains of OMVs were observed less frequently on H23 cells than they were for H19 cells. Similarly, the occasional flagellated H19 cell generally lacked the chains of OMVs (**Fig. 5.3A**). Taken together, these observations suggest the OMV chains failed to form or were not stably associated with the cell when flagella were present.

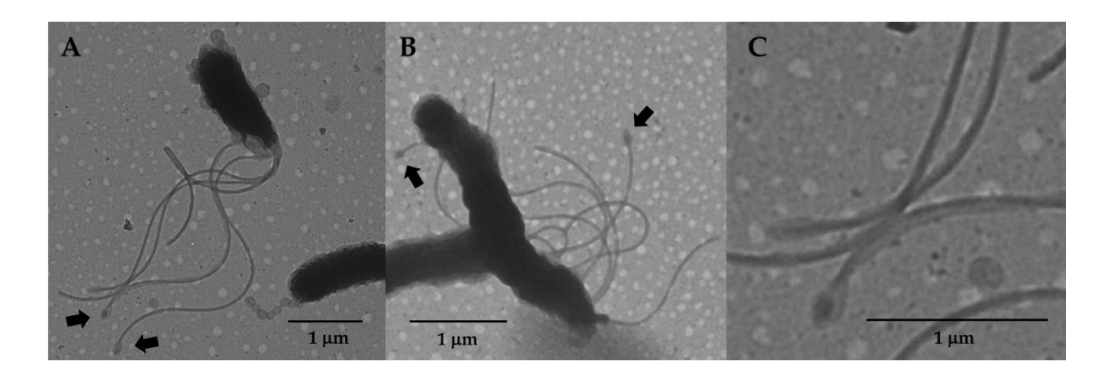


Figure 5.3. Flagella of strains H19 and H23. (A) TEM of a flagellated cell and an aflagelleted cell of strain H19. Note that the flagellated cell has several OMVs on the cell surface, but lacks the chain of OMVs at the cell pole, while the aflagellated cell has a chain of OMVs at the cell pole. (B) TEM of cells of strain H23. In both strains, note that some of the flagella had the characteristic bulb at the end of the filament (indicated by arrows). (C) Close up image of flagella shown in panel A where the bulb-like structures are clearly seen.

Whole genome sequencing of H19 was done to identify a mutation that might account for the aflagellation of the strain. Comparing the genome sequence of H19 with that of the parental, wild-type *H. pylori* B128 strain revealed several single nucleotide polymorphisms (SNPs) and indels (**Table S5.2**). Two of the mutations were in known flagellar genes, motA (encodes a motor stator protein) and *fliP* (encodes a component of the flagellar protein export apparatus). The SNP in motA was a missense mutation that changed Gly-201 to Asp and was present in 98.5% of the reads for that region of the genome. The mutation in *fliP* was a deletion of nucleotide 261, which is within a homopolymeric tract of eight cytidines. The deletion in the poly(C)-tract was present in about 90% of the reads for that region of the genome. Slipped-strand mispairing-mediated mutagenesis within the same poly(C)-tract in *fliP* was reported previously for *H. pylori* 26695, and was proposed as a mechanism for switching between "on" and "off" phases for flagellation and motility (*Josenhans et al. 2000*). It is not known if the phase variation of *fliP* is regulated and it

may be stochastic. Since *H. pylori* motility is required for colonization in animal models (*Eaton et al. 1992, Ottemann and Lowenthal 2002*), there must be a strong selective pressure for the motile phenotype in vivo. Conversely, it may be that following adherence to the gastric epithelium the energy-saving loss of motility is advantageous for the bacterium.

Whole genome sequencing of H23 revealed that the deletion in the poly(C)-tract in *fliP* present in the parental H19 strain had reverted to the 'on' phase. The mutant motA allele identified in H19 was retained in H23, indicating that the MotAG201D variant supported torque generation by the stator unit. Taken together, these observations indicate that mutation in *fliP* was responsible for the aflagellated phenotype of H19. Moreover, these observations indicate that HP0018 is not required for flagellum assembly or motility.

An indel was noted in a third potential flagellar gene, CV725\_07605 (HP0036 homolog), which encodes a predicted PfIC homolog. The indel, a two-nucleotide deletion in a poly(T)-tract that introduced a frameshift mutation at codon 13, was present in both H19 and H23 (**Table S5.2**). PfIC is predicted to form a motor accessory known as the medial disk in the *C. jejuni* flagellar motor (*Drobnič et al. 2023*), but this structure has not been identified in the *H. pylori* motor. If HP0036 does form a motor accessory in *H. pylori*, the frameshift mutation in the hp0036 homolog in H23 suggests that the accessory is not required for motor function.

#### **OMV Proteomes of Strain H19 and H23**

OMVs from H19 and H23 were isolated and compared with those prepared from wild-type *H. pylori* B128. OMVs were prepared by resuspending *H. pylori* cells in buffer, vortexing the cell suspensions to shear the OMVs from the cells, pelleting the cells by centrifugation, and removing any remaining cells by passing the supernatant liquids through a 0.45 µm filter. OMVs from the three *H. pylori* strains were initially examined by TEM (**Fig. 5.4**). Consistent with the prevalence of OMVs on the cells of H19 and H23, these strains yielded denser concentrations of OMVs compared to wild type. In addition to the clusters of OMVs, tubular structures were observed in the samples prepared from H19 and H23 (**Figs. 5.4B and 5.4C**). The tubular structures are not flagellar sheath fragments since most of the H19 cells were aflagellated. Moreover, the tubular structures were not observed in the OMV sample prepared from wild type.

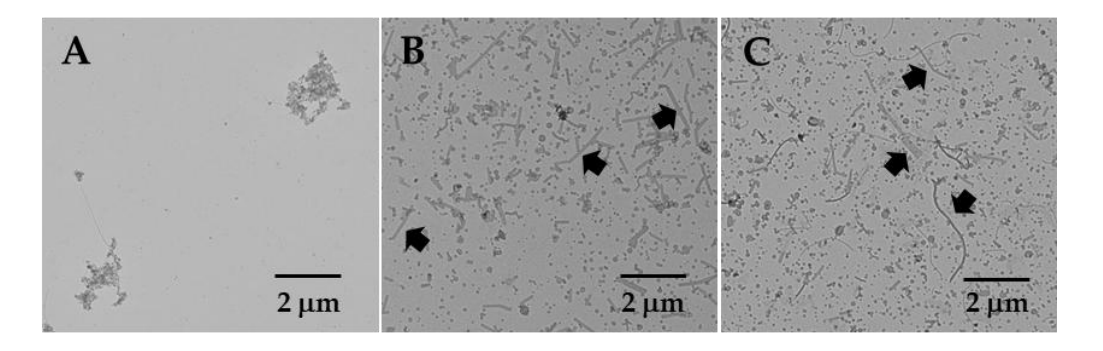


**Figure 5.4. TEM images of OMVs isolated from wild type, H19, and H23**. (**A**) OMV preparation from wild-type *H. pylori* B128. (**B**) OMV preparation from strain H19. (**C**) OMV preparation from strain H23. OMV preparations from H19 and H23 displayed tubular structures (indicated by arrows).

Proteomes of the OMVs prepared from wild-type H. pylori B128, H19, and H23 were analyzed by mass spectroscopy. Each protein identified from the proteomic analysis was assigned a score calculated by the Mascot software package from the combined scores of all mass spectra that matched the amino acid sequence of the protein. While Mascot scores are not quantitative, scores generally correlate with the relative abundance of specific proteins. A total of 226 proteins were identified in the three samples. A complete list of identified proteins in the OMV samples is found in **Table S5.3**. A majority of the proteins identified in the OMV samples (~56%) were outer membrane proteins, predicted lipoproteins, periplasmic proteins, or flagellar proteins (**Table S5.3**). As expected, HP0018 was detected in the OMV sample from wild-type *H. pylori* B128 but not in the OMV samples of the two *Ahp0018* strains. The protein content of the OMVs compared favorably with the proteomes of OMVs reported for two other *H. pylori* strains. Olofsson and co-workers identified 315 proteins in OMVs isolated from H. pylori CCUG17875 (Olofsson et al. 2010), while Zaran and co-workers identified 171 proteins that were significantly enriched in OMVs compared to the parental cell in H. pylori 26695 (Zavan et al. 2019). Eighty-four percent of the proteins that we identified in the H. pylori OMVs had been identified in one or both of the previous studies (Table S5.3).

With the exception of the absence of several flagellar proteins in the OMVs of H19, there were few qualitative differences observed in the protein content of the OMVs isolated from the three strains. Consistent with *fliP* being in the 'off' phase in H19, several flagellar proteins transported across the cell membrane by the flagellar type III secretion system were not detected in the OMVs of this strain. These proteins included FlaB (minor flagellin), FliD (filament cap protein), FlgE (hook protein), FlgL (hook-associated protein), FlgK (hook-associated protein), a

FIgE homolog (HP0908), FIgD (hook cap protein), and FliK (hook length control protein) (**Table S5.3**). The major flagellin of the *H. pylori* flagellum, FlaA, was present in the OMVs of H19, although the Mascot score for FlaA in the sample was substantially lower than that of the other two samples (**Table S5.3**). The presence of FlaA in the OMVs of H19 was likely due to the small proportion of cells in the population where *fliP* was switch to the "on" phase and allowed for flagellum assembly.

A couple of proteins with moderately high Mascot scores (>200) were identified in the OMVs of the two Δhp0018 strains that were not detected in the wild-type OMVs (**Table S5.3**). One of these proteins was ComH (HP1527; accession number: QDY55614.1), a periplasmic protein that is required for natural transformation of *H. pylori* (*Smeets et al. 2000*). The other protein was a DUF1104 domain-containing protein (accession number: QDY56572.1) that corresponds to two open reading frames in *H. pylori* 26695 (HP0719 and HP0720). Both of these proteins were previously identified as being enriched in *H. pylori* 26695 OMVs (*Zavan et al. 2019*), and so it seems unlikely that they have a role in the formation of the OMV chains since the researchers of this previous study did not report on observing OMV chains. Two outer membrane proteins with moderately high Mascot scores (>330) were identified in the OMVs of H23 that were not detected in the OMVs of the other two strains. One of these proteins was FaaA (HP0609/HP0610), which is a VacA-like autotransporter that localizes to the flagellar sheath (*Radin et al. 2013*). The other protein was HofB (HP1083), which is a predicted beta-barrel outer membrane protein. Taken together, there does not appear to be any proteins present in the OMVs of H19 or H23 that might account for the unusual tubular structures observed in **Fig. 5.4**.

#### **HP0018 Localizes to Specific Sites Within the Cell Envelope**

The localization of HP0018 in *H. pylori* was examined by fusing a superfolder green fluorescent protein (sfGFP) to the C-terminus of HP0018 and expressing the fusion protein in H23. Imaging the *H. pylori* cells expressing the HP0018-sfGFP by fluorescence microscopy revealed a strong tendency of the fusion protein to form fluorescent foci at the cell pole and lateral sites (**Figs. 5.5C – 5.5E**). About 33% of the cells had fluorescent foci only at the cell pole, while ~43% of the cells had fluorescent foci only at lateral sites (i.e., non-polar sites) and ~24% of the cells had fluorescent foci at both the cell pole and lateral sites.

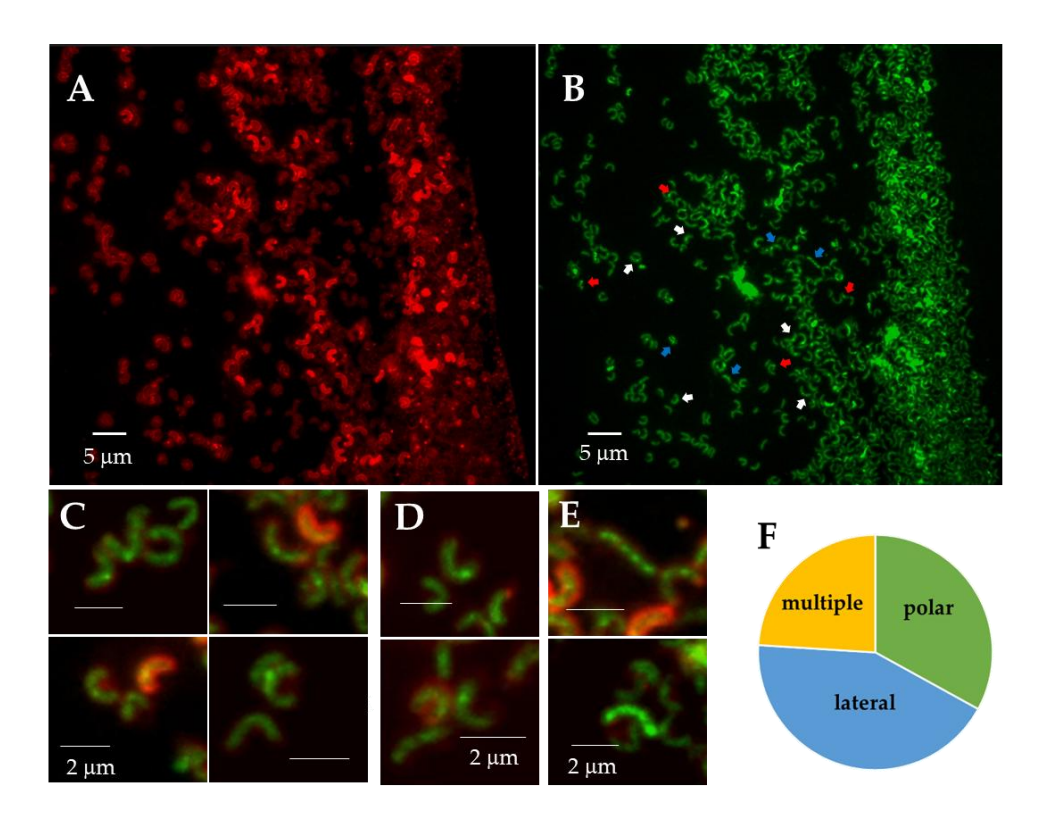


**Figure 5.5.** Localization of a HP0018-sfGFP fusion protein in *H. pylori* by fluorescent microscopy. (**A**, **B**) identical X, Y-planes, slightly different Z-plane of a section of a slide with HP0018-sfGFP. (**A**) Red channel showing membrane staining with FM4-64, (**B**) green channel showing localization of HP0018-sfGFP. White arrows indicate lateral localization of HP0018-sfGFP, red arrows polar, and blue arrows multiple foci. (**C**, **D**, and **E**) Merged channels of red (FM4-64) and green (HP0018-sfGFP) showing (**C**) lateral, (**D**) polar, (**E**) multiple foci. For panels **C-E**, all of the scale bars correspond to 2 μm. (**F**) The frequency of fluorescent foci at the cell pole (polar) and lateral sites was determined, as well as the frequency of cells with four or more fluorescent foci (multiple) (n=133).

#### **Identification of Potential HP0018 Interaction Partners**

To investigate the possible physiological role of HP0018, we attempted to identify HP0018 interaction partners in a co-immunoprecipitation (co-IP) assay using the HP0018-myc fusion protein. The HP0018-myc fusion protein was immunoprecipitated from cell extracts using antibodies directed against the C-myc epitope, and proteins pulled down with the HP0018-myc fusion protein were identified by mass spectroscopy. **Table 5.1** lists the proteins identified from the co-IP assay from one biological replicate, minus ribosomal proteins and ribosomal-associated proteins (e.g., elongation factor-Tu). As a negative control, co-IP assays were done with three

biological replicates of cell extracts prepared from wild-type *H. pylori* B128. For each protein listed in **Table 5.1**, the highest Mascot score from the three replicates of the negative control is indicated.

Table 5.1. Proteins identified from co-IP assay with HP0018-myc-tagged protein.

		HP0018-myc	sample	WT (neg	_
Accession	Description	¹Mascot score	<sup>2</sup> peptid	<sup>1</sup> Mascot	<sup>2</sup> peptid
	-		es	score	es
QDY56472.1	IMP dehydrogenase GuaB, HP0829	1644	25	1659	25
QDY56231.1	RNA helicase RhpA, HP0247	1504	23	316	10
QDY55932.1	hypothetical protein, HP1124	923	17	118	3
QDY56010.1	mechanosensitive ion channel family protein, HP0415	823	19	316	9
QDY56228.1	two-component sensor histidine kinase FlgS, HP0244	748	16	74	1
QDY56734.1	sel1 repeat family protein, HP0519	703	11	561	14
QDY56639.1	outer inflammatory protein OipA, HP0638	475	7	117	6
QDY56525.1	N-acetylmuramoyl-L-alanine amidase AmiA, HP0772	461	13	70	2
QDY56975.1	pyridoxine 5'-phosphate synthase PdxJ, HP1582	437	9	201	5
QDY56071.1	urease subunit alpha UreA, HP0073	416	8	510	9
QDY56955.1	HP0018	372	8	nd	nd
QDY56262.1	mechanosensitive ion channel family protein, HP0284	356	7	104	3
	undecaprenyldiphospho-muramoylpentapeptide	!			
QDY55904.1	beta-N-acetylglucosaminyltransferase MurG, HP1155	288	5	nd	nd
QDY56151.1	Sel1-like repeat protein HcpD, HP0160	252	9	509	9
QDY56984.1	lytic transglycosylase MltD, HP1572	218	7	nd	nd
QDY56970.1	DUF3944 domain-containing protein, HP1588	216	5	527	11
QDY56963.1	molecular chaperone GroEL, HP0010	174	8	1487	31
QDY56571.1	DUF1104 domain-containing protein, HP0721	169	2	116	1
QDY55828.1	hypothetical protein, HP1235	169	5	nd	nd
QDY56232.1	hypothetical protein, HP0248	130	3	525	13
QDY55919.1	chromosome partitioning protein ParB, HP1138	121	4	264	9
QDY56153.1	porphobilinogen synthase HemB, HP0163	117	4	70	2
QDY55781.1	glycosyltransferase family protein, HP1284	102	5	nd	nd

<sup>1</sup>Indicate Mascot scores for proteins that were identified in the co-IP samples prepared with cell extracts from strain H23 expressing the HP0018-myc-tagged protein or wild-type *H. pylori* B128 (WT). Proteins discussed in the text are highlighted in boldface. 2Indicate the number of peptide fragments generated following trypsin digestion that were identified for each protein. nd – not detected.

HP0018 was pulled down specifically in the co-IP assay as it was detected in the cell extract containing the HP0018-myc fusion protein but not in any of the negative control replicates (**Table 5.1**). Four other proteins were detected in the co-IP assay with the sample containing the HP0018-myc fusion protein but not in the negative control replicates, suggesting that these proteins were also pulled down specifically. Two of these proteins, MurG and HP1294, are cytoplasmic proteins and are not likely to interact with HP0018 *in vivo*. The other two proteins, HP1235 and MltD (HP1572), are an integral membrane protein and periplasmic protein, respectively, and are therefore in locations in the cell where they could interact with HP0018 localized in the periplasm. HP1235 is a conserved protein of unknown function that belongs to the dolichyl-phosphatemannose protein mannosyltransferase family (pfam13231). MltD is a lytic transglycosylase that is involved primarily in rearrangement of the peptidoglycan layer (*Chaput et al. 2007*).

Two other proteins, FlgS (HP0224) and AmiA (HP0772), were identified as potential HP0018 interaction partners as they were underrepresented in the negative control replicates compared to the sample containing the HP0018-myc fusion protein (Table 5.1). Both of these proteins were detected in only one of the negative control replicates, and the Mascot scores for these proteins in the negative control were low. FlgS is a histidine kinase of a two-component system that is required for transcription of the RpoN-dependent flagellar genes (Beier and Frank 2000, Niehus et al. 20024). FlgS is a cytoplasmic protein, and so it is unlikely that it interacts with HP0018 in vivo. AmiA is a peptidoglycan hydrolase that is required for the morphological transition of H. pylori cells from spiral to coccoid form (Chaput etl a. 2006). Since AmiA is a periplasmic enzyme, it is in a location in the cell where it could interact with HP0018. Although Chaput and co-workers annotated HP0772 as AmiA (Chaput et al. 2006), the protein is more similar structurally to AmiB and AmiC, two other N-acetylmuramoyl-L-alanine amidases in E. coli. Specifically, E. coli AmiC has an N-terminal, peptidoglycan-binding domain known as an AMIN domain, which consists of a  $\beta$ -sandwich of two symmetrical four-stranded  $\beta$ -sheets (*Rocaboy et al. 2013*). Tertiary structures of E. coli AmiB and HP0772 predicted by AlphaFold indicate both proteins have putative AMIN domains at their N-termini, whereas E. coli AmiA lacks this domain. We will continue to refer to HP0772 as AmiA though to avoid confusion.

Interactions of HP0018 with AmiA and MltD were modeled using AlphaFold2 multimer to obtain supporting evidence for interactions between these proteins. Twenty-five models were examined for each protein pair. In addition to the full-length AmiA, interactions of HP0018 with only the catalytic domain of AmiA were modeled. The energetic likelihood of predicted interactions for each model was evaluated using PISA. Models for interactions between HP0018 and AmiA or MltD predicted by PISA to be the most energetically favorable are presented in **Fig. 5.6**. In the

modeled interactions between HP0018 and the AmiA catalytic domain (**Fig. 5.6A**), PISA values for the interface area,  $\Delta^i G$ , and  $\Delta^i G$  P-value were 1374.8  $\mathring{A}^2$ , -19.4 kcal/mol, and 0.034, respectively. The HP0018-AmiA interface also included 6 hydrogen bonds and 1 salt bridge. In the modeled interactions between HP0018 and MltD (**Fig. 5.6B**), PISA values for the interface area,  $\Delta^i G$ , and  $\Delta^i G$  P-value were 6238.6  $\mathring{A}^2$ , -49.6 kcal/mol, and 0.301, respectively. The HP0018-MltD interface also included 94 hydrogen bonds and 11 salt bridges. Both of the modeled interfaces are predicted by PISA to be energetically favorable, indicating the feasibility of the interactions of HP0018 with AmiA and MltD that were predicted from the co-IP assays.

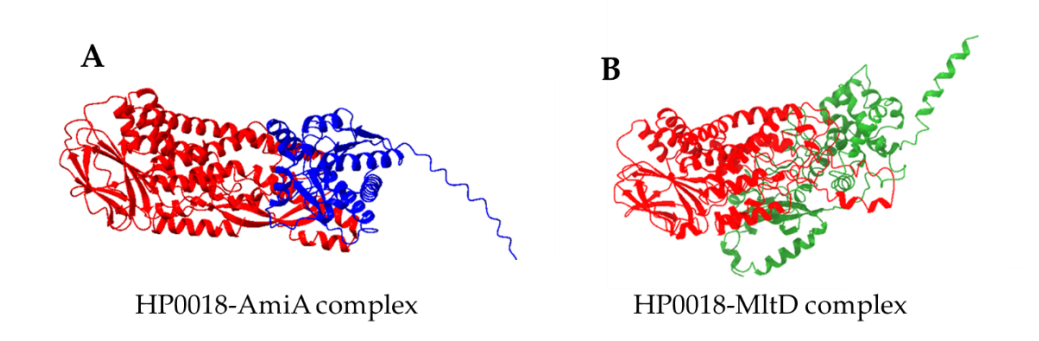


Figure 5.6. AlphaFold2 predictions of protein-protein interactions between HP0018 and AmiA or MItD. (A) Most energetically favorable model for interactions between HP0018 (shown in red) and the catalytic domain of AmiA (shown in blue). (B) Most energetically favorable model for interactions between HP0018 (shown in red) and MItD (shown in green).

# **DISCUSSION**

Flagellar sheath biogenesis in bacteria is a poorly understood process. HP0018 was identified previously as a protein that is present in FS<sup>+</sup> *Helicobacter* species but is absent in FS-*Helicobacter* species (*Gibson et al. 2022*), and we reasoned it may have a role in sheath formation. To address this hypothesis, we deleted *hp0018* in *H. pylori* B128 and characterized the phenotype of the resulting mutant. Although loss of HP0018 in *H. pylori* B128 did not appear to impact sheath formation (**Fig. 5.2**), it did result in increased formation of OMVs that frequently manifested as long chains of OMVs at or near the cell pole in aflagellated cells of strain H19 (**Fig. 5.1**). It was difficult to assess the proportion of H19 cells that had OMV chains since the structures were sheared readily from the cells while preparing the cells for electron microscopy. Nevertheless, cells with OMV chains were easily observed, which suggested a high proportion of

the cells possessed the OMV chains. It will be important to confirm that the hypervesiculation phenotype associated with loss of HP0018 in *H. pylori* B128 is not strain specific by deleting *hp0018* in other *H. pylori* strains and examining the phenotypes of the resulting mutants.

OMVs are formed as a part of normal bacterial growth (*Sartorio et al. 2021*). Previous studies showed that OMV formation by *H. pylori* cells increases as cultures enter stationary phase (*Olofsson et al. 2010, Zavan et al. 2019*). Olofsson and co-workers reported that *H. pylori* strain CCUG17875 grown on Brucella blood agar medium produced small numbers of OMVs during logarithmic growth, but that OMV production increased upon entry into stationary phase, and cells harvested during late stationary phase produced large amounts of OMVs (*Olofsson et al. 2010*). Zavan and co-workers reported the same trend in increased OMV production in *H. pylori* 26695 as cultures progressed from early to late logarithmic phase and then into stationary phase (*Zavan et al. 2019*). While OMV production is a normal part of *H. pylori* growth, the OMV chains observed for the aflagellated cells of strain H19 seems to be a unique phenotype as we are unaware of previous reports describing such morphological features in *H. pylori*.

The chains of OMV were observed infrequently on the flagellated cells of strain H19 where *fliP* had switched to the 'on' phase. A couple of reasons may account for the apparent mutual exclusivity of the OMV chains and flagella in the Δhp0018 mutant (i.e., strain H23 or the occasional cell of strain H19 that was flagellated). Firstly, formation of the OMV chains may have been prevented by the presence of the flagella at the cell pole. For example, the flagellar sheath may affect the surrounding outer membrane region so as to prevent the OMV chains from forming. Alternatively, the *H. pylori* flagellar motor has several accessories that are not present in the archetypal motors of *Escherichia coli* and *Salmonella enterica* (*Qin et al. 2017, Chaban et al. 2018*). Some of the *H. pylori* motor accessories are associated with the outer membrane and may have prevented formation of the OMV chains in strain H23 or the flagellated cells of strain H19. A second possible explanation is the OMV chains were sheared off by rotation of the flagella. Alternatively, HP0018 may have a role in coupling sheath biogenesis with flagellum assembly and the OMV chains may have resulted from sheath formation initiating prematurely in the absence HP0018.

Although FS<sup>-</sup> Helicobacter species lack hp0018 homologs, C. jejuni has sheath-less flagella but possesses a homolog of the hp0018 homolog, Cj0089. Cj0089 is encoded in an operon with two other predicted lipoproteins, Cj0090 and Cj0091. Oakland and co-workers disrupted Cj0089 and Cj0091 in C. jejuni NCTC 11168 and characterized phenotypes related to host colonization for the resulting mutants (**Oakland et al. 2011**). The C. jejuni Cj0091 mutant, but not the Cj0089

mutant, displayed significant reductions in both adherence to human intestinal cell line INT 407 cells and in colonization of the chick cecum (*Oakland et al. 2011*). The researchers did not report on the cellular morphology of the *C. jejuni Cj0089* mutant, so it is not known if disrupting *Cj0089* resulted in hypervesiculation.

Since genes within an operon often have roles in a common function, it is worthwhile to consider the synteny between hp0018 homologs and other genes. Although hp0018 appears to be in an operon by itself in *H. pylori*, in many enterohepatic *Helicobacter* species the *hp0018* homolog is within a predicted operon with a hp1457 homolog and immediately upstream of this gene. HP1457 is a homolog of LpoB, a lipoprotein that is required for activation of the penicillinbinding protein PBP1B (*Typas et al. 2010*). PBP1B is a bifunctional peptidoglycan synthase that has both glycan chain polymerizing and peptide crosslinking activities (Goffin and Ghuysen 1998), and is part of the divisome complex that is responsible for the synthesis and splitting of the cell envelope at the division site (Bertsche et al. 2006). HP1457 is an ortholog of C. jejuni Cj0091. The synteny between the  $\Delta hp0018$  and hp1457 homologs in several Helicobacter species suggests these genes may have roles in a similar biological process. Given that H. pylori HP1457 is a LpoB homolog that may regulate the activity of PBP1B, by extension, HP0018 may have a similar role in remodeling the peptidoglycan layer. Consistent with this idea was the identification of the peptidoglycan hydrolases MItD and AmiA as potential HP0018 interaction partners based on the co-IP assays with the HP0018-myc fusion protein (Table 5.1). The interactions of HP0018 with MltD and AmiA were supported using AlphaFold2 to model complexes between these proteins along with PISA to calculate the energetic likelihood of protein interfaces in the models (Figure 5.6). Future experiments to confirm that HP0018 interacts with MltD and AmiA, however, are needed to clarify the role of HP0018 in *H. pylori*.

The murein sacculus maintains the shape of the cell in bacteria, and several peptidoglycan hydrolases have been identified as having roles in determining the helical shape of cells in *H. pylori* (*Sycuro et al. 2010, Sycuro et al. 2012, Sycuro et al. 2013, Yang et al. 2019*). MItD and AmiA have not been shown to have roles in cell shape determination in *H. pylori*, but given their enzymatic activities it is not unreasonable to postulate that they play a role in remodeling the murein sacculus. HP0018 may regulate the activity of MItD and AmiA, and the unregulated activity of these enzymes in the absence of HP0018 may have been responsible for the decreased helical shape of strains H19 and H23 (Figs. 5.1D-5.1F). Moreover, the slight motility defect of strain H23 in soft agar medium may be due to the altered cell shape of the mutant as *H. pylori* mutants with straight-rod morphology have motility defects in viscous environments (*Martinez et al. 2016*). If

the absence of HP0018 does indeed result in the unregulated activities of MltD or AmiA, a relevant question is how does this relate to the hypervesiculation phenotype of the Δhp0018 mutant? The biogenesis mechanisms for bacterial OMVs formation are poorly understood, although several mechanisms have been proposed (*Sartorio et al. 2021*). One proposed mechanism of OMV production posits that the local accumulation of peptidoglycan fragments or misfolded proteins in the periplasmic induced curvature of the outer membrane to initiate OMV formation (*Sartorio et al. 2021*). Such a mechanism could potentially explain a connection between the unregulated activities of MltD or AmiA and the unusual hypervesiculation phenotype of strain H19. Further investigation into MltD and AmiA and whether HP0018 modulates the activities of these enzymes will likely provide valuable information cell shape determination in *H. pylori*, and may also provide clues on the molecular basis for the unusual hypervesiculation of strain H19.

# **CONCLUSIONS**

H. pylori HP0018 is a predicted lipoprotein that is conserved in many Helicobacter species. Cells of a H. pylori B128 Δhp0018 mutant were less helical in shape compared to wild-type cells, and also produced large amounts of OMVs that frequently formed long chains near the cell pole. Co-IP assays with HP0018 identified two enzymes involved in modification of cell wall peptidoglycan, AmiA and MltD, as potential HP0018 interaction partners. We hypothesize that HP0018 regulates the activity of AmiA and/or MltD, and in the absence of HP0018 the unregulated activity of these enzymes affects the peptidoglycan layer so as to alter the cell shape and stimulate formation of OMVs.

### MATERIALS AND METHODS

#### **Bacterial Strains and Growth Conditions**

*E. coli* NEB® Turbo was used for cloning and plasmid construction. *E. coli* strains were grown in lysogeny broth (LB) broth or LB agar medium supplemented with kanamycin (30  $\mu$ g/mL), ampicillin (100  $\mu$ g/mL), isopropyl β-D-1-thiogalactopyranoside (IPTG; 0.1 mM), or 5-bromo-4-chloro-3-indolyl β-D-galactopyranoside (40  $\mu$ g/mL) when appropriate. *H. pylori* strains used in the study were derived from *H. pylori* B128, which was kindly provided by Dr. Richard M. Peek, Jr. For routine growth of *H. pylori* strains, the cultures were grown in an atmosphere consisting of 10% CO<sub>2</sub>, 6% O<sub>2</sub> and 84% N<sub>2</sub> at 37°C on tryptic soy agar supplemented with 5% heat-inactivated

horse serum (TSA-HS). Liquid cultures of *H. pylori* were grown in brain heart infusion (BHI) medium supplemented with 5% heat-inactivated horse serum with shaking in serum bottles in an atmosphere consisting of 5% CO<sub>2</sub>, 10% H<sub>2</sub>, 10% O<sub>2</sub>, and 75% N<sub>2</sub>. Kanamycin (30 µg/mL) and sucrose (5% wt/vol) were added to the medium when appropriate. Motility of *H. pylori* strains in a soft agar medium consisting of Mueller-Hinton broth, 10% heat-inactivated horse serum, 20 mM 2-(N-morpholino) ethanesulfonic acid (MES; pH 6.0), and 0.4% noble agar was assessed as described (*Chu et al. 2019*).

### Constructing the *H. pylori* ∆hp0018 Mutant

Genomic DNA (gDNA) from *H. pylori* B128 was purified using the Wizard genomic DNA purification kit (Promega, Madison, WI, USA) and used as the template for PCR applications. PCR primers used in the study are listed in **Table S5.1**, as are the plasmids and *H. pylori* strains generated in the study. DNA sequences corresponding to a 533 bp region upstream and a 530 bp region downstream of the *hp0018* homolog were amplified from *H. pylori* B128 gDNA using PrimeSTAR DNA polymerase (Takara Bio, San Jose, CA, USA) together with the primer pairs 51/52 and 53/54, respectively. Primers 52 and 53 are complementary and introduced Xho1 and Nhe1 restriction sites for subsequent cloning of a kanR-sacB cassette. The resulting amplicons were joined together by overlapping PCR using Phusion DNA polymerase (New England Biolabs, Ipswich, MA, USA). The overlapping PCR product was incubated with Taq DNA polymerase (Promega, Madison, WI, USA) to add A-overhangs to the 3'-ends of the amplicon, which was then ligated into pGEM-T Easy (Promega) to generate plasmid pKR12. Insertion of the overlapping PCR product into the plasmid was confirmed by DNA sequencing (Eton Biosciences, Research Triangle Park, NC). A kan<sup>R</sup>-sacB cassette from plasmid pJC038 (*Chu et al. 2019*) was introduced into the Xho1 and Nhe1 sites of plasmid pKR12 to generate plasmid pKR14.

The suicide vector pKR14 was introduced into *H. pylori* B128 by natural transformation as described (*Chu et al. 2019*). Transformants in which *hp0018* had been replaced with the kan<sup>R</sup>-sacB cassette by homologous recombination were enriched by selecting for kanamycin resistance. Using the primers 51 and 54, several kanamycin-resistant isolates were checked by PCR to verify that the kan<sup>R</sup>-sacB cassette was integrated into the *hp0018* locus. One of the strains in which *hp0018* was replaced with the kanR-sacB cassette, which was designated strain H13, was transformed with the suicide vector pKR12. Transformants in which the kan<sup>R</sup>-sacB cassette was replaced with the unmarked deletion of *hp0018* resulting from homologous recombination between plasmid pKR12 and the chromosome were counter-selected on TSA-HS supplemented with 5% sucrose as described (*Copass et al. 1997*). Sucrose-resistant isolates were screened

for kanamycin-sensitivity on TSA-HS supplemented with kanamycin, and deletion of *hp0018* in kanamycin-sensitive isolates was confirmed by PCR using primers 51 and 54, and DNA sequencing of the resulting amplicon. A *H. pylori* B128 strain in which *hp0018* was deleted was designated as strain H19 and stored at -70°C.

### Construction of an Expression Vector for a HP0018-sfGFP Fusion Protein

A gene encoding a super folder green fluorescent protein (sfGFP) described by Dinh and Bernhardt (*Dinh and Bernhardt 2011*) and codon optimized for *H. pylori* was synthesized by Azenta Life Sciences (South Plainfield, NJ, USA). Primers 102 and 103 were used to amplify the coding region of *hp0018* minus the stop codon along with 500 bp of upstream sequence from *H. pylori* B128 gDNA. Primer 102 contained an overhang that included a Nhel site, and primer 103 was complimentary to the 5'-end of the sequence encoding the sfGFP. Primers 104 and 105 were used to amplify the sequence encoding the sfGFP. Primer 104 was complimentary to a portion of primer 103, and primer 105 contained an overhang that included a BamHl site. The resulting amplicons were ligated together and after adding A-overhangs to the 3'-ends, the overlapping PCR product was ligated into pGEM-T Easy to generate plasmid pKR31. Plasmid pKR31 was digested with Nhel and BamHl, and the DNA fragment bearing the *hp0018*-gfp fusion and upstream region was ligated into pHel3 (*Heuermann and Haas 1998*) to generate plasmid pKR40.

#### Construction of c-Myc Tagged HP0018

To facilitate construction of a c-Myc-tagged HP0018 in *H. pylori*, we modified the shuttle vector pHel3 (*Heuermann and Haas 1998*) to allow for the introduction of the c-Myc epitope at the C-terminus of the protein. The modified plasmid, which we designated pHel3-Myc, contains the fliF promoter upstream of the tandem BspQ1 sites for Golden Gate cloning followed by a sequence encoding a flexible linker, c-Myc epitope, and DDDDK epitope. Primers 206 and 207 were used to amplify *hp0018* from *H. pylori* B128 gDNA. The primers introduced BspQ1 sites immediately upstream and downstream of the start and stop codons of *hp0018*, respectively. The resulting amplicon and plasmid pHel3-Myc were digested together with BspQ1 and ligated using Fast-Link DNA ligase as described above. The reaction mix was incubated with BspQ1 to digest uncut pHel3-Myc vector and the reaction mix was then used for transformation of *E. coli*. A plasmid containing the expected insert, designated as pKR66, was verified by restriction enzyme digestion and sequencing of the inserted DNA.

### **Transmission Electron Microscopy (TEM)**

*H. pylori* strains were grown to late-log phase (OD<sub>600</sub> ~1.0) in MHB supplemented with 5% heat-inactivated horse serum. Cells from 1 mL of culture were pelleted by centrifugation (550 x g) then resuspended in 125 μL of phosphate-buffered saline (PBS). Cells were fixed by adding 50 μL of 16% EM grade formaldehyde and 25 μL of 8% EM grade glutaraldehyde to the cell resuspension. Following incubation at room temperature for 5 min, 10 μL of the cell suspension were applied to a 300 mesh, formvar-coated copper grid and incubated at room temperature for 5 min. The cell suspension was wicked off the grids using a filter paper, and the grids were washed 3 times with 10 μL of water. Cells were stained by applying 10 μL of 1% uranyl acetate to the grids for 30 s. After removing the stain with filter paper, the grids were washed three times with 10 μL of water and then air-dried. Cells were visualized using a JEOL JEM 1011 transmission electron microscope.

### Scanning Electron Microscopy (SEM)

*H. pylori* strains were grown, collected, and fixed as described for TEM preparation, then resuspended in ~300 ul PBS. The cell suspension was applied to poly-L-lysine coverslips so as to nearly cover the coverslip, then left overnight at room temperature. The following day, a secondary fixation step was done using a 1:1:1 mixture of distilled water: 4% osmium tetroxide: 2x PBS for 1 h at 4°C. Samples were washed once in PBS for 10 min and then two washes in water to remove excess salts before dehydration in an ethanol series that involved adding ethanol in 25% increments for 10 min each step until reaching 100% ethanol. Samples were washed 3 times in 100% ethanol for 10 min each. Samples were then washed with a 1:1 mixture of hexamethyldisilazane (HMDS) and 100% ethanol for 15 min, followed by washes with 100% HMDS for 5 min then 10 min. The coverslips were dried overnight at room temperature and then added to aluminum SEM stubs using adhesive circles. Samples were coated with gold by sputter coating in a vacuum chamber calibrated to 2 x 10-1 mbar/pa. Stubs were stored under desiccation. SEM was conducted using a FEI Tenio at 5.00kV and a spot size of 7.0.

### **Fluorescence Microscopy**

Cells of strain H93 (motile variant of *H. pylori* B128 Δhp0018 bearing plasmid pKR40, which carries the hp0018::gfp fusion) grown in BHI medium supplemented with heat-inactivated horse serum under microaerobic conditions to mid-logarithmic phase (OD600 ~1.0) were incubated with FM4-64 (5 uM final concentration) and incubated for 5 min at room temperature. Cells were harvested by centrifugation at 8,700 x g k for 1 min, then washed three times by resuspending

the cells and pelleting by centrifugation. Twenty ul of resuspended, stained cells were added to the slide, and after 10 minutes the excess was wiped away. One drop of Prolong Gold antifade mountant (Thermo Fisher Scientific) was added to the sample before placing a 1.5 mm coverslip on the cell sample. Cells were visualized with a Nikon Ti-U fluorescence microscope equipped with a Lumencor SOLA SM II light engine and fitted with a 100X oil immersion objective (NA 1.45) and GFP HISN Zero Shift and Texas Red Longpass filter sets. Image capture was performed with a CoolSNAP Myo camera (Photometrics), controlled via the Nikon NIS-Elements BR software package (v. 4.20.01). Resultant images were processed with the Fiji software package (*Schindelin et al. 2012*, *Schneider et al. 2012*).

### **Preparation and Analysis of OMVs**

Cells of *H. pylori* strains grown on TSA-HS medium were resuspended in 10 ml filter-sterilized PBS, and vortexed for 60 seconds to shear off the OMVs. Cells were removed from the suspension by centrifugation at 8,700 x g for 10 min and the resulting supernatant was passed through a 0.45 um filter to remove any remaining cells. A sample of the filtrate was applied to formvar-coated copper grids and processed for TEM as described above. OMVs were visualized using a JEOL JEM 1011 transmission electron microscope.

Proteins of *H. pylori* outer membrane vesicles (2 to 5 µg total protein) were loaded onto an SDS-polyacrylamide gel and subjected to electrophoresis until the proteins entered the resolving gel. Gel slices containing the proteins were removed and sent to the University of Georgia Proteomics and Mass Spectrometry facility for protein identification. Proteins in the gel slices were digested with trypsin and the resulting peptides were analyzed by LC-MS/MS with a ThermoScientific Orbitrap Velo Elite mass spectrometer coupled with nano-HPLC using a 90-minute elution gradient. Mass spectrometry data were searched against a protein database using Mascot software search engine (Matrix Science) for protein identification.

#### **DNA Sequencing and Analysis**

Genomic DNA from the *H. pylori* strains was purified using the Wizard genomic DNA purification kit (Promega) and submitted to the SeqCenter (Pittsburgh, PA) for genomic library preparation and Illumina sequencing. Reads for *H. pylori* gDNA sequence were mapped using the *breseq* computational pipeline (*Deatherage and Barrick 2014*) with the published NCBI genome for *H. pylori* B128 (Accession no.: NZ\_CP024951.1).

#### **Co-Immunoprecipitation Assay**

Wild-type H. pylori B128 and the H. pylori strain expressing the HP0018-myc fusion protein (strain H141) were grown on TSA-HS plates, harvested, and resuspended in 7 ml phosphate-buffer saline (PBS) with Pierce Protease Inhibitor (Thermo Fisher Scientific, Waltham, MA, USA). Cells were lysed at 18,000 psi with a French press and the resulting cell lysate was centrifuged at 7,700 x g for 10 min to remove unlysed cells and cell debris. The resulting supernatant was centrifuged at 100,000 x g to pellet membrane vesicles, which were subsequently resuspended in PBS buffer containing 50 mM n-dodecyl-β -D-maltoside (DDM) (Chem-Impex International, Wood Dale, IL, USA). The solution was diluted to 20 mM DDM and the insoluble material was pelleted by centrifugation at 10,000 x g for 10 min and the resulting supernatant was used for the co-IP procedure using the Pierce c-Myc Tag Magnetic IP/Co-IP kit (Thermo Fisher Scientific) as described by the supplier. Samples were incubated with the magnetic beads either overnight at 40 C or at room temperature for 30 min. Magnetic beads with bound proteins were washed at least 10 times with a 1:20 solution of Buffer 2 (supplied with the kit) containing 20 mM DDM. Proteins were eluted from the magnetic beads using 100 µl of 1x non-reducing sample buffer (supplied with the kit) followed by incubation at 95-1000 C for 5 to 10 min. Samples were loaded on a 12% SDS-PAGE gel subjected to electrophoresis until the samples entered the top of the resolving gel. The protein band was excised from the gel and submitted to University of Georgia Proteomics and Mass Spectrometry Facility for analysis by in-gel trypsin digestion followed by LC-MS/MS on the Orbitrap mass spectrometer coupled with nano-HPLC using a 90-minute elution gradient.

#### In Silico Modeling of Protein-Protein Interactions

Predicted tertiary structures of HP0018, HP0772 (AmiA), and HP1572 (MltD) were generated by AlphaFold (*Jumper et al. 2021*). AlphaFold2 multimer version 2.3.1 in UCSF ChimeraX 1.5 (*Jumper et al. 2021*) was used to model interactions of the predicted structures using the University of Georgia Sapelo2 high performance computing cluster. For each pair of proteins, 25 ranked models were generated. PISA (Proteins, Interfaces, Structures, and Assemblies; ebi.ac.uk/pdbe/pisa/), an interactive tool for examining protein-protein interfaces and predicting quaternary structures, was used to evaluate the energetic likelihood of predicted interactions for each model. PISA provides information on protein-protein interfaces, including interface area, solvation free energy gain upon formation of the interface ( $\Delta^i$ G), and the P-value of the solvent free energy gain or interface specificity ( $\Delta^i$ G P-value), and also displays all interfacing residues and any bonds that they form. A negative  $\Delta^i$ G value corresponds to hydrophobic interfaces, or positive protein affinity. The P-value is a measure of interface specificity that measures the

probability of getting a lower than observed  $\Delta^i G$  when the interface atoms are picked randomly from the protein surface. A P-value that is <0.5 indicates an interface where the hydrophobicity is greater than would be average for a given structure, and the interface surface is thus potentially interaction-specific. In addition to  $\Delta^i G$  P-values <0.5, calculated values that correspond to energetically favorable protein interfaces include an interface area >1000 Å2 and a  $\Delta^i G$  <0 kcal/mol.

# **SUPPLEMENTARY MATERIALS**

Table S5.1. Strains, plasmids, and primers generated for the study.

H. pylori stra	nins
name	relevant genotype
H13	H. pylori B128 hp0018::kan-sacB
H19	H. pylori B128 Δhp0018 fliP261 (deletion of nucleotide 261 in fliP)
H23	H. pylori B128 Δhp0018 (wild-type fliP allele)
H93	H23 bearing plasmid pKR40
H141	H23 bearing plasmid pKR66
plasmids	
name	description
pRK12	pGEM-T Easy vector containing hp0018 flanking regions; ApR
pRK14	pRK12 derivative with kan <sup>R</sup> -sacB cassette; Ap <sup>R</sup> , Kn <sup>R</sup>
pRK31	pGEM-T Easy vector containing hp0018-gfp fusion; ApR
pKR40	pHel3 containing hp0018-gfp fusion; KnR
pHel3-myc	Modified pHel3 w fliF promoter, c-myc tag, tandem BspQI cloning sites; KnR
pKR66	pHel3-myc derivative that expresses HP0018-myc fusion protein; Kn <sup>R</sup>
primers	
name	sequence
Primer 51	5'-AAACACAATTTCAATGTGCCTTTGA-3'
Primer 52	5'-GAATTCGATTATCCTCGAGTAAAATTACCGACATCAACAGAACG-3'
Primer 53	5'-GATAATCGAATTCGCTAGCTTTTAAAAACGGGTTTGTTTTGAGT-3'
Primer 54	5'-AAAATCCTATCCGCTTCATAGATCC-3'
Primer 102	5'-GCTAGCCTTTTTTAGAAAACACCCCTTTGTA-3'
Primer 103	5'-CATGCTACCGCCACCTTTTAAATGACTCAAAACAAACCCG-3'
Primer 104	5'-GGTGGTGGCGTAGCATGAGCAAAG-3'
Primer 105	5'-GGATCCTTATTTATACAATTCATCCATGCCA-3'
Primer 206	5'-AAGCTCTTCCATGAAAATATTCGTTCTGTTGATGT-3'
Primer 207	5'-AAGCTCTTCAACCTTTTAAATGACTCAAAACAAACCC-3'

Table S5.2. Mutations identified in the original H. pylori  $\Delta$ hp0018 mutant (strain H19) and a motile variant of the  $\Delta$ hp0018 mutant (strain H23) compared to wild-type H. pylori B128.

Strain H19 NCBI designation	Gene/description	Mutation	1Impact	2Frequency
			Thr83lle	
CV725_RS01525	sugar MFS transporter	ACA→ATA		98.7%
CV725_RS02980	DASS family sodium-coupled anion symporter	AGG→GGG	Arg87Gly	98.7%
CV725_RS03080	HAMP domain-containing histidine kinase ArsS	(C)11→14 (1261/1281 nt)	Insertion of a Pro residue	82.4%
CV725_RS03820 hugZ	YbfB/YjiJ family MFS transporter/HugZ family heme oxygenase	(T)15→14 intergenic (-340/+172)	unknown	81.2%
CV725_RS04360	hypothetical protein	(T)7→6 (1040/1251 nt)	Leu347fs	98.0%
CV725_RS04600 CV725_RS04605	TonB-dependent receptor/catalase	(A)5→6 intergenic (-34/-290)	unknown	82.6%
motA	flagellar motor stator protein MotA	GGC→GAC	Gly201Asp	98.5%
fliP	flagellar type III secretion system protein FliP	(G)8→9 (254/747 nt)	Thr88fs	90.1%
CV725_RS06190	hypothetical protein	CCA→TCA	Pro78Ser	94.1%
CV725_RS06350	cag pathogenicity island protein	GTT→ATT	Val1058lle	89.2%
CV725_RS06350	cag pathogenicity island protein	AAA→AGA	Lys921Arg	98.0%
CV725_RS06500	phospholipase A, pseudogene	(G)10→9 (683/1070 nt)	remains phase "off"	86.2%
babA CV725_RS06645	Hop family adhesin BabA/tRNA-Met	(T)13→12 intergenic (-131/+149)	unknown	87.9%
CV725_RS07515	hypothetical	(C)11→10	unknown	92.5%
queF	protein/NADPH-dependent 7-cyano-7-deazaguanine reductase QueF	intergenic (+11/+121)	Ulkilowii	92.376
CV725_RS07605	PDZ domain-containing protein, PfIC homolog	(T)8→6 (31-32/996 nt)	Leu13fs	99.2%
CV725_RS07695	HP0018 homolog	D1338 nt (37-1374/1410 nt)	deletion	98.0%
Strain H23	'			
NCBI designation	Gene/description	Mutation	Impact	Frequency
CV725_RS01525	sugar MFS transporter	ACA→ATA	Thr83lle	98.1%
CV725_RS02390	rod shape-determining protein	GCG→GTG	Ala100Val	99.0%
CV725_RS02980	DASS family sodium-coupled anion symporter	AGG→GGG	Arg87Gly	98.9%
CV725_RS03820 hugZ	YbfB/YjiJ family MFS transporter/HugZ family heme oxygenase	(T)15→14 intergenic (-340/+172)	unknown	80.3%
CV725_RS04360	hypothetical protein	(T)7→6 (1040/1251 nt)	Leu347fs	98.1%
CV725_RS04600 CV725_RS04605	TonB-dependent receptor/catalase	(A)5→6 intergenic (-34/-290)	unknown	81.3%
motA	flagellar motor stator protein MotA	GGC→GAC	Gly201Asp	98.7%
CV725_RS05520	TIGR00366 family protein	(T)7→3 (810-813/1365 nt)	Phe271fs	96.5%
CV725_RS05620	SIR2 family protein, pseudogene	C→T (1752/2474 nt)	remains a pseudogene	98.1%
CV725_RS06350	cag pathogenicity island protein	GTT→ATT	Val1058lle	90.2%
CV725_RS06350	cag pathogenicity island protein	AAA→AGA	Lys921Arg	98.7%
CV725_RS06500	phospholipase A, pseudogene	(G)10→9 (683/1070 nt)	remains phase "off"	84.3%
babA CV725_RS06645	Hop family adhesin BabA/tRNA-Met	(T)13→12 intergenic (-131/+149)	unknown	84.0%

hofG CV725_RS06740	outer membrane protein HofG/TonB-dependent receptor	(A)14→15 intergenic (-71/+258)	unknown	81.0%
CV725_RS07515 queF	hypothetical protein/NADPH-dependent 7-cyano-7-deazaguanine reductase QueF	(C)11→10 intergenic (+11/+121)	unknown	91.8%
CV725_RS07605	PDZ domain-containing protein, PfIC homolog	(T)8→6 (31-32/996 nt)	Leu13fs	99.1%
CV725_RS07695	HP0018 homolog	D1338 nt (37-1374/1410 nt)	deletion	98.7%

<sup>1&</sup>quot;fs" indicates frameshift

Table S5.3. Proteins identified in OMV samples from wild-type H. pylori B128, non-motile  $\Delta hp0018$  mutant (strain H19), and motile  $\Delta hp0018$  isolate (strain H23).

		wild	type	strain	H19	strain	H23	
accession	description	<sup>1</sup> Mas cot score	<sup>2</sup> no. of pept ides	<sup>1</sup> Masc ot score	<sup>2</sup> no. of pept ides	¹Masco t score	<sup>2</sup> no. of pept ides	<sup>3</sup> identified previously
WP_00072 6315.1	Hop family adhesin LabA, HP0025	8563. 26	45	7857.2 0	47	14136.9 1	47	(Olofsson, Vallstrom et al. 2010, Zavan, Bitto et al. 2019)
WP_00088 5488.1	flagellin A, HP0601	6436. 44	30	583.07	2	12027.3 4	33	(Olofsson, Vallstrom et al. 2010, Zavan, Bitto et al. 2019)
WP_14580 1814.1	Hop family adhesin BabA, HP1243	5197. 13	31	6411.5 5	33	6276.06	34	(Olofsson, Vallstrom et al. 2010, Zavan, Bitto et al. 2019)
WP_00075 1499.1	Hop family adhesin HopQ, HP1177	3089. 26	28	3533.0 3	27	2858.25	27	(Olofsson, Vallstrom et al. 2010, Zavan, Bitto et al. 2019)
WP_00001 0021.1	flagellin B, HP0115	2881. 86	22	0.00	0	4904.40	33	(Olofsson, Vallstrom et al. 2010, Zavan, Bitto et al. 2019)
EEC24754.	flagellar filament cap protein FliD, HP0752	2838. 63	38	0.00	0	4190.37	41	(Olofsson, Vallstrom et al. 2010, Zavan, Bitto et al. 2019)
QDY56424.	outer membrane beta-barrel protein HofC, HP0486	2792. 37	22	4676.6 2	25	4547.96	24	(Olofsson, Vallstrom et al. 2010, Zavan, Bitto et al. 2019)
QDY56215.	disulfide isomerase, HP0231	2416. 86	21	3017.5 1	22	2456.88	22	(Olofsson, Vallstrom et al. 2010, Zavan, Bitto et al. 2019)
QDY56165. 1	peptidylprolyl isomerase, HP0175	2160. 94	28	2863.3 4	32	1642.09	24	(Olofsson, Vallstrom et al. 2010)
WP_00079 5968.1	LPP20 family lipoprotein, HP1456	2125. 95	18	2836.6 4	20	3052.54	22	(Olofsson, Vallstrom et al. 2010, Zavan, Bitto et al. 2019)
WP_00059 5790.1	outer membrane beta-barrel protein HorE, HP0472	1759. 30	9	821.63	6	1212.52	9	(Olofsson, Vallstrom et al. 2010, Zavan, Bitto et al. 2019)
QDY55938.	g- glutamyltransferase , HP1118	1752. 60	21	1955.0 3	22	1290.59	19	(Olofsson, Vallstrom et al. 2010)
WP_00104 0308.1	chaperonin GroEL, HP0010	1711. 37	24	1873.0 7	25	1461.94	20	(Olofsson, Vallstrom et al. 2010)

<sup>&</sup>lt;sup>2</sup>Frequency is the number of times the mutation was identified relative to the total number of reads for that sequence.

EEC24951.	predicted lipoprotein, HP0596	1709. 44	14	2554.3 5	15	2861.28	17	(Olofsson, Vallstrom et al. 2010, Zavan, Bitto et al. 2019)
WP_00072 0394.1	LPP20 family lipoprotein, HP1454	1662. 02	24	1321.7 6	21	1030.46	23	(Olofsson, Vallstrom et al. 2010, Zavan, Bitto et al. 2019)
WP_00073 8953.1	Ycel family protein, HP0305	1645. 09	12	1815.6 1	11	1807.77	12	(Olofsson, Vallstrom et al. 2010, Zavan, Bitto et al. 2019)
QDY56091.	predicted lipoprotein, HP0097	1613. 61	10	1891.2 1	15	1839.18	14	(Olofsson, Vallstrom et al. 2010, Zavan, Bitto et al. 2019)
WP_00064 6639.1	flagellar sheath lipoprotein HpaA, HP0797	1581. 04	17	2260.2 3	18	1738.32	21	(Olofsson, Vallstrom et al. 2010, Zavan, Bitto et al. 2019)
WP_00075 1159.1	outer membrane protein HopA, HP0229	1541. 30	13	2132.4 5	16	1900.85	15	(Olofsson, Vallstrom et al. 2010, Zavan, Bitto et al. 2019)
QDY56583.	outer membrane protein HopE, HP0706	1475. 83	14	1964.9 6	14	2033.19	15	(Olofsson, Vallstrom et al. 2010, Zavan, Bitto et al. 2019)
QDY56399.	secreted protease PqqE, HP1012	1462. 35	19	1733.8 6	19	1182.48	18	(Olofsson, Vallstrom et al. 2010, Zavan, Bitto et al. 2019)
QDY56619. 1	secreted protease, HP0657	1440. 76	19	1250.5 4	24	713.89	12	(Olofsson, Vallstrom et al. 2010)
QDY56273.	flagellar biosynthesis protein FlgL, HP0295	1306. 95	27	0.00	0	2055.06	36	(Olofsson, Vallstrom et al. 2010, Zavan, Bitto et al. 2019)
QDY56393.	secreted protease, HP1019	1242. 35	26	1397.2 8	24	1200.73	26	(Olofsson, Vallstrom et al. 2010, Zavan, Bitto et al. 2019)
QDY56824.	outer membrane protein HomA, HP0710	1185. 88	19	2453.3 6	26	2371.84	27	(Olofsson, Vallstrom et al. 2010, Zavan, Bitto et al. 2019)
WP_00102 0067.1	periplasmic binding protein, HP1564	1177. 15	14	1547.9 5	16	1220.54	13	(Olofsson, Vallstrom et al. 2010, Zavan, Bitto et al. 2019)
QDY55779.	polyisoprenoid- binding protein, HP1286	1066. 04	13	1419.2 8	12	745.10	10	(Olofsson, Vallstrom et al. 2010, Zavan, Bitto et al. 2019)
QDY56435. 1	flagellar hook protein FlgE, HP0870	1048. 49	24	0.00	0	3441.91	35	(Olofsson, Vallstrom et al. 2010, Zavan, Bitto et al. 2019)
WP_00071 5700.1	HpaA2 protein, HP0410	1021. 95	11	1404.9 4	13	906.88	11	(Olofsson, Vallstrom et al. 2010, Zavan, Bitto et al. 2019)
QDY55937.	flagellar hook- associated protein FlgK, HP1119	996.7 9	20	0.00	0	1488.03	25	(Olofsson, Vallstrom et al. 2010, Zavan, Bitto et al. 2019)
WP_19294 0664.1	outer inflammatory protein OipA, HP0638	958.4 7	10	1173.6 8	11	1246.73	11	(Olofsson, Vallstrom et al. 2010, Zavan, Bitto et al. 2019)
EEC24262.	ATP synthase subunit B, HP1132	947.1 0	13	1251.5 6	15	601.73	9	(Olofsson, Vallstrom et al. 2010)
QDY56621.	b-barrel assembly factor BamA, HP0655	944.6 4	18	1335.3 4	19	871.91	15	(Olofsson, Vallstrom et al. 2010, Zavan, Bitto et al. 2019)

WP_00084 6456.1	DNA-binding protein Dps, HP0243	943.3 0	10	133.94	3	62.22	2	
QDY55857.	elongation factor Tu, HP1205	901.3 8	17	584.96	14	321.00	6	(Olofsson, Vallstrom et al. 2010)
WP_00073 1326.1	fibronectin type III domain-containing protein, HP0746	895.5 5	17	1133.2 2	18	1128.40	19	(Olofsson, Vallstrom et al. 2010, Zavan, Bitto et al. 2019)
WP_00117 4690.1	thiol peroxidase Tpx, HP0390	886.0 3	9	647.37	9	439.82	5	
WP_00085 6042.1	periplasmic substrate-binding protein, HP1172	876.3 5	12	1153.0 4	16	798.92	13	(Olofsson, Vallstrom et al. 2010)
QDY56995.	periplasmic iron- binding protein, HP1561	876.0 7	10	1281.7 2	12	754.59	9	(Olofsson, Vallstrom et al. 2010, Zavan, Bitto et al. 2019)
WP_00032 3697.1	DUF3944 domain- containing protein, HP1588	870.1 3	13	565.29	11	400.97	8	(Olofsson, Vallstrom et al. 2010)
QDY56671.	ToIC family protein HefA, HP0605	853.4 6	13	1233.7 8	17	749.97	12	(Olofsson, Vallstrom et al. 2010, Zavan, Bitto et al. 2019)
EEC24860.	secreted protease, HP1350	850.7 9	24	1308.3 3	28	880.00	23	(Olofsson, Vallstrom et al. 2010, Zavan, Bitto et al. 2019)
QDY56734.	sel1 repeat family protein, HP0519	800.5 3	11	769.03	10	826.78	11	
QDY56121.	hypothetical protein, HP0130	781.6 4	15	1258.0 4	16	1241.21	17	(Olofsson, Vallstrom et al. 2010, Zavan, Bitto et al. 2019)
QDY56720.	oncogenic effector CagA, HP0547	765.1 3	24	94.47	5	413.06	13	(Olofsson, Vallstrom et al. 2010)
WP_00126 8551.1	SH3 domain- containing peptidase, HP0087	742.4 2	12	760.63	11	703.49	8	(Olofsson, Vallstrom et al. 2010, Zavan, Bitto et al. 2019)
QDY55930.	translocation protein TolB, HP1126	732.3 4	12	1017.5 6	20	601.22	12	(Olofsson, Vallstrom et al. 2010, Zavan, Bitto et al. 2019)
EEC23889.	outer membrane protein FecA-3, HP1400	716.9 0	18	1799.2 8	27	1513.75	22	(Olofsson, Vallstrom et al. 2010, Zavan, Bitto et al. 2019)
QDY56118.	outer membrane protein HorB, HP0127	715.1 6	7	907.78	8	639.32	5	(Olofsson, Vallstrom et al. 2010, Zavan, Bitto et al. 2019)
EEC24215.	hypothetical protein, HP0953	696.6 2	5	795.25	6	701.80	6	(Olofsson, Vallstrom et al. 2010)
QDY56703.	peptidase PepA, HP0570	688.0 4	11	0.00	0	163.12	4	(Olofsson, Vallstrom et al. 2010)
QDY56994.	periplasmic iron- binding protein, HP1562	686.3 6	11	1102.8 9	13	758.00	12	(Olofsson, Vallstrom et al. 2010, Zavan, Bitto et al. 2019)
WP_00078 8701.1	outer membrane protein HopF, HP0252	682.1 5	13	887.03	13	725.36	12	(Olofsson, Vallstrom et al. 2010)
QDY56993. 1	alkyl hydroperoxide reductase TsaA, HP1563	675.4 6	7	1221.8 1	10	754.56	7	(Olofsson, Vallstrom et al. 2010)
WP_00011 7378.1	citrate synthase, HP0026	649.3 3	9	408.33	7	240.07	4	(Olofsson, Vallstrom et al. 2010)

QDY55923. 1	F0F1 ATP synthase subunit alpha, HP1134	647.4 6	16	883.81	23	215.82	10	(Olofsson, Vallstrom et al. 2010)
QDY56423. 1	Catalase, HP0485	645.6 6	11	813.86	13	426.14	11	(Olofsson, Vallstrom et al. 2010, Zavan, Bitto et al. 2019)
QDY56253. 1	pentatricopeptide repeat domain, HP0275	644.5 0	15	844.91	13	364.50	8	(Olofsson, Vallstrom et al. 2010, Zavan, Bitto et al. 2019)
QDY56801. 1	flagellar hook protein FlgE2; HP0908	636.3 7	13	0.00	0	515.79	13	(Olofsson, Vallstrom et al. 2010, Zavan, Bitto et al. 2019)
EEC25266. 1	outer membrane protein HopG, HP0254	613.0 5	12	1068.2 6	12	1000.68	11	(Olofsson, Vallstrom et al. 2010, Zavan, Bitto et al. 2019)
EEC25319.	periplasmic solute- binding protein, HP0298	611.1 0	14	584.32	14	318.31	12	(Olofsson, Vallstrom et al. 2010)
QDY56070. 1	urease beta subunit UreB, HP0072	608.9 6	14	459.84	9	378.15	11	(Olofsson, Vallstrom et al. 2010)
QDY56511.	outer membrane beta-barrel protein HofF, HP0788	596.3 0	10	676.29	10	629.89	8	(Olofsson, Vallstrom et al. 2010, Zavan, Bitto et al. 2019)
QDY56775. 1	neuraminyllactose- binding hemagglutinin, HP0492	540.0 1	11	773.56	11	699.63	9	(Olofsson, Vallstrom et al. 2010, Zavan, Bitto et al. 2019)
QDY57028. 1	outer membrane protein HorL, HP1395	530.6 5	10	746.95	11	558.48	9	(Olofsson, Vallstrom et al. 2010, Zavan, Bitto et al. 2019)
QDY56609. 1	outer membrane protein HorF, HP0671	520.3 2	6	581.97	9	779.94	9	(Olofsson, Vallstrom et al. 2010, Zavan, Bitto et al. 2019)
EEC24629.	hypothetical protein, HP1285	504.5 8	7	674.83	7	695.08	8	(Olofsson, Vallstrom et al. 2010, Zavan, Bitto et al. 2019)
EEC24785. 1	aconitate hydratase, HP0779	503.8 3	10	317.44	5	262.19	3	
QDY56599.	outer membrane protein FecA-1, HP0686	492.8 6	10	1121.5 1	17	698.57	8	(Olofsson, Vallstrom et al. 2010, Zavan, Bitto et al. 2019)
QDY55893. 1	outer membrane beta-barrel protein HofH, HP1167	485.7 1	12	960.24	13	996.76	14	(Olofsson, Vallstrom et al. 2010, Zavan, Bitto et al. 2019)
WP_00120 6904.1	2-oxoglutarate synthase subunit alpha, HP0589	462.6 2	0	284.21	8	144.95	4	(Olofsson, Vallstrom et al. 2010)
WP_00070 9627.1	DUF1104 domain- containing protein; HP0721	455.7 3	4	1369.8 4	4	555.40	4	(Olofsson, Vallstrom et al. 2010, Zavan, Bitto et al. 2019)
QDY55647. 1	ToIC family protein, HP1489	442.7 4	8	536.37	9	480.77	7	(Olofsson, Vallstrom et al. 2010, Zavan, Bitto et al. 2019)
QDY56645.	hydrogenase large subunit, HP0632	439.2 1	12	775.65	13	513.34	11	(Olofsson, Vallstrom et al. 2010)
EEC24175.	predicted lipoprotein, HP1002	438.3 9	10	479.27	12	619.23	11	,
EEC24379.	outer membrane protein Hopl, HP1156	432.6 2	7	892.82	10	689.63	6	(Olofsson, Vallstrom et al. 2010, Zavan, Bitto et al. 2019)

QDY56985.	septal ring lytic transglycosylase RlpA family protein, HP1571	412.7 3	7	762.97	10	500.30	8	(Olofsson, Vallstrom et al. 2010, Zavan, Bitto et al. 2019)
QDY55887.	hypothetical protein, HP1173	404.0	9	812.34	10	476.77	9	(Olofsson, Vallstrom et al. 2010, Zavan, Bitto et al. 2019)
QDY55678.	penicillin-binding protein activator LpoB, HP1457	399.9 0	5	953.29	8	987.80	10	(Olofsson, Vallstrom et al. 2010, Zavan, Bitto et al. 2019)
WP_00122 8615.1	5'-nucleotidase C- terminal domain- containing protein, HP0104	392.9 0	12	413.54	10	264.99	7	(Olofsson, Vallstrom et al. 2010, Zavan, Bitto et al. 2019)
WP_00091 5372.1	outer membrane protein HomD, HP1453	384.2 2	9	867.59	12	491.78	9	(Olofsson, Vallstrom et al. 2010, Zavan, Bitto et al. 2019)
QDY56442.	plasminogen- binding protein PgbB, HP0863	379.0 8	14	641.56	16	448.37	17	(Olofsson, Vallstrom et al. 2010, Zavan, Bitto et al. 2019)
QDY55951. 1	outer membrane protein HorH, HP1107	375.4 3	6	352.89	5	239.51	4	(Zavan, Bitto et al. 2019)
WP_00094 5748.1	TonB-dependent receptor FrpB-3, HP1512	373.5 6	9	1762.4 2	24	1451.37	20	(Olofsson, Vallstrom et al. 2010, Zavan, Bitto et al. 2019)
QDY56476.	thioredoxin- disulfide reductase TrxB, HP0825	372.7 3	6	183.92	5	143.76	5	(Olofsson, Vallstrom et al. 2010)
QDY56296.	periplasmic nuclease NucT, HP0323	368.5 3	5	593.40	9	407.79	6	(Olofsson, Vallstrom et al. 2010, Zavan, Bitto et al. 2019)
QDY56126.	predicted lipoprotein, HP0135	367.0 2	3	501.57	3	533.18	3	(Zavan, Bitto et al. 2019)
QDY55673.	predicted lipoprotein, HP1463	355.5 8	5	382.58	6	340.37	7	(Olofsson, Vallstrom et al. 2010, Zavan, Bitto et al. 2019)
WP_00046 7790.1	hypothetical protein, HP0599	351.4 6	7	415.37	6	409.07	8	(Olofsson, Vallstrom et al. 2010)
QDY55940.	Sel1-like repeat protein, HP1117	346.8 9	7	630.87	0	320.65	5	(Olofsson, Vallstrom et al. 2010, Zavan, Bitto et al. 2019)
WP_00123 6618.1	flagellar motor accessory protein FlgP, HP0836	344.3 9	8	443.26	8	418.92	8	(Zavan, Bitto et al. 2019)
QDY56192.	hypothetical protein, HP0204	334.1 5	5	349.01	4	109.01	2	(Zavan, Bitto et al. 2019)
QDY55739.	copper resistance protein, HP1326	330.3 0	7	663.14	10	430.56	6	(Zavan, Bitto et al. 2019)
QDY55989.	superoxide dismutase SodB, HP0389	320.7 0	7	384.95	10	78.97	2	(Olofsson, Vallstrom et al. 2010)
WP_10493 2432.1	outer membrane protein HopK, HP0477	320.3 3	4	667.87	9	485.91	7	(Olofsson, Vallstrom et al. 2010, Zavan, Bitto et al. 2019)
EEC24290. 1	hypothetical protein, HP0973	319.1 0	5	600.28	9	346.03	6	(Olofsson, Vallstrom et al. 2010)
WP_00003 3534.1	methyl-accepting chemotaxis protein, HP0099	314.0 0	9	193.75	4	0.00	0	(Olofsson, Vallstrom et al. 2010)

EEC24268.	peptidoglycan- associated lipoprotein PalA, HP1125	308.0	5	488.58	7	618.79	7	(Olofsson, Vallstrom et al. 2010)
WP_00053 2521.1	outer membrane beta-barrel protein, HP0726	300.8	6	560.28	8	510.68	6	(Olofsson, Vallstrom et al. 2010, Zavan, Bitto et al. 2019)
QDY56219.	Sel1 repeat protein HcpE, HP0235	298.8 7	5	437.95	7	323.40	5	(Olofsson, Vallstrom et al. 2010, Zavan, Bitto et al. 2019)
QDY56617.	periplasmic chaperone SurA, HP0659	296.6 7	7	557.54	10	401.30	9	(Olofsson, Vallstrom et al. 2010, Zavan, Bitto et al. 2019)
QDY56947.	isocitrate dehydrogenase lcd, HP0027	296.6 6	8	244.73	9	93.43	5	(Olofsson, Vallstrom et al. 2010)
WP_00094 5142.1	plasminogen- binding protein PbgA, HP0508	295.9 2	7	348.13	6	279.35	5	(Olofsson, Vallstrom et al. 2010, Zavan, Bitto et al. 2019)
QDY56799.	flagellar hook- length control protein FliK, HP0906	291.4 5	6	0.00	0	635.27	12	(Zavan, Bitto et al. 2019)
WP_00059 1329.1	outer membrane protein HopL, HP1157	291.1 9	7	398.61	9	456.27	9	(Olofsson, Vallstrom et al. 2010)
QDY56071.	urease subunit alpha UreA, HP0073	276.5 8	8	908.39	5	253.14	2	(Olofsson, Vallstrom et al. 2010)
WP_00006 1442.1	FAD-dependent oxidoreductase, HP0086	274.4 1	5	114.04	4	81.71	3	(Olofsson, Vallstrom et al. 2010)
QDY56597.	acetyl-CoA C- acetyltransferase FadA, HP0690	274.1 7	5	142.94	2	0.00	0	(Olofsson, Vallstrom et al. 2010)
WP_00121 5737.1	aliphatic amidase, HP0294	272.1 7	6	120.60	2	178.64	4	(Olofsson, Vallstrom et al. 2010)
QDY56800.	flagellar hook cap protein FlgD, HP0907	270.6 2	7	0.00	0	205.82	4	(Olofsson, Vallstrom et al. 2010, Zavan, Bitto et al. 2019)
QDY56464. 1	outer membrane protein, HP0839	256.7 2	4	303.81	6	325.92	4	(Olofsson, Vallstrom et al. 2010, Zavan, Bitto et al. 2019)
EEC24940.	membrane fusion protein, HP0606	250.3 1	7	446.78	7	158.04	4	(Olofsson, Vallstrom et al. 2010)
QDY55668. 1	outer membrane protein HorJ, HP1469	233.9 0	6	361.48	7	266.69	6	(Olofsson, Vallstrom et al. 2010, Zavan, Bitto et al. 2019)
QDY55617.	predicted lipoprotein, HP1524	228.5 7	5	449.23	7	350.36	5	(Zavan, Bitto et al. 2019)
EEC24201.	periplasmic solute- binding protein, HP0940	224.8 3	7	163.92	7	221.40	5	(Olofsson, Vallstrom et al. 2010, Zavan, Bitto et al. 2019)
WP_00086 6621.1	peptide-methionine (R)-S-oxide reductase MsrAB, HP0224	208.8	3	734.23	13	223.35	4	(Olofsson, Vallstrom et al. 2010, Zavan, Bitto et al. 2019)
WP_00049 2196.1	thio:disulfide exchange protein DsbC, HP0377	206.4	4	325.52	6	254.90	2	(Olofsson, Vallstrom et al. 2010)

QDY55873.	carbonic anhydrase, HP1186	202.9 5	5	268.57	5	205.07	6	(Olofsson, Vallstrom et al. 2010, Zavan, Bitto et al. 2019)
QDY56593.	hypothetical protein, HP0694	197.0 9	3	417.59	5	161.88	3	(Olofsson, Vallstrom et al. 2010, Zavan, Bitto et al. 2019)
QDY55932.	hypothetical protein, HP1124	196.4 6	4	361.76	10	191.52	7	(Olofsson, Vallstrom et al. 2010, Zavan, Bitto et al. 2019)
WP_00186 1350.1	META domain- containing protein, HP1462	195.3 7	4	437.17	5	340.21	6	(Olofsson, Vallstrom et al. 2010, Zavan, Bitto et al. 2019)
QDY55749.	50S ribosomal protein L2, HP1316	191.5 2	4	97.63	2	0.00	0	(Olofsson, Vallstrom et al. 2010)
QDY55896. 1	NAD(P)/FAD- dependent oxidoreductase, HP1164	190.9 8	4	0.00	0	0.00	0	
EEC24568.	hypothetical protein, HP0563	190.9 2	2	210.98	2	0.00	0	(Olofsson, Vallstrom et al. 2010, Zavan, Bitto et al. 2019)
QDY56806.	outer membrane protein HofG, HP0914	185.8 7	5	432.31	9	587.01	9	(Olofsson, Vallstrom et al. 2010, Zavan, Bitto et al. 2019)
EEC24488.	outer membrane protein HopB, HP0913	171.2 9	3	226.23	3	192.94	3	(Olofsson, Vallstrom et al. 2010, Zavan, Bitto et al. 2019)
WP_00096 0466.1	class II fructose- 1,6-bisphosphate aldolase, HP0176	170.9 3	5	48.46	4	0.00	0	(Olofsson, Vallstrom et al. 2010)
EEC25210. 1	HP0018	165.1 1	2	0.00	0	0.00	0	(Olofsson, Vallstrom et al. 2010, Zavan, Bitto et al. 2019)
EEC24174.	hypothetical protein, HP0118	163.4 9	3	162.53	4	154.22	4	
EEC25339.	hypothetical protein, HP0318	160.0 7	5	76.59	2	0.00	0	
EEC24687.	translation elongation factor EF-G, HP1195	157.0 3	3	107.97	2	0.00	0	(Olofsson, Vallstrom et al. 2010)
QDY56697.	signal peptidase I LepB, HP0576	156.8 9	3	138.33	2	0.00	0	(Olofsson, Vallstrom et al. 2010)
WP_00070 6040.1	fumarate reductase flavoprotein FrdA, HP0192	154.4 3	3	187.20	6	0.00	0	(Olofsson, Vallstrom et al. 2010)
QDY57087.	cag pathogenicity island protein, HP0545	154.0 9	5	246.42	7	176.06	6	(Zavan, Bitto et al. 2019)
WP_00088 5323.1	2-oxoglutarate ferredoxin oxidoreductase subunit beta, HP0590	153.1 5	4	106.59	3	49.71	2	
QDY56711. 1	3-oxoacyl-ACP reductase FabG, HP0561	151.8 8	5	0.00	0	0.00	0	(Olofsson, Vallstrom et al. 2010)
WP_00118 3642.1	fumarate reductase cytochrome b FrdC, HP0193	150.0 5	2	0.00	0	0.00	0	(Olofsson, Vallstrom et al. 2010)

WP_00052 0987.1	molecular chaperone DnaK, HP0109	144.1 5	3	132.41	3	0.00	0	(Olofsson, Vallstrom et al. 2010)
QDY56517.	hypothetical protein, HP0781	141.7 3	2	258.63	5	102.83	3	(Olofsson, Vallstrom et al. 2010, Zavan, Bitto et al. 2019)
WP_00074 3462.1	UPF0323 family lipoprotein, HP0232	141.2 4	4	372.88	8	391.53	6	(Olofsson, Vallstrom et al. 2010, Zavan, Bitto et al. 2019)
EEC23875.	hypothetical protein, HP1108	140.8 5	3	0.00	0	0.00	0	(Olofsson, Vallstrom et al. 2010)
WP_00116 0549.1	fumarate hydratase FumC, HP1325	140.1 0	5	146.43	3	152.85	3	(Olofsson, Vallstrom et al. 2010)
QDY55969.	hypothetical protein, HP0367	137.5 1	4	0.00	0	151.44	4	(Olofsson, Vallstrom et al. 2010, Zavan, Bitto et al. 2019)
WP_00081 3741.1	nucleoside- diphosphate kinase Ndk, HP0198	136.9 5	2	0.00	0	0.00	0	
QDY56411.	molybdate ABC transporter substrate-binding protein, HP0473	135.8 9	3	137.68	2	165.31	3	(Zavan, Bitto et al. 2019)
EEC25054.	predicted cytochrome c peroxidase, HP1461	135.0 1	4	333.48	8	76.29	4	(Olofsson, Vallstrom et al. 2010, Zavan, Bitto et al. 2019)
QDY56580.	acetolactate synthase, HP0709	133.7 4	3	75.68	3	0.00	0	
QDY56623.	non-heme ferritin, HP0653	133.3 8	2	233.65	4	0.00	0	(Olofsson, Vallstrom et al. 2010)
QDY55861. 1	50S ribosomal protein L11, HP1202	130.2 7	4	0.00	0	0.00	0	(Olofsson, Vallstrom et al. 2010)
WP_00046 7393.1	50S ribosomal protein L5, HP1307	128.4 0	3	80.19	2	0.00	0	(Olofsson, Vallstrom et al. 2010)
QDY57056.	outer membrane protein HofA, HP0209	122.0 4	4	217.56	5	284.40	4	(Zavan, Bitto et al. 2019)
QDY56627.	aspartate ammonia-lyase, HP0649	119.9 9	5	0.00	0	0.00	0	(Olofsson, Vallstrom et al. 2010)
QDY56769. 1	DNA polymerase III subunit beta, HP0500	119.7 2	5	0.00	0	0.00	0	
QDY56735.	cag pathogenicity island protein Cag1, HP0520	117.9 6	3	157.66	4	99.17	2	(Olofsson, Vallstrom et al. 2010)
QDY56119.	DUF1104 domain- containing protein; HP0129	113.3 0	3	406.21	5	320.59	5	(Olofsson, Vallstrom et al. 2010, Zavan, Bitto et al. 2019)
QDY56376.	aminopeptidase P family protein, HP1037	106.6 2	5	40.45	2	49.34	2	(Olofsson, Vallstrom et al. 2010)
EEC24050.	ribosome- associated trigger factor, HP0795	103.9 9	4	45.14	2	0.00	0	(Olofsson, Vallstrom et al. 2010)
QDY56205.	YbhB/YbcL family Raf kinase inhibitor-like protein, HP0218	102.0 4	3	52.65	3	126.05	3	

QDY57002.	cytochrome bc complex cytochrome b, HP1539	101.6 5	2	123.08	2	0.00	0	(Olofsson, Vallstrom et al. 2010)
QDY56386.	transcriptional repressor Fur; HP1027	99.25	2	0.00	0	0.00	0	
EEC23825.	hypothetical protein, HP0080	98.73	2	104.28	2	0.00	0	(Olofsson, Vallstrom et al. 2010, Zavan, Bitto et al. 2019)
QDY55924.	ATP synthase subunit gamma, HP1133	97.19	2	206.58	4	108.70	2	(Olofsson, Vallstrom et al. 2010)
QDY56514.	lipoprotein chaperone LoIA, HP0785	95.16	2	215.81	4	132.12	2	(Olofsson, Vallstrom et al. 2010, Zavan, Bitto et al. 2019)
EEC24507.	beta barrel assembly factor BamD, HP1378	94.01	4	181.30	4	57.98	3	(Olofsson, Vallstrom et al. 2010, Zavan, Bitto et al. 2019)
QDY57009.	predicted lipoprotein, HP1546	93.58	2	111.07	2	153.73	3	(Olofsson, Vallstrom et al. 2010, Zavan, Bitto et al. 2019)
QDY57021.	class 1 fructose- bisphosphatase, HP1385	91.71	2	0.00	0	0.00	0	(Olofsson, Vallstrom et al. 2010)
EEC25036.	phospholipid synthesis protein PIsX, HP0201	91.21	7	77.59	3	0.00	0	(Olofsson, Vallstrom et al. 2010)
EEC23979.	glutamine synthetase GlnA, HP0512	89.79	3	0.00	0	0.00	0	(Olofsson, Vallstrom et al. 2010)
EEC25112.	phospholipid biosynthesis protein PlsY, HP1509	86.29	2	0.00	0	0.00	0	
QDY57014. 1	preprotein translocase subunit YajC, HP1551	85.81	2	0.00	0	0.00	0	
QDY56151.	Sel1-like repeat protein, HP0160	84.90	4	253.23	4	231.56	3	(Olofsson, Vallstrom et al. 2010)
WP_00114 8292.1	YkgB family protein, HP0565	84.31	2	0.00	0	0.00	0	
QDY56183. 1	enoyl-[acyl-carrier- protein] reductase Fabl, HP0195	78.85	2	0.00	0	0.00	0	(Olofsson, Vallstrom et al. 2010)
WP_00186 1250.1	outer membrane beta-barrel protein, HP1056	78.65	3	124.09	2	0.00	0	(Olofsson, Vallstrom et al. 2010, Zavan, Bitto et al. 2019)
EEC24155.	methyl-accepting chemotaxis protein, HP0103	77.49	3	291.98	6	0.00	0	(Olofsson, Vallstrom et al. 2010)
EEC23926.	outer membrane protein HofD, HP0487	77.49	2	0.00	0	0.00	0	(Olofsson, Vallstrom et al. 2010, Zavan, Bitto et al. 2019)
QDY55747.	50S ribosomal protein L4, HP1318	77.30	2	0.00	0	0.00	0	(Olofsson, Vallstrom et al. 2010)
QDY55960.	Sel1 repeat protein HcpC, HP1098	74.14	3	163.07	8	144.10	6	(Zavan, Bitto et al. 2019)
QDY55958. 1	phosphogluconate dehydratase, HP1100	73.42	3	0.00	0	0.00	0	

QDY56761.         cag pathogenicity island protein, HP0546         66.93         2         0.00         0         0.00         0           WP_00003 restriction with the control of	
WP_00003 7885.1         subunit beta/beta', HP1198         2         191.97         3         154.95         2         (Olofsson, Value al. 2010, Zalue at	
EEC25102.     protein HorK, HP1501     al. 2010, Za et al.	
WP_00049 oxidase, cbb3-type	
WP_00015         NAD-binding         60.06         5         41.83         2         0.00         0         (Olofsson, Value)           2120.1         protein, HP1398         al. 20	
QDY55836. cytochrome c-553, 59.60 2 234.05 5 139.62 5 (Zavan, Bit 1 HP1227 2019	
General Republic Re	
2-oxoacid:acceptor oxidoreductase	
WP_00116         Hop family outer 0302.1         54.28         2         191.98         2         177.61         2	
EEC25132. hypothetical protein 54.18 3 0.00 0 0.00 0 (Zavan, Bit 1 HP1527 2019	
QDY56646. Ni/Fe hydrogenase, 53.26 2 66.66 3 0.00 0 HP0631	
proline	
WP_00122 dehydrogenase, HP0829 44.24 4 0.00 0 0.00 0 (Olofsson, Value 1.20)	
QDY55772. RNA polymerase subunit alpha, HP1293 (Olofsson, Value 2) (Olofsson, Value 2) (Olofsson, Value 2)	
QDY55614. competence protein 1 598.85 13 209.04 5 (Zavan, Bit 1 ComH, HP1527 0 0 0 2019	
QDY56572. DUF1104 domain- 1 containing protein HP0719/HP0720 0 0 0 273.79 6 (Zavan, Bit 2019	
EEC25038. hypothetical protein 1 269.15 3 285.69 2 (Zavan, Bit 1 HP0203 0 0 2019	
QDY56640. predicted 224.52 2 0.00 0 1 lipoprotein HP0637 0 0	•
WP_00077         outer membrane         172.83         2         0.00         0         (Olofsson, Value)           0228.1         beta-barrel protein, HP1055         0         0         0         al. 20	
WP_00186 TrbG/VirB9 family 145.70 3 141.27 3 1340.1 protein, HP0040 0 0	
QDY56198. Sel1 repeat protein 1 HcpA, HP0211 0 0 137.19 4 46.94 2 (Zavan, Bit	
QDY55899. Flavodoxin FldA, 134.75 4 0.00 0 1 HP1161 0 0	•

EEC24849.	TonB-system		1	134.01	3	0.00	0	
	energizer ExbB,			101.01	ŭ	0.00		
	HP1339	0	0					
	D-amino acid			120.22	2	0.00	0	
	dehydrogenase							
	DadA, HP0943	0	0	444.00	2	0.00	0	(Olofonous Mallatraus at
	hypothetical protein, HP0185	0	0	114.29		0.00	0	(Olofsson, Vallstrom et al. 2010)
	DUF4006 family	0	0	104.19	3	0.00	0	ai. 2010)
_	protein, HP0148	0	0	104.10	ı ı	0.00		
	sel1 repeat family		<u> </u>	102.07	3	0.00	0	
	protein	0	0					
	hypothetical			99.17	3	107.38	2	(Zavan, Bitto et al.
	protein, HP0304	0	0					2019)
	flagellar sheath-			0.00	0	337.80	6	(Olofsson, Vallstrom et
	associated autotransporter							al. 2010)
	FaaA,							
	HP0610/HP0609	0	0					
	outer membrane			96.31	2	334.86	6	(Olofsson, Vallstrom et
I I	protein HofB,							al. 2010, Zavan, Bitto
	HP1083	0	0					et al. 2019)
	DUF2147 domain-			86.72	2	0.00	0	(Zavan, Bitto et al.
	containing protein,	•						2019)
	HP1028	0	0	70.00	0	0.00	0	(Olafaaaa )/allataaaa at
	outer membrane protein FrpB-1,			73.60	2	0.00	0	(Olofsson, Vallstrom et al. 2010)
	HP0876	0	0					ai. 2010)
	hypothetical	0		72.31	2	0.00	0	(Zavan, Bitto et al.
	protein, HP0408	0	0		_			2019)
	hypothetical			68.20	2	0.00	0	(Olofsson, Vallstrom et
1	protein, HP0555							al. 2010, Zavan, Bitto
		0	0					et al. 2019)
	flagellar basal body			0.00	0	99.88	2	
	protein FliL, HP0809	0	0					
	vacuolating	0	0	0.00	0	83.51	3	(Olofsson, Vallstrom et
	cytotoxin domain			0.00		00.01		al. 2010, Zavan, Bitto
	protein, HP0289	0	0					et al. 2019)
	type II 3-			55.12	2	69.16	2	(Olofsson, Vallstrom et
I I	dehydroquinate							al. 2010)
	dehydratase AroQ,	_	_					
	HP1038	0	0	04.00	0	40.40	0	
	ATP F0F1 synthase subunit			64.92	2	49.18	2	
	B', HP1137	0	0					
	TonB-system	0	0	64.81	2	0.00	0	
	energizer ExbB			0	_	0.00		
	homolog, HP1445	0	0					
	hypothetical			62.61	2	0.00	0	(Olofsson, Vallstrom et
	protein, HP0628	0	0					al. 2010)
I I	neuraminyllactose-			61.36	2	0.00	0	
	binding hemagglutinin							
	family protein,							
	HP1081	0	0					
	twin-arginine	•	<u> </u>	54.65	2	0.00	0	
	translocase subunit				-			
	TatA, HP0320	0	0					

EEC25324.	periplasmic solute-			48.26	2	0.00	0	(Olofsson, Vallstrom et
1	binding protein							al. 2010)
	AppD, HP0301	0	0					
EEC25048.	hypothetical			47.59	4	0.00	0	(Zavan, Bitto et al.
1	protein, HP1455	0	0					2019)
EEC25060.	hypothetical			47.11	2	0.00	0	(Olofsson, Vallstrom et
1	protein, HP1467	0	0					al. 2010)
QDY56171.	CvpA family			44.83	2	0.00	0	
1	protein, HP0181	0	0					

<sup>1</sup>Indicate Mascot scores for proteins in the OMV samples prepared from wild-type *H. pylori* B128 and the Δ*hp0018* mutant strains H19 and H23. <sup>2</sup>Indicate the number of peptide fragments generated following trypsin digestion for each protein. <sup>3</sup>Identified as being significantly enriched in OMVs – 171 proteins (*Zavan et al. 2019*); 315 proteins (*Olofsson et al. 2010*) Identified 226 proteins – 84% were identified by Zavan or Olofsson; 52% were identified by Zavan as proteins that were enriched in OMVs.

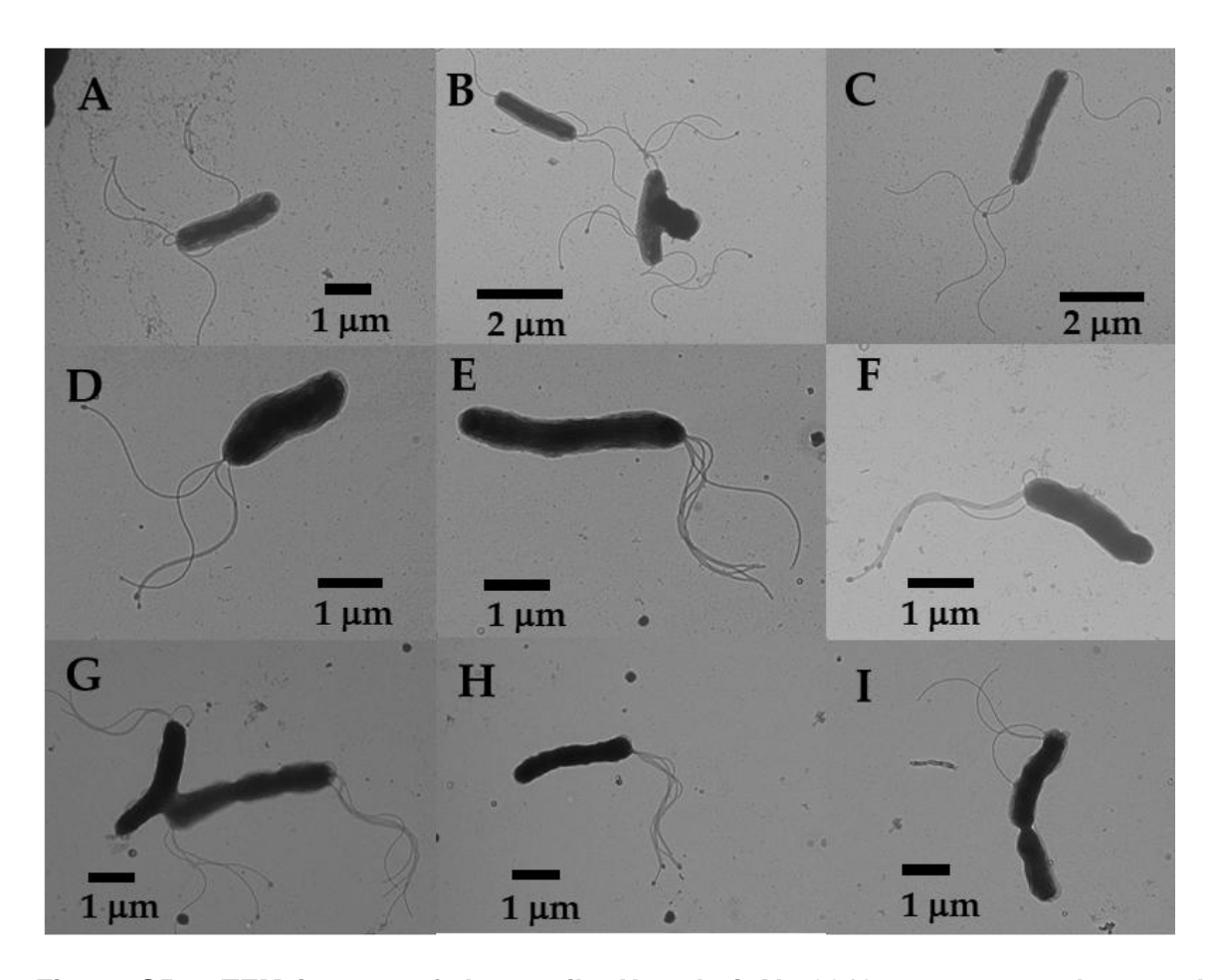


Figure S5.1. TEM images of the motile *H. pylori*  $\Delta hp0018$  mutant complemented with plasmid expressing the HP0018-myc fusion protein. Examples of wild-type *H. pylori* B128 cells are shown in panels A-C, while examples of the *H. pylori*  $\Delta hp0018$  mutant bearing the plasmid encoding the HP0018-myc fusion protein are shown in panels D-I.

Author Contributions: Conceptualization, K.R. and T.R.H.; methodology, K.R. and V.J.S.; formal analysis, K.R.; investigation, K.R.; writing—original draft preparation, K.R.; writing—review and editing, T.R.H. and V.J.S.; supervision, V.J.S. and T.R.H.; project administration, T.R.H.; funding acquisition, T.R.H. All authors have read and agreed to the published version of the manuscript.

Funding: This research was funded by the National Institutes of Health, grant number Al140444. Proteomics data generated in the study were supported by instrument grant NIH S10 OD025118 to the UGA PAMS facility.

Data Availability Statement: The original contributions presented in the study are included in the article and supplementary material, further inquiries can be directed to the corresponding author.

Acknowledgments: We thank Drs. Robert Maier and Stéphane Benoit for use of equipment and laboratory space, and Lindsay Berardi for technical assistance.

Conflicts of Interest: The authors declare no conflicts of interest. The funders had no role in the design of the study; in the collection, analyses, or interpretation of data; in the writing of the manuscript; or in the decision to publish the results.

# **Chapter 6: Conclusions and Future Directions**

# FapH, outer membrane associated flagellar motor accessory structures, and membrane permeability

# **Summary**

The Helicobacter pylori flagellar motor contains several accessory structures that are not found in the archetypal Escherichia coli and Salmonella enterica motors. H. pylori fapH (hp0838) encodes a previously uncharacterized lipoprotein and is in an operon with flgP, which encodes a known motor accessory protein. Chapter 2 detailed how deletion analysis of fapH showed that the gene is not required for motility in soft agar medium, but the mutant displayed a reduced growth rate and an increased sensitivity to bacitracin, which is an antibiotic that is normally excluded by the OM. Introducing a plasmid-borne copy of fapH into the H. pylori ΔfapH mutant suppressed the fitness defect and antibiotic sensitivity of the strain. A variant of the  $\Delta fapH$  mutant containing a frameshift mutation in pflA, which resulted in paralyzed flagella, displayed wild-type growth rate and resistance to bacitracin, suggesting the fitness defect and antibiotic sensitivity of the  $\Delta fapH$  mutant are dependent on flagellar rotation. Comparative analysis of *in-situ* structures of the wild type and  $\Delta fapH$  mutant motors revealed the  $\Delta fapH$  mutant motor lacked a previously undescribed ring-like structure with 18-fold symmetry located near the outer membrane, which was named the FapH ring. The data suggest that the FapH ring helps to preserve OM barrier function during flagellar rotation. Chapter 3 further investigated the isolation and characterization of bacitracin resistant isolates of  $\Delta fapH$  mutants. Two of the isolates had a nonsense mutationin lpxF, which encodes a phosphatase that removes the 4'-phosphate from lipid A. In the absence of LpxF, lipid A is phosphorylated at both the 1 and 4' positions, and we postulate that this modification stabilizes the outer leaflet of the OM and protects the barrier function of the OM in the absence of the FapH ring. The other bacitracin resistant isolate had mutations in the ferric uptake regulator gene, fur. H. pylori Fur is a global regulator and we hypothesize that the

mutations in *fur* alter the expression of one or more genes, which are responsible for the bacitracin resistance.

# **Future Directions: Investigating FapH interaction partners**

Chapter 2 detailed FapH interaction partners that were identified by co-immunoprecipitation and validated by BACTH including HP1454, HP1456, FlgP, and FapH with itself (Fig. 2.5). A Δhp1456 deletion mutant was constructed and characterized by cryo-ET but the motor did not appear to differ from the wild type (**Fig. S2.7**). Introducing a HP1456-myc into  $\Delta hp1456$  and performing coimmunoprecipitation did not yield quality interaction partners or FapH (Fig. S2.7). A BACTH experiment detailed in the Chapter 2 appendix using the known flagellar motor proteins FlgH, FlgI, suspected flagellar motor protein FlgQ, and co-immunoprecipitation candidate HP1457 did not validate any new protein-protein interactions (Fig. A2.1). To further investigate interaction partners of FapH, and identify other protein componenents of the flagellar motor near the OM, additional co-IP experiments should be conducted. In the future, hp1454 and/or hp1457 mutants and myc-tagged proteins may be used to further investigate these interactions. It may be valuable to pursue more sensitive mass spectrometry services that are better able to identify proteins products in SDS-PAGE gel samples. About half of all the samples from FapH-myc, FlgP-myc, HP1456-myc, and wild type that we submitted to the UGA proteomics core were unable to identify any proteins, despite there being discernable bands on the SDS-PAGE with Coomassie staining. I would have liked to have training in mass spectrometry to be better able to interpret the results of the proteomics and troubleshoot the results. Additionally, scaling up the formaldehyde cross lining of whole cell lysates as described in Chapter 2 Appendix may allow for enough sample to be analyzed by mass spectrometry fingerprinting.

# Future Directions: Investigation of outer-membrane associated flagellar motor accessory structures

The purpose of identifying interaction partners of FapH is to identify uncharacterized flagellar motor accessory structures. The structures that we refer to as the basal disk and outer disk (**Fig. 1.4**) are comprised of unknown proteins, although we suspect that FlgP is in there. Besides FlgP, we do not have any candidate proteins for the structures in this region. The flagellar motor of  $\Delta hp1456$  does not differ from wild type (**Fig. S2.7**), and other proteins like HopD and FtsH identified in the proteomics from FapH-myc are unlikely to form flagellar motor structures (**Table S2.3**). At this time, a *flgP::kan-sacB* mutant is being analyzed by cryo-ET and we are awaiting the

results. I think the best path towards investigating the unknown proteins in the outer membrane region is additional co-immunoprecipitation experiments with FapH-myc and FlgP-myc with more sensitivity mass spectrometry.

# Future Directions: Antibiotic sensitivity and membrane permeability

The most interesting result detailed in **Chapter 2** may be the sensitivity of the motile  $\Delta fapH$  to bacitracin (Fig. 2.3). Bacitracin is a large cyclic polypeptide antibiotic that interferes with peptidoglycan biosynthesis by inhibiting the synthesis of lipid II. In the motile  $\Delta fapH$  but not the non-motile ΔfapH the cells are highly sensitive to bacitracin in an efficiency of plating and motility assay (Fig. 2.3). The hypothesis then is that motility, and therefore flagellar rotation, is essential for bacitracin to enter the cell. Bacitracin must pass the outer membrane, so membrane permeability may be increased in the motile  $\Delta fapH$  mutant. Mutations in IpxF and fur detailed in **Chapter 3** appear to rescue the sensitivity of  $\Delta fapH$  to bacitracin by altering membrane permeability and flagellar gene regulation.  $\Delta fapH \Delta lpxF$  mutants (Fig. 3.1) are effectively clean deletions in *lpxF* because the stop codon is introduced within the signal peptide. LpxF is involved in removing the phosphate group from lipid A. Additional experiments could be devised that involve creating deletions in the ΔfapH background of genes involved in lipid A biogenesis and assessing the sensitivity to bacitracin.  $\Delta fapH \Delta fur$  mutants have reduced sensitivity to bacitracin like  $\Delta fapH \Delta lpxF$  mutants (**Fig. 3.5**) but the reason for this is unknown.  $\Delta fapH \Delta fur$  strains have reduced flagellation (Fig. 3.3) and Fur is a known regulator of flagellar gene expression, so this mutant may have either fewer total flagella or partially assembled flagellar basal bodies. Other possibilities include altered gene expression of OM proteins, lipid biogenesis proteins, or proteins involved in LPS biosynthesis, that could be investigated through RNAseg.

At this time, we have no direct evidence that altered membrane permeability is the reason bacitracin is able to enter the cell. An experiment to assess this would involve measuring molecules entering the cell under the condition of flagellar rotation. I attempted to perform this experiment with fluorescently labeled dextrans and imaging with fluorescent microscopy but the result was unspecific binding of the dextran to the wild type cells. I tried to incubate the cells with 1:10 molar concentration fluorescently labeled dextran:unlabeled dextran, but this experiment has proved challenging because the cells are struggling to grow in this condition. I am performing the experiment by inoculating cells to semi-solid agar with the addition of the dextrans, and swim halos are small with the high concentration of unlabeled dextran. I have not yet seen fluorescently labeled  $\Delta fapH$  and unlabeled wild type cells. Liquid culture incubation is another option, but this does not require motility for the cells to grow so it is unclear how many cells have rotating flagella

and if the molecules could enter the cell. If the experiment were successful, flow cytometry provides another method for quantifying the amount of labeled dextran entering the cell.

# Inner membrane associated flagellar motor structures and rod-cage connection

### **SUMMARY**

**Chapter 4** characterized *H. pylori* flagellar motor accessory structures associated with the inner membrane, spanning from the MS-ring to the cage. Comparative analyses of *in-situ* flagellar motor structures from *pflA*, *pflB*, and *flgY* mutants and wild-type *H. pylori* reveal that FlgY forms a 13-fold proximal spoke-ring around the MS-ring, and that PflA and PflB form an 18-fold distal spoke-ring enclosing 18 torque-generating stator complexes. A combination of individual structures predicted by AlphaFold and experimentally confirmed protein-protein interactions with *in-situ* motor structures enabled us to build a pseudo-atomic model of the *H. pylori* motor. Our model suggests that the FlgY spoke-ring functions as a bearing around the rotating MS-ring and as a template for stabilizing the PflA-PflB spoke-ring, thus enabling the recruitment of 18 stator complexes for high-torque generation in each motor. Overall, our study sheds light on how this novel spoke-ring network between the MS-ring and stator complexes enables the unique motility of *H. pylori*. As these accessory proteins are conserved in the phylum Campylobacterota, our findings apply broadly to a better understanding of how polar flagella help bacteria thrive in gastric and enteric niches.

# Future Directions: Investigation of FlgY spoke-ring function

Chapter 4 details the characterization of the FlgY spoke-ring structure located between the MS-ring  $\beta$ -collar and PflA distal spokes. This structure is required for formation of the PflA distal spokes, but is not required for motility, as  $\Delta flgY$  is able to swim out from the point of inoculation (**Fig. 4.2**). We hypothesize in **Chapter 4** that the FlgY spoke-ring functions as a bushing like the LP-ring, as there is a small gap between the FlgY spoke-ring and MS-ring with positively and negatively charged corresponding residues on these structures. Given that the FlgY spoke ring is not required for motor function, I hypothesize that it is required for stability of the motor during flagellar rotation. In the absence of the structure the cells are less than half as motile as wild type

(**Fig. 4.2A**). I hypothesize that the lack of stability during flagellar function results in the motor defect and could be seen by single cell tracking. A single cell tracking experiment using the wild type as a control and  $\Delta flgY$  mutant could be conducted to observe the swimming behavior of the mutant cells. **Chapter 1** describes the swimming behavior of *H. pylori* as run-reverse, where the flagellar bundle functions as a single unit to push or pull the cell. If the motor of the  $\Delta flgY$  mutant is less stable, this may be evident by dissociated flagellar bundles, resulting in cells that are unable to swim in a straight line.

# **Future Directions: Investigating different length PfIA proteins**

The **Chapter 4 Appendix** describes the discovery of a duplication region of pfIA in  $\Delta fapH$  isolates that was also present in a number of other frozen lab strains increasing the length of the protein by 58 amino acids (**Fig. A4.3**). This duplicated region would increase the length of the PfIA distal spoke with unknown effects on the rest of the motor structure. Cryo-ET imaging of motors from strains that contained and lacked this region could determine how the motor architecture differs between these strains. The cage structure may be slightly further away from the center of the motor, or the PfIA distal spoke may be bent to accommodate the longer protein. One issue is that the duplication event may be unstable and the mutations may revert back to wild type at a high rate, making investigations challenging. One solution could be to alter the DNA sequence of pfIA by substituting bases but maintaining the amino acid sequence. This would allow for native translation of the protein, but may eliminate the aspect of the coding sequence that results in the duplication event.

# Role of a candidate cell division protein in outer membrane stability

### **SUMMARY**

**Chapter 5** describes the characterization of a putative cell division protein in *H. pylori*. HP0018 is a predicted lipoprotein of unknown function that is conserved in *Helicobacter* species that have flagellar sheaths but is absent in *Helicobacter* species that have sheath-less flagella. Deletion of *hp0018* in *H. pylori* B128 resulted in formation of long chains of outer membrane vesicles, which

were most evident in an aflagellated variant of the Δhp0018 mutant that had a frameshift mutation in fliP. Flagellated cells of the  $\Delta hp0018$  mutant possessed what appear to be a normal flagellar sheath, suggesting that HP0018 is not required for sheath formation. Cells of the  $\Delta hp0018$  mutant were also less helical in shape compared to wild-type cells. A HP0018-super folder green fluorescent fusion protein expressed in the H. pylori Δhp0018 mutant formed fluorescent foci at the cell poles and lateral sites. Co-immunoprecipitation assays with HP0018 identified two enzymes involved in modification of cell wall peptidoglycan, AmiA and MltD, as potential HP0018 interaction partners. HP0018 may modulate the activity of AmiA or MltD, and in the absence of HP0018 the unregulated activity of these enzymes may alter the peptidoglycan layer in a manner that results in altered cell shape and hypervesiculation. To assess the interaction between HP0018 and AmiA and MltD, proteins could be purified and assayed to assess activity and binding affinity. Purifying only select domains of each protein and assessing activity could inform which domain and residues are responsible for protein activity. Once the important domains and residues are determined, mutants could be constructed to assess if the hypervesiculation phenotype is still present. A hypervesiculation mutant and known binding regions of HP0018-AmiA or HP0018-MltD would inform what each protein is doing during cell division.

# Future Directions: Investigating proteins involved in *H. pylori* cell division

**Chapter 5** describes how HP0018 may localize the cell pole and interact with cell division proteins. Co-immunoprecipitation assays identified AmiA and MltD as possible interaction partners that precipitated with HP0018-myc (**Table 5.1**). AmiA is a peptidoglycan hydrolase involved in conversion of *H. pylori* from spiral to coccoid, while MltD is a lytic transglycosylase involved in the rearrangement of the peptidoglycan. Future work could involve creating deletion mutants and reintroducing myc tagged versions of AmiA and MltD to further investigate interaction partners. Additionally, myc-tagged variants of partially expressed genes would further inform protein interactions, and which region of the protein the interactions are occurring. This may lead to the co-immunoprecipitation of additional cell-wall or cell division proteins, and additional work with interaction partners.

# **Future Directions: Characterizing PfIC**

PfIC is a flagellar motor accessory structure found in *C. jejuni* that has a homologue in *H. pylori* (HP0036). During construction of  $\Delta hp0018$  a mutation arose in *pfIC* where two Ts were deleted

in a run from 8 to 6, at position 31 of 966 (**Table S5.2**) with the result of the gene being put out of frame. The result is effectively a gene deletion in  $\Delta hp0018$  H19 and H23. H23 is the flagellated suppressor strain of H19, which has a frameshift in *fliP* (Table S5.2). Cryo-ET analysis of  $\Delta hp0018$   $\Delta pflC$  (H23) should be performed to investigate if PflC forms a flagellar motor accessory structure. HP0018 is a protein that localizes to the septum and is likely not a flagellar gene. Therefore,  $\Delta hp0018$  should not have an effect on analysis of PflC. We are in discussion with Jun Liu for imaging this strain.

The studies described in this dissertation have made meaningful progress towards characterizing flagellar motor proteins and lipoproteins in *H. pylori*. In 2025 we have characterized less than half of the genes in *H. pylori*, and large protein complexes in the flagellar motor are unknown. The proteins involved in motility and flagellation are critical to the successful colonization of the human stomach, so understanding these proteins in greater detail is important to understanding the pathogenicity of the bacterium. Most lipoproteins are OM-associated and therefore may be candidate targets for antibiotics or modulation by other drugs. Understanding flagellar proteins and lipoproteins is important for our understanding of *H. pylori*.

### References

Abby, S. S. and E. P. Rocha (2012). "The non-flagellar type III secretion system evolved from the bacterial flagellum and diversified into host-cell adapted systems." <u>PLoS Genet</u> **8**(9): e1002983.

Abedrabbo, S., J. Castellon, K. D. Collins, K. S. Johnson and K. M. Ottemann (2017). "Cooperation of two distinct coupling proteins creates chemosensory network connections." <a href="Proc Natl Acad Sci U S A">Proc Natl Acad Sci U S A</a> 114(11): 2970-2975.

Abramson, J., J. Adler, J. Dunger, R. Evans, T. Green, A. Pritzel, O. Ronneberger, L. Willmore, A. J. Ballard, J. Bambrick, S. W. Bodenstein, D. A. Evans, C. C. Hung, M. O'Neill, D. Reiman, K. Tunyasuvunakool, Z. Wu, A. Zemgulyte, E. Arvaniti, C. Beattie, O. Bertolli, A. Bridgland, A. Cherepanov, M. Congreve, A. I. Cowen-Rivers, A. Cowie, M. Figurnov, F. B. Fuchs, H. Gladman, R. Jain, Y. A. Khan, C. M. R. Low, K. Perlin, A. Potapenko, P. Savy, S. Singh, A. Stecula, A. Thillaisundaram, C. Tong, S. Yakneen, E. D. Zhong, M. Zielinski, A. Zidek, V. Bapst, P. Kohli, M. Jaderberg, D. Hassabis and J. M. Jumper (2024). "Accurate structure prediction of biomolecular interactions with AlphaFold 3." <a href="Nature 630">Nature 630</a>(8016): 493-500. Aguilera, L., L. Toloza, R. Gimenez, A. Odena, E. Oliveira, J. Aguilar, J. Badia and L. Baldoma (2014).

"Proteomic analysis of outer membrane vesicles from the probiotic strain Escherichia coli Nissle 1917." Proteomics **14**(2-3): 222-229.

Agulleiro, J. I. and J. J. Fernandez (2015). "Tomo3D 2.0--exploitation of advanced vector extensions (AVX) for 3D reconstruction." J Struct Biol 189(2): 147-152.

Allan, E., N. Dorrell, S. Foynes, M. Anyim and B. W. Wren (2000). "Mutational analysis of genes encoding the early flagellar components of Helicobacter pylori: evidence for transcriptional regulation of flagellin A biosynthesis." J Bacteriol **182**(18): 5274-5277.

Antani, J. D., A. X. Sumali, T. P. Lele and P. P. Lele (2021). "Asymmetric random walks reveal that the chemotaxis network modulates flagellar rotational bias in Helicobacter pylori." <u>Elife</u> **10**.

Arkowitz, R. A. and W. Wickner (1994). "SecD and SecF are required for the proton electrochemical gradient stimulation of preprotein translocation." <u>EMBO J 13(4)</u>: 954-963.

Armbruster, K. M. and T. C. Meredith (2017). "Identification of the Lyso-Form N-Acyl Intramolecular Transferase in Low-GC Firmicutes." J Bacteriol **199**(11).

Arroyo-Pérez, E. E., Hook, J.C., Alvarado, A., Wimmi, S., Glatter, T., Thormann, K.M., and Ringgaard, S (2024). "A conserved cell-pole determinant organizes proper polar flagellum formation." <u>eLife</u> **RP93004**. Arroyo-Perez, E. E. and S. Ringgaard (2021). "Interdependent Polar Localization of FlhF and FlhG and Their Importance for Flagellum Formation of Vibrio parahaemolyticus." <u>Front Microbiol</u> **12**: 655239. Aschtgen, M. S., J. B. Lynch, E. Koch, J. Schwartzman, M. McFall-Ngai and E. Ruby (2016). "Rotation of Vibrio fischeri Flagella Produces Outer Membrane Vesicles That Induce Host Development." <u>J Bacteriol</u> **198**(16): 2156-2165.

Astbury, W. T. B., C.; Weibull, C. (1955). "The structure of bacterial flagella." Symp. Soc. Exp. Biol. 9, 282–305.

Atherton, J. C. and M. J. Blaser (2009). "Coadaptation of Helicobacter pylori and humans: ancient history, modern implications." <u>J Clin Invest</u> **119**(9): 2475-2487.

Atkins, J. F., G. Loughran, P. R. Bhatt, A. E. Firth and P. V. Baranov (2016). "Ribosomal frameshifting and transcriptional slippage: From genetic steganography and cryptography to adventitious use." <u>Nucleic Acids Res</u> **44**(15): 7007-7078.

Attmannspacher, U., B. E. Scharf and R. M. Harshey (2008). "FliL is essential for swarming: motor rotation in absence of FliL fractures the flagellar rod in swarmer cells of Salmonella enterica." <u>Mol Microbiol</u> **68**(2): 328-341.

Auvray, F., J. Thomas, G. M. Fraser and C. Hughes (2001). "Flagellin polymerisation control by a cytosolic export chaperone." J Mol Biol **308**(2): 221-229.

Babu, M. M., M. L. Priya, A. T. Selvan, M. Madera, J. Gough, L. Aravind and K. Sankaran (2006). "A database of bacterial lipoproteins (DOLOP) with functional assignments to predicted lipoproteins." <u>J Bacteriol</u> **188**(8): 2761-2773.

Backert, S., M. Clyne and N. Tegtmeyer (2011). "Molecular mechanisms of gastric epithelial cell adhesion and injection of CagA by Helicobacter pylori." Cell Commun Signal **9**: 28.

Balaban, M. and D. R. Hendrixson (2011). "Polar flagellar biosynthesis and a regulator of flagellar number influence spatial parameters of cell division in Campylobacter jejuni." <u>PLoS Pathog</u> **7**(12): e1002420.

Balaban, M., S. N. Joslin and D. R. Hendrixson (2009). "FlhF and its GTPase activity are required for distinct processes in flagellar gene regulation and biosynthesis in Campylobacter jejuni." <u>J Bacteriol</u> **191**(21): 6602-6611.

Ball, G., H. Antelmann, P. R. Imbert, M. R. Gimenez, R. Voulhoux and B. Ize (2016). "Contribution of the Twin Arginine Translocation system to the exoproteome of Pseudomonas aeruginosa." <u>Sci Rep</u> 6: 27675. Bange, G., N. Kummerer, C. Engel, G. Bozkurt, K. Wild and I. Sinning (2010). "FlhA provides the adaptor for coordinated delivery of late flagella building blocks to the type III secretion system." <u>Proc Natl Acad Sci U S A</u> **107**(25): 11295-11300.

Bange, G., N. Kummerer, P. Grudnik, R. Lindner, G. Petzold, D. Kressler, E. Hurt, K. Wild and I. Sinning (2011). "Structural basis for the molecular evolution of SRP-GTPase activation by protein." <u>Nat Struct Mol Biol</u> **18**(12): 1376-1380.

Bange, G., G. Petzold, K. Wild, R. O. Parlitz and I. Sinning (2007). "The crystal structure of the third signal-recognition particle GTPase FlhF reveals a homodimer with bound GTP." <u>Proc Natl Acad Sci U S A</u> **104**(34): 13621-13625.

- Bansil, R., M. A. Constantino, C. Su-Arcaro, W. Liao, Z. Shen and J. G. Fox (2023). "Motility of Different Gastric Helicobacter spp." <u>Microorganisms</u> **11**(3).
- Barak, R., K. Prasad, A. Shainskaya, A. J. Wolfe and M. Eisenbach (2004). "Acetylation of the chemotaxis response regulator CheY by acetyl-CoA synthetase purified from Escherichia coli." J Mol Biol **342**(2): 383-401.
- Bardy, S. L., A. Briegel, S. Rainville and T. Krell (2017). "Recent advances and future prospects in bacterial and archaeal locomotion and signal transduction." <u>J Bacteriol</u> **199**(18): e00203-00217.
- Bari, W., K. M. Lee and S. S. Yoon (2012). "Structural and functional importance of outer membrane proteins in Vibrio cholerae flagellum." J Microbiol **50**(4): 631-637.
- Bartlett, D. H., B. B. Frantz, and P. Matsumura (1988). "Flagellar transcriptional activators FlbB and Flal: gene sequences and 5' consensus sequences of operons under FlbB and Flal control." <u>J. Bacteriol.</u> **170**: 1575-1581.
- Beatson, S. A., T. Minamino and M. J. Pallen (2006). "Variation in bacterial flagellins: from sequence to structure." <u>Trends Microbiol</u> **14**(4): 151-155.
- Beeby, M., J. L. Ferreira, P. Tripp, S. V. Albers and D. R. Mitchell (2020). "Propulsive nanomachines: the convergent evolution of archaella, flagella and cilia." <u>FEMS Microbiol Rev</u> **44**(3): 253-304.
- Beeby, M., D. A. Ribardo, C. A. Brennan, E. G. Ruby, G. J. Jensen and D. R. Hendrixson (2016). "Diverse high-torque bacterial flagellar motors assemble wider stator rings using a conserved protein scaffold." <u>Proc Natl Acad Sci U S A</u> **113**(13): E1917-1926.
- Behrens, W., T. Schweinitzer, J. Bal, M. Dorsch, A. Bleich, F. Kops, B. Brenneke, X. Didelot, S. Suerbaum and C. Josenhans (2013). "Role of energy sensor TlpD of Helicobacter pylori in gerbil colonization and genome analyses after adaptation in the gerbil." <u>Infect Immun</u> **81**(10): 3534-3551.
- Beier, D. and R. Frank (2000). "Molecular characterization of two-component systems of Helicobacter pylori." <u>J Bacteriol</u> **182**(8): 2068-2076.
- Berg, H. C. E. (2003). E. coli in Motion, Springer.
- Berks, B. C. (2015). "The twin-arginine protein translocation pathway." <u>Annu Rev Biochem</u> **84**: 843-864. Berthenet, E., L. Benejat, A. Menard, C. Varon, S. Lacomme, E. Gontier, J. Raymond, O. Boussaba, O. Toulza, A. Ducournau, A. Buissonniere, A. Giese, F. Megraud, E. Bessede, Q. Jehanne and P. Lehours (2019). "Whole-Genome Sequencing and Bioinformatics as Pertinent Tools to Support Helicobacteracae Taxonomy, Based on Three Strains Suspected to Belong to Novel Helicobacter Species." <u>Front Microbiol</u> **10**: 2820.
- Bertsche, U., T. Kast, B. Wolf, C. Fraipont, M. E. Aarsman, K. Kannenberg, M. von Rechenberg, M. Nguyen-Disteche, T. den Blaauwen, J. V. Holtje and W. Vollmer (2006). "Interaction between two murein (peptidoglycan) synthases, PBP3 and PBP1B, in Escherichia coli." Mol Microbiol 61(3): 675-690. Bi, S. and V. Sourjik (2018). "Stimulus sensing and signal processing in bacterial chemotaxis." Curr Opin Microbiol 45: 22-29.
- Bijlsma, J. J., C. M. Vandenbroucke-Grauls, S. H. Phadnis and J. G. Kusters (1999). "Identification of virulence genes of Helicobacter pylori by random insertion mutagenesis." <u>Infect Immun</u> **67**(5): 2433-2440.
- Biquet-Bisquert, A., G. Labesse, F. Pedaci and A. L. Nord (2021). "The Dynamic Ion Motive Force Powering the Bacterial Flagellar Motor." Front Microbiol **12**: 659464.
- Bishop, R. E., H. S. Gibbons, T. Guina, M. S. Trent, S. I. Miller and C. R. Raetz (2000). "Transfer of palmitate from phospholipids to lipid A in outer membranes of gram-negative bacteria." <u>EMBO J</u> **19**(19): 5071-5080.
- Blaser, M. J. (1994). "Helicobacter pylori: microbiology of a 'slow'bacterial infection." <u>Trends Microbiol</u> **1: 255-260**.
- Blatch GL, L. M. (1999). "The tetratricopeptide repeat: a structural motif mediating protein-protein interactions." <u>bioessays</u> (11):932-9.

Boivin, A. M., L. (1938). "Sur la résistance à l'acide trichloracétique de l'antigène flagellaire (antigène H) du bacille typhique et sur la nature chimique possible de cet antigène." <u>CR Soc. Biol. (Paris)</u> **129, 136–138.** 

Bonny, S. Q., X. Zhou, M. F. Khan, M. M. Rahman, Y. Xin, N. Vankadari, A. Tikhomirova, J. Homman-Ludiye and A. Roujeinikova (2024). "Functional and biochemical characterisation of remote homologues of type IV pili proteins PilN and PilO in Helicobacter pylori." <u>IUBMB Life</u> **76**(10): 780-787.

Botting, J. M., S. Tachiyama, K. H. Gibson, J. Liu, V. J. Starai and T. R. Hoover (2023). "FlgV forms a flagellar motor ring that is required for optimal motility of Helicobacter pylori." <u>PLoS One</u> **18**(11): e0287514.

Brennan, C. A., J. R. Hunt, N. Kremer, B. C. Krasity, M. A. Apicella, M. J. McFall-Ngai and E. G. Ruby (2014). "A model symbiosis reveals a role for sheathed-flagellum rotation in the release of immunogenic lipopolysaccharide." <u>Elife</u> **3**: e01579.

Brimer, C. D. and T. C. Montie (1998). "Cloning and comparison of fliC genes and identification of glycosylation in the flagellin of Pseudomonas aeruginosa a-type strains." <u>J Bacteriol</u> **180**(12): 3209-3217. Browning, D. F., S. A. Matthews, A. E. Rossiter, Y. R. Sevastsyanovich, M. Jeeves, J. L. Mason, T. J. Wells, C. A. Wardius, T. J. Knowles, A. F. Cunningham, V. N. Bavro, M. Overduin and I. R. Henderson (2013). "Mutational and topological analysis of the Escherichia coli BamA protein." <u>PLoS One</u> **8**(12): e84512. Brulle, J. K., T. Grau, A. Tschumi, Y. Auchli, R. Burri, S. Polsfuss, P. M. Keller, P. Hunziker and P. Sander (2010). "Cloning, expression and characterization of Mycobacterium tuberculosis lipoprotein LprF." <u>Biochem Biophys Res Commun</u> **391**(1): 679-684.

Brundage, L., J. P. Hendrick, E. Schiebel, A. J. Driessen and W. Wickner (1990). "The purified E. coli integral membrane protein SecY/E is sufficient for reconstitution of SecA-dependent precursor protein translocation." <u>Cell</u> **62**(4): 649-657.

Buddelmeijer, N. (2015). "The molecular mechanism of bacterial lipoprotein modification--how, when and why?" <u>FEMS Microbiol Rev</u> **39**(2): 246-261.

C. Stewart Goodwin1, J. A. A., Terry Chilvers1, Michelle Peters1, M. David Collins3, Lindsay Sly4, William McConnell1, William E. S. Harper1 (1989). "Transfer of Campylobacter pylori and Campylobacter mustelae to Helicobacter gen. nov. as Helicobacter pylori comb. nov. and Helicobacter mustelae comb, nov., Respectively Free." <a href="INTERNATIONAL JOURNAL OF SYSTEMATIC AND EVOLUTIONARY MICROBIOLOGY logo">INTERNATIONAL JOURNAL OF SYSTEMATIC AND EVOLUTIONARY</a> MICROBIOLOGY logo Vol. 39, No. 4: p. 397405.

C. Su, K. B., W. Liao, View ORCID ProfileM. A. Constantino, S. M. Decker, B. S. Turner, View ORCID ProfileR. Bansil (2020). "Comparison of motility of H. pylori in broth and mucin reveals the interplay of effect of acid on bacterium and the rheology of the medium it swims in." <u>BioRxiv</u>.

Calladine, C. R., B. F. Luisi and J. V. Pratap (2013). "A "mechanistic" explanation of the multiple helical forms adopted by bacterial flagellar filaments." J Mol Biol **425**(5): 914-928.

Cannon, K. S., E. Or, W. M. Clemons, Jr., Y. Shibata and T. A. Rapoport (2005). "Disulfide bridge formation between SecY and a translocating polypeptide localizes the translocation pore to the center of SecY." <u>J</u> <u>Cell Biol</u> **169**(2): 219-225.

Capdevila, S., F. M. Martinez-Granero, M. Sanchez-Contreras, R. Rivilla and M. Martin (2004). "Analysis of Pseudomonas fluorescens F113 genes implicated in flagellar filament synthesis and their role in competitive root colonization." <u>Microbiology (Reading)</u> **150**(Pt 11): 3889-3897.

Capurro, M. I., L. K. Greenfield, A. Prashar, S. Xia, M. Abdullah, H. Wong, X. Z. Zhong, N. Bertaux-Skeirik, J. Chakrabarti, I. Siddiqui, C. O'Brien, X. Dong, L. Robinson, R. M. Peek, Jr., D. J. Philpott, Y. Zavros, M. Helmrath and N. L. Jones (2019). "VacA generates a protective intracellular reservoir for Helicobacter pylori that is eliminated by activation of the lysosomal calcium channel TRPML1." <a href="Nat Microbiol">Nat Microbiol</a> 4(8): 1411-1423.

Carpenter, P. B., D. W. Hanlon and G. W. Ordal (1992). "flhF, a Bacillus subtilis flagellar gene that encodes a putative GTP-binding protein." Mol Microbiol **6**(18): 2705-2713.

- Carroll, B. L. and J. Liu (2020). "Structural Conservation and Adaptation of the Bacterial Flagella Motor." <u>Biomolecules</u> **10**(11).
- Carroll, B. L., T. Nishikino, W. Guo, S. Zhu, S. Kojima, M. Homma and J. Liu (2020). "The flagellar motor of Vibrio alginolyticus undergoes major structural remodeling during rotational switching." <u>Elife</u> **9**.
- Carron, M. A., V. R. Tran, C. Sugawa and J. M. Coticchia (2006). "Identification of Helicobacter pylori biofilms in human gastric mucosa." J Gastrointest Surg **10**(5): 712-717.
- Celebi, N., L. Yi, S. J. Facey, A. Kuhn and R. E. Dalbey (2006). "Membrane biogenesis of subunit II of cytochrome bo oxidase: contrasting requirements for insertion of N-terminal and C-terminal domains." <u>J Mol Biol</u> **357**(5): 1428-1436.
- Celli, J. P., B. S. Turner, N. H. Afdhal, S. Keates, I. Ghiran, C. P. Kelly, R. H. Ewoldt, G. H. McKinley, P. So, S. Erramilli and R. Bansil (2009). "Helicobacter pylori moves through mucus by reducing mucin viscoelasticity." Proc Natl Acad Sci U S A **106**(34): 14321-14326.
- Chaban, B., I. Coleman and M. Beeby (2018). "Evolution of higher torque in Campylobacter-type bacterial flagellar motors." <u>Sci Rep</u> **8**(1): 97.
- Chaddock, A. M., A. Mant, I. Karnauchov, S. Brink, R. G. Herrmann, R. B. Klosgen and C. Robinson (1995). "A new type of signal peptide: central role of a twin-arginine motif in transfer signals for the delta pH-dependent thylakoidal protein translocase." <u>EMBO J 14(12)</u>: 2715-2722.
- Chang, Y., K. H. Moon, X. Zhao, S. J. Norris, M. A. Motaleb and J. Liu (2019). "Structural insights into flagellar stator-rotor interactions." <u>Elife</u> 8.
- Chang, Y., K. Zhang, B. L. Carroll, X. Zhao, N. W. Charon, S. J. Norris, M. A. Motaleb, C. Li and J. Liu (2020). "Molecular mechanism for rotational switching of the bacterial flagellar motor." <u>Nat Struct Mol Biol</u> **27**(11): 1041-1047.
- Chaput, C., C. Ecobichon, N. Cayet, S. E. Girardin, C. Werts, S. Guadagnini, M. C. Prevost, D. Mengin-Lecreulx, A. Labigne and I. G. Boneca (2006). "Role of AmiA in the morphological transition of Helicobacter pylori and in immune escape." PLoS Pathog **2**(9): e97.
- Chaput, C., A. Labigne and I. G. Boneca (2007). "Characterization of Helicobacter pylori lytic transglycosylases Slt and MltD." <u>J Bacteriol</u> **189**(2): 422-429.
- Chatzi, K. E., M. F. Sardis, S. Karamanou and A. Economou (2013). "Breaking on through to the other side: protein export through the bacterial Sec system." <u>Biochem J</u> **449**(1): 25-37.
- Chen, S., M. Beeby, G. E. Murphy, J. R. Leadbetter, D. R. Hendrixson, A. Briegel, Z. Li, J. Shi, E. I. Tocheva, A. Muller, M. J. Dobro and G. J. Jensen (2011). "Structural diversity of bacterial flagellar motors." <u>EMBO J</u> **30**(14): 2972-2981.
- Cherak, S. J. and R. J. Turner (2017). "Assembly pathway of a bacterial complex iron sulfur molybdoenzyme." <u>Biomol Concepts</u> **8**(3-4): 155-167.
- Chimalakonda, G., N. Ruiz, S. S. Chng, R. A. Garner, D. Kahne and T. J. Silhavy (2011). "Lipoprotein LptE is required for the assembly of LptD by the beta-barrel assembly machine in the outer membrane of Escherichia coli." Proc Natl Acad Sci U S A **108**(6): 2492-2497.
- Chong, Z. S., W. F. Woo and S. S. Chng (2015). "Osmoporin OmpC forms a complex with MlaA to maintain outer membrane lipid asymmetry in Escherichia coli." Mol Microbiol **98**(6): 1133-1146.
- Chu, J. (2019). "Understanding the Role of Cardiolipin in Helicobacter Pylori Flagellar Synthesis." <u>Ph.D.</u> Thesis **University of Georgia, Athens, Georgia, 2019**.
- Chu, J., J. Liu and T. R. Hoover (2020). "Phylogenetic Distribution, Ultrastructure, and Function of Bacterial Flagellar Sheaths." <u>Biomolecules</u> **10**(3).
- Cline, K. (2015). "Mechanistic Aspects of Folded Protein Transport by the Twin Arginine Translocase (Tat)." J Biol Chem **290**(27): 16530-16538.
- Clyne, M., A. Labigne and B. Drumm (1995). "Helicobacter pylori requires an acidic environment to survive in the presence of urea." <u>Infect Immun</u> **63**(5): 1669-1673.

Colin, R. and V. Sourjik (2017). "Emergent properties of bacterial chemotaxis pathway." <u>Curr Opin Microbiol</u> **39**: 24-33.

Collins, K. D., T. M. Andermann, J. Draper, L. Sanders, S. M. Williams, C. Araghi and K. M. Ottemann (2016). "The Helicobacter pylori CZB Cytoplasmic Chemoreceptor TlpD Forms an Autonomous Polar Chemotaxis Signaling Complex That Mediates a Tactic Response to Oxidative Stress." J Bacteriol 198(11): 1563-1575.

Collinson, I., R. A. Corey and W. J. Allen (2015). "Channel crossing: how are proteins shipped across the bacterial plasma membrane?" <u>Philos Trans R Soc Lond B Biol Sci</u> **370**(1679).

Constantino, M. A., M. Jabbarzadeh, H. C. Fu and R. Bansil (2016). "Helical and rod-shaped bacteria swim in helical trajectories with little additional propulsion from helical shape." Sci Adv **2**(11): e1601661.

Copass, M., G. Grandi and R. Rappuoli (1997). "Introduction of unmarked mutations in the Helicobacter pylori vacA gene with a sucrose sensitivity marker." <u>Infect Immun</u> **65**(5): 1949-1952.

Correa, N. E., F. Peng and K. E. Klose (2005). "Roles of the regulatory proteins FlhF and FlhG in the Vibrio cholerae flagellar transcription hierarchy." J Bacteriol **187**(18): 6324-6332.

Coticchia, J. M., C. Sugawa, V. R. Tran, J. Gurrola, E. Kowalski and M. A. Carron (2006). "Presence and density of Helicobacter pylori biofilms in human gastric mucosa in patients with peptic ulcer disease." <u>J</u> Gastrointest Surg **10**(6): 883-889.

Cover, T. L. and M. J. Blaser (1992). "Helicobacter pylori and gastroduodenal disease." <u>Annu Rev Med</u> **43**: 135-145.

Crane, J. M. and L. L. Randall (2017). "The Sec System: Protein Export in Escherichia coli." <u>EcoSal Plus</u> **7**(2).

Cranford-Smith, T. and D. Huber (2018). "The way is the goal: how SecA transports proteins across the cytoplasmic membrane in bacteria." <u>FEMS Microbiol Lett</u> **365**(11).

Croxen, M. A., G. Sisson, R. Melano and P. S. Hoffman (2006). "The Helicobacter pylori chemotaxis receptor TlpB (HP0103) is required for pH taxis and for colonization of the gastric mucosa." <u>J Bacteriol</u> **188**(7): 2656-2665.

Cullen, T. W., D. K. Giles, L. N. Wolf, C. Ecobichon, I. G. Boneca and M. S. Trent (2011). "Helicobacter pylori versus the host: remodeling of the bacterial outer membrane is required for survival in the gastric mucosa." <u>PLoS Pathog</u> **7**(12): e1002454.

CXA, X. (2021). "FastTomo: A SerialEM Script for Collecting Electron Tomography Data." <u>bioRxiv</u>. Cymer, F., G. von Heijne and S. H. White (2015). "Mechanisms of integral membrane protein insertion and folding." <u>J Mol Biol</u> **427**(5): 999-1022.

D'Andrea, L. D. and L. Regan (2003). "TPR proteins: the versatile helix." <u>Trends Biochem Sci</u> **28**(12): 655-662.

Dalbey, R. E., A. Kuhn, L. Zhu and D. Kiefer (2014). "The membrane insertase YidC." <u>Biochim Biophys Acta</u> **1843**(8): 1489-1496.

Danielli, A., D. Roncarati, I. Delany, V. Chiarini, R. Rappuoli and V. Scarlato (2006). "In vivo dissection of the Helicobacter pylori Fur regulatory circuit by genome-wide location analysis." <u>J Bacteriol</u> **188**(13): 4654-4662.

Dasgupta, N., S. K. Arora and R. Ramphal (2000). "fleN, a gene that regulates flagellar number in Pseudomonas aeruginosa." J Bacteriol **182**(2): 357-364.

Davies, C., A. J. Taylor, A. Elmi, J. Winter, J. Liaw, A. D. Grabowska, O. Gundogdu, B. W. Wren, D. J. Kelly and N. Dorrell (2019). "Sodium Taurocholate Stimulates Campylobacter jejuni Outer Membrane Vesicle Production via Down-Regulation of the Maintenance of Lipid Asymmetry Pathway." <a href="Front Cell Infect">Front Cell Infect</a> Microbiol **9**: 177.

De Geyter, J., D. Smets, S. Karamanou and A. Economou (2019). "Inner Membrane Translocases and Insertases." <u>Subcell Biochem</u> **92**: 337-366.

- de Juan, D., F. Pazos and A. Valencia (2013). "Emerging methods in protein co-evolution." <u>Nat Rev Genet</u> **14**(4): 249-261.
- De Mot, R. and J. Vanderleyden (1994). "The C-terminal sequence conservation between OmpA-related outer membrane proteins and MotB suggests a common function in both gram-positive and gram-negative bacteria, possibly in the interaction of these domains with peptidoglycan." <u>Mol Microbiol</u> **12**(2): 333-334.
- Deatherage, D. E. and J. E. Barrick (2014). "Identification of mutations in laboratory-evolved microbes from next-generation sequencing data using breseq." <u>Methods Mol Biol</u> **1151**: 165-188.
- Dekker, N. (2000). "Outer-membrane phospholipase A: known structure, unknown biological function." Mol Microbiol **35**(4): 711-717.
- Deme, J. C., S. Johnson, O. Vickery, A. Aron, H. Monkhouse, T. Griffiths, R. H. James, B. C. Berks, J. W. Coulton, P. J. Stansfeld and S. M. Lea (2020). "Structures of the stator complex that drives rotation of the bacterial flagellum." <u>Nat Microbiol</u> **5**(12): 1553-1564.
- DePamphilis, M. L. and J. Adler (1971). "Attachment of flagellar basal bodies to the cell envelope: specific attachment to the outer, lipopolysaccharide membrane and the cyoplasmic membrane." <u>J Bacteriol</u> **105**(1): 396-407.
- Dian, C., S. Vitale, G. A. Leonard, C. Bahlawane, C. Fauquant, D. Leduc, C. Muller, H. de Reuse, I. Michaud-Soret and L. Terradot (2011). "The structure of the Helicobacter pylori ferric uptake regulator Fur reveals three functional metal binding sites." Mol Microbiol **79**(5): 1260-1275.
- Diepold, A., M. Amstutz, S. Abel, I. Sorg, U. Jenal and G. R. Cornelis (2010). "Deciphering the assembly of the Yersinia type III secretion injectisome." EMBO J **29**(11): 1928-1940.
- Diepold, A., U. Wiesand and G. R. Cornelis (2011). "The assembly of the export apparatus (YscR,S,T,U,V) of the Yersinia type III secretion apparatus occurs independently of other structural components and involves the formation of an YscV oligomer." <u>Mol Microbiol</u> **82**(2): 502-514.
- Dik, D. A., D. R. Marous, J. F. Fisher and S. Mobashery (2017). "Lytic transglycosylases: concinnity in concision of the bacterial cell wall." <u>Crit Rev Biochem Mol Biol</u> **52**(5): 503-542.
- Dinh, T. and T. G. Bernhardt (2011). "Using superfolder green fluorescent protein for periplasmic protein localization studies." J Bacteriol **193**(18): 4984-4987.
- Doig, P., N. Kinsella, P. Guerry and T. J. Trust (1996). "Characterization of a post-translational modification of Campylobacter flagellin: identification of a sero-specific glycosyl moiety." <u>Mol Microbiol</u> **19**(2): 379-387.
- Dorrell, N., M. C. Martino, R. A. Stabler, S. J. Ward, Z. W. Zhang, A. A. McColm, M. J. Farthing and B. W. Wren (1999). "Characterization of Helicobacter pylori PldA, a phospholipase with a role in colonization of the gastric mucosa." <u>Gastroenterology</u> **117**(5): 1098-1104.
- Douillard, F. P., K. A. Ryan, D. L. Caly, J. Hinds, A. A. Witney, S. E. Husain and P. W. O'Toole (2008). "Posttranscriptional regulation of flagellin synthesis in Helicobacter pylori by the RpoN chaperone HP0958." J Bacteriol **190**(24): 7975-7984.
- Drobnič, T. e. a. (2023). "Molecular model of a bacterial flagellar motor in situ reveals a "parts-list" of protein adaptations to increase torque." bioRxiv **2023.2009.2008.556779**.
- Dubois, A. and T. Boren (2007). "Helicobacter pylori is invasive and it may be a facultative intracellular organism." Cell Microbiol **9**(5): 1108-1116.
- Dudek, J., S. Pfeffer, P. H. Lee, M. Jung, A. Cavalie, V. Helms, F. Forster and R. Zimmermann (2015). "Protein transport into the human endoplasmic reticulum." <u>J Mol Biol</u> **427**(6 Pt A): 1159-1175.
- Eaton, K. A., D. R. Morgan and S. Krakowka (1992). "Motility as a factor in the colonisation of gnotobiotic piglets by Helicobacter pylori." J Med Microbiol **37**(2): 123-127.
- Eaton, K. A., S. Suerbaum, C. Josenhans and S. Krakowka (1996). "Colonization of gnotobiotic piglets by Helicobacter pylori deficient in two flagellin genes." <u>Infect Immun</u> **64**(7): 2445-2448.

- Eggenhofer, E., M. Haslbeck and B. Scharf (2004). "MotE serves as a new chaperone specific for the periplasmic motility protein, MotC, in Sinorhizobium meliloti." Mol Microbiol **52**(3): 701-712.
- Erhardt, M., H. M. Singer, D. H. Wee, J. P. Keener and K. T. Hughes (2011). "An infrequent molecular ruler controls flagellar hook length in Salmonella enterica." <u>EMBO J</u> **30**(14): 2948-2961.
- Erhardt, M., P. Wheatley, E. A. Kim, T. Hirano, Y. Zhang, M. K. Sarkar, K. T. Hughes and D. F. Blair (2017). "Mechanism of type-III protein secretion: Regulation of FlhA conformation by a functionally critical charged-residue cluster." Mol Microbiol **104**(2): 234-249.
- Ernst, S., A. K. Schonbauer, G. Bar, M. Borsch and A. Kuhn (2011). "YidC-driven membrane insertion of single fluorescent Pf3 coat proteins." J Mol Biol 412(2): 165-175.
- Espitia, C. and R. Mancilla (1989). "Identification, isolation and partial characterization of Mycobacterium tuberculosis glycoprotein antigens." Clin Exp Immunol **77**(3): 378-383.
- Evans, D. G., D. J. Evans, Jr., J. J. Moulds and D. Y. Graham (1988). "N-acetylneuraminyllactose-binding fibrillar hemagglutinin of Campylobacter pylori: a putative colonization factor antigen." <u>Infect Immun</u> **56**(11): 2896-2906.
- Fabiani, F. D., T. T. Renault, B. Peters, T. Dietsche, E. J. C. Galvez, A. Guse, K. Freier, E. Charpentier, T. Strowig, M. Franz-Wachtel, B. Macek, S. Wagner, M. Hensel and M. Erhardt (2017). "A flagellum-specific chaperone facilitates assembly of the core type III export apparatus of the bacterial flagellum." <u>PLoS Biol</u> **15**(8): e2002267.
- Facey, S. J., S. A. Neugebauer, S. Krauss and A. Kuhn (2007). "The mechanosensitive channel protein MscL is targeted by the SRP to the novel YidC membrane insertion pathway of Escherichia coli." <u>J Mol Biol</u> **365**(4): 995-1004.
- Fan, F., K. Ohnishi, N. R. Francis and R. M. Macnab (1997). "The FliP and FliR proteins of Salmonella typhimurium, putative components of the type III flagellar export apparatus, are located in the flagellar basal body." Mol Microbiol **26**(5): 1035-1046.
- Faulds-Pain, A., C. Birchall, C. Aldridge, W. D. Smith, G. Grimaldi, S. Nakamura, T. Miyata, J. Gray, G. Li, J. X. Tang, K. Namba, T. Minamino and P. D. Aldridge (2011). "Flagellin redundancy in Caulobacter crescentus and its implications for flagellar filament assembly." J Bacteriol 193(11): 2695-2707.
- Ferris, H. U., Y. Furukawa, T. Minamino, M. B. Kroetz, M. Kihara, K. Namba and R. M. Macnab (2005). "FlhB regulates ordered export of flagellar components via autocleavage mechanism." <u>J Biol Chem</u> **280**(50): 41236-41242.
- Ferris, H. U. and T. Minamino (2006). "Flipping the switch: bringing order to flagellar assembly." <u>Trends Microbiol</u> **14**(12): 519-526.
- Fischer, W. (2011). "Assembly and molecular mode of action of the Helicobacter pylori Cag type IV secretion apparatus." FEBS J 278(8): 1203-1212.
- Flanagan, J. J., J. C. Chen, Y. Miao, Y. Shao, J. Lin, P. E. Bock and A. E. Johnson (2003). "Signal recognition particle binds to ribosome-bound signal sequences with fluorescence-detected subnanomolar affinity that does not diminish as the nascent chain lengthens." J Biol Chem **278**(20): 18628-18637.
- Foegeding, N. J., R. R. Caston, M. S. McClain, M. D. Ohi and T. L. Cover (2016). "An Overview of Helicobacter pylori VacA Toxin Biology." Toxins (Basel) **8**(6).
- Foynes, S., N. Dorrell, S. J. Ward, R. A. Stabler, A. A. McColm, A. N. Rycroft and B. W. Wren (2000). "Helicobacter pylori possesses two CheY response regulators and a histidine kinase sensor, CheA, which are essential for chemotaxis and colonization of the gastric mucosa." <a href="Infect Immun">Infect Immun</a> 68(4): 2016-2023.
- Fuerst, J. A. (1980). "Bacterial sheathed flagella and the rotary motor model for the mechanism of bacterial motility." <u>J Theor Biol</u> **84**(4): 761-774.
- Fukumura, T., F. Makino, T. Dietsche, M. Kinoshita, T. Kato, S. Wagner, K. Namba, K. Imada and T. Minamino (2017). "Assembly and stoichiometry of the core structure of the bacterial flagellar type III export gate complex." <u>PLoS Biol</u> **15**(8): e2002281.

- Fung, C., S. Tan, M. Nakajima, E. C. Skoog, L. F. Camarillo-Guerrero, J. A. Klein, T. D. Lawley, J. V. Solnick, T. Fukami and M. R. Amieva (2019). "High-resolution mapping reveals that microniches in the gastric glands control Helicobacter pylori colonization of the stomach." <u>PLoS Biol</u> **17**(5): e3000231.
- Furukawa, Y., Y. Inoue, A. Sakaguchi, Y. Mori, T. Fukumura, T. Miyata, K. Namba and T. Minamino (2016). "Structural stability of flagellin subunit affects the rate of flagellin export in the absence of FliS chaperone." Mol Microbiol **102**(3): 405-416.
- G. Karimova, A. U., D. Ladant (2001). "Protein-protein interaction between Bacillus stearothermophilus tyrosyl-tRNA synthetase subdomains revealed by a bacterial two-hybrid system." <u>J Mol Microbiol Biotechnol</u> **3, 73-82**
- Gallusser, A. and A. Kuhn (1990). "Initial steps in protein membrane insertion. Bacteriophage M13 procoat protein binds to the membrane surface by electrostatic interaction." <u>EMBO J</u> **9**(9): 2723-2729.
- Gao, B., M. Lara-Tejero, M. Lefebre, A. L. Goodman and J. E. Galan (2014). "Novel components of the flagellar system in epsilonproteobacteria." <u>mBio</u> **5**(3): e01349-01314.
- Gasiorowski, E., R. Auger, X. Tian, S. Hicham, C. Ecobichon, S. Roure, M. V. Douglass, M. S. Trent, D. Mengin-Lecreulx, T. Touze and I. G. Boneca (2019). "HupA, the main undecaprenyl pyrophosphate and phosphatidylglycerol phosphate phosphatase in Helicobacter pylori is essential for colonization of the stomach." PLoS Pathog **15**(9): e1007972.
- Geis, G., H. Leying, S. Suerbaum, U. Mai and W. Opferkuch (1989). "Ultrastructure and chemical analysis of Campylobacter pylori flagella." J Clin Microbiol **27**(3): 436-441.
- Geis, G., S. Suerbaum, B. Forsthoff, H. Leying and W. Opferkuch (1993). "Ultrastructure and biochemical studies of the flagellar sheath of Helicobacter pylori." J Med Microbiol **38**(5): 371-377.
- Gennity, J. M. and M. Inouye (1991). "The protein sequence responsible for lipoprotein membrane localization in Escherichia coli exhibits remarkable specificity." J Biol Chem **266**(25): 16458-16464.
- Gibson, K., J. K. Chu, S. Zhu, D. Nguyen, J. Mrazek, J. Liu and T. R. Hoover (2022). "A Tripartite Efflux System Affects Flagellum Stability in Helicobacter pylori." Int J Mol Sci **23**(19).
- Gibson, K. H., J. M. Botting, N. Al-Otaibi, K. Maitre, J. Bergeron, V. J. Starai and T. R. Hoover (2023). "Control of the flagellation pattern in Helicobacter pylori by FlhF and FlhG." <u>J Bacteriol</u> **205**(9): e0011023.
- Gillen, K. L. and K. T. Hughes (1991). "Molecular characterization of flgM, a gene encoding a negative regulator of flagellin synthesis in Salmonella typhimurium." J Bacteriol **173**(20): 6453-6459.
- Goddard, T. D., C. C. Huang, E. C. Meng, E. F. Pettersen, G. S. Couch, J. H. Morris and T. E. Ferrin (2018). "UCSF ChimeraX: Meeting modern challenges in visualization and analysis." <u>Protein Sci</u> **27**(1): 14-25.
- Goffin, C. and J. M. Ghuysen (1998). "Multimodular penicillin-binding proteins: an enigmatic family of orthologs and paralogs." Microbiol Mol Biol Rev **62**(4): 1079-1093.
- Gogala, M., T. Becker, B. Beatrix, J. P. Armache, C. Barrio-Garcia, O. Berninghausen and R. Beckmann (2014). "Structures of the Sec61 complex engaged in nascent peptide translocation or membrane insertion." Nature **506**(7486): 107-110.
- Goon, S., J. F. Kelly, S. M. Logan, C. P. Ewing and P. Guerry (2003). "Pseudaminic acid, the major modification on Campylobacter flagellin, is synthesized via the Cj1293 gene." <u>Mol Microbiol</u> **50**(2): 659-671.
- Gouridis, G., S. Karamanou, I. Gelis, C. G. Kalodimos and A. Economou (2009). "Signal peptides are allosteric activators of the protein translocase." <u>Nature</u> **462**(7271): 363-367.
- Grabowicz, M. (2018). "Lipoprotein Transport: Greasing the Machines of Outer Membrane Biogenesis: Re-Examining Lipoprotein Transport Mechanisms Among Diverse Gram-Negative Bacteria While Exploring New Discoveries and Questions." <u>Bioessays</u> **40**(4): e1700187.
- Grabowicz, M. (2019). "Lipoproteins and Their Trafficking to the Outer Membrane." <u>EcoSal Plus</u> **8**(2). Grabowicz, M. and T. J. Silhavy (2017). "Redefining the essential trafficking pathway for outer membrane lipoproteins." <u>Proc Natl Acad Sci U S A</u> **114**(18): 4769-4774.

- Gray, A. N., J. M. Henderson-Frost, D. Boyd, S. Sharafi, H. Niki and M. B. Goldberg (2011). "Unbalanced charge distribution as a determinant for dependence of a subset of Escherichia coli membrane proteins on the membrane insertase YidC." <u>mBio</u> **2**(6).
- Green, J. C., C. Kahramanoglou, A. Rahman, A. M. Pender, N. Charbonnel and G. M. Fraser (2009). "Recruitment of the earliest component of the bacterial flagellum to the old cell division pole by a membrane-associated signal recognition particle family GTP-binding protein." <u>J Mol Biol</u> **391**(4): 679-690.
- Grognot, M. and K. M. Taute (2021). "More than propellers: how flagella shape bacterial motility behaviors." <u>Curr Opin Microbiol</u> **61**: 73-81.
- Guerrero-Ferreira, R. C., P. H. Viollier, B. Ely, J. S. Poindexter, M. Georgieva, G. J. Jensen and E. R. Wright (2011). "Alternative mechanism for bacteriophage adsorption to the motile bacterium Caulobacter crescentus." <a href="Proc Natl Acad Sci U S A 108">Proc Natl Acad Sci U S A 108</a>(24): 9963-9968.
- Guerry, P., R. A. Alm, M. E. Power, S. M. Logan and T. J. Trust (1991). "Role of two flagellin genes in Campylobacter motility." <u>J Bacteriol</u> **173**(15): 4757-4764.
- Guo, S., H. Xu, Y. Chang, M. A. Motaleb and J. Liu (2022). "FliL ring enhances the function of periplasmic flagella." <u>Proc Natl Acad Sci U S A</u> **119**(11): e2117245119.
- Gupta, R. S. (2006). "Molecular signatures (unique proteins and conserved indels) that are specific for the epsilon proteobacteria (Campylobacterales)." <u>BMC Genomics</u> **7**: 167.
- Gupta, S. D., W. Dowhan and H. C. Wu (1991). "Phosphatidylethanolamine is not essential for the Nacylation of apolipoprotein in Escherichia coli." <u>J Biol Chem</u> **266**(15): 9983-9986.
- Gwin, C. M., N. Prakash, J. Christian Belisario, L. Haider, M. L. Rosen, L. R. Martinez and N. W. Rigel (2018). "The apolipoprotein N-acyl transferase Lnt is dispensable for growth in Acinetobacter species." <u>Microbiology</u> (Reading) **164**(12): 1547-1556.
- Halic, M. and R. Beckmann (2005). "The signal recognition particle and its interactions during protein targeting." <u>Curr Opin Struct Biol</u> **15**(1): 116-125.
- Halte, M. and M. Erhardt (2021). "Protein Export via the Type III Secretion System of the Bacterial Flagellum." <u>Biomolecules</u> **11**(2).
- Hamsanathan, S. and S. M. Musser (2018). "The Tat protein transport system: intriguing questions and conundrums." <u>FEMS Microbiol Lett</u> **365**(12).
- Hara, T., S. Matsuyama and H. Tokuda (2003). "Mechanism underlying the inner membrane retention of Escherichia coli lipoproteins caused by Lol avoidance signals." J Biol Chem **278**(41): 40408-40414.
- Hartl, F. U., S. Lecker, E. Schiebel, J. P. Hendrick and W. Wickner (1990). "The binding cascade of SecB to SecA to SecY/E mediates preprotein targeting to the E. coli plasma membrane." Cell **63**(2): 269-279.
- Hathroubi, S., J. Zerebinski and K. M. Ottemann (2018). "Helicobacter pylori Biofilm Involves a Multigene Stress-Biased Response, Including a Structural Role for Flagella." <u>mBio</u> **9**(5).
- Henderson, L. D., T. R. S. Matthews-Palmer, C. J. Gulbronson, D. A. Ribardo, M. Beeby and D. R.
- Hendrixson (2020). "Diversification of Campylobacter jejuni Flagellar C-Ring Composition Impacts Its Structure and Function in Motility, Flagellar Assembly, and Cellular Processes." <u>mBio</u> **11**(1).
- Hendrixson, D. R., B. J. Akerley and V. J. DiRita (2001). "Transposon mutagenesis of Campylobacter jejuni identifies a bipartite energy taxis system required for motility." <u>Mol Microbiol</u> **40**(1): 214-224.
- Hennon, S. W., R. Soman, L. Zhu and R. E. Dalbey (2015). "YidC/Alb3/Oxa1 Family of Insertases." J Biol Chem **290**(24): 14866-14874.
- Heuermann, D. and R. Haas (1998). "A stable shuttle vector system for efficient genetic complementation of Helicobacter pylori strains by transformation and conjugation." <u>Mol Gen Genet</u> **257**(5): 519-528.
- Hillmann, F., M. Argentini and N. Buddelmeijer (2011). "Kinetics and phospholipid specificity of apolipoprotein N-acyltransferase." J Biol Chem **286**(32): 27936-27946.

- Hizlan, D., A. Robson, S. Whitehouse, V. A. Gold, J. Vonck, D. Mills, W. Kuhlbrandt and I. Collinson (2012). "Structure of the SecY complex unlocked by a preprotein mimic." <u>Cell Rep</u> **1**(1): 21-28.
- Hooi, J. K. Y., W. Y. Lai, W. K. Ng, M. M. Y. Suen, F. E. Underwood, D. Tanyingoh, P. Malfertheiner, D. Y. Graham, V. W. S. Wong, J. C. Y. Wu, F. K. L. Chan, J. J. Y. Sung, G. G. Kaplan and S. C. Ng (2017). "Global Prevalence of Helicobacter pylori Infection: Systematic Review and Meta-Analysis." <u>Gastroenterology</u> **153**(2): 420-429.
- Horler, R. S., A. Butcher, N. Papangelopoulos, P. D. Ashton and G. H. Thomas (2009). "EchoLOCATION: an in silico analysis of the subcellular locations of Escherichia coli proteins and comparison with experimentally derived locations." <u>Bioinformatics</u> **25**(2): 163-166.
- Horstmann, J. A., E. Zschieschang, T. Truschel, J. de Diego, M. Lunelli, M. Rohde, T. May, T. Strowig, T. Stradal, M. Kolbe and M. Erhardt (2017). "Flagellin phase-dependent swimming on epithelial cell surfaces contributes to productive Salmonella gut colonisation." <u>Cell Microbiol</u> **19**(8).
- Hosking, E. R., C. Vogt, E. P. Bakker and M. D. Manson (2006). "The Escherichia coli MotAB proton channel unplugged." J Mol Biol **364**(5): 921-937.
- Howitt, M. R., J. Y. Lee, P. Lertsethtakarn, R. Vogelmann, L. M. Joubert, K. M. Ottemann and M. R. Amieva (2011). "ChePep controls Helicobacter pylori Infection of the gastric glands and chemotaxis in the Epsilonproteobacteria." <u>mBio</u> **2**(4).
- Hu, H., M. Santiveri, N. Wadhwa, H. C. Berg, M. Erhardt and N. M. I. Taylor (2022). "Structural basis of torque generation in the bi-directional bacterial flagellar motor." <u>Trends Biochem Sci</u> **47**(2): 160-172. Huang, J. Y., E. G. Sweeney, M. Sigal, H. C. Zhang, S. J. Remington, M. A. Cantrell, C. J. Kuo, K. Guillemin and M. R. Amieva (2015). "Chemodetection and Destruction of Host Urea Allows Helicobacter pylori to
- Hughes, K. T., K. L. Gillen, M. J. Semon and J. E. Karlinsey (1993). "Sensing structural intermediates in bacterial flagellar assembly by export of a negative regulator." <u>Science</u> **262**(5137): 1277-1280.
- lino, T. (1974). "Assembly of Salmonella flagellin in vitro and in vivo." J Supramol Struct 2(2-4): 372-384.
- Ikeda, J. S., C. K. Schmitt, S. C. Darnell, P. R. Watson, J. Bispham, T. S. Wallis, D. L. Weinstein, E. S.

Locate the Epithelium." Cell Host Microbe 18(2): 147-156.

- Metcalf, P. Adams, C. D. O'Connor and A. D. O'Brien (2001). "Flagellar phase variation of Salmonella enterica serovar Typhimurium contributes to virulence in the murine typhoid infection model but does not influence Salmonella-induced enteropathogenesis." <u>Infect Immun</u> **69**(5): 3021-3030.
- Il Kim, M., C. Lee, J. Park, B. Y. Jeon and M. Hong (2018). "Crystal structure of Bacillus cereus flagellin and structure-guided fusion-protein designs." <u>Sci Rep</u> **8**(1): 5814.
- Imada, K., T. Minamino, M. Kinoshita, Y. Furukawa and K. Namba (2010). "Structural insight into the regulatory mechanisms of interactions of the flagellar type III chaperone FliT with its binding partners." <u>Proc Natl Acad Sci U S A</u> **107**(19): 8812-8817.
- Imada, K., T. Minamino, Y. Uchida, M. Kinoshita and K. Namba (2016). "Insight into the flagella type III export revealed by the complex structure of the type III ATPase and its regulator." <a href="Proc Natl Acad Sci U S">Proc Natl Acad Sci U S</a> A **113**(13): 3633-3638.
- Inoue, Y., Y. V. Morimoto, K. Namba and T. Minamino (2018). "Novel insights into the mechanism of well-ordered assembly of bacterial flagellar proteins in Salmonella." Sci Rep **8**(1): 1787.
- Inoue, Y., Y. Ogawa, M. Kinoshita, N. Terahara, M. Shimada, N. Kodera, T. Ando, K. Namba, A. Kitao, K. Imada and T. Minamino (2019). "Structural Insights into the Substrate Specificity Switch Mechanism of the Type III Protein Export Apparatus." <u>Structure</u> **27**(6): 965-976 e966.
- Inouye, S., T. Franceschini, M. Sato, K. Itakura and M. Inouye (1983). "Prolipoprotein signal peptidase of Escherichia coli requires a cysteine residue at the cleavage site." EMBO J **2**(1): 87-91.
- lorgulescu, G. (2009). "Saliva between normal and pathological. Important factors in determining systemic and oral health." J Med Life **2**(3): 303-307.

Ito, Y., K. Kanamaru, N. Taniguchi, S. Miyamoto and H. Tokuda (2006). "A novel ligand bound ABC transporter, LolCDE, provides insights into the molecular mechanisms underlying membrane detachment of bacterial lipoproteins." <u>Mol Microbiol</u> **62**(4): 1064-1075.

Jackowski, S. and C. O. Rock (1986). "Transfer of fatty acids from the 1-position of phosphatidylethanolamine to the major outer membrane lipoprotein of Escherichia coli." <u>J Biol Chem</u> **261**(24): 11328-11333.

Javaheri, A., T. Kruse, K. Moonens, R. Mejias-Luque, A. Debraekeleer, C. I. Asche, N. Tegtmeyer, B. Kalali, N. C. Bach, S. A. Sieber, D. J. Hill, V. Koniger, C. R. Hauck, R. Moskalenko, R. Haas, D. H. Busch, E. Klaile, H. Slevogt, A. Schmidt, S. Backert, H. Remaut, B. B. Singer and M. Gerhard (2016). "Helicobacter pylori adhesin HopQ engages in a virulence-enhancing interaction with human CEACAMs." Nat Microbiol 2: 16189.

Jia, L., M. Dienhart, M. Schramp, M. McCauley, K. Hell and R. A. Stuart (2003). "Yeast Oxa1 interacts with mitochondrial ribosomes: the importance of the C-terminal region of Oxa1." <u>EMBO J</u> **22**(24): 6438-6447. Jimenez-Pearson, M. A., I. Delany, V. Scarlato and D. Beier (2005). "Phosphate flow in the chemotactic response system of Helicobacter pylori." <u>Microbiology (Reading)</u> **151**(Pt 10): 3299-3311.

Johnson, S., J. C. Deme, E. J. Furlong, J. J. E. Caesar, F. F. V. Chevance, K. T. Hughes and S. M. Lea (2024). "Structural basis of directional switching by the bacterial flagellum." <u>Nat Microbiol</u> **9**(5): 1282-1292. Johnson, S., Y. H. Fong, J. C. Deme, E. J. Furlong, L. Kuhlen and S. M. Lea (2020). "Symmetry mismatch in the MS-ring of the bacterial flagellar rotor explains the structural coordination of secretion and rotation." <u>Nat Microbiol</u> **5**(7): 966-975.

Johnson, S., E. J. Furlong, J. C. Deme, A. L. Nord, J. J. E. Caesar, F. F. V. Chevance, R. M. Berry, K. T. Hughes and S. M. Lea (2021). "Molecular structure of the intact bacterial flagellar basal body." <u>Nat Microbiol</u> **6**(6): 712-721.

Jones, A. S., J. I. Austerberry, R. Dajani, J. Warwicker, R. Curtis, J. P. Derrick and C. Robinson (2016). "Proofreading of substrate structure by the Twin-Arginine Translocase is highly dependent on substrate conformational flexibility but surprisingly tolerant of surface charge and hydrophobicity changes." <u>Biochim Biophys Acta</u> **1863**(12): 3116-3124.

Josenhans, C., K. A. Eaton, T. Thevenot and S. Suerbaum (2000). "Switching of flagellar motility in Helicobacter pylori by reversible length variation of a short homopolymeric sequence repeat in fliP, a gene encoding a basal body protein." Infect Immun **68**(8): 4598-4603.

Josenhans, C., E. Niehus, S. Amersbach, A. Horster, C. Betz, B. Drescher, K. T. Hughes and S. Suerbaum (2002). "Functional characterization of the antagonistic flagellar late regulators FliA and FlgM of Helicobacter pylori and their effects on the H. pylori transcriptome." Mol Microbiol 43(2): 307-322. Jumper, J., R. Evans, A. Pritzel, T. Green, M. Figurnov, O. Ronneberger, K. Tunyasuvunakool, R. Bates, A. Zidek, A. Potapenko, A. Bridgland, C. Meyer, S. A. A. Kohl, A. J. Ballard, A. Cowie, B. Romera-Paredes, S. Nikolov, R. Jain, J. Adler, T. Back, S. Petersen, D. Reiman, E. Clancy, M. Zielinski, M. Steinegger, M. Pacholska, T. Berghammer, S. Bodenstein, D. Silver, O. Vinyals, A. W. Senior, K. Kavukcuoglu, P. Kohli and D. Hassabis (2021). "Highly accurate protein structure prediction with AlphaFold." Nature 596(7873): 583-589.

Kamiya, R., S. Asakura and S. Yamaguchi (1980). "Formation of helical filaments by copolymerization of two types of 'straight' flagellins." <u>Nature</u> **286**(5773): 628-630.

Kang, S. M., H. S. Kang, W. H. Chung, K. T. Kang and D. H. Kim (2024). "Structural Perspectives on Metal Dependent Roles of Ferric Uptake Regulator (Fur)." <u>Biomolecules</u> **14**(8).

Kaparakis, M., L. Turnbull, L. Carneiro, S. Firth, H. A. Coleman, H. C. Parkington, L. Le Bourhis, A. Karrar, J. Viala, J. Mak, M. L. Hutton, J. K. Davies, P. J. Crack, P. J. Hertzog, D. J. Philpott, S. E. Girardin, C. B. Whitchurch and R. L. Ferrero (2010). "Bacterial membrane vesicles deliver peptidoglycan to NOD1 in epithelial cells." <u>Cell Microbiol</u> **12**(3): 372-385.

Kaplan, M., P. Subramanian, D. Ghosal, C. M. Oikonomou, S. Pirbadian, R. Starwalt-Lee, S. K. Mageswaran, D. R. Ortega, J. A. Gralnick, M. Y. El-Naggar and G. J. Jensen (2019). "In situ imaging of the bacterial flagellar motor disassembly and assembly processes." <u>EMBO J</u> **38**(14): e100957.

Kaplan, M., M. J. Sweredoski, J. Rodrigues, E. I. Tocheva, Y. W. Chang, D. R. Ortega, M. Beeby and G. J. Jensen (2020). "Bacterial flagellar motor PL-ring disassembly subcomplexes are widespread and ancient." Proc Natl Acad Sci U S A **117**(16): 8941-8947.

Karim, Q. N., R. P. Logan, J. Puels, A. Karnholz and M. L. Worku (1998). "Measurement of motility of Helicobacter pylori, Campylobacter jejuni, and Escherichia coli by real time computer tracking using the Hobson BacTracker." J Clin Pathol **51**(8): 623-628.

Karimova, G., J. Pidoux, A. Ullmann and D. Ladant (1998). "A bacterial two-hybrid system based on a reconstituted signal transduction pathway." <u>Proc Natl Acad Sci U S A</u> **95**(10): 5752-5756.

Karlinsey, J. E., A. J. Pease, M. E. Winkler, J. L. Bailey and K. T. Hughes (1997). "The flk gene of Salmonella typhimurium couples flagellar P- and L-ring assembly to flagellar morphogenesis." <u>J Bacteriol</u> **179**(7): 2389-2400.

Keilberg, D., Y. Zavros, B. Shepherd, N. R. Salama and K. M. Ottemann (2016). "Spatial and Temporal Shifts in Bacterial Biogeography and Gland Occupation during the Development of a Chronic Infection." mBio **7**(5).

Khanra, N., P. Rossi, A. Economou and C. G. Kalodimos (2016). "Recognition and targeting mechanisms by chaperones in flagellum assembly and operation." <a href="Proc Natl Acad Sci U S A">Proc Natl Acad Sci U S A</a> 113(35): 9798-9803. Kiefer, D. and A. Kuhn (2018). "YidC-mediated membrane insertion." <a href="FEMS Microbiol Lett">FEMS Microbiol Lett</a> 365(12). Kihara, A., Y. Akiyama and K. Ito (1995). "FtsH is required for proteolytic elimination of uncomplexed forms of SecY, an essential protein translocase subunit." <a href="Proc Natl Acad Sci U S A">POC Natl Acad Sci U S A</a> 92(10): 4532-4536.

Kim, D., J. M. Paggi, C. Park, C. Bennett and S. L. Salzberg (2019). "Graph-based genome alignment and genotyping with HISAT2 and HISAT-genotype." <u>Nat Biotechnol</u> **37**(8): 907-915.

Kim, I. J. and S. R. Blanke (2012). "Remodeling the host environment: modulation of the gastric epithelium by the Helicobacter pylori vacuolating toxin (VacA)." Front Cell Infect Microbiol 2: 37.

Kim, S. Y., X. T. Thanh, K. Jeong, S. B. Kim, S. O. Pan, C. H. Jung, S. H. Hong, S. E. Lee and J. H. Rhee (2014). "Contribution of six flagellin genes to the flagellum biogenesis of Vibrio vulnificus and in vivo invasion." <a href="Infect Immun">Infect Immun</a> 82(1): 29-42.

Kobayashi, T., J. N. Rinker and H. Koffler (1959). "Purification and chemical properties of flagellin." <u>Arch Biochem Biophys</u> **84**: 342-362.

Kojima, S. and D. F. Blair (2001). "Conformational change in the stator of the bacterial flagellar motor." Biochemistry **40**(43): 13041-13050.

Kojima, S., H. Terashima and M. Homma (2020). "Regulation of the Single Polar Flagellar Biogenesis." <u>Biomolecules</u> **10**(4).

Kolich, L. R., Y. T. Chang, N. Coudray, S. I. Giacometti, M. R. MacRae, G. L. Isom, E. M. Teran, G. Bhabha and D. C. Ekiert (2020). "Structure of MlaFB uncovers novel mechanisms of ABC transporter regulation." Elife 9.

Kondo, S., Y. Imura, A. Mizuno, M. Homma and S. Kojima (2018). "Biochemical analysis of GTPase FlhF which controls the number and position of flagellar formation in marine Vibrio." Sci Rep 8(1): 12115. Koniger, V., L. Holsten, U. Harrison, B. Busch, E. Loell, Q. Zhao, D. A. Bonsor, A. Roth, A. Kengmo-Tchoupa, S. I. Smith, S. Mueller, E. J. Sundberg, W. Zimmermann, W. Fischer, C. R. Hauck and R. Haas (2016). "Helicobacter pylori exploits human CEACAMs via HopQ for adherence and translocation of CagA." Nat Microbiol 2: 16188.

Konovalova, A., D. E. Kahne and T. J. Silhavy (2017). "Outer Membrane Biogenesis." <u>Annu Rev Microbiol</u> **71**: 539-556.

Konovalova, A. and T. J. Silhavy (2015). "Outer membrane lipoprotein biogenesis: Lol is not the end." Philos Trans R Soc Lond B Biol Sci **370**(1679).

Kostrzynska, M., J. D. Betts, J. W. Austin and T. J. Trust (1991). "Identification, characterization, and spatial localization of two flagellin species in Helicobacter pylori flagella." <u>J Bacteriol</u> **173**(3): 937-946. Kostrzynska, M., P. W. O'Toole, D. E. Taylor and T. J. Trust (1994). "Molecular characterization of a conserved 20-kilodalton membrane-associated lipoprotein antigen of Helicobacter pylori." <u>J Bacteriol</u> **176**(19): 5938-5948.

Kremer, J. R., D. N. Mastronarde and J. R. McIntosh (1996). "Computer visualization of three-dimensional image data using IMOD." J Struct Biol 116(1): 71-76.

Kubori, T., S. Yamaguchi and S. Aizawa (1997). "Assembly of the switch complex onto the MS ring complex of Salmonella typhimurium does not require any other flagellar proteins." <u>J Bacteriol</u> **179**(3): 813-817.

Kuhn, A. and D. Kiefer (2017). "Membrane protein insertase YidC in bacteria and archaea." <u>Mol</u> Microbiol **103**(4): 590-594.

Kuhn, A., H. G. Koch and R. E. Dalbey (2017). "Targeting and Insertion of Membrane Proteins." <u>EcoSal Plus</u> **7**(2).

Kuhn, M. J., F. K. Schmidt, N. E. Farthing, F. M. Rossmann, B. Helm, L. G. Wilson, B. Eckhardt and K. M. Thormann (2018). "Spatial arrangement of several flagellins within bacterial flagella improves motility in different environments." Nat Commun **9**(1): 5369.

Kuipers, E. J. (1997). "Helicobacter pylori and the risk and management of associated diseases: gastritis, ulcer disease, atrophic gastritis and gastric cancer." Aliment Pharmacol Ther **11 Suppl 1**: 71-88.

Kumazaki, K., S. Chiba, M. Takemoto, A. Furukawa, K. Nishiyama, Y. Sugano, T. Mori, N. Dohmae, K. Hirata, Y. Nakada-Nakura, A. D. Maturana, Y. Tanaka, H. Mori, Y. Sugita, F. Arisaka, K. Ito, R. Ishitani, T. Tsukazaki and O. Nureki (2014). "Structural basis of Sec-independent membrane protein insertion by YidC." Nature **509**(7501): 516-520.

Kusumoto, A., N. Nishioka, S. Kojima and M. Homma (2009). "Mutational analysis of the GTP-binding motif of FlhF which regulates the number and placement of the polar flagellum in Vibrio alginolyticus." <u>J Biochem</u> **146**(5): 643-650.

Kusumoto, A., A. Shinohara, H. Terashima, S. Kojima, T. Yakushi and M. Homma (2008). "Collaboration of FlhF and FlhG to regulate polar-flagella number and localization in Vibrio alginolyticus." <u>Microbiology</u> (Reading) **154**(Pt 5): 1390-1399.

Kuzniatsova, L., T. M. Winstone and R. J. Turner (2016). "Identification of protein-protein interactions between the TatB and TatC subunits of the twin-arginine translocase system and respiratory enzyme specific chaperones." <u>Biochim Biophys Acta</u> **1858**(4): 767-775.

Lam, K. H., T. K. Ling and S. W. Au (2010). "Crystal structure of activated CheY1 from Helicobacter pylori." <u>J Bacteriol</u> **192**(9): 2324-2334.

Lamb, J. R., S. Tugendreich and P. Hieter (1995). "Tetratrico peptide repeat interactions: to TPR or not to TPR?" Trends Biochem Sci **20**(7): 257-259.

Langklotz, S., U. Baumann and F. Narberhaus (2012). "Structure and function of the bacterial AAA protease FtsH." <u>Biochim Biophys Acta</u> **1823**(1): 40-48.

Lappann, M., A. Otto, D. Becher and U. Vogel (2013). "Comparative proteome analysis of spontaneous outer membrane vesicles and purified outer membranes of Neisseria meningitidis." <u>J Bacteriol</u> **195**(19): 4425-4435.

Lasisi, T. J., Y. R. Raji and B. L. Salako (2016). "Salivary creatinine and urea analysis in patients with chronic kidney disease: a case control study." <u>BMC Nephrol</u> **17**: 10.

LaVallie, E. R. and M. L. Stahl (1989). "Cloning of the flagellin gene from Bacillus subtilis and complementation studies of an in vitro-derived deletion mutation." <u>J Bacteriol</u> **171**(6): 3085-3094. Leake, M. C., J. H. Chandler, G. H. Wadhams, F. Bai, R. M. Berry and J. P. Armitage (2006). "Stoichiometry and turnover in single, functioning membrane protein complexes." <u>Nature</u> **443**(7109): 355-358.

- Lee, H. C. and H. D. Bernstein (2001). "The targeting pathway of Escherichia coli presecretory and integral membrane proteins is specified by the hydrophobicity of the targeting signal." <a href="Proc Natl Acad">Proc Natl Acad</a> Sci U S A **98**(6): 3471-3476.
- Lee, L. K., M. A. Ginsburg, C. Crovace, M. Donohoe and D. Stock (2010). "Structure of the torque ring of the flagellar motor and the molecular basis for rotational switching." <u>Nature</u> **466**(7309): 996-1000. Lee, S. H. and J. E. Galan (2004). "Salmonella type III secretion-associated chaperones confer secretion-
- Leipe, D. D., Y. I. Wolf, E. V. Koonin and L. Aravind (2002). "Classification and evolution of P-loop GTPases and related ATPases." J Mol Biol **317**(1): 41-72.
- Leonard-Rivera, M. and R. Misra (2012). "Conserved residues of the putative L6 loop of Escherichia coli BamA play a critical role in the assembly of beta-barrel outer membrane proteins, including that of BamA itself." J Bacteriol **194**(17): 4662-4668.
- Lertsethtakarn, P., M. R. Howitt, J. Castellon, M. R. Amieva and K. M. Ottemann (2015). "Helicobacter pylori CheZ(HP) and ChePep form a novel chemotaxis-regulatory complex distinct from the core chemotaxis signaling proteins and the flagellar motor." Mol Microbiol **97**(6): 1063-1078.
- Lertsethtakarn, P., K. M. Ottemann and D. R. Hendrixson (2011). "Motility and chemotaxis in Campylobacter and Helicobacter." <u>Annu Rev Microbiol</u> **65**: 389-410.

pathway specificity." Mol Microbiol 51(2): 483-495.

- Lewenza, S., M. M. Mhlanga and A. P. Pugsley (2008). "Novel inner membrane retention signals in Pseudomonas aeruginosa lipoproteins." J Bacteriol **190**(18): 6119-6125.
- Li, G. and J. X. Tang (2006). "Low flagellar motor torque and high swimming efficiency of Caulobacter crescentus swarmer cells." Biophys J **91**(7): 2726-2734.
- Li, Y. E., Y. Wang, X. Du, T. Zhang, H. Y. Mak, S. E. Hancock, H. McEwen, E. Pandzic, R. M. Whan, Y. C. Aw, I. E. Lukmantara, Y. Yuan, X. Dong, A. Don, N. Turner, S. Qi and H. Yang (2021). "TMEM41B and VMP1 are scramblases and regulate the distribution of cholesterol and phosphatidylserine." J Cell Biol 220(6).
- Liao, Y., G. K. Smyth and W. Shi (2014). "featureCounts: an efficient general purpose program for assigning sequence reads to genomic features." <u>Bioinformatics</u> **30**(7): 923-930.
- Lienlaf, M., J. P. Morales, M. I. Diaz, R. Diaz, E. Bruce, F. Siegel, G. Leon, P. R. Harris and A. Venegas (2010). "Helicobacter pylori HopE and HopV porins present scarce expression among clinical isolates." World J Gastroenterol **16**(3): 320-329.
- Lill, R., K. Cunningham, L. A. Brundage, K. Ito, D. Oliver and W. Wickner (1989). "SecA protein hydrolyzes ATP and is an essential component of the protein translocation ATPase of Escherichia coli." <u>EMBO J</u> **8**(3): 961-966.
- Liu, A. N., K. W. Teng, Y. Chew, P. C. Wang, T. T. H. Nguyen and M. C. Kao (2022). "The Effects of HP0044 and HP1275 Knockout Mutations on the Structure and Function of Lipopolysaccharide in Helicobacter pylori Strain 26695." <u>Biomedicines</u> **10**(1).
- Liu, J., B. Hu, D. R. Morado, S. Jani, M. D. Manson and W. Margolin (2012). "Molecular architecture of chemoreceptor arrays revealed by cryoelectron tomography of Escherichia coli minicells." <a href="Proc Natl">Proc Natl</a> Acad Sci U S A **109**(23): E1481-1488.
- Liu, X. and K. M. Ottemann (2022). "Methylation-Independent Chemotaxis Systems Are the Norm for Gastric-Colonizing Helicobacter Species." J Bacteriol **204**(9): e0023122.
- Liu, X., A. Roujeinikova and K. M. Ottemann (2023). "FliL Functions in Diverse Microbes to Negatively Modulate Motor Output via Its N-Terminal Region." <u>mBio</u> **14**(2): e0028323.
- Liu, X., S. Tachiyama, X. Zhou, R. A. Mathias, S. Q. Bonny, M. F. Khan, Y. Xin, A. Roujeinikova, J. Liu and K. M. Ottemann (2024). "Bacterial flagella hijack type IV pili proteins to control motility." <u>Proc Natl Acad Sci</u> U S A **121**(4): e2317452121.
- Livak, K. J. and T. D. Schmittgen (2001). "Analysis of relative gene expression data using real-time quantitative PCR and the 2(-Delta Delta C(T)) Method." <u>Methods</u> **25**(4): 402-408.

- Logan, S. M., J. F. Kelly, P. Thibault, C. P. Ewing and P. Guerry (2002). "Structural heterogeneity of carbohydrate modifications affects serospecificity of Campylobacter flagellins." <u>Mol Microbiol</u> **46**(2): 587-597.
- Loh, J. T. and T. L. Cover (2006). "Requirement of histidine kinases HP0165 and HP1364 for acid resistance in Helicobacter pylori." Infect Immun **74**(5): 3052-3059.
- Lorenz, C., T. J. Dougherty and S. Lory (2019). "Correct Sorting of Lipoproteins into the Inner and Outer Membranes of Pseudomonas aeruginosa by the Escherichia coli LolCDE Transport System." <u>mBio</u> **10**(2). LoVullo, E. D., L. F. Wright, V. Isabella, J. F. Huntley and M. S. Pavelka, Jr. (2015). "Revisiting the Gramnegative lipoprotein paradigm." <u>J Bacteriol</u> **197**(10): 1705-1715.
- Lowenthal, A. C., C. Simon, A. S. Fair, K. Mehmood, K. Terry, S. Anastasia and K. M. Ottemann (2009). "A fixed-time diffusion analysis method determines that the three cheV genes of Helicobacter pylori differentially affect motility." <u>Microbiology (Reading)</u> **155**(Pt 4): 1181-1191.
- Lundstrom, A. M., K. Blom, V. Sundaeus and I. Bolin (2001). "HpaA shows variable surface localization but the gene expression is similar in different Helicobacter pylori strains." <u>Microb Pathog</u> **31**(5): 243-253. Lutkenhaus, J. (2012). "The ParA/MinD family puts things in their place." <u>Trends Microbiol</u> **20**(9): 411-418.
- Macnab, R. M. (2003). "How bacteria assemble flagella." Annu Rev Microbiol 57: 77-100.
- Malinverni, J. C. and T. J. Silhavy (2009). "An ABC transport system that maintains lipid asymmetry in the gram-negative outer membrane." <u>Proc Natl Acad Sci U S A</u> **106**(19): 8009-8014.
- Malinverni, J. C., J. Werner, S. Kim, J. G. Sklar, D. Kahne, R. Misra and T. J. Silhavy (2006). "YfiO stabilizes the YaeT complex and is essential for outer membrane protein assembly in Escherichia coli." <u>Mol Microbiol</u> **61**(1): 151-164.
- Manson, M. D. (2010). "Dynamic motors for bacterial flagella." <u>Proc Natl Acad Sci U S A</u> **107**(25): 11151-11152.
- Manson MD, T. P., Berg HC, Harold FM, Van der Drift C. (1977). "A protonmotive force drives bacterial flagella." <u>Proc Natl Acad Sci U S A</u> **74(7):3060-4**.
- Mao, G., Y. Zhao, X. Kang, Z. Li, Y. Zhang, X. Wang, F. Sun, K. Sankaran and X. C. Zhang (2016). "Crystal structure of E. coli lipoprotein diacylglyceryl transferase." <u>Nat Commun</u> **7**: 10198.
- Marshall, B. J. and J. R. Warren (1984). "Unidentified curved bacilli in the stomach of patients with gastritis and peptic ulceration." Lancet **1**(8390): 1311-1315.
- Martinez, L. E., J. M. Hardcastle, J. Wang, Z. Pincus, J. Tsang, T. R. Hoover, R. Bansil and N. R. Salama (2016). "Helicobacter pylori strains vary cell shape and flagellum number to maintain robust motility in viscous environments." Mol Microbiol **99**(1): 88-110.
- Mastronarde, D. N. (2005). "Automated electron microscope tomography using robust prediction of specimen movements." J Struct Biol 152(1): 36-51.
- Mastronarde, D. N. and S. R. Held (2017). "Automated tilt series alignment and tomographic reconstruction in IMOD." J Struct Biol 197(2): 102-113.
- Matlack, K. E., B. Misselwitz, K. Plath and T. A. Rapoport (1999). "BiP acts as a molecular ratchet during posttranslational transport of prepro-alpha factor across the ER membrane." Cell **97**(5): 553-564.
- Matsunami, H., C. S. Barker, Y. H. Yoon, M. Wolf and F. A. Samatey (2016). "Complete structure of the bacterial flagellar hook reveals extensive set of stabilizing interactions." Nat Commun **7**: 13425.
- Matsuyama, S., N. Yokota and H. Tokuda (1997). "A novel outer membrane lipoprotein, LolB (HemM), involved in the LolA (p20)-dependent localization of lipoproteins to the outer membrane of Escherichia coli." <u>EMBO J</u> **16**(23): 6947-6955.
- McClain, M. S., W. E. Boeglin, H. M. S. Algood and A. R. Brash (2024). "Fatty acids of Helicobacter pylori lipoproteins CagT and Lpp20." <u>Microbiol Spectr</u>: e0047024.
- McClain, M. S., B. J. Voss and T. L. Cover (2020). "Lipoprotein Processing and Sorting in Helicobacter pylori." <u>mBio</u> **11**(3).

McGee, D. J., M. L. Langford, E. L. Watson, J. E. Carter, Y. T. Chen and K. M. Ottemann (2005). "Colonization and inflammation deficiencies in Mongolian gerbils infected by Helicobacter pylori chemotaxis mutants." <u>Infect Immun</u> **73**(3): 1820-1827.

McGee, K., P. Horstedt and D. L. Milton (1996). "Identification and characterization of additional flagellin genes from Vibrio anguillarum." J Bacteriol **178**(17): 5188-5198.

Meuskens, I., A. Saragliadis, J. C. Leo and D. Linke (2019). "Type V Secretion Systems: An Overview of Passenger Domain Functions." <u>Front Microbiol</u> **10**: 1163.

Michie, K. A., A. Boysen, H. H. Low, J. Moller-Jensen and J. Lowe (2014). "LeoA, B and C from enterotoxigenic Escherichia coli (ETEC) are bacterial dynamins." <u>PLoS One</u> **9**(9): e107211.

Mimori, Y., I. Yamashita, K. Murata, Y. Fujiyoshi, K. Yonekura, C. Toyoshima and K. Namba (1995). "The structure of the R-type straight flagellar filament of Salmonella at 9 A resolution by electron cryomicroscopy." J Mol Biol **249**(1): 69-87.

Minamino, T. and K. Imada (2015). "The bacterial flagellar motor and its structural diversity." <u>Trends Microbiol</u> **23**(5): 267-274.

Minamino, T. and R. M. Macnab (1999). "Components of the Salmonella flagellar export apparatus and classification of export substrates." <u>J Bacteriol</u> **181**(5): 1388-1394.

Minamino, T. and R. M. MacNab (2000). "Interactions among components of the Salmonella flagellar export apparatus and its substrates." <u>Mol Microbiol</u> **35**(5): 1052-1064.

Minamino, T., Y. V. Morimoto, N. Hara, P. D. Aldridge and K. Namba (2016). "The Bacterial Flagellar Type III Export Gate Complex Is a Dual Fuel Engine That Can Use Both H+ and Na+ for Flagellar Protein Export." PLoS Pathog **12**(3): e1005495.

Minamino, T., Y. V. Morimoto, N. Hara and K. Namba (2011). "An energy transduction mechanism used in bacterial flagellar type III protein export." <u>Nat Commun</u> **2**: 475.

Minamino, T., Y. V. Morimoto, M. Kinoshita and K. Namba (2021). "Membrane voltage-dependent activation mechanism of the bacterial flagellar protein export apparatus." <u>Proc Natl Acad Sci U S A</u> **118**(22).

Mine, T., Y. Morita, A. Kataoka, T. Mizushima and T. Tsuchiya (1999). "Expression in Escherichia coli of a new multidrug efflux pump, MexXY, from Pseudomonas aeruginosa." <u>Antimicrob Agents Chemother</u> **43**(2): 415-417.

Mizote, T., H. Yoshiyama and T. Nakazawa (1997). "Urease-independent chemotactic responses of Helicobacter pylori to urea, urease inhibitors, and sodium bicarbonate." <a href="Infect Immun">Infect Immun</a> 65(4): 1519-1521. Mizutani, M., K. Mukaiyama, J. Xiao, M. Mori, R. Satou, S. Narita, S. Okuda and H. Tokuda (2013). "Functional differentiation of structurally similar membrane subunits of the ABC transporter LolCDE complex." <a href="FEBS Lett">FEBS Lett</a> 587(1): 23-29.

Moon, K. H., X. Zhao, A. Manne, J. Wang, Z. Yu, J. Liu and M. A. Motaleb (2016). "Spirochetes flagellar collar protein FlbB has astounding effects in orientation of periplasmic flagella, bacterial shape, motility, and assembly of motors in Borrelia burgdorferi." Mol Microbiol **102**(2): 336-348.

Morado, D. R., B. Hu and J. Liu (2016). "Using Tomoauto: A Protocol for High-throughput Automated Cryo-electron Tomography." J Vis Exp(107): e53608.

Moreno, Y. and M. A. Ferrus (2012). "Specific detection of cultivable Helicobacter pylori cells from wastewater treatment plants." Helicobacter **17**(5): 327-332.

Moss, S. F. (2017). "The Clinical Evidence Linking Helicobacter pylori to Gastric Cancer." <u>Cell Mol Gastroenterol Hepatol</u> **3**(2): 183-191.

Mukherjee, S. and D. B. Kearns (2014). "The structure and regulation of flagella in Bacillus subtilis." <u>Annu</u> Rev Genet **48**: 319-340.

Muller, M., H. G. Koch, K. Beck and U. Schafer (2001). "Protein traffic in bacteria: multiple routes from the ribosome to and across the membrane." <u>Prog Nucleic Acid Res Mol Biol</u> **66**: 107-157. Munch, R. (2003). "Robert Koch." Microbes Infect **5**(1): 69-74.

Murray, T. S. and B. I. Kazmierczak (2006). "FlhF is required for swimming and swarming in Pseudomonas aeruginosa." J Bacteriol **188**(19): 6995-7004.

Nagamori, S., I. N. Smirnova and H. R. Kaback (2004). "Role of YidC in folding of polytopic membrane proteins." J Cell Biol **165**(1): 53-62.

Nakamura, S., A. Leshansky, Y. Magariyama, K. Namba and S. Kudo (2014). "Direct measurement of helical cell motion of the spirochete leptospira." Biophys J **106**(1): 47-54.

Narita, S. and H. Tokuda (2009). "Biochemical characterization of an ABC transporter LptBFGC complex required for the outer membrane sorting of lipopolysaccharides." <u>FEBS Lett</u> **583**(13): 2160-2164. Narita, S. I. and H. Tokuda (2017). "Bacterial lipoproteins; biogenesis, sorting and quality control."

Biochim Biophys Acta Mol Cell Biol Lipids 1862(11): 1414-1423.

Necchi, V., P. Sommi, A. Vanoli, R. Fiocca, V. Ricci and E. Solcia (2017). "Natural history of Helicobacter pylori VacA toxin in human gastric epithelium in vivo: vacuoles and beyond." <u>Sci Rep</u> **7**(1): 14526. Nedeljkovic, M., D. E. Sastre and E. J. Sundberg (2021). "Bacterial Flagellar Filament: A Supramolecular Multifunctional Nanostructure." <u>Int J Mol Sci</u> **22**(14).

Neumann, S., C. H. Hansen, N. S. Wingreen and V. Sourjik (2010). "Differences in signalling by directly and indirectly binding ligands in bacterial chemotaxis." <u>EMBO J</u> **29**(20): 3484-3495.

Niehus, E., H. Gressmann, F. Ye, R. Schlapbach, M. Dehio, C. Dehio, A. Stack, T. F. Meyer, S. Suerbaum and C. Josenhans (2004). "Genome-wide analysis of transcriptional hierarchy and feedback regulation in the flagellar system of Helicobacter pylori." <u>Mol Microbiol</u> **52**(4): 947-961.

Nishijima, M., S. Nakaike, Y. Tamori and S. Nojima (1977). "Detergent-resistant phospholipase A of Escherichia coli K-12. Purification and properties." <u>Eur J Biochem</u> **73**(1): 115-124.

Noland, C. L., M. D. Kattke, J. Diao, S. L. Gloor, H. Pantua, M. Reichelt, A. K. Katakam, D. Yan, J. Kang, I. Zilberleyb, M. Xu, S. B. Kapadia and J. M. Murray (2017). "Structural insights into lipoprotein N-acylation by Escherichia coli apolipoprotein N-acyltransferase." <a href="Proc Natl Acad Sci U S A">Proc Natl Acad Sci U S A</a> 114(30): E6044-E6053. Nord, A. L., Y. Sowa, B. C. Steel, C. J. Lo and R. M. Berry (2017). "Speed of the bacterial flagellar motor near zero load depends on the number of stator units." <a href="Proc Natl Acad Sci U S A">Proc Natl Acad Sci U S A</a> 114(44): 11603-11608. Norqvist, A. and H. Wolf-Watz (1993). "Characterization of a novel chromosomal virulence locus involved in expression of a major surface flagellar sheath antigen of the fish pathogen Vibrio anguillarum." <a href="Infect Immun">Infect Immun</a> 61(6): 2434-2444.

O'Brien, E. J. and P. M. Bennett (1972). "Structure of straight flagella from a mutant Salmonella." <u>J Mol</u> Biol **70**(1): 133-152.

O'Toole, P. W., L. Janzon, P. Doig, J. Huang, M. Kostrzynska and T. J. Trust (1995). "The putative neuraminyllactose-binding hemagglutinin HpaA of Helicobacter pylori CCUG 17874 is a lipoprotein." <u>J Bacteriol</u> **177**(21): 6049-6057.

O'Toole, P. W., M. Kostrzynska and T. J. Trust (1994). "Non-motile mutants of Helicobacter pylori and Helicobacter mustelae defective in flagellar hook production." <u>Mol Microbiol</u> **14**(4): 691-703.

O'Toole, P. W., M. C. Lane and S. Porwollik (2000). "Helicobacter pylori motility." <u>Microbes Infect</u> **2**(10): 1207-1214.

Oakland, M., B. Jeon, O. Sahin, Z. Shen and Q. Zhang (2011). "Functional characterization of a lipoprotein-encoding operon in Campylobacter jejuni." <u>PLoS One</u> **6**(5): e20084.

Odenbreit, S., M. Till, D. Hofreuter, G. Faller and R. Haas (1999). "Genetic and functional characterization of the alpAB gene locus essential for the adhesion of Helicobacter pylori to human gastric tissue." <u>Mol Microbiol</u> **31**(5): 1537-1548.

Ohnishi, N., H. Yuasa, S. Tanaka, H. Sawa, M. Miura, A. Matsui, H. Higashi, M. Musashi, K. Iwabuchi, M. Suzuki, G. Yamada, T. Azuma and M. Hatakeyama (2008). "Transgenic expression of Helicobacter pylori CagA induces gastrointestinal and hematopoietic neoplasms in mouse." <a href="Proc Natl Acad Sci U S A">Proc Natl Acad Sci U S A</a> 105(3): 1003-1008.

Ojemalm, K., S. C. Botelho, C. Studle and G. von Heijne (2013). "Quantitative analysis of SecYEG-mediated insertion of transmembrane alpha-helices into the bacterial inner membrane." <u>J Mol Biol</u> **425**(15): 2813-2822.

Okuda, S., D. J. Sherman, T. J. Silhavy, N. Ruiz and D. Kahne (2016). "Lipopolysaccharide transport and assembly at the outer membrane: the PEZ model." <u>Nat Rev Microbiol</u> **14**(6): 337-345.

Okuda, S. and H. Tokuda (2009). "Model of mouth-to-mouth transfer of bacterial lipoproteins through inner membrane LolC, periplasmic LolA, and outer membrane LolB." <u>Proc Natl Acad Sci U S A</u> **106**(14): 5877-5882.

Olofsson, A., A. Vallstrom, K. Petzold, N. Tegtmeyer, J. Schleucher, S. Carlsson, R. Haas, S. Backert, S. N. Wai, G. Grobner and A. Arnqvist (2010). "Biochemical and functional characterization of Helicobacter pylori vesicles." <u>Mol Microbiol</u> **77**(6): 1539-1555.

Ono, H., A. Takashima, H. Hirata, M. Homma and S. Kojima (2015). "The MinD homolog FlhG regulates the synthesis of the single polar flagellum of Vibrio alginolyticus." <u>Mol Microbiol</u> **98**(1): 130-141.

Orfanoudaki, G. and A. Economou (2014). "Proteome-wide subcellular topologies of E. coli polypeptides database (STEPdb)." Mol Cell Proteomics **13**(12): 3674-3687.

Ortega, A., I. B. Zhulin and T. Krell (2017). "Sensory Repertoire of Bacterial Chemoreceptors." <u>Microbiol</u> <u>Mol Biol Rev</u> **81**(4).

Ortega, D. R. and I. B. Zhulin (2016). "Evolutionary Genomics Suggests That CheV Is an Additional Adaptor for Accommodating Specific Chemoreceptors within the Chemotaxis Signaling Complex." <u>PLoS Comput Biol</u> **12**(2): e1004723.

Ottemann, K. M. and A. C. Lowenthal (2002). "Helicobacter pylori uses motility for initial colonization and to attain robust infection." Infect Immun **70**(4): 1984-1990.

Pallen, M. J. and N. J. Matzke (2006). "From The Origin of Species to the origin of bacterial flagella." <u>Nat</u> Rev Microbiol **4**(10): 784-790.

Palmer, T., F. Sargent and B. C. Berks (2010). "The Tat Protein Export Pathway." <u>EcoSal Plus</u> **4**(1). Pandza, S., M. Baetens, C. H. Park, T. Au, M. Keyhan and A. Matin (2000). "The G-protein FlhF has a role in polar flagellar placement and general stress response induction in Pseudomonas putida." <u>Mol</u> Microbiol **36**(2): 414-423.

Paraskevopoulou, V., M. Schimpl, R. C. Overman, S. Stolnik, Y. Chen, L. Nguyen, G. S. Winkler, P. Gellert, J. S. Klassen and F. H. Falcone (2021). "Structural and binding characterization of the LacdiNAc-specific adhesin (LabA; HopD) exodomain from Helicobacter pylori." <u>Curr Res Struct Biol</u> **3**: 19-29.

Park, E., J. F. Menetret, J. C. Gumbart, S. J. Ludtke, W. Li, A. Whynot, T. A. Rapoport and C. W. Akey (2014). "Structure of the SecY channel during initiation of protein translocation." <u>Nature</u> **506**(7486): 102-106

Park, E. and T. A. Rapoport (2011). "Preserving the membrane barrier for small molecules during bacterial protein translocation." <u>Nature</u> **473**(7346): 239-242.

Parkinson, J. S., G. L. Hazelbauer and J. J. Falke (2015). "Signaling and sensory adaptation in Escherichia coli chemoreceptors: 2015 update." <u>Trends Microbiol</u> **23**(5): 257-266.

Partridge, J. D., Y. Dufour, Y. Hwang and R. M. Harshey (2023). "Flagellar motor remodeling during swarming requires FliL." <u>Mol Microbiol</u> **120**(5): 670-683.

Paul, K., M. Erhardt, T. Hirano, D. F. Blair and K. T. Hughes (2008). "Energy source of flagellar type III secretion." <u>Nature</u> **451**(7177): 489-492.

Pereira, L. and T. R. Hoover (2005). "Stable accumulation of sigma54 in Helicobacter pylori requires the novel protein HP0958." J Bacteriol **187**(13): 4463-4469.

Peterson, J. H., C. A. Woolhead and H. D. Bernstein (2003). "Basic amino acids in a distinct subset of signal peptides promote interaction with the signal recognition particle." <u>J Biol Chem</u> **278**(46): 46155-46162.

- Pettersen, E. F., T. D. Goddard, C. C. Huang, E. C. Meng, G. S. Couch, T. I. Croll, J. H. Morris and T. E. Ferrin (2021). "UCSF ChimeraX: Structure visualization for researchers, educators, and developers." Protein Sci **30**(1): 70-82.
- Pinas, G. E., V. Frank, A. Vaknin and J. S. Parkinson (2016). "The source of high signal cooperativity in bacterial chemosensory arrays." Proc Natl Acad Sci U S A **113**(12): 3335-3340.
- Pittman, M. S., M. Goodwin and D. J. Kelly (2001). "Chemotaxis in the human gastric pathogen Helicobacter pylori: different roles for CheW and the three CheV paralogues, and evidence for CheV2 phosphorylation." <u>Microbiology (Reading)</u> **147**(Pt 9): 2493-2504.
- Plummer, M., S. Franceschi, J. Vignat, D. Forman and C. de Martel (2015). "Global burden of gastric cancer attributable to Helicobacter pylori." <u>Int J Cancer</u> **136**(2): 487-490.
- Popham, D. L., D. Szeto, J. Keener and S. Kustu (1989). "Function of a bacterial activator protein that binds to transcriptional enhancers." <u>Science</u> **243**(4891): 629-635.
- Porwollik, S., B. Noonan and P. W. O'Toole (1999). "Molecular characterization of a flagellar export locus of Helicobacter pylori." <u>Infect Immun</u> **67**(5): 2060-2070.
- Powers, M. J. and M. S. Trent (2018). "Phospholipid retention in the absence of asymmetry strengthens the outer membrane permeability barrier to last-resort antibiotics." <u>Proc Natl Acad Sci U S A</u> **115**(36): E8518-E8527.
- Praefcke, G. J. and H. T. McMahon (2004). "The dynamin superfamily: universal membrane tubulation and fission molecules?" Nat Rev Mol Cell Biol 5(2): 133-147.
- Prashar, A., M. I. Capurro and N. L. Jones (2022). "Under the Radar: Strategies Used by Helicobacter pylori to Evade Host Responses." Annu Rev Physiol **84**: 485-506.
- Price, C. E. and A. J. M. Driessen (2010). "Conserved negative charges in the transmembrane segments of subunit K of the NADH:ubiquinone oxidoreductase determine its dependence on YidC for membrane insertion." J Biol Chem **285**(6): 3575-3581.
- Price, C. E., A. Otto, F. Fusetti, D. Becher, M. Hecker and A. J. Driessen (2010). "Differential effect of YidC depletion on the membrane proteome of Escherichia coli under aerobic and anaerobic growth conditions." <u>Proteomics</u> **10**(18): 3235-3247.
- Prouty, M. G., N. E. Correa and K. E. Klose (2001). "The novel sigma54- and sigma28-dependent flagellar gene transcription hierarchy of Vibrio cholerae." <u>Mol Microbiol</u> **39**(6): 1595-1609.
- Qi, H. Y. and H. D. Bernstein (1999). "SecA is required for the insertion of inner membrane proteins targeted by the Escherichia coli signal recognition particle." J Biol Chem **274**(13): 8993-8997.
- Qin, Z., W. T. Lin, S. Zhu, A. T. Franco and J. Liu (2017). "Imaging the motility and chemotaxis machineries in Helicobacter pylori by cryo-electron tomography." J Bacteriol **199**(3): e00695-00616.
- Quarantini, S., L. Cendron and G. Zanotti (2014). "Crystal structure of the secreted protein HP1454 from the human pathogen Helicobacter pylori." <u>Proteins</u> **82**(10): 2868-2873.
- Rader, B. A., C. Wreden, K. G. Hicks, E. G. Sweeney, K. M. Ottemann and K. Guillemin (2011).
- "Helicobacter pylori perceives the quorum-sensing molecule AI-2 as a chemorepellent via the chemoreceptor TlpB." Microbiology (Reading) **157**(Pt 9): 2445-2455.
- Radin, J. N., J. A. Gaddy, C. Gonzalez-Rivera, J. T. Loh, H. M. Algood and T. L. Cover (2013). "Flagellar localization of a Helicobacter pylori autotransporter protein." <u>mBio</u> **4**(2): e00613-00612.
- Radomska, K. A., M. Wosten, S. R. Ordonez, J. A. Wagenaar and J. P. M. van Putten (2017). "Importance of Campylobacter jejuni FliS and FliW in Flagella Biogenesis and Flagellin Secretion." <u>Front Microbiol</u> **8**: 1060.
- Rain, J. C., L. Selig, H. De Reuse, V. Battaglia, C. Reverdy, S. Simon, G. Lenzen, F. Petel, J. Wojcik, V. Schachter, Y. Chemama, A. Labigne and P. Legrain (2001). "The protein-protein interaction map of Helicobacter pylori." Nature **409**(6817): 211-215.
- Rapoport, T. A. (2007). "Protein translocation across the eukaryotic endoplasmic reticulum and bacterial plasma membranes." <u>Nature</u> **450**(7170): 663-669.

- Reid, S. W., M. C. Leake, J. H. Chandler, C. J. Lo, J. P. Armitage and R. M. Berry (2006). "The maximum number of torque-generating units in the flagellar motor of Escherichia coli is at least 11." <u>Proc Natl</u> Acad Sci U S A **103**(21): 8066-8071.
- Renault, T. T., A. O. Abraham, T. Bergmiller, G. Paradis, S. Rainville, E. Charpentier, C. C. Guet, Y. Tu, K. Namba, J. P. Keener, T. Minamino and M. Erhardt (2017). "Bacterial flagella grow through an injection-diffusion mechanism." Elife 6.
- RICHARD A. ALM, P. G., 2 AND TREVOR J. TRUST" (1993). "Distribution and Polymorphism of the Flagellin Genes from Isolates of Campylobacter coli and Campylobacter jejuni." <u>Journal of Bacteriology</u> **Vol. 175. No. 10**: p. 3051-3057.
- Robinson, M. D., D. J. McCarthy and G. K. Smyth (2010). "edgeR: a Bioconductor package for differential expression analysis of digital gene expression data." <u>Bioinformatics</u> **26**(1): 139-140.
- Rocaboy, M., R. Herman, E. Sauvage, H. Remaut, K. Moonens, M. Terrak, P. Charlier and F. Kerff (2013). "The crystal structure of the cell division amidase AmiC reveals the fold of the AMIN domain, a new peptidoglycan binding domain." <u>Mol Microbiol</u> **90**(2): 267-277.
- Roier, S., F. G. Zingl, F. Cakar, S. Durakovic, P. Kohl, T. O. Eichmann, L. Klug, B. Gadermaier, K. Weinzerl, R. Prassl, A. Lass, G. Daum, J. Reidl, M. F. Feldman and S. Schild (2016). "A novel mechanism for the biogenesis of outer membrane vesicles in Gram-negative bacteria." <u>Nat Commun</u> **7**: 10515.
- Rolig, A. S., J. Shanks, J. E. Carter and K. M. Ottemann (2012). "Helicobacter pylori requires TlpD-driven chemotaxis to proliferate in the antrum." <u>Infect Immun</u> **80**(10): 3713-3720.
- Roney, I. J. and D. Z. Rudner (2023). "The DedA superfamily member PetA is required for the transbilayer distribution of phosphatidylethanolamine in bacterial membranes." <u>Proc Natl Acad Sci U S A</u> **120**(20): e2301979120.
- Roney, I. J. and D. Z. Rudner (2023). "Two broadly conserved families of polyprenyl-phosphate transporters." Nature **613**(7945): 729-734.
- Rosinke, K., V. J. Starai and T. R. Hoover (2024). "Helicobacter pylori HP0018 Has a Potential Role in the Maintenance of the Cell Envelope." <u>Cells</u> **13**(17).
- Rosinke, K., S. Tachiyama, J. Mrasek, J. Liu and T. R. Hoover (2025). "A Helicobacter pylori flagellar motor accessory is needed to maintain the barrier function of the outer membrane during flagellar rotation." <u>PLoS Pathog</u> **21**(1): e1012860.
- Roujeinikova, A. (2008). "Cloning, purification and preliminary X-ray analysis of the C-terminal domain of Helicobacter pylori MotB." <u>Acta Crystallogr Sect F Struct Biol Cryst Commun</u> **64**(Pt 4): 277-280.
- Roujeinikova, A. (2008). "Crystal structure of the cell wall anchor domain of MotB, a stator component of the bacterial flagellar motor: implications for peptidoglycan recognition." <u>Proc Natl Acad Sci U S A</u> **105**(30): 10348-10353.
- Ruiz, N., R. M. Davis and S. Kumar (2021). "YhdP, TamB, and YdbH Are Redundant but Essential for Growth and Lipid Homeostasis of the Gram-Negative Outer Membrane." <u>mBio</u> **12**(6): e0271421. Ruiz, N., L. S. Gronenberg, D. Kahne and T. J. Silhavy (2008). "Identification of two inner-membrane proteins required for the transport of lipopolysaccharide to the outer membrane of Escherichia coli." <u>Proc Natl Acad Sci U S A</u> **105**(14): 5537-5542.
- Rust, M., S. Borchert, E. Niehus, S. A. Kuehne, E. Gripp, A. Bajceta, J. L. McMurry, S. Suerbaum, K. T. Hughes and C. Josenhans (2009). "The Helicobacter pylori anti-sigma factor FlgM is predominantly cytoplasmic and cooperates with the flagellar basal body protein FlhA." <u>J Bacteriol</u> **191**(15): 4824-4834. Ryan, K. A., N. Karim, M. Worku, S. A. Moore, C. W. Penn and P. W. O'Toole (2005). "HP0958 is an essential motility gene in Helicobacter pylori." FEMS Microbiol Lett **248**(1): 47-55.
- Saijo-Hamano, Y., H. Matsunami, K. Namba and K. Imada (2019). "Architecture of the Bacterial Flagellar Distal Rod and Hook of Salmonella." <u>Biomolecules</u> **9**(7).

Saito, A., Y. Hizukuri, E. Matsuo, S. Chiba, H. Mori, O. Nishimura, K. Ito and Y. Akiyama (2011). "Post-liberation cleavage of signal peptides is catalyzed by the site-2 protease (S2P) in bacteria." <u>Proc Natl</u> Acad Sci U S A **108**(33): 13740-13745.

Sakamoto, C., R. Satou, H. Tokuda and S. Narita (2010). "Novel mutations of the LolCDE complex causing outer membrane localization of lipoproteins despite their inner membrane-retention signals." <u>Biochem Biophys Res Commun</u> **401**(4): 586-591.

Salama, N. R., M. L. Hartung and A. Muller (2013). "Life in the human stomach: persistence strategies of the bacterial pathogen Helicobacter pylori." Nat Rev Microbiol **11**(6): 385-399.

Samatey, F. A., K. Imada, S. Nagashima, F. Vonderviszt, T. Kumasaka, M. Yamamoto and K. Namba (2001). "Structure of the bacterial flagellar protofilament and implications for a switch for supercoiling." <a href="Nature 410(6826)">Nature 410(6826)</a>: 331-337.

Samatey, F. A., H. Matsunami, K. Imada, S. Nagashima, T. R. Shaikh, D. R. Thomas, J. Z. Chen, D. J. Derosier, A. Kitao and K. Namba (2004). "Structure of the bacterial flagellar hook and implication for the molecular universal joint mechanism." <u>Nature</u> **431**(7012): 1062-1068.

Sanders, L., T. M. Andermann and K. M. Ottemann (2013). "A supplemented soft agar chemotaxis assay demonstrates the Helicobacter pylori chemotactic response to zinc and nickel." <u>Microbiology (Reading)</u> **159**(Pt 1): 46-57.

Sankaran, K. and H. C. Wu (1994). "Lipid modification of bacterial prolipoprotein. Transfer of diacylglyceryl moiety from phosphatidylglycerol." J Biol Chem **269**(31): 19701-19706.

Santini, C. L., B. Ize, A. Chanal, M. Muller, G. Giordano and L. F. Wu (1998). "A novel sec-independent periplasmic protein translocation pathway in Escherichia coli." EMBO J **17**(1): 101-112.

Santiveri, M., A. Roa-Eguiara, C. Kuhne, N. Wadhwa, H. Hu, H. C. Berg, M. Erhardt and N. M. I. Taylor (2020). "Structure and Function of Stator Units of the Bacterial Flagellar Motor." <u>Cell</u> **183**(1): 244-257 e216.

Saraogi, I. and S. O. Shan (2014). "Co-translational protein targeting to the bacterial membrane." <u>Biochim Biophys Acta</u> **1843**(8): 1433-1441.

Sartorio, M. G., E. J. Pardue, M. F. Feldman and M. F. Haurat (2021). "Bacterial Outer Membrane Vesicles: From Discovery to Applications." <u>Annu Rev Microbiol</u> **75**: 609-630.

Sawant, P., K. Eissenberger, L. Karier, T. Mascher and M. Bramkamp (2016). "A dynamin-like protein involved in bacterial cell membrane surveillance under environmental stress." Environ Microbiol **18**(8): 2705-2720.

Schiebel, E., A. J. Driessen, F. U. Hartl and W. Wickner (1991). "Delta mu H+ and ATP function at different steps of the catalytic cycle of preprotein translocase." Cell **64**(5): 927-939.

Schindelin, J., I. Arganda-Carreras, E. Frise, V. Kaynig, M. Longair, T. Pietzsch, S. Preibisch, C. Rueden, S. Saalfeld, B. Schmid, J. Y. Tinevez, D. J. White, V. Hartenstein, K. Eliceiri, P. Tomancak and A. Cardona (2012). "Fiji: an open-source platform for biological-image analysis." Nat Methods **9**(7): 676-682.

Schirm, M., E. C. Soo, A. J. Aubry, J. Austin, P. Thibault and S. M. Logan (2003). "Structural, genetic and functional characterization of the flagellin glycosylation process in Helicobacter pylori." <u>Mol Microbiol</u> **48**(6): 1579-1592.

Schmitz, A., C. Josenhans and S. Suerbaum (1997). "Cloning and characterization of the Helicobacter pylori flbA gene, which codes for a membrane protein involved in coordinated expression of flagellar genes." J Bacteriol 179(4): 987-997.

Schneider, C. A., W. S. Rasband and K. W. Eliceiri (2012). "NIH Image to ImageJ: 25 years of image analysis." Nat Methods **9**(7): 671-675.

Schuhmacher, J. S., F. Rossmann, F. Dempwolff, C. Knauer, F. Altegoer, W. Steinchen, A. K. Dorrich, A. Klingl, M. Stephan, U. Linne, K. M. Thormann and G. Bange (2015). "MinD-like ATPase FlhG effects location and number of bacterial flagella during C-ring assembly." <a href="Proc Natl Acad Sci U S A">Proc Natl Acad Sci U S A</a> 112(10): 3092-3097.

- Schuhmacher, J. S., K. M. Thormann and G. Bange (2015). "How bacteria maintain location and number of flagella?" <u>FEMS Microbiol Rev</u> **39**(6): 812-822.
- Schulze, R. J. and W. R. Zuckert (2006). "Borrelia burgdorferi lipoproteins are secreted to the outer surface by default." <u>Mol Microbiol</u> **59**(5): 1473-1484.
- Seitl, I., S. Wickles, R. Beckmann, A. Kuhn and D. Kiefer (2014). "The C-terminal regions of YidC from Rhodopirellula baltica and Oceanicaulis alexandrii bind to ribosomes and partially substitute for SRP receptor function in Escherichia coli." <u>Mol Microbiol</u> **91**(2): 408-421.
- Serek, J., G. Bauer-Manz, G. Struhalla, L. van den Berg, D. Kiefer, R. Dalbey and A. Kuhn (2004).
- "Escherichia coli YidC is a membrane insertase for Sec-independent proteins." EMBO J 23(2): 294-301.
- Seydel, A., P. Gounon and A. P. Pugsley (1999). "Testing the '+2 rule' for lipoprotein sorting in the Escherichia coli cell envelope with a new genetic selection." Mol Microbiol **34**(4): 810-821.
- Sharma, C. M., S. Hoffmann, F. Darfeuille, J. Reignier, S. Findeiss, A. Sittka, S. Chabas, K. Reiche, J.
- Hackermuller, R. Reinhardt, P. F. Stadler and J. Vogel (2010). "The primary transcriptome of the major human pathogen Helicobacter pylori." <u>Nature</u> **464**(7286): 250-255.
- Shibata, S., H. Matsunami, S. I. Aizawa and M. Wolf (2019). "Torque transmission mechanism of the curved bacterial flagellar hook revealed by cryo-EM." <u>Nat Struct Mol Biol</u> **26**(10): 941-945.
- Shibata, S., N. Takahashi, F. F. Chevance, J. E. Karlinsey, K. T. Hughes and S. Aizawa (2007). "FliK regulates flagellar hook length as an internal ruler." <u>Mol Microbiol</u> **64**(5): 1404-1415.
- Shruthi, H., P. Anand, V. Murugan and K. Sankaran (2010). "Twin arginine translocase pathway and fast-folding lipoprotein biosynthesis in E. coli: interesting implications and applications." <u>Mol Biosyst</u> **6**(6): 999-1007.
- Sidhu, V. K., F. J. Vorholter, K. Niehaus and S. A. Watt (2008). "Analysis of outer membrane vesicle associated proteins isolated from the plant pathogenic bacterium Xanthomonas campestris pv. campestris." BMC Microbiol **8**: 87.
- Silhavy, T. J., D. Kahne and S. Walker (2010). "The bacterial cell envelope." <u>Cold Spring Harb Perspect</u> <u>Biol</u> **2**(5): a000414.
- Silverman, M., J. Zieg and M. Simon (1979). "Flagellar-phase variation: isolation of the rh1 gene." <u>J</u> Bacteriol **137**(1): 517-523.
- Simon, S. M., C. S. Peskin and G. F. Oster (1992). "What drives the translocation of proteins?" <u>Proc Natl</u> Acad Sci U S A **89**(9): 3770-3774.
- Sjoblad, R. D., C. W. Emala and R. N. Doetsch (1983). "Invited review: bacterial flagellar sheaths: structures in search of a function." <u>Cell Motil</u> **3**(1): 93-103.
- Smeets, L. C., J. J. Bijlsma, S. Y. Boomkens, C. M. Vandenbroucke-Grauls and J. G. Kusters (2000). "comH, a novel gene essential for natural transformation of Helicobacter pylori." J Bacteriol **182**(14): 3948-3954.
- Smith, H. C., K. L. May and M. Grabowicz (2023). "Teasing apart the evolution of lipoprotein trafficking in gram-negative bacteria reveals a bifunctional LolA." <u>Proc Natl Acad Sci U S A</u> **120**(6): e2218473120.
- Smith, T. G. and T. R. Hoover (2009). "Deciphering bacterial flagellar gene regulatory networks in the genomic era." <u>Adv Appl Microbiol</u> **67**: 257-295.
- Snijder, H. J., I. Ubarretxena-Belandia, M. Blaauw, K. H. Kalk, H. M. Verheij, M. R. Egmond, N. Dekker and B. W. Dijkstra (1999). "Structural evidence for dimerization-regulated activation of an integral membrane phospholipase." Nature **401**(6754): 717-721.
- Snyder, L. A., N. J. Loman, K. Futterer and M. J. Pallen (2009). "Bacterial flagellar diversity and evolution: seek simplicity and distrust it?" <u>Trends Microbiol</u> **17**(1): 1-5.
- Sommerlad, S. M. and D. R. Hendrixson (2007). "Analysis of the roles of FlgP and FlgQ in flagellar motility of Campylobacter jejuni." J Bacteriol **189**(1): 179-186.
- Spohn, G. and V. Scarlato (1999). "Motility of Helicobacter pylori is coordinately regulated by the transcriptional activator FlgR, an NtrC homolog." <u>J Bacteriol</u> **181**(2): 593-599.

- Srikumar, R., T. Kon, N. Gotoh and K. Poole (1998). "Expression of Pseudomonas aeruginosa multidrug efflux pumps MexA-MexB-OprM and MexC-MexD-OprJ in a multidrug-sensitive Escherichia coli strain." Antimicrob Agents Chemother **42**(1): 65-71.
- Stark, R. M., G. J. Gerwig, R. S. Pitman, L. F. Potts, N. A. Williams, J. Greenman, I. P. Weinzweig, T. R. Hirst and M. R. Millar (1999). "Biofilm formation by Helicobacter pylori." <u>Lett Appl Microbiol</u> **28**(2): 121-126.
- Stead, C. M., A. Beasley, R. J. Cotter and M. S. Trent (2008). "Deciphering the unusual acylation pattern of Helicobacter pylori lipid A." <u>J Bacteriol</u> **190**(21): 7012-7021.
- Steinberg, R., L. Knupffer, A. Origi, R. Asti and H. G. Koch (2018). "Co-translational protein targeting in bacteria." <u>FEMS Microbiol Lett</u> **365**(11).
- Stern, A. S. and H. C. Berg (2013). "Single-file diffusion of flagellin in flagellar filaments." <u>Biophys J</u> **105**(1): 182-184.
- Stevens, C. M. and M. Paetzel (2012). "Purification of a Tat leader peptide by co-expression with its chaperone." <u>Protein Expr Purif</u> **84**(1): 167-172.
- Stone KJ, S. J. (1971). "Mechanism of action of bacitracin: complexation with metal ion and C 55 isoprenyl pyrophosphate." <u>Proc Natl Acad Sci U S A</u> **68(12):3223-7**.
- Strict, J. (1996). <u>Swimming against the Tide: Adrianus Pijper and the Debate over Bacterial Flagella, 1946-1956</u>.
- Sycuro, L. K., Z. Pincus, K. D. Gutierrez, J. Biboy, C. A. Stern, W. Vollmer and N. R. Salama (2010). "Peptidoglycan crosslinking relaxation promotes Helicobacter pylori's helical shape and stomach colonization." <u>Cell</u> **141**(5): 822-833.
- Sycuro, L. K., C. S. Rule, T. W. Petersen, T. J. Wyckoff, T. Sessler, D. B. Nagarkar, F. Khalid, Z. Pincus, J. Biboy, W. Vollmer and N. R. Salama (2013). "Flow cytometry-based enrichment for cell shape mutants identifies multiple genes that influence Helicobacter pylori morphology." <u>Mol Microbiol</u> **90**(4): 869-883.
- Sycuro, L. K., T. J. Wyckoff, J. Biboy, P. Born, Z. Pincus, W. Vollmer and N. R. Salama (2012). "Multiple peptidoglycan modification networks modulate Helicobacter pylori's cell shape, motility, and colonization potential." <u>PLoS Pathog</u> **8**(3): e1002603.
- Tachiyama, S., K. L. Chan, X. Liu, S. Hathroubi, B. Peterson, M. F. Khan, K. M. Ottemann, J. Liu and A. Roujeinikova (2022). "The flagellar motor protein FliL forms a scaffold of circumferentially positioned rings required for stator activation." <u>Proc Natl Acad Sci U S A</u> **119**(4).
- Tajima, T., N. Yokota, S. Matsuyama and H. Tokuda (1998). "Genetic analyses of the in vivo function of LolA, a periplasmic chaperone involved in the outer membrane localization of Escherichia coli lipoproteins." FEBS Lett **439**(1-2): 51-54.
- Takekawa, N., M. Isumi, H. Terashima, S. Zhu, Y. Nishino, M. Sakuma, S. Kojima, M. Homma and K. Imada (2019). "Structure of Vibrio FliL, a New Stomatin-like Protein That Assists the Bacterial Flagellar Motor Function." <u>mBio</u> **10**(2).
- Tambalo, D. D., D. E. Bustard, K. L. Del Bel, S. F. Koval, M. F. Khan and M. F. Hynes (2010).
- "Characterization and functional analysis of seven flagellin genes in Rhizobium leguminosarum bv. viciae. Characterization of R. leguminosarum flagellins." <u>BMC Microbiol</u> **10**: 219.
- Tan, J., X. Zhang, X. Wang, C. Xu, S. Chang, H. Wu, T. Wang, H. Liang, H. Gao, Y. Zhou and Y. Zhu (2021). "Structural basis of assembly and torque transmission of the bacterial flagellar motor." <u>Cell</u> **184**(10): 2665-2679 e2619.
- Tanaka, K., S. I. Matsuyama and H. Tokuda (2001). "Deletion of lolB, encoding an outer membrane lipoprotein, is lethal for Escherichia coli and causes accumulation of lipoprotein localization intermediates in the periplasm." J Bacteriol **183**(22): 6538-6542.
- Tanaka, S. Y., S. Narita and H. Tokuda (2007). "Characterization of the Pseudomonas aeruginosa Lol system as a lipoprotein sorting mechanism." J Biol Chem **282**(18): 13379-13384.
- Tang, H., T. F. Braun and D. F. Blair (1996). "Motility protein complexes in the bacterial flagellar motor." <u>J</u> Mol Biol **261**(2): 209-221.

Taniguchi, N. and H. Tokuda (2008). "Molecular events involved in a single cycle of ligand transfer from an ATP binding cassette transporter, LolCDE, to a molecular chaperone, LolA." <u>J Biol Chem</u> **283**(13): 8538-8544.

Tannaes, T., N. Dekker, G. Bukholm, J. J. Bijlsma and B. J. Appelmelk (2001). "Phase variation in the Helicobacter pylori phospholipase A gene and its role in acid adaptation." <u>Infect Immun</u> **69**(12): 7334-7340.

Team, R. C. (2020). "R: A language and environment for statistical

computing." from <a href="https://www.R-project.org/">https://www.R-project.org/</a>.

Terada, M., T. Kuroda, S. I. Matsuyama and H. Tokuda (2001). "Lipoprotein sorting signals evaluated as the LolA-dependent release of lipoproteins from the cytoplasmic membrane of Escherichia coli." <u>J Biol Chem</u> **276**(50): 47690-47694.

Terashima, H., N. Li, M. Sakuma, M. Koike, S. Kojima, M. Homma and K. Imada (2013). "Insight into the assembly mechanism in the supramolecular rings of the sodium-driven Vibrio flagellar motor from the structure of FlgT." Proc Natl Acad Sci U S A **110**(15): 6133-6138.

Terry, K., A. C. Go and K. M. Ottemann (2006). "Proteomic mapping of a suppressor of non-chemotactic cheW mutants reveals that Helicobacter pylori contains a new chemotaxis protein." <u>Mol Microbiol</u> **61**(4): 871-882.

Terry, K., S. M. Williams, L. Connolly and K. M. Ottemann (2005). "Chemotaxis plays multiple roles during Helicobacter pylori animal infection." <u>Infect Immun</u> **73**(2): 803-811.

Teufel, F., J. J. Almagro Armenteros, A. R. Johansen, M. H. Gislason, S. I. Pihl, K. D. Tsirigos, O. Winther, S. Brunak, G. von Heijne and H. Nielsen (2022). "SignalP 6.0 predicts all five types of signal peptides using protein language models." <u>Nat Biotechnol</u> **40**(7): 1023-1025.

Thibault, P., S. M. Logan, J. F. Kelly, J. R. Brisson, C. P. Ewing, T. J. Trust and P. Guerry (2001).

"Identification of the carbohydrate moieties and glycosylation motifs in Campylobacter jejuni flagellin." <u>J</u> Biol Chem **276**(37): 34862-34870.

Thomashow, L. S. and S. C. Rittenberg (1985). "Isolation and composition of sheathed flagella from Bdellovibrio bacteriovorus 109J." J Bacteriol **163**(3): 1047-1054.

Thong, S., B. Ercan, F. Torta, Z. Y. Fong, H. Y. Wong, M. R. Wenk and S. S. Chng (2016). "Defining key roles for auxiliary proteins in an ABC transporter that maintains bacterial outer membrane lipid asymmetry." Elife **5**.

Thormann, K. M., C. Beta and M. J. Kuhn (2022). "Wrapped Up: The Motility of Polarly Flagellated Bacteria." Annu Rev Microbiol **76**: 349-367.

Tikhonova, E. B., Q. Wang and H. I. Zgurskaya (2002). "Chimeric analysis of the multicomponent multidrug efflux transporters from gram-negative bacteria." J Bacteriol **184**(23): 6499-6507.

Tokunaga, M., H. Tokunaga and H. C. Wu (1982). "Post-translational modification and processing of Escherichia coli prolipoprotein in vitro." <u>Proc Natl Acad Sci U S A</u> **79**(7): 2255-2259.

Tomkiewicz, D., N. Nouwen, R. van Leeuwen, S. Tans and A. J. Driessen (2006). "SecA supports a constant rate of preprotein translocation." J Biol Chem **281**(23): 15709-15713.

Tsang, J., T. Hirano, T. R. Hoover and J. L. McMurry (2015). "Helicobacter pylori FlhA Binds the Sensor Kinase and Flagellar Gene Regulatory Protein FlgS with High Affinity." J Bacteriol **197**(11): 1886-1892.

Tsang, J. and T. R. Hoover (2014). "Requirement of the flagellar protein export apparatus component FliO for optimal expression of flagellar genes in Helicobacter pylori." J Bacteriol 196(15): 2709-2717.

Tsang, J., T. G. Smith, L. E. Pereira and T. R. Hoover (2013). "Insertion mutations in Helicobacter pylori flhA reveal strain differences in RpoN-dependent gene expression." <u>Microbiology (Reading)</u> **159**(Pt 1): 58-67.

Tsirigotaki, A., J. De Geyter, N. Sostaric, A. Economou and S. Karamanou (2017). "Protein export through the bacterial Sec pathway." <u>Nat Rev Microbiol</u> **15**(1): 21-36.

Tsukahara, J., K. Mukaiyama, S. Okuda, S. Narita and H. Tokuda (2009). "Dissection of LolB function-lipoprotein binding, membrane targeting and incorporation of lipoproteins into lipid bilayers." <u>FEBS J</u> **276**(16): 4496-4504.

Tsukazaki, T., H. Mori, Y. Echizen, R. Ishitani, S. Fukai, T. Tanaka, A. Perederina, D. G. Vassylyev, T. Kohno, A. D. Maturana, K. Ito and O. Nureki (2011). "Structure and function of a membrane component SecDF that enhances protein export." Nature **474**(7350): 235-238.

Typas, A., M. Banzhaf, B. van den Berg van Saparoea, J. Verheul, J. Biboy, R. J. Nichols, M. Zietek, K. Beilharz, K. Kannenberg, M. von Rechenberg, E. Breukink, T. den Blaauwen, C. A. Gross and W. Vollmer (2010). "Regulation of peptidoglycan synthesis by outer-membrane proteins." <u>Cell</u> **143**(7): 1097-1109. Ureta, A. R., R. G. Endres, N. S. Wingreen and T. J. Silhavy (2007). "Kinetic analysis of the assembly of the outer membrane protein LamB in Escherichia coli mutants each lacking a secretion or targeting factor in a different cellular compartment." <u>J Bacteriol</u> **189**(2): 446-454.

Vallese, F., N. M. Mishra, M. Pagliari, P. Berto, G. Codolo, M. de Bernard and G. Zanotti (2017). "Helicobacter pylori antigenic Lpp20 is a structural homologue of Tipalpha and promotes epithelial-mesenchymal transition." <u>Biochim Biophys Acta Gen Subi</u> **1861**(12): 3263-3271.

van Amsterdam, K. and A. van der Ende (2004). "Helicobacter pylori HP1034 (ylxH) is required for motility." Helicobacter **9**(5): 387-395.

Van den Berg, B., W. M. Clemons, Jr., I. Collinson, Y. Modis, E. Hartmann, S. C. Harrison and T. A. Rapoport (2004). "X-ray structure of a protein-conducting channel." <u>Nature</u> **427**(6969): 36-44. van der Laan, M., M. L. Urbanus, C. M. Ten Hagen-Jongman, N. Nouwen, B. Oudega, N. Harms, A. J. Driessen and J. Luirink (2003). "A conserved function of YidC in the biogenesis of respiratory chain complexes." Proc Natl Acad Sci U S A **100**(10): 5801-5806.

van der Sluis, E. O., E. van der Vries, G. Berrelkamp, N. Nouwen and A. J. Driessen (2006). "Topologically fixed SecG is fully functional." <u>J Bacteriol</u> **188**(3): 1188-1190.

van Vliet, A. H., E. J. Kuipers, J. Stoof, S. W. Poppelaars and J. G. Kusters (2004). "Acid-responsive gene induction of ammonia-producing enzymes in Helicobacter pylori is mediated via a metal-responsive repressor cascade." <u>Infect Immun</u> **72**(2): 766-773.

Varadi, M., S. Anyango, M. Deshpande, S. Nair, C. Natassia, G. Yordanova, D. Yuan, O. Stroe, G. Wood, A. Laydon, A. Zidek, T. Green, K. Tunyasuvunakool, S. Petersen, J. Jumper, E. Clancy, R. Green, A. Vora, M. Lutfi, M. Figurnov, A. Cowie, N. Hobbs, P. Kohli, G. Kleywegt, E. Birney, D. Hassabis and S. Velankar (2022). "AlphaFold Protein Structure Database: massively expanding the structural coverage of protein-sequence space with high-accuracy models." <u>Nucleic Acids Res</u> **50**(D1): D439-D444.

Velez-Gonzalez, F., A. Marcos-Vilchis, B. Vega-Baray, G. Dreyfus, S. Poggio and L. Camarena (2024). "Rotation of the Fla2 flagella of Cereibacter sphaeroides requires the periplasmic proteins MotK and MotE that interact with the flagellar stator protein MotB2." <u>PLoS One</u> **19**(3): e0298028.

Vogeley, L., T. El Arnaout, J. Bailey, P. J. Stansfeld, C. Boland and M. Caffrey (2016). "Structural basis of lipoprotein signal peptidase II action and inhibition by the antibiotic globomycin." <u>Science</u> **351**(6275): 876-880.

von Heijne, G. (1990). "The signal peptide." J Membr Biol 115(3): 195-201.

Wadhwa, N., R. Phillips and H. C. Berg (2019). "Torque-dependent remodeling of the bacterial flagellar motor." Proc Natl Acad Sci U S A **116**(24): 11764-11769.

Wagner, S., I. Grin, S. Malmsheimer, N. Singh, C. E. Torres-Vargas and S. Westerhausen (2018). "Bacterial type III secretion systems: a complex device for the delivery of bacterial effector proteins into eukaryotic host cells." <u>FEMS Microbiol Lett</u> **365**(19).

Wagner, S., L. Konigsmaier, M. Lara-Tejero, M. Lefebre, T. C. Marlovits and J. E. Galan (2010). "Organization and coordinated assembly of the type III secretion export apparatus." <u>Proc Natl Acad Sci U</u> S A **107**(41): 17745-17750.

- Wagner, S., O. I. Pop, G. J. Haan, L. Baars, G. Koningstein, M. M. Klepsch, P. Genevaux, J. Luirink and J. W. de Gier (2008). "Biogenesis of MalF and the MalFGK(2) maltose transport complex in Escherichia coli requires YidC." J Biol Chem 283(26): 17881-17890.
- Waite, D. W., I. Vanwonterghem, C. Rinke, D. H. Parks, Y. Zhang, K. Takai, S. M. Sievert, J. Simon, B. J. Campbell, T. E. Hanson, T. Woyke, M. G. Klotz and P. Hugenholtz (2017). "Comparative Genomic Analysis of the Class Epsilonproteobacteria and Proposed Reclassification to Epsilonbacteraeota (phyl. nov.)." <u>Front Microbiol</u> **8**: 682.
- Waldo, G. S., B. M. Standish, J. Berendzen and T. C. Terwilliger (1999). "Rapid protein-folding assay using green fluorescent protein." <u>Nat Biotechnol</u> **17**(7): 691-695.
- Wang, F., A. M. Burrage, S. Postel, R. E. Clark, A. Orlova, E. J. Sundberg, D. B. Kearns and E. H. Egelman (2017). "A structural model of flagellar filament switching across multiple bacterial species." <u>Nat Commun</u> **8**(1): 960.
- Wassenaar, T. M., N. M. Bleumink-Pluym, D. G. Newell, P. J. Nuijten and B. A. van der Zeijst (1994). "Differential flagellin expression in a flaA flaB+ mutant of Campylobacter jejuni." <u>Infect Immun</u> **62**(9): 3901-3906
- Watts, G. (2005). "Nobel prize is awarded to doctors who discovered H pylori." <u>BMJ</u> **331**(7520): 795. Wehmeier, S., A. S. Varghese, S. S. Gurcha, B. Tissot, M. Panico, P. Hitchen, H. R. Morris, G. S. Besra, A. Dell and M. C. Smith (2009). "Glycosylation of the phosphate binding protein, PstS, in Streptomyces coelicolor by a pathway that resembles protein O-mannosylation in eukaryotes." <u>Mol Microbiol</u> **71**(2): 421-433.
- Weibull, C. (1948). "Some chemical and physico-chemical properties of the flagella of Proteus vulgaris." <u>Biochim. Biophys</u> **2, 351–361.**
- Weibull, C. (1949). "Chemical and physicochemical properties of the flagella of Proteus vulgaris and Bacillus subtilis a comparison." <u>Biochim. Biophys. Acta</u> **3, 378–382**.
- Weibull, C. (1950). "Electrophoretic and Titrimetric Measurements on Bacterial Flagella." <u>Acta Chem.</u> Scand **4, 260–267.**
- Weibull, C. (1953). "The Free Amino Groups of the Proteus Flagella Protein-Quantitative Determination of Dinitrophenyl Amino Acids Using Paper Chromatography." Acta Chem. Scand **7**, **335–339**.
- Wickles, S., A. Singharoy, J. Andreani, S. Seemayer, L. Bischoff, O. Berninghausen, J. Soeding, K. Schulten, E. O. van der Sluis and R. Beckmann (2014). "A structural model of the active ribosome-bound membrane protein insertase YidC." Elife **3**: e03035.
- Wickstrom, D., S. Wagner, P. Simonsson, O. Pop, L. Baars, A. J. Ytterberg, K. J. van Wijk, J. Luirink and J. W. de Gier (2011). "Characterization of the consequences of YidC depletion on the inner membrane proteome of E. coli using 2D blue native/SDS-PAGE." J Mol Biol 409(2): 124-135.
- Wiktor, M., D. Weichert, N. Howe, C. Y. Huang, V. Olieric, C. Boland, J. Bailey, L. Vogeley, P. J. Stansfeld, N. Buddelmeijer, M. Wang and M. Caffrey (2017). "Structural insights into the mechanism of the membrane integral N-acyltransferase step in bacterial lipoprotein synthesis." Nat Commun **8**: 15952.
- Williams, A. W., S. Yamaguchi, F. Togashi, S. I. Aizawa, I. Kawagishi and R. M. Macnab (1996). "Mutations in flik and flhB affecting flagellar hook and filament assembly in Salmonella typhimurium." <u>J Bacteriol</u> **178**(10): 2960-2970.
- Williams, S. M., Y. T. Chen, T. M. Andermann, J. E. Carter, D. J. McGee and K. M. Ottemann (2007). "Helicobacter pylori chemotaxis modulates inflammation and bacterium-gastric epithelium interactions in infected mice." <u>Infect Immun</u> **75**(8): 3747-3757.
- Winkler, H. (2007). "3D reconstruction and processing of volumetric data in cryo-electron tomography." J Struct Biol **157**(1): 126-137.
- Winkler, H., P. Zhu, J. Liu, F. Ye, K. H. Roux and K. A. Taylor (2009). "Tomographic subvolume alignment and subvolume classification applied to myosin V and SIV envelope spikes." J Struct Biol 165(2): 64-77.

- Wolgemuth, C. W. (2015). "Flagellar motility of the pathogenic spirochetes." <u>Semin Cell Dev Biol</u> **46**: 104-112.
- Worku, M. L., Q. N. Karim, J. Spencer and R. L. Sidebotham (2004). "Chemotactic response of Helicobacter pylori to human plasma and bile." J Med Microbiol **53**(Pt 8): 807-811.
- Wroblewski, L. E., R. M. Peek, Jr. and K. T. Wilson (2010). "Helicobacter pylori and gastric cancer: factors that modulate disease risk." Clin Microbiol Rev **23**(4): 713-739.
- Wu, H. C., J. S. Lai, S. Hayashi and C. Z. Giam (1982). "Biogenesis of membrane lipoproteins in Escherichia coli." Biophys J **37**(1): 307-315.
- Wu, T., A. C. McCandlish, L. S. Gronenberg, S. S. Chng, T. J. Silhavy and D. Kahne (2006). "Identification of a protein complex that assembles lipopolysaccharide in the outer membrane of Escherichia coli." <u>Proc Natl Acad Sci U S A</u> **103**(31): 11754-11759.
- Wuichet, K., R. P. Alexander and I. B. Zhulin (2007). "Comparative genomic and protein sequence analyses of a complex system controlling bacterial chemotaxis." <u>Methods Enzymol</u> **422**: 1-31.
- Wuichet, K. and I. B. Zhulin (2010). "Origins and diversification of a complex signal transduction system in prokaryotes." Sci Signal **3**(128): ra50.
- Wunder, C., Y. Churin, F. Winau, D. Warnecke, M. Vieth, B. Lindner, U. Zahringer, H. J. Mollenkopf, E. Heinz and T. F. Meyer (2006). "Cholesterol glucosylation promotes immune evasion by Helicobacter pylori." Nat Med **12**(9): 1030-1038.
- Xie, K., T. Hessa, S. Seppala, M. Rapp, G. von Heijne and R. E. Dalbey (2007). "Features of transmembrane segments that promote the lateral release from the translocase into the lipid phase." <u>Biochemistry</u> **46**(51): 15153-15161.
- Xing, Q., K. Shi, A. Portaliou, P. Rossi, A. Economou and C. G. Kalodimos (2018). "Structures of chaperone-substrate complexes docked onto the export gate in a type III secretion system." <u>Nat</u> Commun **9**(1): 1773.
- Xiong, Q., M. K. Morphew, C. L. Schwartz, A. H. Hoenger and D. N. Mastronarde (2009). "CTF determination and correction for low dose tomographic tilt series." <u>J Struct Biol</u> **168**(3): 378-387. Yahr, T. L. and W. T. Wickner (2001). "Functional reconstitution of bacterial Tat translocation in vitro." EMBO J **20**(10): 2472-2479.
- Yakushi, T., K. Masuda, S. Narita, S. Matsuyama and H. Tokuda (2000). "A new ABC transporter mediating the detachment of lipid-modified proteins from membranes." <u>Nat Cell Biol</u> **2**(4): 212-218. Yakushi, T., T. Tajima, S. Matsuyama and H. Tokuda (1997). "Lethality of the covalent linkage between mislocalized major outer membrane lipoprotein and the peptidoglycan of Escherichia coli." <u>J Bacteriol</u> **179**(9): 2857-2862.
- Yamaguchi, K., F. Yu and M. Inouye (1988). "A single amino acid determinant of the membrane localization of lipoproteins in E. coli." <u>Cell</u> **53**(3): 423-432.
- Yamaguchi, T., F. Makino, T. Miyata, T. Minamino, T. Kato and K. Namba (2021). "Structure of the molecular bushing of the bacterial flagellar motor." Nat Commun **12**(1): 4469.
- Yang, D. C., K. M. Blair, J. A. Taylor, T. W. Petersen, T. Sessler, C. M. Tull, C. K. Leverich, A. L. Collar, T. J. Wyckoff, J. Biboy, W. Vollmer and N. R. Salama (2019). "A Genome-Wide Helicobacter pylori
- Morphology Screen Uncovers a Membrane-Spanning Helical Cell Shape Complex." J Bacteriol **201**(14). Yao, R., D. H. Burr, P. Doig, T. J. Trust, H. Niu and P. Guerry (1994). "Isolation of motile and non-motile
- insertional mutants of Campylobacter jejuni: the role of motility in adherence and invasion of eukaryotic cells." Mol Microbiol **14**(5): 883-893.
- Yeow, J., K. W. Tan, D. A. Holdbrook, Z. S. Chong, J. K. Marzinek, P. J. Bond and S. S. Chng (2018). "The architecture of the OmpC-MlaA complex sheds light on the maintenance of outer membrane lipid asymmetry in Escherichia coli." J Biol Chem **293**(29): 11325-11340.
- Yonekura, K., S. Maki-Yonekura and K. Namba (2002). "Growth mechanism of the bacterial flagellar filament." Res Microbiol **153**(4): 191-197.

- Yoon, S. S. and J. J. Mekalanos (2008). "Decreased potency of the Vibrio cholerae sheathed flagellum to trigger host innate immunity." <u>Infect Immun</u> **76**(3): 1282-1288.
- Zavan, L., N. J. Bitto, E. L. Johnston, D. W. Greening and M. Kaparakis-Liaskos (2019). "Helicobacter pylori Growth Stage Determines the Size, Protein Composition, and Preferential Cargo Packaging of Outer Membrane Vesicles." <u>Proteomics</u> **19**(1-2): e1800209.
- Zhang, K. (2016). "Gctf: Real-time CTF determination and correction." <u>J Struct Biol</u> **193**(1): 1-12. Zhao, X., S. J. Norris and J. Liu (2014). "Molecular architecture of the bacterial flagellar motor in cells." Biochemistry **53**(27): 4323-4333.
- Zheng, S. Q., E. Palovcak, J. P. Armache, K. A. Verba, Y. Cheng and D. A. Agard (2017). "MotionCor2: anisotropic correction of beam-induced motion for improved cryo-electron microscopy." <u>Nat Methods</u> **14**(4): 331-332.
- Zhou, J. and D. F. Blair (1997). "Residues of the cytoplasmic domain of MotA essential for torque generation in the bacterial flagellar motor." <u>J Mol Biol</u> **273**(2): 428-439.
- Zhou, X., M. F. Khan, Y. Xin, K. L. Chan and A. Roujeinikova (2024). "Biochemical characterization of paralyzed flagellum proteins A (PfIA) and B (PfIB) from Helicobacter pylori flagellar motor." <u>Biosci Rep</u> **44**(9).
- Zhu, L., H. R. Kaback and R. E. Dalbey (2013). "YidC protein, a molecular chaperone for LacY protein folding via the SecYEG protein machinery." J Biol Chem **288**(39): 28180-28194.
- Zhu, L., A. Wasey, S. H. White and R. E. Dalbey (2013). "Charge composition features of model single-span membrane proteins that determine selection of YidC and SecYEG translocase pathways in Escherichia coli." J Biol Chem 288(11): 7704-7716.
- Zimmer, J., Y. Nam and T. A. Rapoport (2008). "Structure of a complex of the ATPase SecA and the protein-translocation channel." <u>Nature</u> **455**(7215): 936-943.
- Zoufaly, S., J. Frobel, P. Rose, T. Flecken, C. Maurer, M. Moser and M. Muller (2012). "Mapping precursor-binding site on TatC subunit of twin arginine-specific protein translocase by site-specific photo cross-linking." J Biol Chem 287(16): 13430-13441.